QUEEN MARY UNIVERSITY OF LONDON

Novel approaches for Ru-promoted C–H arylation methods

Submitted in partial fulfilment of the requirements of the Degree of Doctor of Philosophy

Marco Simonetti

2015

Statement of originality

I, Marco Simonetti, confirm that the research included within this thesis is my own work or that where it has been carried out in collaboration with, or supported by others, that this is duly acknowledged below and my contribution indicated. Previously published material is also acknowledged below.

I attest that I have exercised reasonable care to ensure that the work is original, and does not to the best of my knowledge break any UK law, infringe any third party's copyright or other Intellectual Property Right, or contain any confidential material.

I accept that the College has the right to use plagiarism detection software to check the electronic version of the thesis.

I confirm that this thesis has not been previously submitted for the award of a degree by this or any other university.

The copyright of this thesis rests with the author and no quotation from it or information derived from it may be published without the prior written consent of the author.

Signature: 

Date: 21/12/2015

Details of collaboration and publications:

2. M. Simonetti, G. J. P. Perry, X. C. Cambeiro, F. Juliá-Hernández, J. N. Arokianathar and I. Larrosa, "Ru-catalyzed C–H Arylation of Fluoroarenes with Aryl Halides"
Submitted

1. F. Juliá-Hérnandez, M. Simonetti and I. Larrosa, "Metalation Dictates Remote Regioselectivity: Ruthenium-Catalysed Functionalization of *meta* C_{Ar}–H Bonds" *Angew. Chem. Int. Ed.* **2013**, *52*, 11458

Abstract

The development of new procedures for the production of biologically and industrially relevant compounds still remains a big challenge in chemistry. The biaryl motif is ubiquitous among a wide range of compounds of industrial importance. For example, the biaryl skeleton is found in molecular switches and motors, agrochemicals or medicines such as antifungal, anticancer, antibiotics, anti-inflammatory treatments. These properties make the biaryl functionality a highly desirable synthetic target, for both commercial and research purposes. In this context, C–H arylation has been acknowledged as a useful alternative to traditional cross-couplings, replacing the organometallic coupling partner by a non-prefunctionalised substrate in the reaction with a haloarene.

Approaches for the development of Ru-catalysed C–H arylation methodologies are presented herein.

The introduction provides a general overview about different strategies employed in metal-catalysed direct C–H arylation methods. The rational behind selectivity and reactivity are also thoroughly discussed.

The second chapter describes studies on the C–H activation of perfluorinated arenes by Ru(II)-species. The synthesis of unprecedented aryl rutyhenium complexes and mechanistic considerations on the metalation of the arene are presented. In the last part of the second chapter the development of a bis-cationic rutehium(II) complex able to catalyse direct C–H arylation of electron-poor arenes with bromoarenes in the absence of any directing group is described. A complete mechanistic analysis, along with the scope of the methodology, is therefore given.

Table of Contents

Notations and Abbreviations

Ac	Acyl
Ar	Aryl
Ad	1-Adamantyl
AcOH	Acetic acid
Bn	Benzyl
BQ	1,4-Benzoquinone
Bzq	Benzo[*h*]quinoline
coe	Cyclooctene
cod	1,5-Cyclooctadiene
Cp*	1,2,3,4,5-pentamethylcyclopentadienyl
CPME	Cyclopentyl methyl ether
CSA	Camphorsulfonic acid
CMD	**C**oncerted **M**etalation **D**eprotonation
Cy	Cyclohexyl
DCE	1,2-Dichloroethane
DMPU	1,3-Dimethyl-3,4,5,6-tetrahydro-2(1*H*)-pyrimidinone
dppb	1,4-Bis(diphenylphosphino)butane
dppe	1,2-Bis(diphenylphosphino)ethane
dtpy	2,6-Di-*tert*-butylpyridine
DG	Directing group
DME	1,2-Dimethoxyethane
DMEDA	1,2-Bis(methylamino)ethane

DMF	*N*,*N*-Dimethylformamide
DMSO	Dimethylsulfoxide
DTBP	di-*tert*-butyl peroxide
EDG	Electron-donating group
equiv	Equivalent
EWG	Electron-withdrawing group
Gly	Glycine
HFIP	1,1,1,3,3,3-Hexafluoro-2-propanol
HMPT	Tris(dimethylamino)phosphine
Ile	Isoleucine
Ind	Indenyl
L	Ligand
MPA	Mono-protected amino acid
Mes	Mesityl
MS	Molecular sieves
MTBE	2-Methoxy-2-methylpropane
NMR	Nuclear magnetic resonance
NBS	*N*-Bromosuccinimide
NCS	*N*-Chlorosuccinimide
OTf	Trifluoromethansulfonate
OAc	Acetate
PC	Propylene carbonate
PEPPSI	**P**yridine-**e**nhanced **p**recatalyst **p**reparation **s**tabilization and **i**nitiation

Ph	Phenyl
Phen	1,10-Phenanthroline
PhDavehos	2-diphenylphosphino-2-(*N*,*N*-dimethylamino)biphenyl
Piv	Pivaloyl
rt	Room temperature
S_EAr	Electrophilic aromatic substitution
TEMPO	(2,2,6,6-Tetramethyl-piperidin-1-yl)oxyl
TBAB	*tert*-Butylammonium bromide
TBATB	tetrabutylammonium tribromide
Tf	Triflyl
TFA	Trifluoroacetic acid
THF	Tetrahydrofuran
TIPS	Triisopropylsilyl
Ts	Tosyl
Val	Valine

Chapter 1. Metal-Catalysed Direct C_{Ar}–C_{Ar} C–H Arylation: Strategies and Methods

1.1. Introduction

The development of new methodologies for the production of biologically and industrially relevant compounds still remains a big challenge in Chemistry. The biaryl motif is ubiquitous among the wide range of industrially important compounds.[1] For example, the biaryl skeleton is found in molecular switches, motors, agrochemicals, and medicines such as antifungal, anticancer, antibiotics, anti-inflammatory treatments (Figure 1.1). This potential makes the biaryl functionality a highly desirable synthetic target, for both commercial and research purposes.

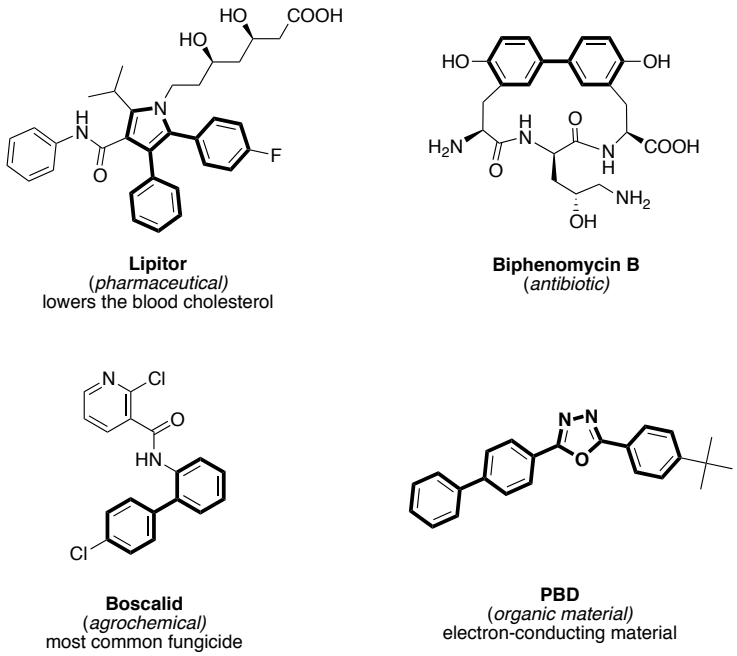

Figure 1.1. Selected industrially important bi(hetero)aryls.

Over the past decade Lipitor generated $115 billion in cumulative global revenue. Boscalid is registered for foliar feeding on a wide range of vegetables, fruits and nut crops and is one of the most commonly employed fungicides. Other examples of biaryl-containing molecules are Biphenomicyn B (inhibits the protein biosynthesis) and PBD (a component of OLEDs, organic light emitting diode). Thus, approaches for the synthesis of the biaryl unit have attracted tremendous interest from the synthetic community in the past few decades.

1.2. Traditional transition metal-catalysed cross coupling reactions

Based on pioneering studies by Ullmann and Goldberg,[2] regioselective synthesis of biaryls mostly takes advantage of transition metal-catalysed cross-coupling reactions between organic (pseudo)halides and stoichiometric amounts of organometallic reagents.[3] This methodology is still the modern method of choice for the formation of C_{Ar}–C_{Ar} bonds, its importance was recognised with the 2010 Nobel Prize in Chemistry, awarded to three of the main contributors (Suzuki, Negishi and Heck).[4] As shown in Scheme 1.1, the identity of the metal **M** varies, depending on the specific case. The name of the reaction assumes different names after the chemist who developed it.

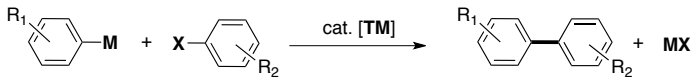

TM = Transition Metal
M = B (Suzuki), Zn (Negishi), Sn (Stille), Mg (Kumada), Si (Hiyama)
X = (pseudo)halide

Scheme 1.1. General scheme for traditional cross-coupling reactions.

The most commonly accepted mechanism for this transformation is described in Scheme 1.2. The first step is the oxidative addition of the (pseudo)haloarene into the $L_y\mathbf{TM}^n$ forming **I**. This transmetalates with a molecule of organometallic reagent to form species **II** which, after reductive elimination, provides the biaryl with concomitant regeneration of the catalyst.

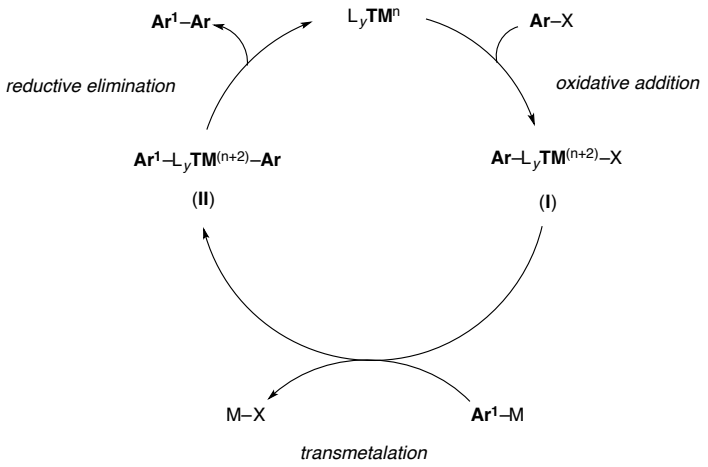

Scheme 1.2. Mechanism of traditional metal-catalysed cross-coupling reactions.

Although highly effective, traditional cross-couplings have intrinsic limitations: 1) the requirement of organometallic nucleophilic reagents which, if they are functionalised, are seldom commercially available or are relatively expensive; 2) their preparation from the corresponding arenes involves several steps, during which undesired by-products might be formed; and 3) at the end of each catalytic cycle a molecule of frequently toxic waste material (M-X) is produced.

1.3. Metal-catalysed direct C–H bond arylation

In the past years, the concept of sustainability has become one of the main guiding principles in several areas of science and engineering,[5] therefore "green chemistry" is of increasing importance. In view of this, more attention has been redirected towards developing synthetic chemistry that is energy and resource efficient. Catalysis, indeed, has been shown to be a powerful tool that can fulfil the sustainability requirement: high yields, selectivity, atom economy and reaction efficiency.[6]

In recent years, transition-metal-catalysed direct arylation *via* C–H bond activation (Scheme 1.3, *pathway B*), the coupling of an arene (C_{Ar}–H) with an aryl halide (C_{Ar}–X), has

been deeply studied and it has shown to be an alternative to traditional cross-coupling reactions (Scheme 1.3, *pathway A*).[7]

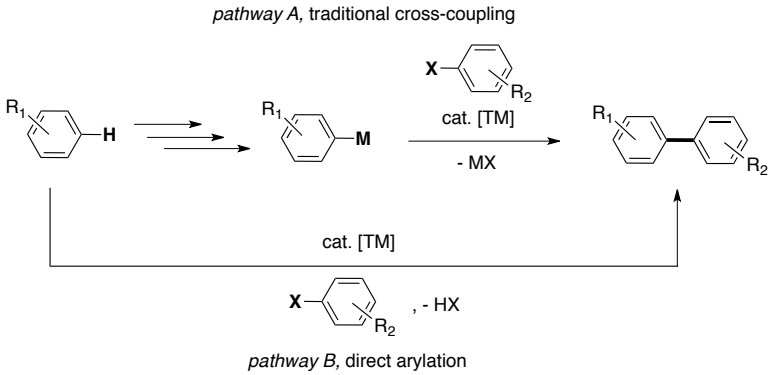

Scheme 1.3. Comparison between classical cross-coupling and direct arylation.

Metal-catalysed direct C–H arylations can be differentiated, on the basis of the nature of the coupling partners into, 1) oxidative arylation and 2) reaction with aryl (pseudo)halides as electrophilic coupling partners (Scheme 1.4). Oxidative arylation requires the presence of an oxidant and can be achieved with either a stoichiometric amount of organometallic reagent (Scheme 1.4, equation *a*) or (hetero)arenes as coupling partner (Scheme 1.4, equation *b*). Since the use of organometallic reagents is associated with the formation of undesired by-products, the dehydrogenative arylation represents what may be considered the ultimate aim of C–H activation, without the need for either "M" or "X" activating groups. However, since the C–H bond is ubiquitous in organic compounds, the inherent difficulty of differentiating and activating one specific position, and cross *versus* homo-coupling selectivity still constitute major challenges. Instead, the direct arylation with (pseudo)halides (Scheme 1.4) can constitute a good alternative for overcoming these disadvantages, which makes it arguably the reaction of greatest impact on bi(hetero)aryls synthesis since the development of traditional cross couplings.

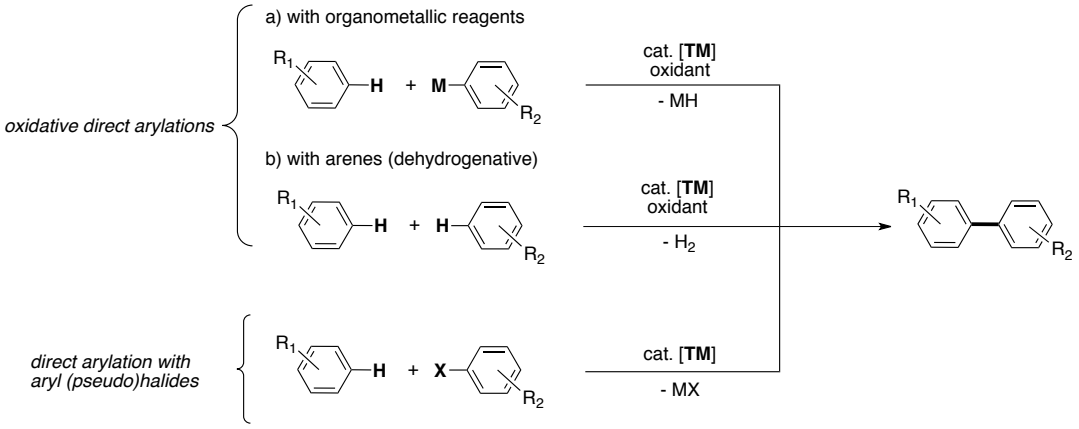

Scheme 1.4. Strategies for catalytic direct arylation for the synthesis of biaryls.

From a mechanistic point of view, TM-catalysed direct arylation processes are often proposed to occur *via* oxidative addition of the aryl halide to the transition metal (to give **III**), followed by one of the possible key carbon-metal bond forming steps shown in Scheme 1.5.

a) *Oxidative addition*. C–H bond undergoes oxidative addition to the metal forming the metal hydride species **IV**.
b) *Heck-type*. The aryl metal species **III** undergoes dearomatasing carbometalation to provide **V** which, after isomerisation (to **VI**) and β-hydride elimination, affords the biaryl.
c) *σ-Bond metathesis*. The C–M bond is formed *via* a 4-membered transition state (**VII**) in a concerted manner.
d) *Electrophilic aromatic substitution* (S_EAr). The arene attacks **III** displacing an ionic ligand from the catalyst to form the Wheland intermediate **VIII**. Deprotonation by the anionic ligand gives the biaryl product.
e) *Concerted metalation-deprotonation* (CMD). The C–M bond is formed *via* a 6-membered transition state (**IX**) in which the key role of proton abstraction from the arene is played by a carboxylic acid.

The type of mechanism operating in each particular case depends on the substrate,

transition metal, ligands and reaction conditions.

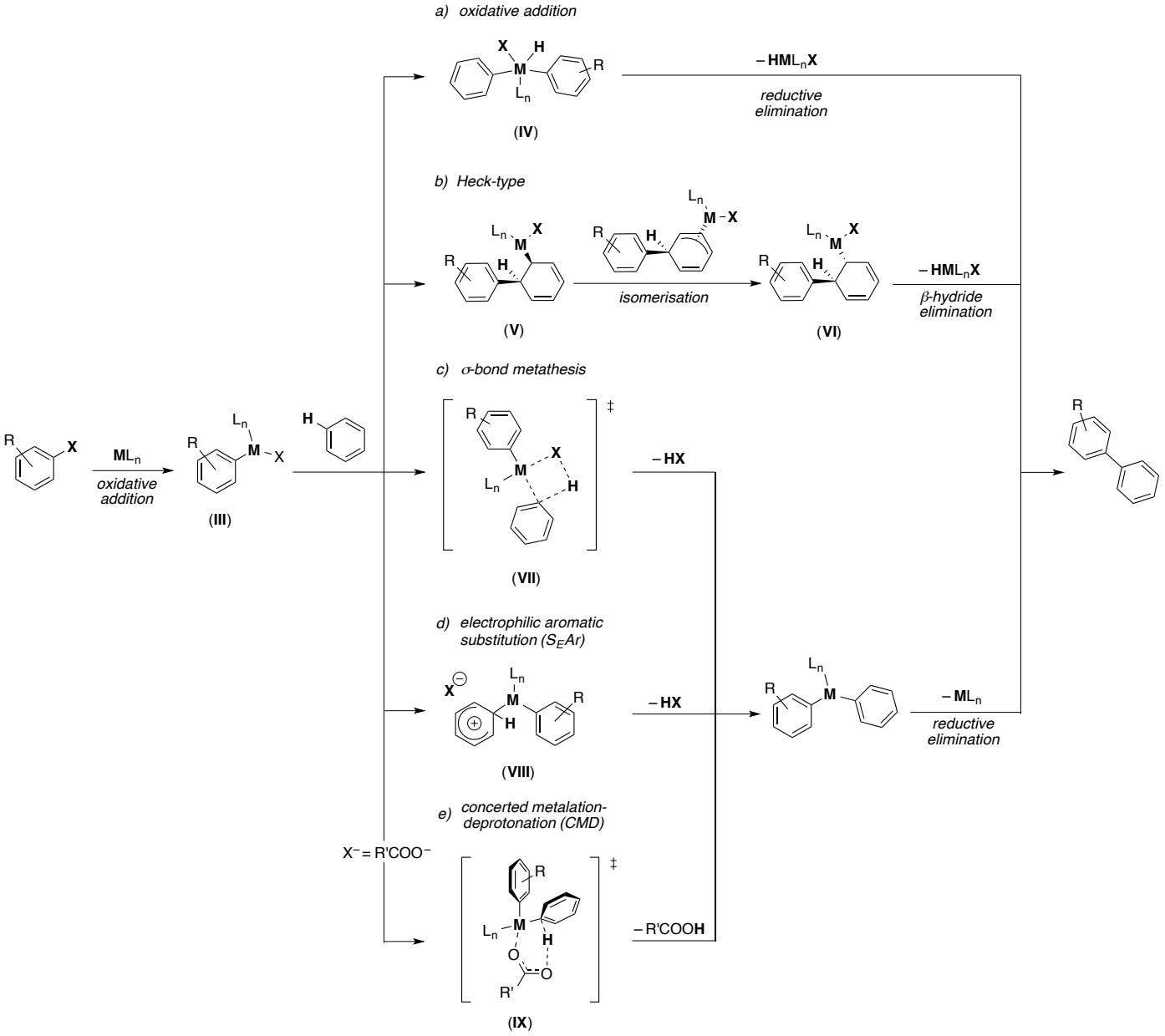

Scheme 1.5. Different mechanisms form metal-catalysed direct arylation of arenes.

1.4. Strategies for metal-catalysed direct C–H arylation

Although C–H arylation methodologies address the main drawbacks of traditional cross-couplings, they still suffer from two main challenges. The first one is derived from the high dissociation energy of the C–H bond (413 KJ/mol). To overcome this thermodynamic barrier, harsh reaction conditions and long reaction times are often required. The second is controlling the arylation regioselectivity at one specific C–H amongst others.

The strategies most commonly used to achieve regioselectivity are based on electronic and/or steric properties of the substrates, or on the presence of coordinating groups able to assist the metalation of the arene at a given position. As previously mentioned, the mechanism of the C–H activation and the arylation site-selectivity is deeply driven by the nature of the substrate. For this reason, and in view of all the literature that has been published about C–H arylation processes, it is possible to give a rationalisation of the arylation regioselectivity of different substrates by understanding the factors that govern the mechanism of the process.

1.4.1. Electronic-controlled arylation methods

In the following sections, only selected examples of Pd-, Rh-, Cu- and Au-catalysed direct arylation methodologies, where the reactivity/selectivity of the process is driven by the electronic properties of the arenes, will be discussed. Nevertheless, other metals such as Ni[8a,b]and Ir[9] and have been revealed to be valuable catalysts in various C–H arylation protocols especially in the direct arylation of heterocycles.

1.4.1.1. C–H arylation of electron-rich (hetero)arenes

Electron-rich (hetero)arenes are likely to react *via* S_EAr in which the most nucleophilic position(s) of the ring will be arylated. Therefore, the natural S_EAr selectivity, where this type of mechanism can be evoked, is generally followed.

In 2004 Sames and Lane reported the Pd-catalysed direct C-2 arylation of *N*-substituted indoles with aryl iodides in DMA solvent with CsOAc base (Scheme 1.6).[10]

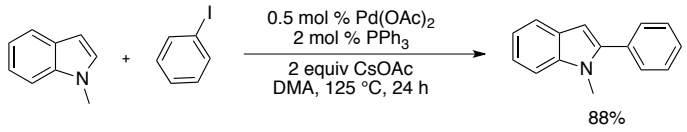

Scheme 1.6. Sames and Lane C2 arylation of indole.

Surprisingly, the method developed by Sames does not follow the expected "electrophilic" regiochemistry, instead the C2 position is arylated selectively. One year later, the same author described mechanistic experiments supporting an electrophilic palladation.[11] The reaction was shown to be first order with respect to both catalyst and indole substrate. Additionally, a Hammet plot of a variety of 6-substituted *N*-methylindoles demonstrated that increasing electron density on the indole ring led to a faster reaction rate. Lastly, the observation of a clear unsually large secondary kinetic isotopic effect (KIE) at C3 position (Scheme 1.7, equation *a*) in the reaction, leading to the C2-arylation of *N*-methylindole, led the authors to propose that both C2- and C3- arylation pathways proceed *via* electrophilic metalation at the more nucleophilic C3. The C3-palladated indole can either undergo deprotonation and reductive elimination, giving the 3-arylindole, or experience a C3 to C2 Pd migration, affording the 2-arylindole (Scheme 1.7, equation *b*). The authors, in order to rationalise the regioselectivity observed in their original study (Scheme 1.7, equation *c*),[10] suggested that sterically congested haloarenes slow the C3–C2 migration consequently decreasing the C2 selectivity.

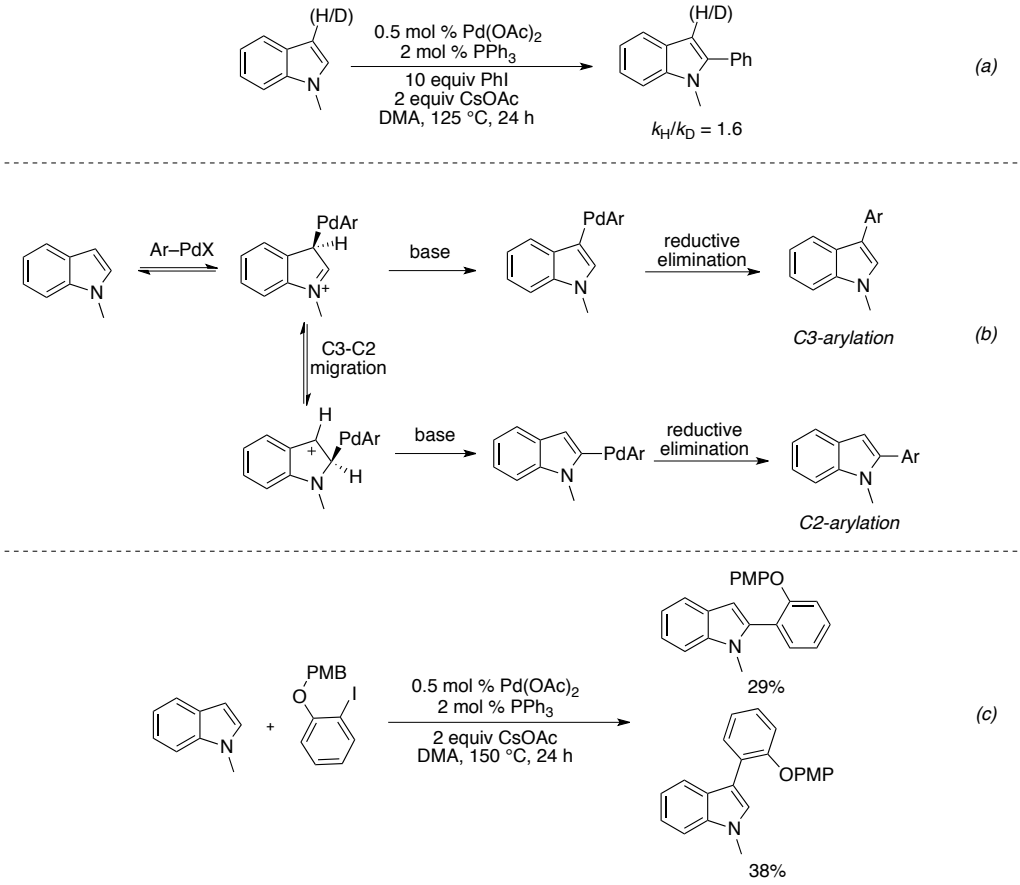

Scheme 1.7. Sames' mechanistic experiments (equations *a* and *c*) and C3 to C2 Pd migration (equation *b*)

An example of rhodium-catalysed C–H arylation of arenes through electrophilic metalation was reported by the Itami group in 2006.[12] The rhodium(I) complex *trans*-$L_2Rh(CO)Cl$, L= $P[OCH(CF_3)_2]_3$, was successfully used in the arylation of nucleophilic arenes with idodoarenes in the presence of a stoichiometric amount of silver carbonate and dimethoxyethane (DME, 1 equiv). Higher yields were observed with combinations of more nucleophilic arenes and more highly oxidising iodoarenes (Scheme 1.8).

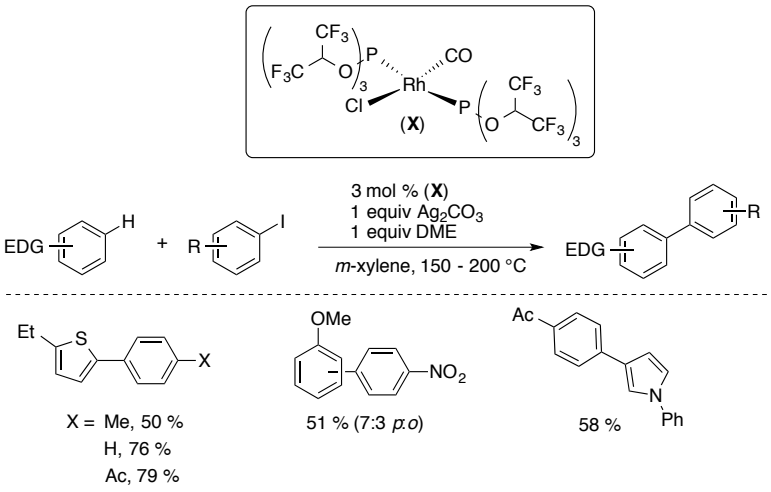

Scheme 1.8. Rhodium-catalysed direct arylation of electron-rich (hetero)arenes with aryl iodides.

Use of the strongly π -accepting $P[OCH(CF_3)_2]_3$ ligand was found to be crucial in the catalytic system. For example, when $P[OCH(CF_3)_2]_3$ was replaced with more weakly π–accepting ligands, such as $P(C_6H_5)[OCH(CF_3)_2]_2$, $P(OC_6H_5)_3$, $P[OCH(CH_3)_2]_3$, or $P(C_6H_5)_3$ for the arylation of 3-methoxythiophene with *p*-iodoacetophenone, the yield of the corresponding biaryl decreased from 94% to 31, 6, 9, and 0%, respectively. A clear correlation between the arylation efficiency and the π–accepting ability of the ligand, judged by electronic parameters based on the carbonyl stretching frequency (ν CO) in *trans*-$L_2RhCl(CO)$ complexes, was observed. The absence of a significant KIE for the intramolecular competition arylation of 2-deuteriothiophene with iodobenzene, lends support to the electrophilic nature of the metalation. Although the role of silver was not established, the *in situ* formation of a cationic Rh(III) complex by halide abstraction, along with assistance in the oxidative addition step, are plausible roles of silver(I) in this reaction. Interestingly, the DME additive was found to suppress the formation of the bis-arylated adduct. A possible mechanism could be a Rh(I)/Rh(III) cycle in which rhodium(I) species (**X**), in the presence of the aryl iodide and silver(I), undergoes oxidative addition with consequent halide abstraction to generate the highly electrophilic Rh(III) complex (**XI**). This intermediate performs C–H activation on the electron-rich (hetero)arenes (Ar^1–H) *via*

electrophilic metalation forming (**XII**), which, after reductive elimination, affords the biaryl and the initial Rh(I) species (Scheme 1.9)

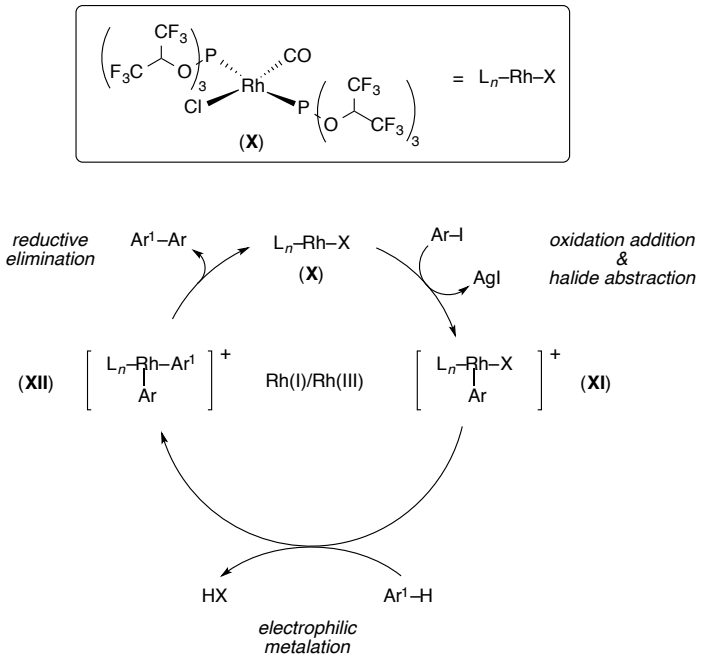

Scheme 1.9. Proposed mechanism for the Rh-catalysed arylation of electron-rich arenes.

In 2011 Gaunt *et al*. reported the development of a copper-catalysed highly *para*-selective Friedel–Crafts-type arylation of phenol and aniline derivatives, employing bis(aryliodonium) salts as the electrophiles (Scheme 1.10).[13]

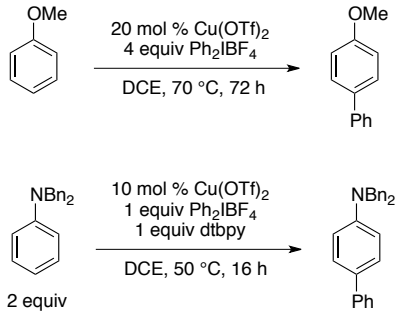

Scheme 1.10. *para*-Selective C–H arylation of phenol and aniline derivatives.

The original mechanistic proposal was a Cu(I)/Cu(III) catalytic cycle, proceeding by electrophilic metalation (Scheme 1.11, equation *a*). Previous studies from the same authors towards the development of a *meta*-selective arylation of anilides[14a] and α-aryl carbonyl motifs,[14b] with $Cu(OTf)_2$ and hypervalent iodine(III) species, revealed a non-irrelevant amount of arylation in the absence of the copper catalyst. In fact, the arylation of *N*,*N*-dibenzylaniline and anisole proceeded without copper, albeit at higher temperature and in lower yield. In view of this, a metal-free arylation promoted by the iodine(III) species cannot be ruled out (Scheme 1.11, equation *b*).[15]

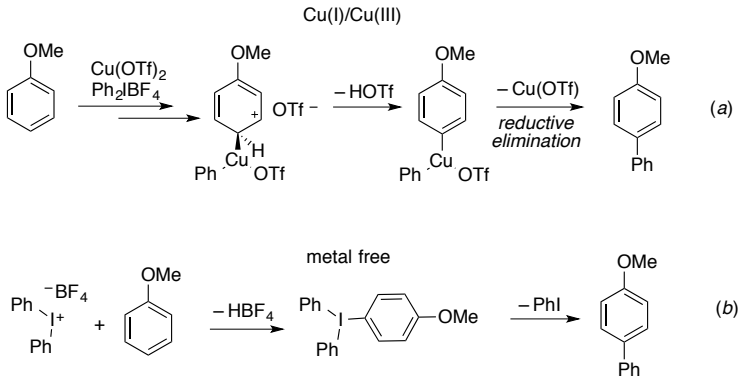

Scheme 1.11. Plausible mechanisms for the arylation of anisole with Ph_2IBF_4.

Another example of arylation, in which the regioselectivity is driven by the nucleophilicity of the arene undergoing C–H activation, is the gold-catalysed arylation of arenes with aryltrimethylsilanes reported by Lloyd-Jones, Russell *et al*. in 2012 (Scheme 1.12).[16]

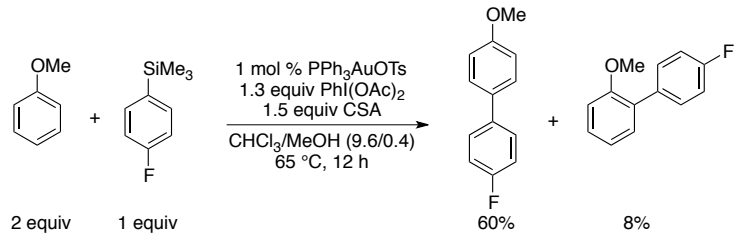

Scheme 1.12. Gold-catalysed arylation of anisole with aryltrimethylsilane.

The Au(I) catalyst (**XIII**) is oxidised by the iodine(III) to form a the Au(III) intermediate

(**XIV**), which transmetalates with the arylmethylsilane, affording aryl gold(III) species (**XV**). The auration of the electron-rich arene *via* S_EAr, followed by deprotonation, lead to the formation of the cationic bis-aryl gold(III) complex (**XVI**). Facile reductive elimination affords the biaryl product, regenerating the catalyst (**XIII**) and closing the cycle (Scheme 1.13).

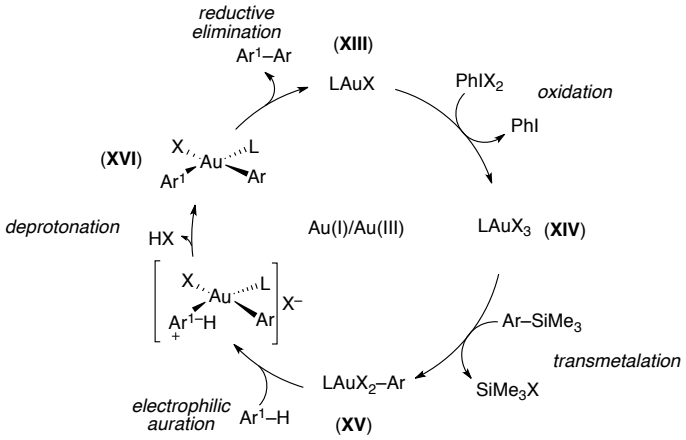

Scheme 1.13. Proposed mechanism for the Au-catalysed direct arylation.

1.4.1.2. C–H arylation of electron-poor (hetero)arenes

In 2005 Davies and Macgregor reported a computational study on the cyclometalation mechanism of *N*,*N*-dimethylbenzylamine by $Pd(OAc)_2$. Their aim was to expand upon and gain greater insight into Rybov and co-workers' mechanistic studies on the reactivity of palladium toward C–H bond activation.[17] Their investigations suggested that the reaction proceeds *via* an agostic C–H complex, rather than a Wheland intermediate.[18] The metalation is assisted by a facile intramolecular H-transfer *via* a six-membered transition state to coordinated acetate. Therefore the amphiphilic $Pd(OAc)_2$ provides electrophilic activation of a C–H bond and acts as an intramolecular base for the deprotonation (Figure 1.2).

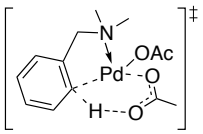

Figure 1.2. Proposed transition state for the palladation of *N*,*N*-dimethylbenzylamine.

Around the same period in 2005, Fagnou and co-workers developed a palladium catalysed direct arylation of pyridine *N*-oxides (Scheme 1.14),[19a] which was also further expanded for a vast array of diazine, azole and thiazole *N*-oxides.[19b-d]

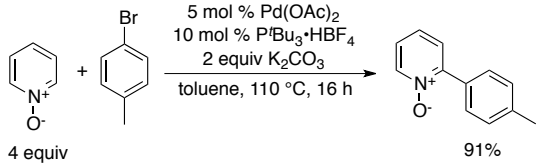

Scheme 1.14. Direct C–H arylation of pyridine *N*-oxide with aryl halides.

Competition reactions showed that electron-deficient 4-nitropyridine *N*-oxide reacts more readily than the more electron-rich 4-methoxypyridine *N*-oxide (Scheme 1.15, equation *a*). This evidence, along with a large primary KIE of 4.7 (Scheme 1.15, equation *b*), cannot be explained by an S_EAr type reaction.

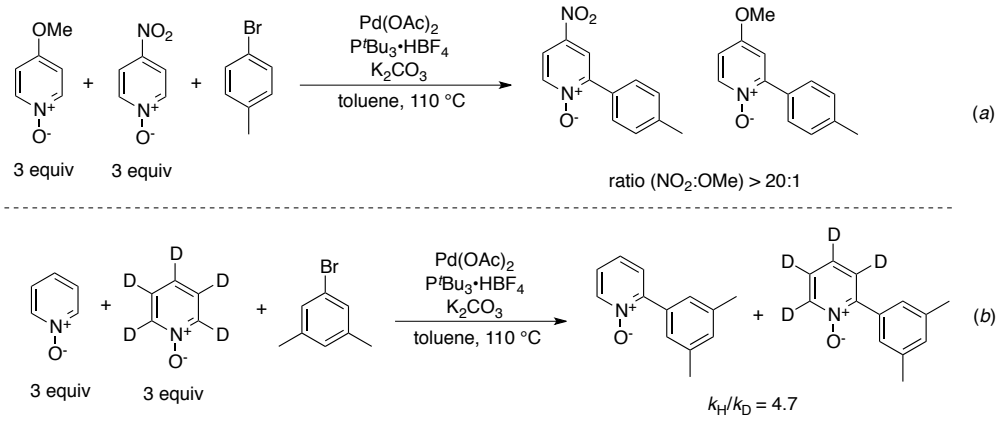

Scheme 1.15. Mechanistic competition and KIE experiments for the arylation of pyridine *N*-oxide.

In 2006 Echavarren and Maseras [20] studied the mechanism of the Pd-catalysed intramolecular C–H arylation, employing reaction conditions previously developed by Fagnou and co-workers.[21] Intramolecular competition arylations (Scheme 1.16., equations *a* and *b*), along with the KIE experiment (Scheme 1.16., equation *c*), suggested that the process does not proceed through an S_EAr pathway. In fact, in Scheme 1.16. equation *b*, the most electron-deficient ring underwent arylation selectively (ratio 25:1) when compared to the example shown in equation *a*, where both rings were arylated with a similar ratio (1.1:1).

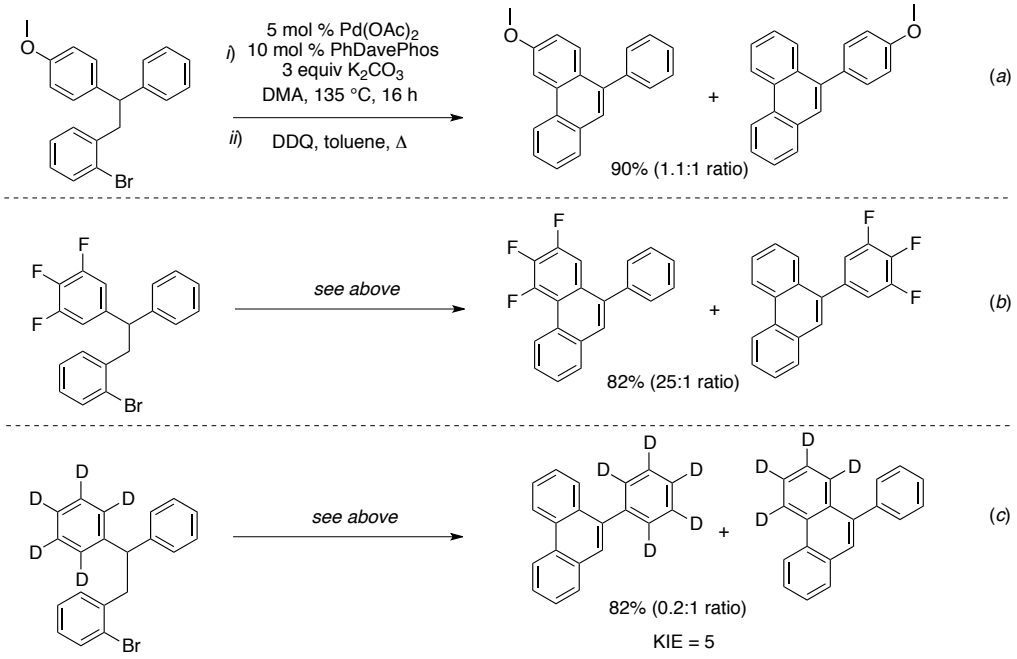

Scheme 1.16. Mechanistic investigations for the intramolecular arylation.

A computational investigation on the C–H activation mode supports a proton abstraction, by a carbonate ligand, providing a rational explanation for the experimental data (Figure 1.3).

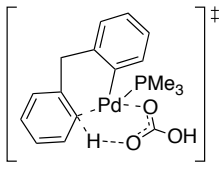

Figure 1.3. Proposed transition state for the intramolecular Pd-catalysed arylation.

A few months later, in 2006, Fagnou *et al*. extended the intermolecular arylation of electron-deficient arenes to perfluorobenzene derivatives.[22] The reaction shows complete inversion of reactivity relative to the electrophilic pathway, the less nucleophilic position being the site for arylation (Scheme 1.17., equations *a*). A k_H/k_D of 3.0 was found confirming the kinetic relevance of breaking the C–H bond in the arylation. Competition experiments, performed to establish the relative reactivity of different perfluoroarenes, revealed that arenes with more acidic C–H bonds reacted preferentially (Scheme 1.17., equation *b*).

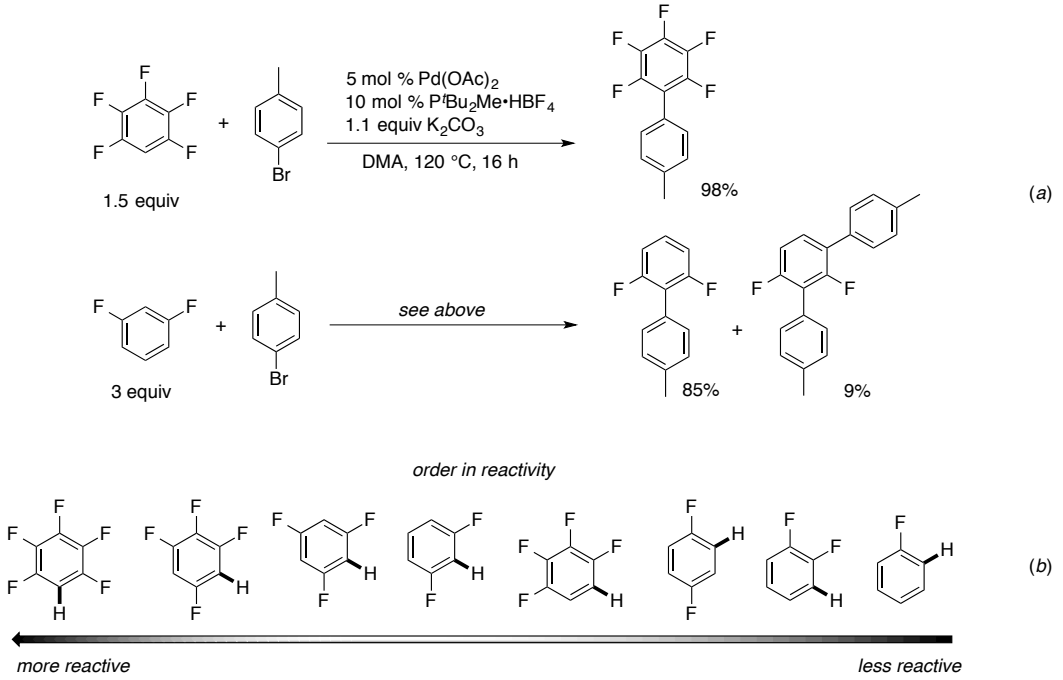

Scheme 1.17. Direct C–H arylation of perfluorobenzene derivatives and their order of reactivity.

The mechanism proposed by Fagnou involves the oxidative addition of the ArBr at a Pd(0) centre generating the aryl palladium(II) bromide species (**XVII**), which undergoes ligand exchange with the carbonate ligand forming (**XVIII**). This active intermediate is capable of performing C–H activation on the perfluoroarene *via* a concerted metalation-deprotonation transition state (CMD, **XIX**). The resulting bisaryl palladium(II) complex (**XX**), after reductive elimination, generates the biaryl product. Computational data in support of a six-membered transition state for the C–H activation mode, over a more classic four-membered

(σ-bond metathesis, **XXI**) were provided. Additionally, other C–H activation pathways such as electrophilic palladation, oxidative addition leading to a Pd(IV)–H complex, and proton abstraction by an external carbonate were computed to have higher activation barriers.

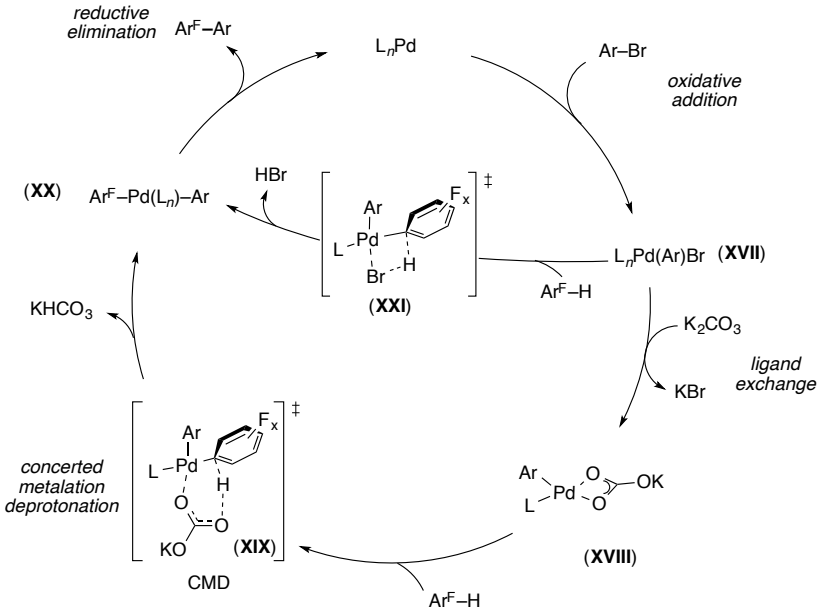

Scheme 1.18. Proposed mechanism for the Pd-catalysed direct arylation of polyfluoroarenes.

The relative reactivities and site selectivities disclosed by the authors suggest that C–H acidity is an important reaction parameter to be considered in direct arylation. In view of this, Fagnou concluded his work stating: "*This is an entirely different way of considering the design of intermolecular direct arylation reactions*".[22]

The addition of a carboxylate co-catalyst to direct C–H arylation has been shown to generate highly active catalytic systems. Larrock in 2004[23] and Sames in 2005[24] have successfully used stoichiometric amounts of pivalate salts in palladium and rhodium systems. Fagnou, however, in 2006 was the first to use pivalic acid as a co-catalyst in the Pd-catalyst C–H arylation of simple arenes (such as benzene) with aryl halides.[25] The pivalate is believed to act as a proton shuttle aiding the CMD in a similar fashion to the carbonate/bicarbonate ligand, which was originally proposed in the arylation of the polyfluoroarenes. The use of pivalic acid as an additive allowed a more facile cleavage of the

C–H bond (computationally the CMD transition state is 1.3 kcal/mol lower when compared to the bicarbonate anion), fuelling the development of many intramolecular direct arylation,[20b,26] as well as in the functionalisation of electron-deficient arenes,[19c-d,27] and electron-rich heteroarenes.[27a,28]

Until recently, it was generally accepted that electron-rich heteroarenes reacted through a S_EAr mechanism due to their high nucleophilicity. However, Gorelsky and Fagnou demonstrated that the C–H bond cleavage for a wide range of (hetero)arenes, including electron-rich (hetero)arenes, proceed by the CMD pathway.[29] Using computational methods, they were able to obtain calculated activation barriers matching the regioselectivity observed experimentally for the palladium-catalysed direct arylation of each (hetero)arene. Moreover, for the oxidative cross-coupling of indole with benzene, both C–H bond cleavages were explained by the same CMD mechanism.[30]

Efforts towards the understanding of the origins of the regioselectivity of the palladium-catalysed C_{Ar}–H bond metalation-deprotonation by Gorelsky, Fagnou and Lapointe,[29a,31] have set the basis in evaluating the parameters that govern the barrier for the cleavage of the C–H bond for a diverse set of (hetero)arenes. The distortion-interaction analysis was the main computational tool used for the purpose (Scheme 1.19).

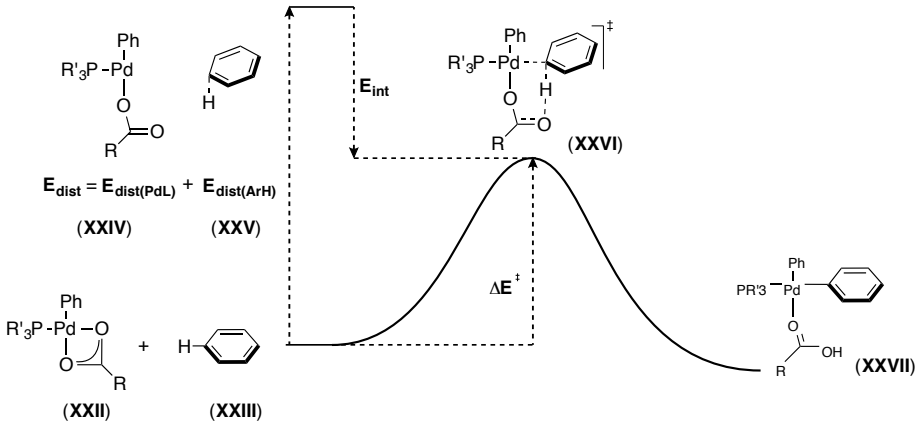

Scheme 1.19. Distortion-interaction analysis for the CMD transition state.

The analysis quantifies different contributions to the CMD barrier (**XXVI**). The energetic cost associated with distortion of the arene and palladium complex, from their ground state structures (**XXII, XXIII**) to their geometries (**XXIV**, **XXV**) in the optimised CMD transition states (**XXVI**), is called distortion energy (ΔE_{dist}). The energy gained from electronic interaction of **XXIV** and **XXV**, to form the TS **XXVI**, is named interaction energy (ΔE_{int}). This distortion-analysis has allowed the classification of the arenes in three different categories (Figure 1.4).[31b]

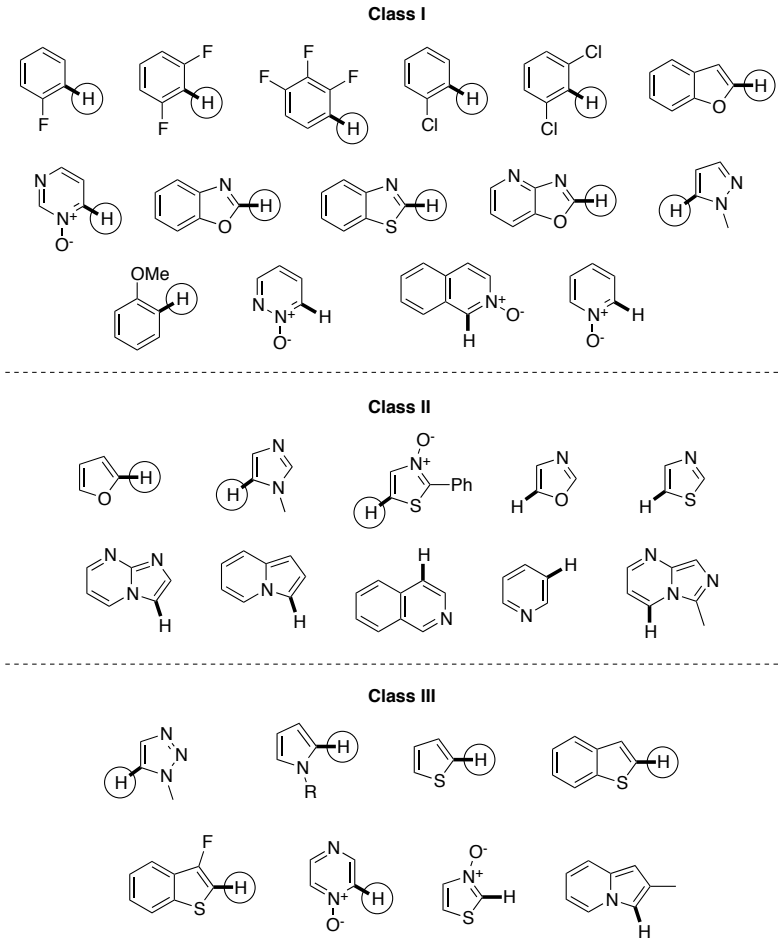

Figure 1.4. Classification of (hetero)arenes in terms of contributions to regioselectivity of C–H bond metalation *via* CMD, based on their reactivity with [Pd(C_6H_5)(PMe_3)(OAc)] complex.[29a,31a,32] C–H in bold represents that with the lowest activation energy for the CMD transition state; if the H atom is circled it indicates that the lowest CMD barrier corresponds with the lowest gas-phase electronic energy of heterolytic dissociation.

For class I arenes the regioselectiviy of the C–H bond functionalisation is controlled by the difference in the (hetero)arene distortion energies, ΔE_{dist} (ArH). Class II includes (hetero)arenes for which both interaction energies (ΔE_{int} (PdL+ArH)) are determining factors in defining the most reactive C–H bond. In class III belong (hetero)arenes in which both the distortion and interaction energies influence the choice of the C–H bond. For most of the arenes in class I and in class III, the arylation occurs at the most acidic C–H bond. π-Electron-rich arenes benefit from large negative E_{int} values, however this gain in energy is balanced out by a large E_{dist} penalty. On the other hand, electron-deficient arenes do not benefit from large E_{int} values, but the TS remains accessible due to a low E_{dist}, arising from less energetic demand for arene distortion. The energetic cost for distorting the arene, into the geometry adopted in the CMD transition state, can be separated into two components: 1) the C–H bond stretching and 2) the out-of-plane bending. The energetic penalty for the out-of-plane bending for different arenes has a fairly constant value, hence does not play a major role in determining the selectivity. However, there is a relationship between the distortion energies and the deprotonation energies of the C–H bonds (C–H acidities). In fact, for most of the (hetero)arenes in class I and III, the C–H bond with lowest distortion energy at the CMD TS is the most acidic one. As a result of this, electron-deficient arenes exhibit less C–H bond elongation in the CMD TS than electron-rich arenes. The reactivity is also tuned by metal coordination. Much like to the effect of an electron-withdrawing group, metal coordination to the heteroarene activates C–H bonds by lowering the distortion energy of the arene.

In 2008, Daugulis *et al*. introduced an alternative to the palladium-catalysed processes, developing a general method for the copper-catalysed arylation of electron-deficient arenes.[33] The reaction is thought to proceed *via* deprotonation of an acidic (hetero)arene by a strong lithium or potassium base, followed by lithium/potassium-copper transmetalation and reaction of the organocopper species with aryl iodide (Scheme 1.20).

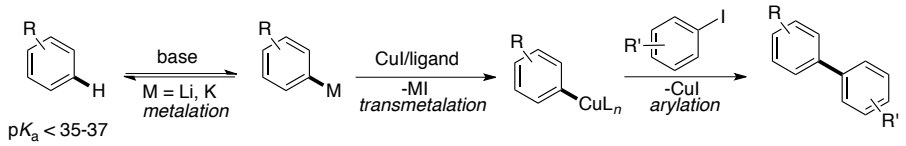

Scheme 1.20. Proposed mechanism for the Cu-catalysed direct arylation of electron-deficient arenes.

The choice of base is dependent on the acidity of the C–H bond to be arylated. Acidic C–H bonds (pK_a below 27) can be arylated by employing K_3PO_4, whereas stronger lithium or potassium alkoxide bases are needed for less acidic protons (pK_a 27-35). A variety of electron-rich and electron-poor (hetero)arenes, including polyfluorobenzene derivatives, azoles, caffeine, thiophenes, benzofuran, pyridine, pyridine oxides, pyridazines and pyrimidine were successfully arylated (Scheme 1.21).

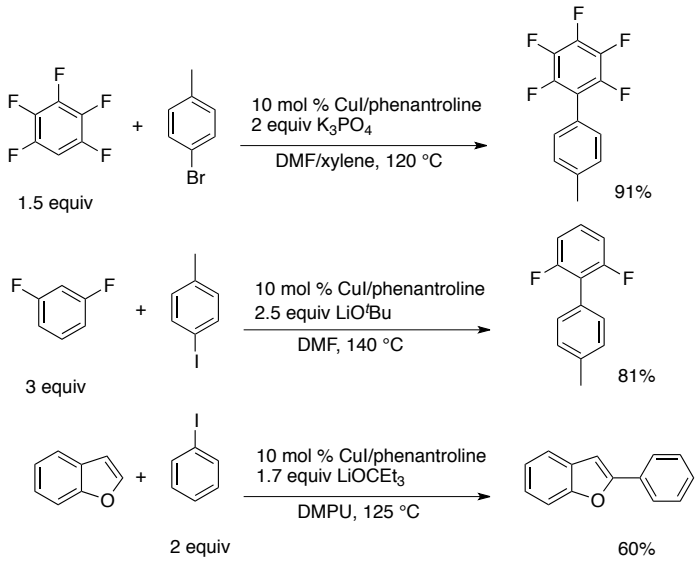

Scheme 1.21. Cu-catalysed direct arylation of arenes with acidic C_{Ar}–H.

In 2010 Larrosa *et al*. reported the first general protocol for direct C–H activation of electron-poor arenes, with Au(I) complexes, for the preparation of Au(I) arenes (Scheme 1.22).[34] Furthermore, the observation of a primary KIE of 5 indicates that the C–H breaking step occurs during the rate-limiting step of the reaction. Reminiscent of the work of Fagnou and Gorelsky,[22,25,28,31] and Echavarren and Maseras,[20] this kinetic data suggested that a CMD

pathway for the C–H activation step is operating. Selectivity towards the most acidic proton was also observed.

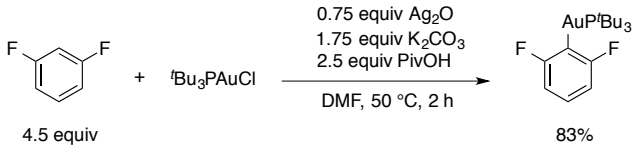

Scheme 1.22. Gold C–H activation of electron-poor arenes.

Three years later, Larrosa and co-workers displayed the potential of gold(I) aryl complexes developing a gold-catalysed oxidative cross-coupling, between electron-poor and electron-rich arenes (Scheme 1.23). The selectivity of the two C–H activation steps is controlled by switching the oxidation state of the Au species. Au(I) and Au(III) species have orthogonal selectivity for C–H activation: Au(I) complexes activate electron-poor arenes with acidic protons, while electrophilic Au(III) species is selective for electron-rich arenes.[35]

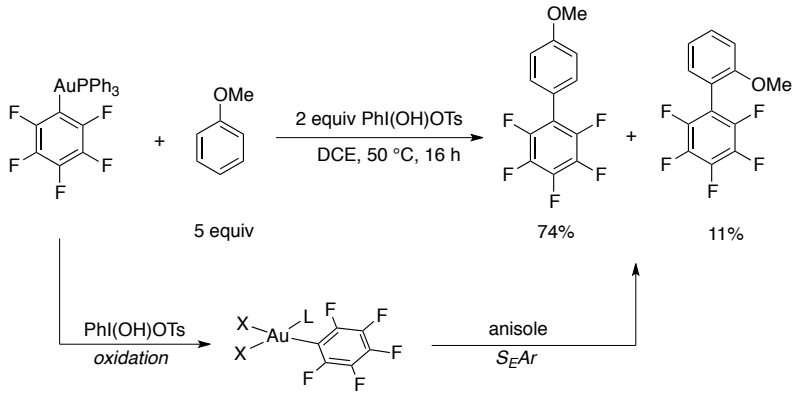

Scheme 1.23. Oxidative cross-coupling of gold(I) pentafluorophenyl complex with anisole.

Very recently, Larrosa *et al*. reported the first methodology for Au(I/III)-catalysed oxidative cross coupling of arenes *via* double C–H activation. As previously reported by the same group,[35] the reaction has shown to be fully selective for the cross-coupling between electron-poor and electron-rich (hetero)arenes (Scheme 1.24).[36] Although the mechanism of the transformation is still under investigation, initial experiments suggest that the active gold

species is a phosphine-free complex and the silver salt might be involved in the C–H activation of the electron-poor arene.

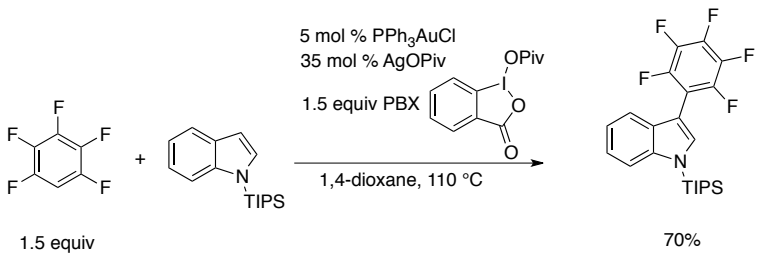

Scheme 1.24. Gold-catalysed oxidative cross-coupling of arenes.

1.4.2. C–H arylation of (hetero)arenes *via* chelate-assisted metalation

The most powerful tool to induce regioselectivity and reactivity in C–H arylation methodologies, which is not related to the electron properties of the aromatic ring, is the use of directing groups. Usually a directing group is a substituent connected to the ring, which contains a heteroatom (commonly O, N or S) in γ, δ or ε with respect to the C–H bond that will be arylated. Thus it is able to coordinate transition metals favouring their approach to the *ortho* C–H bond (Scheme 1.25, equation *a*).[7] Recently, tremendous progress in engineering directing groups has also made possible the direct C–H functionalisation at the *meta* position (Scheme 1.25, equation *b*).[37] This coordination can be interpreted as Lewis acid–base adduct formation, in which the metal complex acts as the Lewis acid by accepting electrons from the Lewis base directing group. The formation of this adduct is affected by several factors, such as the metal complex, functional group, solvent, and temperature.

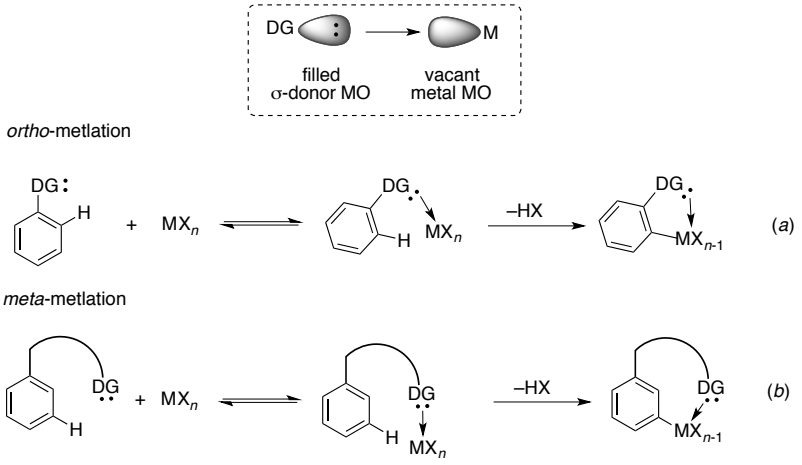

Scheme 1.25. General scheme for *ortho* and *meta* C–H metalation employing a directing group.

1.4.2.1. *ortho* C–H Arylation of (hetero)arenes bearing a directing group (DG)

Directing group-assisted *ortho* C–H arylation methodologies have been described with a large number of transition metals. The most successfully exploited ones are Pd, Ru and Rh which will be discussed in the following sections. However related methodologies with Co,[38] Fe[39] Ni,[8c,d] Cu[40] and Ir[41] catalysts have also been reported.

1.4.2.1.1. Chelate-assisted Pd-catalysed *ortho* C–H Arylation of (hetero)arenes

In a ground-breaking paper dated 1984, Tremont described $Pd(OAc)_2$ promoted anilide alkylation by alkyl iodides. The author proposed that the reaction proceeds *via* Pd(II)/Pd(IV) system, although a σ-bond metathesis mechanism was not discarded (Scheme 1.26).[42]

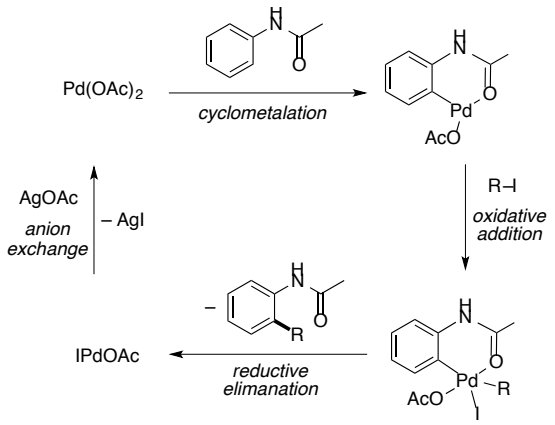

Scheme 1.26. Catalytic cycle for *ortho*-alkylation of anilides.

In 2005, inspired by this pioneering work, Sanford[43] and Daugulis[44] independently developed approaches for the preparation of *ortho*-substituted anilides and 2-phenylpyridines derivatives *via* a Pd(II)/Pd(IV) catalytic cycle.

Sanford reported methodologies for direct *ortho*-arylation of different anilides/carbamates and pyridine/quinoline derivatives using hypervalent iodine compounds as the oxidising arylation reagent (Scheme 1.27).[43]

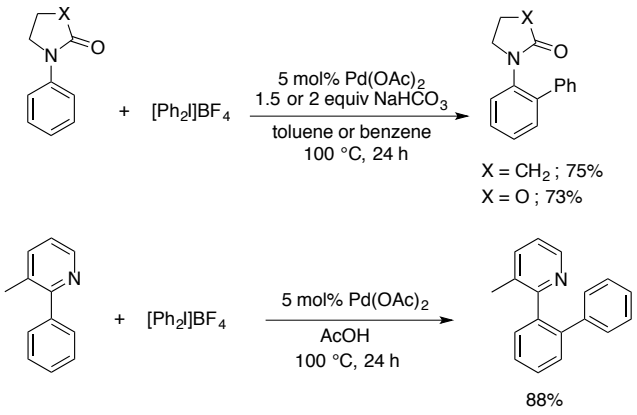

Scheme 1.27. Pd-catalysed direct arylation of amides and pyridine derivatives developed by Sanford.

Interestingly, when the Pd-dimer **1** was subjected to the arylation conditions shown in Scheme 1.28, the biaryl product was only formed in the presence of the more oxidising

bisaryliodonium salt. Iodobenzene and phenyl triflate resulted to be ineffective.

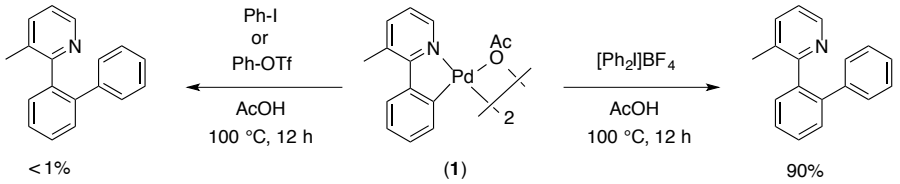

Scheme 1.28. Single-turnover arylation of **1** with various electrophiles.

In 2004 Canty and co-workers reported the crystal structure of a Pd(IV) complex in which a "Ph" and a "OTf" group have been transferred from an hypervalent iodine(III) species to the Pd(II) starting complex,[45] therefore bisaryliodonium salts are powerful enough to oxidise Pd(II) to Pd(IV).[46]

In 2011, Vicente *et al*. reported the first crystal structure of a Pd(IV) complex generated by oxidative addition of an aryl iodide.[47] The importance of this finding from a conceptual point of view is of great significance, because it demonstrates that Pd(II) complexes can undergo oxidative addition with aryl iodides. On the other hand, the aryl iodide and the Pd-ligands system employed for the synthesis of the Pd(IV) complex were highly unique, being designed *ad hoc*. In addition, this oxidative addition is proposed to be intramolecular. Therefore, generalising that aryl iodides are able to insert into Pd(II), and thus able to oxidise Pd(II) to Pd(IV), is a conclusion to be approached with caution.

According to Daugulis' protocol, the arylation of pivaloyl anilides can be performed either using $[Ph_2I]PF_6$ in AcOH or with aryl iodides and AgOAc in TFA (Scheme 1.29). Monoarylated products were exclusively obtained when *ortho* or *meta* substituted anilides were used.[44a]

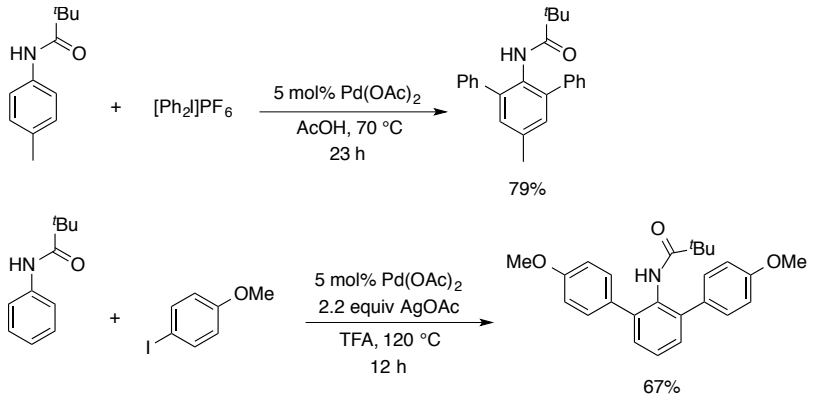

Scheme 1.29. Pd-catalysed arylation of pivaloyl anilides developed by Daugulis.

A few months later, Daugulis proposed an alternative for the *ortho* arylation assisted by nitrogen chelation developed by Sanford, replacing the hypervalent iodine(III) species with iodoarenes. A stoichiometric amount of silver(I) acetate, slightly higher temperature and longer reaction times were needed (Scheme 1.30).[44b]

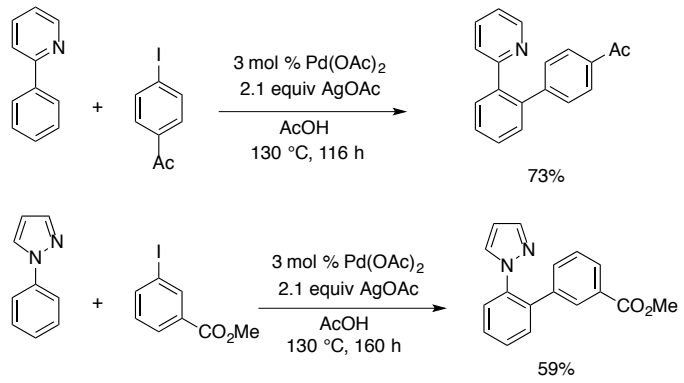

Scheme 1.30. *ortho*-Arylation assisted by nitrogen chelation with aryl iodides.

Since these reactions are faster with electron-rich aryl iodides, Daugulis proposed that a Pd(0)/Pd(II) process was unlikely. For this reason a Pd(II)/Pd(IV) mechanism was evoked.[44a,48] In a 2009 review, the author suggested that: "*The aryl iodide enters the catalytic cycle at the stage of oxidative addition to Pd(II), which is most likely the rate-determining step since arylation rate depends on ArI and reductive elimination from Pd(IV) is expected to be fast. The oxidative addition step must be faster for electron-rich aryl iodides, which is*

different from the usual Pd(0)-Pd(II) coupling cycle where electron-deficient aryl halides are more reactive."[49]

Well established studies on the oxidative addition at a Pd(0) centre with aryl halides have demonstrated that the process is favoured when electron-poor aryl iodides are employed.[50] A similar study on a Pd(II) system has not yet been reported. However, it might be reasonable to expect that the electronic properties of the aryl halide influencing the oxidative addition at the Pd(0) centre should parallel the one for the oxidative addition at Pd(II).

A further explanation about Daugulis' arylation system occurring *via* a Pd(II)/Pd(IV) catalytic cycle, can be proposed from the studies reported by Cheng and co-workers on the Pd-catalysed *ortho* arylation of aromatic oximes.[51,52] In 2008, they reported a facile route for the synthesis of fluorenones from aromatic aldoxime ethers and aryl halides by a dual Pd-catalysed C–H arylation and Heck cyclisation. A combination of $Pd(OAc)_2$ catalyst, Ag_2O, and TFA as solvent provided excellent conversion towards the target products (Scheme 1.31).[51]

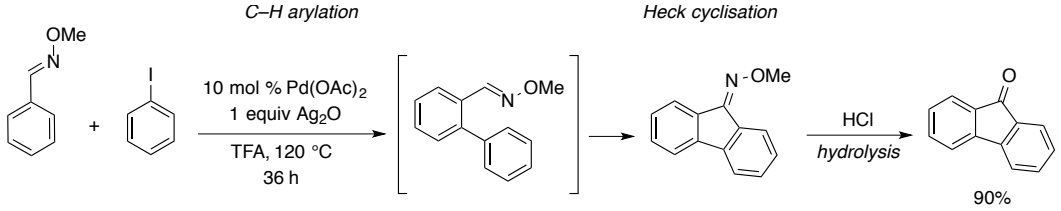

Scheme 1.31. Pd-catalysed *tandem* C–H arylation-cyclisation of aldoxime ethers.

Mechanistic studies, mainly based on the synthesis and characterisation by single-crystal X-ray diffraction of an unusual anionic Pd(II) complex (**2**), formed by treating the *O*-methyl oxime with $Pd(OAc)_2$ and Ag_2O in TFA, demonstrate that aryl iodides can oxidatively insert at the Pd(II) centre with the aid of a silver(I) halide scavenger, affording after reductive elimination, the corresponding biaryl product (Scheme 1.32, equation *a*). Additionally, the cyclisation was propesed to occur *via* a Pd-catalysed Heck, in which Ag_2O acts as the terminal oxidant (Scheme 1.32, equation *b*).

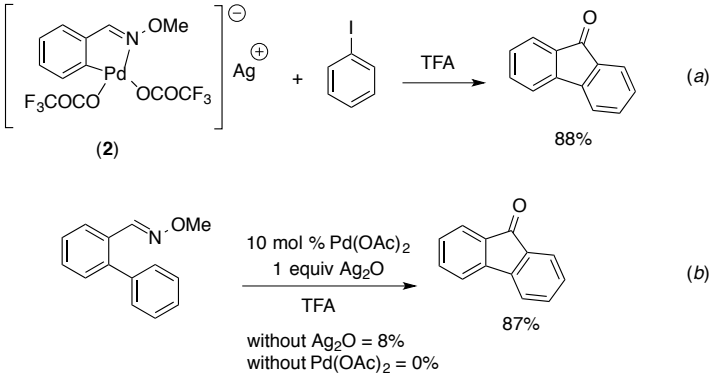

Scheme 1.32. Mechanistic investigations on the *tandem* C–H arylation-cyclisation Pd-catalysed of aldoxime ethers. (a) Stoichiometric arylation of **2** with iodobenzene. (b) Oxidative Heck-type intramolecular arylation.

The same group expanded this methodology developing a chelate-assisted cross-dehydrogenative palladium-catalysed dual C–H arylation and Heck cyclisation of aromatic aldoxime ethers. The process employs simple arenes as the coupling partner and potassium persulfate as the terminal oxidant (Scheme 1.33).[52]

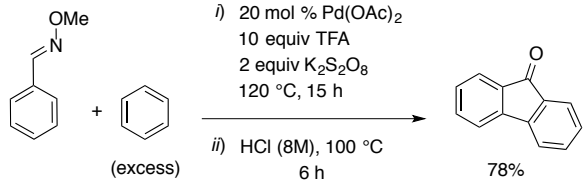

Scheme 1.33. *Tandem* cross-dehydrogenative C–H arylation-cyclisation Pd-catalysed of aldoxime ethers with simple arenes.

Interestingly, the treatment of *O*-methyl oxime with $Pd(OAc)_2$ in TFA (without any silver) afforded the dinuclear Pd(II)species **3**. This complex reacts with benzene only in the presence of potassium persulfate oxidant to generate the product (Scheme 1.34). Therefore, the oxidation of Pd(II) to Pd(IV) triggers the second metalation. Competition experiments have also revealed that electron-rich arenes react faster, suggesting an S_EAr mode for the C–H activation at the Pd(IV) centre.

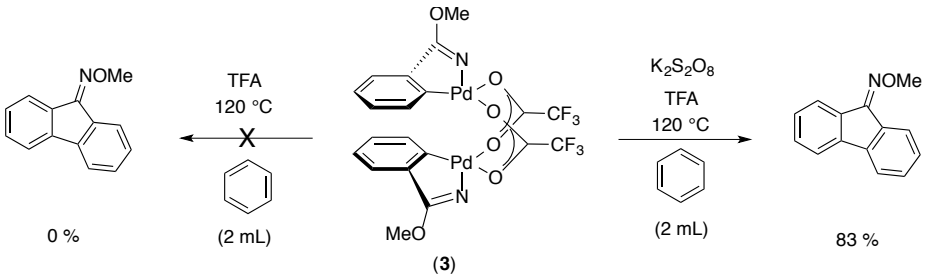

Scheme 1.34. Mechanistic investigations on the *tandem* C–H arylation-cyclisation Pd-catalysed of aldoxime ethers. Single-turnover arylation of **3** with potassium persulfate and benzene.

In light of these papers, it is reasonable assuming that Daugulis' conditions for the *ortho*-arylation of arylamides,[44a,48b] benzamides,[48a] or phenylpyridines derivatives[44b] are similar to those developed by Cheng for the arylation/cyclisation of aldoxime ethers with aryl iodides (Scheme 1.31).[51] The main differences are the use of Ag_2O rather than AgOAc, and in same cases, the employment of TFA in place of AcOH. It is well known that the treatment of a directing group-containing arene with $Pd(OAc)_2$ in AcOH or TFA solvents, leads to the formation of dinuclear Pd(II)species (**XXIX**).[43,52] Based on the mechanistic investigations conducted by Cheng,[51] an anionic Pd(II) complex (**XXX**) is formed as well in the presence of silver (Scheme 1.35).

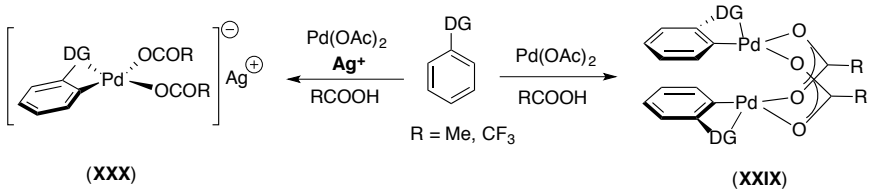

Scheme 1.35. Possible dual reactivity in the presence or in the absence of silver.

In view of Sanford's experimental observations,[43] a complex of the type **XXIX** only reacts with bisaryliodonium salts. Whereas, according to Cheng's investigation,[51] a complex of the type **XXX** does react with aryl iodides. This could be rationalised as follows. The anionic Pd(II) complex (**XXX**) would more readily undergo oxidative addition, therefore aryl iodides might be strong enough to oxidise **XXX** to **XXXI**, the anionic Pd(IV) complex arising from oxidative addition. The latter being a reversible process, the role of silver may

be to remove the iodide from **XXXI**, irreversibly forming, in the presence of a monodentate ligand (L), the neutral Pd(IV) complex **XXXII**, which would readily reductive eliminate the product (Scheme 1.36). Alternatively, the halide abstraction could also happen after reductive elimination.

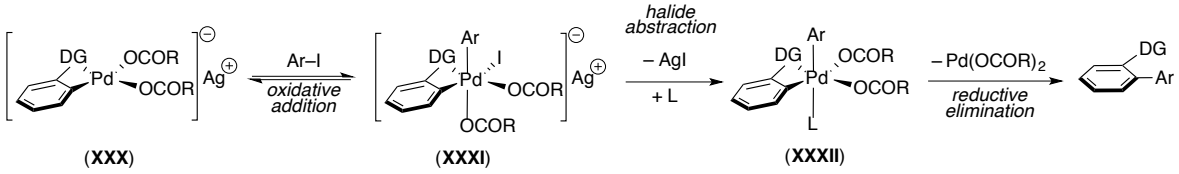

(**XXX**) (**XXXI**) (**XXXII**)

Scheme 1.36. Plausible Pd(II)/Pd(IV) chelated-assisted arylation with aryl iodides.

Although it would not be appropriate to make any sort of generalisation, this could provide a logical explanation when Pd(II)/Pd(IV) catalytic cycles are evoked with ArI/Ag(I) systems.

In 2007 Daugulis and co-workers reported two Pd-catalysed methods for direct *ortho*-arylation of free benzoic acids.[53] The first method employs aryl iodides as the coupling partner, stoichiometric silver acetate for iodide removal and acetic acid solvent (Scheme 1.37, equation *a*). The second method, instead, involves the use of aryl chloride, Cs_2CO_3 base, *n*-butyl-di-1-adamantylphosphine ligand and DMF solvent in strictly anhydrous conditions (Scheme 1.37, equation *b*).

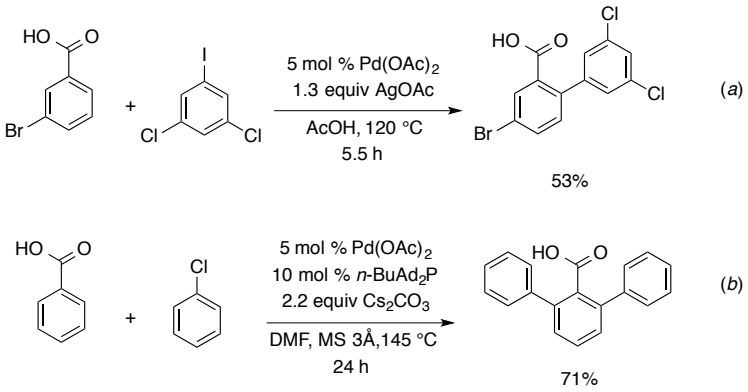

Scheme 1.37. Two methods for *ortho*-arylation of carboxylic acids under palladium catalysis.

No examples of direct arylation of *ortho*-substituted carboxylic acids were reported when aryl iodides were employed as the coupling partners. Mechanistic studies of the second method point to the heterolytic C–H bond cleavage as the rate-determining step.

Four years later, Larrosa *et al*. reported that *ortho*-substituted benzoic acids can undergo a tandem *ortho*-arylation/protodecarboxylation process that lead to *meta*-substituted biaryl compounds (Scheme 1.38).[54] In the same paper they also demonstrated that Pd complexes (and not Ag salts) are able to perform the decarboxylation of *ortho*-arylated disubstituted benzoic acids.

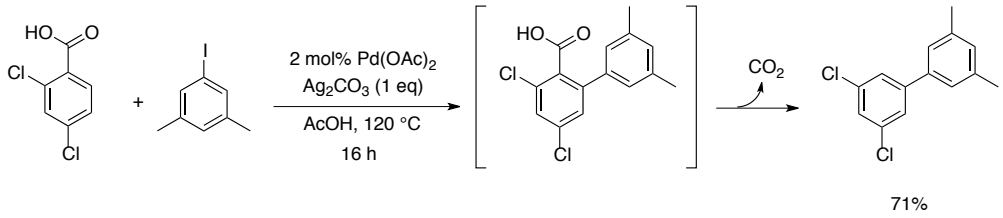

Scheme 1.38. Tandem *ortho*-selective arylation/protodecarboxylation process leading to formal *meta*-selective C–H arylation.

The same group has put this methodology to further use in the development of the first direct *meta*-arylation of phenols. The group took advantage of the well-known ability of phenols to fix CO_2 *ortho* to the hydroxyl group (Kolbe-Schmitt reaction). This allows for a selective C–H functionalisation to proceed followed by removal of the directing group by decarboxylation. Thus, CO_2 acts as a transient/traceless directing group for *meta*-arylation of arenes with aryl iodides (Scheme 1.39).[55]

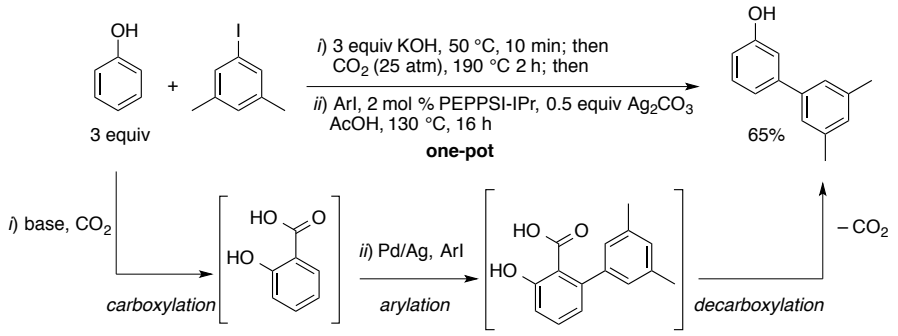

Scheme 1.39. One-pot carboxylation, tandem *ortho*-arylation/protodecarboxylation process leading to formal *meta*-selective C–H arylation of phenols.

A recent publication by Larrosa and co-workers has successfully shown the *ortho*-arylation of *ortho*-substituted benzoic acids.[56] Their previous reports revealed that sterically hindered *ortho*-disubstituted benzoic acids readily undergo protodecarboxylation under Pd-catalysis. However, here the authors found that the presence of K_2CO_3 prevents the otherwise facile protodecarboxylation (Scheme 1.40).

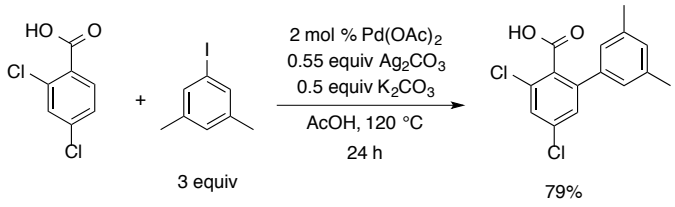

Scheme 1.40. *ortho*-Arylation of *ortho*-substituted benzoic acids under palladium catalysis.

The Larrosa group was able to develop a Pd-catalysed silver-free protocol for the arylation of benzoic acids with aryl iodides. Taking advantage of the low solubility of $(NMe_4)I$, the right combination of KOAc, NMe_4Cl and AcOH were found to be effective components in a system where of $(NMe_4)OAc$ plays the key role of regenerating the catalyst (Scheme 1.41).[57]

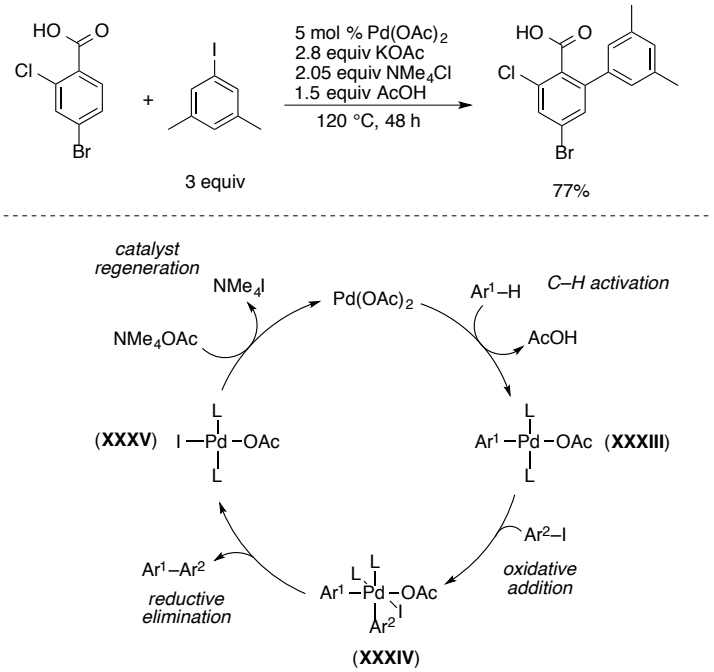

Scheme 1.41. Silver-free *ortho*-arylation of benzoic acids with aryl iodides.

Arising from cyclometalation of the benzoic acid, intermediate **XXXIII** undergoes oxidative addition generating **XXXIV** in the presence of the aryl iodide. Facile reductive elimination frees the biaryl product and forms the Pd–I species **XXXV**. Finally, halide abstraction from **XXXV** by NMe_4OAc restores the active $Pd(OAc)_2$. The same protocol was efficaciously applied to the direct arylation of electron-poor and electron-rich (hetero)arenes, and for other nitrogen-containing arenes with directing groups.

The first oxidative coupling of carboxylic acids with phenylboronate was reported in 2007 by Yu *et* al. (Scheme 1.42).[58] In this manuscript, Pd-catalysed methylation and arylation of sp^2 and sp^3 C–H bonds were described.

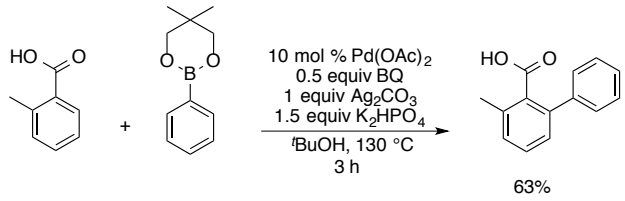

Scheme 1.42. *ortho*-Arylation of benzoic acids with phenylboranate.

The following year, the same group published a methodology for the *ortho*-arylation of benzoic and arylacetic acids with potassium aryltrifluoroborates as the coupling partners employing oxygen as the terminal oxidant (Scheme 1.43).[59] Under these reaction conditions, the use of air or O_2 as the terminal oxidant, instead of Ag_2CO_3, was made possible.

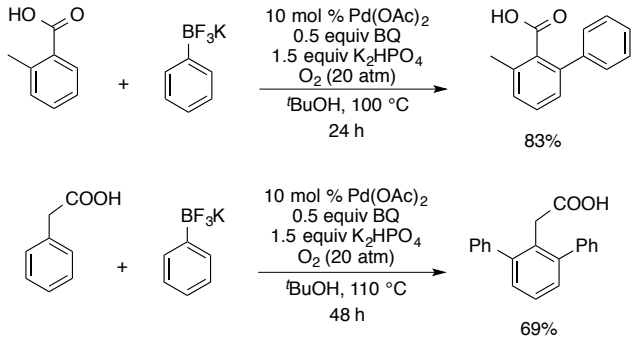

Scheme 1.43. *ortho*-Arylation of aryl acetic and benzoic acids with aryltrifluoroborates.

In 2015, Su and co-workers reported the room temperature Pd-catalysed arylation of benzoic acids with aryl iodides by using a mono-protected amino acid ligand (MPAA). The use of HFIP as a solvent was found to be the key for to achieving mild reaction conditions, and caesium carbonate base was important for improving the yield of the process. Finally, mechanistic studies revealed that Ac-Ile-OH (MPAA) enhanced the efficiency of the system, accelerating the C–H activation process and improving the catalyst lifetime. Interestingly, a KIE experiment determined by initial rates revealed a primary KIE only in the absence of the MPAA-ligand. This indicates that the C–H activation event ceases to be kinetically significant when the Ac-Ile-OH ligand assists the Pd catalyst in the metalation of the substrate (Scheme 1.44)[60]

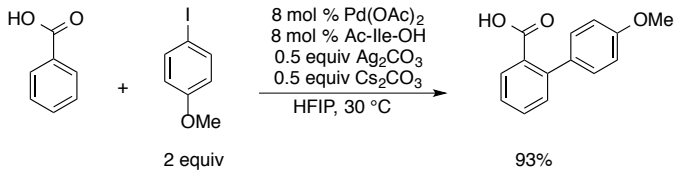

Scheme 1.44. Room temperature direct C–H arylation of benzoic acids.

Many other examples of Pd-catalysed direct C–H arylation *ortho* to a directing group have been developed, including oxidative couplings employing organometallic reagents, oxidative double C–H activation methods and coupling with (pseudo)halide reagents. Anilides,[43,44a,48b, 61] benzamides,[48a, 62] oximes,[51,52, 63] nitrogen-containing heterocycles,[43,44b, 64] carboxylic acids,[53-60] carbamates,[65] ureas,[66] guanidines,[67] ketones,[68] aldehydes,[68b,69] phenols,[70] benzyl alcohols,[71] phosphates[72] and benzyl amines[73] have shown to be valuable directing groups for the direct arylation methods under palladium catalysis.

1.4.2.1.2. Chelate-assisted Ru-catalysed *ortho* C–H Arylation of (hetero)arenes.

Many chelate-assisted ruthenium-catalysed direct arylation methods have been reported over the course of the last two decades, often providing a solid alternative to palladium catalysis.[7g, 74]

Inspired by a pioneering work by Lewis and Smith showing the ability of ruthenium complexes to catalyse hyrdoarylation with ethylene,[75] Murai *et al*. reported the use of a Ru(0) catalyst precursor for the direct *ortho*-alkylation of aromatic ketones with olefins (Scheme 1.45).[76a]

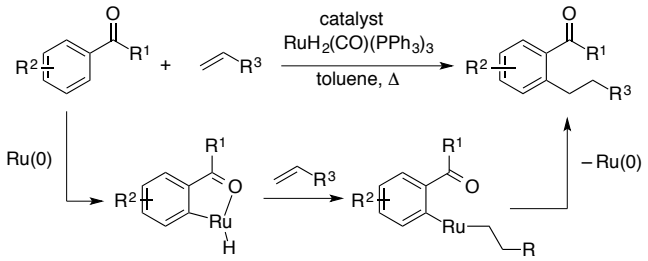

Scheme 1.45. Ruthenium-catalysed hydroarylation of aromatic ketones with alkenes.

Ten years later, Kakiuchi, Murai *et al*. reported the first Ru-catalysed arylation of aromatic ketones with phenyl boronic ester *via* the oxidative addition of C–H bonds. Experimental evidence highlighted that the reaction requires 2 equivalents of the ketone substrate in order to obtain a synthetically useful yield of the biaryl product.

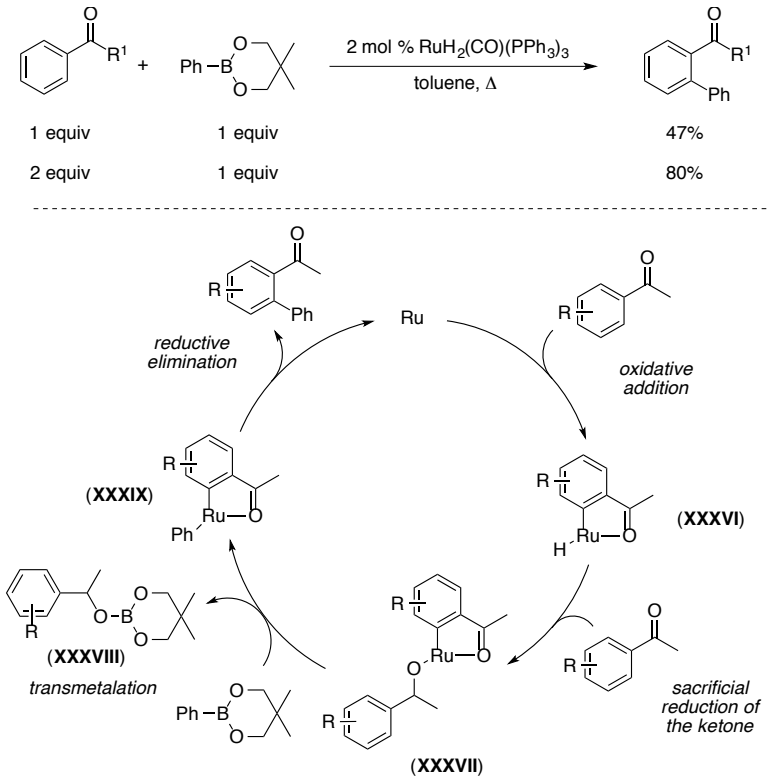

Scheme 1.46. Ru-catalysed arylation of aromatic ketones with boronic esters.

Mechanistic investigations deriving from *in-situ* ^{11}B- and ^{1}H-NMR allowed the authors to elucidate the steps of the catalytic process. The *ortho* C–H bond is cleaved by ruthenium(0) complex to give *ortho* the metalated intermediate **XXXVI**. The addition of a Ru–H bond in **XXXVI** to the hydride acceptor ketone carbonyl group leads to the production of an (alkoxy)-ruthenium intermediate **XXXVII**. Transmetalation, between the phenyl-boronate and intermediate **XXXVII**, results in the formation of the (diaryl)ruthenium complex **XXXVIII** and the trialkoxyborane(borinate) **XXXIX**. Reductive elimination, leading to C–C bond formation, then provides the arylation product and regenerates the catalyst (Scheme 1.46).[77a] In a following paper, the same authors were able to improve the arylation conditions by employing pinacolone (3,3-dimethyl-2-butanone) as the solvent. In fact, pinacolone was revealed to be an efficient H and B($OCH_2C(CH_3)_2$–CH_2O) acceptor moiety, allowing the use of an equimolar *ratio* between the aromatic ketone and phenyl-boronate.[77b]

In 2001, Oi and co-workers introduced the use of Ru(II) catalysts for the direct arylation of 2-phenylpyridine derivatives with aryl (pseudo)halides (X = Cl, Br, I, OTs). $[RuCl_2(\eta^6\text{-}C_6H_6)]_2$ catalyst in combination with PPh_3 ligand, K_2CO_3 base and NMP solvent was found to be the right combination of additives for the methodology. The original mechanistic proposal put forward by the authors suggested the oxidative addition of the aryl (pseudo)halide at a Ru(II) centre forming the aryl ruthenium(IV) species **XL**. *ortho*-Directed electrophilic ruthenation of the 2-PhPy generates the anionic (diaryl)ruthenium complex **XLI**, which after deprotonation affords **XLII**. Finally, reductive elimination frees the biaryl product closing the cycle (Scheme 1.47).[78a]

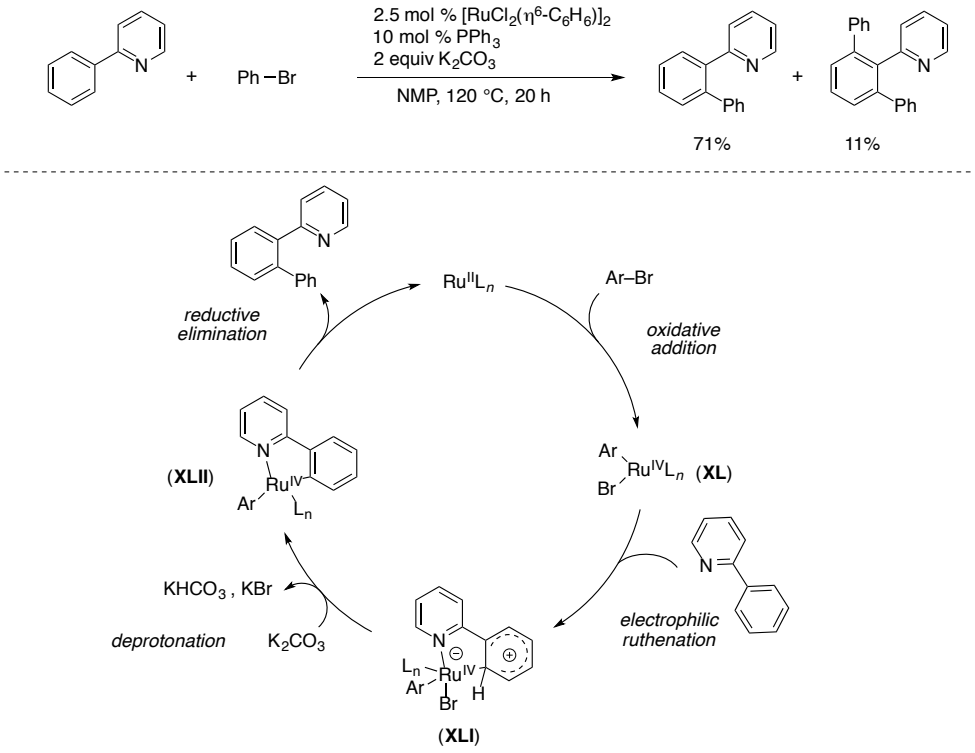

Scheme 1.47. *ortho*-Arylation of 2-phenylpyridine with aryl halides catalysed by Ru(II) species.

The same group, a year later, expanded the arylation protocol to aromatic imines applying identical reaction conditions.[78b] Although the proposed mechanism for the arylation is now considered incorrect, in 2001 the knowledge in C–H activation was extremely limited

especially in ruthenium catalysis. Besides, the mechanism for such transformations is nowadays still a topic of debate.

In 2005-2006, Ackermann *et. al.* introduced the use of phosphine oxide additives (**R_2P(O)H)** in Ru(II)-catalysed arylation of functional arenes with (pseudo)halides (X = Cl, OTs). The reaction conditions developed by Ackermann resemble those reported by Oi and Inoue,[78] with exception of the phosphine oxide additive, which was used in replacement of PPh_3 (Scheme 1.48).[79]

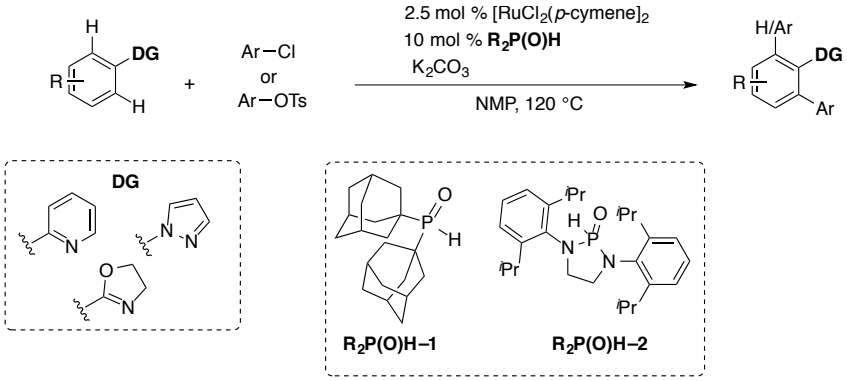

Scheme 1.48. Ru(II)/**R_2P(O)H**-catalysed arylation of DG-containing arenes with (pseudo)halides.

In this study the role of **R_2P(O)H** was considered simply as a preligand, as a possible anionic phosphorus ligand precursor. However, the C–H bond activation with ruthenium(II) was later established as a base(carbonate/carboxylate)-assisted CMD process (**XLIV**).[80] Similarly to McGregor,[18] Echavarren,[20] and Fagnou [22] reported with palladium, Ackermann proposed that **R_2P(O)H** plays the role of a Ru(II) coordinating ligand for deprotonation of arene C–H bonds in a similar way as carboxylate (**XLIII**, Figure 1.5).[81]

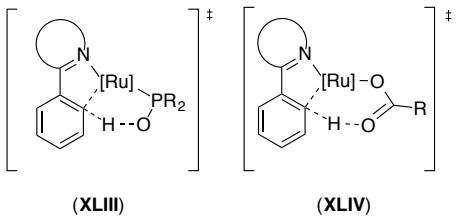

Figure 1.5. Proposed transition states for the ligand-assisted C–H activation with Ru(II) species.

In 2007, density functional theory (DFT) calculations by Maseras and Dixneuf showed that coordination of phenylpyridine to a $RuCl_2$(NHC) unit (**XLV**) led to a species containing an *ortho*-C–H agostic interaction (**XLVI**). C–H activation *via* oxidative addition, forming the Ru(IV)–H species **XLVII**, was determined to be unrealistic as its energy is +28.2 kcal/mol above **XLVI**. When a hydrogen carbonate unit ($HOCO_2^-$) was computed with **XLVI**, a new species (**XLVIII**) was formed, having an energy of 22.9 kcal/mol below that of the two separate fragments. Optimisation towards a suitable transition state for the C–H activation starting from **XLVIII**, led to the establishment of a barrier of 13.9 kcal/mol for the carbonate-assisted metalation of arene (**XLIX**). The final cycloruthenated species (**L**) was consequently formed (Scheme 1.49). In the same manuscript, empirical evidence for the direct C–H arylation of 2-PhPy with aryl halides, employing Ru(II)/NHC system, were shown.[80]

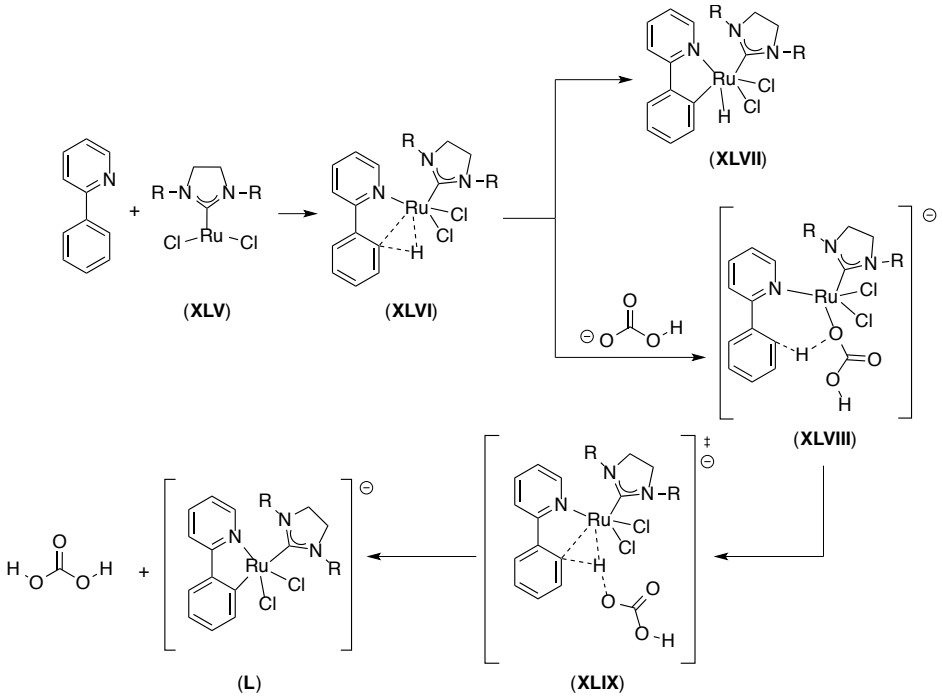

Scheme 1.49. DFT studies by Maseras *et al*. on the carbonate-assisted C–H activation of 2-PhPy with **XLV**.

In 2008, Ackerman introduced the use of 2-mesitylenecarboxylic acid ($MesCO_2H$) as an additive for the arylation of DG-containing arenes.[81] By employing this hindered benzoic

acid or **$R_2P(O)H$–1** (see Scheme 1.48) additives, arylation conditions in apolar solvents, such as toluene, were achieved for the first time. Ackermann suggested that the role of the benzoate/ phosphine oxide additives is to aid the chelate-assisted metalation of the substrate (Figure 1.5).

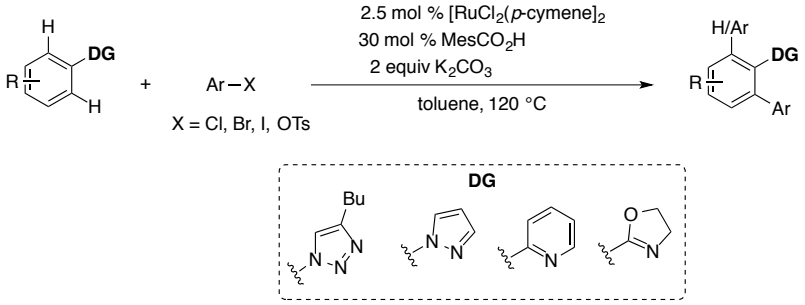

Scheme 1.50. Ru(II)/$MesCO_2H$-catalysed arylation of DG-containing arenes with (pseudo)halides.

The most accepted mechanism for the Ru(II)-catalysed chelate-assisted arylation with aryl halides involves the reversible cyclometalation of the arene by the Ru(II) catalyst, *via* concerted metalation-deprotonation (**XLIV**). The cycloruthenated species **LI** undergoes oxidative addition, in the presence of the aryl halide, affording the Ru(IV) intermediate **LII**. After reductive elimination, this intermediate frees the biaryl product regenerating the starting catalyst.[7g]

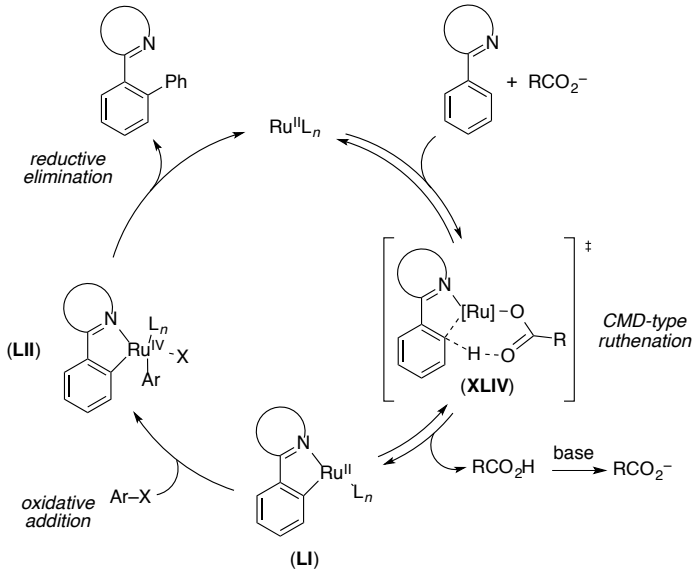

Scheme 1.51. Proposed mechanism for the Ru(II)-chelate-assisted arylation of arenes with aryl halides.

In 2012, the first oxidative arylation of DG-containing arenes with aryl boronic acids catalysed by Ru(II) was reported by Jeganmohan and co-workers. Benzamides were successfully arylated employing $[RuCl_2(p\text{-cymene})]_2$ catalyst precursor, $AgSbF_6$ as halide scavenger, Ag_2O as the terminal oxidant and THF solvent (Scheme 1.52, equation *a*).[82a]

The following year the same authors were able to report the oxidative arylation of acetanilides with boronic acid. Although the reaction conditions resemble those developed for the arylation of the benzamides, 20 mol % of $Cu(OTf)_2$ additive was needed to improve the arylation yield (Scheme 1.52, equation *b*).[82b]

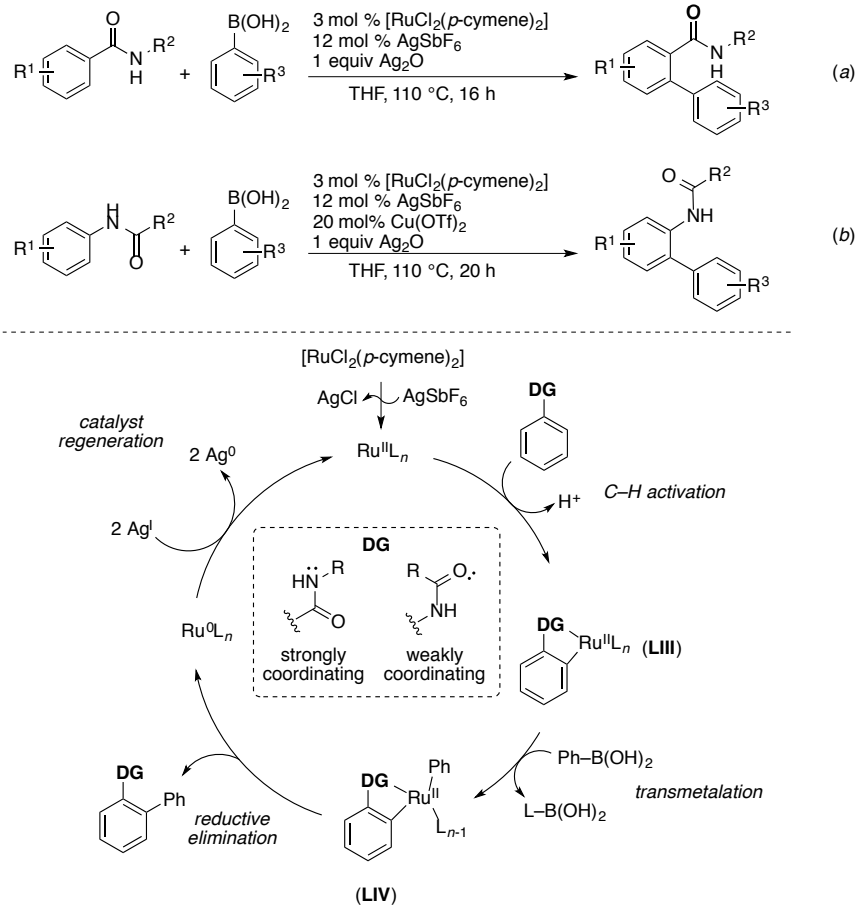

Scheme 1.52. Ru(II)-catalysed arylation of benzanilides and acetanilides with boronic acids.

This methodology is the first protocol in which weakly-coordinating DGs, such as anilides, were successfully used under Ru(II) catalysis. In fact, Ru(II)-catalysed arylation was limited to 2-pyridyl, oxazoline, azole, amide and oxime substituted arenes with aromatic electrophiles. The mechanism involved C–H activation of the arene by the Ru(II) complex, forming the cyclometalated intermediate **LIII**, which undergoes transmetalation with the boronic acid affording the (biaryl)Ru(II) species **LIV**. Reductive elimination generates the product and a Ru(0) intermediate that is oxidised by the Ag(I) salt restoring the original Ru(II) species (Scheme 1.52).

Although many reports display the potential of Ru-catalysis in direct arylation methodologies, to date they are limited to arenes bearing directing groups. Therefore more studies will be required in order to increase the already vast array of C–H functionalisations that ruthenium can deliver.[83]

1.4.2.1.3. Chelate-assisted Rh-catalysed *ortho* C–H Arylation of (hetero)arenes.

In 1998 the Oi group developed the first rhodium-catalysed chelate-assisted arylation method. The selective *ortho*-arylation of 2-aryl pyridines with arylstannanes was achieved using a catalytic amount of a Rh(I)/PPh_3 catalyst such as Wilkinson's catalyst, and with chlorinated solvents (Scheme 1.53, equation *a*).[84] Trichloroethylene is formed during the arylation with 1,1,2,2-tetrachloroethane solvent, which suggested that the chlorinated solvent is essential for catalytic turnover acting as the oxidising agent (Scheme 1.54, equation *b*).

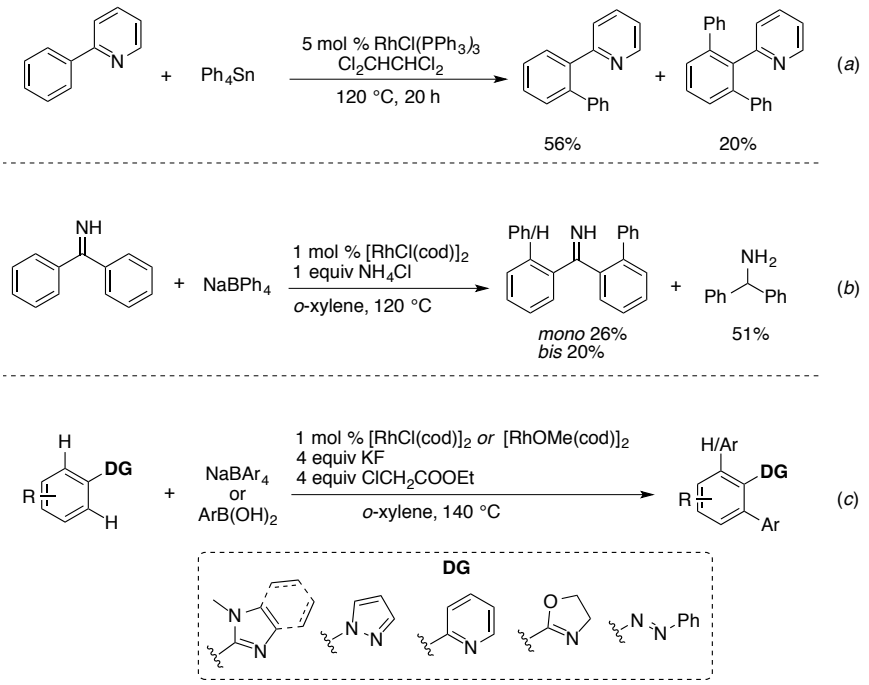

Scheme 1.53. Rh-catalysed chelate-assisted *ortho*-arylation of arenes with organometallics reagents.

In 2005, Miura and co-workers developed a Rh(I)-catalysed *ortho*-arylation of imines with sodium tetraphenylborate and ammonium chloride as additive (Scheme 1.53, equation *b*).[85a] The process provided only low yields of mono- and di-arylated adduct due to reduction of the starting imine to the corresponding benzyl amine, which acts as an oxidant regenerating the catalyst (Scheme 1.54, equation *a*). In a follow-up paper, the Miura group improved the

arylation conditions by using KF additive and α-chloroacetate as the terminal oxidant (Scheme 1.53, equation *c* and Scheme 1.54, equation *b*).[85b]

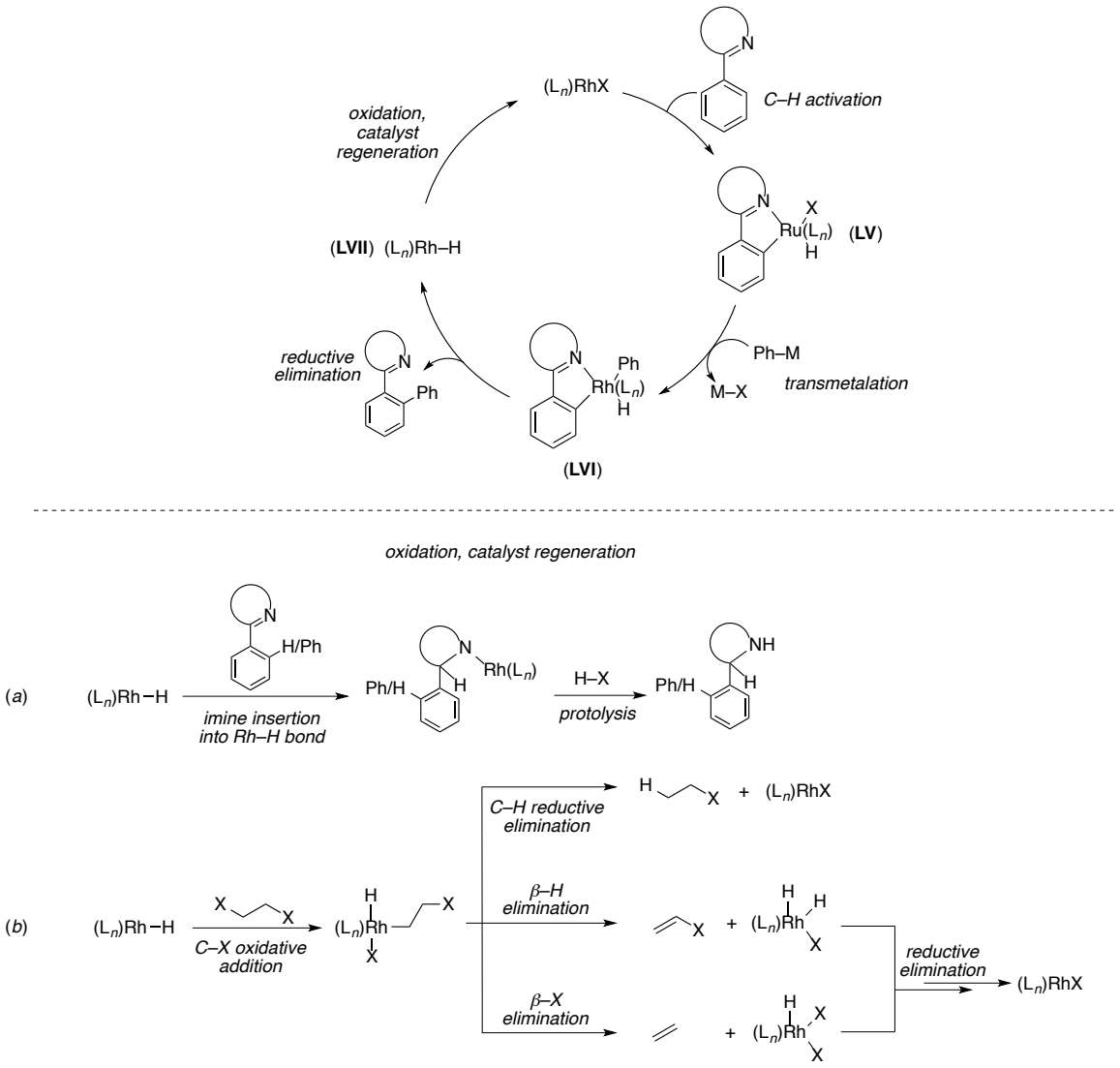

Scheme 1.54. Mechanism of the Rh(I)-catalysed arylation with organometallic reagents.

The mechanism of Rh(I)-catalysed arylation with organometallic reagents involves the oxidative addition at Rh(I) centre forming the Rh(III)–H species (**LV**). Transmetalation with organometallic reagent generates the (diaryl)Ru(III)–H complex **LVI**, which reductively eliminates giving the biaryl product and the Rh(I)–H intermediate **LVII**. Insertion of the

imine into the Ru–H of **XLVII** followed by protolysis (Scheme 1.54, equation *a*), or C–X oxidative addition of the halogenated solvent/additive with consequent C–H reductive elimination or β-hydride / halogen elimination with successive reductive elimination, restores the starting Rh(I) catalyst (Scheme 1.54, equation *b*).

In 2008, Vogler and Studer reported that Rh(I)/(4-$CF_3C_6H_4)_3P$ in combination with 2,2,6,6-tetramethylpyperidine-*N*-oxyl radical (TEMPO) oxidant is a valuable catalytic system for the arylation of 2-pyridylarenes with boronic acids (Scheme 1.55). [86]

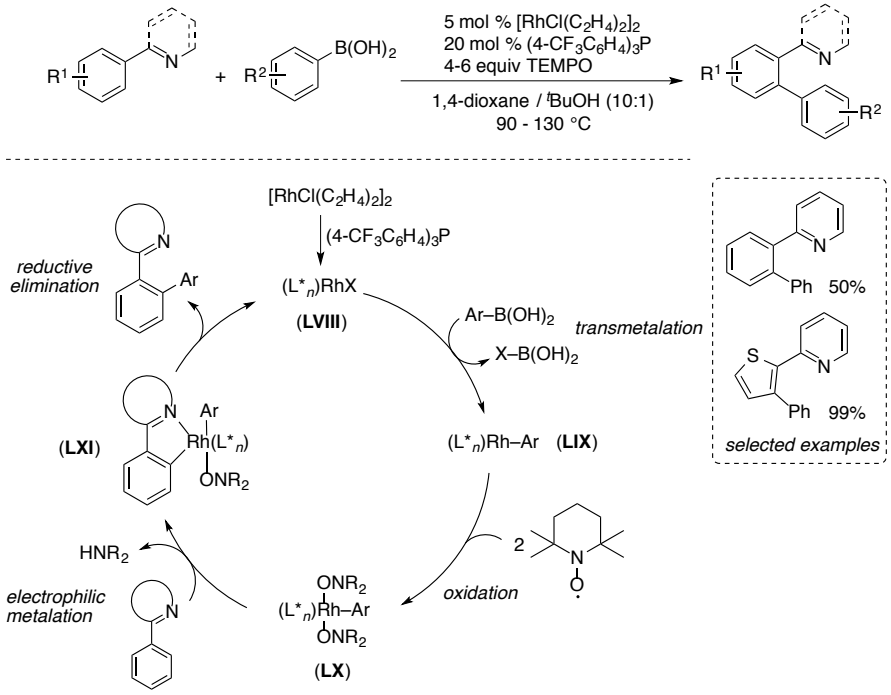

Scheme 1.55. Rh(I)/(4-$CF_3C_6H_4)_3P$/TEMPO catalytic system for the arylation of 2-pyridylarenes.

Among the ligands tested, electron-deficient triarylphosphines were found to be the best. Additionally, more nucleophilic arenes, such as 2-(thiophen-2-yl)pyridine, were the most reactive. These observations are consistent with an electrophilic C–H metalation process requiring a highly electron-deficient Rh(III) centre. Although the mechanism has not been fully elucidated, a plausible catalytic process could start from transmetalation of Ru(I) catalyst **LVIII** with the organoboron reagent to give the aryl ruthenium(I) species **LIX**. The

latter is likely to be oxidised by TEMPO, to afford a rhodium(III) complex **LX** that performs electrophilic C–H activation on the 2-pyridylarene, generating (diaryl)ruthenium(III) **LXI** intermediate. Reductive elimination frees the product restoring the original Rh(I) species. Since the C–H activation event is likely to occur at Rh(III) centre, this report fuelled the design of Rh(III)-catalysed arylation methods of closely related substrates with organometallic reagents.[87]

In 2003, the groups of Bedford[88] and Oi[89] independently developed Rh(I)-catalysed methods for *ortho*-arylation of phenols with haloarenes that rely on the reversible transesterification of phosphorus(III) species with phenols/phenoxides. The *ortho*-selectivity derived from the ability of aryl dialkylphosphinites and phosphorodiamidates to undergo C–H activation with rhodium complexes leading to 5-membered metallacycles. Bedford's conditions for *ortho*-arylation of phenols consist of: $Rh(Cl)(PPh)_3$ catalyst precursor, diisopropylphosphinite ($ArOP^iPr_2$) as the phosphnyl-transfer agent, Cs_2CO_3 base and aryl bromide coupling partner. Although these conditions were compatible with a vast array of functional groups, the phenol must have an *ortho* bulky substituent (^{t}Bu, ^{i}Pr, 1-naphthol) in order to react. Phenol derivatives with less bulky *ortho* groups (Et, Me) were poorly reactive (Scheme 1.56, equation *a*). Oi and co-workers, developed a system where hexamethylphosphotriamide (HMPT) acts as the phosphinyl group transfer agent that enables the cyclometalation of the aryl phosphorodiamidate. Oi's system does not require an *ortho* group on the phenol for the reaction to proceed, *ortho*- and *meta*- substituted phenols provides exclusively mono-arylation, instead *para*-substituted ones mainly give bisarylation (Scheme 1.56, equation *b*). The mechanism involves oxidative insertion of haloarene at Rh(I) centre to form an aryl-Rh(III) complex (**LXII**). Phenyl phosphite (**LXIII**) formation *via* (trans)esterification permits the cyclometalation of the phenol derivative (**LXIV**). Reductive elimination generates the (diaryl)phosphite **LXV** and restores the initial Rh(I) catalyst. Transfers of phosphinyl group from **LXV** to a phenol allows the catalytic use of the phosphorus(III) tether.

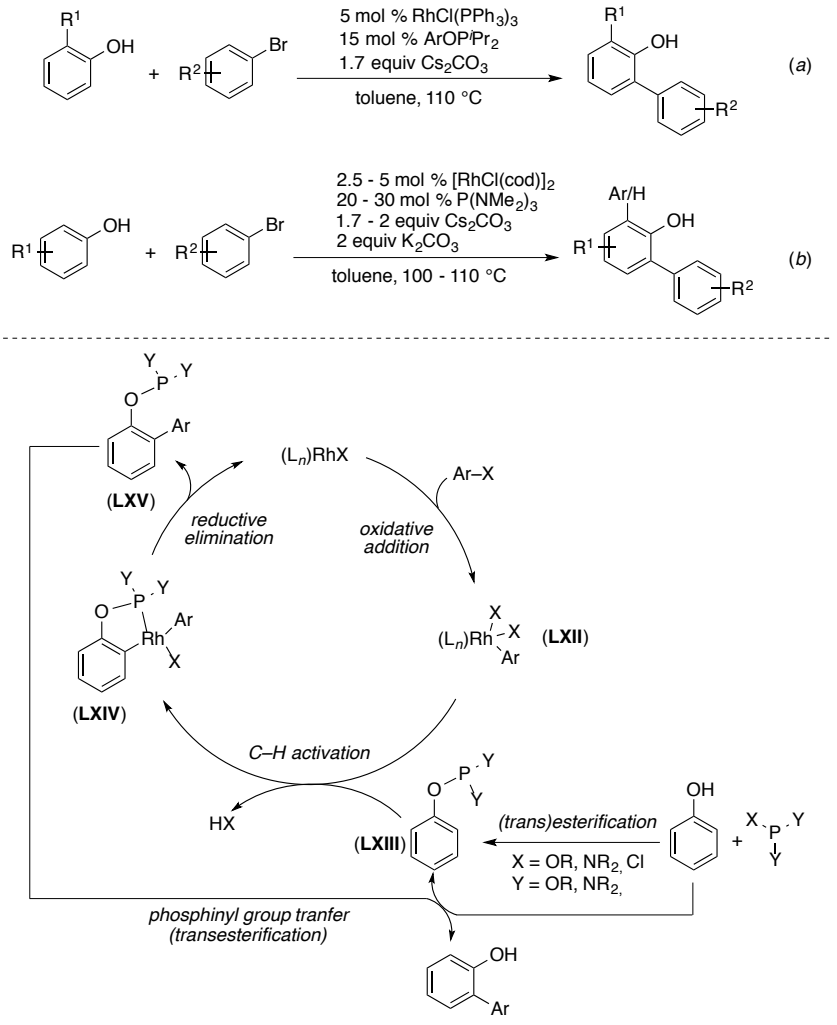

Scheme 1.56. Bedford and Oi's protocols for the *ortho*-arylation of phenols with ArBrs catalysed by Rh(I).

In 2008, Zhao and Yu described a Rh(I)-catalysed decarbonylative arylation of 2-pyridyl arenes and analogues with acyl chlorides.[90] Under typical reaction conditions, the 2-substituted pyridines were efficiently arylated with $[RhCl(cod)]_2$ catalyst precursor, Na_2CO_3 base, 4Å molecular sieves in xylene as the solvent. The mechanism of the reaction is proposed to be oxidative addition of the acyl chloride to a Rh(I) centre to give **LXVI,** decarbonylation to form **LXVIII**, electrophilic metalation to generate **LXVIII** and reductive elimination to close the cycle affording the final product (Scheme 1.57).

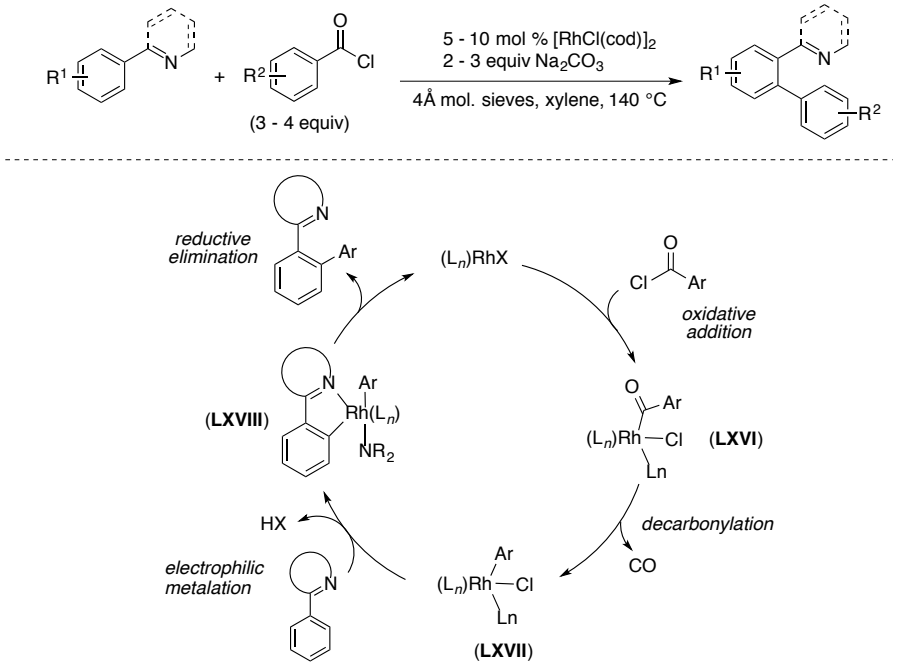

Scheme 1.57. Rh(I)-catalysed decarbonylative arylation of 2-pyridilarenes with acylchlorides

More recently, the Glorius group developed the Rh(III)-catalysed oxidative arylation *via* double C–H activation.[91 a] $Rh[Cp^*Cl_2]_2$ catalyst precursor in combination with sub-stoichiometric amounts of halide abstractor $AgSbF_6$, catalytic CsOPiv, stoichiometric quantities of PivOH and $Cu(OAc)_2$, shaped an efficient system for the cross dehydrogenative coupling (CDC) of benzamide-type arenes and simple arenes. Although several examples were reported, the CDC requires high loading of the simple arene coupling partner (≈ 50 equiv), which ends up being the solvent of the reaction. More interestingly, only simple arenes bearing halogen(s) (X, X ≠ F) were efficiently arylated with a preference for the *meta* and *para* positions (Scheme 1.58, equation *a*), as already seen for other Rh- and Ir-catalysed C–H functionalisation.[92] Synthetically useful biaryl were mostly obtained using *meta*-substituted haloarenes (Scheme 1.58, equation *b*). Although the mechanism is still under investigation, efforts towards the understanding of the step of the catalytic cycle were made by deuterium-labelling experiments on both coupling partners. The results provided strong evidence on the reversible nature of C–H activation process occuring on both benzamide and bromobenzene. KIE experiments revealed that the breaking of the C–H on both arenes is

kinetically relevant. In a closely related paper, the same authors developed a CDC of furan and thiophene derivatives.[91b]

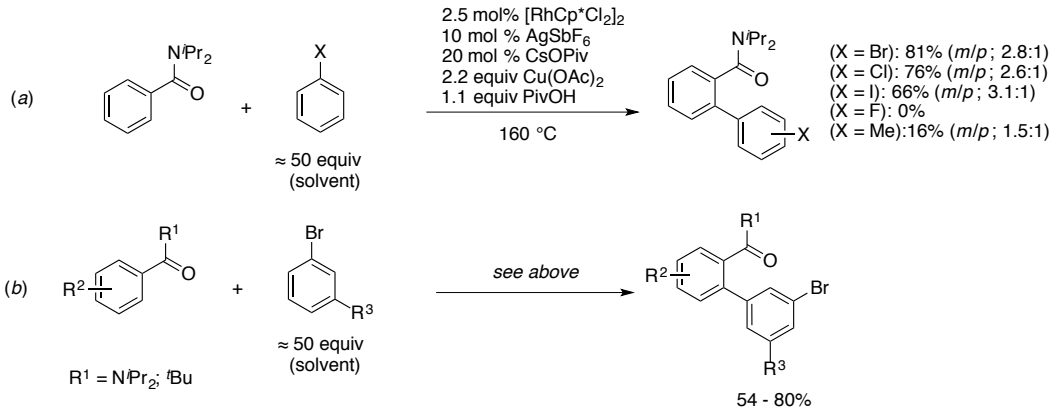

Scheme 1.58. Rh(III)-catalysed CDC between benzamide derivatives and halorenes.

A few months later, the same group improved the substrate scope and the reaction conditions of the CDC methodology thanks to the presence of 2 equivalents of hexabromobenzene additive and 2-chloro-*p*-xylene as the solvent.[91c] The latter allowed a decreased arene loading (20 equiv) and to couple simple arenes, which do not bear a halogen substituent. Hetreoarenes like (benzo)furans and (benzo)thiophenes were also found to be suitable coupling partners (Scheme 1.59, equations *a* and *b*). More deuterium labelling mechanistic investigations were conducted, confirming the reversible nature and the kinetic relevance of both C–H activation events. The KIE results suggests that the non-chelate-assisted C–H activation is likely to be involved in the rate determining step of the catalytic cycle. Competition experiments aimed to gain information about the influence of the electronic properties of each coupling partner were conducted. Treatment of 1:1 mixtures of differently substituted benzamides with benzene showed that the CDC is enhanced for electron-rich benzamides. In contrast, the electronic influence on the non-directed C–H activation step is much less pronounced. This data indicates that neither an Ar–H deprotonation pathway nor a S_EAr mechanism is plausible for this step, leading the authors to suggest a σ-bond metathesis-type mechanism. Interestingly, the product formation was always associated with the formation of C_6HBr_5 derived from the protodehalogenation of

C_6Br_6, which indicates the role of C_6Br_6 as an oxidant. Stoichiometric/mechanistic reactions in order to cast light on the role of $Cu(OAc)_2$ and C_6Br_6 revealed that the omission of one of the two led to a significant decrease in the reaction efficiency. In the absence of both the reaction does not take place. These results suggest that both reagents are not only involved in the reoxidation of the catalyst. H/D scrambling experiments with D_2O in the absence of the simple arene coupling partner showed a slightly enhanced deuteration of the benzamide in the presence of C_6Br_6. When *p*-xylene-d_{10} was used as the only source of D atoms, D incorporation on the benzamide was instead highly enhanced with C_6Br_6. These observations could be interpreted as indirect proof of the key role of C_6Br_6 in the "activation" of the rhodium catalyst for the undirected C–H activation.

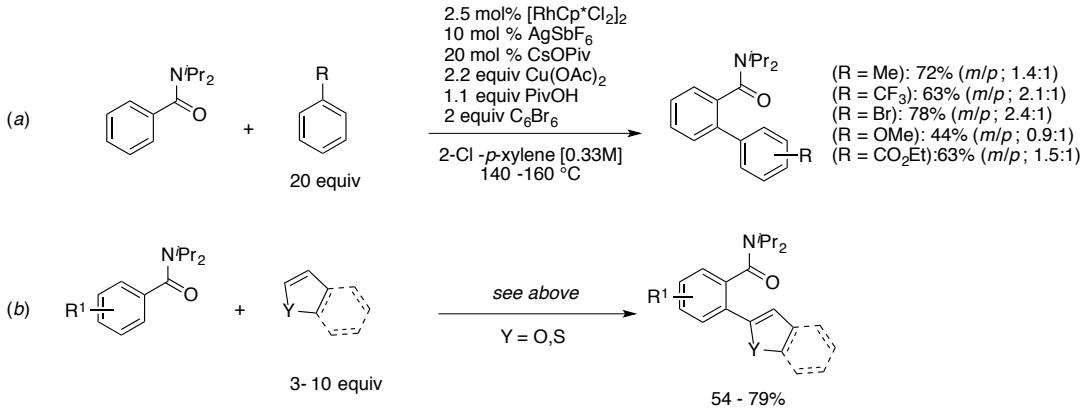

Scheme 1.59. Rh(III)-catalysed CDC between benzamide derivatives and (hetero)arenes.

In 2013, the You group independently developed a similar methodology for CDC of closely-related substrates. $[RhCp^*Cl_2]_2$ catalyst precursor in combination of sub-stoichiometric amount of halide abstractor $AgSbF_6$, $Cu(OAc)_2$ in DCE solvent, were found to be the optimised conditions for the cross coupling of 2-pyridylarenes with (hetero)aromatic compounds (Scheme 1.60, equation *a*).[93] H/D scrambling reactions with D_2O as source of D atoms, revealed the reversibility of the C–H activation on both arenes, although the D-incorporation on the thiophene was less pronounced respect to the 2-PhPy coupling partner.

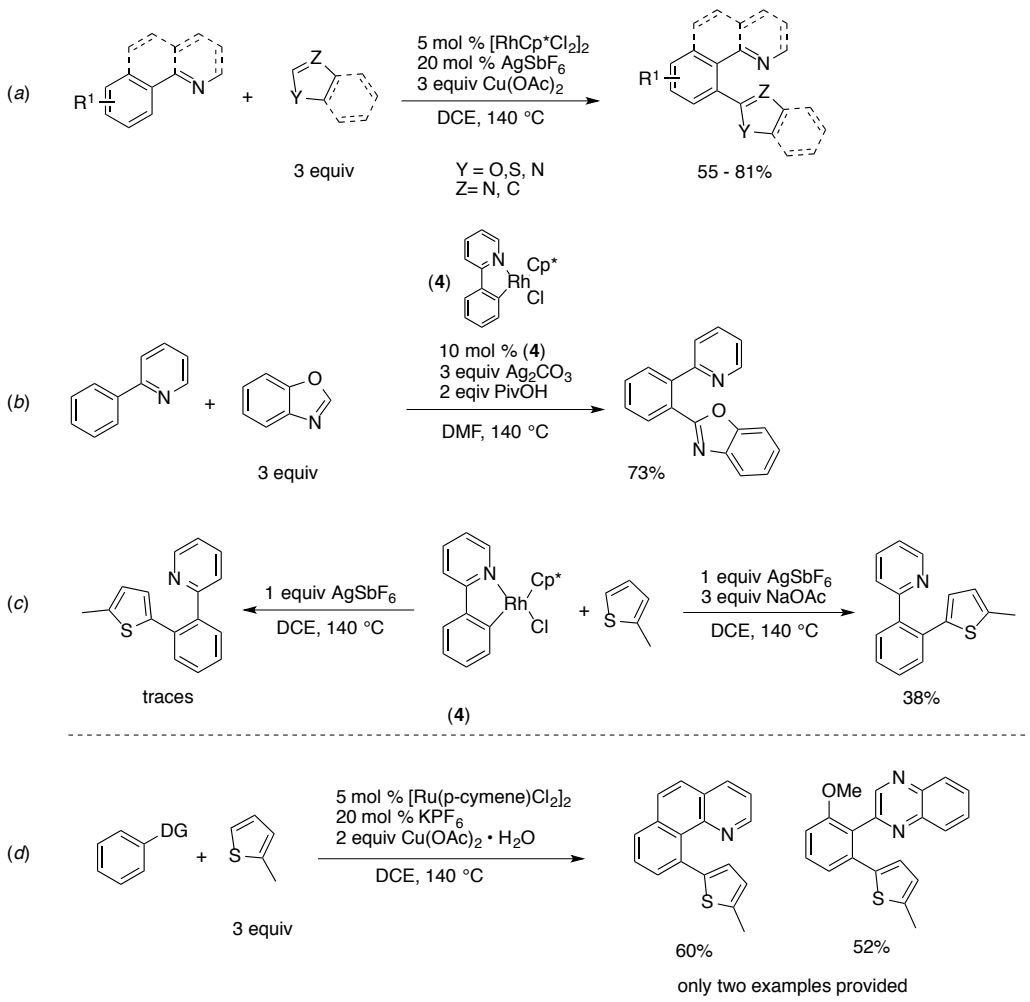

Scheme 1.60. CDC catalysed by Rh(III)- and Ru(II) of DG-containing arenes with (hetero)arenes.

Although under slightly different reaction conditions, an independently prepared cyclometalatated Rh(III) complex (**4**), catalysed the arylation of 2-Phy with benzoxazole, suggesting that a similar intermediate might be formed under standard conditions (Scheme 1.60, equation *b*). In a single turn-over reaction, complex (**4**) reacts with the thiophene only if acetates are present as additive, suggesting that they are essential for the non-directed C–H activation to take place (Scheme 1.60, equation *c*). Additionally, the negligible effect on the addition of catalytic amount of TEMPO appears to preclude a radical involvement. In the same manuscript, You and co-workers reported two examples for an analogue arylation method catalysed by Ru(II), proving the ability of ruthenium to catalyse similar processes.

[Ru(*p*-cymene)Cl_2]$_2$ with KPF_6 additive and stoichiometric amount of $Cu(OAc)_2$ in DCE solvent, proved to be efficient conditions for the cross coupling of two DG-containing arenes with a thiophene derivative (Scheme 1.60, equation *d*).

1.4.2.2. *meta* C–H Arylation of (hetero)arenes bearing a directing group (DG)

Different approaches with Cu, Pd and Ru catalysts have been used in order to achieve *meta*-selectivity. In some cases the installation of a directing group drives the metalation at the *meta* position where the functionalisation will take place. In other cases, the initial *ortho*-metalation dictated by a chelating group is re-directed at the *meta*-position where the coupling will finally happen. Lastly, particular *ortho*-cyclometalated complexes can promote functionalisations at *ortho*- or *para*- positions with respect to the metalation site, thus enabling functionalisations in *meta* position to the directing group. In the following sections these cases will discussed.

1.4.2.2.1. *meta* C–H Arylation dictated by the metalation site

In 2009 Gaunt and co-workers, inspired by their previous studies on the arylation of indoles catalysed by copper(II) using bis(aryl) iodonium salts as oxidant, [94] reported the first example of direct C–H *meta*-arylation. The pivalamide group, which is classically *ortho*/*para*-directing for S_EAr or a powerful *ortho*-directing group in chelate-assisted C–H functionalisation, was instead discovered to direct *meta*-arylation with Ar_2IOTf under $Cu(OTf)_2$ catalysis (Scheme 1.61, equation *a*).[95] The mechanism of the reaction was proposed to proceed *via* an aryl-Cu(III) (**LXIX**) species deriving form oxidation of Cu(I) (which is proposed to be formed by *in situ* reduction or disproportionation) by the (bis)aryliodonium salt. These highly electrophilic species promotes an antioxycupration (**LXX**) that, after re-aromatisation (**LXXI**) and reductive elimination, generates the biaryl product. A DFT study by Wu's group disfavoured that proposal, suggesting insterad an initial metal attack at the *ortho*-position followed by a four-membered transition state to finally

give the arylation at *meta* position.[96] Subsequent studies by *Gaunt et al*. showed that other α-aryl carbonyl compounds, such as Weinreb amides, esters and ketones, also underwent the Cu-catalysed *meta*-arylation.[14b] During this study, the authors observed that the *meta*-arylation also proceeded under metal free conditions at slightly higher temperature in a low yield compared to the metal catalysed process (Scheme 1.61, equation *b*).

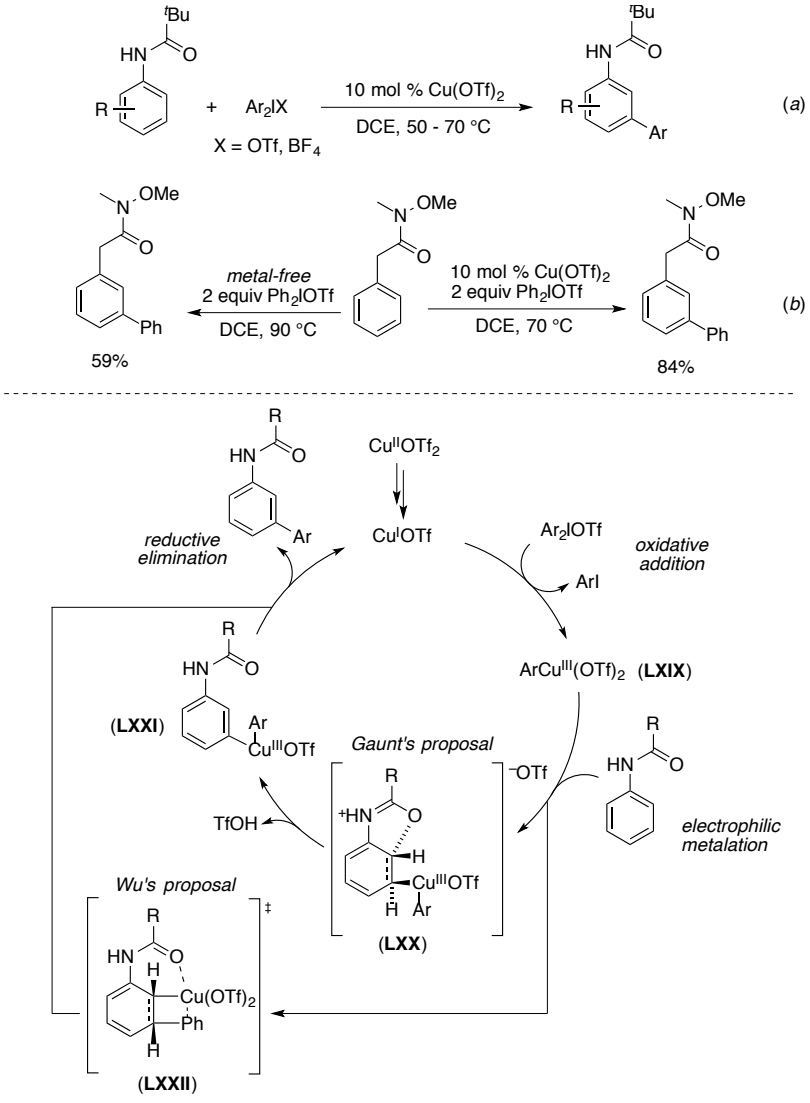

Scheme 1.61. *meta*-Selective arylation developed by the Gaunt group.

In a breakthrough paper Yu and co-workers introduced the concept of remote C–H bond activation assisted by an "*end-on*" template, in which a weak coordination between a nitrile group present on the template and the catalyst, Pd(II), made the remote C–H bond activation possible. The extensively engineered aryl spacing group was reported to be essential for the directing effect. Thus, a high level of rigidity on the template was indispensable for the purpose. A big advantage of this new approach is that the regioselectivity is not substrate-dependant; in fact a template-directed *meta*-selective C–H olefination of simple arenes was described.[97] Interestingly, a recent DFT study suggested a bimetallic (*i.e.* Pd–Pd or Pd–Ag) cyclophane-type transition state (**LXXIII**) rather that a monometallic one (**LXXII**) (Scheme 1.62).[98]

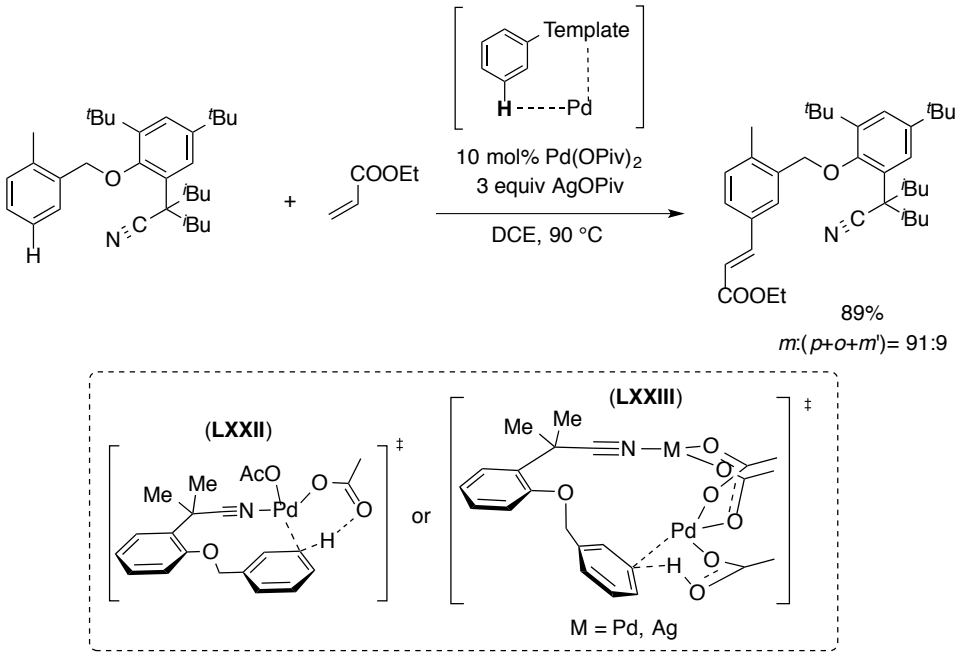

Scheme 1.62. Template-directed *meta*-selective Pd-catalysed alkenylation.

In following papers the same group, applying the same template-directed strategy with modified nitrile-containing-directing groups, developed a Pd-catalysed *meta*-direct C–H arylation of phenylpropionic acid[99] and indolines[100] derivatives with aryl boronates (Scheme 1.63). A MPAA-ligand (Ac-Gly-OH) was a valuable additive for assisting the concerted

metalation-deprotonation (**LXXIV**), thus decreasing the C–H activation barrier which was found to be rate-determining by KIE experiments.[101]

Various other methods have been reported for *meta*-alkenylation and/or hydroxylation, which rely on similar cyanide directing groups.[102]

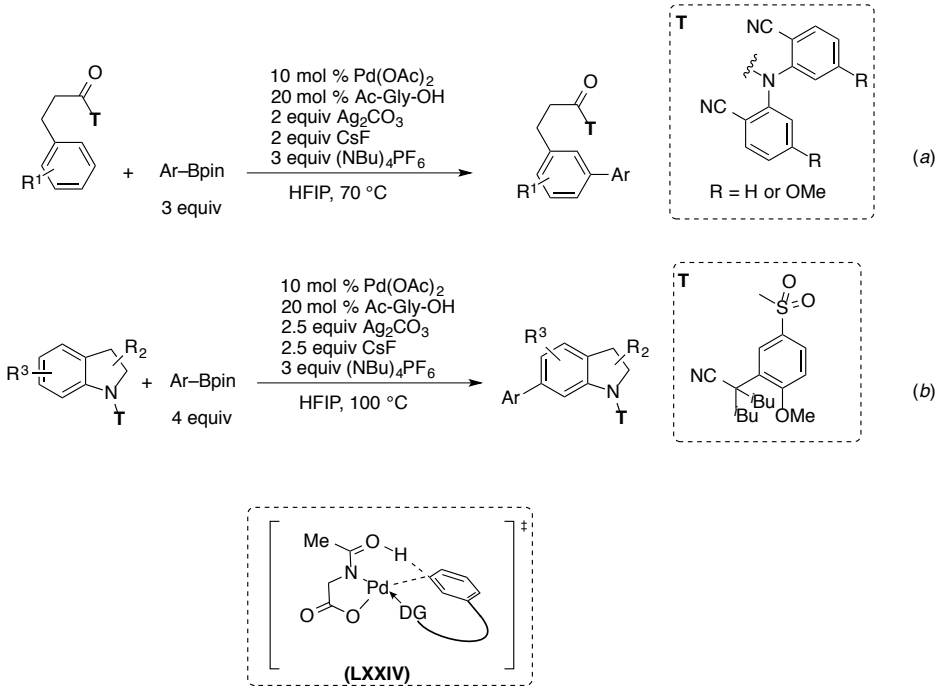

Scheme 1.63. Template-directed *meta*-arylation of phenylpropionic acid and indolines derivatives with phenyl boronates under Pd catalysis.

1.4.2.2.2. *meta* C–H Arylation by hijacking the metalation site

A totally different approach for tackling the *meta*-position involves the catalytic system Pd/norbornene introduced by Catellani in the mid 1980s. The reactivity of the Catellani reaction arises from the ability of norbornene to initiate a competitive reaction pathway and form a rigid catalyst scaffold placing the palladium catalyst in proximity to a C–H bond. The unique reactivity of norbornene is accompanied by a catalytic cycle involving multiple oxidation state transitions of palladium between (0), (II), and (IV).[103]

Very recently, inspired by Catellani's reaction, the Yu[104] and the Dong[105] groups have simultaneously developed a direct C–H *meta*-arylation of arenes bearing *ortho*-directing group with aryl iodides. The mechanism involves an *ortho*-directed C–H activation to give the cyclometalated species **LXXV** followed by carbopalladation of norbornene (NBE) to form a norbornylpalladium(II) intermediate **LXXVI**. With no possibility of *syn*-β-hydride elimination, a second C–H activation occurs forming palladacycle **LXXVII**.

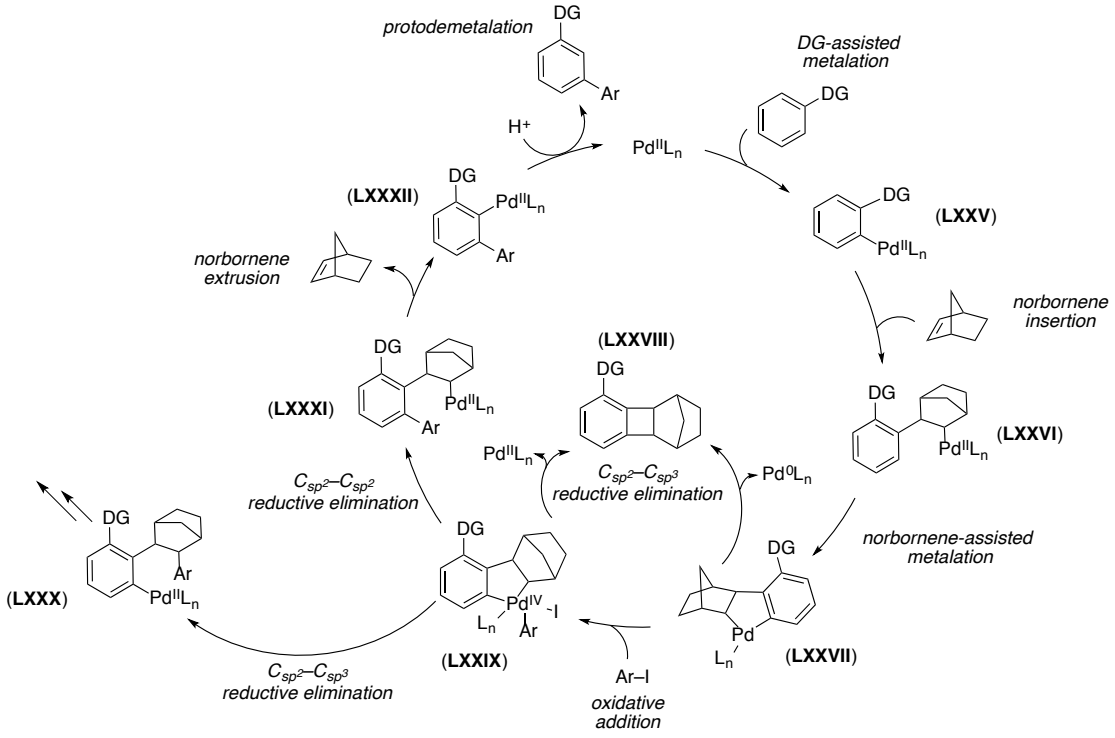

Scheme 1.64. Mechanism of the Pd/NBE catalysed direct *meta*-arylation of arenes bearing an *ortho*-DG.

This palladium(II) complex can either undergo reductive elimination forming cyclobutane adduct **LXXVIII** or react further in the presence an aryl halide affording the Pd(IV) intermediate **LXXIX**. This species can reductively eliminate forming the C–C bond in three different ways. The two C_{sp^2}–C_{sp^3} reductive eliminations provide undesired species **LXXVIII** or **LXXX**, instead the C_{sp^2}–C_{sp^2} elimination forms the on-cycle intermediate **LXXXI**. Catellani noticed that *ortho*-substituted aryl iodides have the tendency to selectively promote the C_{sp^2}–C_{sp^2} reductive elimination. This is known as the *ortho*-effect in the Catellani

reaction.[106] Norbornene extrusion from **LXXXI** forms the (diaryl)palladium(II) species that, after the fundamental step of protodemetalation, frees the biaryl product restoring the initial Pd(II) catalyst (Scheme 1.64).

The Yu approach consists of using derivatives of phenylacetic acids as the arenes bearing an *ortho*-directing group, aryl iodide coupling partners (alkyl iodides and benzyl bromides were also suitable electrophiles), highly optimised pyridine ligand (**5**), AgOAc base and halide abstractor, MTBE solvent with $Pd(OAc)_2$ and norbornene catalysts. The authors disclosed that pyridine-type ligands were essential for promoting the norborne's insertion after cyclometalation (**LXXVI**). Although the system is exclusively *meta*-selective, only *ortho*-substituted electron poor aryl iodides and *ortho*-substituted arenes were found to be suitable coupling partners (Scheme 1.65, equation *a*).[104a]

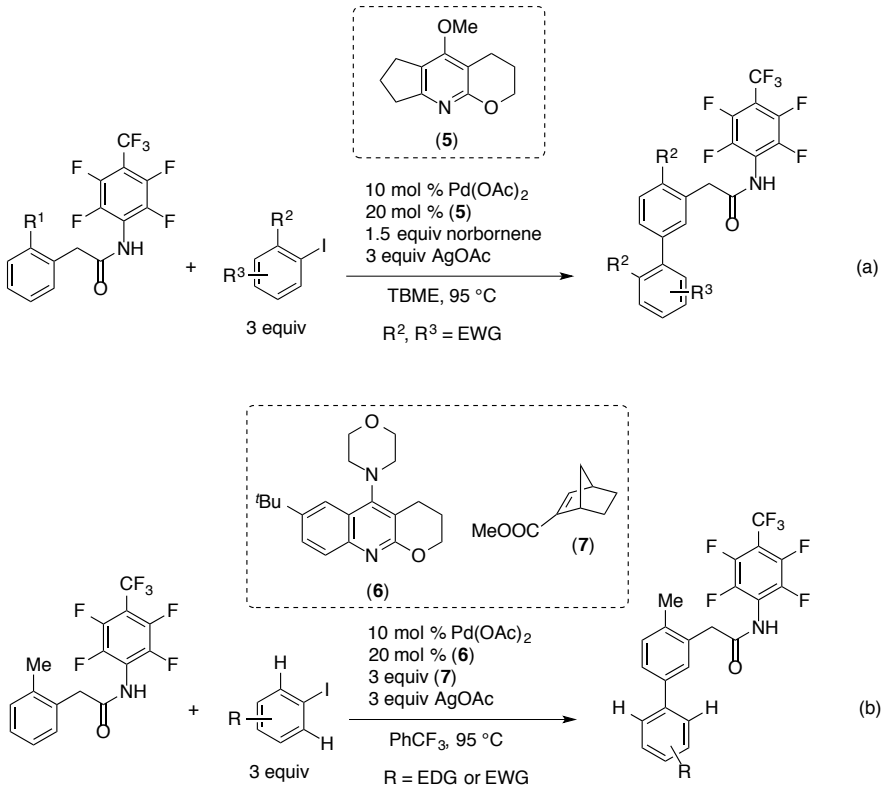

Scheme 1.65. Yu's protocols for the Pd/NBE-mediated *meta* arylation.

This is most likely due to the *ortho*-effect of the Catellani reaction and also to ease the oxidative addition at Pd(II) centre. Remarkably, in a following report Yu *et al*. were able to substantially improve the scope of the arylation by introducing the norbornene derivative (**7**), which was demonstrated to promote the selective C_{sp^2}–C_{sp^2} over the C_{sp^2}–C_{sp^2} reductive elimination. Under slightly modified conditions, by using pyridine ligand **6**, norbornene derivative **7** and trifluorotoluene solvent, *para*- and *meta*-substituted aryl iodides bearing electron-withdrawing or electron-donating groups were successfully used in the arylation (Scheme 1.65, equation *b*).[104b]

Dong and co-workers independently developed the norbornene-mediated Pd(II)-catalysed *meta*-C–H arylation of simple benzylamines derivatives. $Pd(OAc)_2$/$AsPh_3$/NBE catalytic system, AgOAc along with a combination of acetates as an "acetate cocktail" (CsOAc, $LiOAc \cdot 2H_2O$, $CuOAc \cdot 2H_2O$, AcOH) in chlorobenzene solvent were the optimised reaction conditions leading to the formation of the *meta*-arylated adduct. Although the reasons behind the need of so many acetate-containing additives remain unclear, the omission or partial omission of any of them is detrimental for the arylation. Also for the Dong's protocol, only *ortho*-substituted electron poor aryl iodides were reactive in the system (Scheme 1.66).[105]

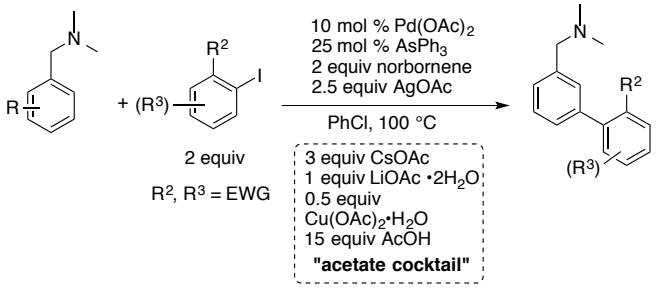

Scheme 1.66. Dong's protocols for the Pd/NBE-mediated *meta* arylation.

1.4.2.2.3. *meta* C–H functionalization: metalation dictates remote regioselectivity

This approach is based on forming a cyclometalated ruthenium complex containing a σ–aryl bond, which steers an electrophilic attack to the *para* position by inductive and mesomeric effects, providing a formal *meta* incorporation of an electrophile in the metalated aromatic ring (Figure 1, *d*). The metal is therefore acting as a "pseudo-protecting group" for the *ortho* position, directing the attack to *para*, thus affording a selective *meta* activation.[107] This concept has been successfully applied for the *meta*-sulfonation, *meta*-alkylation and *meta*-bromination of arenes containing traditional *ortho*-directing groups by Frost,[108] Ackermann,[109] Greaney[110] and Huag[111] (Scheme 1.67).

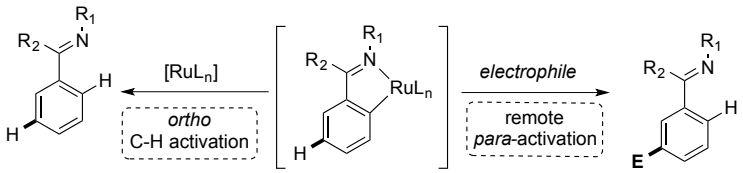

Frost et al. *Sulfonation with* **ArSO$_2$Cl**; Alkylation with **R^{1}R^{2}R^{3}C**Br
Ackermann et al. *Alkylation with* **R^{1}R^{2}CH**Br and **R^{1}R^{2}R^{3}C**Br
Greaney et al. *Bromination with* NBu$_4$**Br**$_3$
Huang et al. *Bromination with* N**B**S

Scheme 1.67. Ruthenium-catalysed *meta*-functionalisations through remote *para*-activation.

Late transition metal cyclometalated complexes containing σ–carbon-to-metal bonds have been shown to posses an interesting reactivity on the aromatic ligands. The electron density on this aryl group is increased at the *ortho* and *para* positions, exhibiting an interesting regioselectivity on transformations such as C–H oxidative dimerization and S_EAr.[112] Dimerisation,[113] nitration,[114] chlorination,[113c-e, 115] bromination,[114b-c, 115b-c, 116] iodination,[115b-c,116b] sulfonation,[117] acylation[116c] and formylation[118] reactions on ligands of cyclometalated complexes of Ru, Os, Rh, Ir, Pd and Pt have have been accomplished under mild conditions, where the M–C_{ipso} bond have been shown to be kinetically inert (Scheme 1.68). Interestingly, ligand dimerisation reactions and halogenation of cycloruthenated complexes have been shown to occur by a radical pathway, in which an aryl radical is induced by oxidation of the metal centre to Ru(III).[113e]

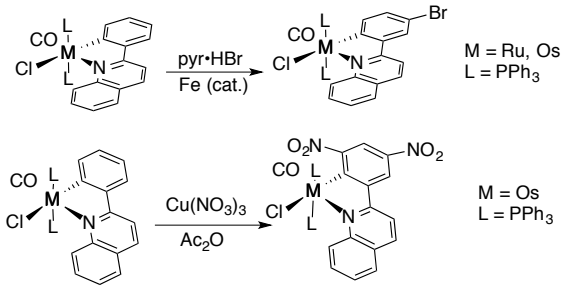

Scheme 1.68. Examples of *para*- and- *ortho* bromination/nitration with cyclometalated Ru/Os complexes.[114c]

Almost two decades have passed since Frost and co-workers discovered the first catalytic *meta* C–H transformation.[108a] Arising from unexpected results, the selective catalytic *meta*-sulfonation of 2-phenylpyridine was found to occur in the presence of dichloro(*p*-cymene)Ru(II) dimer, K_2CO_3 base upon reaction with sulfonyl chlorides in MeCN solvent (Scheme 1.69, equation *a*). No reaction occurred in the absence of the catalyst, and no products arising from *ortho* or *para* positions were observed. Additional experiments showed that the reaction tolerates electron withdrawing or donating groups on the sulfonyl chlorides and substituents in position 4 on the phenyl ring of the 2-phenylpyridine. In order to provide a better understanding of the mechanism, a plausible intermediate of the process (*ortho*-ruthenated phenylpyridine, **8**) was isolated through an alternative pathway. The complex was submitted to the reaction conditions observing quantitative conversion towards the *meta* adduct (Scheme 1.69, equation *b*). Complex **8** was also employed as catalyst to determine if demetalation, which is essential for the catalyst turnover, was taking place under reaction conditions, and indeed, the *meta*-sulfonation product was isolated (Scheme 1.69, equation *c*).

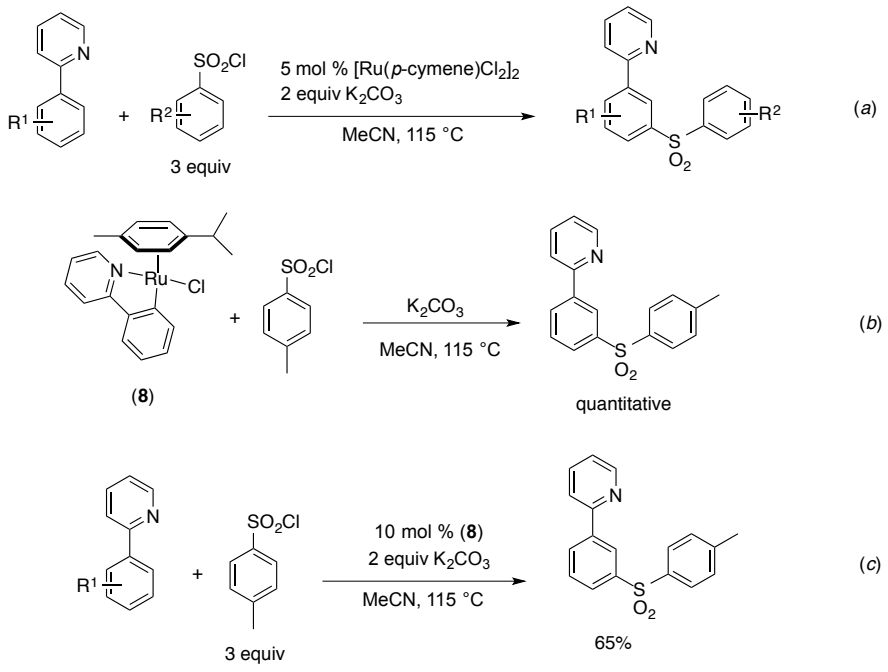

Scheme 1.69. Ru-catalysed *meta*-sulfonation of 2-arylpyridine derivatives.

Although only speculation can be made, it is likely that Ackermann *et al*. produced but may not have noticed, *meta*-alkylation of 2-PhPy with secondary alkyl bromides in 2009.[119] Four years later, Hofmann and Ackermann described the *meta*-selective C–H bond alkylation of 2-phenyl-pyridines, azole-substituted arenes, and pyrimidine derivatives with secondary alkyl bromides (Scheme 1.70, equations *a*). Ruthenium(II) carboxylate complexes were essential for promoting the direct alkylation. The catalyst can be generated *in situ* from [Ru(*p*-cymene)Cl_2]$_2$ and a carboxylate, with 2,4,6-trimethylbenzoate ($MesCO_2H$) proving to be particularly active. Substituents at C3' and C4' of the 2-phenylpyridine were well tolerated, thus yielding the functionalised products in moderate to good yields. However, C2'-substituted substrates led to a mixture of the two possible *meta* regioisomers derived from the attack at the *ortho* and *para* positions with respect to the metalation site (Scheme 1.70, equations *b*). Interestingly, whereas secondary alkyl bromides afford complete *meta* selectivity, primary substrates lead exclusively to the *ortho*-alkylated product.[119] This selectivity was further demonstrated by reaction of 2-phenylpyridine with an equimolecular

mixture of secondary and primary alkylbromides, which showed complete chemoselectivity (Scheme 1.70, equations *c*).

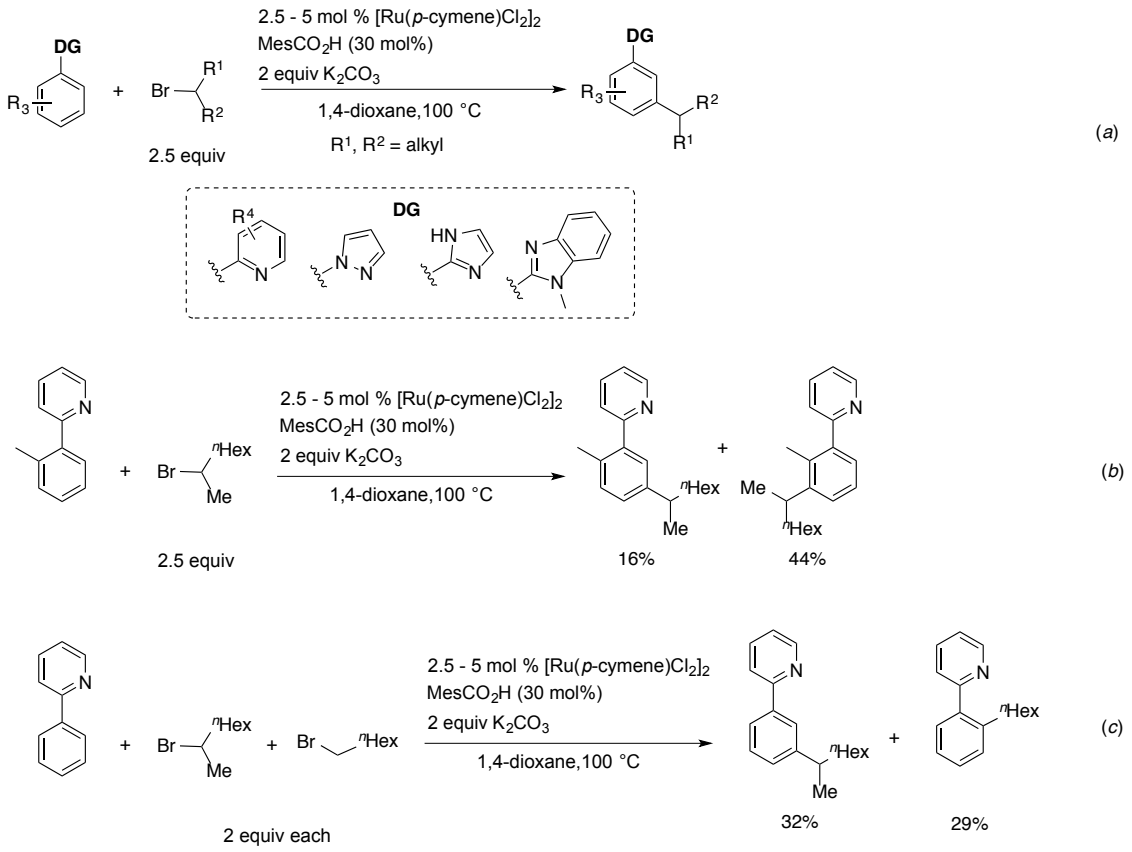

Scheme 1.70. Ru-catalysed *meta*-alkylation of 2-arylpyridine derivatives with secondary alkylbromides.

Intermolecular competition experiments for the *meta*-alkylation of 4'-methoxy-2-phenylpyridine and 4'-fluoro-2-phenylpyridine with 2-bromooctane showed the former to react 2.6 times faster, and is suggestive of an S_EAr. Also consistent with an S_EAr, the authors report a KIE of 1.0 for the *meta* C–H bond in 2-(3,4,5-trideuterophenyl)pyridine. Although most of the experimental evidence points towards an S_EAr pathway, TEMPO is reported to negatively affect the alkylation reaction, thus a radical mechanism cannot be completely ruled out.

Very recently, Frost and co-workers reported a similar method for the Ru-catalysed alkylation of 2-arylpyridines derivatives with tertiary alkyl bromides (Scheme 1.71, equation *a*). Electron-withdrawing or donating substituents at C4' of the 2-phenylpyridine are well tolerated. Instead substituents at C2' and C3' positions did not provide the target *meta*-alkylated adduct, but the C2'–C2' homocoupled 2-phenylpyridine (Scheme 1.71, equations *b*). A related reactivity was previously observed in Ru(II)-catalysed *ortho*-arylation when bulky *ortho*-substituted aryl halides promoted homocoupling of the arene rather than cross-coupling with the electrophile.[120] Interestingly, when ethyl 2-bromoisobutrate (**9**) was used as the electrophile, alkylated products **10** and **11** were formed. The authors suggested that the formation of **11** is consistent with a radical conjugate polymerisation. If traces of the elimination product of **9** are formed, a tertiary carbon centred radical species can add onto it and the resulting radical species can enter in the alkylation catalytic cycle, forming **11** (Scheme 1.71, equations *c*). Moreover, oxygen and TEMPO proved to be detrimental to the reaction.

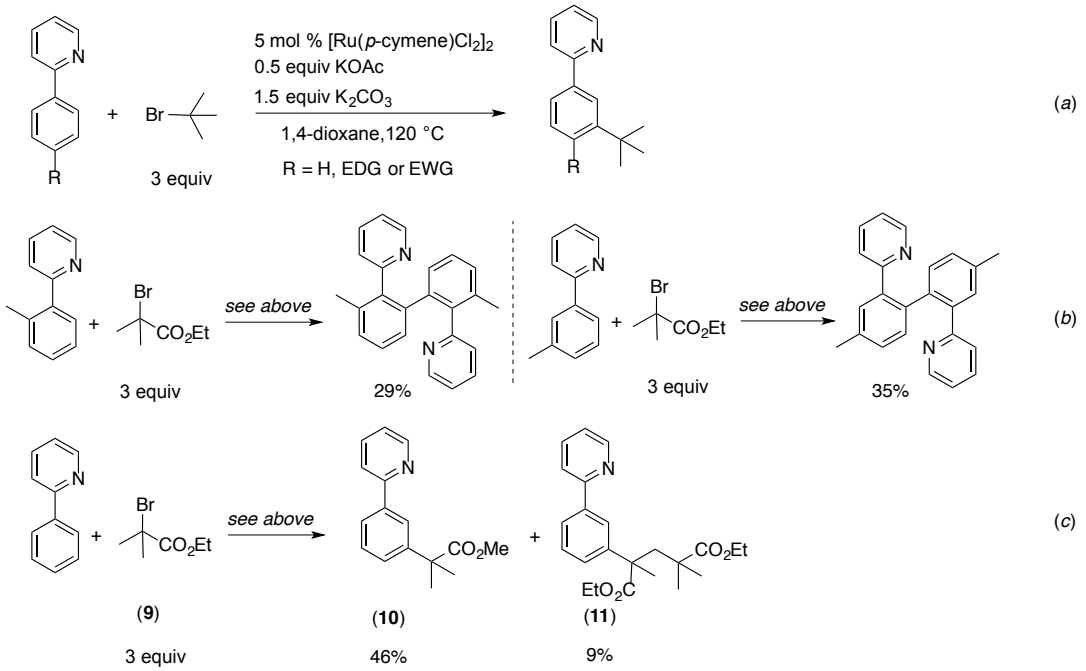

Scheme 1.71. Frost's *meta*-alkylation of 2-arylpyridine derivatives with tertiary alkylbromides

In view of this evidence the authors proposed a radical mechanism. Initial *ortho*-metalation generates cyclometalated species **LXXXIII**. A single electron transfer from a Ru(II) species to the electrophile, generates a tertiary alkyl radical (**LXXXIV**) and the corresponding Ru(III)X compound (**LXXXV**). Radical addition of the alkyl radical **LXXXIV** at position *para* to the metalation site of complex **LXXXIII**, forms the cyclohexadienyl radical intermediate **LXXXVI**. Rearomatisation of the latter *via* single-electron oxidation from **LXXXV** followed by consequent deprotonation, and protodemetalation frees the biaryl closing the cycle (Scheme 1.72).

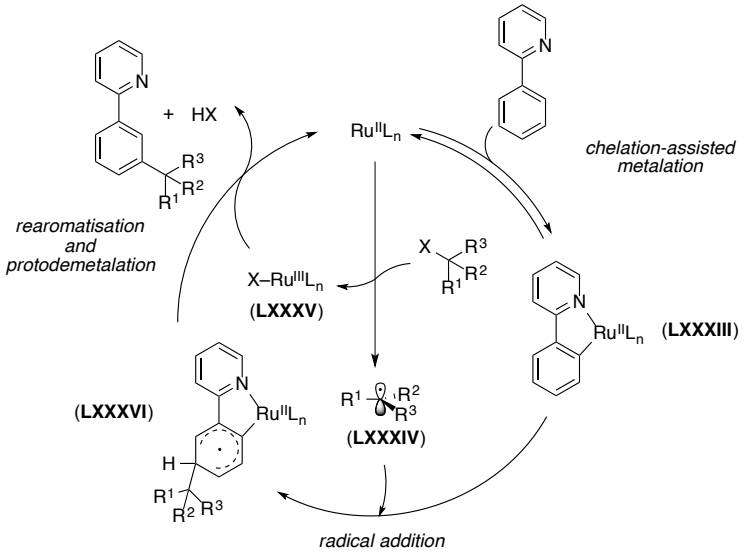

Scheme 1.72. Frost's proposed mechanism for the Ru-catalysed *meta*-alkylation.

Soon after this report by Frost, Ackermann *et. al.* described a related methodology for the Ru(II)-catalysed *meta*-alkylation of aniline-protected with a removable directing group and for pyridyl-, pyrimydyl- and pyrazolyl-substituted arenes. The catalytic activity of the system derived from the use of the MPAA-ligand, which enabled the functionalisation to take place. The alkylation does not occur in the absence of MPPA-ligand and more conventional carboxylate-type additive resulted to be less active. Substituents at the *para* position are compatible with the system, instead only few examples of *ortho*- and *meta*-

substituted arenes were reported, probably due to the formation of homocoupling of the arene as seen in Frost's case (Scheme 1.73).[109b]

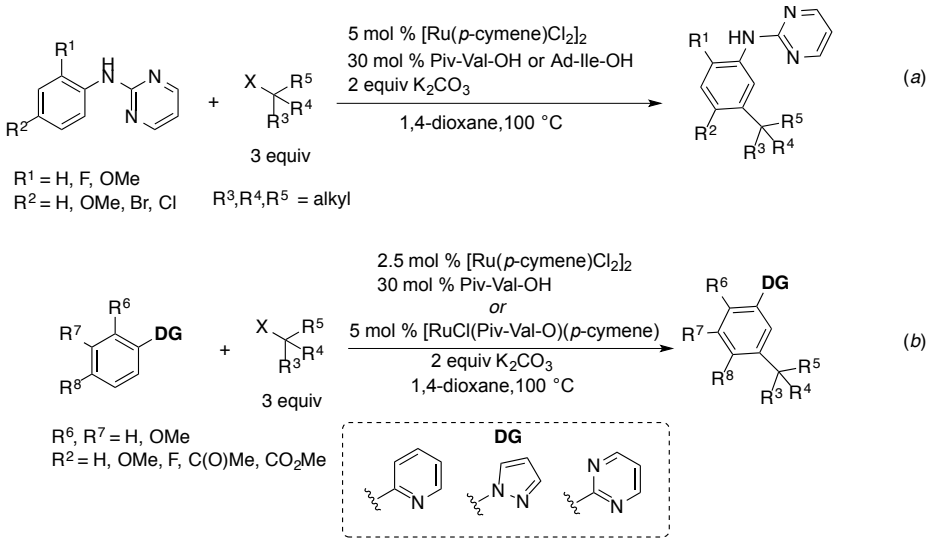

Scheme 1.73. Ackermann's *meta*-alkylation of DG-containing arenes with tertiary alkylbromides.

Counter to what has been reported for the *meta*-alkylation with secondary alkybromides,[109a] competition experiments of C4'-substituited 2-PhPy revealed that more electron-poor substrates are more reactive in the system. Other intermolecular competition reactions disclosed that tertiary alkyl bromides react faster than secondary ones. Deuterium labelling scrambling experiments showed that the *ortho*-C–H activation is reversible, instead the addition of the alkyl group at position *meta* is instead irreversible. Interestingly, when [D_9]-*tert*-butyl bromide was used as the only source of D atoms, deuterium incorporation at position *ortho,* where the metalation occurs, was noticed. This experiment reveals that the organic electrophile does not act only as alkylating agent, but also as proton source for the protodemetalation step. KIE experiments aimed to understand the kinetic relevance of the breaking of *meta*-C–H bond were also investigated. The KIE measured by initial rates was 1.6, whereas 1.4 was calculated for an intermolecular completion reaction. These results indicate that the cleavage of the *meta*-C–H bond is kinetically relevant. When the well-defined cycloruthenated complex **12** was used as catalyst, it proved to be catalytically

inactive unless the MPAA-ligand was added (Scheme 1.74, equation *a*). Moreover, ^{t}BuBr was claimed to be indispensable when complex **13** was subjected to a stoichiometric protodemetalation reaction. However, the control experiment without ^{t}BuBr was not shown.

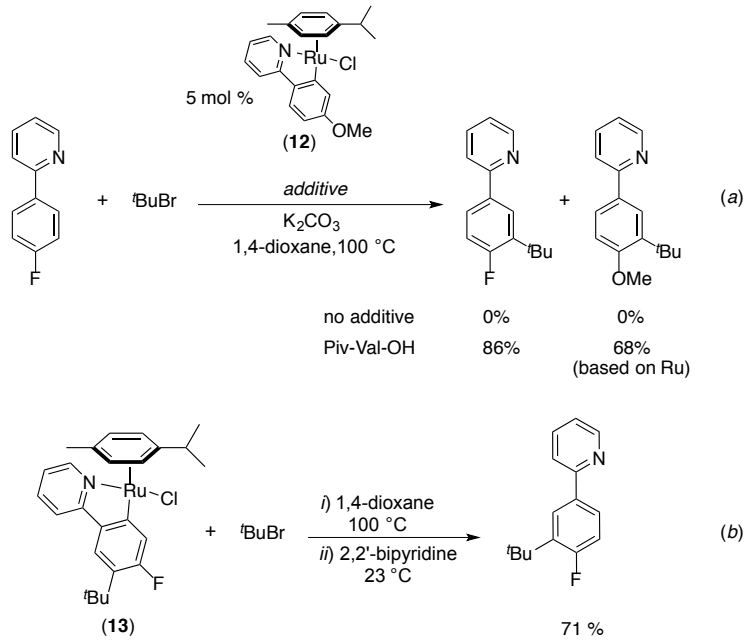

Scheme 1.74. Reactions with cyclometalated Ru(II) complexes.

Experiments aimed to understand the activation mode of C–Br bond were also conducted. An independently prepared alkylpyridium salt was tested as coupling partner under standard conditions (Scheme 1.75, equation *a*). No coupling product was observed ruling out the *in situ* formation of a similar electrophile. Also, methylencyclohexane did not afford any product, which renders a β-elimination followed by hydroarylation unlikely (Scheme 1.75, equation *b*). When well-defined *cis*- and *trans*-1-bromo-4-phenylcyclohexanes were utilised as coupling partner in independent alkylation reactions, both delivered the same diastereoisomeric product mixture, which suggests a homolytic C–Br cleavage (Scheme 1.75, equation *c* and *d*). Lastly, an experiment with a radical clock confirmed the radical nature of the process (Scheme 1.75, equation *e*).

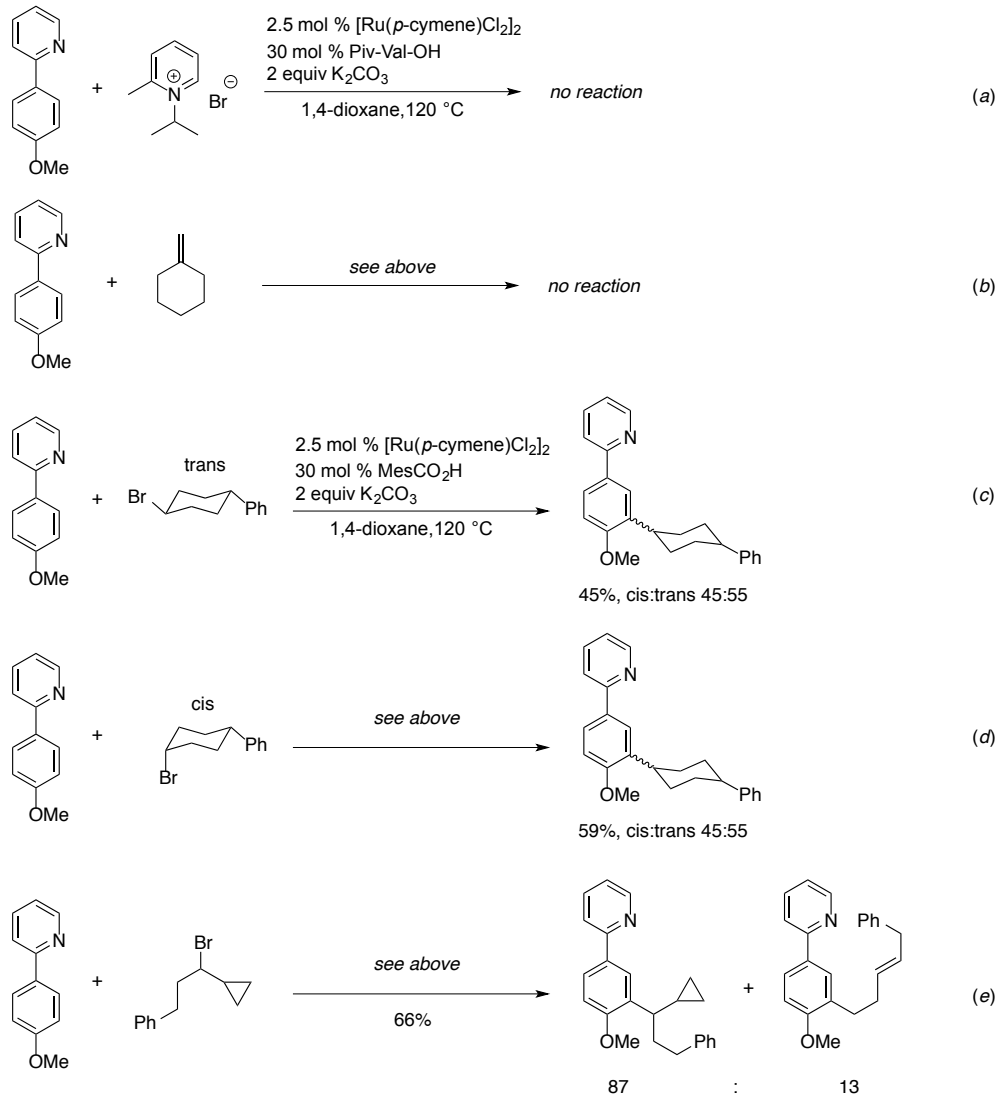

Scheme 1.75. Investigation on the *meta*-C–C formation.

The authors reported a kinetic investigation of the *meta*-alkylation, proposing a second-order dependence on the concentration of the ruthenium catalyst. However, analysis of the data reported in the paper seems to be instead consistent with a first order-dependence in the catalyst. Nevertheless, the proposed catalytic cycle resembles the one suggested by Frost.[108b] Reversible C–H activation by Ru(II)-MPAA complex (**LXXXVII**) forms the cyclometalated intermediate **LXXXVIII**. SET activation of the alkyl halide and subsequent radical addition generates complex **LXXXIX**. Rearomatisation promoted by the Ru(III)X species with

consequent hydrogen abstraction leads to intermediate **XC**. Finally, protodemetalation with an additional molecule of the alkyl halide liberates the product, regenerating **LXXXVII** (Scheme 1.76).

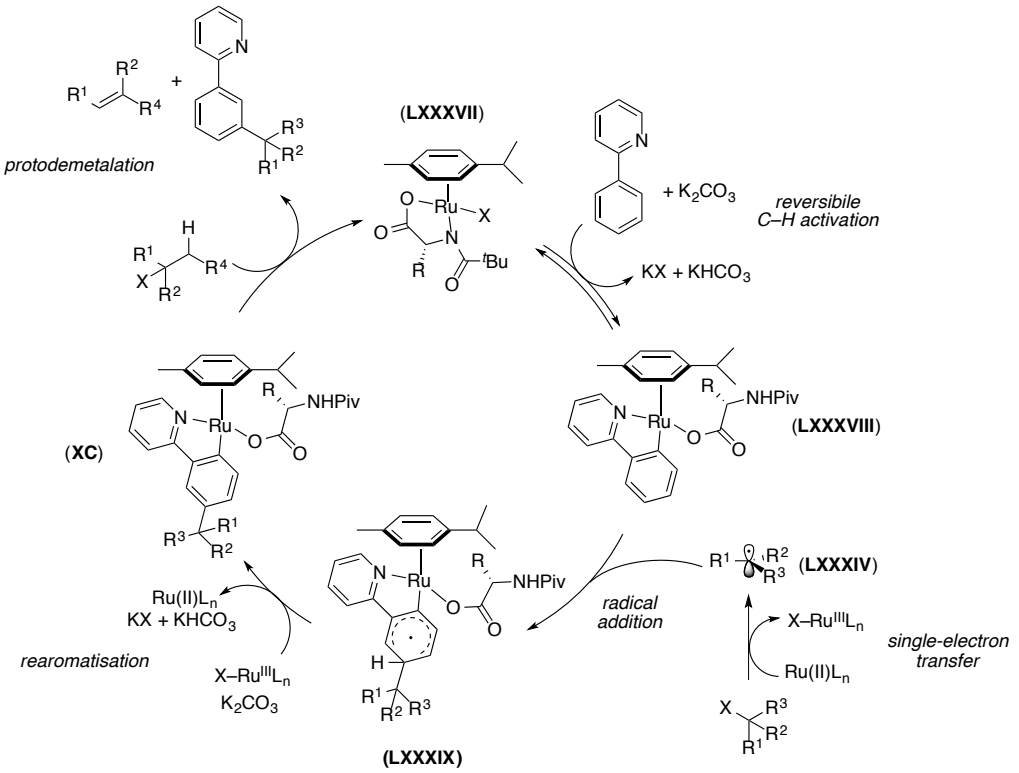

Scheme 1.76. Ackermann's proposed mechanism for the Ru-catalysed *meta*-alkylation.

The Greaney group, using a similar approach, developed a Ru(II)-catalysed direct C–H bromination of 2-arylpyridinine derivatives. Dichloro(*p*-cymene)Ru(II) dimer catalyst precursor, $MesCO_2H$ additive, tetrabutylammonium tribromide (TBATB) as the bromine source, K_2CO_3 base in dioxane solvent were found to be the optimal conditions for the process. As seen in Frost's *meta*-alkylation, only substituent at C4' of the 2-PhPy were compatible with the system (Scheme 1.77, equation *a*). Moreover, by combining the Ru-catalysed *meta*-bromination with Pd-catalysed Suzuki and Heck couplings in a one-pot fashion, the authors developed an overall *meta*-alkenylation and arylation protocol of 2-phenylpyridine analogues (Scheme 1.77, equation *b* and *c*).[110]

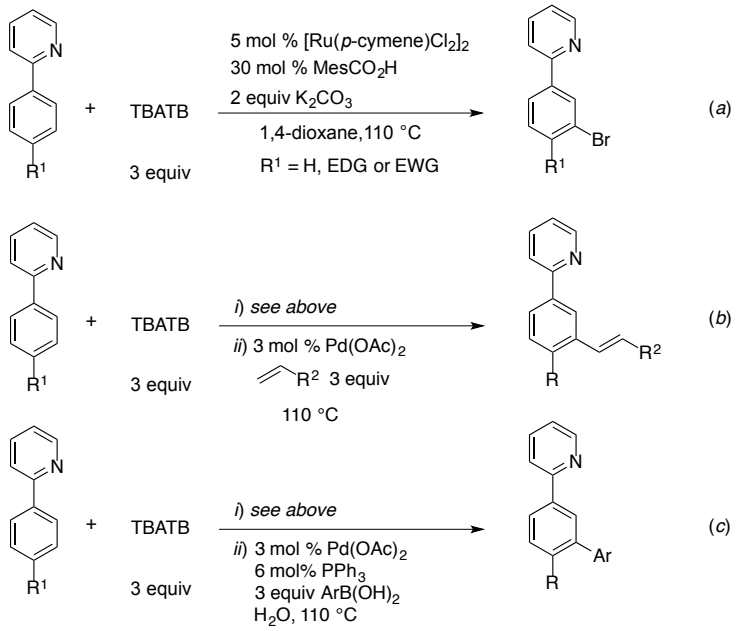

Scheme 1.77. Ru-catalysed *meta*-bromination and one-pot Pd-catalysed alkenylation and arylation.

A few months later, Huang and co-workers reported an analogous methodology for the *meta*-bromination of arenes bearing pyridyl, pyriminidyl or pyrazolyl directing groups. Interestingly, the reaction conditions developed by the authors are different compared the other *meta*-functionalisation. In fact, only ruthenium catalysts, NBS brominating agent and DMA solvent, in absence of any other additives, were found to be the optimal reaction conditions. Although the screening of various Ru catalysts revealed that several Ru(II) and Ru(III) complexes with different ligand environment were able to promote the bromination, $[Ru(p\text{-cymene})Cl_2]_2$ was found to be most effective (Scheme 1.78).[111]

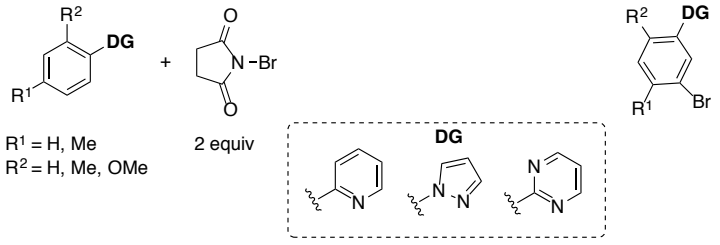

Scheme 1.78. Huang's *meta*-bromination of DG-containing arenes with NBS.

Similarly to Greany *et al*., the authors combined the *meta*-brominated adduct in Pd-catalysed coupling reactions with various coupling partners. Additionally, the method was applied in the synthesis of the anti-cancer drug Vismodegib (Scheme 1.79).

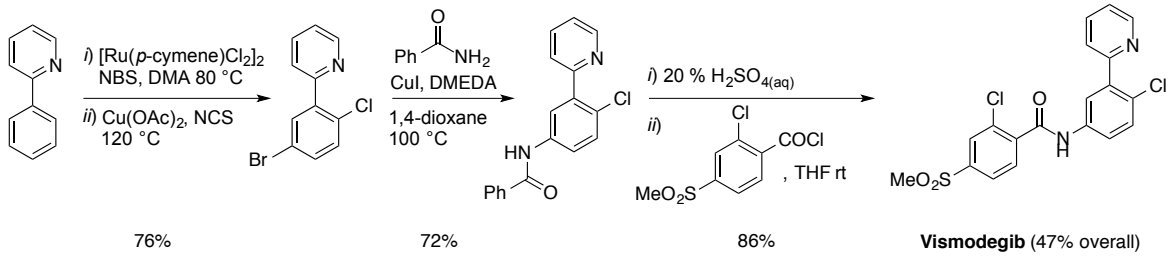

Scheme 1.79. Synthesis of Vismodegib.

H/D scrambling experiments might indicate a different C–H activation mode respect to the others Ru-catalysed *meta*-functionalisations. When 2-PhPy **14** with 92% of D at C2'/C2" positions was subjected to standard reaction conditions, no H incorporation at C2'/C2" was detected in product **15** (Scheme 1.80, equation *a*). This indicates that no D/H exchange occurs between positions C2' and C3'. Instead cross-over experiments in the absence of NBS between **16** and **17** displayed that D/H scrambling at position C2' happens (Scheme 1.80, equation *b*). This result led the authors to suggest that a di(hydride) Ru(IV) species like **19**, arising from reaction of a putative cyclometalated Ru(II)-H complex **18** with **17**, might be involved in the process (Scheme 1.80, equation *b-1*). Alternatively, transmetalation between cyloruthenated intermediates **18** and **20** followed by cross-reductive elimination would provide an alternative explanation (Scheme 1.80, equation *b-2*). Intermolecular KIE at C2' was evaluated to be 1.43, instead at C3' position was 1.56 indicating that both metalation and C–Br bond formation/rearomatisation are kinetically relevant in the process.

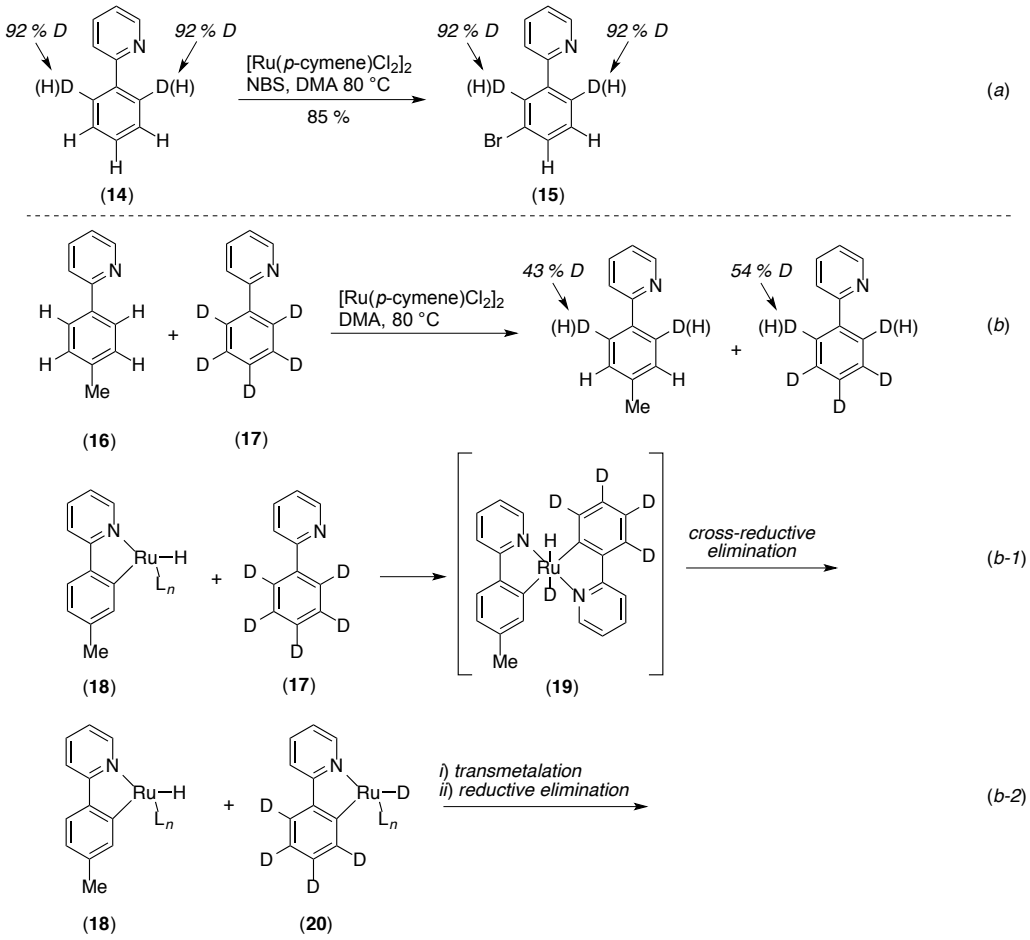

Scheme 1.80. H/D exchange experiments reported by Huang and co-workers.

Intriguingly, when the cyclometalated complex **8** was subjected to a stoichiometric bromination reaction only trace of product were observed (Scheme 1.81, equation *a*). Contrary to what Frost[108] and Ackermann[109] reported, this result indicates that an intermediate like **8** is not part of the catalytic cycle. Instead, complex **8** is a suitable catalyst precursor implying that the active species is being generated *in situ* with an excess of 2-PhPy (Scheme 1.81, equation *b*). On the other hand, $[Ru(p\text{-cymene})Cl_2]_2$ forms nanoparticles when heated a 135 °C in DMF,[121] thus a heterogeneous system cannot be ruled out.

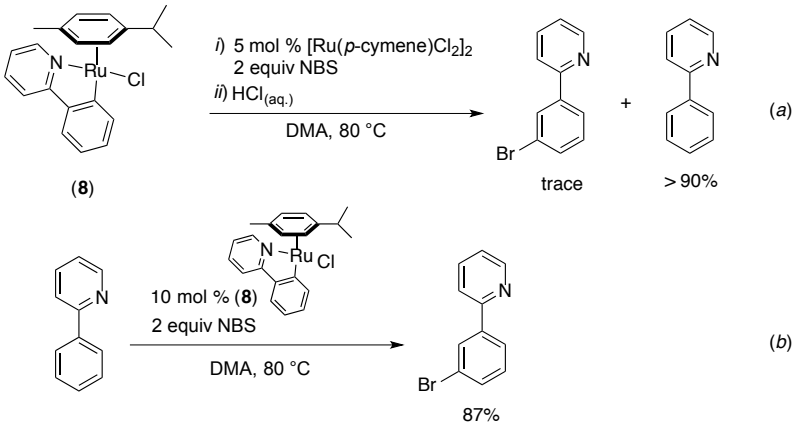

Scheme 1.81. Experiments using the well-defined cyclometalated Ru(II) complex **8**.

1.4.3. Steric-controlled C–H functionalisation methods

In 2007, Sanford and Hull reported Pd-catalysed oxidative C–H cross coupling of benzo[*h*]quinoline (Bzq) with simple arenes in the presence of Ag_2CO_3, 1,4-benzoquinone (BQ), and DMSO.[64c] The reaction proceeded with high levels of chemoselectivity despite the possibility for competing homo-dimerisation of substrates. In fact, the C–H activation of non-coordinating arenes proceeded under steric control. Mono-substituted arenes gave mixtures of *meta*- and *para*- coupling products, instead regioselective cross coupling was observed with symmetrical 1,2- and 1,3-disubstituted arenes. However, the cross coupling using 1,4-disubstituted benzene derivatives led to a lower yield, possibly due to the steric hindrance of the substituents. The proposed reaction pathway included: chelation-assisted cyclometallation of Bzq at Pd(II) centre to form **XCI**, 1,4-BQ coordinated with cyclometallated Pd(II), promoting the direct C–H activation of the non-coordinating arene affording **XCII**. Reductive elimination frees the cross-coupled product and Pd(0). Finally, re-oxidation of Pd(0) by Ag(I) re-establishes the original Pd(II) species (Scheme 1.82).

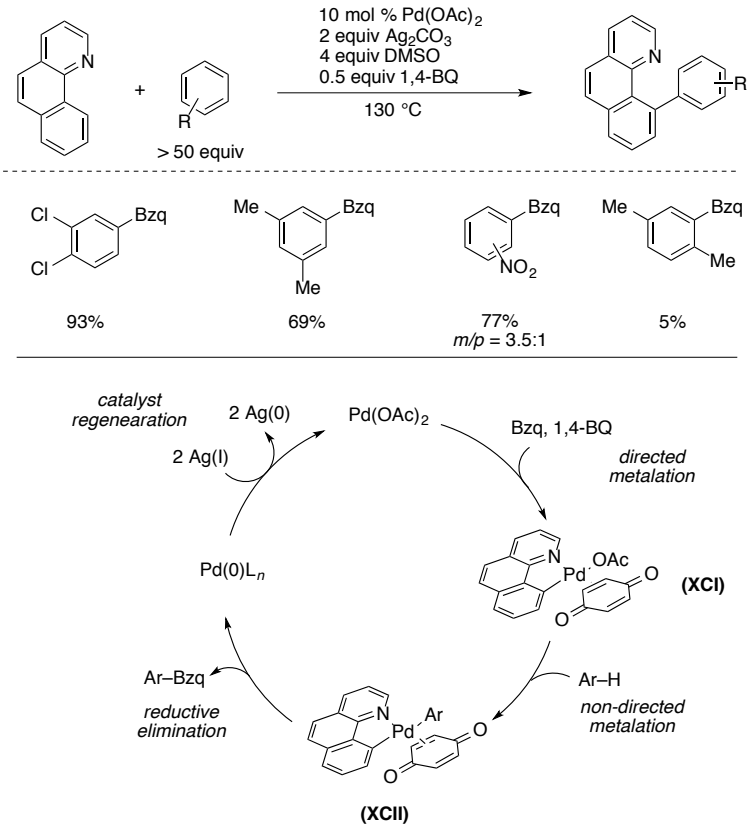

Scheme 1.82. Regioselectivy cross-coupling between benzo[*h*]quinolone and simple arenes.

Organoboron and organosilicon reagents are valuable intermediates for several organic transformations, consequently methodology for C–H silylation[122] and borylation[123] of simple arenes are particularly attractive.[124] Rhodium and Iridium catalysts have proved to be the most active, although more recently Ni,[125] Fe,[126] Co[127] and Pt[128] catalysts provided robust alternatives. The regioselectivity of these methods is predictable based on steric factors, where the least sterically hindered positions are the ones preferentially functionalised.[129]

In 2002, Smith and co-workers reported a selective and convenient method for the borylation of simple arenes using (Ind)Ir(cod) precatalyst, 1,2-bis(diphenylphosphino)ethane (dppe) ligand, pinacolborane (HBPin) borylating agents in cyclohexane solvents. 1,3- and 1,2-disubstituited benzene derivatives were selectively borylated at *meta* position, whereas monosubstituted arenes led to statistical mixture of *meta*- and *ortho*- borylated adducts (Scheme 1.83, equation *a*). The synthetic utility was shown by the one-pot C–H borylation

followed by palladium-catalysed Suzuki-Miyaura cross-coupling with 3-bromotoluene coupling partner (Scheme 1.83, equation *b*).[123d]

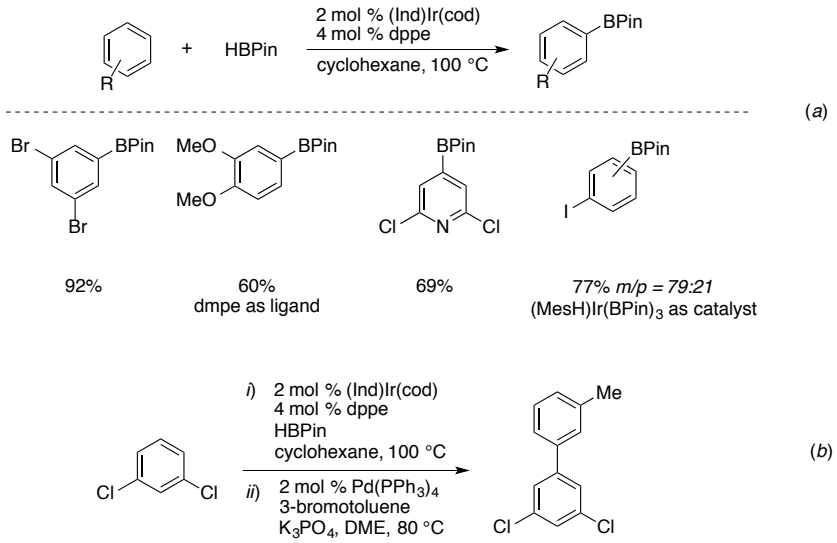

Scheme 1.83. Smith's iridium-catalysed borylation of arenes.

These initial reports on Ir-catalysed C–H borylation,[123a,c,d] led the development of a series of studies by the group of Hartwig, Ishiyama, and Miyaura where $[IrOMe(cod)]_2$ was identified as the optimal precatalyst for this transformation when used in combination with 4,4'-di-*tert*-butyl-2,2'-bipyridine (dtby) ligand.

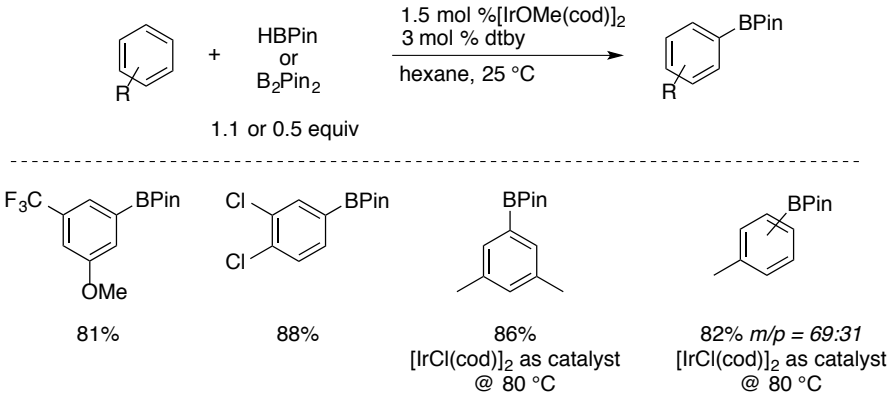

Scheme 1.84. Hartwig, Ishiyama, and Miyaura direct C–H borylation.

The catalytic system Ir/dtby allowed the borylation of a wide range of electron-rich and electron-deficient arenes with high yields without using an excess of the arene at room temperature.[123e-g] Detailed mechanistic studies identified the *in situ* formation of triborylated Ir(III) complex **22** after coe (cyclooctene) ligand dissociation from **21**. The tris(boryl)iridium intermediate **22** performs C–H activation on the arene *via* oxidative addition forming the Ir(V) intermediate **XCIII**, which, after reductive elimination, frees the borylated product generating the Ir(III)–H species **23**. The latter undergoes transmetalation with B_2Pin_2 restoring the active Ir(III) intermediate **22** (Scheme 1.85).[123e,h,i]

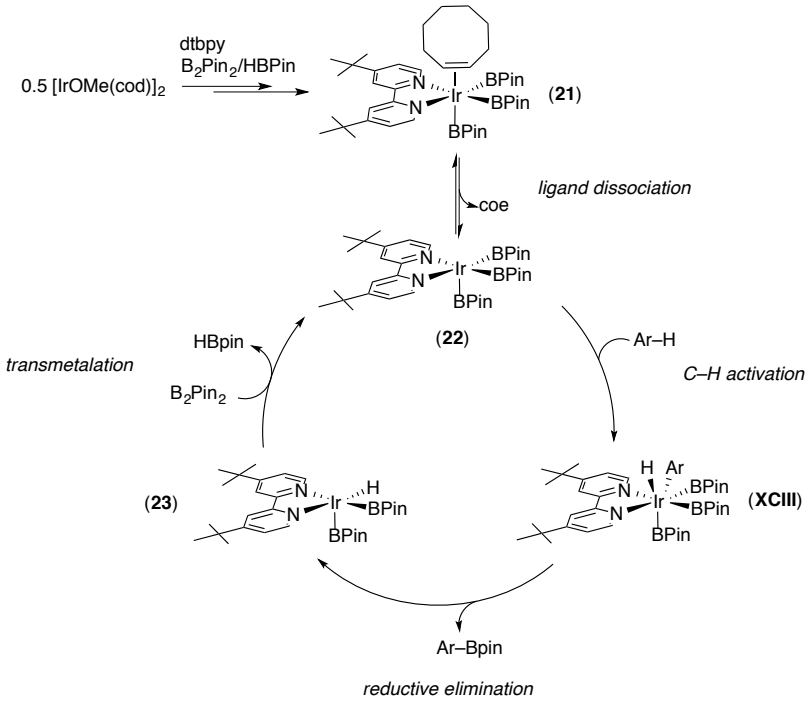

Scheme 1.85. Mechanism of the Ir-catalysed direct C–H borylation of arenes.

Although the Ir/Rh direct C–H silylation/borylation of arenes without directing groups represents the state-of-the-art of the field; the level of selectivity of monosubstituted arenes is poor since a statistical distribution of *meta*- and *para*- isomers is usually yielded. Also non-symmetrical 1,2-disubstituited arenes suffers of scarce selectivity. Recently the groups of Hartwig and Itami were able to increase the selectivity towards the *para* position by using

bulky bidentate phosphine as ligands, namely for the Rh-catalysed silylation[122g,h] and Ir-catalysed borylation.[123l] Hartwig's *para*-selective silylation relies on the use of $[Rh(coe)OH]_2$ precatalyst with ligands **24** or **25** where the intermediate **XCIV** performs the C–H activation on the arene (Scheme 1.86, *top a*). Instead, Itami's *para*-selective borylation utilises $[Ir(cod)OH]_2$ precatalyst with ligands **26** where the Ir(III) species **27** performs the C–H activation on the arene (Scheme 1.86, *bottom b*).

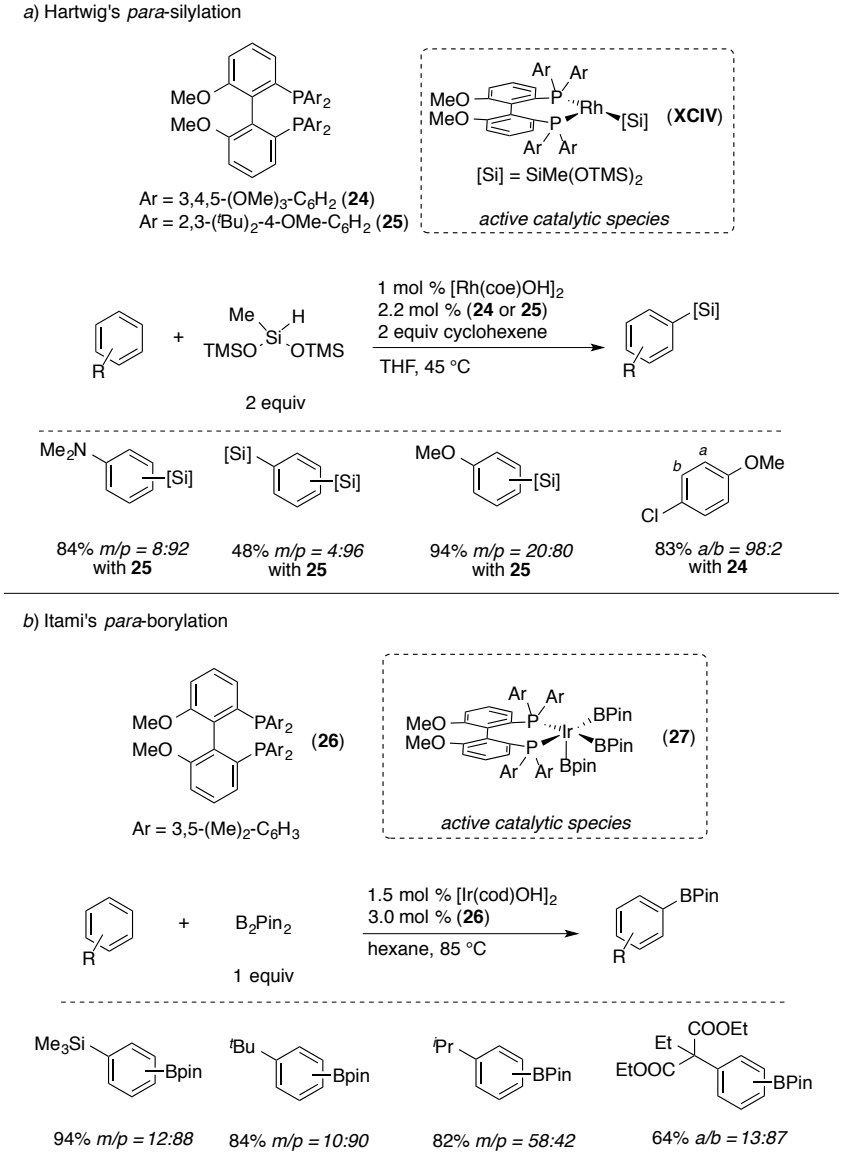

Scheme 1.86. Hartwig's *para*-selective silylation and Itami's *para*-selective borylation

1.4.4. Ligand-substrate interaction C–H functionalisation method

Kuninobu and Kanai drastically increased the level of *meta*-selectivity in direct C–H borylation of arenes by introducing a secondary interaction between ligand and substrate. More specifically, an iridium catalyst gets directed into close proximity of the *meta*-C–H bond by hydrogen bonding between a carbonyl group in the substrate (H–bond acceptor) and a *N,N*'-disubstituted urea ligand (H–bond donor). In other words, the hydrogen-bonding donor site of the ligand recognises the hydrogen-bonding acceptor site of the substrate and orients the *meta*-C–H bond of the substrates to the catalytic site (Figure 1.6).[130] This strategy for inducing selectivity in C–H functionalisation represents a breakthrough because only catalytic amount of a ligand, which serves as a directing group, is required.

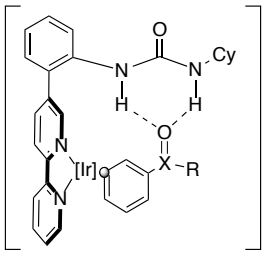

Figure 1.6. Secondary interaction between ligand and substrate.

The concept was successfully applied for the C–H borylation of aromatic amides, esters, phosphonates, phosphonic diamide and phosphine oxides. The level of *meta*-selectivity was greatly enhanced when ligand **28** was used in place of the classical dtpy in combination of $[Ir(cod)OMe]_2$ precatalyst and *p*-xylene solvent (Scheme 1.87).

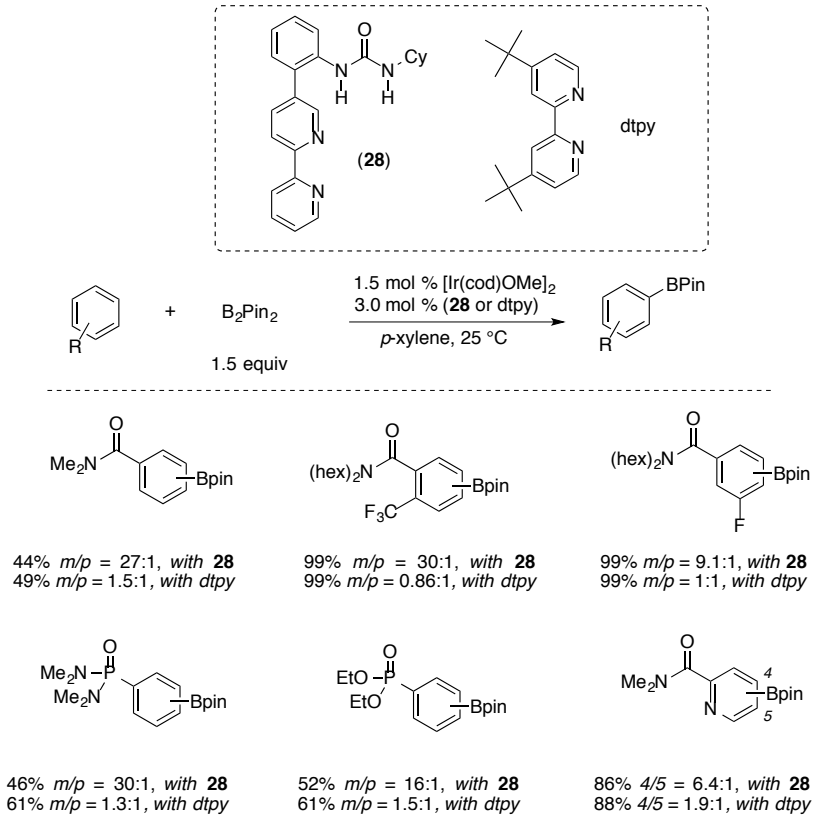

Scheme 1.87. *meta*-Selective borylation *via* ligand-substrate interaction.

1.5. Conclusion

Metal-catalysed C–H activation has emerged as a promising route toward the formation of a specific aryl-aryl bond and has maturated into a progressively viable alternative to traditional cross-coupling reactions as a most elegant, cost-effective, and environmentally friendly approach to functionalise benzene derivatives. Indeed, methods for direct arylation with aryl (pseudo)halides and for oxidative direct arylation with either organometallic reagents or simple arenes have been reported.

Although major progress has been made in developing new methods for enhancing reactivity and selectivity in C–H functionalisation, the installation of a directing group, capable of precoordinating the catalyst nearby the activating C–H bond, still remains the most reliable approach. However, the directing group is seldom a necessity after the C–H functionalisation event and may have to be removed decreasing the overall atom economy of the method. Moreover, the activation of simple arenes represents a significant challenge. In these cases, a large stoichiometric excesses of the arene is needed. The efficiency and site-selectivity of the C–H functionalisation is mainly governed by the electronic and steric profile of the arene and poor levels of selectivity are often encountered. The development of more general methods for *meta* or *para* regioselective C–H arylation would greatly expand the scope of this new C–C bond forming reactions.

For these reasons C–H activation cannot yet compete with traditional cross-coupling reactions, which have shown to be highly reliable and practical. In this context, a number of major challenges must still be overcome before these reactions find broad applicability. For example, reducing the catalyst loading, reactions temperatures and time, and employing cheap electrophiles such as aryl chlorides, would make these methodologies more appealing to the chemical industries. Also, the development of highly efficient catalytic systems that use air as the sole oxidant rather then co-oxidants such as copper(II) or silver(I) salts, from the view of atom economy and overall cost, would be ideal.

Chapter 2. Ruthenium-Catalysed Direct C–H Arylation of Fluoroarenes with Aryl Halides

2.0. Collaboration and acknowledgments

The work described in this chapter was also made possible thanks to the help of:

1) Gregory J. P. Perry, who has been collaborating during the isolation and characterisation of the biaryl compounds;
2) Dr. Xacobe C. Cambeiro, who performed and wrote the theoretical computational part;
3) Dr. Francisco Juliá-Hernández, who actively contributed in the initial stage of the project;
4) Jude N. Arokianathar, who, under my supervision, started investigating the stoichiometric C–H activation of perfluoroarenes with $Ru(OPiv)_2$(*p*-cymene) complex during his master project.

2.1. Introduction

As discussed in Chapter 1, the development of new chemical transformations based on metal-catalysed C–H activation has been shown to considerably simplify the synthesis of organic molecules.[7] Among all the transition metals, palladium is definitely leading the field, however ruthenium chemistry, which has lagged behind palladium's by almost a quarter of a century, is growing exponentially and it is revealing itself to be a valid and cheaper alternative.[7g,74]

Despite the natural abundance of ruthenium ($1.0 \cdot 10^{-3}$ ppm) being fifteen times lower than that of palladium ($1.5 \cdot 10^{-2}$ ppm),[131] the difference in price between these two metals does not reflect their relative availabilities. As reported in Graph 2.1, ruthenium is considerably cheaper than palladium.[132] However, as price reflects the real balance between demand and offer, the palladium market is over ten times higher than that of ruthenium (Graph 2.2)[132] and this factor inevitably contributes to its actual cost. More specifically, palladium is widely employed in the manufacturing of catalytic converters for automobiles, while ruthenium sees its main applications in the electrical sector (Graph 2.3).[132]

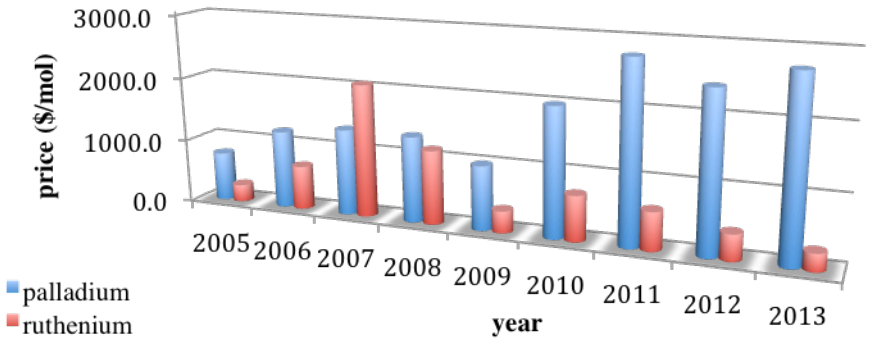

Graph 2.1. Average price for Pd and Ru ($/mol) from 2005 to 2013.

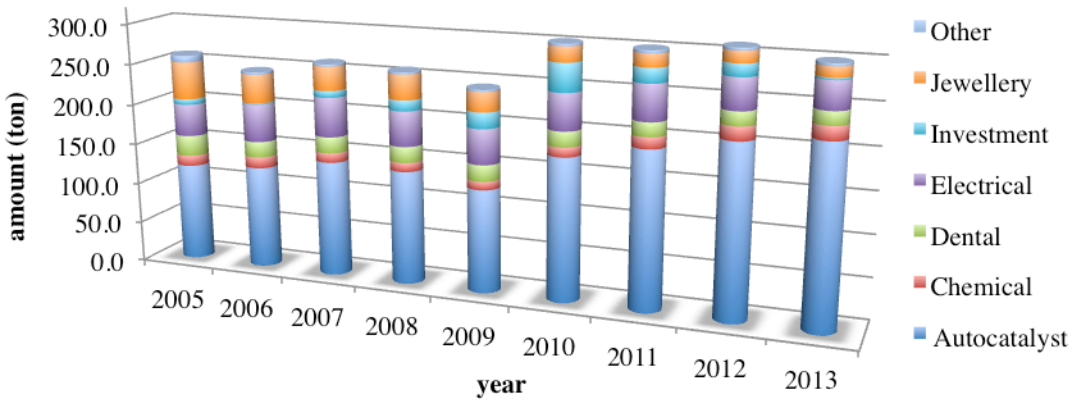

Graph 2.2. Palladium global demand from 2005 to 2013.

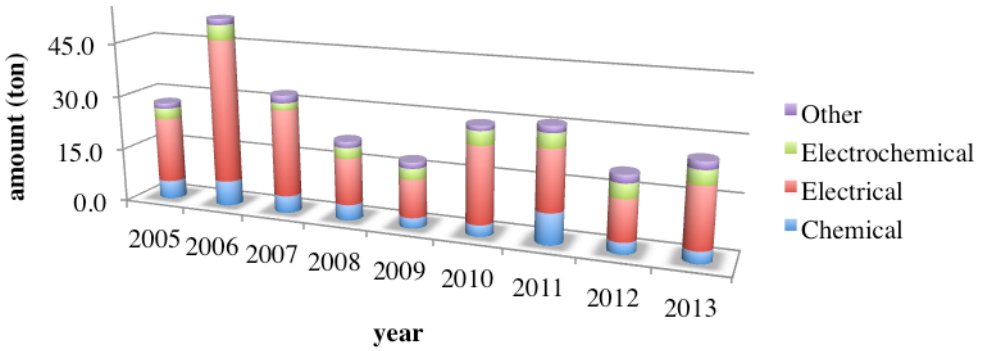

Graph 2.3. Ruthenium global demand from 2005 to 2013.

A closer inspection of their respective demands in the chemical industry (Graph 2.4) might partially explain the higher price of palladium.[132] The scarcity of ruthenium-promoted chemical transformations is perhaps a consequence of the lack of generality and predictability of its behaviour, compared to that exhibited by palladium catalysis. In this context, the work in this chapter seeks to partially fill the gap in this knowledge of ruthenium coordination chemistry. Efforts towards the understanding of the foremost and basic mechanistic factors driving new chemical transformations triggered by ruthenium, along with its relatively lower price compared to palladium, would provide the chemical industry with a viable transition metal alternative.

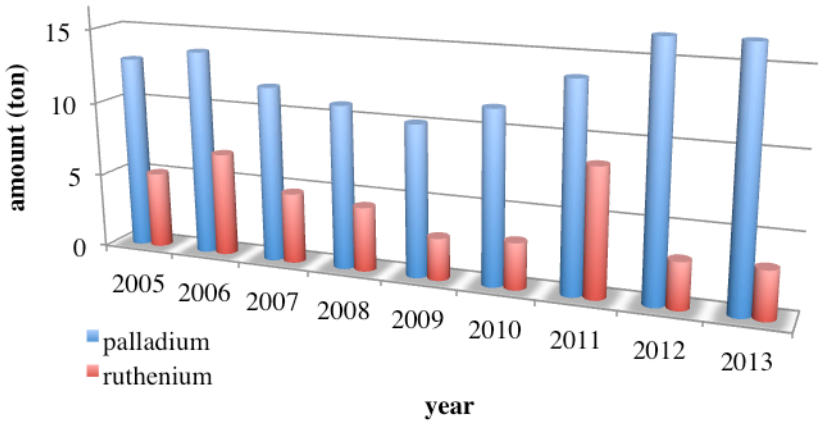

Graph 2.4. Ru *Vs* Pd global demand for chemical purposes from 2005 to 2013.

2.2. Ru-catalysed C_{Ar}–H functionalisation

Notwithstanding the tremendous progresses in Ru-catalysed C_{Ar}–H functionalisation, the majority of the reported methods are based on chelate-assisted metalation of the substrate (see section 1.4.2.1.2).[7g,74b] Directing groups have consistently been required for the functionalisation of arenes by ruthenium, ever since Lewis and Smith reported the first Ru-catalysed C–C bond formation in 1986.[75] Murai, Chatani, Kakiuchi *et al*., initiated the use of ruthenium(0) catalyst precursors, showing the utility of *ortho*-ruthenated species as catalytic intermediates for hydroalkylation and hydroalkenylation,[76] silylation,[133] and arylation with aryl boronic esters.[77] More recently, significant progress has been made considering the direct arylation of arenes possessing a chelating group, employing ruthenium(II) catalysts, by Oi and Inoue,[78] Ackermann,[79] Maseras and Dixneuf.[80] However, examples where ruthenium catalysts were employed in absence of chelating groups are rare.[134]

Processes catalysed by ruthenium in absence of directing groups include:

1) Inter-and intramolecular hydroarylation of arenes with alkenes and alkynes

In 2003/4 Gunnoe *et al*. reported the ability of complex TpRu(CO)(NCMe)(Me) (**29**) to catalyse alkylation of simple arenes, furane and thiophene derivatives with olefins (Scheme 2.1, *left hand side*).[134a,c] Sames and co-workers reported approximately in the same period an intramolecular version of the hydroarylations with alkenes.[134b] The readily available $RuCl_3$, in combination with halide scavenger AgOTf, was found to provide a suitable catalytic system (Scheme 2.1, *right hand side*). High valent Ru(IV)/(III) complexes **30** and **31** were effectively used to catalyse hydroarylations of indole and pyrrole analogues with alkynes (Scheme 2.1, *bottom*).[134d-e]

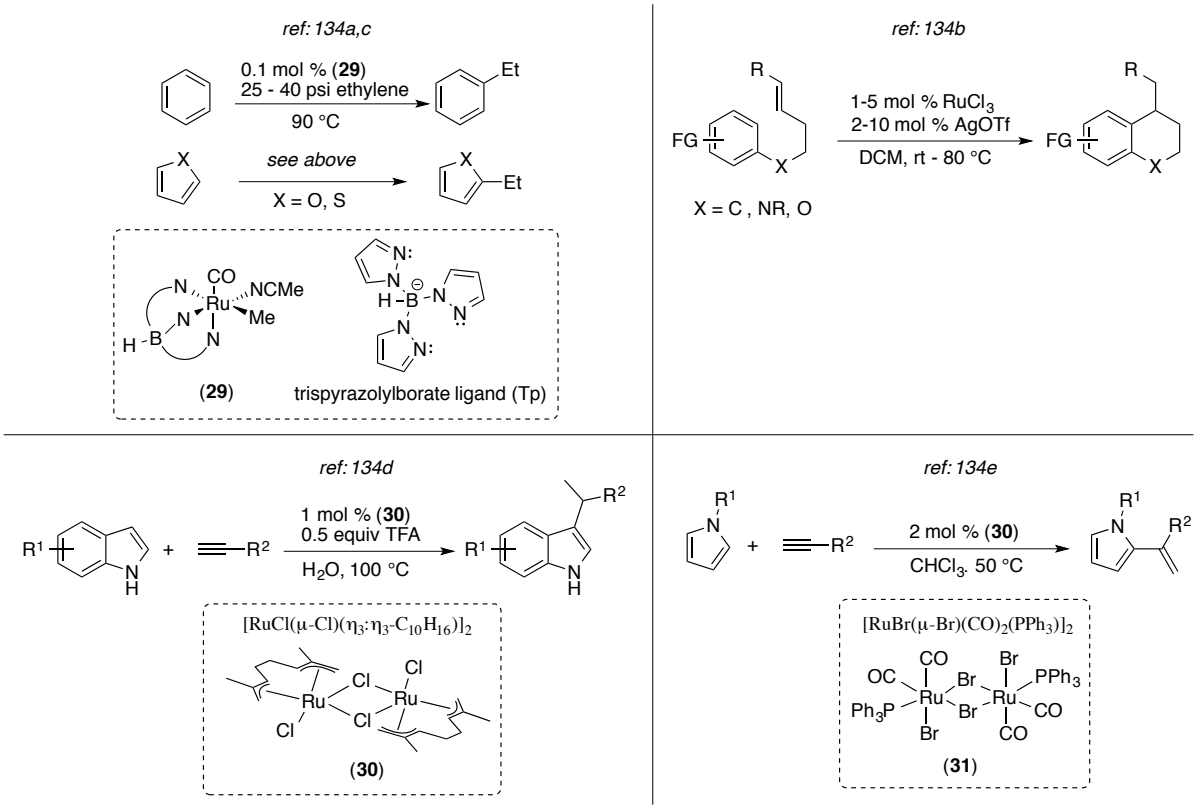

Scheme 2.1. Hydroarylation of arenes with alkenes and alkynes catalysed by ruthenium.

2) Allylation of simple arenes with alkynes

A pioneering work by Hidai and co-workers dated 1997 set the beginning of the ruthenium-catalysed C–H allylation of arenes. The convoluted Ru(III) complex **32** was in fact found to promote the process.[134f] Later, Pregosin *et al*. served the first example of Ru(IV)-catalysed C–H allylation employing catalyst **33 (**Scheme 2.2**)**.[134g] A more recent review by Bruneau and Achard depicted the potential of allylic ruthenium(IV) complexes in catalysis.[134h]

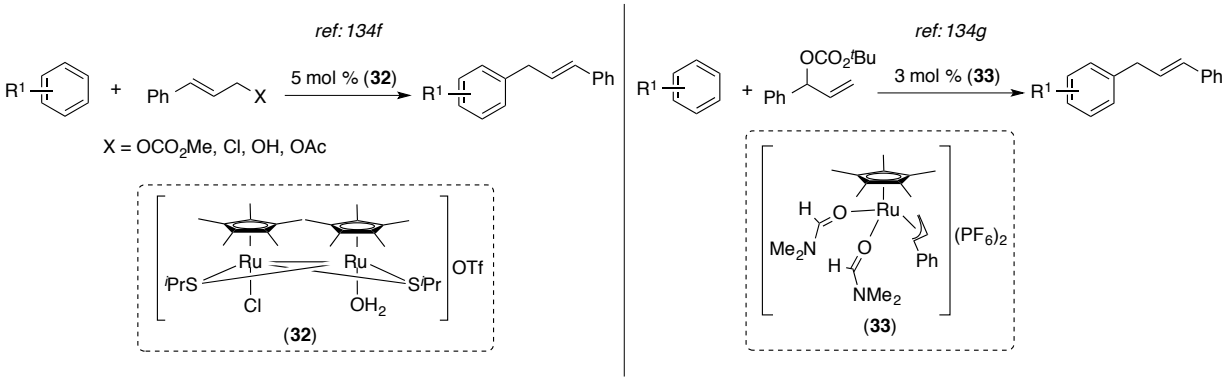

Scheme 2.2. Ru-catalysed direct C–H allylation of benzene derivatives.

3) Propargylation of aromatic compounds with propargyl alcohols

Dixneuf and co-workers in 2005 illustrated the ability of (η^6-arene)-Ru(II) (**34**-**37**) catalysts to promote C2 propargylation of furane derivatives with propargyl alcohol. The reaction was proposed to proceed *via* an allenylidene intermediate Ru=C=C=CHR, followed by nucleophilic attack of the arene (Scheme 2.3).[134i-j] Haack *et al*. in 2012 reported related transformations employing indole and pyrrole as nucleophiles.[134k]

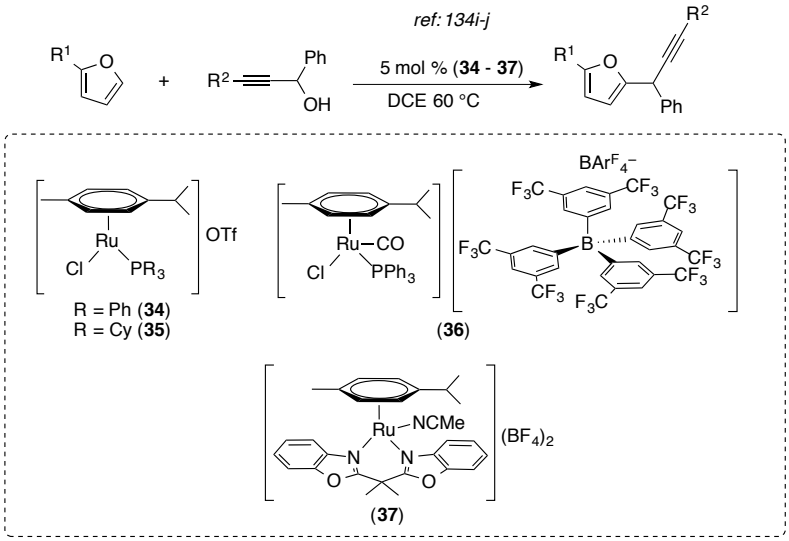

Scheme 2.3. Ru-catalysed propargylation of heteroaromatic compounds with propargyl alcohols.

4) Oxidative cross-coupling of benzene derivatives with cycloalkenes

A work by Li and Guo dated 2011 described the CDC between arenes and cycloalkanes. Substoichiometric amount of $Ru_3(CO)_{12}$, catalytic amount of 1,4-bis(diphenylphosphino)butane (dppb) ligand and di-*tert*-butyl peroxide oxidant (DTBP) were the components needed for the process. A marked *para*- selectivity was encountered for mono-substituted aromatics with carbonyl-containing functional groups and 2-prydyl moiety. Lower selectivity was observed for halogen-, OMe- and CN-substituted benzenes (Scheme 2.4).[134l]

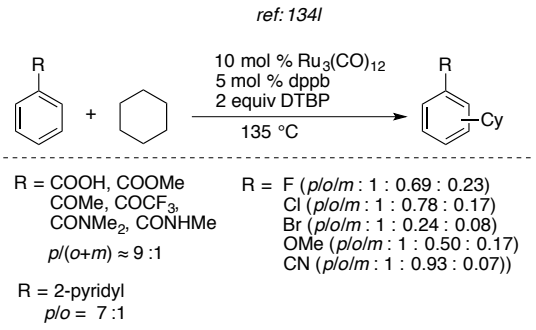

Scheme 2.4. Ru-catalysed CDC between cycloalkanes and arenes.

5) Oxidative Heck-type alkenylation

As early as 2001 Milstein and co-workers illustrated the oxidative Heck-type reaction of simple arenes with alkene, using molecular oxygen as the terminal oxidant. Several Ru(III) and Ru(II) precatalyst were found to be have similar catalytic activity, therefore simple $RuCl_3$ was chosen as the favoured catalyst (Scheme 2.5).[134m]

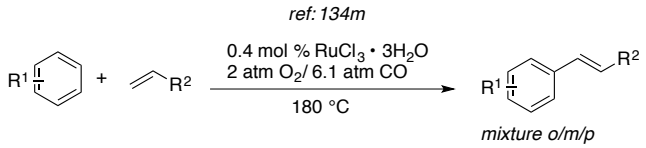

Scheme 2.5. Ru-catalysed oxidative Heck-type process.

6) Direct C3 sylilation of indole derivatives

Oestreich, Ohki and Tatsumi found the unique catalytic ability of complex **38** to promote direct C3 silylation of indole-type substrates with tri-substituted silanes. The authors proposed a synergic Ru–S catalytic system. The Si–H bond is heterolytically split by the Ru–S bond of a coordinatively unsaturated cationic ruthenium(II) complex, forming a sulfur-stabilised silicon electrophile. The Wheland intermediate, of the subsequent Friedel-Crafts-type process, is assumed to be deprotonated by the sulfur atom. The overall catalysis proceeds without solvent at low temperature, only liberating molecular hydorgen (Scheme 2.6).[134n]

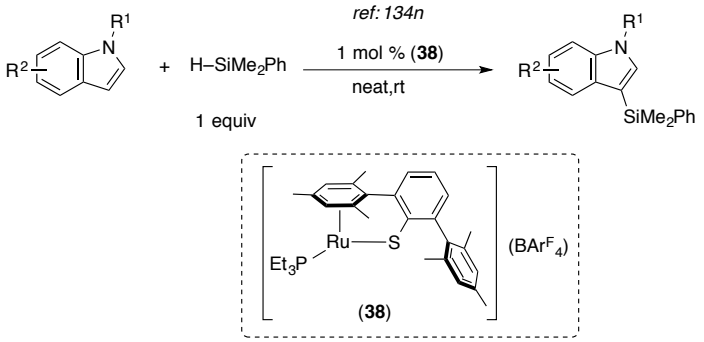

Scheme 2.6. Ru-catalysed oxidative Heck-type process.

7) Oxidative C–N homo- and cross-couplings of carbazole-type derivatives

Patureau and co-workers developed the oxidative Ru(II)-catalysed C–N homocoupling of 9*H*–carbazole derivatives, employing air and catalytic $Cu(OAc)_2$ as oxidants. A ternary solvent system formed by chlorobenzene, tetrachloroethylene and AcOH was essential for the reaction to proceed (Scheme 2.7, equation *a*).[134o] By using a similar approach, one year later the same group introduced the C–N cross-dehydrogenative coupling of carbazoles with diphenylamines. Stoichiometric amounts of $Cu(OAc)_2$ and oxygen were required as terminal oxidants (Scheme 2.7, equation *b*).[134p]

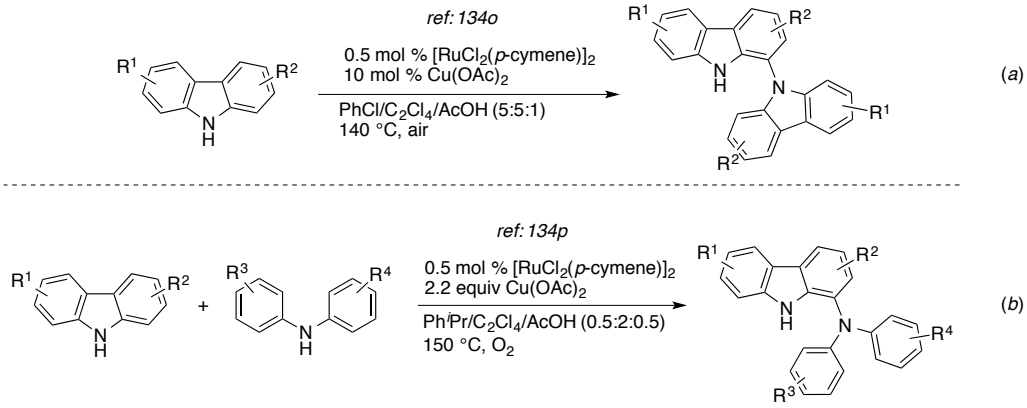

Scheme 2.7. Ru-catalysed oxidative C–N coupling of carbazole and diphenylamines.

8) para-Selective hydroxylation of anisole type

Finally, Ackermann *et al*. described a highly *para*-selective Ru(II)-hydroxylation of anisole derivatives employing the hypervaletent iodine(III) species $PhI(TFA)_2$ as both oxidant and oxygen source (Scheme 2.8).[134q]

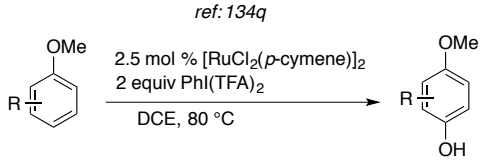

Scheme 2.8. Ru-catalysed *para*-hydroxylation of anisole derivatives.

As discussed in Chapter 1 (see sections 1.4.1), an alternative method for *site*-selective C–H activation is utilising the intrinsic reactivity of a given arene. In particular, studies with Pd,[22] Au[34-36] and Cu[33] have revealed that C–H activation on fluoroarenes occurs preferentially at the most acidic C–H bond (Scheme 1). Fundamental studies on Pd-catalysed C–H arylation led to the hypothesis that the C–H cleavage is assisted by basic ligands such as carboxylates or carbonates, in a concerted metalation-deprotonation (CMD).[18-20, 22, 31] Dixneuf and Maseras,[80] and Ackermann[81, 135] also reported the benefits of such additives in ruthenium-catalysed chelation-assisted C–H arylation (see section 1.4.2.1.2).

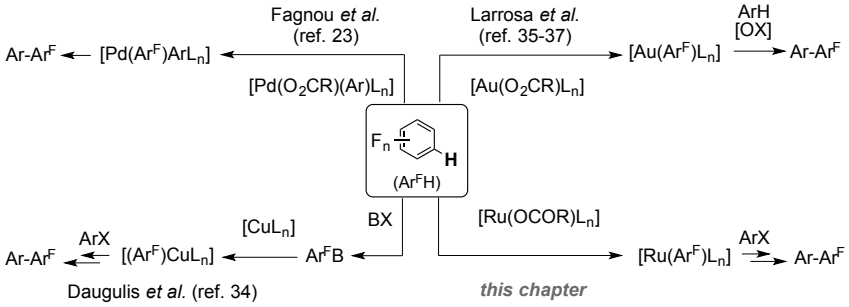

Scheme 2.9. C–H activation/arylation of perfluoroarenes by Pd, Au, Cu and Ru.

Remarkably, a directing-group-free Ru-catalysed direct C_{Ar}–H arylation methodology was yet to be discovered. Therefore, using fluoroarenes as model substrates, we set out to investigate the possibility of developing a DG-free Ru-catalysed arylation.

The first part of this chapter discloses that (*p*-cymene)-Ru(II) complexes, with the aid of carboxylates, are capable of C–H activation on fluoroarenes by D/H labeling experiments. Isolation of unprecedented aryl Ru(II) species generated from C–H activation of several fluoroarenes is also reported. The second part of Chapter 2 reports that benzoic acids can be used as surrogates of DGs, in order to enable the C–H arylation of fluoroarenes with aryl halides. Furthermore, it describes mechanistic insights concerning the C–H activation and the formal oxidative addition/reductive elimination steps, as well as studies towards the understanding of an unprecedented arylation *site*-selectivity together with preliminary kinetic data.

2.3. Ru-promoted C–H activation of fluoroarenes

H/D exchange processes can be used to explore the potential of a transition-metal catalyst towards the cleavage/formation of C–H bonds.[136] Given the often reversible nature of the C–H metalation step in ruthenium catalysis,[81, 135, 137] we decided to attempt the ruthenium-catalysed D/H scrambling on the non-volatile perfluorinated arene **d_1-39a**. When a 98:2 mixture of **d_1-39a**/**39a** was subjected to the reaction conditions described in Table 2.1, using 5 mol % of ruthenium-precatalyst $[RuCl_2(p\text{-cymene})]_2$, a net 9% of H incorporation was detected. Conversely, a control experiment in the absence of ruthenium showed no scrambling. This result suggests that Ru(II) complexes are able to activate C–H bonds in perfluorinated arenes. A closer inspection, using ^{19}F- and ^{1}H-NMR spectroscopy, revealed the formation of an unprecedented aryl-ruthenium intermediate (**Ru1-39a**, see Figure 2.1), suggesting that the D/H scrambling occurs *via* C–H/C–D activation, most likely involving the participation of pivalates in the metalation step.

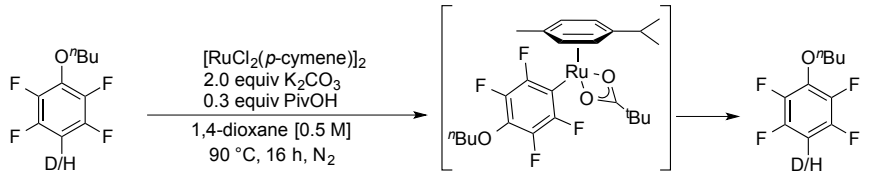

entry	[Ru] (mol %)	**d_1-39a**/**39a** (*initial ratio*)	**d_1-39a**/**39a** (*final ratio*)	**Ru1-39a** (%)
1	none	98:2	98:2	none
2	$[RuCl_2(p\text{-cymene})]_2$ (5)	98:2	89:11	1

[a] Reaction conditions: **d_1-39a** / **39a** (98:2 mixture, 1.0 equiv, 0.50 mmol), $[RuCl_2(p\text{-cymene})]_2$ (see above), PivOH (0.3 equiv), Na_2CO_3 (2.0 equiv), 1,4-dioxane [0.5 M] were stirred under N_2 in a closed vessel at 90 °C for 16h; yield and ratio of **d_1-39a** / **39a** was evaluated by ^{1}H-NMR using 1,3,5-trimethoxybenzene as internal standard.

Table 2.1. D/H scrambling of **d_1-39a**/**39a** via **Ru1-39a** by reversible C–D / C–H activation.

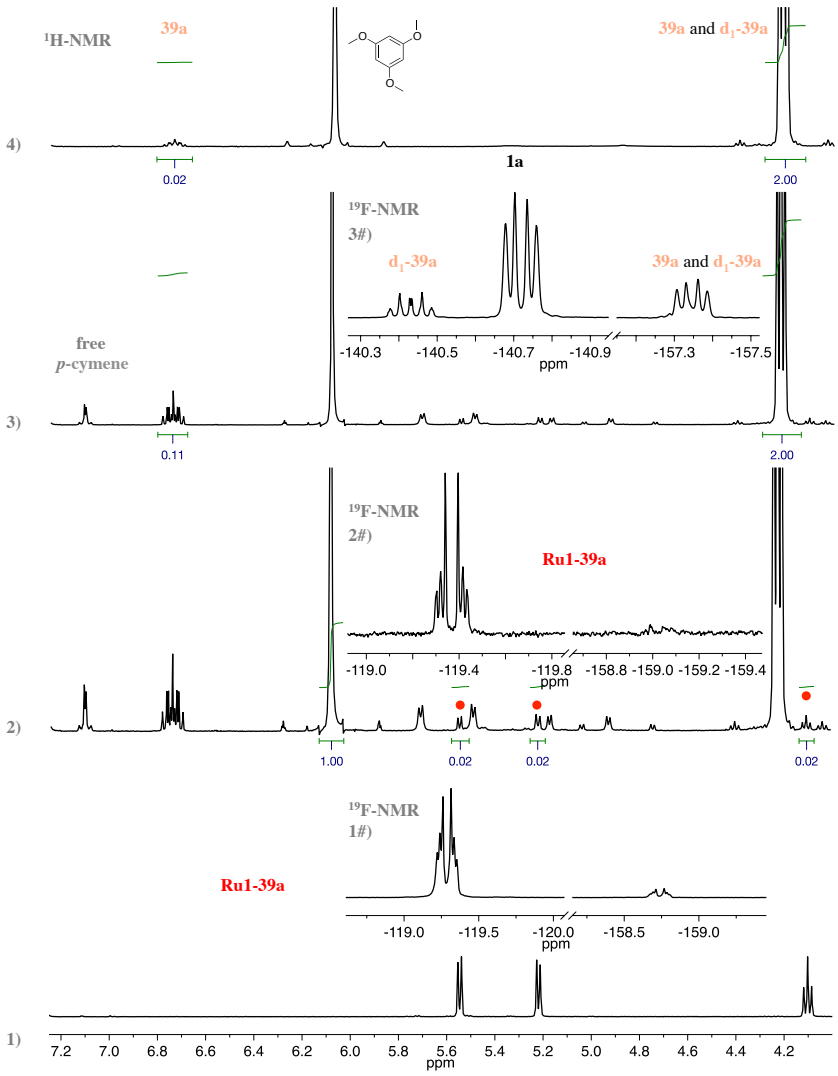

Figure 2.1. 1) ^{1}H-NMR expansion of *p*-cymene and O-$CH_2C_3H_7$ region for independently isolated **Ru1-39a**. 1#) ^{19}F-NMR expansion for independently isolated **Ru1-39a**. 2) ^{1}H-NMR expansion of the reaction described in Table 2.1 entry 2, showing: *p*-cymene and O-$CH_2C_3H_7$ regions for **Ru1-39a**, and aromatic singlet for internal standard 1,3,5-trimethoxybenzene; relative integration of signals corresponding to **Ru1-39a** with respect to the standard gives the yield of **Ru1-39a**. 2#) ^{19}F-NMR expansion of reaction described in Table 2.1 entry 2, showing **Ru1-39a**. 3) ^{1}H-NMR expansion of reaction described in Table 2.1 entry 2, showing the aromatic proton for **39a** and O-$CH_2C_3H_7$ protons for **d_1-39a** and **39a**; relative integration of the aromatic proton of **39a** with respect to O-$CH_2C_3H_7$ protons gives the ratio between for **d_1-39a** and for **39a**. 3#) ^{19}F-NMR expansion of the reaction described in Table 2.1 entry 2, showing **d_1-39a** and **39a**. 4) ^{1}H-NMR expansion of reaction described in Table 2.1 entry 2, showing the aromatic proton of **39a** and O-$CH_2C_3H_7$ protons for **d_1-39a** and **39a**; relative integration of the aromatic proton of **39a** with respect to O-$CH_2C_3H_7$ protons gives the ratio between **d_1-39a** and **39a**.

We then shifted our attention towards the optimisation of the C–H activation of **39a** to **Ru-39a**, with the well-defined complex Ru(OPiv)$_2$(*p*-cymene) (**Ru-C1**). As shown in Table 2.2, we initially screened bases at different temperatures aiming to suppress protodemetalation.

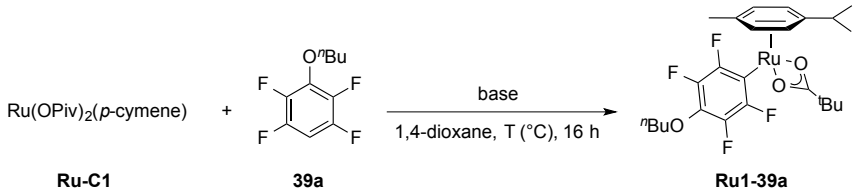

entry	base	T (°C)	**Ru-C1** (%)	**Ru1-39a**(%)
1	none	60	80	8
2	KOPiv	60	85	11
3	none	90	83	6
4	KOPiv	90	87	6
5	Li_2CO_3	60	90	8
6	Na_2CO_3	60	84	11
7	K_2CO_3	60	40	14
8	Cs_2CO_3	60	6	0
9	$(NMe_4)OC(CF_3)_3$	60	85	10
10	Li_2CO_3	90	78	12
11	Na_2CO_3	90	62	25
12	K_2CO_3	90	20	33
13	Cs_2CO_3	90	2	3
14	$(NMe_4)OC(CF_3)_3$	90	57	28
15	**Na_2CO_3**	**120**	**32**	**55**
16	$(NMe_4)OC(CF_3)_3$	120	48	30
17[b]	Na_2CO_3	120	24	54
18	Na_2CO_3	140	18	22

[a] Reaction conditions: **Ru-C1** (1.0 equiv, 0.05 mmol), **39a** (5.0 equiv), base (2.0 equiv) and 1,4-dioxane [0.2 M] were stirred under argon in a closed vessel at the specified temperature for 16 h; yield is evaluated by ^{1}H-NMR using 1,3,5-trimethoxybenzene as internal standard. [b] Base (0.10 mmol, 2.0 equiv).

Table 2.2. Temperature and base optimisation of the C–H activation of **39a** with **Ru-C1**.

As we would expect from a reversible process, either at 60 or 90 °C in the absence of base or with KOPiv (entries 1-4) low conversion of the desired complex was detected. Examination of alkali carbonate bases at 60 °C (entries 5-8) revealed that more soluble Cs_2CO_3 and K_2CO_3 bases led to low mass recovery, whereas the less soluble Li_2CO_3 and Na_2CO_3 provided excellent mass balance giving maximum 11% of **Ru1-39a** (entry 6). Examination of the of ^{1}H-NMRs suggests that a high concentration of carbonates, in place of the pivalate ligand(s), generation of Ru(II) carbonate/bicarbonate *p*-cymene complexes might occur. Indeed, when only caesium and potassium carbonates were employed, new ruthenium species were formed. The absence of any peaks by ^{19}F-NMR, with the exception of those related to **Ru1-39a**, indicates that none of these compounds are aryl ruthenium complexes. Therefore, we might assume that Ru(II) carbonate/bicarbonate *p*-cymene complexes are less capable of C–H activation respect to Ru(OPiv)$_2$(*p*-cymene) (**Ru-C1**).

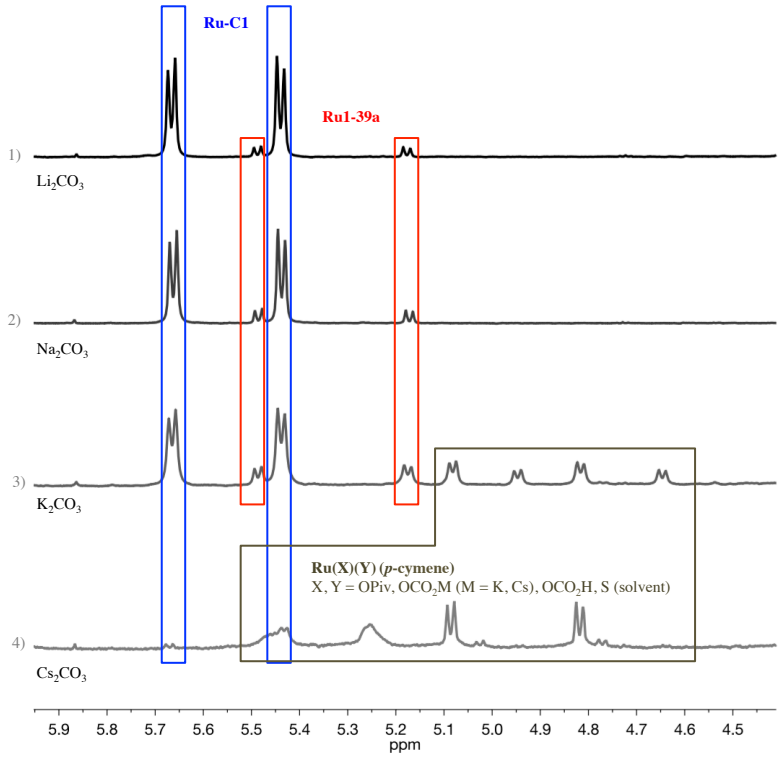

Figure 2.2. ^{1}H-NMR expansion of *p*-cymene ruthenium complexes region of reactions described in **Table 2.2**: 1) entry 5; 2) entry 6; 3) entry 7; 4) entry 8.

Our venture of finding a weakly coordinating base led us to test tetramethylammonium perfluoro-*tert*-butoxide, which revealed itself to be compatible with the C–H activation providing 10% product (entry 9, Table 2.2). The corresponding alcohol, perfluoro-*tert*-butyl alcohol, has a pKa of 5.4[138] and so perfluoro-*tert*-butoxide is basic enough to deprotonate pivalic acid (pKa 5.0).[139] Additionally, the boiling point of this perfluorinated alcohol (45 °C)[138] being below the working temperature of the reaction, a scenario of high concentration of the base and a low concentration of its conjugated acid is likely to be achieved in solution. At 90 °C (entries 10-13), a similar behaviour of the alkali carbonate bases was observed. In fact, the most suitable base was found to be the moderately soluble Na_2CO_3 giving a promising conversion towards **Ru1-39a** (25%, entry 11) along with good mass recovery (62 + 52 = 87%, entry 11). The poorly soluble Li_2CO_3 and the highly soluble Cs_2CO_3 were not suitable namely because they provided low conversation and terrible mass recovery (entries 10 and 13). Although K_2CO_3 led to the formation of the product in 33% (entry 12), the overall poor mass balance (53%) renders this base unsuitable. An alternative to Na_2CO_3 is given by $(NMe)_4OC(CF_3)_3$, which provided 28% of conversion and good mass recovery (85%, entry 14). Raising the temperature to 120 °C, Na_2CO_3 revealed itself to be superior to the alkoxide base, delivering 55% of **Ru1-39a** (entry 15). Finally, higher loading of Na_2CO_3 (4 equiv) or higher temperature (140 °C) did not increase the efficiency of the process (entries 17-18).

A screening of solvents revealed that 1,4-dioxane led to the highest yield (Table 2.3). Among the solvents that have been tested (mesitylene, Bu_2O, CPME, Bu_2O, PC entries 1-5), none was found to be better than 1,4-dioxane (entry 1). The concentration of the reaction has also an important effect (entries 1, 6-8). In Fact, concentrations above 0.5 M and below 0.2 M led to a reduction of both yield and mass recovery. At an optimal concentration of 0.5 M (entry 7), **Ru1-39a** was formed in 55%.

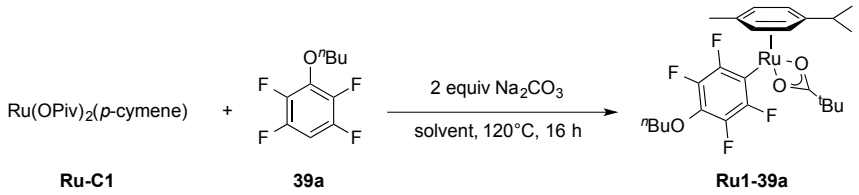

entry	solvent	concentration [M]	**Ru-C1** (%)	**Ru1-39a**(%)
1	1,4-dioxane	0.2	32	55
2	mesitylene	0.2	43	26
3	CPME	0.2	26	46
4	Bu_2O	0.2	60	4
5	propylene carbonate	0.2	2	0
6	1,4-dioxane	0.1	39	32
7	**1,4-dioxane**	**0.5**	**33**	**55**
8	1,4-dioxane	1	12	44

[a] Reaction conditions: **Ru-C1** (1.0 equiv, 0.05 mmol), **39a** (5.0 equiv), Na_2CO_3 (2.0 equiv) and the specified solvent at the stated concentration were stirred under argon in a closed vessel at 120 °C for 16 h; yield is evaluated by ^{1}H-NMR using 1,3,5-trimethoxybenzene as internal standard.

Table 2.3. Solvents screening for the C–H activation of **39a** with **Ru-C1**.

In order to gain a better insight to the kinetics of the C–H activation, the time profile of the process was examined (Table 2.4 and Graph 2.5). The analysis disclosed that 16 h are needed for the reaction to reach a maximum yield of 55% (entry 8, Table 2.4). Leaving the C–H activation for 24 h lead to decomposition of both **Ru-C1** and **Ru1-39a**.

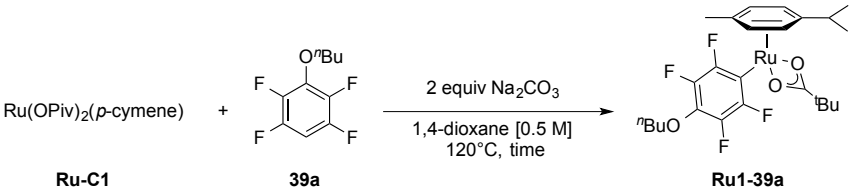

entry	time (h)	**Ru-C1** (%)	**Ru1-39a**(%)
1	0.5	79	18
2	1	70	25
3	2	60	34
4	3	48	42
5	5	40	47
6	7	36	50
7	10	35	54
8	**16**	**33**	**55**
9	24	16	39

[a] Reaction conditions: **Ru-C1** (1.0 equiv, 0.05 mmol), **39a** (5.0 equiv), Na^2CO^3 (2.0 equiv) and 1,4-dioxane [0.5 M] were stirred under argon in a closed vessel at 120 °C for the specified time; yield is evaluated by ^{1}H-NMR using 1,3,5-trimethoxybenzene as internal standard.

Table 2.4. Time-scan of the C–H activation of **39a** with **Ru-C1**.

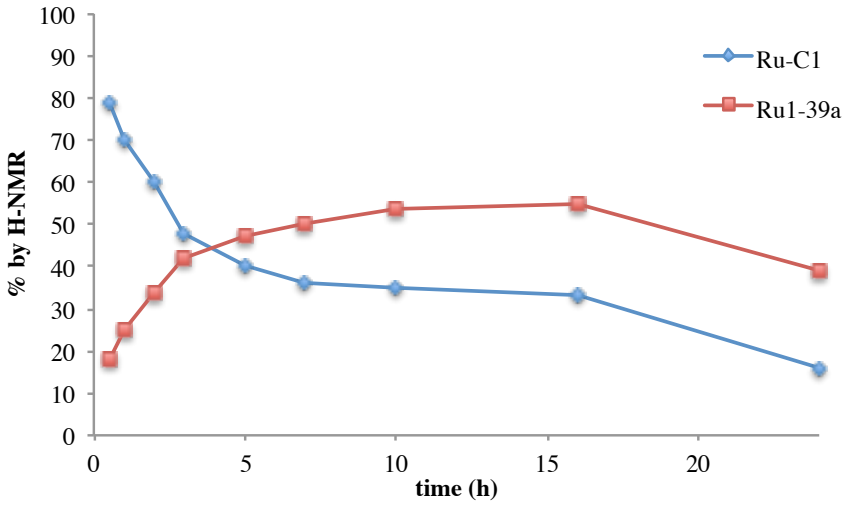

Graph 2.5. Time profile of the C–H activation of **39a** with **Ru-C1**.

We then shifted our attention towards the optimisation of the loading of perfluoroarene **39a**. In accordance with an equilibrium process, the yield of **Ru1-39a** improved from 55 to 68% (entry 4, Table 2.5) when the loading of **39a** was increased from 5 to 20 equiv. Isolation of **Ru1-39a** by column chromatography, afforded the title complex in 60% yield as orange solid.

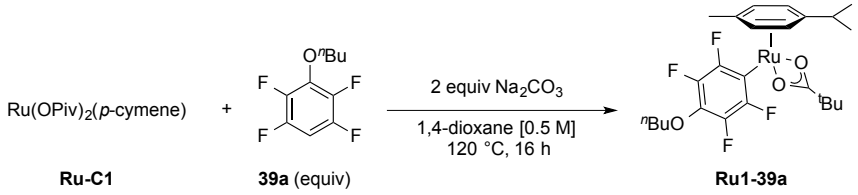

entry	**39a** (equiv)	**Ru-C1** (%)	**Ru1-39a**(%)
1	5	33	55
2[b]	10	20	58
3[b]	15	18	62
4[b]	**20**	**14**	**68 (60)**

[a] Reaction conditions: **Ru-C1** (1.0 equiv, 0.05 mmol), **39a** (see above), Na_2CO_3 (2.0 equiv) and the 1,4-dioxane [0.5 M] were stirred under argon in a closed vessel at the 120 °C for 16 h; yield is evaluated by ^{1}H-NMR using 1,3,5-trimethoxybenzene as internal standard. [b] **Ru-C1** (1.0 equiv, 0.2 mmol). Yield in parenthesis refers to isolated material.

Table 2.5. Optimal loading of the perfluoroarene for the C–H activation of **39a** with **Ru-C1**.

Having identified satisfactory reaction conditions for the synthesis of **Ru1-39a**, we applied them to the C–H activation of pentafluorobenzene (**39b**) and 1,2,4,5-tetrafluorobenzene (**39c**) with **Ru-C1** (Scheme 2.10). The corresponding aryl ruthenium complexes **Ru1-39b** and **Ru1-39c** were obtained in 75% and 77% yield as yellow solids, after purification.

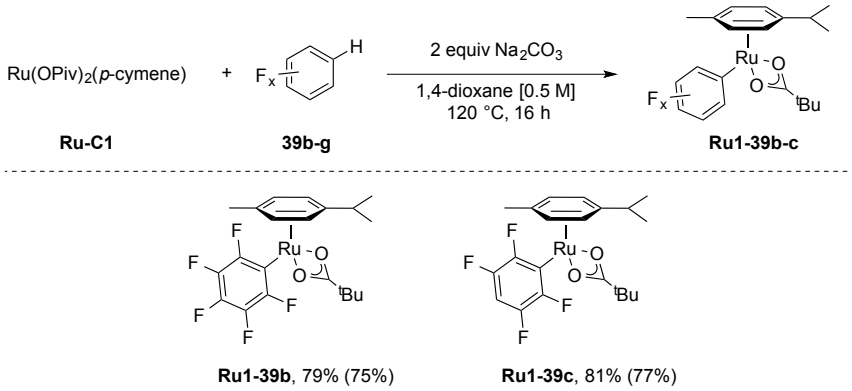

[a] Reaction conditions: **Ru-C1** (1.0 equiv, 0.2 mmol), **39a-c** (20.0 equiv), Na_2CO_3 (2.0 equiv) and the 1,4-dioxane [0.5 M] were stirred under argon in a closed vessel at 120 °C for 16 h; yield is evaluated by ^{1}H-NMR using 1,3,5-trimethoxybenzene as internal standard. [b] **Ru-C1** (1.0 equiv, 0.2 mmol). Yield in parenthesis refers to isolated material.

Scheme 2.10. C–H activation of **39b** and **39c** with **Ru-C1.**

Slow evaporation from a concentrated solution of **Ru1-39c** in $CHCl_3$, provided suitable crystals for X-ray analysis. Indeed, its structure was further confirmed by single crystal X-ray analysis (Figure 2.3).

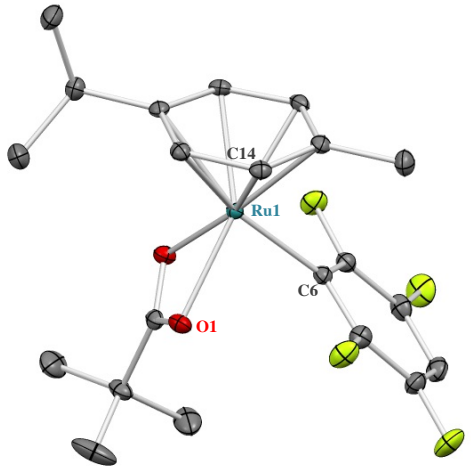

Figure 2.3. ORTEP diagram of **Ru1-39c** at 50% ellipsoids. Selected bond lengths [Å]: Ru(1)–O(1) 2,156; Ru(1)–C(6) 2,156; Ru(1)–C(14) 2,170. Selected bond angle [°]: O(1)–Ru(1)–C(6) 83,59.[140]

Finally, the kinetic isotope effect measured in two independent set of experiments conducted in parallel, revealed that the rate of formation of **Ru1**-**39a** is 2.4 times faster for non-deuterated **39a** compared to **d_1**-**39a** (KIE = 2.4). This result is in agreement with a CMD-type C–H bond cleavage mode where the C–H activation step is kinetically significant.[18-20, 22, 31]

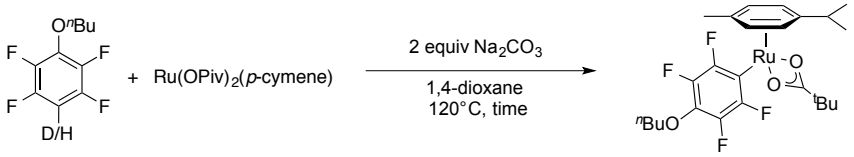

39a or **d_1-39a** **Ru-C1** **Ru1-39a**

entry	**39a** or **d_1-39a**	**time (min)**	**Ru1-39a**(%)
1	**39a**	5	3.3
2	**39a**	10	4.9
3	**39a**	15	6.4
4	**39a**	20	8.9
5	**d_1-39a**	5	0.9
6	**d_1-39a**	10	2.0
7	**d_1-39a**	15	2.6
8	**d_1-39a**	20	3.2

[a] Reaction conditions: **Ru-C1** (1.0 equiv, 0.1 mmol), **39a** or **d_1-39a** (5.0 equiv), Na_2CO_3 (2.0 equiv, 0.2 mmol), 1,4-dioxane [0.1 M] were stirred under Ar in a closed vessel at 120 °C for the appropriate time; yield is evaluated by ^{1}H-NMR using 1,3,5-trimethoxybenzene as internal standard.

Table 2.6. KIE experiment for the C–H activation of **39a / d_1-39a** with **Ru-C1**.

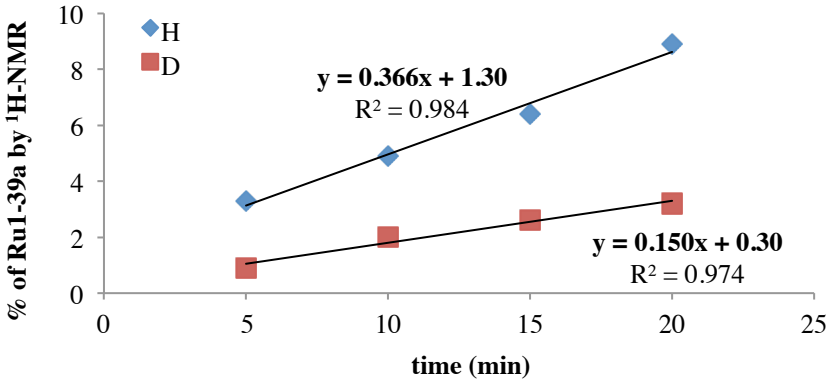

Graph 2.6. Rates of formation of **Ru1-39a** for C–H/D activation of **39a** and **d_1-39a** with Ru-C1 (%/min).

$$\mathbf{KIE} = \frac{k\mathrm{H}}{k\mathrm{D}} = \frac{0.366}{0.150} = \mathbf{2.4}$$

2.3.1 Ru-promoted C–H activation of fluoroarenes: conclusion

In order to develop a ruthenium catalysed C–H arylation methodology in the absence of directing groups, we decided to start our investigation by determining whether (η^6-arene)-Ru(II) complexes are capable of C–H activation on fluoroarenes. Indeed, D/H labelling experiments revealed that (*p*-cymene)Ru species, with the aid of pivalates, are able to promote a reversible C–H/C–D activation on polyfluoroarenes. Furthermore, the detection of an unprecedented aryl Ru(II) complex arising from C–H/D activation during the D/H scrambling experiments, led to the development of a novel and straightforward methodology for the synthesis of perfluoroaryl (*p*-cymene)RuOPiv complexes. Finally, by evaluating the KIE of the process, we postulated a concerted metalation deprotonation (CMD) for the C–H activation mode.

2.4. [(η^6-arene)-Ru(OCOR)$_2$]-catalysed C–H arylation of fluoroarenes with aryl halides

Having demonstrated that Ru-catalysts are capable of performing C−H activation on electron-deficient arenes, we shifted our attention to the development of a catalytic system for the C−H arylation of these substrates.

To gain an idea about the stability of (η^6-arene)Ru(II) bis-carboxylates catalysts in the arylation process, the amount of decomplexed, free arene-ligand recovered at the end of the reaction was systematically monitored by ^{1}H-NMR. Although at this stage of our investigations we did not have a full understanding of the meaning of these data, the recovery of free arene-ligand could either indicate catalyst decomposition or that (η^6-arene)Ru(OCO_2R)$_2$ are pre-catalysts. A satisfactory explanation for this matter will be provided in the next epigraph.

As a starting point, we chose to examine direct arylation of **39a** with 4-bromoanisole (**40a**) employing conditions under which the perfluoroaryl Ru(II) species **Ru1-39a** is generated efficiently (Table 2.7). When Na_2CO_3, KOPiv or (NMe_4)$OC(CF_3)_3$ were used with catalyst Ru(OPiv)$_2$(*p*-cymene) (**Ru-C1**), no biaryl **41aa** was detected (entries 1-3). Encouragingly, when Ru(OBz)$_2$(*p*-cymene) (**Ru-C2**) was tested, **41aa** formed in traces with Na_2CO_3 and in 19% of yield with perfluoro-*tert*-butoxide (entries 5, 7). A discussed in Chapter 1 (see section 1.4.2.1), our group recently reported the ability of tetramethylammonium salts of abstracting iodides in palladium-catalysed direct arylation.[57] Similarly, (NMe_4)$OC(CF_3)_3$ might be involved in catalyst regeneration *via* halide abstraction from a Ru-Br species. This could provide a plausible explanation for the high activity of tetramethylammonium perfluoro-*tert*-butoxide. Finally, the amount of free *p*-cymene detected varies from base to base, catalyst **Ru-C2** seems to be less stable than its analogue **Ru-C1.**

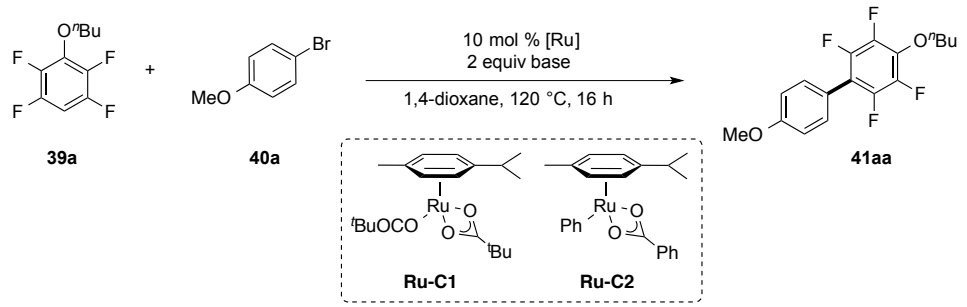

entry	[Ru] (10 mol %)	base (2 equiv)	free *p*-cymene (%)	**41aa** (%)
1	**Ru-C1**	Na_2CO_3	26	0
2	**Ru-C1**	KOPiv	11	0
3	**Ru-C1**	$(NMe_4)OC(CF_3)_3$	44	0
5	**Ru-C2**	Na_2CO_3	41	< 1
6	**Ru-C2**	KOPiv	27	0
7	**Ru-C2**	$(NMe_4)OC(CF_3)_3$	69	19

[a] Reaction conditions: **40a** (1.0 equiv, 0.10 mmol), **39a** (5.0 equiv), specified [Ru] catalyst (10 mol%), appropriate base (2.0 equiv), 1,4-dioxane [0.5 M] were stirred under N_2 in a closed vessel at 120 °C for 16 h; yield is evaluated by ^{1}H-NMR using 1,3,5-trimethoxybenzene as internal standard; % of free *p*-cymene is based on the loading of [Ru].

Table 2.7. Initial optimisation of the ruthenium source and base for the arylation of **40a** with **39a**.

Aiming to find the most suitable electrophile coupling partner, a screening of (pseudo)aryl halides was conducted in the arylation of **39a** with catalyst **Ru-C2** (Table 2.8). 4-Iodoanisole (**I-40a**), 4-choloroanisole (**Cl-40a**) and 4-methoxyphenyl triflate (**OTf-40a**) proved to be more poorly yielding than 4-bromoansiole **40a** (entries 1-3). Therefore **40a** was kept as the standard aryl bromide for the following optimisations.

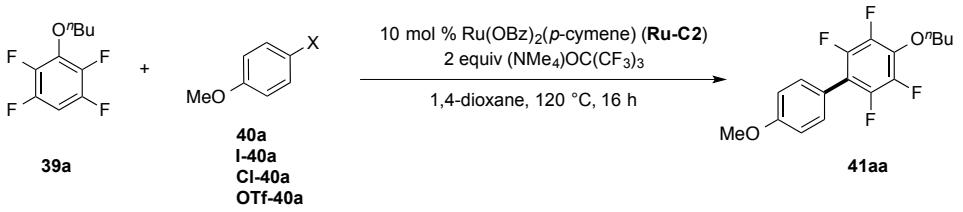

entry	Ar–X	free *p*-cymene (%)	**41aa** (%)
1	4-OMe-C_6H_4-Br (**40a**)	69	19
2	4-OMe-C_6H_4-I (**I-40a**)	61	11
3	4-OMe-C_6H_4-Cl (**Cl-40a**)	55	4
4	4-OMe-C_6H_4-OTf (**OTf-40a**)	60	0

[a] Reaction conditions: appropriate Ar–X (1.0 equiv, 0.10 mmol), **39a** (5.0 equiv), **Ru-C2** catalyst (10 mol%), $(NMe)_4OC(CF_3)_3$ (2.0 equiv), 1,4-dioxane [0.5 M] were stirred under N_2 in a closed vessel at 120 °C for 16 h; yield is evaluated by ^{1}H-NMR using 1,3,5-trimethoxybenzene as internal standard; % of free *p*-cymene is based on the loading of **Ru-C2**.

Table 2.8. (Pseudo)halides screening for the arylation of **39a** with **40a** with catalyst **Ru-C2**.

Several solvents were screened for the Ru-catalysed arylation of **39a** with **40a** (Table 2.9). 1,2-dichloroethane (DCE) and toluene did not provide any product, which was disappointing as **Ru-C2** catalyst proved to be exceptionally stable in toluene solvent (% free *p*-cymene < 1%, entry 3). The more polar *N*,*N*-dimethylacetamide (DMA) provided 15% of biaryl **41aa** (entry 14). When the coordinating acetonitrile (MeCN) was tested in place of 1,4-dioxane, a substantial increase from 19% to 34% yield was noticed (entry 5). The bulkier and less volatile pivalonitrile (^{t}BuCN) further improved the yield, providing 37% of **41aa** (entry 7). Notably, with either MeCN or ^{t}BuCN all of the *p*-cymene ligand was recovered as free arene at the end of the reaction.

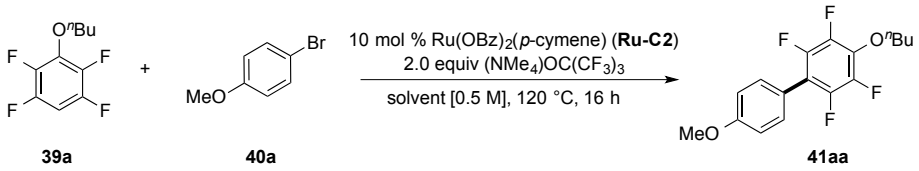

entry	solvent	free *p*-cymene (%)	**41aa** (%)
1	1,4-dioxane	69	19
2	DCE	76	0
3	toluene	< 1	0
4	DMA	65	15
5	MeCN	99	34
6	^{t}BuCN	99	37

[a] Reaction conditions: **40a** (1.0 equiv, 0.10 mmol), **39a** (5.0 equiv), **Ru-C2** (10 mol%), (NMe$_4$)OC(CF$_3$)$_3$ (2.0 equiv), appropriate solvent [0.5 M] were stirred under N_2 in a closed vessel at 120 °C for 16 h; yield is evaluated by ^{1}H-NMR using 1,3,5-trimethoxybenzene as internal standard; % of free *p*-cymene is based on the loading of **Ru-C2**.

Table 2.9. Solvent screening for the arylation of **40a** with **39a** with catalyst **Ru-C2**

Subsequently, owing the ability of nitrogen donors to coordinate metals,[137,141] a screening of the optimal loading of pivalonitrile was investigated (Table 2.10). Decreasing the concentration from 0.5 M (≈ 18 equiv of ^{t}BuCN) to 0.25 M (≈ 36 equiv) caused a drop in yield from 37% to 22% (entry 1). Diminishing the loading of pivalonitrile to 15 equiv improved the amount of biaryl **41aa** to 42% (entry 2). Further reduction of ^{t}BuCN to 8 equiv provided a maximum arylation yield of 46%. Finally, additional decrease to 5 equiv of the bulky nitrile solvent reduced the yield of **41aa** to 44%.

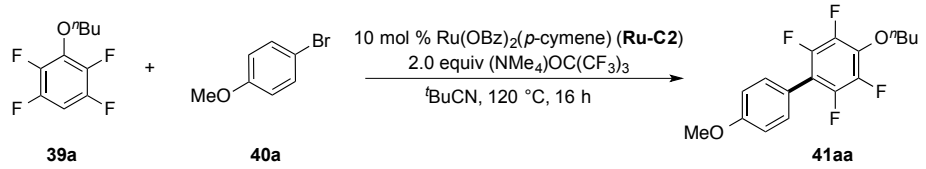

entry	^{t}BuCN	free *p*-cymene (%)	**41aa** (%)
1	[0.25 M] ≈ 36 equiv	99	22
2	[0.5 M] ≈ 18 equiv	99	37
2	15 equiv	99	42
3	8 equiv	99	46
4	5 equiv	99	44

[a] Reaction conditions: **40a** (1.0 equiv, 0.10 mmol), **39a** (5.0 equiv), **Ru-C2** (10 mol%), (NMe$_4$)OC(CF$_3$)$_3$ (2.0 equiv), ^{t}BuCN (see above) were stirred under N_2 in a closed vessel at 120 °C for 16 h; yield is evaluated by ^{1}H-NMR using 1,3,5-trimethoxybenzene as internal standard; % of free *p*-cymene is based on the loading of [Ru].

Table 2.10. Loading of pivalonitrile for the arylation **39a** with **40a** with catalyst **Ru-C2**

The addition of aliphatic carboxylates, in Ru(OBz)$_2$(*p*-cymene) (**Ru-C2**) catalysed arylation of **39a** with 4-bromoanisole in ^{t}BuCN solvent, was explored (Table 2.11, entries 2-4). Gratifyingly, potassium acetate (KOAc), adamantoate (KOAd) and pivalate (KOPiv) helped the process by namely increasing the yield from 46% to 50%, 53% and 54%. As discussed in sections 1.4.1.2 and 1.4.2.1.2 (Chapter 1), carboxylates were found to be valuable additives for Pd-catalysed C–H arylation of electron-poor arenes and for chelation-assisted Ru-catalysed arylation methods *via* CMD transition state. Thus, similarly to previous investigations, carboxylates might be involved in assisting the concerted ruthenation-deprotonation of the perfluoroarene. When Ru(OPiv)$_2$(*p*-cymene) (**Ru-C1**) was tested again in the absence of any additives, only 6% arylation was detected (entry 5). Instead, when **Ru-C1** was used in combination of 20 mol % of KOBz, establishing equivalent conditions of entry 4 in which **41aa** was formed in 54%, the biaryl product was detected in 57% (entry 6). Not surprisingly, when catalyst **Ru-C1** was employed with 20 mol % benzoic acid (**CA-50**, PhCO$_2$H) and 2.2 equiv of perfluoro-*tert*-butoxide, 57% product was observed (entry 7). These experimental results are quite unexpected because an

outstanding difference in reactivity (from 6% to 46%, entries 5 and 1) occurs when the bis-pivalate catalyst **Ru-C1** is used in place of the bis-benzoate analogue **Ru-C2**. A similar trend was observed in entries 3 and 7 of Table 2.7 at the beginning of the epigraph. Although the reasons behind this remarkable switch in reactivity are still not elucidated, assuming that the less coordinating and basic benzoate is more efficient than pivalate in assisting the metalation of the arene would be a poorly convincing hypothesis.

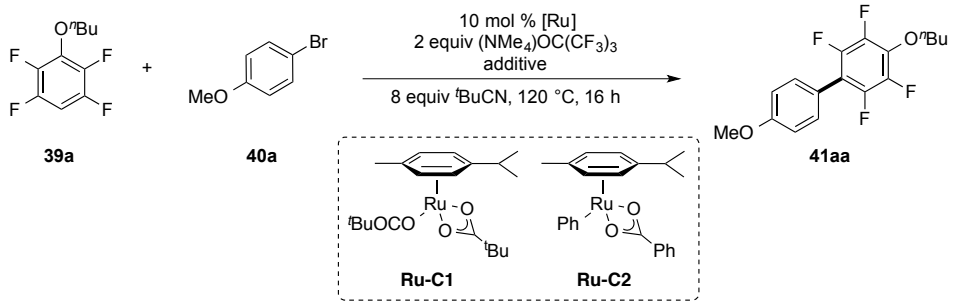

entry	[Ru] (10 mol %)	additive (equiv)	**41aa** (%)
1	**Ru-C2**	none	46
2	**Ru-C2**	KOAc (0.2)	50
3	**Ru-C2**	KOAd (0.2)	53
4	**Ru-C2**	KOPiv (0.2)	54
5	**Ru-C1**	none	6
6	**Ru-C1**	KOBz (0.2)	57
7[b]	**Ru-C1**	$PhCO_2H$ (0.2)	57

[a] Reaction conditions: **40a** (1.0 equiv, 0.10 mmol), **39a** (5.0 equiv), appropriate [Ru] (10 mol%), $(NMe_4)OC(CF_3)_3$ (2.0 equiv), specified additive (see above), ^{t}BuCN (8 equiv) were stirred under N_2 in a closed vessel at 120 °C for 16 h; yield is evaluated by ^{1}H-NMR using 1,3,5-trimethoxybenzene as internal standard; 99% of free *p*-cymene based on the loading of [Ru] was detected in all the entries. [b] $(NMe_4)OC(CF_3)_3$ (2.2 equiv).

Table 2.11. The role of benzoate additive for the arylation **39a** with **40a**.

In view of the dramatic effect of the benzoate additive in the arylation, a vast screening of benzoic acids, possessing diverse electronic and steric properties, was conducted (Table 2.12). Benzoic acids from entry 1 to 21 have negative or no effect on the final yield of biaryl **41aa**. Benzoic acids from entry 22 to 49 are less active than benzoic acid (**CA-50**, entry 50), although they have a positive effect on the amount of biaryl product detected after 16 h with respect to the control reaction without any additive (entry 60). Finally benzoic acids from entry 51 to 59 were the most active. Particularly, 3-acetylbenzoic acid (entry 57), 4-fluorobenzoic acid (entry 58), 3-benzoylbenzoic acid (entry 59) and 4-methylsulphonylbenzoic acid (entry 58) which provided 67%, 67%, 68% and 68.5% yield of **41aa**, respectively.

From the results shown below, we could not find any trend in the reactivity with variation of the electron properties on the acid ring. For example, 3-fluorobenzoic acid (entry 49) and 4-methoxybenzoic acid (entry 51) afforded comparable amount of product, respectively 54.5% and 58%, despite having nearly opposite Hammet constants: $\sigma_{p\text{-OMe}} = -0.27$, $\sigma_{m\text{-F}} = 0.34$.[142] The only unequivocal factor affecting the final yield of biaryl product seems to be the steric hindrance around the COOH group. In fact, a closer inspection of the toluic acids serie (entries 49, 29 and 11) indicates that the yield drops form 49% (*p*-toluic acid) to 29% (*m*-toluic acid), reaching a minimum of < 3% for the *o*-toluic acid.

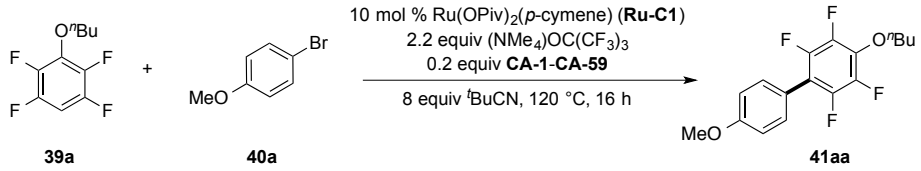

39a **40a** **41aa**

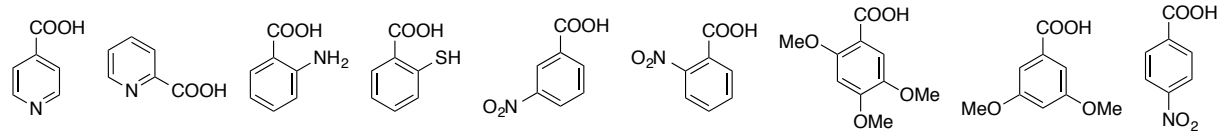

CA-1 **CA-2** **CA-3** **CA-4** **CA-5** **CA-6** **CA-7** **CA-8** **CA-9**

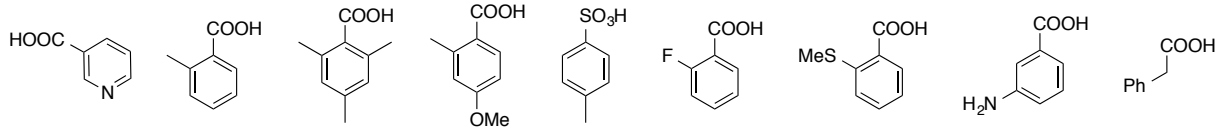

CA-10 **CA-11** **CA-12** **CA-13** **CA-14** **CA-15** **CA-16** **CA-17** **CA-18**

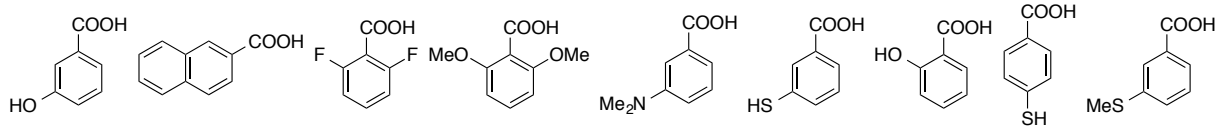

CA-19 **CA-20** **CA-21** **CA-22** **CA-23** **CA-24** **CA-25** **CA-26** **CA-27**

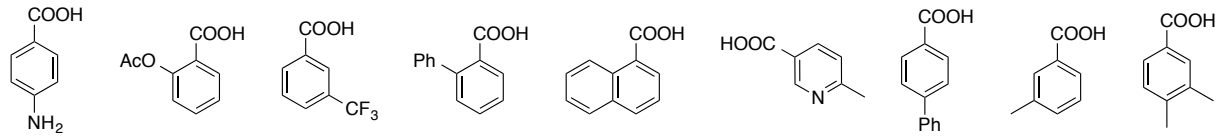

CA-28 **CA-29** **CA-30** **CA-31** **CA-32** **CA-33** **CA-34** **CA-35** **CA-36**

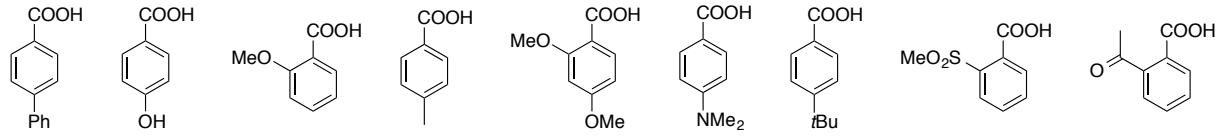

CA-37 **CA-38** **CA-39** **CA-40** **CA-41** **CA-42** **CA-43** **CA-44** **CA-45**

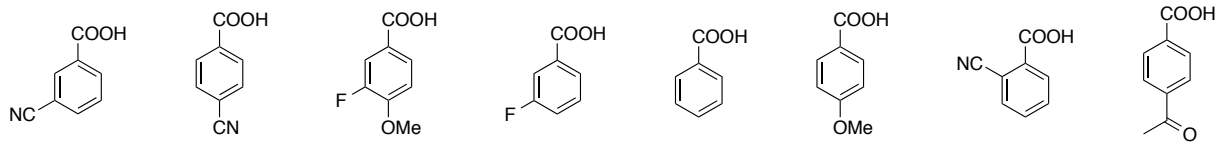

CA-46 **CA-47** **CA-48** **CA-49** **CA-50** **CA-51** **CA-52** **CA-53**

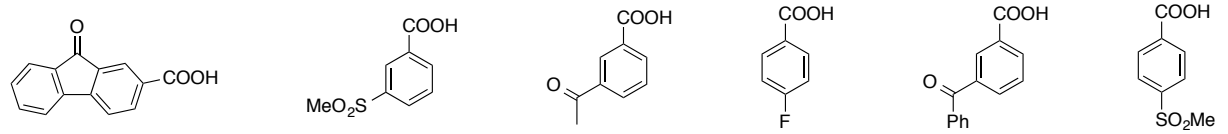

CA-54 **CA-55** **CA-56** **CA-57** **CA-58** **CA-59**

entry	**CA-1-30**	**41aa** (%)	*entry*	**CA-31-59**	**3ae** (%)
1	**CA-1**	0	*31*	**CA-31**	18
2	**CA-2**	0	*32*	**CA-32**	21
3	**CA-3**	0	*33*	**CA-33**	25
4	**CA-4**	0	*34*	**CA-34**	26
5	**CA-5**	0	*35*	**CA-35**	29
6	**CA-6**	0	*36*	**CA-36**	29
7	**CA-7**	0	*37*	**CA-37**	31
8	**CA-8**	0	*38*	**CA-38**	33.5
9	**CA-9**	< 1	*39*	**CA-39**	46
10	**CA-10**	< 2	*40*	**CA-40**	49
11	**CA-11**	< 3	*41*	**CA-41**	49
12	**CA-12**	3.5	*42*	**CA-42**	49
13	**CA-13**	3.5	*43*	**CA-43**	49
14	**CA-14**	3.5	*44*	**CA-44**	50
15	**CA-15**	4	*45*	**CA-45**	50
16	**CA-16**	4	*46*	**CA-46**	51
17	**CA-17**	4	*47*	**CA-47**	51
18	**CA-18**	5.5	*48*	**CA-48**	54
19	**CA-19**	5.5	*49*	**CA-49**	54.5
20	**CA-20**	6	*50*	**CA-50**	57
21	**CA-21**	6.5	*51*	**CA-51**	58
22	**CA-22**	8.5	*52*	**CA-52**	59
23	**CA-23**	8.5	*53*	**CA-53**	60
24	**CA-24**	9.5	*54*	**CA-54**	63
25	**CA-25**	11.5	*55*	**CA-55**	63.5
26	**CA-26**	12	*56*	**CA-56**	67
27	**CA-27**	13	*57*	**CA-57**	67
28	**CA-28**	16	*58*	**CA-58**	68
29	**CA-29**	18	*59*	**CA-59**	68.5
30	**CA-30**	18	*60*	none	6

[a] Reaction conditions: **40a** (1.0 equiv, 0.10 mmol), **39a** (5.0 equiv), **Ru-C1** (10 mol%), $(NMe_4)OC(CF_3)_3$ (2.2 equiv), appropriate carboxylic acid (**CA**, see above), ^{t}BuCN (8 equiv) were stirred under N_2 in a closed vessel at 120 °C for 16 h; yield is evaluated by ^{1}H-NMR using 1,3,5-trimethoxybenzene as internal standard; 99% of free *p*-cymene based on the loading of **Ru-C1** was detected in all the entries.

Table 2.12. Screening of benzoic acid for the arylation **39a** with **40a** with catalyst **Ru-C1**

The optimal loading of benzoate additive in the ruthenium-catalysed arylation of **39a** with **40a** was evaluated employing 3-acetylbenzoic acid (**CA-56**) and catalyst **Ru-C1** adjusting the amount of perfluoro-*tert*-butoxide base (Table 2.13). When the loading of **CA-56** increases from 0 to 0.1 equiv, the yield of **41aa** raises from 6% to 32% (entries 1-2). A further addition of 3-acetylbenzoic acid (0.2 /0.3 equiv, entries 3-4) allowed the biaryl to be formed in 66% and 67% of yield. At higher loadings of **CA-54** (0.4 to 0.75 equiv, entries 5-7) the final yield of product decreases. In entry 8, when the reaction was left for 24 h, no improvement in the final amount of **41aa** was noticed, indicating that the reaction has already stop after 16 h.

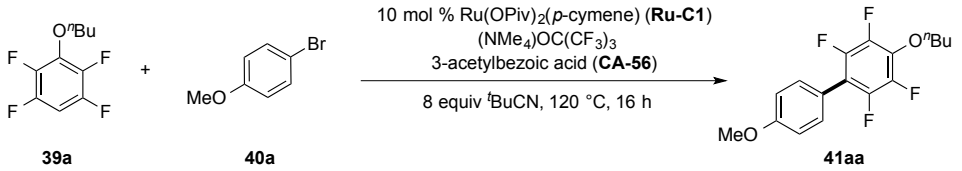

39a **40a** **41aa**

entry	3-acetylbenzoic acid **CA-56** (equiv)	$(NMe_4)OC(CF_3)_3$ (equiv)	**41aa** (%)
1	0	2.0	6
2	0.1	2.1	32
3	**0.2**	**2.2**	**67**
4	**0.3**	**2.3**	**66**
5	0.4	2.4	64
6	0.5	2.5	62
7	0.75	2.75	60
8[b]	0.3	2.3	66

[a] Reaction conditions: **40a** (1.0 equiv, 0.10 mmol), **39a** (5.0 equiv), **Ru-C1** (10 mol%), $(NMe_4)OC(CF_3)_3$ (2.0 equiv), 3-acetylbenzoic acid (see above), ^{t}BuCN (8 equiv) were stirred under N_2 in a closed vessel at 120 °C for 16 h; yield is evaluated by ^{1}H-NMR using 1,3,5-trimethoxybenzene as internal standard; 99% of free *p*-cymene based on the loading of **Ru-C1** was detected in all the entries. [b] Reaction run for 24 h.

Table 2.13. Loading of 3-acetylbenzoic acid (**CA-56**) for the arylation of **39a** with **40a** with catalyst **Ru-C1.**

A temperature screening for the arylation of **39a** with **40a** is shown in Table 2.14. At temperatures below (entries 1-3) and above 120 °C (entries 5-6), the process is lower yielding, providing less that 66% of biaryl product.

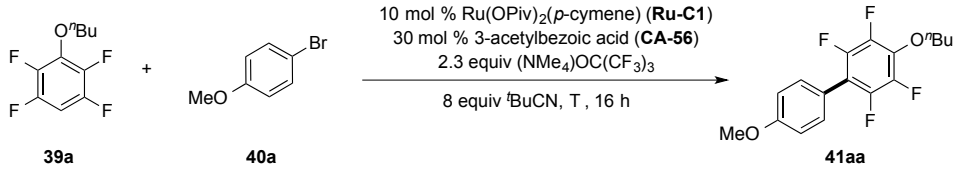

entry	T (° C)	**41aa** (%)
1	90	23
2	100	49
3	110	59
4	**120**	**66**
5	130	64
6	140	56

[a] Reaction conditions: **40a** (1.0 equiv, 0.10 mmol), **39a** (5.0 equiv), **Ru-C1** (10 mol%), $(NMe_4)OC(CF_3)_3$ (2.0 equiv), 3-acetylbenzoic acid (30 mol %), ^{t}BuCN (8 equiv) were stirred under N_2 in a closed vessel at the specified temperature for 16 h; yield is evaluated by ^{1}H-NMR using 1,3,5-trimethoxybenzene as internal standard; 99% of free *p*-cymene based on the loading of **Ru-C1** was detected in all the entries. [b] Reaction run for 24 h.

Table 2.14. Temperature screening for the arylation **39a** with **40a** with catalyst **Ru-C1**

2.5. Role of the (η^6-arene)-ligand and development of a new catalyst

During the optimisation of the reaction, we observed that when using nitrile solvents the *p*-cymene ligand of the ruthenium catalyst was quantitatively recovered as free arene at the end of the reaction.

The thermal- and photo-substitution of (η^6-arenes) in Ru(II) complexes by σ- or π-donor ligands has been known for over 30 years.[143] Particularly, Pfeffer *et al*. in 1999 studied cyclometalation reactions of *N*,*N*-dimethylbenzylamine and 2-phenyl pyridines derivatives using $[Ru(\eta^6\text{-}C_6H_6)Cl_2]_2$ in MeCN solvent for the synthesis of aryl ruthenium species **Ru1-42** and **Ru1-43** (Scheme 2.11). Moreover, they reported arene displacement on [Ru(*o*-C_6H_4-Py)(benzene)(MeCN)]$^+$ (**Ru1-43**) by three MeCN ligands to form [Ru(*o*-C_6H_4-Py)$(MeCN)_4$]$^+$ (**Ru2-43**) and the usefulness of such labile nitriles for ligand-substitution reactions (Scheme 2.11, equation *b*). Intriguingly, *o*-ruthenated *N*,*N*-dimethylbenzylamine did not undergo arene displacement by MeCN, leading the same authors to suggest that the more strongly coordinating character of pyridine is necessary to weaken the benzene–ruthenium bond, thus allowing arene displacement (Scheme 2.11, equation *b*).[141]

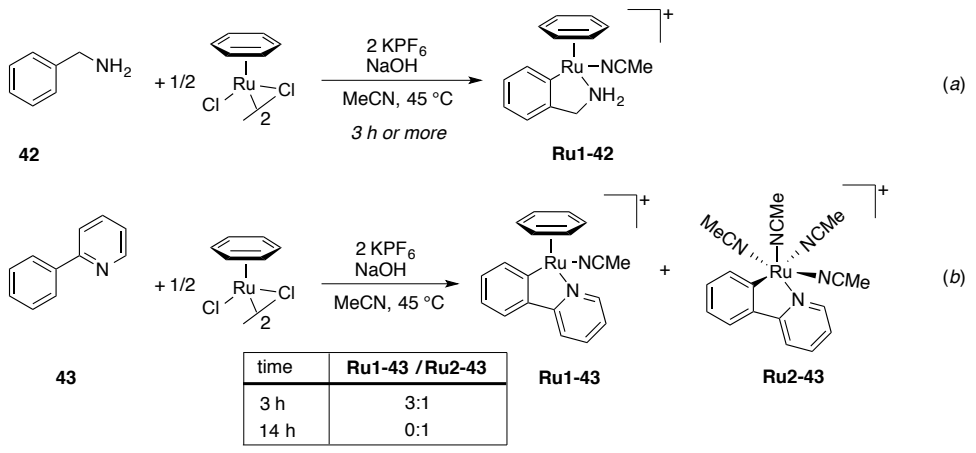

time	Ru1-43 / Ru2-43
3 h	3:1
14 h	0:1

Scheme 2.11. Cyclometalation reactions of **42** and **43** using $[Ru(\eta^6\text{-}C_6H_6)Cl_2]_2$ in MeCN.

Dixneuf, Jutand and co-workers observed identical behaviour on cycloruthenated compounds in MeCN, even at room temperature. Moreover, they established that whereas

the *p*-cymene-containing complex [Ru(*o*-C_6H_4-Py)(*p*-cymene)MeCN]$^+$ (**Ru1'-43**) was able to react with iodobenzene (**I-40b**) to form the cross-coupled biaryl **43b-bis** (Scheme 2.12, equation *a*), the *p*-cymene-free complex [Ru(*o*-C_6H_4-Py)(MeCN)^4]$^+$ (**Ru2-43**) was inert under identical conditions (Scheme 2.12, equation *b*).[137]

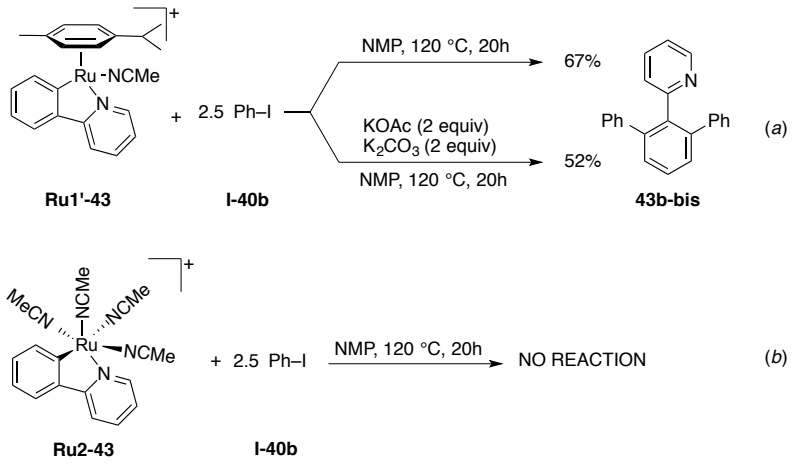

Scheme 2.12. Stoichiometric reactions of **Ru1'-43** and **Ru2-43a** with iodobenzene.

In view of this literature precedent, suggesting that arene dissociation is detrimental to the arylation reaction, we attempted to improve the efficiency of our catalytic system by increasing the stability of the (η^6-arene)-ligand. Towards this aim, since 99% of the (η^6-arene)-ligand of catalysts **Ru-C1** or **Ru-C2** was recovered as free arene after 16 h when nitrile solvents were used in the arylation, Ru(OPiv)$_2$(C_6Me_6) (**Ru-C3**) was prepared and tested. Surprisingly, this catalyst provided **41aa** in only 31% yield, despite being significantly more stable under the reaction conditions, with only 16% of the total C_6Me_6 ligand detected as the free compound at the end of the reaction (Table 2.15, entry 2). Moreover, when Ru(OPiv)$_2$(C_6H_6) (**Ru-C4**) catalyst was tested under identical conditions, biaryl **41aa** was formed in 65% yield along with 99% of free benzene deriving form catalyst **Ru-C4** (entry 3). A matching behaviour was observed when 4-fluorobenzoic acid (**CA-57**) was used in place of 3-acetylbenzoic acid (**CA-56**, entries 4-6).

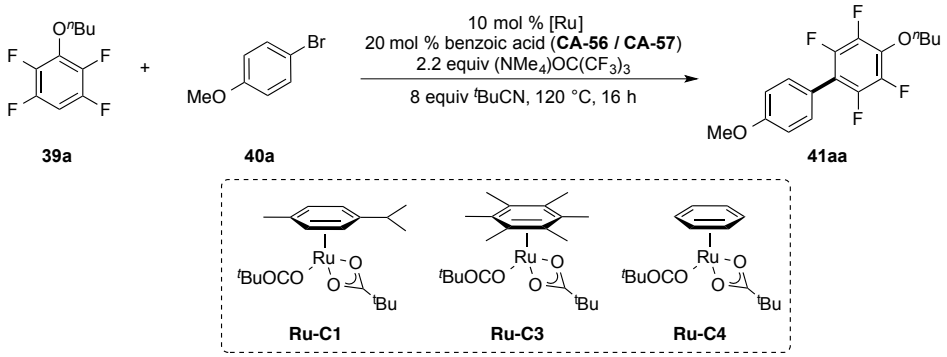

entry	[Ru] (10 mol%)	benzoic acid (20 mol%)	free (η^6-arene) (%)	**41aa** (%)
1	**Ru-C1**	3-acetylbenzoic acid	99	67
2	**Ru-C3**	3-acetylbenzoic acid	16	31
3	**Ru-C4**	3-acetylbenzoic acid	99	65
4	**Ru-C1**	4-fluorobenzoic acid	99	67
5	**Ru-C3**	4-fluorobenzoic acid	14	32
6	**Ru-C4**	4-fluorobenzoic acid	99	66

[a] Reaction conditions: **40a** (1.0 equiv, 0.10 mmol), **39a** (5.0 equiv), specified [Ru] catalyst (10 mol %), $(NMe_4)OC(CF_3)_3$ (2.3 equiv), ^{t}BuCN (8 equiv) were stirred under N_2 in a closed vessel at 120 °C for 16 h; yield is evaluated by ^{1}H-NMR using 1,3,5-trimethoxybenzene as internal standard; % of free (η^6-arene) is based on the loading of [Ru].

Table 2.15. $Ru(OPiv)_2(\eta^6$-arene) catalyst screening for the arylation **39a** with **40a**.

These results serve as first evidence for the detrimental effect of the coordination of the (η^6-arene)-ligand on the Ru-catalyst for the arylation, leading us to hypothesise that, under our reaction conditions, dissociation of the arene ligand could be necessary for the reaction to take place.

Recently, Pilarski *et al*. observed that in the $[RuCl_2(p$-cymene$)]_2$-catalysed arylation of *N*-pyrimidine-protected indoles with boronic acids, observed that some catalytic activity was maintained even after full dissociation of the *p*-cymene ligand (Scheme 2.13).[144]

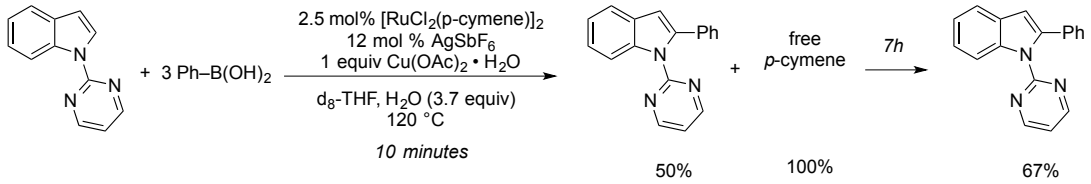

Scheme 2.13. Pilarski mechanistic investigation on the role of the *p*-cymene ligand.

To test this theory, the kinetic profile of the reaction was examined (Table 2.16, Graph 2.7, and Figure 2.4). As shown in Graph 2.7, when 10 mol % of the *p*-cymene-containing catalyst **Ru-C1** was employed, an induction period in formation of **41aa** (purple squares) was observed. This induction period was associated with dissociation of the *p*-cymene ligand (black circles).

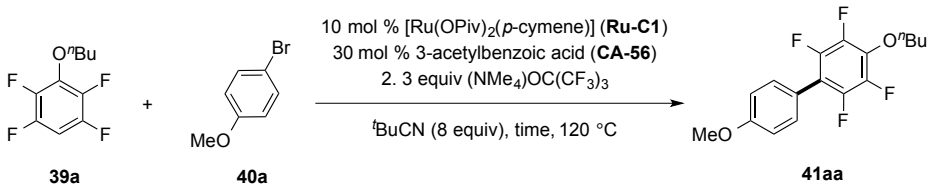

entry	time (min)	free *p*-cymene	**41aa**(%)
1	2	0.8	0.2
2	5	3.8	1.5
3	8	6.0	3.9
4	10	7.0	6.8
5	15	8.4	16.7
6	30	9.9	34.3
7	16 h	9.9	66.2

[a] Reaction conditions: **40a** (1.0 equiv, 0.1 mmol), **39a** (5.0 equiv), **Ru-C2** (10 mol %), 3-acetylbenzoic acid (0.3 equiv), $(NMe_4)OC(CF_3)_3$ (2.3 equiv), ^{t}BuCN (8.0 equiv) were stirred under N_2 in a closed vessel at 120 °C for the appropriate time; yield is evaluated by ^{1}H-NMR using 1,3,5-trimethoxybenzene as internal standard; % of free (η^6-arene) is based on the loading of **Ru-C2**.

Table 2.16. Kinetic profile for the arylation of **39a** with **40a** employing catalyst **Ru-C1**.

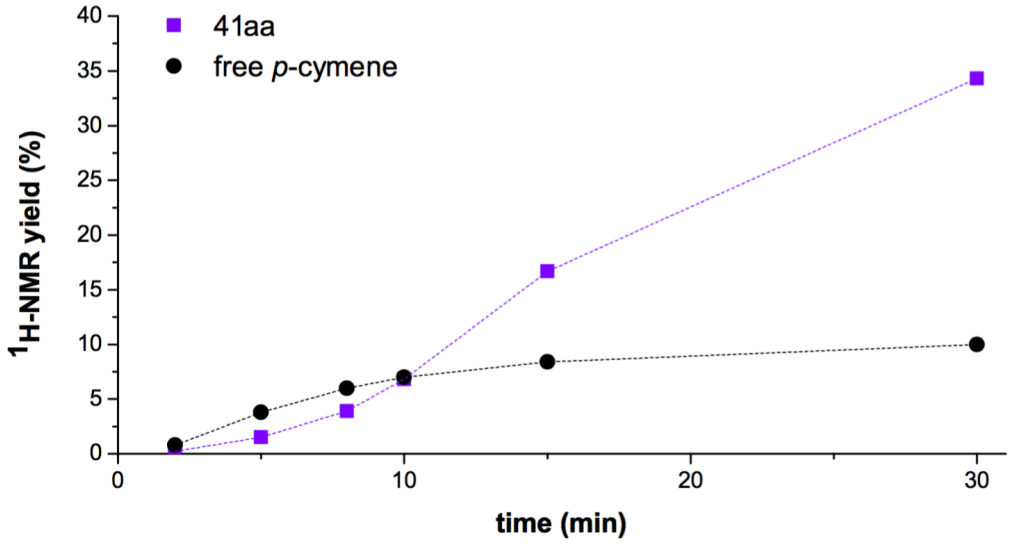

Graph 2.7. Cross-coupling of **39a** and **40a** with *p*-cymene-containing catalyst **Ru-C1**. Reaction conditions: see **Table 2.16**.

^{1}H-NMR analysis (Figure 2.4, *left hand side*) shows the quick formation of several unknown ruthenium *p*-cymene complexes together with **Ru1-39a**. **Ru-C1** is rapidly consumed after 5 min, while **Ru1-39a**, which starts forming at the very beginning of the reaction, has disappeared after 30 min. ^{19}F-NMR (Figure 2.4, *right hand side*) confirms the formation of **Ru1-39a** and its consumption with the concomitant appearance of a new aryl-Ru complex (**Ru2-39a**).

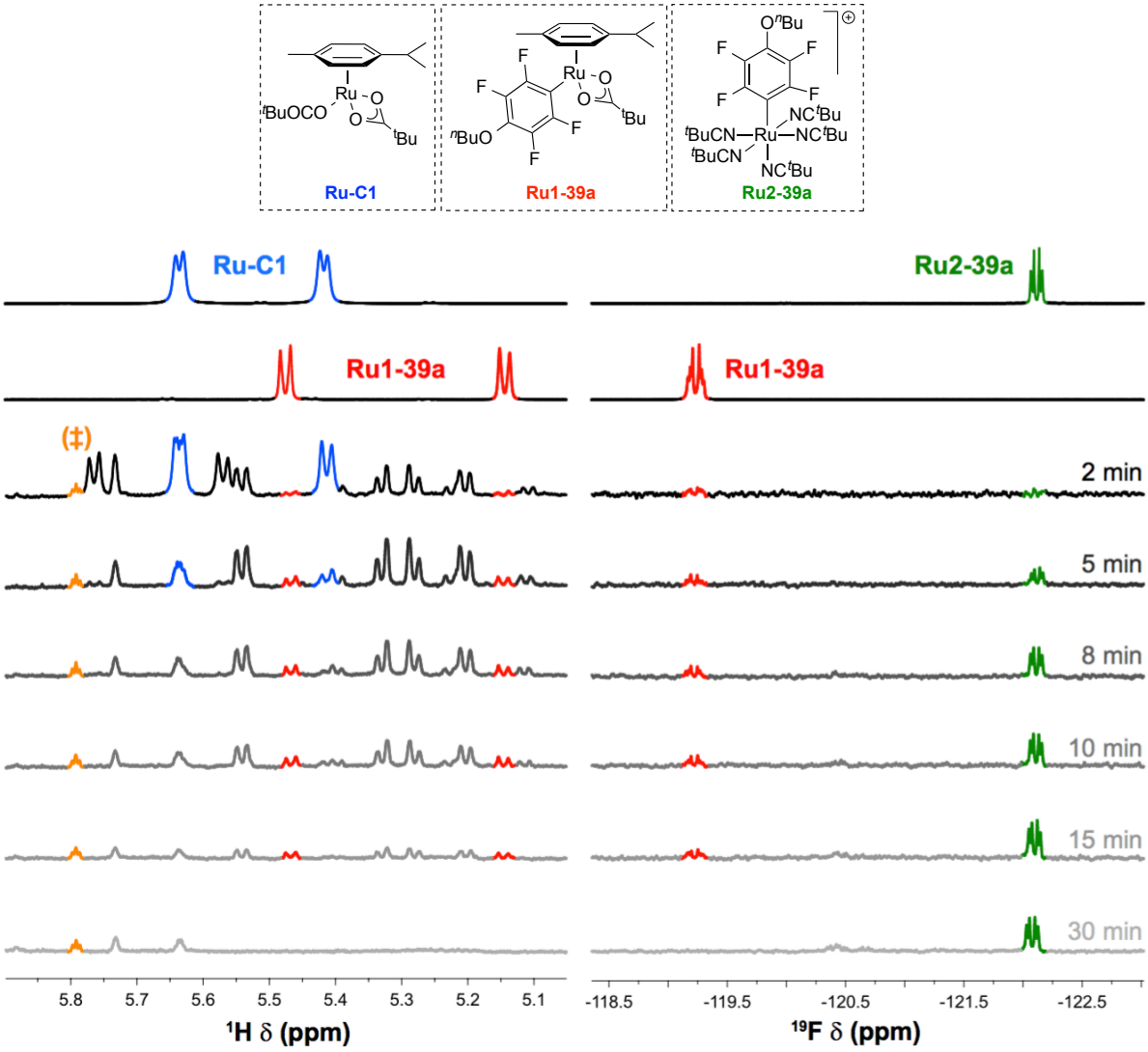

Figure 2.4. Time-dependent NMR experiments (reaction conditions as described in **Table 2.16**). *Left-hand side*: ^{1}H-NMR expansion of the AB system region of Ru-coordinated *p*-cymene: **Ru-C1** (blue), **Ru1-39a** (red), ‡ satellite peak of the singlet associated to 1,3,5-trimethoxybenzene internal standard. *Right-hand side*: ^{19}F-NMR expansion of fluoroaryl-ruthenium complexes region: **Ru1-39a** (red), **Ru2-39a** (green).

Independent synthesis, by thermal replacement of the *p*-cymene ligand of **Ru1-39a** with ^{t}BuCN, confirmed the newly formed species to be *p*-cymene-free aryl-Ru complex **Ru2-39a**.

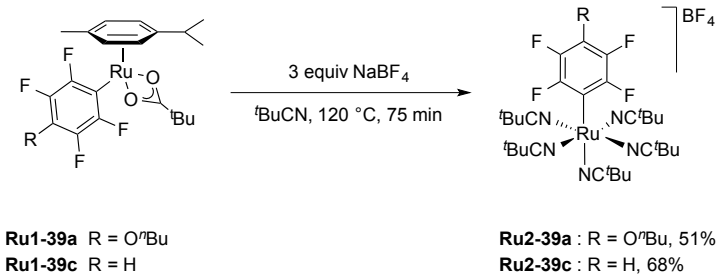

Scheme 2.14. Synthesis of **Ru2-39a** and **Ru2-39c** by thermal ligand substitution.

Furthermore, the structure of the cationic nitrile-containing intermediate was confirmed by X-ray analysis of the analogous complex **Ru2-39c** (Figure 2.5).

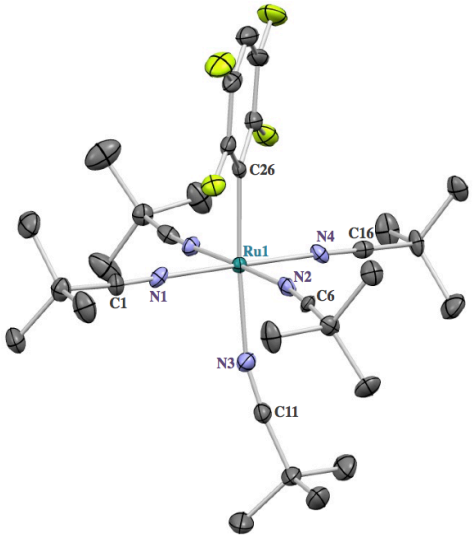

Figure 2.5. ORTEP diagram of **Ru2-39c** at 50% ellipsoids. Selected bond lengths [Å]: Ru(1)–C(26) 2.074; Ru(1)–N(1) 2.009; Ru(1)–N(2) 2.020; Ru(1)–N(3) 2.105; N(1)–C(1) 1.132; N(2)–C(6) 1.147; N(3)–C(11) 1.142. Selected bond angles [°]: C(26)–Ru(1)–N(4) 90.48; N(4)–Ru(1)–N(2) 91.96; N(1)–Ru(1)–N(2) 88.47; N(1)–Ru(1)–N(3) 92.69; C(6)–N(2)–Ru(1) 171.71; C(1)–N(1)–Ru(1) 174.94; C(11)–N(3)–Ru(1) 165.76.[145]

These data indicate that Ru(OPiv)$_2$(*p*-cymene) (**Ru-C1**) is able to perform C−H activation on perfluoroarene **39a** generating the aryl ruthenium species **Ru1-39a** in ^{t}BuCN. **Ru1-39a**, in turn, must lose its *p*-cymene ligand forming cationic intermediate **Ru2-39a**, which then reacts with 4-bromoanisole **40a**, yielding the biaryl product **41aa**. Formation of **41aa** continues after complete loss of *p*-cymene, so a nitrile-coordinated Ru(II) species should also perform C−H activation in the absence of *p*-cymene.

This experimental observation led us to design a (η^6-arene)-ligand free Ru(II) catalyst to simplify and potentially improve our catalytic system. Hence, we synthesised [Ru(^{t}BuCN)$_6$][BF$_4$]$_2$ (**Ru-C5**) from RuCl$_3$ · ×H$_2$O, the structure of which was confirmed by single crystal X-ray analysis.

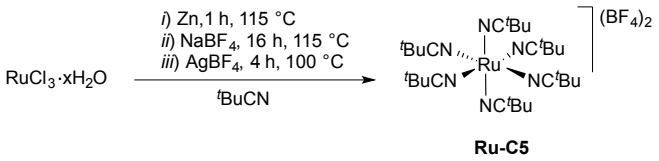

Scheme 2.15. Synthesis of hexakis(pivalonitrile-*k*-*N*)ruthenium(II) bis(tetrafluoroborate) **(Ru-C5)**.

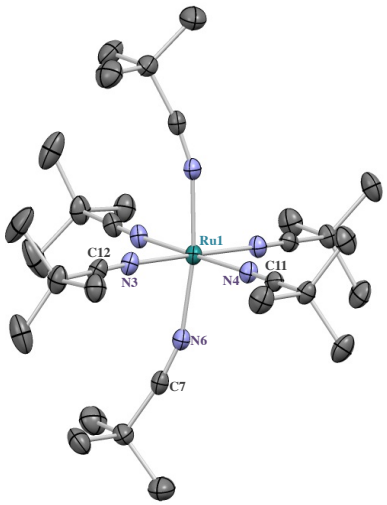

Figure 2.6. ORTEP diagram of **Ru-C5** at 50% ellipsoids. Selected bond lengths [Å]: Ru(1)–N(3) 2.012; Ru(1)–N(4) 2.025; Ru(1)–N(6) 2.015. Selected bond angles [°]: C(11)–N(4)–Ru(1) 172.55; C(12)–N(3)–Ru(1) 173.45; C(7)–N(6)–Ru(1) 162.29.[146]

Subsequently, time-dependent experiments with catalyst **Ru-C5**, under comparable reaction conditions to those used with catalyst **Ru-C1**, were conducted (Table 2.17, Graph 2.8, and Figure 2.7).

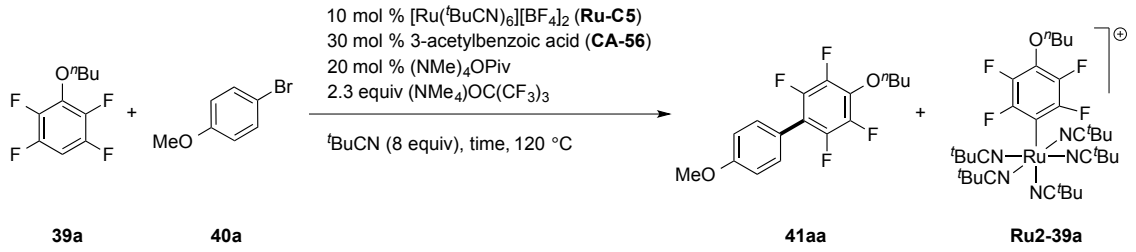

entry	time (min)	**41aa**(%)	**Ru2-39a** (%)
1	2	0.8	NA
2	5	8.4	NA
3	8	13.4	NA
4	10	16.7	NA
5	15	23.9	NA
6	30	38.1	5.0
7	16 h	72.4	NA

[a] Reaction conditions: **40a** (1.0 equiv, 0.1 mmol), **39a** (5.0 equiv), **Ru-C5** (10 mol %), 3-acetylbenzoic acid (0.3 equiv), $(NMe_4)OPiv$ (0.2 equiv), $(NMe_4)OC(CF_3)_3$ (2.3 equiv), ^{t}BuCN (8.0 equiv) were stirred under N_2 in a closed vessel at 120 °C for the appropriate time; yield is evaluated by ^{1}H-NMR using 1,3,5-trimethoxybenzene as internal standard and also by quantitative ^{19}F-NMR using hexafluorobenzene as internal standard for entry 6.

Table 2.17. Kinetic profile for the arylation of **39a** with **40a** employing catalyst **Ru-C5**.

Graph 2.8 (reaction conditions A, purple triangles) shows the formation of biaryl **41aa** from the very start of the reaction without an evident induction period. ^{19}F-NMR spectra in Figure 2.7 (*top left*) display **Ru2-39a** as the only visible aryl ruthenium species throughout the reaction. Inspection of the ^{19}F-NMR spectrum of the reaction after 30 min (Figure 2.7, *full figure*), reveals that 50% of the ruthenium loaded at the beginning of the reaction is in the form of **Ru2a**, suggesting that this complex may be a resting state of the catalytic cycle (Table 2.17, entry 6).

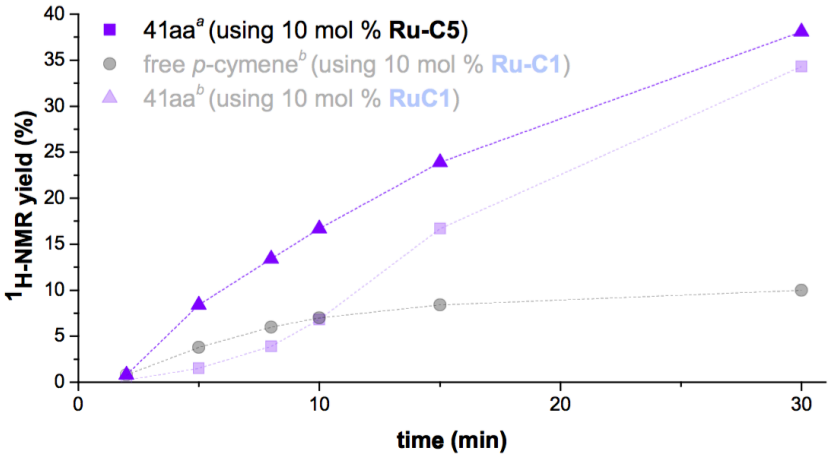

Graph 2.8. Cross-coupling of **39a** and **40a** with nitrile-containing catalyst **Ru-C5**. [a] Reaction conditions: see **Table 2.17**. [b] Reaction conditions: see **Table 2.16**.

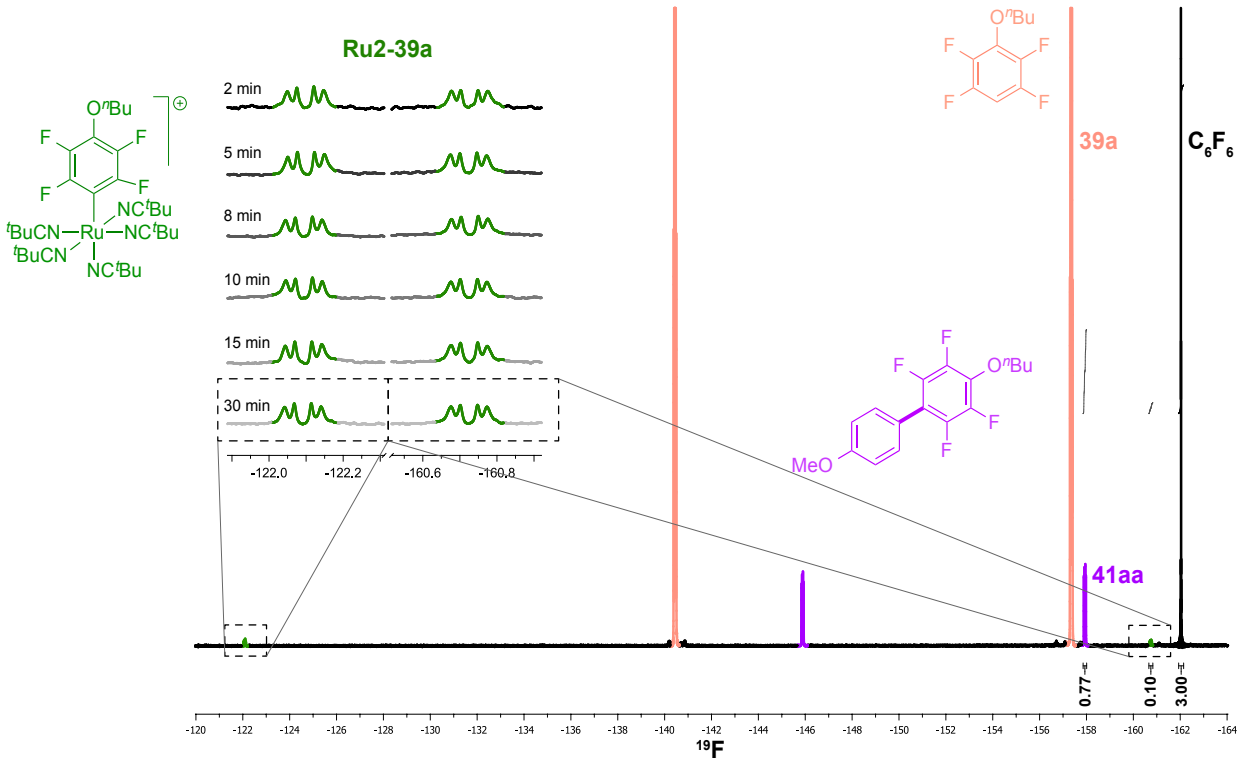

Figure 2.7. Time-dependent experiments (see **Table 2.17**). *Top left*: ^{19}F-NMR expansion of **Ru2-39a** region (green). *Full figure*: ^{19}F-NMR of the reaction stopped after 30 min (entry 6), showing **Ru2-39a**, **41aa** (purple), **39a** (pink) and C_6F_6 (black) used as internal standard (0.5 equiv, 0.05 mmol).

2.6. $[Ru(^tBuCN)_6][BF_4]_2$-catalysed C–H arylation of fluoroarenes with aryl halides

Having established that the catalytic system formed by $[Ru(^tBuCN)_6][BF_4]_2$ (**Ru-C5**)/$(NMe_4)OPiv$ is superior to the one constituted by $Ru(OPiv)_2$(*p*-cymene) (**Ru-C1**) (Scheme 2.16, and entries 6 of Table 2.16/Table 2.17), we then returned to the optimisation of the arylation conditions employing the bench-stable and easy-to-prepare nitrile-containing catalyst **Ru-C5**. We chose the equally reactive and readily available 4-fluorobenzoic acid over 3-acetylbenzoic acid and we prepared its corresponding tetramethylammonium salt in order to ease the screening. Also, bromobenzene (**40b**) was selected as the coupling partner, in place of the more electron-rich 4-bromoanisole (**40a**).

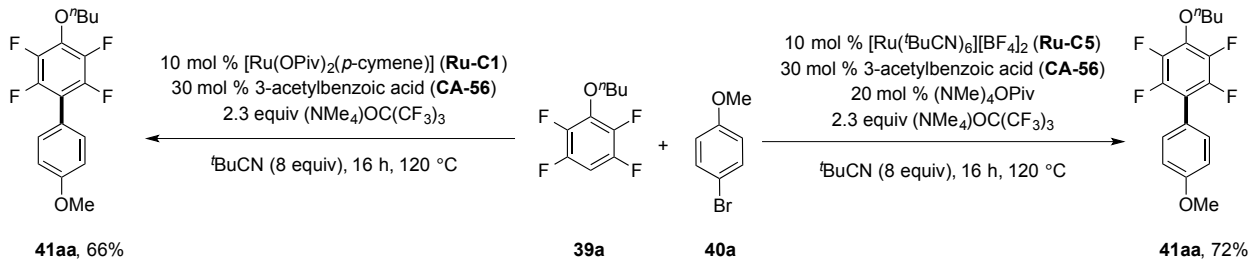

Scheme 2.16. Comparison of catalysts **Ru-C1** and **Ru-C5**.

Similarly to $Ru(OBz)_2$(*p*-cymene) (**Ru-C2**) in Table 2.11, when catalyst **Ru-C5** was used without pivalate (Table 2.18 entry 1, 59% yield of biaryl **41ab**) the arylation efficiency was lower than in entry 2 where 0.2 equiv of $(NMe_4)OPiv$ were added (entry 2, 72% yield).

We then decided to screen the loading of perfluoroarene **39a**, aiming to increase the atom economy of the process (Table 2.18). Gratifyingly, 3 or 5 equiv of **39a** provided identical amounts of biaryl **41ab** (entries 5 and 2). However, a lower loading of perfluoroarene **39a** (1 or 2 equiv, entries 3-4) led to a reduction of the yield.

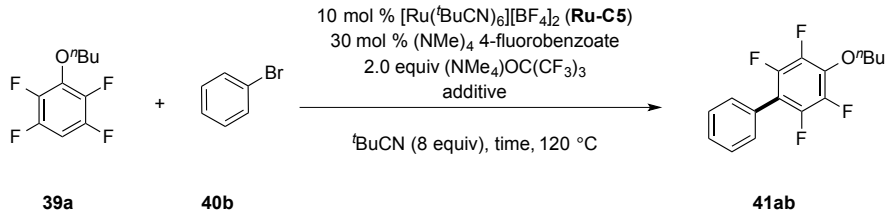

entry	**39a** (equiv)	additive (equiv)	**41ab**(%)
1	5	none	59
2	5	$(NMe_4)OPiv$ (0.2)	72
3	1	$(NMe_4)OPiv$ (0.2)	45
4	2	$(NMe_4)OPiv$ (0.2)	63
5	3	$(NMe_4)OPiv$ (0.2)	72

[a] Reaction conditions: **40b** (1.0 equiv, 0.5 mmol), **39a** (see above), **Ru-C5** (10 mol %), (NMe_4) 4-fluorobenzoate (0.3 equiv), the appropriate additive (see above), $(NMe_4)OC(CF_3)_3$ (2.0 equiv), ^{t}BuCN (8.0 equiv) were stirred under N_2 in a closed vessel at 120 °C for 16 h; yield is evaluated by ^{1}H-NMR using 1,4-dintrobenzene as internal standard.

Table 2.18. The role of the pivalate additive for the arylation of **39a** with **40b** employing catalyst **Ru-C5** and the screening of the loading of perfluoroarene **39a**.

When 2.5 mol % of **Ru-C5**, 0.6 equiv of (NMe_4) 4-fluorobenzoate, 0.4 equiv of $(NMe_4)OPiv$, 2.2 equiv of $(NMe_4)OC(CF_3)_3$ and 8 equiv of ^{t}BuCN were used, biaryl **41ab** was formed in 62% yield (Table 2.19, entry 1). Fine-tuning of the loading of pivalonitrile solvent/ligand revealed that 3 equiv was the optimal amount, increasing the yield of **41ab** to 72% (Table 2.19, entry 5). However, when the loading of ^{t}BuCN was higher or lower than 3 equiv a drop in yield was observed.

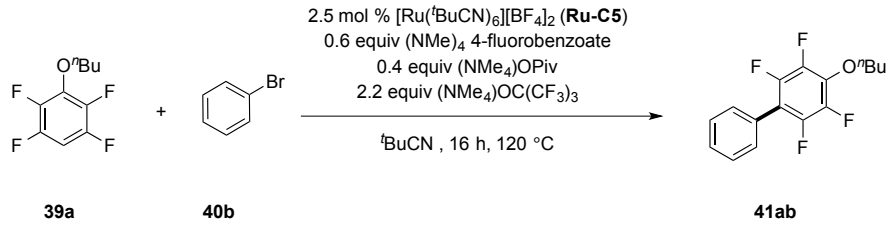

entry	^{t}BuCN (equiv)	**41ab**(%)
1	8	61
2	0	4
3	1	20
4	2	60
5	3	72
6	4	66
8	6	64
10	10	60

[a] Reaction conditions: **40b** (1.0 equiv, 0.5 mmol), **39a** (3.0 equiv), **Ru-C5** (2.5 mol %), (NMe_4) 4-fluorobenzoate (0.6 equiv), (NMe_4)OPiv (0.4 equiv), (NMe_4)$OC(CF_3)_3$ (2.2 equiv), ^{t}BuCN (see aboove) were stirred under N_2 in a closed vessel at 120 °C for 16 h; yield is evaluated by ^{1}H-NMR using 1,4-dintrobenzene as internal standard.

Table 2.19. Screening of the loading of pivalonitrile in the arylation of **39a** with **40b** employing catalyst **Ru-C5**.

The loading of **Ru-C5** was also screened. The yield of product **41ab** constantly improved from 66% up to 80% as we increased the amount of **Ru-C5** from 2.0 to 4.0 mol % (Table 2.20, entries 1-5). Higher loading of catalyst proved to be ineffective for improving the yield of biaryl **41ab**.

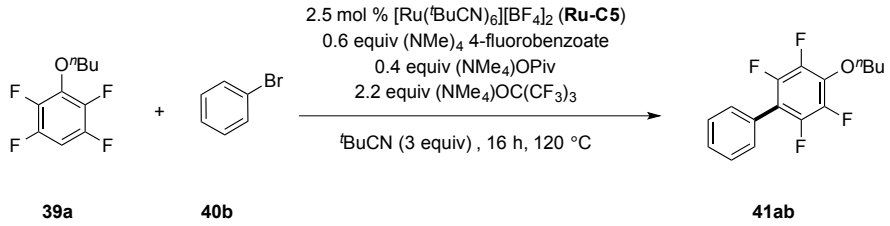

entry	$[Ru(^tBuCN)_6][BF_4]$ (**Ru-C5**) (mol %)	**41ab**(%)
1	2.0	66
2	2.5	72
3	3.0	75
4	3.5	77
5	4.0	80
6	4.5	80
7	5.0	80

[a] Reaction conditions: **40b** (1.0 equiv, 0.5 mmol), **39a** (3.0 equiv), **Ru-C5 (**see above), (NMe_4) 4-fluorobenzoate (0.6 equiv), $(NMe_4)OPiv$ (0.4 equiv), $(NMe_4)OC(CF_3)_3$ (2.2 equiv), ^{t}BuCN (3.0 equiv) were stirred under N_2 in a closed vessel at 120 °C for 16 h; yield is evaluated by ^{1}H-NMR using 1,4-dintrobenzene as internal standard.

Table 2.20. Screening of the loading of catalyst **Ru-C5** in the arylation of **39a** with **40b**

By keenly adjusting the relative amounts of (NMe_4) 4-fluorobenzoate, $(NMe_4)OPiv$ and $(NMe_4)OC(CF_3)_3$ to 0.35, 0.4, and 2.5 equiv a further improvement in the yield of biaryl **41ab** was accomplished (82%, Table 2.21, entry 1). Adopting identical reaction conditions, a screening of reaction temperatures was carried out. Temperatures between 105 and 120 °C led to comparable amount of biaryl **41ab** (Table 2.21, entries 1-5). 115 °C was found to be the best compromise providing 82% NMR and 76% isolated yield of **41ab** (entry 1).

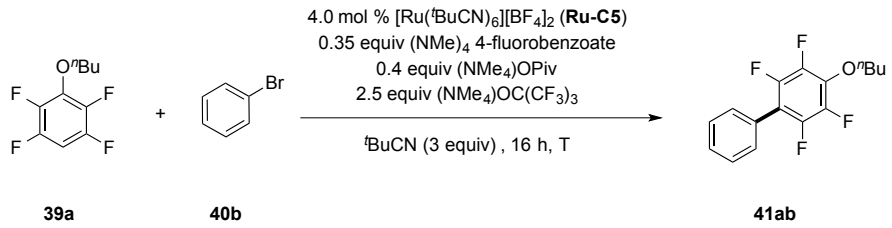

entry	T (° C)	**41ab**(%)
1	120	82
2	100	74
3	105	80
4	110	81
5	115	82 (76)
6	130	74

[a] Reaction conditions: **40b** (1.0 equiv, 0.5 mmol), **39a** (3.0 equiv), **Ru-C5** (4.0 mol %), (NMe_4) 4-fluorobenzoate (0.35 equiv), (NMe_4)OPiv (0.4 equiv), (NMe_4)$OC(CF_3)_3$ (2.5 equiv), ^{t}BuCN (3.0 equiv) were stirred under N_2 in a closed vessel at 120 °C for 16 h. Yield is evaluated by ^{1}H-NMR using 1,4-dintrobenzene as internal standard; yield in parenthesis refers to isolated material.

Table 2.21. Screening of the temperature for the arylation of **39a** with **40b** employing catalyst **Ru-C5**.

When the arylation of **39a** with **40b** was conducted under strictly anhydrous conditions in a glove box, the yield of biaryl **41ab** was comparable with a normal reaction run employing standard Schlenk techniques (Table 2.22, entry 2). Instead the process is not compatible with the presence of oxygen or TEMPO (entries 3-4). Finally, similarly our obesrvations in Table 2.21 (entry 5), the arylation was completely shut down when (NMe_4) 4-fluorobenzoate was omitted from the standard reaction conditions.

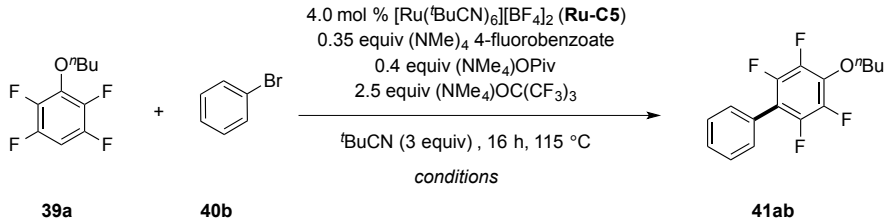

39a **40b** **41ab**

entry	*conditions*	**41ab**(%)
1[a]	standard	82 (76)
2[b]	glove box	81
3[c]	under air	0
4[d]	TEMPO (1 equiv)	< 1
5[e]	without (NMe_4) 4-fluorobenzoate	0

[a] Standard reaction conditions: **40b** (1.0 equiv, 0.5 mmol), **39a** (3.0 equiv), **Ru-C5** (4.0 mol %), (NMe_4) 4-fluorobenzoate (0.35 equiv), (NMe_4)OPiv (0.4 equiv), (NMe_4)$OC(CF_3)_3$ (2.5 equiv), ^{t}BuCN (3.0 equiv) were stirred under N_2 in a closed vessel at 115 °C for 16 h. [b] Glove box. [c] Under air. [d] TEMPO (1 equiv). [e] Without (NMe_4) 4-fluorobenzoate. Yield is evaluated by ^{1}H-NMR using 1,4-dintrobenzene as internal standard; yield in parenthesis refers to isolated material.

Table 2.22. Effect of water, oxygen or TEMPO in the arylation of **39a** with **40b** employing catalyst **Ru-C5**.

2.7. Reactivity of aryl ruthenium species Ru1-39c and Ru2-39c

To further probe the surprising role of the benzoate additive, we attempted a stoichiometric reaction between the preformed cationic tetrafluorophenyl-Ru complex **Ru2-39c** and 5-bromo-*m*-xylene (**40c**) (Table 2.23). Interestingly, the cationic intermediate **Ru2-39c** does not react with the aryl bromide unless the benzoate additive is present in the mixture (entry 4), giving 35.0 % yield of biaryl **41cc** and 13.5% of the bis-arylated adduct **41cc'**. In fact it proved to be inert with no additive, $(NMe_4)OPiv$ or $(NMe_4)OC(CF_3)_3$ (entries 1-3). This implies that the benzoate additive is fundamental to the formal oxidative addition step, but not for the metalation of the substrate.

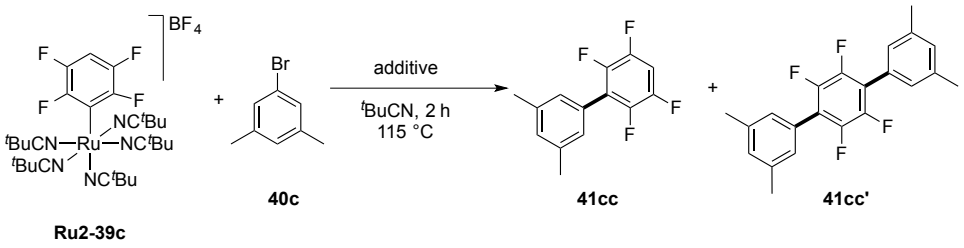

entry	additive (2.5 equiv)	**41cc (%)**	**41cc'** (%)
1	no additive	0	0
2	$(NMe_4)OC(CF_3)_3$	0	0
3	$(NMe_4)OPiv$	0	0
4	(NMe_4) 4-fluorobenzoate	35	13.5

[a] Reaction conditions: **Ru-39c** (1.0 equiv, 0.03 mmol), **40c** (3.0 equiv), additive (if any, 2.5 equiv) were stirred under N_2 in a closed vessel at 115 °C for 2 h. yield is evaluated by quantitative ^{19}F-NMR using octafluorotoluene as internal standard.

Table 2.23. Reactivity of **Ru2-39c** with bromoarene **40c** under stoichiometric conditions

In stark contrast with the observations of Dixneuf and Jutand, a *p*-cymene-free aryl-Ru(II) complex can react with aryl halides (see Scheme 2.12).[137] However, the same authors reported in a follow up paper that a *p*-cymene-containing cycloruthenated 1-phenylpyrazole

species reacted with iodobenzene only in the presence of K_2CO_3 and KOAc additives (Scheme 2.17).[147] Although an explanation for this behaviour was not given, decomposition of the aryl ruthenium species, leading to catalytic-like conditions cannot be ruled out. Interestingly, the analogous cycloruthenated 2-PhPy complex reacted under similar conditions, also in the absence of any additives (see Scheme 2.12).[137]

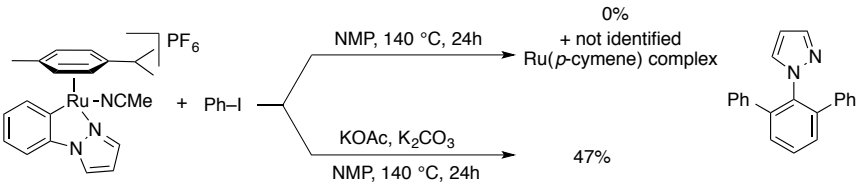

Scheme 2.17. Stoichiometric arylation experiments of cyclometalated 1-phenylpyrazole with Ph-I.

To confirm the intermediacy of the fluoroaryl-Ru complexes in the reaction, the direct arylation of tetrafluorotoluene **39d** with *m*-bromoxylene (**40c**) was studied using the tetrafluorophenyl- containing unit species **Ru2-39c** and **Ru1-39c** as catalysts (Table 2.24). In entry 1, even in the presence of a large excess of **39d** (30 equiv with respect to the cationic catalyst **Ru2-39c**), nearly quantitative formation of the products from arylation of tetrafluorobenzene (**41cc** and **41cc'**) was observed, along with 78% yield of biaryl product deriving from tetrafluorotoluene (**41dc**). This result strongly supports that the fluoroaryl-Ru complex is an active intermediate in the reaction. Analogous behaviour was also observed for catalyst **Ru1-39c**, although it revealed itself to be less efficient than **Ru2-39c** because of its requirement to lose its *p*-cymene ligand before entering in the arylation catalytic cycle (entry 2).

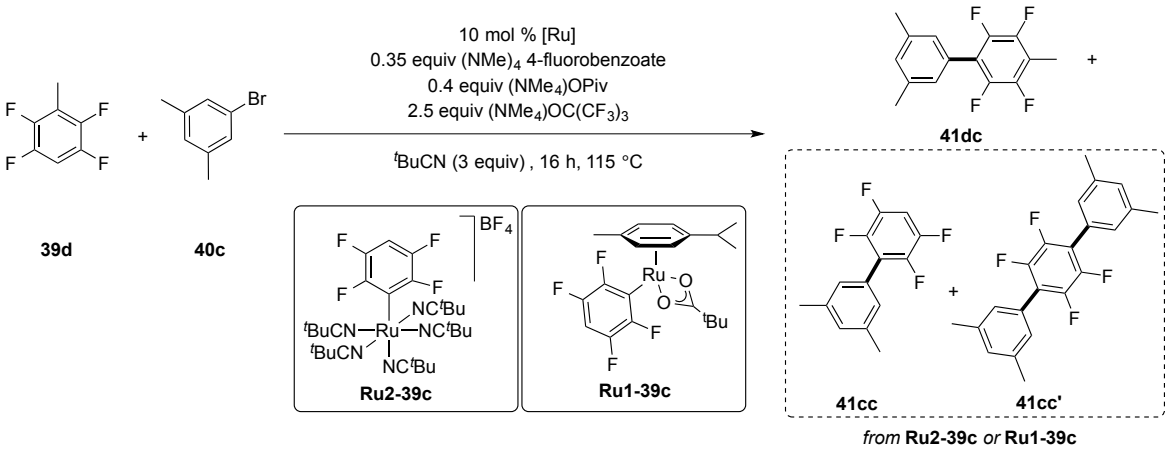

entry	[Ru] (10 mol%)	**41dc (%)**	**41cc (%)**	**41cc'** (%)
1	**Ru2-39c**	78.0	4.0	4.0
2[b]	**Ru1-39c**	70.5	2.5	1.5

[a] Reaction conditions: **40c** (1.0 equiv, 0.5 mmol), **39d** (3.0 equiv), [Ru] see above (10 mol %), (NMe_4) 4-fluorobenzoate (0.35 equiv), (NMe_4)OPiv (0.4 equiv), (NMe_4)$OC(CF_3)_3$ (2.5 equiv), ^{t}BuCN (3.0 equiv) were stirred under N_2 in a closed vessel at 115 °C for 16 h. Yield is evaluated by quantitative ^{19}F-NMR using C_6F_6 as internal standard. [b] (NMe_4)OPiv (0.3 equiv).

Table 2.24. Reactivity of **Ru2-39c** and **Ru1-39c** with bromoarene **40c** under catalytic conditions.

2.8. Scope of the Ru-catalysed direct arylation of fluoroarenes with aryl halides

With the optimal reaction conditions in hand, we explored the compatibility of our protocol with a variety of functionalities on the aryl bromide coupling partner for the arylation of pentafluorobenzene (**39b**) (Scheme 2.18). The reaction works in the presence of a wide range of substituents in the *ortho*, *meta*, and *para* positions, affording the corresponding biaryl products **41ba**-**41bv** in moderate to excellent yields. Generally, *ortho*-substituted bromides and electron-poor aryl halides are less reactive. Notably, sensitive functional groups such as COMe (**41bn**), COOMe (**41bo**), SMe (**41bl**), NMe_2 (**41bm**) as well as terminal (**41br**) and internal alkenes (**41bs**) are tolerated. Some reactivity is also observed with a cyano substituent (**41bv**), however -NO_2, -CHO, -OH groups and terminal alkynes (**41bw**-**41bz**) are not compatible with the system. In addition to aryl bromides, iodides and chlorides can also be used as coupling partners (**41bb**). Conversely, pseudohalides PhOTs and PhOMs did not afford biaryl **41bb**. *o*,*o*-Disubstituted aryl halides are unreactive in our system, allowing the iodine-containing product **41bq** to be formed in good yield. The latter could be further functionalised by other coupling reactions. Finally, bromoarenes **40a'**-**40c'**, which are prone to cyclise under palladium[148] or base/phenanthroline catalysis,[149] to form 5- or 6-membered adducts *via* intramolecular C–H arylation, exhibited complete selectivity towards the intermolecular process (**41ba'**-**41bc'**) displaying a unique characteristic of our system. Contrary to what is seen with palladium, with ruthenium the metalation of the substrate occurs before the formal oxidative addition step. The reverse sequence of these fundamental steps is the reason behind the total selectivity towards the intermolecular C–H arylation process.

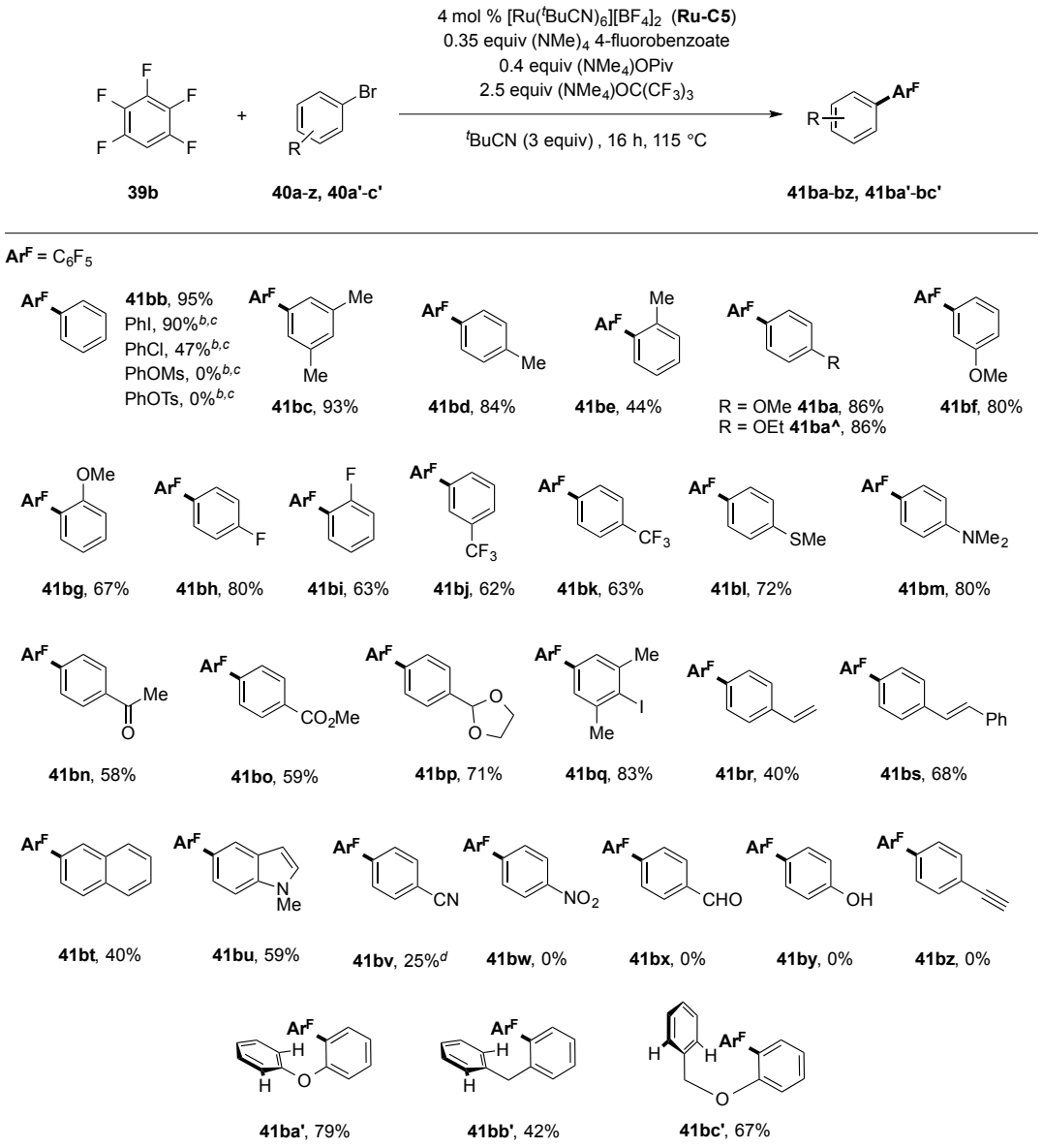

[a] Reaction conditions: Bromoarene **40** (1.0 equiv, 0.5 mmol), **39b** (3.0 equiv), (NMe_4) 4-fluorobenzoate (0.35 equiv), $(NMe_4)OPiv$ (0.4 equiv), $(NMe_4)OC(CF_3)_3$ (2.5 equiv), **Ru-C5** (4 mol %) and ^{t}BuCN (3.0 equiv) stirred at 115 °C under N_2 in a closed vessel for 16 h. Yields of pure, isolated products. [b] Yield estimated by ^{1}H-NMR with dibromomethane as internal standard. [c] Performed with 1.0 equiv of the stated PhX instead of **40b**. [d] **Ru-C5** (8 mol %), reaction time 1 h.

Scheme 2.18. Scope of the Ru-catalysed arylation of **39b** with bromoarenes **40a-z**, **40a'-c'**.

We then turned our attention to the generality of this methodology, with respect to the (fluoro)arene partner (Scheme 2.19). The functional group tolerance is the same as for the aryl bromides (**41dc**-**41ic**). Interestingly, the regioselectivity of arylation is different from

that reported by Fagnou[22] and Daugulis[33] for Pd and Cu catalysis. For Cu the most acidic proton preferentially undergoes C−H arylation. In fact, the methodology introduced by Daugulis is a base-promoted C–H activation, which relies on alkali metal bases to deprotonate the C_{Ar}–H bond. In view of this, two *ortho* electron-withdrawing groups are required to increase the acidity of C_{Ar}–H bond and strong bases such as *tert*-butoxide are sometimes needed. Fagnou's protocol is based on a concerted metalation-deprotonation, in which an aryl palladium(II) generated by oxidative addition from an aryl halide, is responsible for the C–H activation. As discussed in Chapter 1 (see section 1.4.1.2), for most of the arenes in Class I (this class includes fluoroarenes) and in Class II, the arylation occurs at the most acidic C–H bond.[31] Instead, with ruthenium the selectivity for the most acidic proton is less pronounced, with the substrate's steric bulk also having an important effect. This may be attributed to the larger steric demand of the octahedral Ru(II) species, when compared with the four-coordinate Cu and Pd complexes. A similar behaviour has been described for octahedral rhodium and iridium complexes, which display a sterically-controlled selectivity (Chapter 1, see section 1.4.3). Under our conditions, tetrafluorobenzene derivatives display excellent reactivity (**41aa**, **41cc**-**41kc**). 1,2,3,5- and 1,2,3,4-tetrafluorobenzene, selectively provided the mono arylated products in good yield (**41jc** and **41kc**). In contrast, 1,2,3,5-tetrafluorobenzene generates bis-arylated adduct with either Pd or Cu. Similarly, 1,2,3,4-tetrafluorobenzene, having only one *ortho* fluorine atom, is poorly reactive with Cu, and with Pd the bis-arylation cannot be avoided. Further differences can be observed for the tri- and di-fluorobenzene series (**41lc**-**41oc**, **41uc**-**41vc**). Symmetric 1,3,5-trifluorobenzene and 1,4-difluorobezene do not give bis/tris-arylation (**41lc** and **41uc**) as otherwise seen with Pd. 1,2,4-trifluorobenzene provides three isomers in a 1:0.95:0.13 ratio with 5% of bisarylated adduct (**41mc**), 1,2,3-trifluorobenzene affords two isomers in a 1:0.3 ratio (**41nc**) and 1,3-difluorobenzene generates three isomers in a ratio 1:0.63:0.25 (**41vc**). Additionally, when tri- and di-fluorobenzene analogues bearing a trifluoromethyl group where tested (**41pc**-**41tc**), the arylation selectively took place at the least hindered position of those having one *ortho* fluorine substituent. Only traces of **41wc** were observed with fluorobenzene, and benzene (**41xc**) was completely inert. Heteroaromatic compounds bearing an acidic proton, such as benzo[*b*]thiophene and

caffeine, underwent arylation under identical reaction conditions (**44b**, **45c**), proving to be unreactive when (NMe_4) 4-fluorobenzoate was omitted.

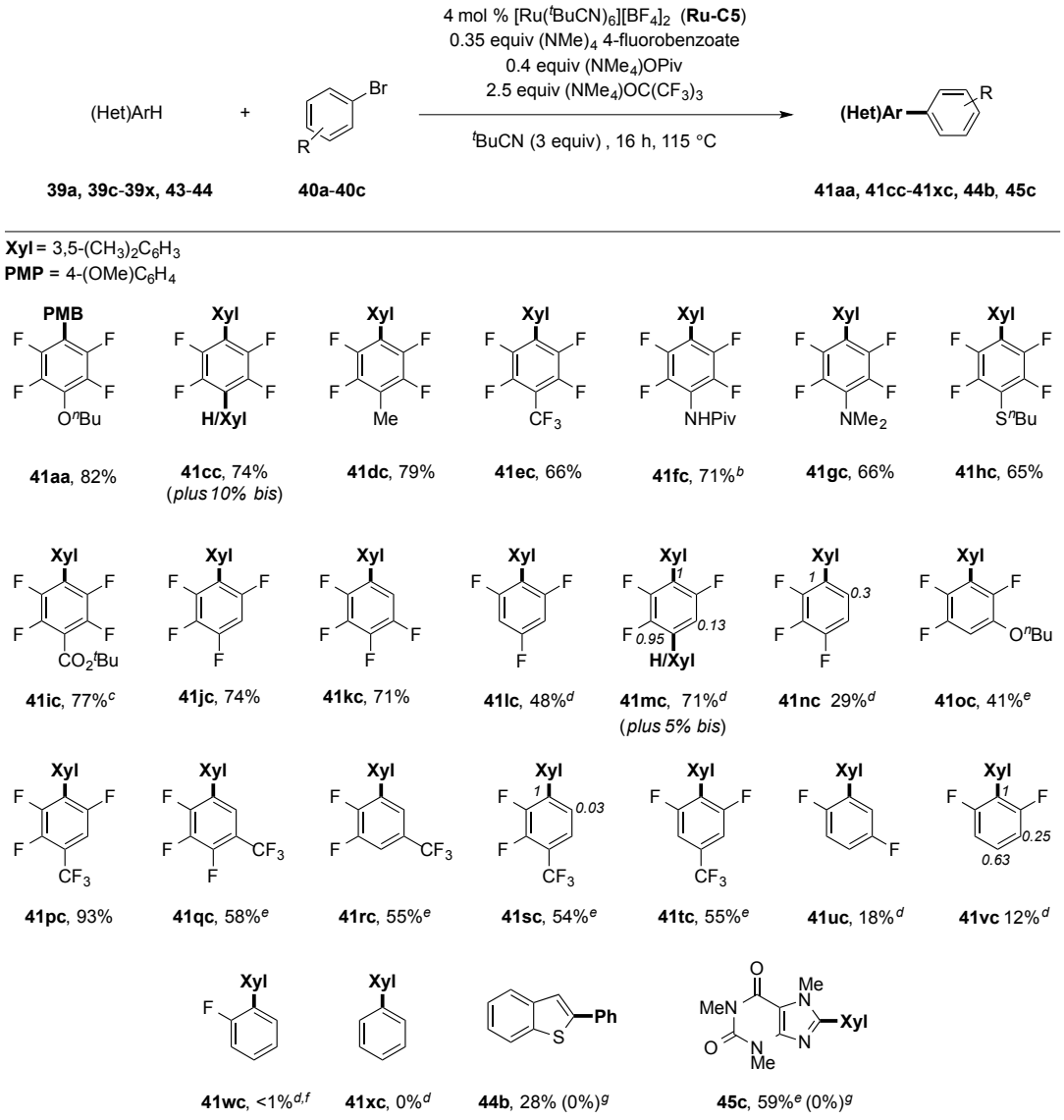

[a] Reaction conditions: Bromoarene **40a**-**40c** (1.0 equiv, 0.5 mmol), **39**, **44**-**45** (3.0 equiv), (NMe_4) 4-fluorobenzoate (0.35 equiv), (NMe_4)OPiv (0.4 equiv), (NMe_4)$OC(CF_3)_3$ (2.5 equiv), **Ru-C5** (4 mol %) and ^{t}BuCN (3.0 equiv) stirred at 115 °C under N_2 in a closed vessel for 16 h. Yields of pure, isolated products. [b] ^{t}BuCN (6.0 equiv). [c] Reaction time was 2 h. [d] **39** (10.0 equiv). [e] **39** (5.0 equiv). [f] Detected in traces by ^{19}F-NMR. [g] Performed without (NMe_4) 4-fluorobenzoate.

Scheme 2.19. Scope of the Ru-catalysed arylation of (hetero)aromatics **39**, **43**-**44** with bromoarenes **40a-40c**.

Finally, the conditions developed for the arylation of fluoroarenes were also applied to substrates containing classical *ortho* directing groups (Scheme 2.20). 2-phenylpyridine (**43**), benzo[*h*]quinoline (**46**), 1-phenylpyrazole (**47**), 2-phenyl-2-oxazoline (**48**), 2-aryloxypyridine (**49**), 1-benzyl-5-phenyltetrazole (**50**), *N*-pyrimidine-indole (**51**) were successfully arylated with an equimolar stoichiometry of bromoarenes **40a**-**40c**, under otherwise identical standardised conditions.

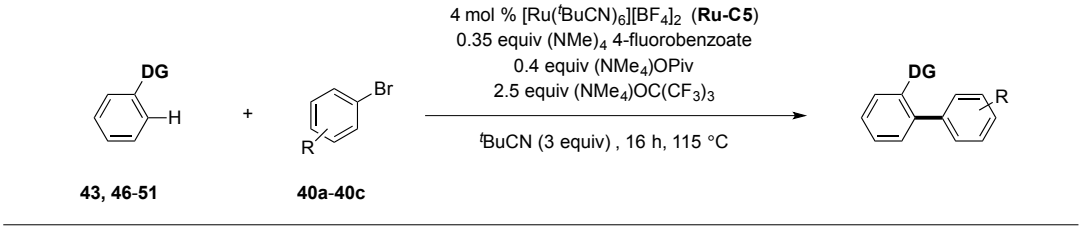

Xyl = 3,5-$(CH_3)_2C_6H_3$; **PMP** = 4-$(OMe)C_6H_4$

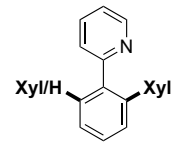

43c
32% *plus 30% bis*
(32% *plus 31% bis*)[b,c]

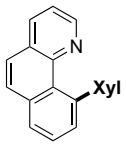

46c
97% (96%)[b,c]

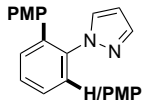

47a
31% *plus 34% bis*
(30% *plus 33% bis*)[b,c]

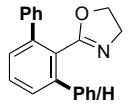

48b
10%[c] *plus 36% bis*
(12% *plus 40% bis*)[b,c]

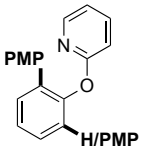

49a
43% *plus 21% bis*
(47% *plus 20% bis*)[b,c]

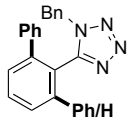

50b
62% *plus 3% bis*
(62% *plus 3% bis*)[b,c]

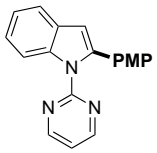

51a
32% (26%)[b,c]

[a] Reaction conditions: Bromoarene **40a**-**40c** (1.0 equiv, 0.5 mmol), **43**, **46**-**51** (1.0 equiv, 0.5 mmol), (NMe_4) 4-fluorobenzoate (0.35 equiv), $(NMe_4)OPiv$ (0.4 equiv), $(NMe_4)OC(CF_3)_3$ (2.5 equiv), **Ru-C5** (4 mol %) and ^{t}BuCN (3.0 equiv) stirred at 115 °C under N_2 in a closed vessel for 16 h. Yields of pure, isolated products. [b] Performed without (NMe_4) 4-fluorobenzoate. [c] Yield estimated by ^{1}H-NMR with dibromomethane as internal standard.

Scheme 2.20. Scope of the Ru-catalysed arylation for substrates containing an *ortho* directing group with bromoarenes **40a**-**40c**.

Remarkably, all of these substrates exhibited equivalent reactivity, even without the benzoate additive. These results further emphasise that the benzoate additive is only needed when the arene does not contain a directing group, suggesting that both the directing group and the benzoate additive may play similar redox roles in facilitating the reaction of the aryl-ruthenium intermediate with the aryl bromide. Therefore, it is tempting to speculate that the benzoate ligand may be playing an important role in facilitating an oxidative addition or a SET process. However, further mechanistic studies will be necessary to fully understand its role.

2.9. D/H labelling experiments

To assess the reversibility of the C–H activation without altering the arylation conditions, equimolar amounts of **d_1-39a** and pentafluorobenzene (**39b**) were subjected to reaction with bromobenzene (**40b**) (Scheme 2.21). Biaryls **41ab**, **41bb** as well as d_1-pentafluorobenzene (**d_1-39b**) and non-deuterated **39a** were detected, confirming the reversible nature of the ruthenation step. Moreover, comparing the overall amount of arylation with the sum of H/D exchange, we speculate that the rate of proto/deuterodemetalation and that observed for arylation, must be of a similar order of magnitude.

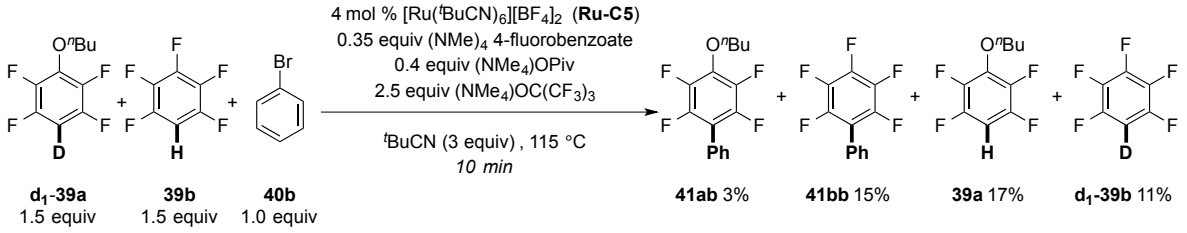

[a] Reaction conditions: Bromobenzene **40b** (1.0 equiv, 0.25 mmol), fluoroarenes **d_1-39a** and **39b** (1.5 equiv each), (NMe_4) 4-fluorobenzoate (0.35 equiv), (NMe_4)OPiv (0.4 equiv), (NMe_4)$OC(CF_3)_3$ (2.5 equiv), **Ru-C5** (4 mol %) and ^{t}BuCN (3.0 equiv) stirred at 115 °C under N_2 in a closed vessel for 10 min. Yields were evaluated by quantitative ^{19}F-NMR using octafluorotoluene as internal standard.

Scheme 2.21. Reversibility of the metalation under arylation conditions: competition arylation experiment of **d_1-39a** and **39b** with bromobenzene **40b**.

We then conducted a competition KIE experiment employing 2,3,5,6-tetrafluoroanisole (**39y**) and **d_1-39a** under the conditions described in Scheme 2.22. A KIE of 2.2 was observed in addition to H/D scrambling between the perfluorinated arenes. Thus, the C–H activation, albeit reversible, is kinetically significant.

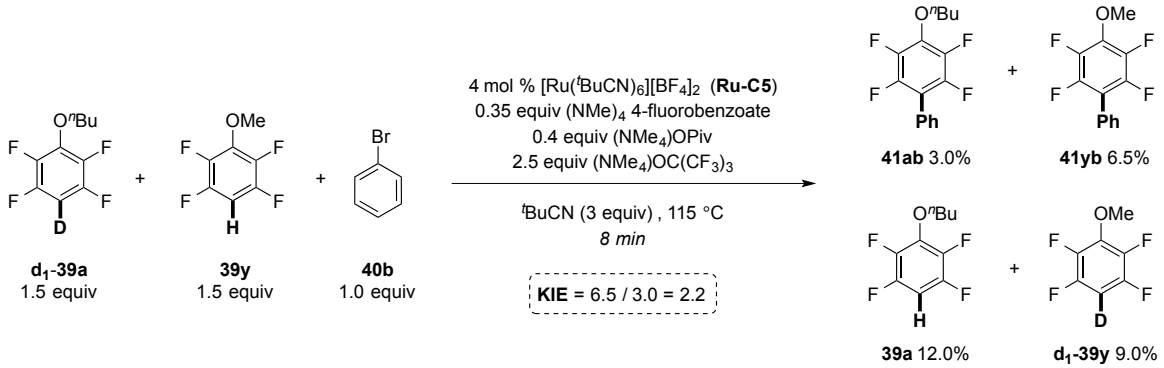

[a] Reaction conditions: Bromobenzene **40b** (1.0 equiv, 0.25 mmol), fluoroarenes **d_1-39a** and **39y** (1.5 equiv each), (NMe_4) 4-fluorobenzoate (0.35 equiv), $(NMe_4)OPiv$ (0.4 equiv), $(NMe_4)OC(CF_3)_3$ (2.5 equiv), **Ru-C5** (4 mol %) and ^{t}BuCN (3.0 equiv) stirred at 115 °C under N_2 in a closed vessel for 8 min. Yields were evaluated by quantitative ^{19}F-NMR using octafluorotoluene as internal standard.

Scheme 2.22. Competition KIE experiment between **d_1-39a** and **39y** with bromobenzene **40b**.

Finally, a KIE measured in two independent parallel experiments between fluoroarenes **d_1-39a** and **39a**, confirmed that the rate of arylation for non-deuterated arene is 2.4 times faster compared to that of **d_1-39a** (Table 2.25).

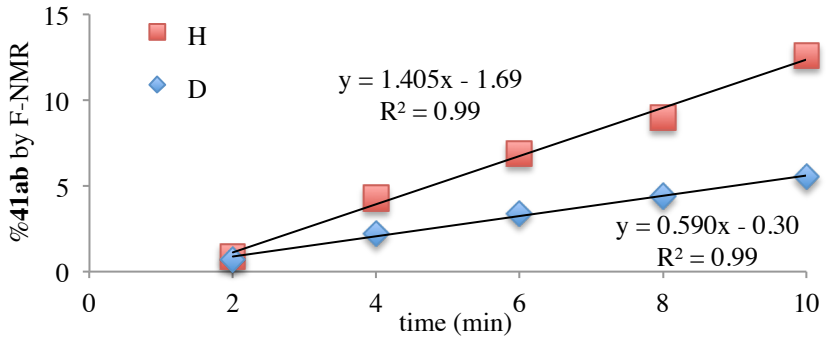

Graph 2.9. Rates of formation of **41ab** for the arylation of **39a** and **d_1-39a** with bromobenzene **40b** (%/min).

$$\textbf{KIE} = \frac{k\mathrm{H}}{k\mathrm{D}} = \frac{1.405}{0.590} = \mathbf{2.4}$$

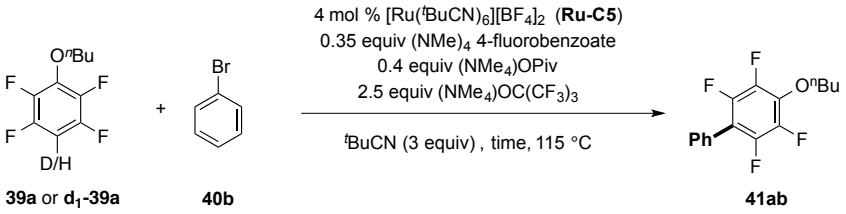

entry	**39a** or **d_1-39a**	time (min)	**41ab**(%)
1	**39a**	2	0.9
2	**39a**	4	4.3
3	**39a**	6	6.9
4	**39a**	8	9.0
5	**39a**	10	12.6
6	**d_1-39a**	2	0.7
7	**d_1-39a**	4	2.2
8	**d_1-39a**	6	3.4
9	**d_1-39a**	8	4.4
10	**d_1-39a**	10	5.5

[a] Reaction conditions: Bromobenzene **40b** (1.0 equiv, 0.25 mmol), fluoroarene **d_1-39a** or **39a** (3.0 equiv), (NMe_4) 4-fluorobenzoate (0.35 equiv), (NMe_4)OPiv (0.4 equiv), (NMe_4)$OC(CF_3)_3$ (2.5 equiv), **Ru-C5** (4 mol %) and ^{t}BuCN (3.0 equiv) stirred at 115 °C under N_2 in a closed vessel for the appropriate time (see above). Yields were evaluated by quantitative ^{19}F-NMR using hexafluorobenzene as internal standard.

Table 2.25. KIE experiments measured in parallel reactions for the arylation of **39a** and **d_1-39a** with **40b**.

2.10. Competition experiments among aryl halides

Intermolecular competition experiments between Cl-, Br- and I- *para*-substituted anisole-type arenes with pentafluorobenzene (**39b**), revealed that iodoarene **I-40a^** was more reactive than bromoarene **40a** and, in turn, its analogue **40a^** (4-bromophenetole) was more reactive than choloroarene **Cl-40a** (Scheme 2.23). This order of reactivity suggests that the formal oxidative insertion, of the putative arene(II)ruthenium intermediate into the carbon–halogen bond, is kinetically significant.[50]

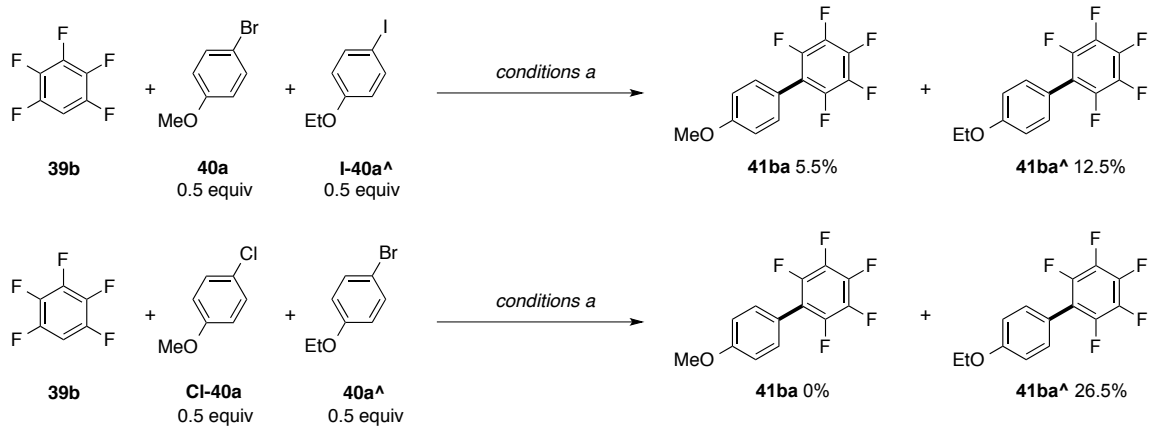

[a] *Conditions a*: haloarenes (see above 0.5.0 equiv each, 0.25 mmol each) pentaflorobenzene **39b** (3.0 equiv), (NMe_4) 4-fluorobenzoate (0.35 equiv), (NMe_4)OPiv (0.4 equiv), (NMe_4)$OC(CF_3)_3$ (2.5 equiv), **Ru-C5** (4 mol %) and ^{t}BuCN (3.0 equiv) stirred at 115 °C under N_2 in a closed vessel for 15 min. Yields were evaluated by ^{1}H-NMR using dibromomethane as internal standard.

Scheme 2.23. Competition arylation between haloarenes **40a** and **I-40a^**, and **Cl-40a** and **40a^**.

When three different set of Cl- Br- I- arenes, each individual triad bearing a distinctive *para*- electron-withdrawing and electron-donating group, reacted in a competition experiment with pentafluorobenzene **39b**, an unusual reactivity dependent on the nature of the halide was observed (Scheme 2.24). The detected order in reactivity is the following: electron-poor aryl chlorides are more reactive than electron-rich ones, electron-poor and electron-rich aryl bromides are equally reactive, whereas electron-poor aryl iodides are less reactive than electron-rich ones. This atypical comportment suggests a change in the mechanism depending on the nature of the aryl halide. Thus, the step in which the

electrophile enters the catalytic cycle is gaining or losing kinetic relevance. Although, our empirical results could be theoretically rationalised in terms of oxidative addition as rate-determining for aryl chlorides and the reductive elimination in the case of aryl iodides, a more in depth study on the matter will need to be provided.

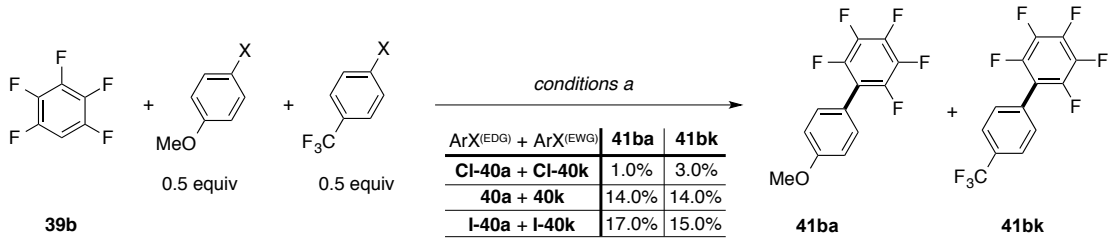

ArX(EDG) + ArX(EWG)	41ba	41bk
Cl-40a + Cl-40k	1.0%	3.0%
40a + 40k	14.0%	14.0%
I-40a + I-40k	17.0%	15.0%

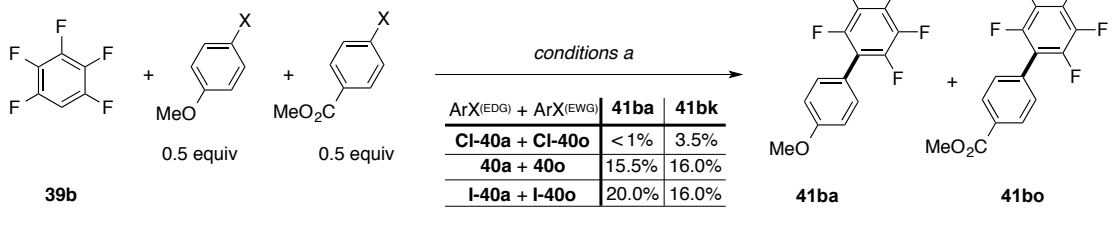

ArX(EDG) + ArX(EWG)	41ba	41bk
Cl-40a + Cl-40o	< 1%	3.5%
40a + 40o	15.5%	16.0%
I-40a + I-40o	20.0%	16.0%

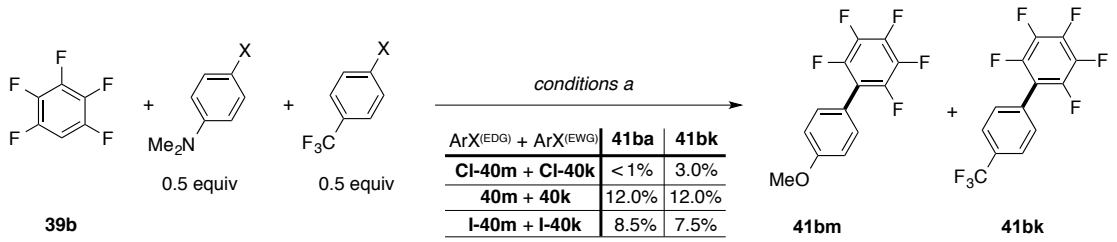

ArX(EDG) + ArX(EWG)	41ba	41bk
Cl-40m + Cl-40k	< 1%	3.0%
40m + 40k	12.0%	12.0%
I-40m + I-40k	8.5%	7.5%

[a] *Conditions a*: haloarenes (see above 1.0 equiv, 0.25 mmol) pentaflorobenzene **39b** (3.0 equiv each), (NMe_4) 4-fluorobenzoate (0.35 equiv), $(NMe_4)OPiv$ (0.4 equiv), $(NMe_4)OC(CF_3)_3$ (2.5 equiv), **Ru-C5** (4 mol %) and ^{t}BuCN (3.0 equiv) stirred at 115 °C under N_2 in a closed vessel for 15 min. Yields were evaluated by ^{1}H-NMR using dibromomethane as internal standard.

Scheme 2.24. Competition arylation between haloarenes having diverse electronic properties with **39b**.

Our experimental observation is in contrast with that reported by Ackermann *et al*. for the arylation of a 2-phenylpyridine derivative with an excess of differently substituted electrophiles. In their study, electron-deficient aryl halides always reacted preferentially over electron-rich ones and the chemoselectivity was not dependent on the nature of the leaving group or the solvent (Scheme 2.25).[150]

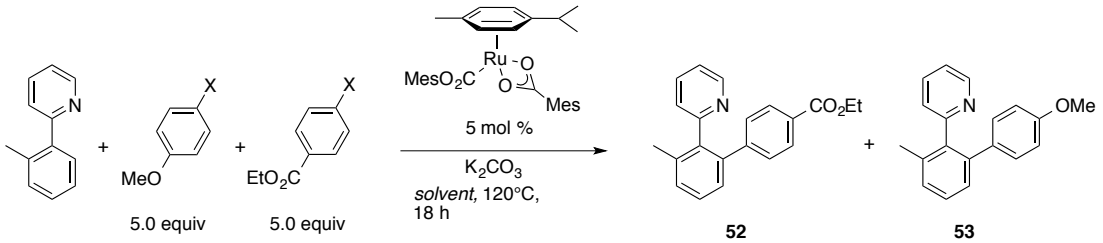

halogen	*solvent*	**52**	**53**
X = Cl	toluene	86%	6%
X = Br	toluene	55%	24%
X = Cl	NMP	56%	5%
X = Br	NMP	28%	19%

Scheme 2.25. Competition arylation between electron-deficient and electron-rich aryl halides reported by Ackermann and co-workers.[150]

Classically, the rate of a two-electron oxidative addition step is faster for electron-deficient aryl halides.[50] Indeed, only a few examples in which electron-rich aryl halides display greater reactivity than the electron-deficient ones have been reported in literature.

Daugulis *at al*. illustrated one example in the Pd-catalysed arylation of benzamides.[48a] Chatani *et al*. studied the Ru-catalysed arylation of aromatic amide (**54**) having an 8-aminoquinoline moiety with an electronically different set of *para*-substituted aryl bromides. A "V"-shaped Hammett plot was observed when correlating single data kinetic points with σ_p values (Figure 2.8). The analysis showed two segments with ρ values of –0.5 and +2.1, respectively. The negative slope of –0.5 indicates that electron-donating groups facilitate the C–H arylation, although electron withdrawing CO_2Me and COMe were not a good fit for this slope. This led the authors to suggest that the mechanism or rate-determining step for the reaction was dependent on the nature of the aryl bromide substituent.[151]

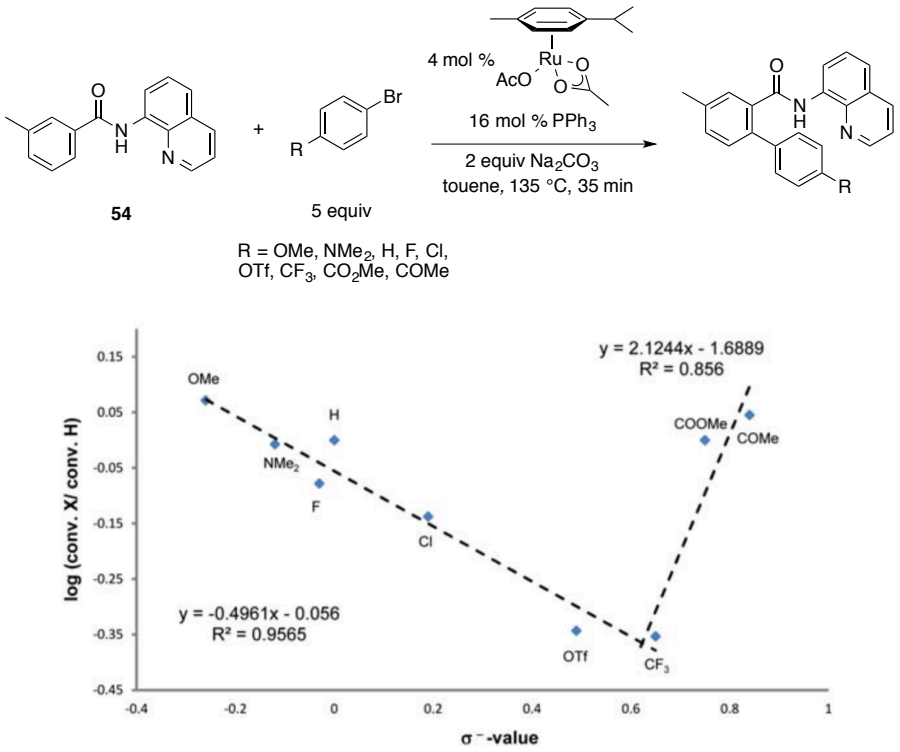

Figure 2.8. Hammett plot study for the arylation of **54** with various substituted aryl bromides.[151]

Additionally, competition experiments using 4-dimethylaminophenyl bromide (**40o**) and methyl 4-bromobenzoate (**40m**) were carried out. Not surprisingly, since the Hammett plot in Figure 2.8 revealed **40m** to have higher arylation rate than **40o,** it was observed that arylated adduct (**55**), deriving from cross coupling with the more electron-poor aryl bromide, gave higher yields than **56**, regardless of the electronic of the substituent at the *meta* position of the aromatic amide. However, the ratio of **55** and **56** decreased to close to 1:1 when the electron-donating nature of the substituents became stronger (Scheme 2.26). Other competition experiments revealed that more highly electron withdrawing groups, at the *meta* position of the aromatic amide, facilitated the arylation. These results suggest that the electronic nature of a substituent in the aromatic amide is also a dominant factor.

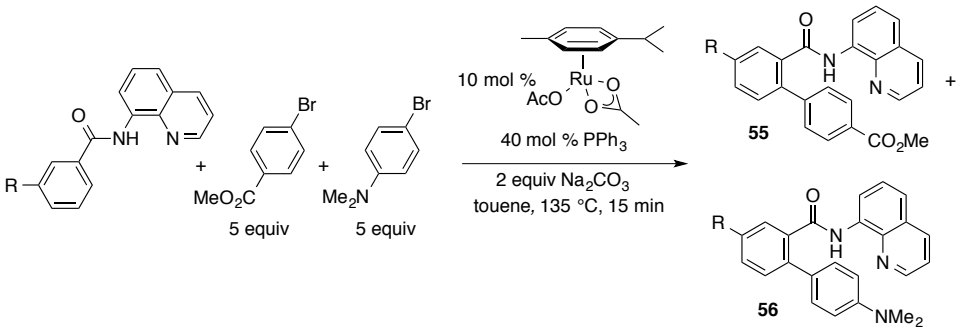

R	ratio 55	56
CF_3	5.6	1
Me	2.6	1
$OSiR_3$	2.3	1
NMe_2	1.6	1

Scheme 2.26. Competition arylation between haloarenes having diverse electronic properties with **39b**.

Recently, Ackermann and co-workers described the Ru(II)-catalysed arylation of azoarenes, in which electron-rich arylbromides displayed superior arylation rates.[152] A Hammett plot was constructed from the correlation between the initial rates and the σ_p values. The plot resulted in a linear fit with a negative slope of –0.21, indicating that electron-donating groups ease the C–H arylation. This observation led the authors to suggest a rate-determining reductive elimination.

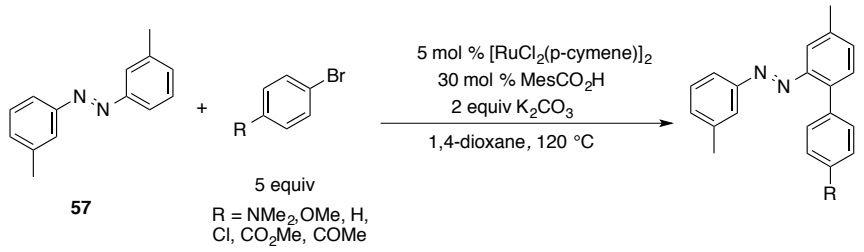

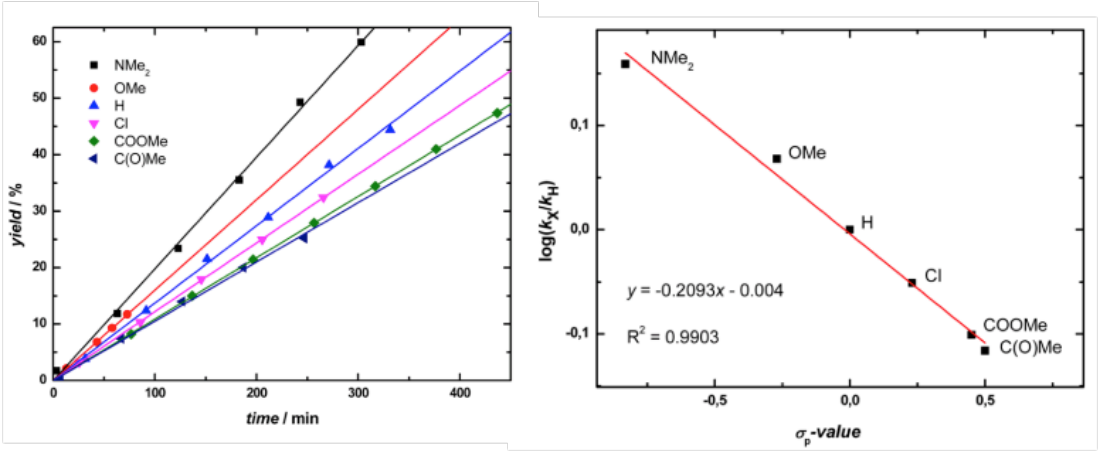

Figure 2.9. Kinetic data and Hammet plot for the arylation of **57** with various substituted aryl bromides.[152]

2.11. Computational investigation

To obtain more information on the factors influencing the Ru-promoted C–H activation, we performed a DFT study on several models of potentially relevant Ru(II) complexes.[153] $Ru(OAc)_2$(benzene) (**M1**) was used as a model of **Ru-C1**, while monocationic $[Ru(OAc)(MeCN)_4]^+$ (**M2**) was used to model the nitrile-containing complex likely formed from reaction of **Ru-C5** with pivalate.[154] For both models, CMD-type transition states (**TS1** and **TS2**, respectively, Figure 2.10) were found with very similar energies (29.5 and 28.8 kcal/mol, respectively), consistently with both complexes being active in the C–H activation reaction. Also, both aryl-Ru(II) products (**P1** and **P2**) were less stable than the starting materials, which explains the experimental requirement for a stoichiometric base to drive the process forward.

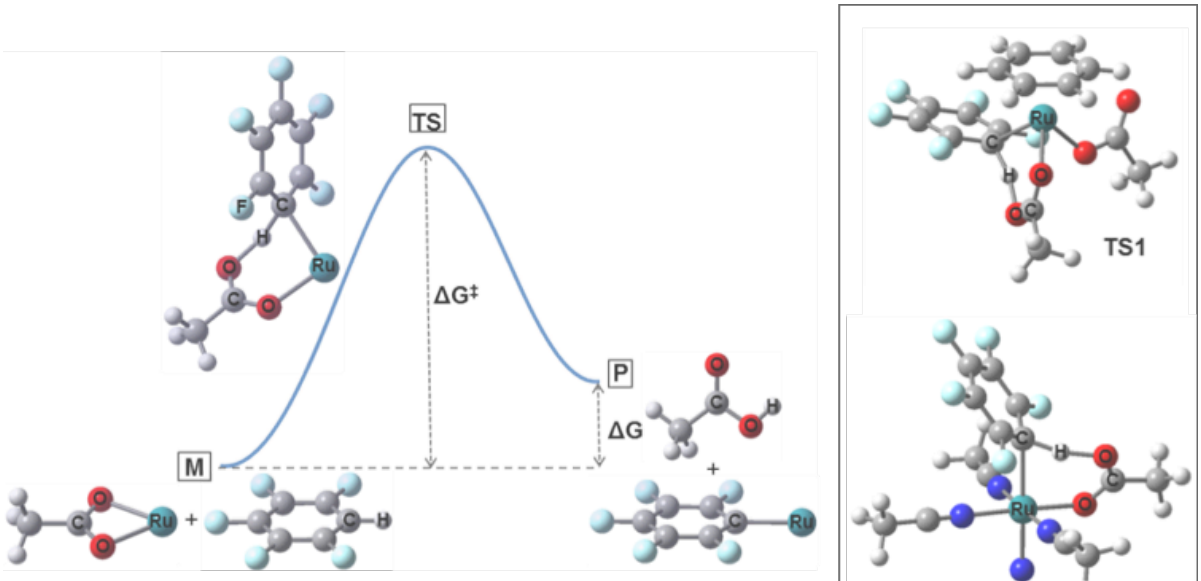

Relative energies (kcal/mol)	TS1	P1	TS2	P2[a]
ΔG	29.5	7.2	28.8	12.1
ΔE	18.2	7.2	15.8	-1.8

[a] P2 contains one additional molecule of MeCN compared to M2

Figure 2.10. *Left-hand side:* Schematic profile for the C–H activation step (ligands on Ru omitted for clarity) and calculated energies. *Right-hand side:* Optimised structures for the transition states with the *p*-cymene-containing catalyst (**TS1**) and the cationic nitrile-containing catalyst (**TS2**).

Regioselectivity was studied using substrate **39r** (Scheme 2.27), which has three C–H sites with different electronic and steric properties. With **M2**, the computed barriers for each position matched the experimental results, with the least sterically hindered position (**c**) being favoured, followed by the most electron-deficient (**a**, 3.3 kcal/mol higher). Interestingly, analogous calculations with a Pd-based system[22] [Pd(OCOH)(Ph)(PMe_3)] provided a different selectivity, favouring the most electron-deficient position (**a**) although with a lower selectivity over **c** (2.4 kcal/mol). Experimentally, both Ru and Pd[22] catalysts provided as the major product **41rc**, resulting from arylation at position **c**, but while with Ru this was the only product, a significant amount of arylation at position **a** was obtained with Pd. The difference between the calculated and experimental result with Pd can be explained by the model being less sterically congested than the real system, particularly due to the use of PMe_3 as a surrogate of P^tBu_2Me. A different experimental regioselectivity for substrate **39r** was also found with Cu (see SI, section 2.14).

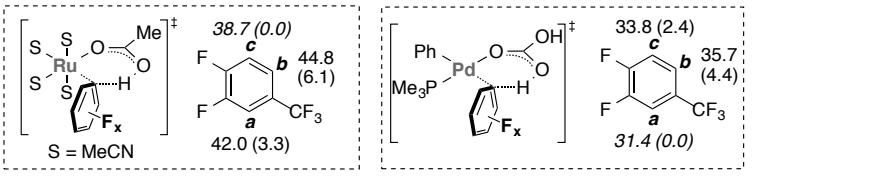

	41rc (%)	**41rc'** (%)	**41rc''** (%)	ratio
[Ru]	55	0	0	1 : 0 : 0
[Pd]	39	13	17	1 : 0.33 : 0.44

Scheme 2.27. *Top:* Predicted barriers for the three C–H sites in **39r** with Ru and Pd catalysts ($\Delta G^{\ddagger}$ in kcal/mol, numbers in brackets are $\Delta\Delta G^{\ddagger}$ relative to the lowest barrier). *Bottom*: Experimental results for direct arylation of 1r with Ru and Pd catalysts.

Previously published studies on Pd-catalysed C–H activation,[22,31] have shown that the regioselectivity in the case of fluoroarene-type substrates (Class I) is controlled by the acidity of the different C–H bonds present in the substrate, which correlates with the energetic cost of distorting the arene geometry to that adopted in the TS (see section 1.4.1.2). Surprisingly, a distortion-interaction analysis on the Ru system showed that the favoured position **c** had in this case the lowest distortion energy for the arene (Table 2.26). Thus, in the Ru system the distortion energy is not directly correlated with the acidity of each hydrogen, and the lower $\Delta E_{dist}(Ar^FH)$ for position **c** shall be explained by a less distorted geometry in this TS when compared to the other regioisomers. Indeed, the C–H distance in the TS for **c** was the shortest compared with **b** and **a**. Moreover, all three TS with Ru displayed shorter C–H distances than their Pd counterparts (1.30-1.32 for Ru against 1.38 to 1.41 for Pd), and consistently lower $\Delta E_{dist}(Ar^FH)$ (25.5-29.5 kcal/mol for Ru against 34.4-40.1 for Pd). This suggests that with Ru a more early TS is found, thus the cost of breaking the C–H bond is less relevant relative to other factors. In the Ru-based system both distortion and interaction energies contributed significantly to the discrimination between **a** and **c** ($\Delta\Delta$Eint = 0.7 kcal/mol, $\Delta\Delta E_{dist}(Ar^FH)$ = 1.1 kcal/mol), while in the case of Pd the regioselectivity was mainly controlled by distortion ($\Delta\Delta$Eint = 0.9 kcal/mol, $\Delta\Delta$Edist(ArFH) = 3.9 kcal/mol). The higher contribution of interaction energy to regioselectivity is consistent with a larger influence of steric factors for the Ru-based system as compared with the Pd one. A more detailed study will be required for extracting specific conclusions on the exact nature of the factors determining regioselectivity with Ru and their relative weights.

	$\Delta G^{‡}$	$\Delta E^{‡}$	$\Delta E_{dist}(M)$	$\Delta E_{dist}(Ar^FH)$	ΔE_{dist} (tot)	ΔE_{int}
a-Ru	42.0	27.0	29.9	26.6	56.5	-29.5
c-Ru	38.7	25.0	29.7	25.5	55.2	-30.2
a-Pd	31.4	19.7	19.7	34.4	54.4	-34.4
c-Pd	33.8	23.4	20.5	38.3	58.7	-35.3

[a] Calculated energies in kcal/mol

Table 2.26. Distortion and interaction energies for the C–H activation of **39r** with Ru and Pd catalysts.

2.12. Initial rate kinetic analysis

To shed more light on the reaction mechanism, a kinetic analysis based on initial rates method[155] was conducted. This allowed us to estimate the order of each individual component in the rate equation. The results presented in this epigraph, however, are only preliminary, and larger set of data will be necessary for extracting definitive conclusions.

The reactions were followed by taking small aliquots from the crude, and analysed by GC-FID employing an internal standard. Therefore, in order to dilute the concentration of the reaction, 10 equiv of ^{t}BuCN, along with the use of a compatible co-solvent (ethylpivalate), were employed. Both the exceptionally fast arylation rate at the very beginning of the reaction (see Graph 2.8) and the high sensitivity towards traces of oxygen (see Table 2.22, entry 3), have required the reaction to be carried out in a glove box, withdrawing small samples from mixture every minute. Additionally, quantitative results could only be compared among data acquired from a series of experiments performed in parallel. Consequently, not more than three reactions were possible to be followed simultaneously. Moreover, when high loading of (NMe_4) 4-fluorobenzoate, (NMe_4)OPiv and (NMe_4)$OC(CF_3)_3$ were used, the partial insolubility of these species under the reaction conditions might have led to further loss of accuracy in the evaluation of their actual concentration. These intrinsic limitations have made the acquirement of the kinetic data more restricted and perhaps less reliable.

The time-course data for each single run show clear evidence of an initial kinetic burst[156] followed by a slower, steady-state rate (Graph 2.10-Graph 2.16). For this reasons, two different regimes were separately considered for our kinetic analysis: *1° regime* = initial burst; *2° regime* = steady-state. These initial-rate data suggest a change in mechanism and/or a kinetically relevant catalyst regeneration step, after the first product formation during the initial burst.

Particularly in the case of the kinetic order in [Ru], the linear fit of the steady-state reaction regime intersects the vertical axis at a concentration of biaryl **41ab** matching approximately the concentration of **Ru-C5** (2° regimes Graph 2.10 and Table 2.28). This implies that the

burst corresponds to a single turnover of the Ru(II) catalyst. Nevertheless, the rate during both periods exhibits a first-order dependence on [Ru] (Table 2.28).

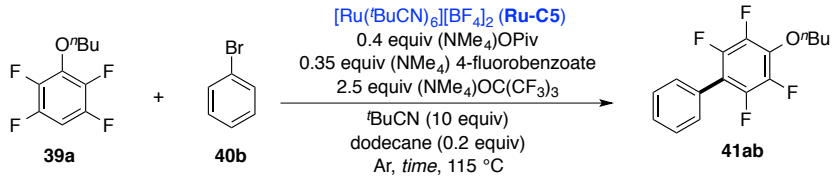

	1 mol% **Ru-C5**		2.25 mol% **Ru-C5**		5 mol% **Ru-C5**	
time (min)	**[41ab]** (mM)	**41ab** (%)	**[41ab]** (mM)	**41ab** (%)	**[41ab]** (mM)	**41ab** (%)
1	0.27	0.05	0.07	0.01	0.03	0.01
2	0.28	0.05	1.84	0.33	1.60	0.29
3	2.28	0.41	11.86	2.13	13.48	2.42
4	5.22	0.94	24.32	4.37	32.00	5.75
5	8.22	1.48	34.87	6.26	52.51	9.43
8	17.62	3.16	56.99	10.23	87.44	15.71
10	20.86	3.75	69.29	12.45	104.31	18.73
13	25.89	4.65	84.81	15.23	125.62	22.56
16	30.30	5.44	99.05	17.79	151.71	27.25
20	36.59	6.57	120.46	21.63	175.59	31.54

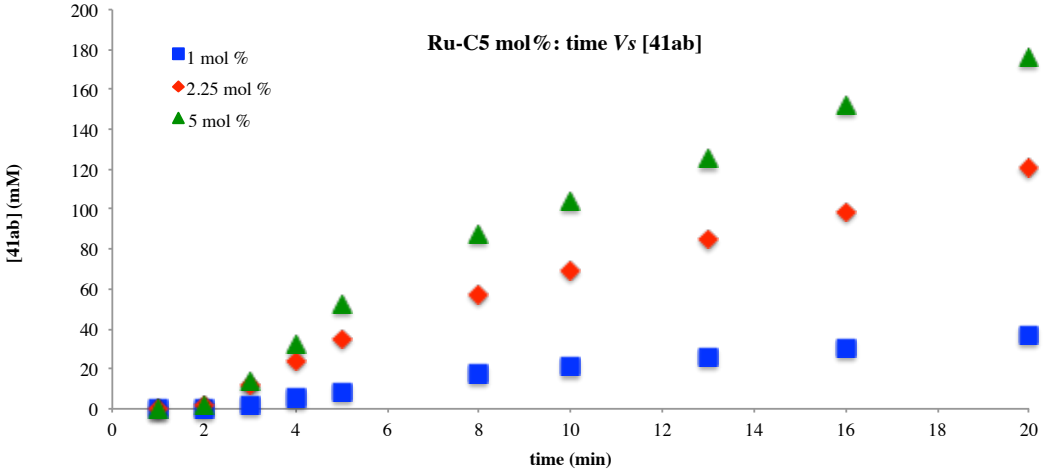

[a] Reaction conditions: Bromobenzene **40b** (1.0 equiv, 0.50 mmol), fluoroarene **39a** (3.0 equiv), (NMe_4) 4-fluorobenzoate (0.35 equiv), $(NMe_4)OPiv$ (0.4 equiv), $(NMe_4)OC(CF_3)_3$ (2.5 equiv), **Ru-C5** (see above), ^{t}BuCN (10.0 equiv) and dodecane (0.2 equiv) were stirred at 115 °C under N_2 in a closed vessel. Small aliquots were taken at the each stated time (see above). Yields were evaluated by GC-FID with dodecane as internal standard.

Table 2.27. Arylation data and concentration *Vs* time plots for the arylation of **39a** with **40b** at different concentration of **Ru-C5**.

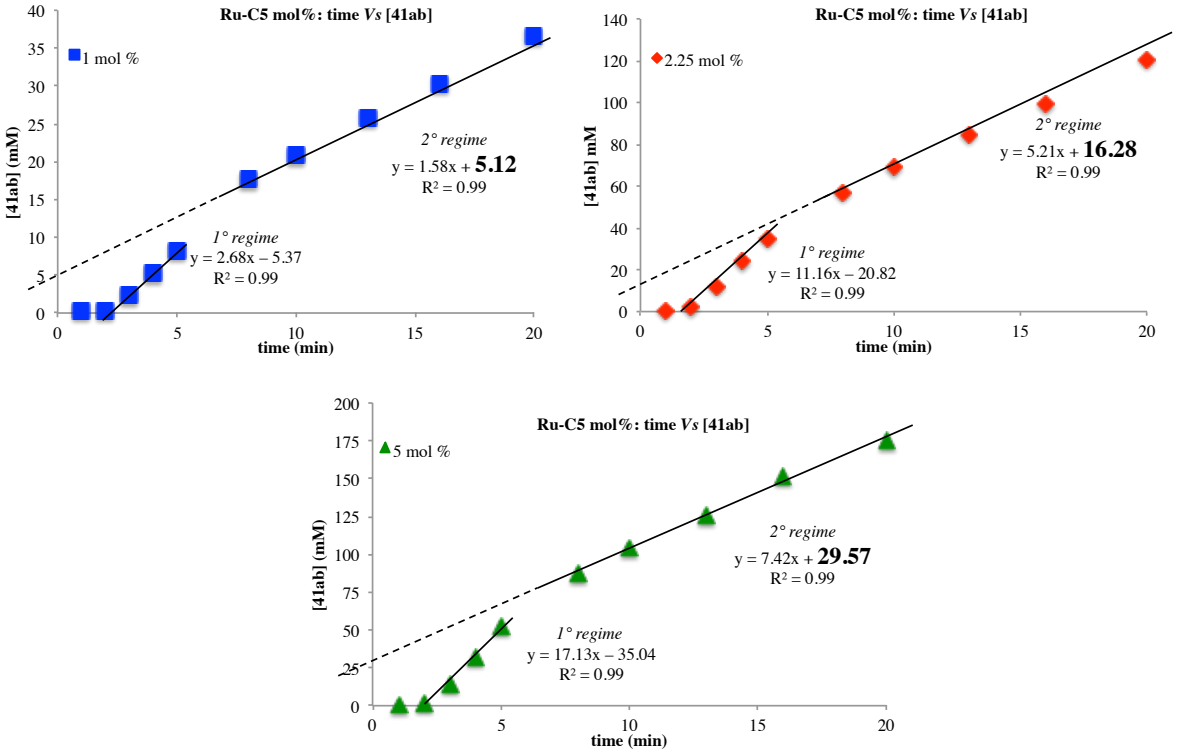

Graph 2.10. Rates of formation for **41ab** (mM/min); two different regimes are shown for each concentration of **Ru-C5** for the arylation of **39a** with **40b**.

			1° regime		*2° regime*	
	[**Ru-C5**] (mM)	ln[**Ru-C5**]	r_{obs} (mM/min)	ln(r_{obs})	r_{obs} (mM/min)	ln(r_{obs})
1 mol %	5.57	1.72	2.68	0.99	1.58	0.46
2.25 mol %	12.53	2.53	11.16	2.41	5.21	1.65
5 mol %	27.84	3.33	17.13	2.84	7.42	2.00

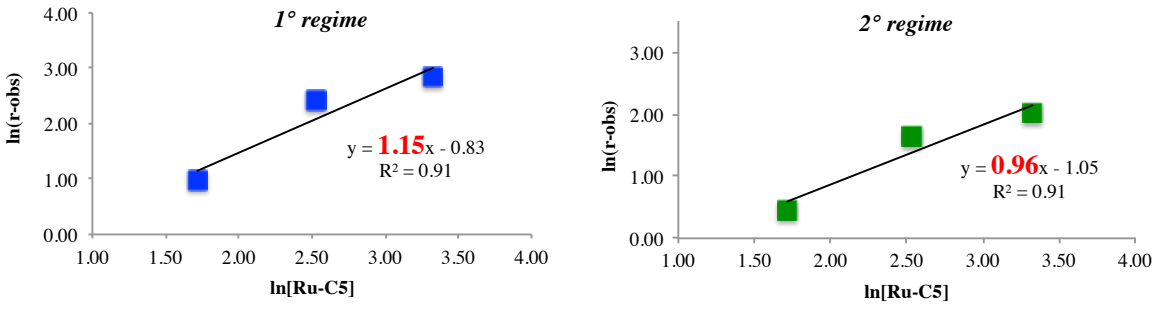

Table 2.28. Kinetic order with respect to **Ru-C5** for the arylation **39a** with **40b**.

The kinetic order in fluoroarene **39a** was evaluated to be ≈ 0.7 for both regimes (Table 2.29, Table 2.30 and Graph 2.11). The KIE experiments pointed out that the C–H bond cleavage is a kinetically relevant step in the arylation (see section 2.9). The first order in ruthenium, along with the positive order in the perfluoroarene substrate, are in agreement with the C–H activation being the rate-determining step of the reaction. In a simple system, order one would be expected. However, the experimentally fractional order observed in fluoroarene **39a** might indicate that the substrate is involved in an off-cycle equilibrium, providing inverse order in **39a**. Thus, the detected < 1 value would arise from a combination of these processes.

Another aspect that needs to be taken into consideration is the reversible nature of the C–H activation under standard reaction conditions (see section 2.9), which led us to suggest that the overall arylation rate and the rate of protodemetalation must be of similar order of magnitude. The computational investigation (see section 2.11) indicates that a pivalate-containing ruthenium(II) species performs the CMD, with consequent formation of PivOH. Assuming that the rate of deprotonation of PivOH by the perfluoro-*tert*-butoxide base is greater than the rate of protodemetalation caused by PivOH itself, the only source of H-atoms accountable for protoderuthenation would be fluoroarene **39a**. Therefore, assuming that the rates of the rate-determining step (C–H activation) and that of the opposite process (protodemetalation) are similar, the reversible nature of the metalation should not affect the order in fluoroarene **39a**. However, if the concentration of H-atoms increases because of the presence of adventitious water in the reaction, the protodemetalation process might then gain kinetic relevance. Therefore, more kinetic data obtained after thorough drying of all the reagents might be necessary to cast further light on the matter.

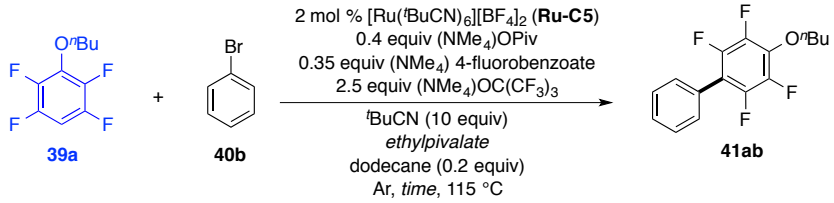

time (min)	1 equiv **39a** [41ab] (mM)	1 equiv **39a** 41ab (%)	3 equiv **39a** [41ab] (mM)	3 equiv **39a** 41ab (%)	5 equiv **39a** [41ab] (mM)	5 equiv **39a** 41ab (%)
1	0.03	0.01	0.01	0.00	0.02	0.01
2	1.00	0.24	1.63	0.38	1.75	0.41
3	5.11	1.20	8.65	2.04	10.19	2.40
4	8.81	2.08	19.18	4.52	22.11	5.21
5	12.65	2.98	27.47	6.47	34.07	8.03
8	19.44	4.58	42.62	10.04	52.17	12.29
10	24.34	5.73	55.76	13.14	69.03	16.26
13	31.15	7.34	67.15	15.82	88.29	20.80
16	34.77	8.19	76.26	17.97	97.38	22.94
20	39.88	9.40	88.92	20.95	111.68	26.31

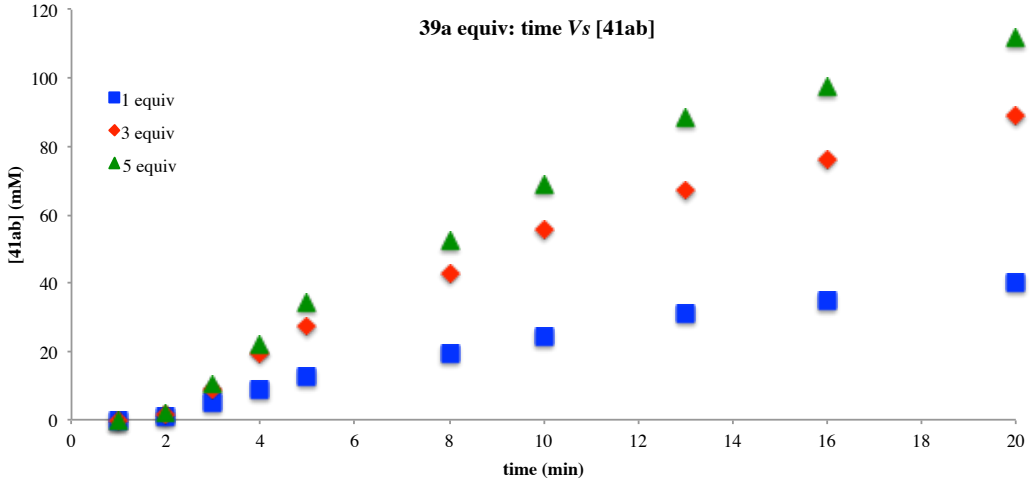

[a] Reaction conditions: Bromobenzene **40b** (1.0 equiv, 0.50 mmol), fluoroarene **39a** (see above), (NMe_4) 4-fluorobenzoate (0.35 equiv), (NMe_4)OPiv (0.4 equiv), (NMe_4)$OC(CF_3)_3$ (2.5 equiv), **Ru-C5** (2.0 mol %), ^{t}BuCN (10.0 equiv), dodecane (0.2 equiv), and ethylpivalate co-solvent (the amount was adjusted in order to keep an identical concentration for each case, see SI for details) were stirred at 115 °C under N_2 in a closed vessel. Small aliquots were taken at the each stated time (see above). Yields were evaluated by GC-FID with dodecane as internal standard.

Table 2.29. Arylation data and concentration *Vs* time plots for the arylation of **39a** with **40b** at different concentration of **Ru-C5**.

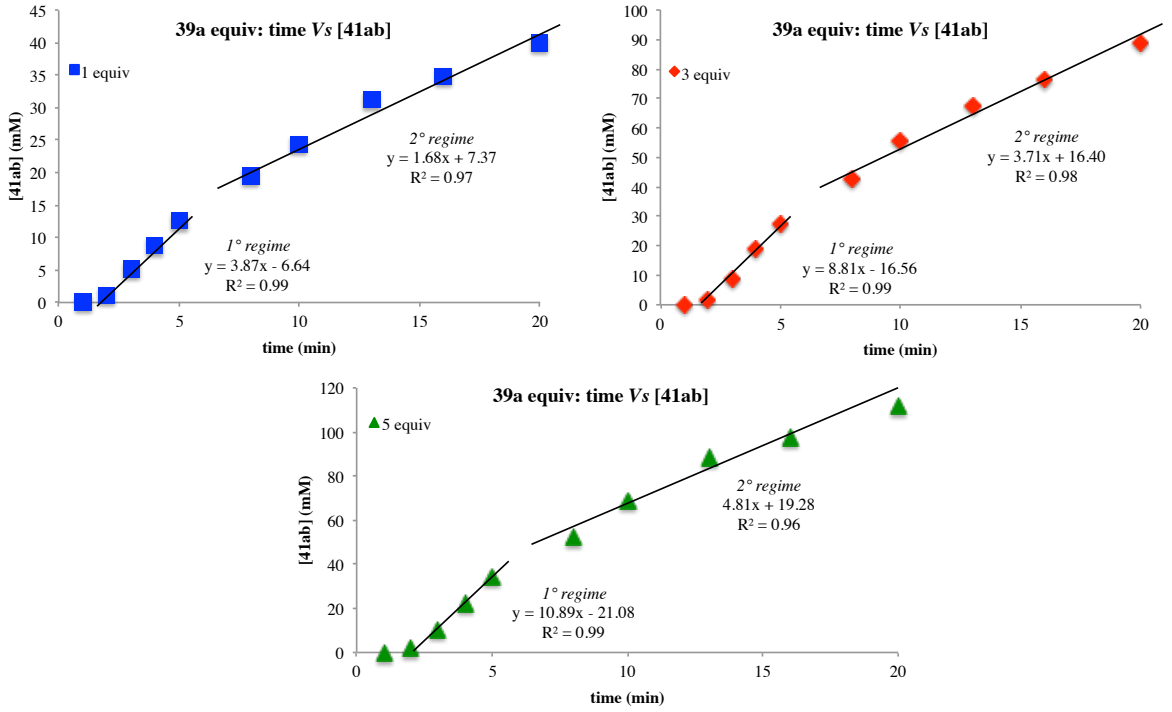

Graph 2.11. Rates of formation for **41ab** (mM/min); two different regimes are shown for each concentration of **39a** for the arylation of **39a** with **40b**.

			1° regime		*2° regime*	
	[**39a**] (mM)	ln[**39a**]	r_{obs} (mM/min)	$ln(r_{obs})$	r_{obs} (mM/min)	$ln(r_{obs})$
1 equiv	424.45	6.05	3.87	1.35	1.68	0.52
3 equiv	1273.34	7.15	8.81	2.18	3.71	1.31
5 equiv	2122.24	7.66	10.89	2.39	4.81	1.57

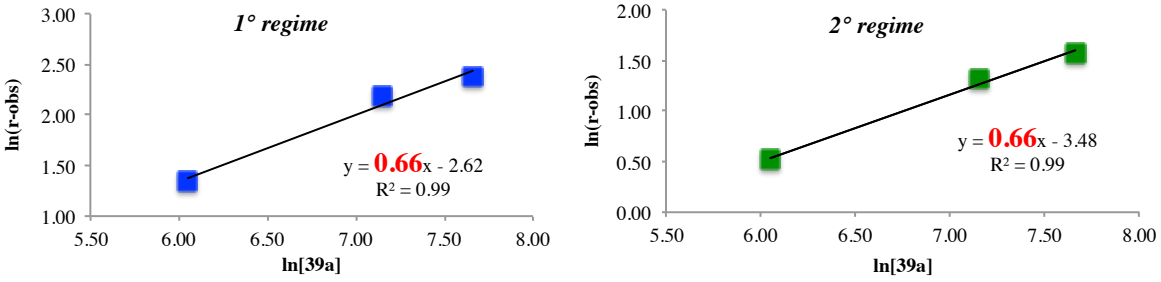

Table 2.30. Kinetic order with respect to fluoroarene **39a** for the arylation **39a** with **40b**.

The kinetic orders in bromobenzene **40b** (Table 2.31, Table 2.32, Graph 2.12) and (NMe_4) 4-fluorobenzoate (Table 2.33, Table 2.34, Graph 2.12) were assessed to be ≈ 0 for both regimes. From the stoichiometric experiments conducted in section 2.7, we disclosed that the benzoate additive is fundamental to the formal oxidative addition step. The kinetic orders in these two reagents, along with the stoichiometric experiments, suggest that both components are entering the catalytic cycle after the rate-determining C–H activation, most likely in the same or in a consecutive step.

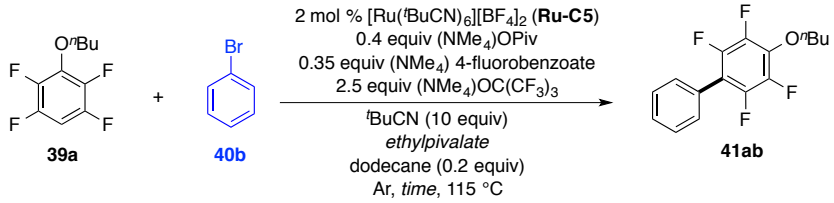

	0.5 equiv **40b**		1 equiv **40b**		2 equiv **40b**	
time (min)	**[41ab]** (mM)	**41ab** (%)	**[41ab]** (mM)	**41ab** (%)	**[41ab]** (mM)	**41ab** (%)
1	0.02	0.01	0.02	0.00	0.03	0.01
2	1.55	0.37	1.63	0.38	0.86	0.20
3	7.90	1.86	8.75	2.06	7.70	1.81
4	16.14	3.80	19.04	4.49	16.21	3.82
5	24.67	5.81	27.58	6.50	24.64	5.81
8	36.51	8.60	42.64	10.04	36.41	8.58
10	45.88	10.81	55.76	13.14	47.84	11.27
13	57.57	13.56	67.15	15.82	60.65	14.29
16	65.33	15.39	76.26	17.97	67.03	15.79
20	77.43	18.24	88.92	20.95	80.07	18.86

[a] Reaction conditions: Bromobenzene **40b** (see above), fluoroarene **39a** (1.5 mmol, 3.0 equiv), (NMe_4) 4-fluorobenzoate (0.35 equiv), (NMe_4)OPiv (0.4 equiv), (NMe_4)$OC(CF_3)_3$ (2.5 equiv), **Ru-C5** (2.0 mol %), ^{t}BuCN (10.0 equiv), dodecane (0.2 equiv), and ethylpivalate co-solvent (the amount was adjusted in order to keep an identical concentration for each case, see SI for details) were stirred at 115 °C under N_2 in a closed vessel. Small aliquots were taken at the each stated time (see above). Yields were evaluated by GC-FID with dodecane as internal standard.

Table 2.31. Arylation data and concentration *Vs* time plots for the arylation of **39a** with **40b** at different concentration of bromoarene **40b**.

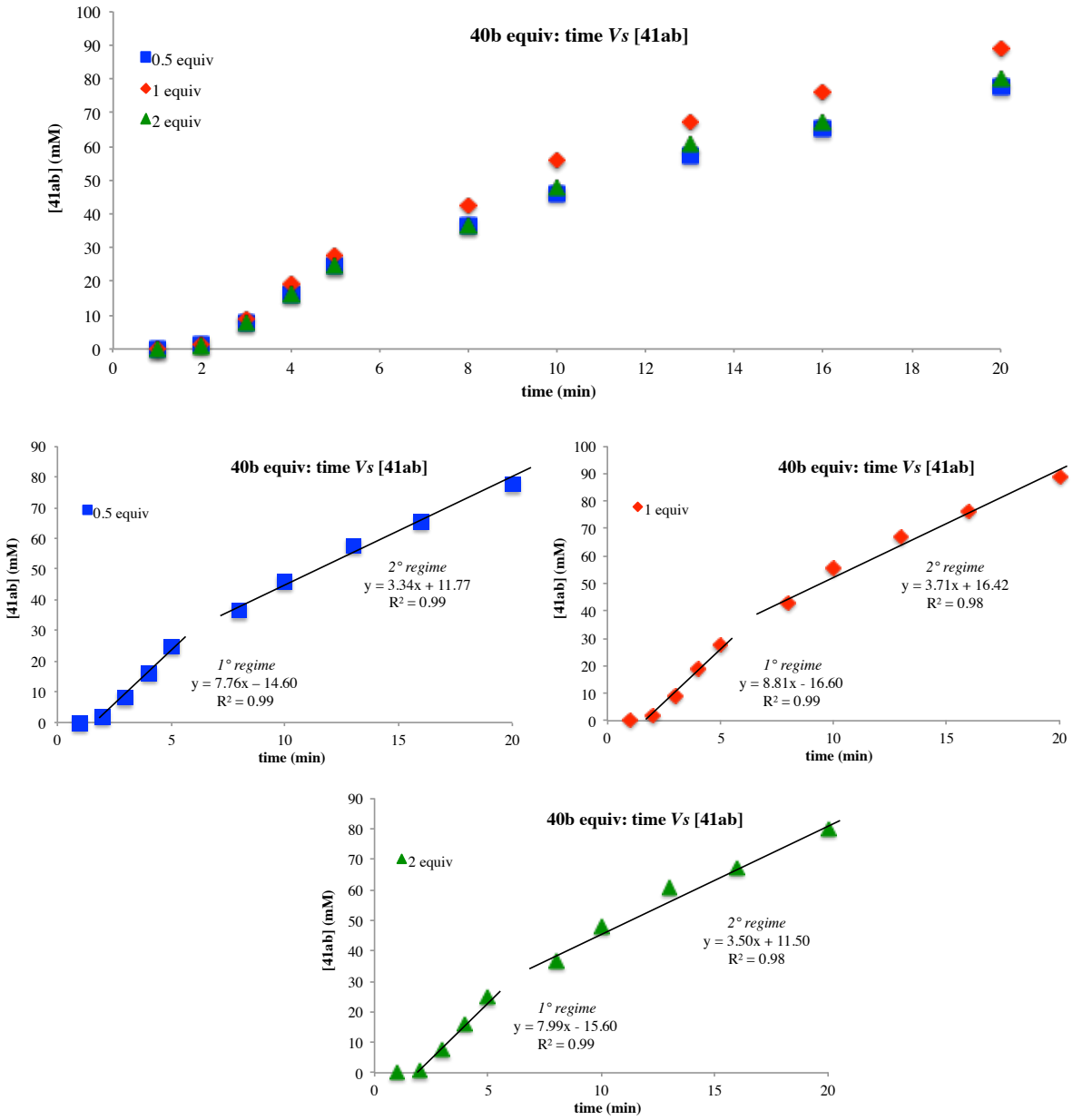

Graph 2.12. Rates of formation for **41ab** (mM/min); two different regimes are shown for each concentration of **40b** for the arylation of **39a** with **40b**.

			1° regime		*2° regime*	
	[**40b**] (mM)	ln[**40b**]	r_{obs} (mM/min)	ln(r_{obs})	r_{obs} (mM/min)	ln(r_{obs})
0.5 equiv	212.22	5.36	7.76	2.05	3.34	1.21
1 equiv	424.45	6.05	8.81	2.18	3.71	1.31
2 equiv	848.90	6.74	7.99	2.08	3.50	1.25

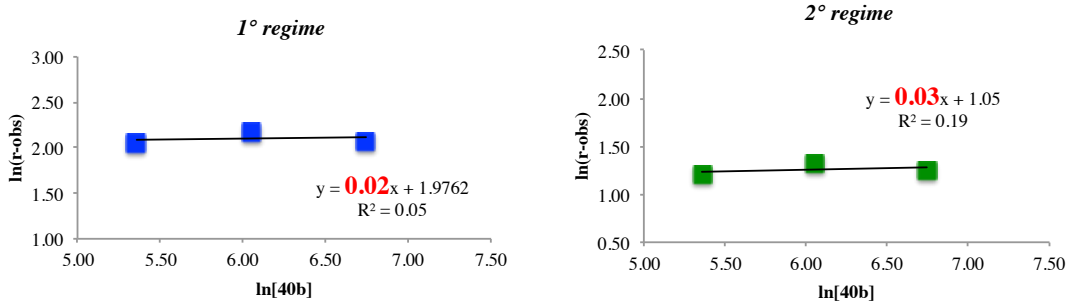

Table 2.32. Kinetic order with respect to bromobenzene **40b** for the arylation **39a** with **40b**.

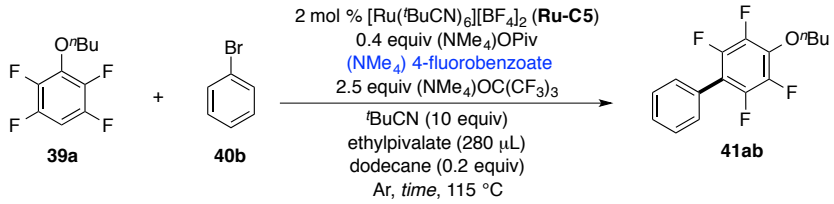

	0.175 equiv (NMe$_4$) 4-fluorobenzoate		0.35 equiv (NMe$_4$) 4-fluorobenzoate		0.7 equiv (NMe$_4$) 4-fluorobenzoate	
time (min)	**[41ab]** (mM)	**41ab** (%)	**[41ab]** (mM)	**41ab** (%)	**[41ab]** (mM)	**41ab** (%)
1	0.02	0.00	0.01	0.00	0.01	0.00
2	0.93	0.22	1.63	0.38	1.37	0.32
3	4.62	1.09	8.65	2.04	6.66	1.57
4	9.69	2.28	19.18	4.52	11.79	2.78
5	12.80	3.02	27.47	6.47	18.09	4.26
7	20.01	4.71	42.62	10.04	25.63	6.04
10	33.87	7.98	55.76	13.14	39.61	9.33
13	43.25	10.19	67.15	15.82	50.39	11.87
16	52.37	12.34	76.26	17.97	59.94	14.12
20	66.07	15.57	88.92	20.95	70.90	16.70

[a] Reaction conditions: Bromobenzene **40b** (0.5 mmol, 1.0 equiv), fluoroarene **39a** (1.5 mmol, 3.0 equiv), (NMe$_4$) 4-fluorobenzoate (see above), (NMe$_4$)OPiv (0.4 equiv), (NMe$_4$)OC(CF$_3$)$_3$ (2.5 equiv), **Ru-C5** (2.0 mol %), ^{t}BuCN (10.0 equiv), dodecane (0.2 equiv), and ethylpivalate co-solvent (280 µL) were stirred at 115 °C under N_2 in a closed vessel. Small aliquots were taken at the each stated time (see above). Yields were evaluated by GC-FID with dodecane as internal standard.

Table 2.33. Arylation data and concentration *Vs* time plots for the arylation of **39a** with **40b** at different concentration of (NMe$_4$) 4-fluorobenzoate.

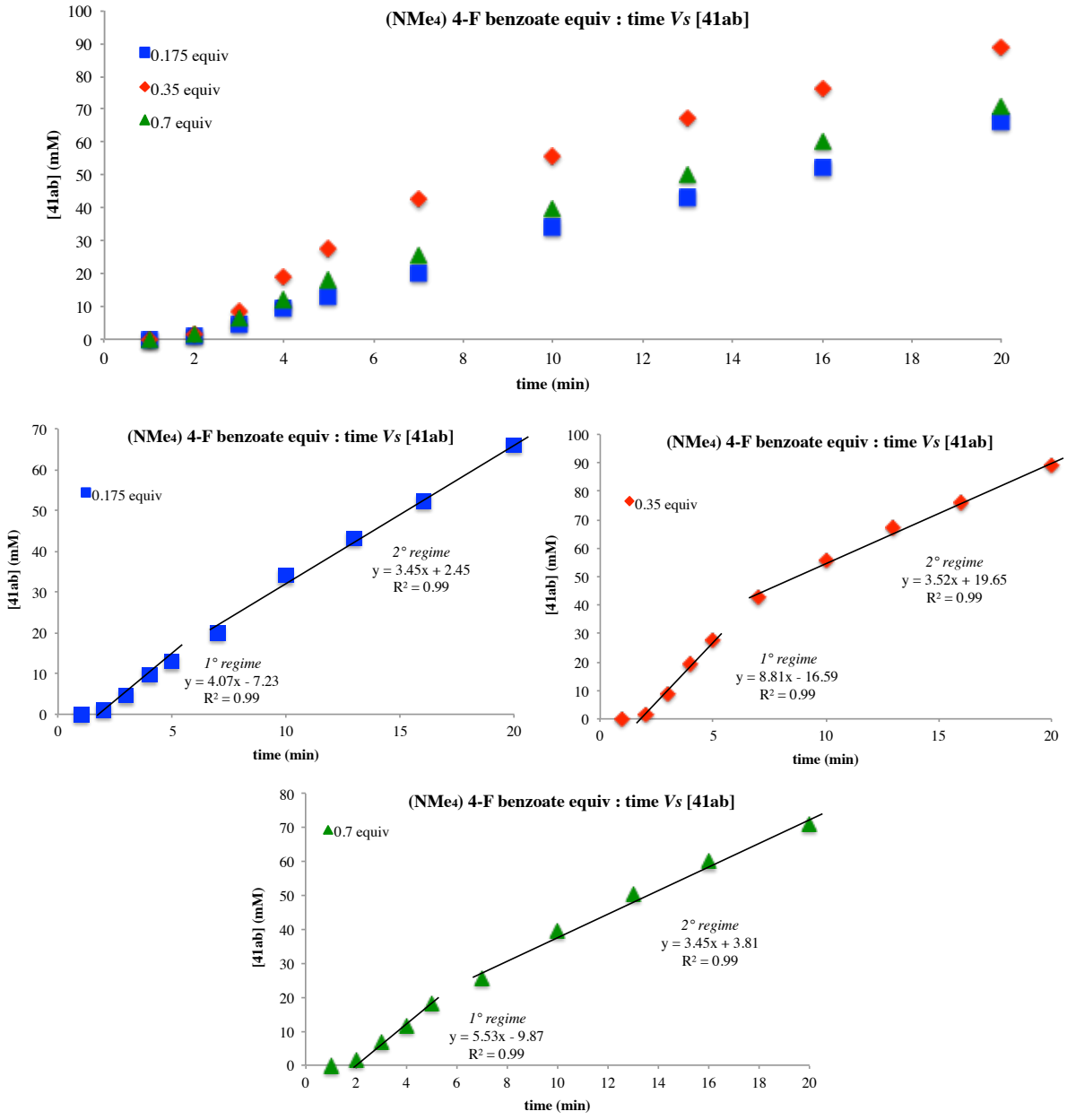

Graph 2.13. Rates of formation for **41ab** (mM/min); two different regimes are shown for each concentration of (NMe_4) 4-fluorobenzoate for the arylation of **39a** with **40b**.

			1° regime		*2° regime*	
	[**4F-OBz**] (mM)	ln[**4F-OBz**]	r_{obs} (mM/min)	ln(r_{obs})	r_{obs} (mM/min)	ln(r_{obs})
0.175 equiv	74.28	4.31	4.07	1.40	3.45	1.24
0.35 equiv	148.56	5.00	8.81	2.18	3.52	1.26
0.7 equiv	297.11	5.69	5.53	1.71	3.45	1.24

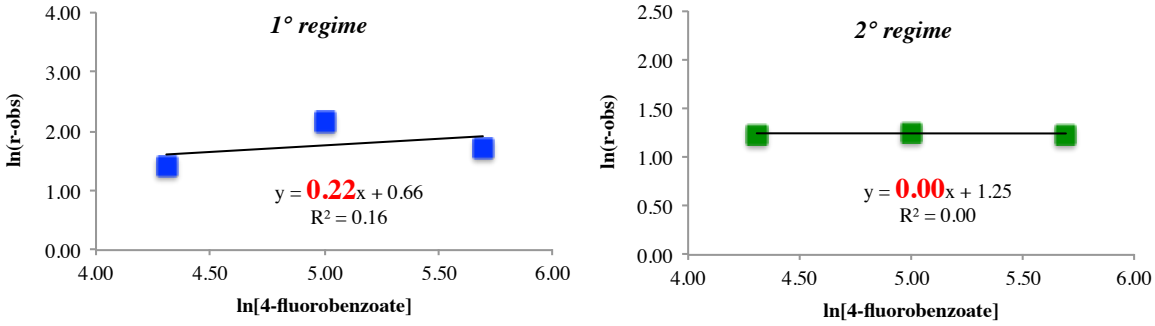

Table 2.34. Kinetic order with respect to (NMe_4) 4-fluorobenzoate for the arylation **39a** with **40b**.

The kinetic orders in (NMe_4)OPiv were found to be positive, specifically ≈ 0.4 for both regimes (Table 2.35, Table 2.36, Graph 2.14). These data are less intuitive and perhaps more cryptic to be rationalised.

Similarly to our reasoning concerning the fractional positive order in fluoroarene **39a**, the pivalate might participate in the formation of an off-cycle equilibrium. A (bis)perfluoroaryl Ru(II) species, arising from a second C–H activation event promoted by pivalate, would explain the observed < 1 value.

Moreover, although the pivalate additive has a positive outcome on the kinetic profile of the process, the benzoate additive is crucial for the reaction to proceed. If we assume that the role of pivalate is to assist the metalation of the fluoroarene substrate while the benzoate helps the formal oxidative addition step, the different coordination ability of these two carboxylates might need to be taken into consideration for the fractional positive orders in (NMe_4)OPiv. As the arylation is a complex and delicate weave of reversible steps until the irreversible formation of the C_{Ar}– C_{Ar} bond in biaryl **41ab**, the more coordinating pivalate might outcompete the available coordination site(s) on the Ru centre when the benzoate needs to be involved in triggering the redox susceptibility of the perfluoroaryl Ru(II) arising

from C–H activation. However, more time-dependent studies at different concentration of pivalate will need to be performed in order to average out possible experimental errors.

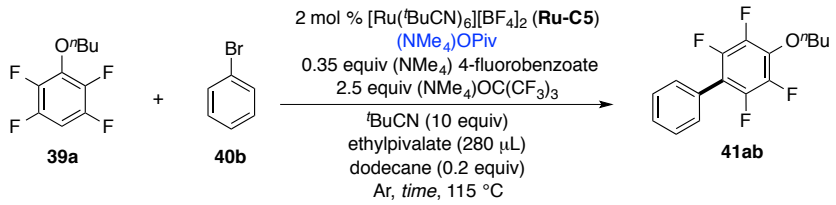

time (min)	0.2 equiv (NMe$_4$)OPiv [41ab] (mM)	0.2 equiv (NMe$_4$)OPiv 41ab (%)	0.4 equiv (NMe$_4$)OPiv [41ab] (mM)	0.4 equiv (NMe$_4$)OPiv 41ab (%)	0.8 equiv (NMe$_4$)OPiv [41ab] (mM)	0.8 equiv (NMe$_4$)OPiv 41ab (%)
1	0.01	0.03	0.01	0.00	0.01	0.00
2	1.07	0.25	1.63	0.38	1.45	0.34
3	4.73	1.11	8.65	2.04	6.90	1.63
4	8.37	1.97	19.18	4.52	13.38	3.15
5	11.90	2.80	27.47	6.47	20.15	4.75
7	19.85	4.68	42.62	10.04	33.84	7.97
10	30.17	7.11	55.76	13.14	47.25	11.13
13	37.61	8.86	67.15	15.82	64.96	15.30
16	45.42	10.70	76.26	17.97	79.49	18.73
20	58.36	13.75	88.92	20.95	95.32	22.47

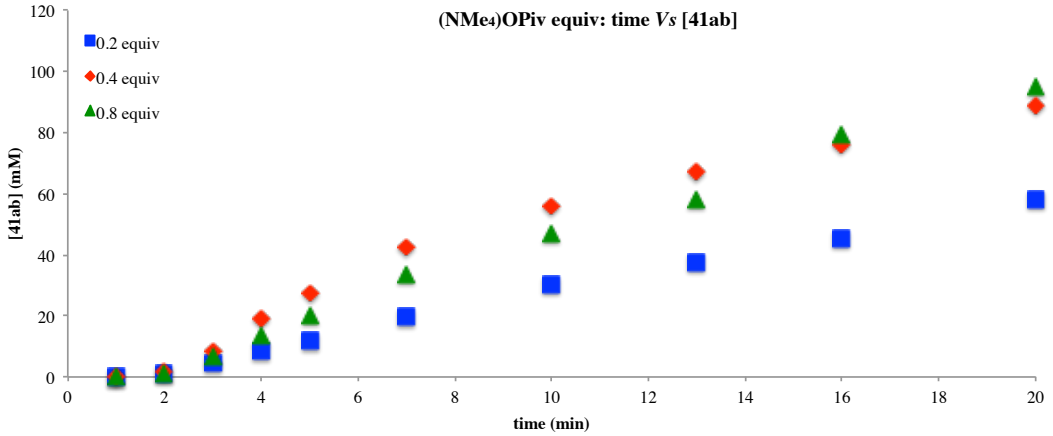

[a] Reaction conditions: Bromobenzene **40b** (0.5 mmol, 1.0 equiv), fluoroarene **39a** (1.5 mmol, 3.0 equiv), (NMe$_4$) 4-fluorobenzoate (0.35 equiv), (NMe$_4$)OPiv (see above), (NMe$_4$)OC(CF$_3$)$_3$ (2.5 equiv), **Ru-C5** (2.0 mol %), ^{t}BuCN (10.0 equiv), dodecane (0.2 equiv), and ethylpivalate co-solvent (280 µL) were stirred at 115 °C under N_2 in a closed vessel. Small aliquots were taken at the each stated time (see above). Yields were evaluated by GC-FID with dodecane as internal standard.

Table 2.35. Arylation data and concentration *Vs* time plots for the arylation of **39a** with **40b** at different concentration of (NMe$_4$)OPiv.

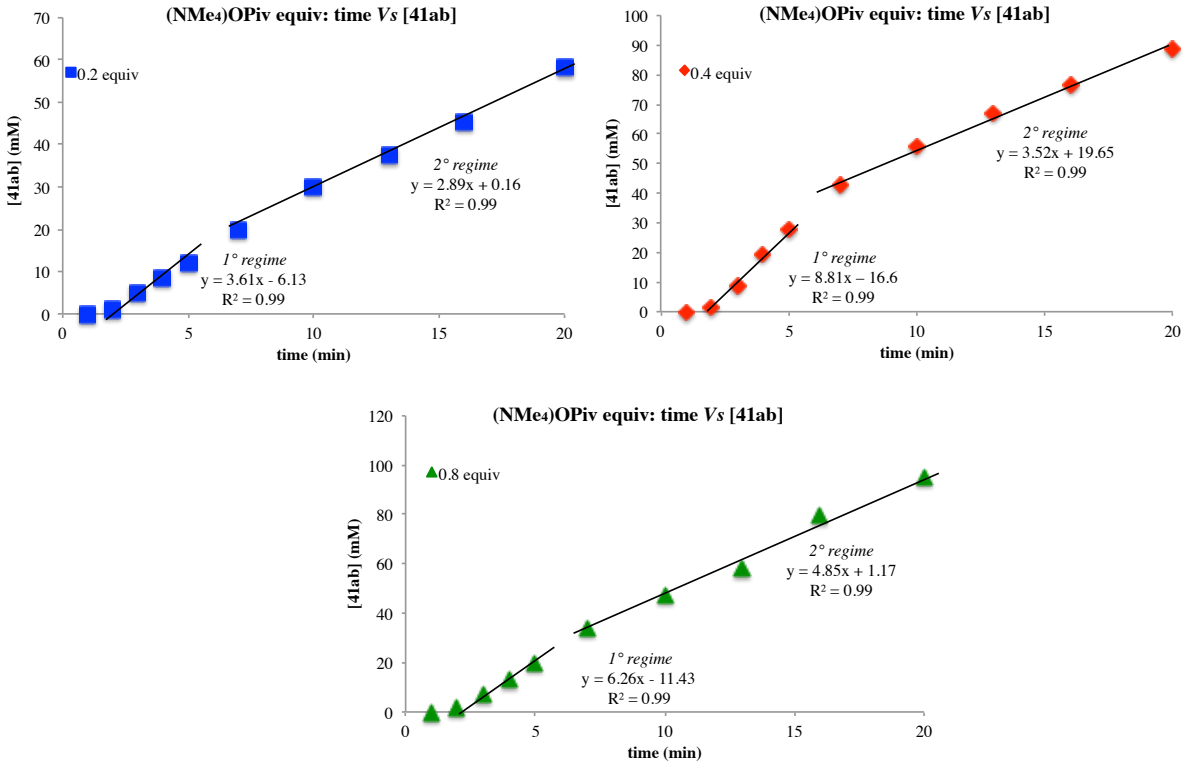

Graph 2.14. Rates of formation for **41ab** (mM/min); two different regimes are shown for each concentration of (NMe_4)OPiv for the arylation of **39a** with **40b**.

			1° regime		*2° regime*	
	[**OPiv**] (mM)	ln[**OPiv**]	r_{obs} (mM/min)	ln(r_{obs})	r_{obs} (mM/min)	ln(r_{obs})
0.2 equiv	84.89	4.44	3.61	1.28	2.89	1.06
0.4 equiv	169.78	5.13	8.81	2.18	3.52	1.26
0.8 equiv	339.56	5.83	6.26	1.83	4.85	1.58

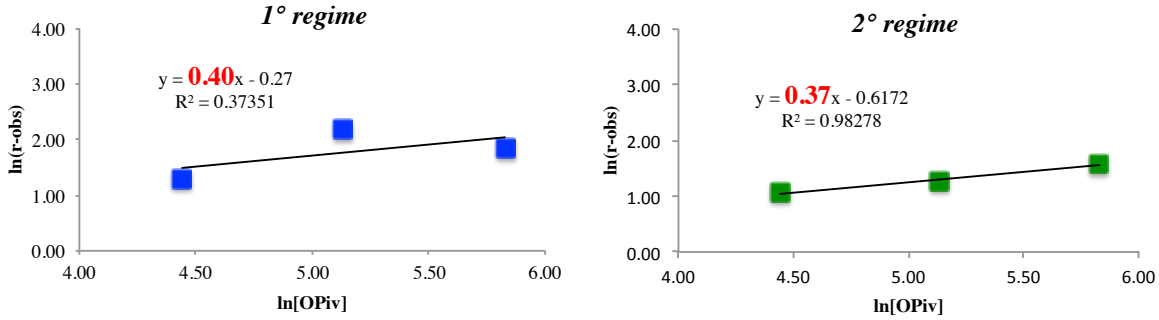

Table 2.36. Kinetic order with respect to (NMe_4)OPiv for the arylation **39a** with **40b**.

The kinetic order in $(NMe_4)OC(CF_3)_3$ (Table 2.37, Table 2.38, Graph 2.15) was assessed to be substantially different for the burst period and for the steady-state regime. In fact the order for the 1° regime was ≈ –0.7, whereas the order for the 2° regime was ≈ 0.7.

Although of difficult and debatable interpretation, these data might give a hint towards the understanding of the activation mode of catalyst **Ru-C5**. An initial scenario where the visually more soluble $(NMe_4)OC(CF_3)_3$ promotes a fast counteranion exchange, forming $[Ru(^tBuCN)_6][OC(CF_3)_3]_2$ by $(NMe_4)BF_4$ precipitation, might be likely to occur. Therefore high concentration of perfluoro-*tert*-butoxide could prevent pivalate coordination and somehow interfere with the kinetic relevant C–H activation step, possibly explaining the negative order in $(NMe_4)OC(CF_3)_3$ during the initial burst.

Owing the kinetic importance of the C–H activation step, during the steady-state period the order in perfluoro-*tert*-butoxide was positive. In fact, the prevention of protodemetalation, by deprotonation of PivOH, readily increases the rate of formation of biaryl **41ab**.

Fractional orders might be due to a combination of both of these contrasting effects. However, more kinetic points might need to be acquired to have a clearer understanding on the matter.

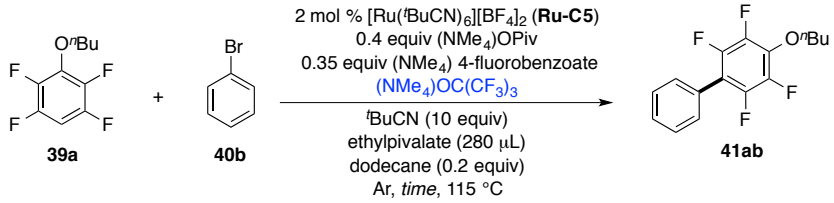

time (min)	0.2 equiv (NMe4)OC(CF3)3 [41ab] (mM)	0.2 equiv (NMe4)OC(CF3)3 41ab (%)	0.4 equiv (NMe4)OC(CF3)3 [41ab] (mM)	0.4 equiv (NMe4)OC(CF3)3 41ab (%)	0.8 equiv (NMe4)OC(CF3)3 [41ab] (mM)	0.8 equiv (NMe4)OC(CF3)3 41ab (%)
1	0.01	0.00	0.01	0.00	0.04	0.01
2	3.13	0.74	1.63	0.38	0.65	0.15
3	10.51	2.48	8.65	2.04	3.58	0.84
4	18.97	4.47	19.18	4.52	8.10	1.91
5	26.23	6.18	27.47	6.47	12.05	2.84
7	34.22	8.06	42.62	10.04	20.06	4.73
10	52.58	12.39	55.76	13.14	31.05	7.32
13	63.89	15.05	67.15	15.82	42.88	10.10
16	64.18	15.12	76.26	17.97	54.76	12.90
20	73.90	17.41	88.92	20.95	66.81	15.74

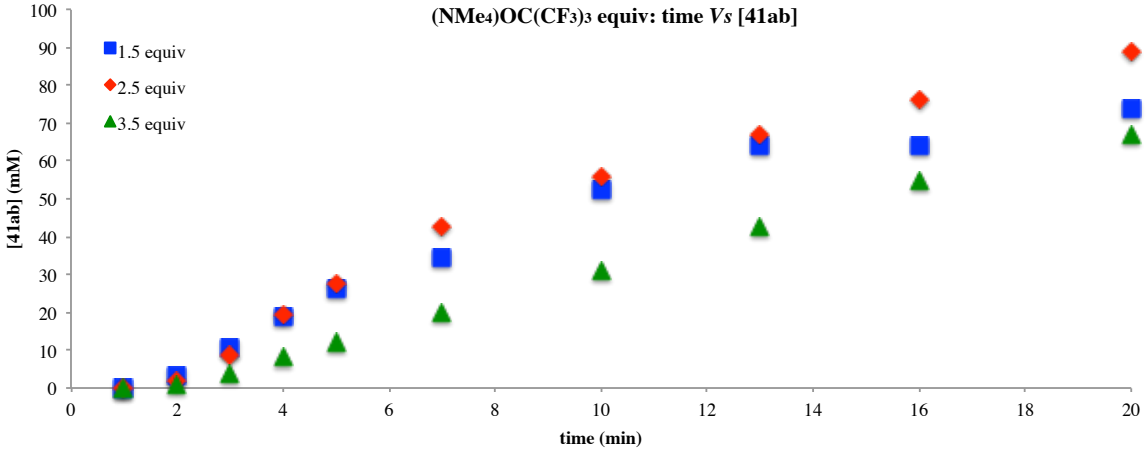

[a] Reaction conditions: Bromobenzene **40b** (0.5 mmol, 1.0 equiv), fluoroarene **39a** (1.5 mmol, 3.0 equiv), (NMe_4) 4-fluorobenzoate (0.35 equiv), $(NMe_4)OPiv$ (0.4 equiv), $(NMe_4)OC(CF_3)_3$ (see above), **Ru-C5** (2.0 mol %), ^{t}BuCN (10.0 equiv), dodecane (0.2 equiv), and ethylpivalate co-solvent (280 μL) were stirred at 115 °C under N_2 in a closed vessel. Small aliquots were taken at the each stated time (see above). Yields were evaluated by GC-FID with dodecane as internal standard.

Table 2.37. Arylation data and concentration *Vs* time plots for the arylation of **39a** with **40b** at different concentration of $(NMe_4)OC(CF_3)_3$.

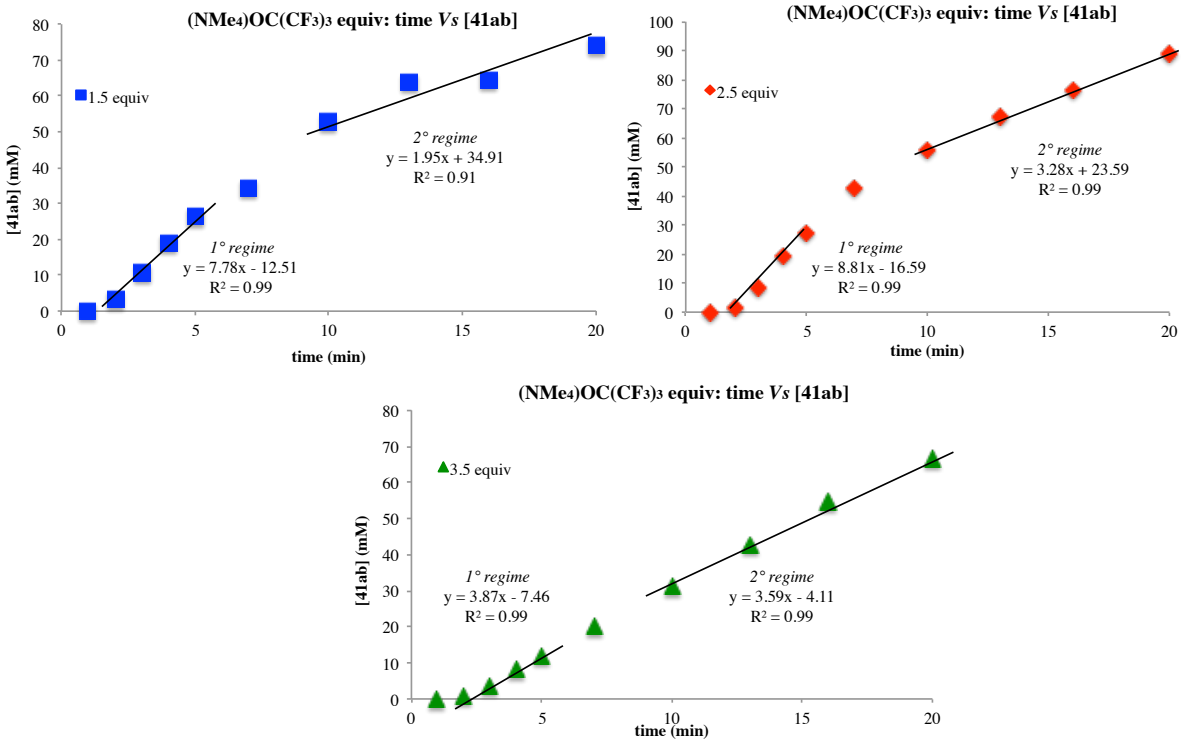

Graph 2.15. Rates of formation for **41ab** (mM/min); two different regimes are shown for each concentration of $(NMe_4)OC(CF_3)_3$ for the arylation of **39a** with **40b**.

			1° regime		*2° regime*	
	[**alkoxide**] (mM)	ln[**alkoxide**]	r_{obs} (mM/min)	ln(r_{obs})	r_{obs} (mM/min)	ln(r_{obs})
1.5 equiv	636.67	6.46	7.78	2.05	1.95	0.67
2.5 equiv	1061.12	6.97	8.81	2.18	3.28	1.19
3.5 equiv	1485.57	7.30	3.87	1.35	3.59	1.28

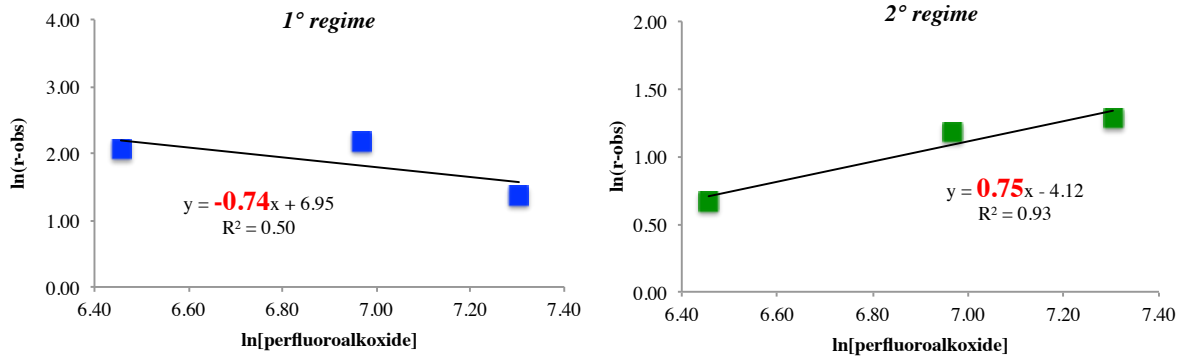

Table 2.38. Kinetic order with respect to $(NMe_4)OC(CF_3)_3$ for the arylation **39a** with **40b**.

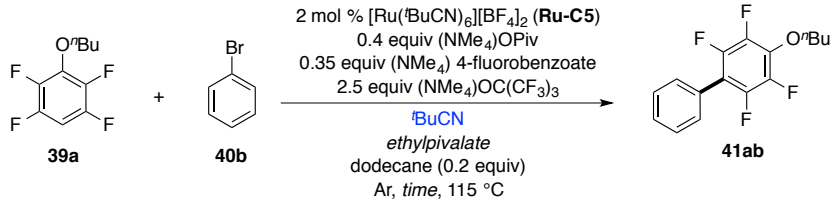

time (min)	2.71 equiv ^{t}BuCN [41ab] (mM)	2.71 equiv ^{t}BuCN 41ab (%)	5.42 equiv ^{t}BuCN [41ab] (mM)	5.42 equiv ^{t}BuCN 41ab (%)	9.03 equiv ^{t}BuCN [41ab] (mM)	9.03 equiv ^{t}BuCN 41ab (%)
1	0.02	0.00	0.08	0.02	0.01	0.00
2	6.28	1.20	3.48	0.66	1.50	0.28
3	21.22	4.04	14.00	2.67	7.33	1.40
4	34.67	6.60	24.48	4.66	14.13	2.69
5	47.12	8.97	34.18	6.51	20.40	3.88
7	67.73	12.90	58.59	11.16	34.78	6.62
10	88.14	16.78	79.65	15.17	50.40	9.60
13	101.22	19.27	100.54	19.14	69.32	13.20
16	110.34	21.01	113.53	21.62	81.32	15.48
20	121.94	23.22	131.51	25.04	97.11	18.49

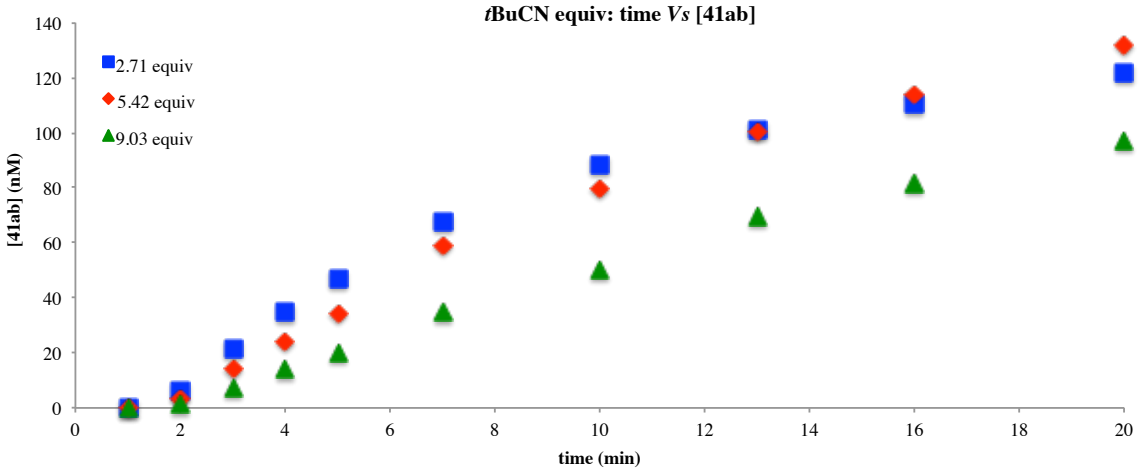

[a] Reaction conditions: Bromobenzene **40b** (0.5 mmol, 1.0 equiv), fluoroarene **39a** (1.5 mmol, 3.0 equiv), (NMe_4) 4-fluorobenzoate (0.35 equiv), $(NMe_4)OPiv$ (0.4 equiv), $(NMe_4)OC(CF_3)_3$ (2.5 equiv), **Ru-C5** (2.0 mol %), ^{t}BuCN (see above), dodecane (0.2 equiv), and ethylpivalate co-solvent (the amount was adjusted in order to keep an identical concentration for each case, see SI for details) were stirred at 115 °C under N_2 in a closed vessel. Small aliquots were taken at the each stated time (see above). Yields were evaluated by GC-FID with dodecane as internal standard.

Table 2.39. Arylation data and concentration *Vs* time plots for the arylation of **39a** with **40b** at different concentration of ^{t}BuCN.

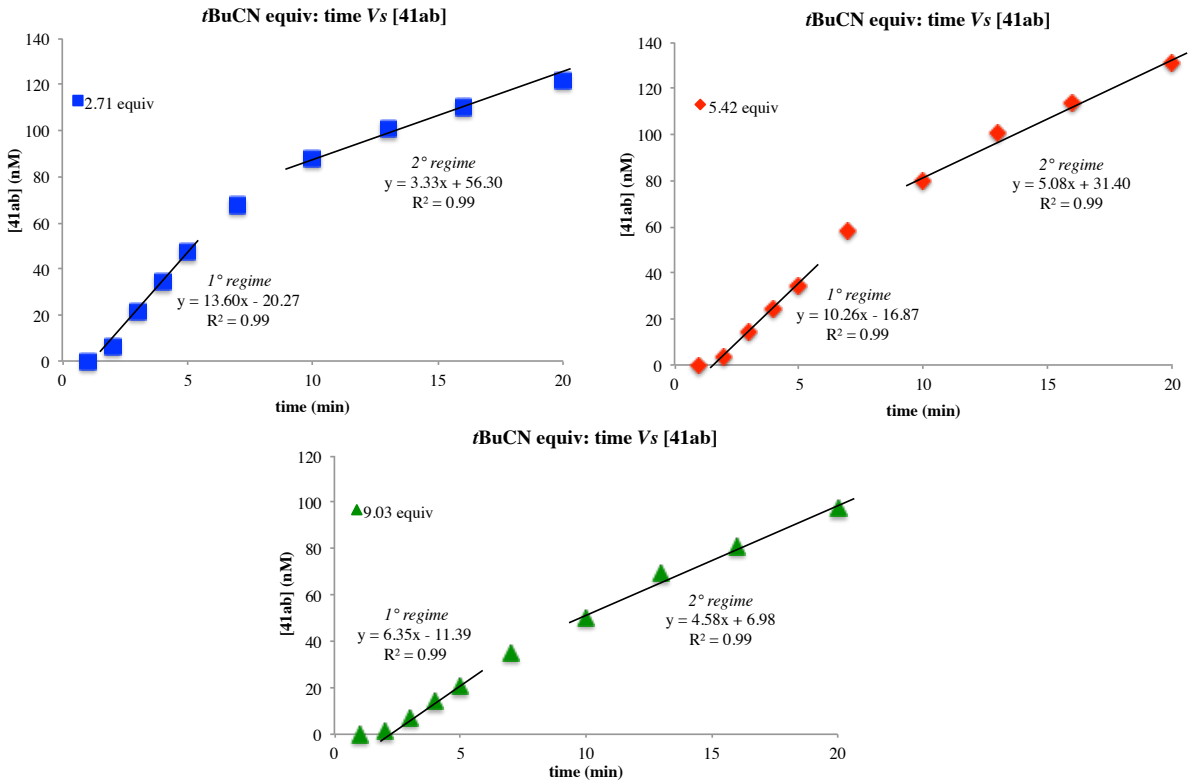

Graph 2.16. Rates of formation for **41ab** (mM/min); two different regimes are shown for each concentration of ^{t}BuCN for the arylation of **39a** with **40b**.

			1° regime		*2° regime*	
	[^{t}**BuCN**] (mM)	ln[^{t}**BuCN**]	r_{obs} (mM/min)	ln(r_{obs})	r_{obs} (mM/min)	ln(r_{obs})
2.71 equiv	1422.42	7.26	13.60	2.61	3.30	1.19
5.42 equiv	2897.41	7.97	10.26	2.33	5.08	1.63
9.03 equiv	4741.39	8.46	6.35	1.85	4.58	1.52

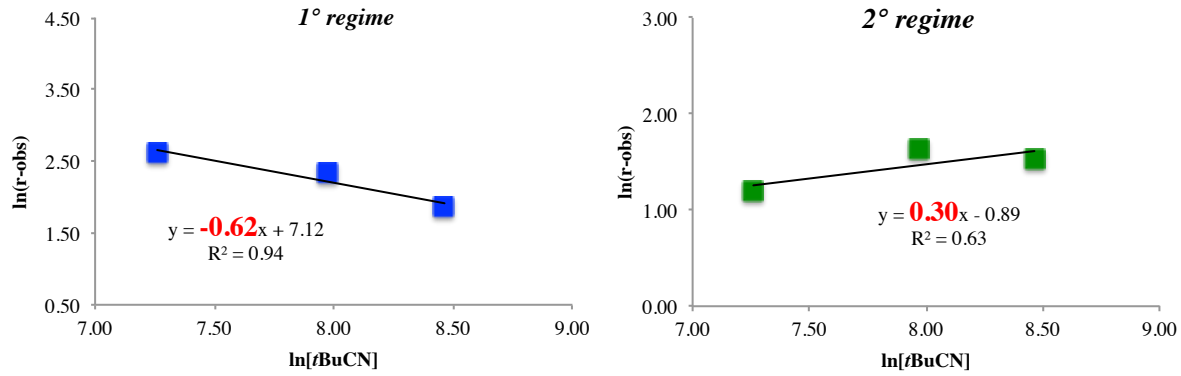

Table 2.40. Kinetic order with respect to ^{t}BuCN for the arylation **39a** with **40b**.

Similarly to our previous analysis, the kinetic order in ^{t}BuCN (Table 2.39,Table 2.40, Graph 2.16) was measured to be different for the burst period and for the steady-state regime. In fact, the order for the 1° regime was ≈ –0.6, whereas the order for the 2° regime was = 0.3, with a much worse linear fitting.

Analogously to the negative order encountered in the initial burst with perfluoro-*tert*-butoxide, the negative order during the 1° regime of ^{t}BuCN could be rationalised by a similar approach. During the first catalytic turnover, high concentration of pivalonitrile ligand might prevent the formation of the pivalate-containing ruthenium species able to perform C–H activation, reducing the overall arylation rate. However, more data points need to be taken in order to confirm the nearly zero order dependence in the concentration of pivalonitrile on the rateof formation of biaryl **41ab** during the steady-state period.

On the basis of our experimental and computational observations, a plausible catalytic cycle is described in Scheme 2.28. Perfluoro-*tert*-butoxide irreversibly promotes counteranion exchange from catalyst $[Ru(^tBuCN)_6)][BF_4]_2$ (**Ru-C5**), generating $[Ru(^tBuCN)_6][OC(CF_3)_3]_2$ (**XCV**) by precipitation of the highly insoluble $(NMe_4)BF_4$. An equilibrium established among $(NMe_4)OPiv$, $(NMe_4)OC(CF_3)_3$, ^{t}BuCN and species **XCV** lead to the formation of the active cationic ruthenium(II) intermediate (**XCVI**). The formation of this equilibrium might explain the negative order dependence of rate on the concentration of ^{t}BuCN and $(NMe_4)OC(CF_3)_3$ during the burst regime. The cationic species **XCVI** performs reversible C–H activation on the perfluoroarene (**Ar^F**H) *via* concerted metalation-deprotonation (**XCVII**) affording aryl ruthenium complex **XCVIII**. This species, in the presence of $(NMe_4)OPiv$ and another molecule of **Ar^F**H, could potentially generate the (bis)aryl ruthenium(II) species **XCIX**, providing one potential rationalisation for the fractional positive order in fluoroarene and pivalate measured during the kinetic analysis. Intermediate **XCVIII** becomes redox-active in the presence of the benzoate additive, undergoing a formal oxidative addition/reductive elimination steps with the aryl halide. This forms the biaryl product (**Ar^F**–**Ar**) and the Br-containing Ru(II)-complex (**C**) (burst kinetic, *1° regime*). Finally, catalyst regeneration promoted by $(NMe_4)OPiv$ *via* $(NMe_4)Br$

precipitation restores the active intermediate **XCVI** and leads to the next catalytic cycle (steady-state rate, *2° regime*). Therefore, the catalyst regeneration step might provide a reasonable explanation regarding the initial kinetic burst detected during the kinetic analysis.

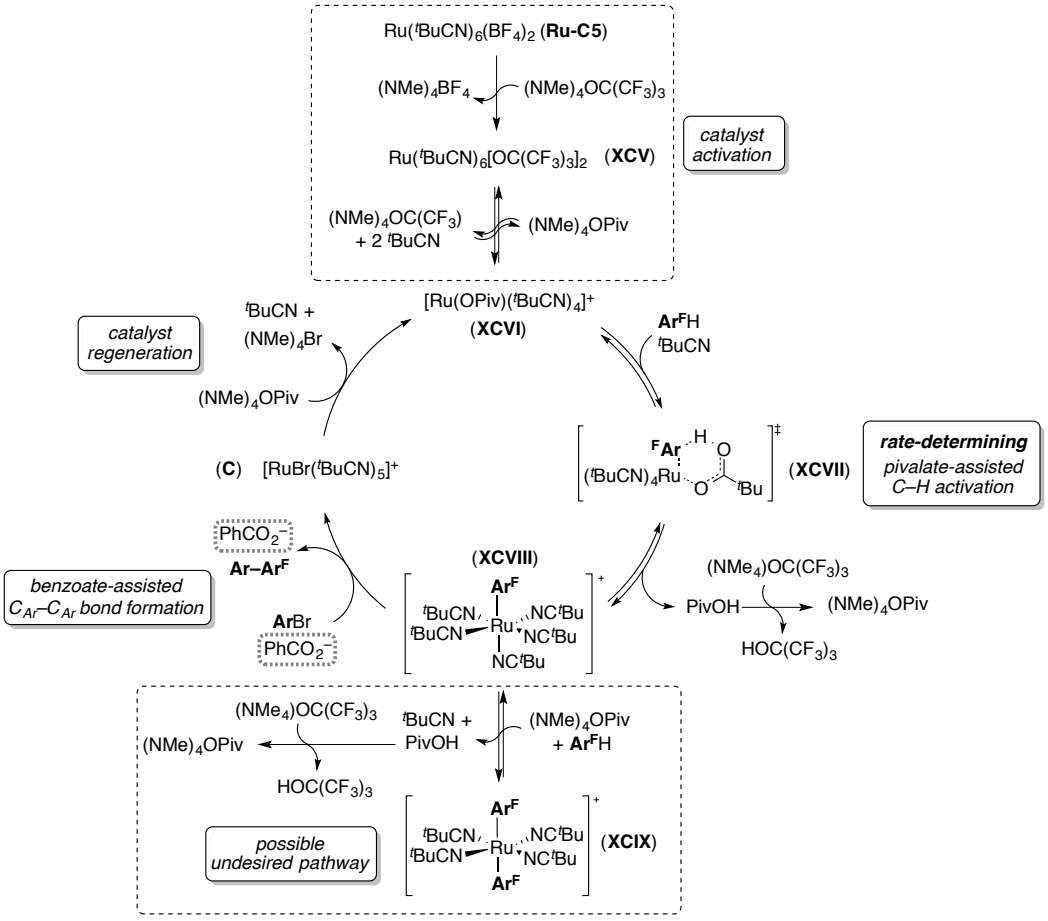

Scheme 2.28. Proposed catalytic cycle for the Ru-catalysed C–H arylation of polyfluoroarenes with aryl halides.

2.13. Conclusion

We have described the first ruthenium-catalysed system capable of C–H arylation of arenes without the need for a directing group. This methodology is applicable to a wide array of (hetero)arenes bearing an acidic proton and presents a broad functional group tolerance. Contrarily to previous reports on Pd, Cu and Au-catalysis, the metalation/arylation site-selectivity on the electron-deficient arene seems to be governed by both electronic and steric factors.

^{19}F-NMR and ^{1}H-NMR studies have demonstrated that Ru(II)biscarboxylate(η^6-arene) complexes are able to perform C–H activation on arenes without a chelating group, but the resulting aryl ruthenium(II) species does not react with the electrophile unless the (η^6-arene)-ligand is displaced by the nitrile solvent. As a consequence of this, solvated Ru(II) species are capable of C–H activation as well. The synthesis and characterisation of unprecedented aryl-Ru(II) intermediates confirmed the spectroscopic data, permitting us to design a novel, more effective nitrile-containing Ru(II) catalyst. The aryl-Ru(II) species, generated from metalation of the perfluorinated arene, reacts with aryl halides to form biaryl product in both single-turnover and catalytic manners, but only if a benzoate additive is present in the reaction mixture. On the other hand, DG-containing arenes do not require this additive, suggesting that the benzoic acid triggers the redox susceptibility of the ruthenated species in a similar fashion to *ortho*-metalated Ru(II) complexes.

D/H labelling experiments demonstrated the reversibility of the C–H activation under the reaction conditions. Nevertheless, KIE experiments revealed the ruthenation of the substrate to be kinetically significant. This implies that the rates of protoderuthenation and arylation of the Ru(II) intermediate generated from C–H activation, must be similar.

Competition arylation experiments among electronically diverse aryl halides suggest a change in the mechanism of the formal oxidative addition/reductive elimination steps dependant on the nature of the halogen.

The catalytic system shows relevant differences in terms of regioselectivity with previously described Pd catalysts. DFT calculations suggest that the difference between both systems arise mainly from a larger relevance of steric factors in the Ru system.

A kinetic analysis based on initial rate method disclosed an initial burst kinetic regime followed by a steady-state reaction. The initial burst was related to the first catalytic turnover in Ru-catalyst, suggesting that the catalyst regeneration step was accountable for the lower arylation in rate in the steady-state regime. The kinetic order for each single component of the reaction was also determined. Particularly, the zero order dependence in the concentration of the aryl bromide and in 4-fluorobenzoate, along with the positive orders in Ru and fluoroarene, suggest that the C–H activation is the rate-determining step of the reaction.

Further investigations on the mechanism aimed to understand the role of action of the benzoate additive, shedding light on the mechanism of the formal oxidative addition/reductive elimination steps, would be the main focus of our future studies.

2.14. Experimental procedures and characterisation of the compounds

General Information

Unless otherwise indicated, all reactions were carried out in Schlenk vials using reagents obtained from commercial sources and used without further purification. All solid reagents were kept under vacuum in a desiccator for 24 h prior to use and stored under vacuum in a desiccator, unless otherwise stated. All other starting materials and solvents were purchased from Acros, Aldrich, Alfa Aesar, Fluorochem, Apollo Scientific and Manchester Organics, and used without further purification unless otherwise stated. 2,3,5,6-tetrafluoro-*N*,*N*-dimethylaniline (**39g**), [157] 1-bromo-2-phenoxybenzene (**40a'**), [158] 1-(benzyloxy)-2-bromobenzene (**40c'**),[159] 2-phenoxypyridine (**48**),[160] 1-benzyl-5-phenyl-*1H*-tetrazole (**50**),[161] and 1-(pyrimidin-2-yl)-*1H*-indole (**51**)[162] were prepared according to reported methods. Column chromatography was carried out on silica gel, particle size 40-63 μm, using flash techniques. Melting points were obtained using a Stuart SMP11 apparatus and are uncorrected. IR spectra were recorded using a Thermo Scientific Nicolet iS5 FTIR machine, relevant bands are quoted in cm^{-1}. High resolution mass spectra were performed at the EPSRC National Mass Spectrometry Service Centre (Swansea) or by the School of Chemistry Mass Spectrometry Service (University of Manchester) employing a Thermo Finnigan MAT95XP spectrometer. Mass spectra for the characterization of ruthenium complexes were performed by the School of Chemistry Mass Spectrometry Service (University of Manchester) employing a Waters SQD2 spectrometer. Elemental analyses were performed by the School of Chemistry Microanalysis Laboratory (University of Manchester) using a Flash 2000 elemental analyzer machine. ^{1}H NMR, ^{19}F NMR and ^{13}C NMR spectra were recorded at 400 or 500 MHz on Bruker machines. ^{1}H NMR are referenced to the residual solvent peak at 7.26 ppm ($CDCl_3$), 2.05 ppm ($(CD_3)_2CO$), 5.32 ppm (CD_2Cl_2), 4.79 ppm (D_2O) and quoted in ppm to 2 decimal places with coupling constants (*J*) to the nearest 0.1 Hz. ^{13}C NMR spectra, recorded at 100 MHz or 126 MHz, are referenced to the solvent peak at 77.16 ppm ($CDCl_3$), 29.84 ppm ($(CD_3)_2CO$) or 53.84 ppm (CD_2Cl_2) and quoted in ppm to 1 decimal place with coupling constants (*J*) to the nearest 0.1

Hz. ^{19}F NMR spectra were recorded at 376 or 471 MHz in $CDCl_3$, $(CD_3)_2CO$, CD_2Cl_2 or D_2O, and quoted in ppm to 2 decimal places and with coupling constants (*J*) to the nearest 0.1 Hz.

General Procedure 1 for the C–H arylation of (hetero)aromatic arenes with aryl halides

$[Ru(^tBuCN)_6](BF_4)_2$ (**Ru-C5**) (15.5 mg, 0.020 mmol), aryl bromide (if solid, 0.50 mmol), arene (if solid, 1.50 mmol), $(NMe_4)OC(CF_3)_3$ (386.5 mg, 1.250 mmol), (NMe_4) 4-fluorobenzoate (37.3 mg, 0.175 mmol) and (NMe_4)OPiv (35.1 mg, 0.20 mmol) were weighed in the open air and placed in a crimp-cap Schlenk microwave vial (10 mL) with a magnetic stirrer bar, unless otherwise stated. The reaction vessel was capped, evacuated and backfilled with N_2 three times, then left under vacuum for 30 min. The vial was then backfilled with N_2 and aryl bromide (if liquid, 0.50 mmol), arene (if liquid, 1.50 mmol) and pivalonitrile (166.3 μL, 1.50 mmol) were added *via* syringe unless otherwise stated. The vial was resealed with a new cap under a stream of N_2 and the mixture was stirred for 16 h at 115 °C. On completion of the reaction, the mixture was diluted with Et_2O and filtered through a cotton plug. Evaporation of the solvent and purification by silica gel column chromatography afforded the corresponding biaryls.

Procedure 2 for D/H scrambling of d_1-39a/39a *via* Ru1-39a by reversible C–D / C–H activation

PivOH (0.3 equiv, 0.15 mmol), K_2CO_3 (2.0 equiv, 1.00 mmol) and $[RuCl_2(p\text{-cymene})]_2$ (5 mol %, 0.05 mmol) were weighed in a Schlenk microwave vial (10 mL) with a magnetic stirrer bar. The reaction vessel was capped, evacuated and backfilled with N_2 three times, then left under vacuum for 30 min. The vial was then backfilled with N_2 and 1.0 mL of a 0.5 M solution of a 98:2 mixture of **d_1-39a**:**39a** (1.0 equiv, 0.50 mmol) in 1,4-dioxane was then added *via* syringe. The vial was resealed with a new cap under a stream of N_2 and the mixture was heated to 90 ºC for 16 h. Upon completion, the reaction mixture was cooled to

room temperature diluted with 3 mL of Et_2O, filtered through a cotton plug and evaporated *in vacuo* to give a residue, to which 1,3,5-trimethoxybenzene (0.33 equiv, 0.167 mmol) was added as internal standard in $CDCl_3$.

General Procedure 3 of the C–H Activation of Fluoroarenes with Complex Ru-C1

$Ru(OPiv)_2$(*p*-cymene) (**Ru-C1**) (1.0 equiv) and the appropriate base (if any, *see section 2.3*) were weighed in the open air and placed in a crimp-cap Schlenk microwave vial (10 mL) with a magnetic stirrer bar. The reaction vessel was capped, evacuated and backfilled with Ar three times, then left under vacuum for 30 min. The vial was then backfilled with Ar and the appropriate perfluoroarene (*see section 2.3*) and solvent (*see section 2.3*) were added *via* syringe. The vial was resealed with a new cap under a stream of Ar and the reaction was heated at the stated temperature (*see section 2.3*) for the specified time (*see section 2.3)*. Upon completion, the reaction mixture was cooled to room temperature and a given amount of 1,3,5-trimethoxybenzene was added as internal standard in $CDCl_3$. The crude mixture was then filtered through a cotton plug directly to an NMR tube. If purification was needed after NMR analysis, the crude was evaporated, dissolved in hexane and loaded on a silica column. The column was flushed with a 0-15% Et_2O-hexane gradient using N_2 in replacement of compressed air. The yellow band observed was eluted and evaporated *in vacuo* to give the desired aryl ruthenium complex as a yellow/orange solid. The final complexes are stable under air for a few days, but decompose if exposed to oxygen for longer. Storage in a desiccator under vacuum or in a glove box is needed. Suitable crystals of **Ru1-39c** for X-ray crystallography (see crystallographic section) were grown by slow evaporation from a concentrated solution of the complex in $CDCl_3$.

Characterization data of Ru1-39a, Ru1-39b and Ru1-39c

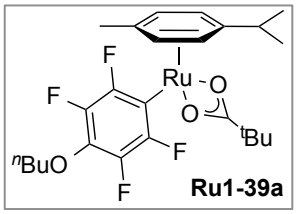

The General Procedure 3 was applied with $Ru(OPiv)_2$(*p*-cymene) (**Ru-C1**) (1.0 equiv, 87.5 mg, 0.20 mmol), 3-butoxy-1,2,4,5-tetrafluorobenzene (**39a**) (888.8 mg, 4.00 mmol), Na_2CO_3 (42.4 mg, 0.4 mmol), 1,4-dioxane (0.4 mL, 0.5 M), 120 °C, 16 h. Column chromatography afforded the title product as a dark yellow/orange solid (66.9 mg, 60%).

^{1}H NMR (400 MHz, $CDCl_3$): δ 5.55 (d, *J* = 5.9 Hz, 2H), 5.22 (d, *J* = 5.9 Hz, 2H), 4.10 (t, *J* = 6.8 Hz, 2H), 2.85 (septet, *J* = 6.9 Hz, 1H), 2.10 (s, 3H), 1.72 (app quintet, *J* = 7.0 Hz, 2H), 1.49 (app sextet, *J* = 7.4 Hz, 2H), 1.34 (d, *J* = 6.8 Hz, 6H), 0.95 (t, *J* = 7.4 Hz, 3H), 0.76 (s, 9H); ^{13}C NMR (100 MHz, $CDCl_3$): δ 196.0, 148.0 (dm, *J* = 224.9 Hz), 140.3 (dm, *J* = 249.3 Hz), 133.3 - 133.0 (m), 130.6 - 129.5 (m), 106.3, 93.3, 80.6, 78.1, 74.8 (t, *J* = 2.6 Hz), 40.1, 32.1, 27.8, 26.1, 22.6, 19.1, 19.0, 13.9; ^{19}F NMR (376 MHz, $CDCl_3$) δ –119.2 - –119.3 (m, 2F), –158.7 - –158.8 (m, 2F); IR (ATR) 2962, 1489, 1439; 1080; m.p. 77 - 80 °C. Anal. Calcd. for $C_{25}H_{32}F_4O_3Ru$: C, 53.85; H, 5.78. Found: C, 53.76; H, 5.84. HRMS (APCI) *m/z* calcd. $C_{25}H_{32}F_4O_3Ru$ $[M]^+$ 558.1331; found $[M]^+$ 558.1316.

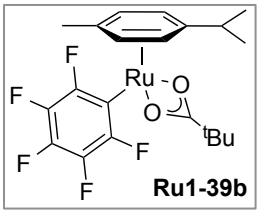

The General Procedure 3 was applied with $Ru(OPiv)_2$(*p*-cymene) (**Ru-C1**) (1.0 equiv, 87.5 mg, 0.20 mmol), pentafluorobenzene (**39b**) (444.0 μL, 4.00 mmol), Na_2CO_3 (42.4 mg, 0.4 mmol), 1,4-dioxane (0.4 mL, 0.5 M), 120 °C, 16 h. Column chromatography afforded the title product as a yellow solid (75.5 mg, 75%).

^{1}H NMR (400 MHz, $CDCl_3$): δ 5.56 (d, *J* = 5.8 Hz, 2H), 5.22 (d, *J* = 5.8 Hz, 2H), 2.84 (septet, *J* = 6.9 Hz, 1H), 2.09 (s, 3H), 1.34 (d, *J* = 6.9 Hz, 6H), 0.77 (s, 9H); ^{13}C NMR (126 MHz, $CDCl_3$): δ 196.3, 147.5 (dm, *J* = 225.3 Hz), 137.3 (dm, *J* = 240.3 Hz), 136.1 (dm, *J* = 251.8 Hz), 131.0 - 130.0 (m), 106.6, 93.5, 80.8, 78.1, 40.1, 32.1, 26.1, 22.6, 19.1; ^{19}F NMR (376 MHz, $CDCl_3$) δ –117.1 - –117.3 (m, 2F), 160.9 (t, *J* = 19.8 Hz, 1F), –164.0 - –164.2 (m, 2F); IR (ATR) 2966, 1488, 1438, 732; m.p. 139 -142 °C. Anal. Calcd for $C_{21}H_{23}F_5O_2Ru$:

C, 50.10; H, 4.60. Found: C, 50.21; H, 4.60. HRMS (APCI) *m/z* calcd. $C_{21}H_{23}F_5O_2Ru$ $[M]^+$ 504.0662; found $[M]^+$ 504.0656.

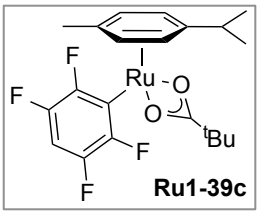

Ru1-39c

The General Procedure 3 was applied with $Ru(OPiv)_2$(*p*-cymene) (**Ru-C1**) (1.0 equiv, 87.5 mg, 0.20 mmol), 1,2,4,5-tetrafluorobenzene (**39c**) (446.6 μL, 4.00 mmol), Na_2CO_3 (42.4 mg, 0.4 mmol), 1,4-dioxane (0.4 mL, 0.5 M), 120 °C, 16 h. Column chromatography afforded the title product as a yellow/orange solid (74.9 mg, 77%).

^{1}H NMR (400 MHz, $CDCl_3$): δ 6.64 (tt, *J* = 9.5, 6.9 Hz, 1H), 5.56 (d, *J* = 6.0 Hz, 2H), 5.22 (d, *J* = 6.0 Hz, 2H), 2.85 (septet, *J* = 6.9 Hz, 1H), 2.10 (s, 3H), 1.34 (d, *J* = 6.9 Hz, 6H), 0.76 (s, 9H); ^{13}C NMR (100 MHz, $CDCl_3$): δ 196.1, 148.0 (dm, *J* = 225.2 Hz), 144.9 (dm, *J* = 248.7 Hz), 141.2 – 140.1 (m), 106.5, 101.4 (t, *J* = 23.5 Hz), 93.4, 80.8, 78.1, 40.1, 32.0, 26.1, 22.6, 19.1; ^{19}F NMR (376 MHz, $CDCl_3$) δ –119.3 - –119.4 (m, 2F), –142.3 - –142.4 (m, 2F); IR (ATR) 2966, 1489, 1443, 729; m.p. 141 - 145 °C. Anal. Calcd for $C_{21}H_{24}F_4O_2Ru$: C, 51.95; H, 4.98. Found: C, 51.86; H, 5.03. HRMS (APCI) *m/z* calcd. $C_{21}H_{24}F_4O_2Ru$ $[M]^+$ 486.0756; found $[M]^+$ 486.0745.

General Procedure 4 of the C–H activation of fluoroarenes 39a and d_1-39a with Complex Ru-C1 for the KIE experiment

$Ru(OPiv)_2$(*p*-cymene) (**Ru-C1**) (43.8 mg, 0.10 mmol), Na_2CO_3 (21.2 mg, 0.20 mmol) were weighed in the open air and placed in a crimp-cap Schlenk microwave vial (10 mL) with a magnetic stirrer bar. The reaction vessel was capped, evacuated and backfilled with Ar three times, then left under vacuum for 30 min. The vial was backfilled with Ar then **39a** or **d_1-39a** (111.1 or 111.6 mg, 0.50 mmol) and 1.4-dioxane (1.0 mL, 0.1 M with respect to **Ru-C1**) were added *via* syringe. The vial was resealed with a new cap under a stream of Ar and the mixture was stirred for 5 min at room temperature. The vial was then heated at 120 °C for the appropriate time (*see* Table 2.6). Upon completion, the vial was quickly cooled in a dry ice/acetone bath and a given amount of 1,3,5-trimethoxybenzene was added as internal

standard in $CDCl_3$. The crude was then filtered through a cotton plug directly into an NMR tube for analysis.

General Procedure 5 of the C–H arylation of 39a with bromoarene 40a or 40b

The appropriate ruthenium catalyst (**Ru-C1** – **Ru-C5**) (*see sections 2.4-2-7*), base (*see sections 2.4-2-7*) and additive(s) (if any, *see sections 2.4-2-7*) were weighed in a crimp-cap Schlenk microwave vial (10 mL) with a magnetic stirrer bar. The reaction vessel was capped, evacuated and backfilled with N_2 three times, then left under vacuum for 30 min. The vial was backfilled with N_2 then **39a** (*see sections 2.4-2-7*), **40a** or **40b** (1.0 equiv) and the appropriate solvent (*see sections 2.4-2-7)* were added *via* syringe. The vial was resealed with a new cap under a stream of N_2 and the reaction was heated at the stated temperature (*see sections 2.4-2-7*) for the specified time (*see sections 2.4-2-7*). Upon completion, the reaction mixture was cooled to room temperature and a given amount of 1,3,5-trimethoxybenzene or 1,3-dinitrobenzene was added as internal standard in $CDCl_3$. The crude was then filtered through a cotton plug directly into an NMR tube. If purification was needed after NMR analysis, the crude was evaporated, dissolved in hexane and loaded on a silica column for flash chromatography to afford the corresponding biaryls.

Procedure 6 for the C–H arylation of 39a with 40b (see Table 2.22[b])

All solid reagents, except **Ru-C5**, were dried at 70 °C in a vacuum oven over night. All liquid reagents were dried over 4 Å molecular sieves and degassed with 3 freeze-pump-thaw cycles. In a glove box, **Ru-C5** (0.02 mmol, 15.5 mg), (NMe_4) 4-fluorobenzoate (0.175 mmol, 37.3 mg), (NMe_4)OPiv (0.2 mmol, 35.1 mg), (NMe_4)$OC(CF_3)_3$ (1.25 mmol, 386.5 mg), bromobenzene (0.5 mmol, 53.5 μL), **39a** (1.50 mmol, 333.3 mg) and pivalonitrile (1.50 mmol, 166.3 μL) were loaded in a crimp-cap microwave vial with a stirrer bar. The vial was sealed and the mixture was stirred at 115 °C for 16 h. On completion, a given amount of 1,3-

dinitrobenzene was added as internal standard in $CDCl_3$. The crude was then filtered through a cotton plug directly into an NMR tube for analysis.

Procedure 7 for the C–H arylation of 39a with 40b (see Table 2.22[c])

Ru-C5 (0.02 mmol, 15.5 mg), (NMe_4) 4-fluorobenzoate (0.175 mmol, 37.3 mg), (NMe_4)OPiv (0.2 mmol, 35.1 mg), (NMe_4)$OC(CF_3)_3$ (1.25 mmol, 386.5 mg), bromobenzene (0.5 mmol, 53.5 μL), **39a** (333.3 mg, 1.50 mmol) and pivalonitrile (166.3 μL, 1.50 mmol) were loaded in a crimp-cap microwave vial with a stirrer bar. The vial was capped and the mixture was stirred at 115 °C for 16 h. On completion, a given amount of 1,3-dinitrobenzene was added as internal standard in $CDCl_3$. The crude mixture was then filtered through a cotton plug directly into an NMR tube for analysis.

General Procedure 8 for time-dependent C–H Arylation of 39a with 4-bromoanisole 40a with catalyst Ru-C1 (see Table 2.16)

Ru-C1 (0.01 mmol, 4.4 mg), 3-acetylbenzoic acid (0.03 mmol, 4.9 mg), (NMe_4)$OC(CF_3)_3$ (0.23 mmol, 71.1 mg) were weighed in the open air and placed in a crimp-cap Schlenk microwave vial (10 mL) with a magnetic stirrer bar. The reaction vessel was capped, evacuated and backfilled with N_2 three times, then left under vacuum for 30 min. The vial was backfilled with N_2 then **39a** (111.1 mg, 0.5 mmol), **40a** (12.5 μL, 0.1 mmol) and pivalonitrile (88.4 μL, 0.8 mmol) were added *via* syringe. The vial was resealed with a new cap under a stream of N_2 and the reaction was heated at 120 °C for the appropriate time. Upon completion, the vial was quickly cooled in a dry ice/acetone bath and a given amount of 1,3,5-trimethoxybenzene was added as internal standard in $CDCl_3$. The crude was then filtered through a cotton plug directly to an NMR tube for analysis.

General Procedure 9 for time-dependent C–H Arylation of 39a with 4-bromoanisole 40a with catalyst Ru-C5 (see Table 2.17)

Ru-C5 (0.01 mmol, 7.7 mg), 3-acetylbenzoic acid (0.03 mmol, 4.9 mg), $(NMe_4)OPiv$ (0.02 mmol, 3.5 mg), $(NMe_4)OC(CF_3)_3$ (0.23 mmol, 71.1 mg) were weighed in the open air and placed in a crimp-cap Schlenk microwave vial (10 mL) with a magnetic stirrer bar. The reaction vessel was capped, evacuated and backfilled with N_2 three times, then left under vacuum for 30 min. The vial was backfilled with N_2 then **39a** (111.1 mg, 0.5 mmol), **40a** (12.5 μL, 0.1 mmol) and pivalonitrile (88.4 μL, 0.8 mmol) were added *via* syringe. The vial was resealed with a new cap under a stream of N_2 and the reaction was heated at 120 °C for the appropriate time. Upon completion, the vial was quickly cooled in a dry ice/acetone bath and a given amount of 1,3,5-trimethoxybenzene (and C_6F_6 if needed, 0.5 equiv, 0.05 mmol, 5.8 μL) was added as internal standard in $CDCl_3$. The crude was then filtered through a cotton plug directly to an NMR tube for analysis.

Procedure 10 for the arylation of Ru2-39c with bromoarene 40c (Table 2.23)

All solid reagents, except **Ru2-39c**, were dried at 70 °C in a vacuum oven over night. All liquid reagents were dried over 4 Å molecular sieves and degassed with 3 freeze-pump-thaw cycles. In a glove box, **Ru2-39c** (0.03 mmol, 22.6 mg), additive (if any, see Table 2.23), **40c** (12.2 μL, 0.09 mmol) and pivalonitrile (100 μL, 0.3 M) were loaded in a crimp-cap microwave vial with a stirrer bar. The vial was sealed and the mixture was stirred at 115 °C for 16 h. On completion, the mixture was filtered through a plug of silica with Et_2O, the solvent was evaporated and octafluorotoluene (8.5 μL, 0.06 mmol, 2.0 equiv) was added as internal standard in $CDCl_3$ for quantitative ^{19}F-NMR analysis.

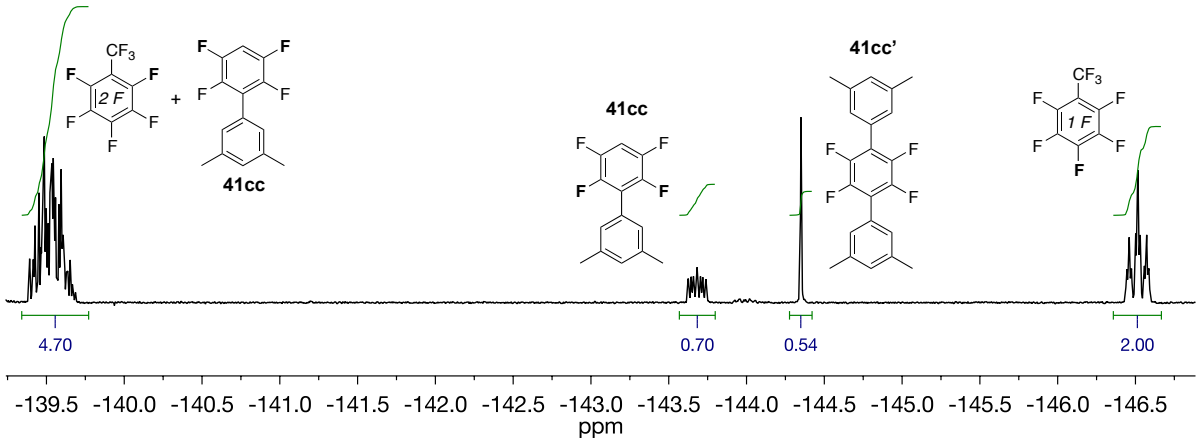

Figure 2.11. ^{19}F-NMR expansion of the reaction described in entry 4 of **Table 2.23** displaying **41cc** and **41cc'** with relative integration with respect to the internal standard octafluorotoluene.

Procedure 11 for arylation of fluoroarene 39d employing catalyst Ru2-39c or Ru1c-39c with bromoarene 40c (see Table 2.24).

All solid reagents, except for **Ru2-39c** and **Ru1-39c**, were dried at 70 °C in a vacuum oven over night. All liquid reagents were dried over 4Å molecular sieves and degassed with 3 freeze-pump-thaw cycles. In glove box, **Ru2-39c** or **Ru1-39c** (0.05 mmol, 38.7 mg or 24.2 mg, or 10 mol %), (NMe_4) 4-fluorobenzoate (0.175 mmol, 37.3 mg), (NMe_4)OPiv (0.4 or 0.3 equiv: 0.20 mmol, 35.1 mg or 0.15 mmol, 26.3 mg, see Table 2.24), (NMe_4)$OC(CF_3)_3$ (1.25 mmol, 386.5 mg), **40c** (0.50 mmol, 67.9 μL), **39d** (182.7 μL, 1.50 mmol) and pivalonitrile (166.3 μL, 1.50 mmol) were loaded in a crimp-cap microwave vial with a stirrer bar. The vial was sealed, taken outside the box and the mixture was stirred at 115 °C for 16 h. On completion, the mixture was filtered through a plug of silica with Et_2O, the solvent evaporated and hexafluorobenzene (28.9 μL, 0.25 mmol, 0.5 equiv) was added as internal standard in $CDCl_3$ for quantitative ^{19}F-NMR analysis.

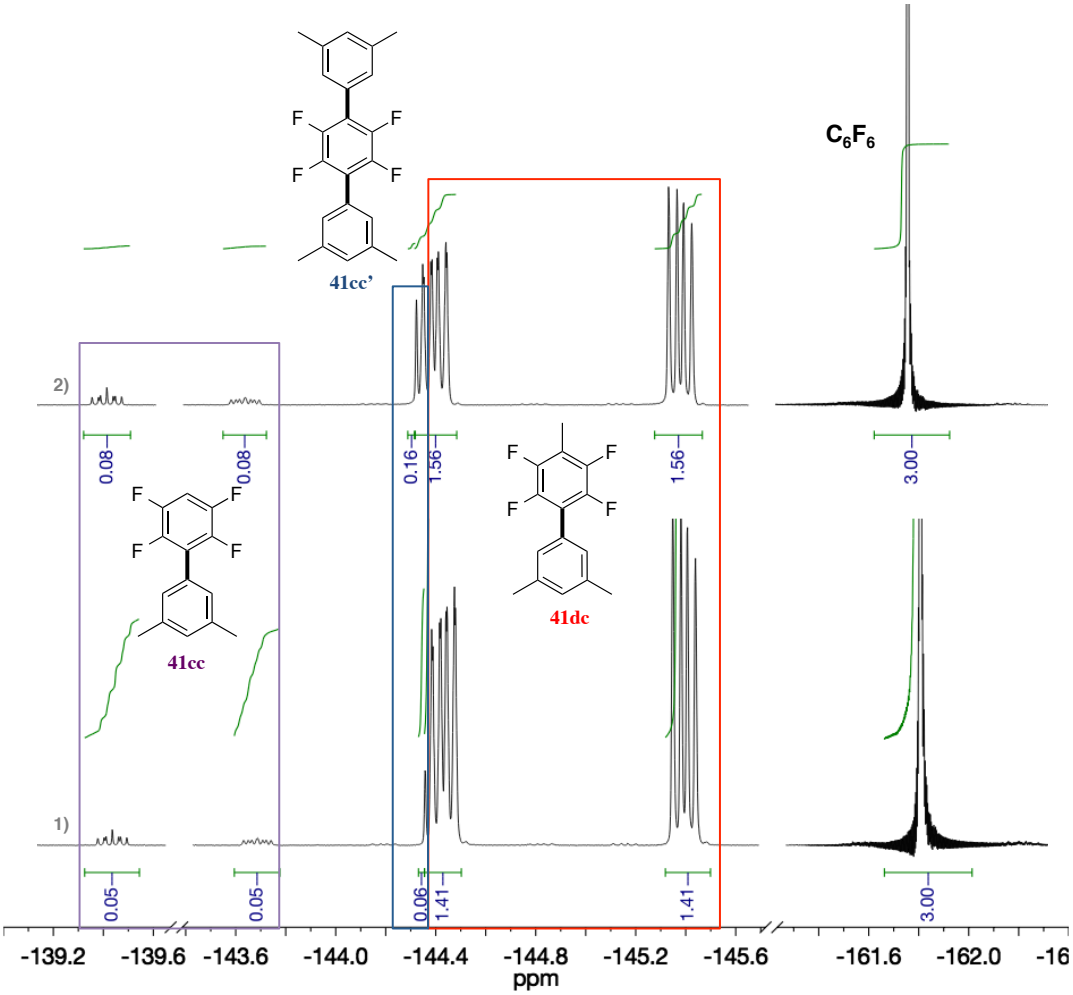

Figure 2.12. ^{19}F-NMR NMR expansion of the reactions illustrated in Table 2.24: 2) entry 1; 1) entry 2, displaying **41dc**, **41cc** and **41cc'** with relative integrations with respect to the internal standard C_6F_6.

Procedure 12 for D/H – H/D scrambling experiment with fluoroarenes d_1-39a and 39b under arylation conditions with bromobenzene 40b (see Scheme 2.21)

All solid reagents, except **Ru-C5**, were dried at 70 °C in a vacuum oven over night. All liquid reagents were dried over 4Å molecular sieves and degassed with 3 freeze-pump-thaw cycles. In a glove box, **Ru-C5** (7.7 mg, 0.01 mmol), (NMe_4) 4-fluorobenzoate (0.0875 mmol, 18.7 mg), (NMe_4)OPiv (17.6 mg, 0.100 mmol), (NMe_4)$OC(CF_3)_3$ (193.3 mg, 0.625 mmol), **40b** (26.3 µL, 0.250 mmol), **d_1-39a** (83.7 mg, 0.375 mmol), **39b** (41.6 µL, 0.375

mmol) and pivalonitrile (58.2 μL, 0.750 mmol) were loaded in a crimp-cap microwave vial with a stirrer bar. The vial was sealed, taken outside the box and the mixture was stirred at 115 °C for 10 min. On completion, the vial was quickly cooled in a dry ice/acetone bath and octafluorotoluene (17.7 μL, 0.125 mmol, 0.5 equiv) was added as internal standard in $CDCl_3$. The crude mixture was then filtered through a cotton plug directly into an NMR tube for quantitative ^{19}F-NMR analysis.

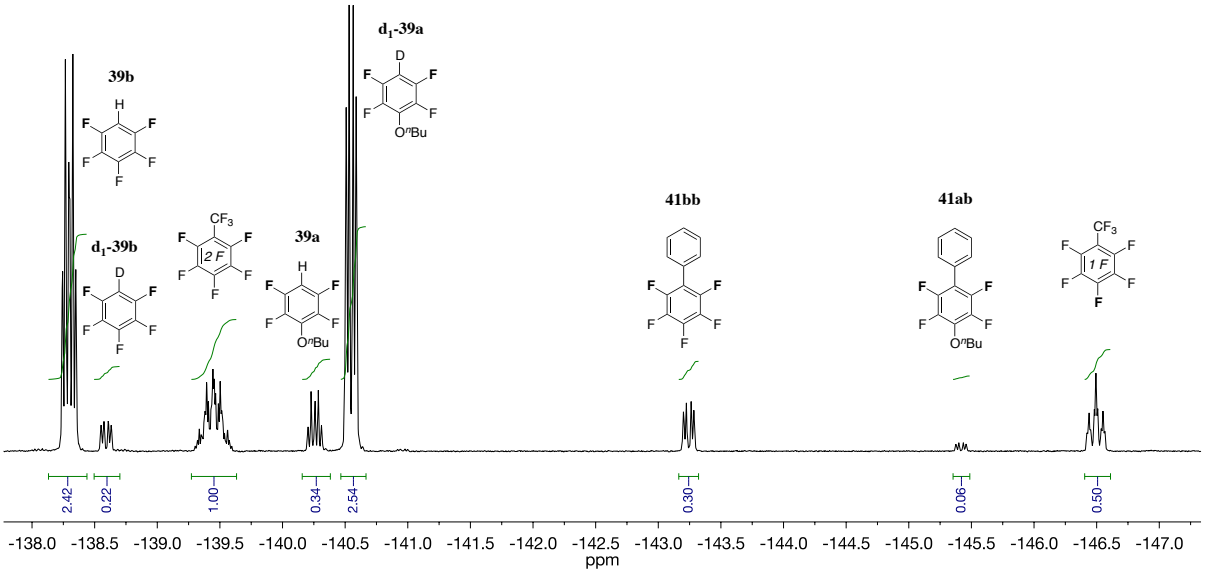

Figure 2.13. ^{19}F-NMRexpansion of the reaction illustrated in **Scheme 2.21**, displaying **39a**, **d_1-39a**, **39b**, **d_1-39b**,[163] **41bb**, **41ab** with relative integrations with respect to the internal standard octafluorotoluene.

Procedure 13 for KIE experiment between fluoroarenes d_1-39a and 39y with bromobenzene 40b (see Scheme 2.22)

All solid reagents, except **Ru-C5**, were dried at 70 °C in a vacuum oven over night. All liquid reagents were dried over 4Å molecular sieves and degassed with 3 freeze-pump-thaw cycles. In a glove box, **Ru-C5** (7.7 mg, 0.01 mmol), (NMe_4) 4-fluorobenzoate (0.0875 mmol, 18.7 mg), (NMe_4)OPiv (17.6 mg, 0.100 mmol), (NMe_4)$OC(CF_3)_3$ (193.3 mg, 0.625 mmol), **40b** (26.3 μL, 0.250 mmol), **d_1-39a** (83.7 mg, 0.375 mmol), **39y** (52.2 μL, 0.375

mol) and pivalonitrile (58.2 μL, 0.75 mmol) were loaded in a crimp-cap microwave vial with a stirrer bar. The vial was sealed, taken outside the box and the mixture was stirred at 115 °C for 8 min. Upon completion, the vial was quickly cooled in a dry ice/acetone bath and hexafluorobenzene (14.4 μL, 0.125 mmol, 0.5 equiv.) was added as internal standard in $CDCl_3$. The crude was then filtered through a cotton plug directly into an NMR tube for quantitative ^{19}F-NMR analysis.

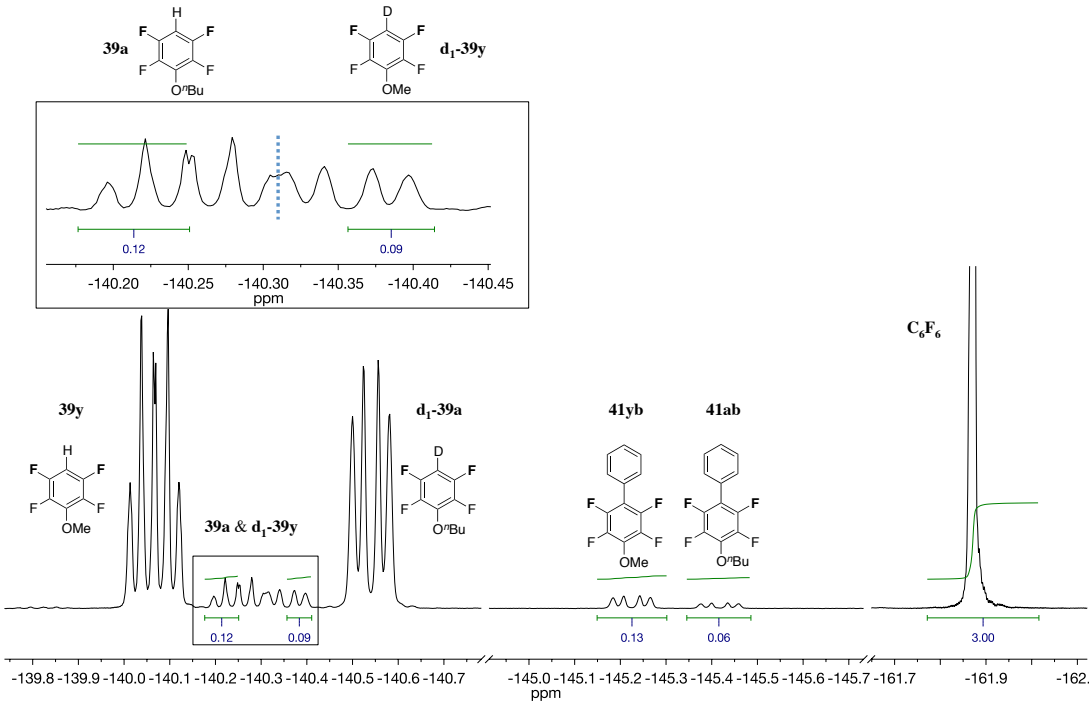

Figure 2.14. ^{19}F-NMRexpansion of the reaction illustrated in **Scheme 2.22**, displaying **39a**, **d_1-39a**, **39y**, **d_1-39y**,[22] **41yb**, **41ab** with relative integrations with respect to the internal standard octafluorotoluene.

General Procedure 14 for KIE experiment of fluoroarenes d_1-39a and 39a with bromobenzene 40b in separate flasks (see Table 2.25)

All solid reagents, except **Ru-C5**, were dried at 70 °C in a vacuum oven over night. All liquid reagents were dried over 4Å molecular sieves and degassed with 3 freeze-pump-thaw cycles. In a glove box, **Ru-C5** (7.7 mg, 0.01 mmol), (NMe_4) 4-fluorobenzoate (0.0875

mmol, 18.7 mg), $(NMe_4)OPiv$ (17.6 mg, 0.100 mmol), $(NMe_4)OC(CF_3)_3$ (193.3 mg, 0.625 mmol), **40b** (26.3 μL, 0.250 mmol), **39a** or **d_1-39a** (166.6 mg or 167.4 mg, 0.750 mmol) and pivalonitrile (58.2 μL, 0.750 mmol) were loaded in a crimp-cap microwave vial with a stirrer bar. The vial was sealed, taken outside the box and the mixture was stirred at 115 °C for the appropriate time. Upon completion, the vial was quickly cooled in a dry ice/acetone bath and a given amount of hexafluorobenzene was added as internal standard in $CDCl_3$. The crude mixture was then filtered through a cotton plug directly into an NMR tube for quantitative ^{19}F-NMR analysis.

General Procedure 15 for competition arylation among various substituted aryl halides with pentafluorobenzene 39b (see Scheme 2.23 and Scheme 2.24)

Ru-C5 (0.01 mmol, 7.7 mg), (NMe_4) 4-fluorobenzoate (0.0875 mmol, 18.7 mg), $(NMe_4)OPiv$ (17.6 mg, 0.100 mmol), $(NMe_4)OC(CF_3)_3$ (193.3 mg, 0.625 mmol), the appropriate of aryl halide(s) (if solid, 0.5 equiv each, 0.125 mmol each) were weighed in the open air and placed in a crimp-cap Schlenk microwave vial (10 mL) with a magnetic stirrer bar. The reaction vessel was capped, evacuated and backfilled with N_2 three times, then left under vacuum for 30 min. The vial was backfilled with N_2 then **39b** (88.3 μL, 0.750 mmol), the appropriate of aryl halide(s) (if liquid, 0.5 equiv each, 0.125 mmol each) and pivalonitrile (88.4 μL, 0.8 mmol) were added *via* syringe. The vial was resealed with a new cap under a stream of N_2 and the reaction was heated at 120 °C for the appropriate time. Upon completion, the vial was quickly cooled in a dry ice/acetone bath and a given amount of dibromomethane was added as internal standard in $CDCl_3$. The crude was then filtered through a cotton plug directly to an NMR tube for analysis.

General Procedure 16 for the preparation of Ru(OCOR)$_2$(η^6-arene) Ru-C1 – Ru-C4.

[RuCl$_2$(η^6-arene)]$_2$ (1.0 equiv, 0.5 mmol) and KOCOR (20.0 equiv, 10 mmol) were weighed in a Schlenk flask with a magnetic stirrer bar. The reaction vessel was evacuated and backfilled with N_2 three times, then left under vacuum for 30 min. The vial was backfilled with N_2 then dry toluene (20.0 mL, 0.025 M), which was degassed with 3 freeze-pump-thaw cycles, was added *via* syringe. The reaction was then heated at 70 °C for 12 h. Note: if the reaction is left longer than 12 h, partial decomposition and lower yields were observed. Upon completion, the reaction mixture was cooled to room temperature, and evaporated to dryness under reduced pressure. 50 mL of CH_2Cl_2 were added to the crude, then the resulting mixture was filtered through a plug of Celite® and the remaining yellow/orange solution evaporated under reduced pressure affording the final complex as a yellow/orange solid. If needed, crystallization from CH_2Cl_2/hexane or cold Et_2O was effectuated.

Characterisation data of Ru-C1 – Ru-C4

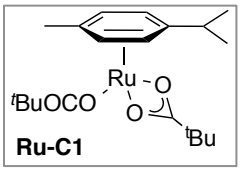

Ru-C1

The General Procedure 16 was applied with [RuCl$_2$(*p*-cymene)]$_2$ (306.2 mg, 0.5 mmol) and KOPiv (1.40 g, 10.0 mmol). Crystallization from CH_2Cl_2/hexane afforded Ru(OPiv)$_2$(*p*-cymene) (**Ru-C1**) as a yellow solid (371.9 mg, 85%).

Spectroscopic data matched those previously reported.[164]

^{1}H NMR (500 MHz; $CDCl_3$): δ 5.71 (d, *J* = 5.5 Hz, 2H), 5.49 (d, *J* = 5.5 Hz, 2H), 2.88 (septet, *J* = 6.9 Hz, 1H), 2.24 (s, 3H), 1.32 (d, *J* = 6.9 Hz, 6H), 1.06 (s, 18H); ^{13}C NMR: (126 MHz; $CDCl_3$): δ 192.0, 98.7, 94.3, 78.3, 76.9, 40.0, 31.6, 27.7, 22.6, 18.6.

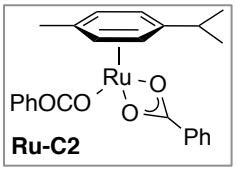

Ru-C2

The General Procedure 16 was applied with [RuCl$_2$(*p*-cymene)]$_2$ (306.2 mg, 0.5 mmol) and KOBz (1.60 g, 10.0 mmol). Crystallization from cold Et_2O afforded Ru(OBz)$_2$(*p*-cymene) (**Ru-C2**) as an orange solid (277.0 mg, 58%).

^{1}H NMR (400 MHz, $CDCl_3$): δ 7.86 - 7.83 (m, 4H), 7.37 (tt, *J* = 7.4, 1.5 Hz, 2H), 7.28 - 7.24 (m, 4H), 5.99 (d, *J* = 6.1 Hz, 2H), 5.78 (d, *J* = 6.1 Hz, 2H), 2.97 (septet, *J* = 6.9 Hz, 1H), 2.36 (s, 3H), 1.41 (d, *J* = 6.9 Hz, 6H); ^{13}C NMR (126 MHz, $CDCl_3$): δ 178.9, 134.3, 131.7, 129.2, 128.2, 98.5, 93.5, 79.5, 78.1, 32.0, 22.7, 18.9. IR (ATR) 3082, 2964, 1633, 829; m.p. 105-110 ºC. Anal. Calcd for $C_{24}H_{24}O_4Ru$: C, 60.37; H, 5.07. Found: C, 60.41; H, 5.11. MS (ES^-, MeCN) *m/z* 477.1 (10%) $[M - (H)]^-$, MS (ES^+, MeCN) *m/z* 398.1 (100%) $[M - (C_7H_5O_2+MeCN)]^+$.

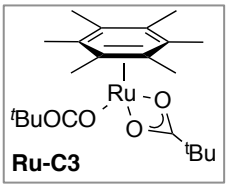

Ru-C3

The General Procedure 16 was applied with $[RuCl_2(C_6Me_6)]_2$ (334.2 mg, 0.5 mmol) and KOPiv (1.40 g, 10.0 mmol) affording $Ru(OPiv)_2(C_6Me_6)$ (**Ru-C3**) as a dark orange solid (419.0 mg, 90%).

^{1}H NMR (500 MHz, $CDCl_3$): δ 2.08 (s, 18H), 1.07 (s, 18H); ^{13}C NMR (126 MHz, $CDCl_3$): δ 190.0, 88.4, 40.0, 28.1, 15.4. IR (ATR) 2953, 2923, 1557, 866; m.p. 95-100 ºC. Anal. Calcd for $C_{22}H_{36}O_4Ru$: C, 56.75; H, 7.79. Found: C, 56.80; H, 7.84. MS (ES^+, MeCN) *m/z* 365.2 (100%) $[M - (C_5H_9O_2)]^+$, *m/z* 447.2 (50%) $[M - (C_5H_9O_2 + 2MeCN)]^+$.

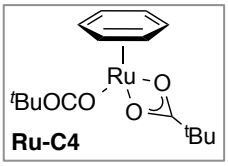

Ru-C4

The General Procedure 16 was applied with $[RuCl_2(benzene)]_2$ (250.1 mg, 0.5 mmol) and KOPiv (1.40 g, 10.0 mmol). Crystallization from CH_2Cl_2/hexane afforded $Ru(OPiv)_2$(benzene) (**Ru-C4**) as a yellow solid (267.0 mg, 70%).

^{1}H NMR (500 MHz; $CDCl_3$): δ 5.71 (s, 6H), 1.09 (s, 18H); ^{13}C NMR: (126 MHz; $CDCl_3$): δ 193.0, 79.1, 40.2, 27.7. IR (ATR) 2923, 2901, 15601, 877; m.p. 90-95 ºC. Anal. Calcd for $C_{16}H_{24}O_4Ru$: C, 50.38; H, 6.34. Found: C, 50.22; H, 6.41. MS (ES^+, MeCN) *m/z* 281.1 (100%) $[M - (C_5H_9O_2)]^+$, *m/z* 363.1 (50%) $[M - (C_5H_9O_2 + 2MeCN)]^+$.

Procedure 17 for the Synthesis of hexakis(pivalonitrile-κN)ruthenium(II) bis(tetrafluoroborate) Ru-C5

Neither Schlenk nor anhydrous conditions are needed for the synthesis of **C5**. 1.0 g $RuCl_3 \cdot \times H_2O$ (Reagent Grade purity ≥ 95%, 4.6 mmol based on anhydrous molecular weight), 1.0 g of Zn dust (<10 μm, 15.3 mmol) and 70.0 mL of pivalonitrile were loaded in a 100 mL Ace pressure tube and heated for 1 h at 115 °C. Note: 1) a change in colour from dark green to blue and finally to deep yellow/brown is observed; 2) if the mixture is left longer than 1 h, lower yields were observed. Then, the reaction mixture was cooled to room temperature, filtered through a plug of Celite® and the resulting solution was loaded again into an Ace pressure tube with 1.5 g of $NaBF_4$ (13.7 mmol). After heating the mixture for 16 h at 115 °C, the reaction was cooled to room temperature, filtered through a plug of Celite® and evaporated to dryness. Note: the solvent pivalonitrile can be easily distilled, recovered and reused at this stage. The crude was dissolved in CH_2Cl_2, filtered through a plug of Celite® and the pale green solution was reduced *in vacuo*. Crystallization of the crude with CH_2Cl_2/Et_2O gave a white/grey solid, which was filtered and washed with Et_2O. Repetition of the crystallization procedure a further 3 times provided 1.6 g of a white solid. This compound is a mixture of the desired complex **Ru-C5** and of **Ru-C5'** [hexakis(pivalonitrile-κ*N*)ruthenium(II)]di-μ-chlorobis[chlororuthenium(II)]. The molecular structure of **C5'** ($[Ru(^tBuCN)_6][Ru_2Cl_6]$) was determined by X-ray (see crystallographic section, suitable crystals were grown by slow crystallization from CH_2Cl_2/Et_2O). Subsequently, the mixture of **Ru-C5** and **C5'** (1.6 g) was mixed with $AgBF_4$ (9.5 mmol, 1.85 g), and pivalonitrile (50 mL) in an Ace pressure tube and heated for 4 h at 100 °C. After this time, the reaction was cooled to room temperature, filtered through a plug of Celite® and evaporate to dryness. Note: the solvent pivalonitrile can be distilled and recovered again at this stage. The crude was dissolved in CH_2Cl_2, filtered through a plug of Celite® and the pale yellow solution was reduced *in vacuo*. Crystallization of the crude with CH_2Cl_2/Et_2O gave an off-white solid, which was filtered and washed with Et_2O. Repetition of the crystallization procedure an additional 2 times provided title complex **Ru-C5** as a bench stable white solid (1.55 g, 2.0

mmol, 43.5%). Suitable crystals of **Ru-C5** for X-ray crystallography were grown by slow crystallization from CH_2Cl_2/Et_2O (see crystallographic section).

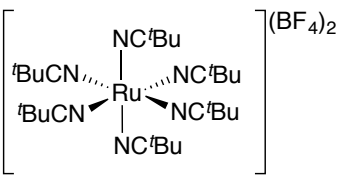

Ru-C5

^{1}H NMR (400 MHz, $(CD_3)_2CO$): δ 1.56 (s, 54H); ^{13}C NMR (126 MHz, $(CD_3)_2CO$): δ 134.7, 31.3, 28.1; ^{19}F NMR (376 MHz, $(CD_3)_2CO$) δ –151.2 (s), –151.2 (s); IR (ATR) 1097, 1055; m.p. > 230 °C decomposition. Anal. Calcd for $C_{30}H_{54}B_2F_8N_6Ru$: C, 46.59; H, 7.04; N, 10.87. Found: C, 46.50; H, 7.14; N, 10.81. MS (ES^+, CH_2Cl_2) *m/z* 687.5 (100%) $[M – (BF_4)]^+$.

General Procedure 18 for the preparation of Ru2-39a and Ru2-39c

Ru1-39a or **Ru1-39c** (1.0 equiv, 0.25 mmol) and $NaBF_4$ (82.4 mg, 0.75 mmol) were weighed in a crimp-cap Schlenk microwave vial (20 mL) with a magnetic stirrer bar. Note: the use of an oversized stirrer bar is advised. The reaction vessel was capped, evacuated and backfilled with N_2 three times, then left under vacuum for 30 min. The vial was backfilled with N_2 then pivalonitrile (5.0 mL, 0.05 M), which was dried over 4Å molecular sieves and degassed with 3 freeze-pump-thaw cycles, was added *via* syringe. The vial was resealed with a new cap under a stream of N_2 and the reaction was heated at 120 °C for 75 min with vigorous stirring. Upon completion, the reaction mixture was cooled to room temperature, diluted with 3 mL of pivalonitrile, filtered through a plug of Celite® and the remaining pale yellow/greenish solution evaporated under reduced pressure. The crude was then purified by crystallization from ^{t}BuCN/Et_2O affording the final products as white solids, which were washed with Et_2O. The final complexes are stable under air for a few hours, but decompose if exposed to oxygen for longer. Storage of **Ru2-39a** and **Ru2-39c** in a desiccator under vacuum or in glove box is needed. Suitable crystals of **Ru2-39c** for X-ray crystallography were grown by slow crystallization from CH_2Cl_2/Et_2O (see crystallographic section).

Characterisation data of Ru2-39a and Ru2-39c

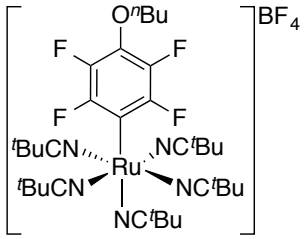

Ru2-39a

The General Procedure 18 was applied with **Ru1-39a** (139.4 mg, 0.25 mmol) affording **Ru2-39a** (105.1 mg, 51%).

^{1}H NMR (400 MHz, $CDCl_3$): δ 4.14 (t, *J* = 6.5 Hz, 2H), 1.78 (app quintet, *J* = 7.0 Hz, 2H), 1.57 (s, 9H), 1.52 (app t, *J* =7.5 Hz, 2H), 1.42 (s, 36H), 0.98 (t, *J* = 7.4 Hz, 3H); ^{13}C NMR (126 MHz, $CDCl_3$): δ 153.4 (dm, *J* = 226.2 Hz), 140.2 (dm, *J* = 246.3 Hz), 132.1 - 131.8 (m), 131.3, 129.2, 124.3 - 123.5 (m), 74.9, 32.2, 30.3, 29.8, 28.6, 28.5, 19.1, 14.0; ^{19}F NMR (471 MHz, $CDCl_3$) δ –121.8 (dd, *J* = 26.9, 9.5 Hz, 2F), –154.0 (s), –154.1 (s), –160.9 (dd, *J* = 26.6, 9.3 Hz, 2F); IR (ATR) 2954, 2252, 1424, 999; m.p. 160 ºC decomposition; Anal. Calcd for $C_{35}H_{54}BF_8N_5ORu$: C, 50.97; H, 6.60; N, 8.49. Found: C, 51.04; H, 6.67; N, 8.43. MS (ES$^+$, CH_2Cl_2) *m/z* 655.4 (35%) [M – (BF_4 + ^{t}BuCN)]$^+$.

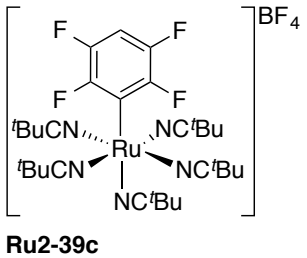

Ru2-39c

The General Procedure 18 was applied with **Ru1-39c** (121.4 mg, 0.25 mmol) affording **Ru2-39c** (127.9 mg, 68%).

^{1}H NMR (400 MHz, CD_2Cl_2): δ 6.67 - 6.58 (m, 1H), 1.53 (s, 9H), 1.39 (s, 36H); ^{13}C NMR (101 MHz, CD_2Cl_2): δ 153.7 (dddd, *J* = 226.3, 19.3, 9.8, 2.5 Hz), 144.8 (dddd, *J* = 246.0, 22.7, 9.4, 2.2 Hz), 136.0 (tt, *J* = 44.1, 3.7 Hz), 131.5, 129.1, 99.7 (t, *J* = 23.6 Hz), 30.4, 29.9, 28.6, 28.4; ^{19}F NMR (376 MHz, CD_2Cl_2) δ –121.4 - –121.6 (m), –144.9 - –145.0 (m), –153.7 (s), –153.2 (s); IR (ATR) 2929, 2272, 1436, 1052; m.p. 170 ºC decomposition ; Anal. Calcd for $C_{31}H_{46}BF_8N_5Ru$: C, 49.47; H, 6.16; N, 9.31. Found: C, 49.52; H, 6.20; N, 9.25. MS (ES$^+$, CH_2Cl_2) *m/z* 583.4 (50%) [M – (BF_4 + ^{t}BuCN)]$^+$.

General procedure 19 for the preparation of tetramethylammonium salts

A round bottom flask equipped with a magnetic stirrer bar was loaded with 50.0 mL (50.0 mmol) of $(NMe_4)OH \cdot 5H_2O$ solution (1.0 M in EtOH) and placed in an ice bath. Subsequently, a solution of the acid, or $(CF_3)_3COH$ in EtOH (50 mL, 50 mmol, 1.0 M) was added at 0 °C. Then the ice bath was removed and the solution allowed to stir at room temperature of 1 h. The solvent was removed under reduced pressure affording the salts as white solid in quantitative yield.

Characterisation data of tetramethylammonium salts

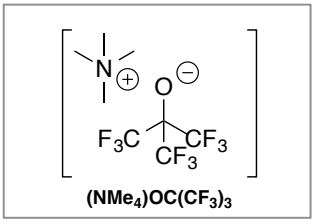

The General Procedure 19 was applied with perfluoro-*tert*-butyl alcohol affording tetramethylammonium perfluoro-*tert*-butyl alkoxide (15.44 g, 100%).

^{1}H NMR (400 MHz, D_2O): δ 3.14 (s, 12H); ^{13}C NMR (126 MHz, $CDCl_3$): δ 122.6 (q, J = 294.3 Hz), 82.1 - 81.0 (m), 55.1 - 55.1 (m); ^{19}F NMR (376 MHz, $CDCl_3$) δ –75.4 (s); IR (ATR) 1249, 1194, 949, 721; m.p. 170 – 175 ºC.

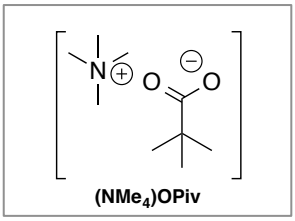

The General Procedure 19 was applied with pivalic acid affording tetramethylammonium pivalate (8.75 g, 100%).

^{1}H NMR (400 MHz, D_2O): δ 3.14 (s, 12H), 1.06 (s, 9H); ^{13}C NMR (126 MHz, $CDCl_3$): δ 188.7, 55.2 - 55.1 (m), 39.7, 27.4; IR (ATR) 1609, 1356, 920, 780; m.p. 235 – 240 ºC.

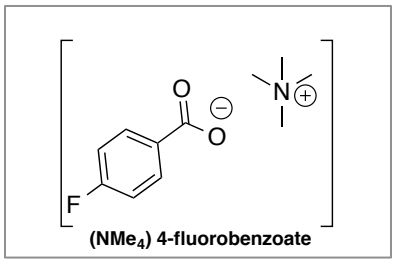

The General Procedure 19 was applied with 4-fluorobenzoic acid affording tetramethylammonium 4-fluorobenzoate (10.6 g, 100%).

^{1}H NMR (400 MHz, D_2O): δ 7.84 (dd, J = 8.9, 5.6 Hz, 2H), 7.12 (app t, J = 8.9 Hz, 2H), 3.14 (s, 12H); ^{13}C NMR (126

MHz, $CDCl_3$): δ 174.5, 164.3 (d, *J* = 248.0 Hz), 132.4 (d, *J* = 2.7 Hz), 131.2 (d, *J* = 9.1 Hz), 114.9 (d, *J* = 21.8 Hz), 55.1 - 55.1 (m); ^{19}F NMR (376 MHz, $CDCl_3$) δ –110.4 - –110.4 (m, 1F); IR (ATR) 2944, 1565, 1348, 951; m.p. 225 – 230 °C.

General procedure 20 for the preparation of 39a, 39o, and 39h

1-bromobutane (23.5 mmol) was added to a stirred suspension of perfluoro(thio)phenol (25.0 mmol) and K_2CO_3 (30.0 mmol) in MeCN (40.0 mL) under reflux conditions and stirred for a further 5 h. Upon completion, the reaction mixture was allowed to cool to ambient temperature; then H_2O (100 mL) and pentane (200 mL) were added. After phase separation, the organic layer was washed with 1 M NaOH (100 mL), H_2O (2 × 100 mL) and brine (100 mL), dried over $MgSO_4$ and evaporated to dryness affording a pale yellow oil. Purification *via* a silica plug eluted with pentane gave the title product as a colourless oil. For the synthesis of **39a** and **39o** the reaction can be carried out under air. Schlenk conditions and lower temperatures are required for the synthesis of **39h** (50 °C for 5 h after addition of the electrophile).

Characterisation data of 39a, 39o and 39h

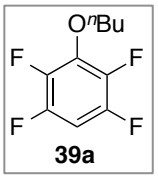

39a

The General Procedure 20 was applied with 2,3,5,6-tetrafluorophenol (4.15 g 25.0 mmol) affording 3-butoxy-1,2,4,5-tetrafluorobenzene (**39a**) (4.39 g, 84%). Spectroscopic data matched those previously reported.[165]

^{1}H NMR (500 MHz, $CDCl_3$): δ 6.74 (tt, *J* = 10.0, 7.0 1H), 4.22 (t, *J* = 6.7 Hz, 2H), 1.76 (app quintet, *J* = 7.0 Hz, 2H), 1.51 (app sextet, *J* = 7.5 Hz, 2H), 0.97 (t, *J* = 7.5 Hz, 3H); ^{13}C NMR (126 MHz, $CDCl_3$): δ 146.5 (dtd, *J* = 246.5, 12.6, 4.0 Hz), 141.4 (ddt, *J* = 246.7, 14.6, 3.9 Hz), 138.5 (tt, *J* = 12.1, 3.6 Hz), 99.3 (t, *J* = 23.1 Hz), 75.2 (t, *J* = 3.2 Hz), 32.1, 18.9, 13.7; ^{19}F NMR (471 MHz, $CDCl_3$) δ –140.5 - –140.6 (m, 2F), –157.4 - –157.4 (m, 2F); IR (ATR) 2964, 1488, 1171, 1087, 713; HRMS (APCI) *m/z* calcd. $C_{10}H_{10}F_4O$: 222.0668; found $[M+H]^+$ 223.0737.

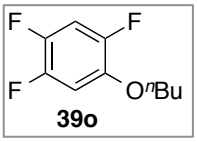

39o

The General Procedure 20 was applied with 2,4,5-trifluorophenol (3.70 g 25.0 mmol) affording 1-butoxy-2,4,5-trifluorobenzene (**39o**) (3.89 g, 81%). ^{1}H NMR (500 MHz, $CDCl_3$): δ 6.97 - 6.91 (m, 1H), 6.79 (app dt, *J* = 11.5, 7.7 Hz, 1H), 3.96 (t, *J* = 6.5 Hz, 2H), 1.78 (app quintet, *J* = 7.1 Hz, 2H), 1.49 (app sextet, *J* = 7.5 Hz, 2H), 0.97 (t, *J* = 7.4 Hz, 3H); ^{13}C NMR (126 MHz, $CDCl_3$): δ 147.9 (ddd, *J* = 245.1, 9.0, 3.3 Hz), 146.2 (ddd, *J* = 243.8, 13.2, 3.8 Hz), 143.6 - 143.5 (m), 143.3 (ddd, *J* = 242.9, 14.1, 10.5 Hz), 105.9 (app t, *J* = 23.0 Hz), 104.1 (d, *J* = 22.1 Hz), 70.1, 31.2, 19.2, 13.8; ^{19}F NMR (471 MHz, $CDCl_3$) δ –136.3 - –136.4 (m, 1F),–141.3 - –141.5 (m, 1F), –145.4 (app dt *J* = 21.3, 8.9 Hz, 1F); IR (ATR) 2962, 1485, 1173, 912, 712. HRMS (APCI) *m/z* calcd. $C_{10}H_{10}F_4O$: 204.0757; found $[M]^+$ 204.0749.

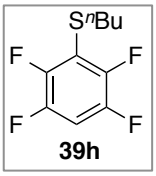

39h

The General Procedure 20 was applied with 2,3,5,6-tetrafluorobenzenethiol (4.55 g, 25.0 mmol) affording butyl(2,3,5,6-tetrafluorophenyl)sulfane (**39h**) (4.37 g, 78%).

^{1}H NMR (500 MHz, $CDCl_3$): δ 7.05 - 6.98 (m, 1H), 2.93 (t, *J* = 7.4 Hz, 2H), 1.54 (app quintet, *J* = 7.4 Hz, 2H), 1.42 (app sextet, *J* = 7.4 Hz, 2H), 0.89 (t, *J* = 7.4 Hz, 3H); ^{13}C NMR (126 MHz, $CDCl_3$): δ 147.0 (app ddt, *J* = 244.8, 13.6, 3.3 Hz), 146.0 (dm, *J* = 249.6 Hz), 115.8 (t, *J* = 20.2 Hz), 105.7 (t, *J* = 22.9 Hz), 34.4, 32.0, 21.6, 13.6; ^{19}F NMR (471 MHz, $CDCl_3$) δ –134.0 - –134.1 (m, 2F), –138.4 - –138.6 (m, 2F); IR (ATR) 2962, 1524, 1217, 1167, 855. HRMS (EI) *m/z* calcd. $C_{10}H_{10}F_4S$: $[M]^+$ 238.0434; found: $[M]^+$ 238.0438.

Procedure 21 for the preparation of 3-butoxy-1,2,4,5-tetrafluorobenzene-6-*d* d_1-39a

Compound **39a** (5.00 g, 22.5 mmol) was dissolved in anhydrous THF (70 mL, 0.33 M) in a flame-dried Schlenk flask under a N_2 atmosphere. The stirred solution was left to cool to –78 °C then a solution of ^{t}BuLi in pentane (15.5 mL, 24.8 mmol, 1.6 M) was added dropwise. The mixture was allowed to stir at –78 °C for an additional 15 min before being quenched with D_2O [10 M in anhydrous THF] (22.5 mL, 225 mmol). The reaction mixture was then allowed to warm to ambient temperature and stirred for a further 30 min. After this time, the solution was diluted with TBME (150 mL), pentane (50 mL) and H_2O (150 mL). The organic phase was separated, washed with H_2O (3×100 mL) and brine (100 mL), dried over $MgSO_4$ and evaporated under reduced pressure affording a pale yellow oil. Purification *via* a silica plug eluted with pentane gave the title product as a colourless oil (4.25 g, 84%, > 99 atom % D).

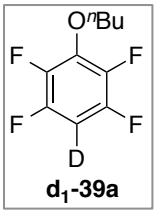

d_1-39a

^{1}H NMR (500 MHz, $CDCl_3$): δ 4.22 (t, *J* = 6.5 Hz, 2H), 1.76 (app quintet, *J* = 7.0 Hz, 2H), 1.50 (app sextet, *J* = 7.5 Hz, 2H), 1.97 (t, *J* = 7.4 Hz, 3H); ^{13}C NMR (126 MHz, $CDCl_3$): δ 146.5 (dtd, *J* = 246.7, 12.6, 3.9 Hz), 141.4 (app ddt, *J* = 246.3, 14.5, 3.7 Hz), 138.5 (tt, *J* = 12.1, 3.6 Hz), 99.5 - 99.7 (m), 75.16 (t, *J* =3.1 Hz), 32.0, 18.9, 13.8; ^{19}F NMR (471 MHz, $CDCl_3$) δ –140.7 (dd, *J* = 21.3, 9.1 Hz, 2F), –157.3 (dd, *J* = 21.0, 9.1 Hz, 2H); IR (ATR) 2966, 1491, 1167, 1094, 708;HRMS (APCI) *m/z* calcd. $C_{10}H_9DF_4O$: 223.0731; found $[M+H]^+$ 224.0801.

Procedure 22 for the preparation of *N*-(2,3,5,6-tetrafluorophenyl)pivalamide 39f

NEt_3 (1.4 mL, 10.0 mmol) and trimethylacetyl chloride (553.6 μL, 4.5 mmol) were added *via* syringe to a solution containing 2,3,5,6-tetrafluoroaniline (825.5 mg, 5.0 mmol) in toluene (15.0 mL, 0.33 M), and the mixture was heated to reflux for 16 h. After this time, the reaction mixture was allowed to cool to ambient temperature and concentrated under reduced pressure to dryness. CH_2Cl_2 (100 mL) and H_2O (100 mL) were added to the crude, the organic phase phase was separated, washed with 1 M NaOH (100 mL), H_2O (100 mL) and brine (100 mL), dried over $MgSO_4$ and evaporated under reduced pressure. Purification by

flash chromatography with a 0-30% CH_2Cl_2-hexane gradient afforded the product as a white solid (997.0 mg, 89 %).

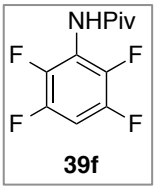

39f

^{1}H NMR (500 MHz, $CDCl_3$): δ 7.03 (br s, 1H), 6.91 (tt, *J* = 9.7, 7.3 Hz, 1H), 1.27 (s, 9H); ^{13}C NMR (126 MHz, $CDCl_3$): δ 176.9, 146.0 (app dtd, *J* = 247.6 12.3, 4.0 Hz), 142.4 (app ddt, *J* = 249.1, 14.7, 3.5 Hz), 117.4 (tt, *J* = 14.6, 3.1 Hz), 103.8 (t, *J* = 22.8 Hz), 39.7, 27.6; ^{19}F NMR (376 MHz, $CDCl_3$) δ –139.3 - –139.4 (m, 2F), –145.9 - –146.0 (m, 2F); IR (ATR) 3246, 2975, 1670, 1494, 1177, 858, 713; m.p. 147 - 151 ºC; HRMS (EI) *m/z* calcd. $C_{11}H_{11}ONF_4$: $[M]^+$ 249.0771; found: $[M]^+$ 249.0779.

Procedure 23 for the preparation of *tert*-butyl 2,3,5,6-tetrafluorobenzoate 39i

Tosyl chloride (1.91 g, 10.0 mmol) was added to an ice-cold solution of 2,3,5,6-tetrafluorobenzoic acid (970.0 mg, 5.0 mmol) in pyridine (10.0 mL, 0.5 M). After 10 min, *tert*-butanol (741.2 mg, 10.0 mmol) was added and the solution was stirred for a further 1 h at 0 °C. Then, the reaction mixture was allowed to warm to room temperature and stirred for an additional 16 h. The solvent was evaporated to dryness and the residue was partitioned between EtOAc (100 mL) and saturated $NaHCO_3$ (100 mL). The organic layer was separated, washed with saturated $NaHCO_3$ (2×100 mL) and brine (100 mL) and dried over $MgSO_4$ giving a pale yellow oil. Purification *via* silica plug with 5% of CH_2Cl_2 in hexane afforded the title compound as colourless oil (1.20 g, 96%).

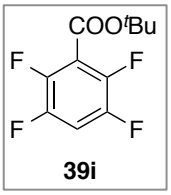

39i

^{1}H NMR (400 MHz, $CDCl_3$): δ 7.13 (tt, *J* = 9.5, 7.2 Hz, 1H), 1.60 (s, 9H); ^{13}C NMR (126 MHz, $CDCl_3$): δ 158.7, 146.0 (dm, *J* = 249.9 Hz), 144.2 (dm, *J* = 254.2 Hz), 115.7 (t, *J* = 17.3 Hz), 107.9 (t, *J* = 22.6 Hz), 85.0, 28.2; ^{19}F NMR (376 MHz, $CDCl_3$) δ –137.8 - –137.9 (m, 2F), –141.0 - –141.2 (m, 2F); IR (ATR) 2984, 2360, 1731, 1500, 1306, 1177, 1152, 949. HRMS (EI) *m/z* calcd. $C_{11}H_{10}O_2F_4$: $[M]^+$ 250.0611; found: $[M]^+$ 250.0615.

Kinetic section: supplementary information

Kinetic order in catalyst Ru-C5 (see Table 2.27)

$[Ru(^tBuCN)_6](BF_4)_2$ (**Ru-C5**) (1, 2.25 or 5 mol %; 3.9, 8.7 or 19.3 mg), $(NMe_4)OC(CF_3)_3$ (386.5 mg, 1.250 mmol), (NMe_4) 4-fluorobenzoate (37.3 mg, 0.175 mmol) and (NMe_4)OPiv (35.1 mg, 0.20 mmol) were weighed in the open air and placed in a crimp-cap Schlenk microwave vial (10 mL) with a magnetic stirrer bar. The reaction vessel was capped, evacuated and backfilled with N_2 three times, then left under vacuum for 30 min. The vial was then backfilled with N_2 and bromobenzene **40b** (52 μL, 0.50 mmol, 1.0 equiv), arene **39a** (270 μL, 1.50 mmol), pivalonitrile (553 μL, 5.0 mmol) and dodecane (23 μL, 0.1 mmol) were added *via* syringe (total volume of liquids = 898 μL). The vial was resealed with a new cap under a stream of N_2 and brought inside a glove box. Then the mixture was stirred at 115 °C and small aliquots were taken *via* syringe at the appropriate time. The samples for the GC-FID analysis were prepared by flushing the syringe used for withdrawing the small amount of the crude with 2 mL of EtOAc directly inside a GC vial.

Kinetic order in fluoroarene 39a (see Table 2.29)

$[Ru(^tBuCN)_6](BF_4)_2$ (**Ru-C5**) (2 mol %, 7.8 mg), $(NMe_4)OC(CF_3)_3$ (386.5 mg, 1.250 mmol), (NMe_4) 4-fluorobenzoate (37.3 mg, 0.175 mmol) and (NMe_4)OPiv (35.1 mg, 0.20 mmol) were weighed in the open air and placed in a crimp-cap Schlenk microwave vial (10 mL) with a magnetic stirrer bar. The reaction vessel was capped, evacuated and backfilled with N_2 three times, then left under vacuum for 30 min. The vial was then backfilled with N_2 and bromobenzene **40b** (52 μL, 0.50 mmol, 1.0 equiv), arene **39a** (1.0, 3.0 or 5.0 equiv; 90, 270 or 450 μL), pivalonitrile (553 μL, 5.0 mmol), dodecane (23 μL, 0.1 mmol) and ethylpivalate (460, 280 or 100 μL) were added *via* syringe (total volume of liquids = 1178 μL). The vial was resealed with a new cap under a stream of N_2 and brought inside a glove box. Then the mixture was stirred at 115 °C and small aliquots were taken *via* syringe at the appropriate time. The samples for the GC-FID analysis were prepared by flushing the syringe used for withdrawing the small amount of the crude with 2 mL of EtOAc directly inside a GC vial.

Kinetic order in bromobenzene 40b (see Table 2.31)

$[Ru(^tBuCN)_6](BF_4)_2$ (**Ru-C5**) (2 mol %, 7.8 mg), $(NMe_4)OC(CF_3)_3$ (386.5 mg, 1.250 mmol), (NMe_4) 4-fluorobenzoate (37.3 mg, 0.175 mmol) and (NMe_4)OPiv (35.1 mg, 0.20 mmol) were weighed in the open air and placed in a crimp-cap Schlenk microwave vial (10 mL) with a magnetic stirrer bar. The reaction vessel was capped, evacuated and backfilled with N_2 three times, then left under vacuum for 30 min. The vial was then backfilled with N_2 and bromobenzene **40b** (0.5, 1.0 or 2.0 equiv; 26, 52 or 104 μL), arene **39a** (270 μL, 1.50 mmol), pivalonitrile (553 μL, 5.0 mmol), dodecane (23 μL, 0.1 mmol) and ethylpivalate (306, 280 or 228 μL) were added *via* syringe (total volume of liquids = 1178 μL). The vial was resealed with a new cap under a stream of N_2 and brought inside a glove box. Then the mixture was stirred at 115 °C and small aliquots were taken *via* syringe at the appropriate time. The samples for the GC-FID analysis were prepared by flushing the syringe used for withdrawing the small amount of the crude with 2 mL of EtOAc directly inside a GC vial.

Kinetic order in (NMe_4) 4-fluorobenzoate (see Table 2.33)

$[Ru(^tBuCN)_6](BF_4)_2$ (**Ru-C5**) (2 mol %, 7.8 mg), $(NMe_4)OC(CF_3)_3$ (386.5 mg, 1.250 mmol), (NMe_4) 4-fluorobenzoate (0.175, 0.35 or 0.7 equiv; 18.7, 37.3 or 74.6 mg) and (NMe_4)OPiv (35.1 mg, 0.20 mmol) were weighed in the open air and placed in a crimp-cap Schlenk microwave vial (10 mL) with a magnetic stirrer bar. The reaction vessel was capped, evacuated and backfilled with N_2 three times, then left under vacuum for 30 min. The vial was then backfilled with N_2 and bromobenzene **40b** (0.5 mmol, 1.0 equiv, 52 μL), arene **39a** (270 μL, 1.50 mmol), pivalonitrile (553 μL, 5.0 mmol), dodecane (23 μL, 0.1 mmol) and ethylpivalate (280 μL) were added *via* syringe (total volume of liquids = 1178 μL). The vial was resealed with a new cap under a stream of N_2 and brought inside a glove box. Then the mixture was stirred at 115 °C and small aliquots were taken *via* syringe at the appropriate time. The samples for the GC-FID analysis were prepared by flushing the syringe used for withdrawing the small amount of the crude with 2 mL of EtOAc directly inside a GC vial.

Kinetic order in $(NMe_4)OPiv$ (see Table 2.35)

$[Ru(^tBuCN)_6](BF_4)_2$ (**Ru-C5**) (2 mol %, 7.8 mg), $(NMe_4)OC(CF_3)_3$ (386.5 mg, 1.250 mmol), (NMe_4) 4-fluorobenzoate (37.3 mg, 0.175 mmol) and $(NMe_4)OPiv$ (0.2, 0.4 or 0.8 equiv; 17.5, 35.0 or 70.0 mg) were weighed in the open air and placed in a crimp-cap Schlenk microwave vial (10 mL) with a magnetic stirrer bar. The reaction vessel was capped, evacuated and backfilled with N_2 three times, then left under vacuum for 30 min. The vial was then backfilled with N_2 and bromobenzene **40b** (0.5 mmol, 1.0 equiv, 52 μL), arene **39a** (270 μL, 1.50 mmol), pivalonitrile (553 μL, 5.0 mmol), dodecane (23 μL, 0.1 mmol) and ethylpivalate (280 μL) were added *via* syringe (total volume of liquids = 1178 μL). The vial was resealed with a new cap under a stream of N_2 and brought inside a glove box. Then the mixture was stirred at 115 °C and small aliquots were taken *via* syringe at the appropriate time. The samples for the GC-FID analysis were prepared by flushing the syringe used for withdrawing the small amount of the crude with 2 mL of EtOAc directly inside a GC vial.

Kinetic order in $(NMe_4)OC(CF_3)_3$ (Table 2.37)

$[Ru(^tBuCN)_6](BF_4)_2$ (**Ru-C5**) (2 mol %, 7.8 mg), $(NMe_4)OC(CF_3)_3$ (1.5, 2.5 or 3.0 equiv; 231.8, 386.4 or 541 mg), (NMe_4) 4-fluorobenzoate (37.3 mg, 0.175 mmol) and $(NMe_4)OPiv$ (35.1 mg, 0.20 mmol) were weighed in the open air and placed in a crimp-cap Schlenk microwave vial (10 mL) with a magnetic stirrer bar. The reaction vessel was capped, evacuated and backfilled with N_2 three times, then left under vacuum for 30 min. The vial was then backfilled with N_2 and bromobenzene **40b** (0.5 mmol, 1.0 equiv, 52 μL), arene **39a** (270 μL, 1.50 mmol), pivalonitrile (553 μL, 5.0 mmol), dodecane (23 μL, 0.1 mmol) and ethylpivalate (280 μL) were added *via* syringe (total volume of liquids = 1178 μL). The vial was resealed with a new cap under a stream of N_2 and brought inside a glove box. Then the mixture was stirred at 115 °C and small aliquots were taken *via* syringe at the appropriate time. The samples for the GC-FID analysis were prepared by flushing the syringe used for withdrawing the small amount of the crude with 2 mL of EtOAc directly inside a GC vial.

Kinetic order in ^{t}BuCN (Table 2.39)

$[Ru(^t BuCN)_6](BF_4)_2$ (**Ru-C5**) (2 mol %, 7.8 mg), $(NMe_4)OC(CF_3)_3$ (386.5 mg, 1.250 mmol), (NMe_4) 4-fluorobenzoate (37.3 mg, 0.175 mmol) and (NMe_4)OPiv (35.1 mg, 0.20 mmol) were weighed in the open air and placed in a crimp-cap Schlenk microwave vial (10 mL) with a magnetic stirrer bar. The reaction vessel was capped, evacuated and backfilled with N_2 three times, then left under vacuum for 30 min. The vial was then backfilled with N_2 and bromobenzene **40b** (0.5 mmol, 1.0 equiv, 52 μL), arene **39a** (270 μL, 1.50 mmol), pivalonitrile (2.71, 5.52 or 9.03 equiv; 150.0, 300.0 or 500.0 μL), dodecane (23 μL, 0.1 mmol) and ethylpivalate (457, 307 or 107 μL) were added *via* syringe (total volume of liquids = 952 μL). The vial was resealed with a new cap under a stream of N_2 and brought inside a glove box. Then the mixture was stirred at 115 °C and small aliquots were taken *via* syringe at the appropriate time. The samples for the GC-FID analysis were prepared by flushing the syringe used for withdrawing the small amount of the crude with 2 mL of EtOAc directly inside a GC vial.

Characterisation data of biaryl compounds

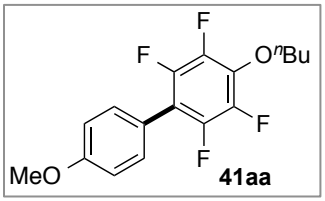

4-butoxy-2,3,5,6-tetrafluoro-4'-methoxy-1,1'-biphenyl (**41aa**).

The General Procedure 1 was applied with 4-bromoanisole (**40a**) (62.6 μL, 0.50 mmol) and 3-butoxy-1,2,4,5-tetrafluorobenzene (**39a**) (333.3 mg, 1.50 mmol). Column chromatography (hexane 100%) afforded the title product as a white solid (134.6 mg, 82%).

^{1}H NMR (400 MHz, $CDCl_3$): δ 7.38 (d, *J* = 8.9 Hz, 2H), 7.00 (d, *J* = 8.9 Hz, 2H), 4.25 (t, *J* = 6.5 Hz, 2H), 3.86 (s, 3H), 1.79 (app quintet, *J* = 7.0 Hz, 2H), 1.52 (app sextet, *J* = 7.5 Hz, 2H), 1.99 (t, *J* = 7.4 Hz, 3H); ^{13}C NMR (126 MHz, $CDCl_3$): δ 160.0, 144.4 (dm, *J* = 245.1 Hz), 141.7 (app ddt, *J* = 246.5, 15.7, 4.3 Hz), 136.6 - 136.4 (m), 131.6, 119.6, 114.2 - 114.0 (m, 2C), 75.2 (t, *J* = 3.0 Hz), 55.5, 32.1, 19.0, 13.9; ^{19}F NMR (376 MHz, $CDCl_3$) δ –145.7 (dd, *J* = 22.4, 8.8 Hz, 2F), 157.7 (dd, *J* = 22.4, 8.8 Hz, 2F); IR (ATR) 2934, 1476, 1080, 974, 826. m.p. 49 - 51 ºC; HRMS (EI) *m/z* calcd. $C_{17}H_{16}F_4O_2$: $[M]^+$ 328.1081 found: $[M]^+$ 328.1077.

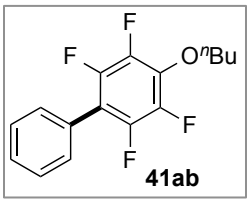

4-butoxy-2,3,5,6-tetrafluoro-1,1'-biphenyl (**41ab**).

The General Procedure 1 was applied with bromobenzene (**40b**) (52.7 μL, 0.50 mmol) and 3-butoxy-1,2,4,5-tetrafluorobenzene (**39a**) (333.3 mg, 1.50 mmol). Column chromatography (hexane 100%) afforded the title product as a white solid (113.4 mg, 76%).

^{1}H NMR (500 MHz, $CDCl_3$): δ 7.51 - 7.40 (m, 5H), 4.29 (t, *J* = 6.5 Hz, 2H), 1.85 - 1.79 (m, 2H), 1.59 - 1.52 (m, 2H), 1.02 (t, *J* = 7.4 Hz, 3H); ^{13}C NMR (126 MHz, $CDCl_3$): δ 144.4 (dm, *J* = 245.7 Hz), 141.6 (ddt, *J* = 246.6, 15.6, 4.4 Hz), 137.0 (tt, *J* = 12.3, 3.5 Hz), 130.3, 128.9, 128.7, 127.5, 114.3 (t, *J* = 17.2 Hz), 75.2, 32.1, 19.0, 13.8; ^{19}F NMR (471 MHz, $CDCl_3$) δ –145.4 (dd, *J* = 21.9, 8.9 Hz, 2F), –157.6 (dd, *J* = 22.2, 8.7 Hz, 2F); IR (ATR) 2962, 1482, 1438, 1077, 987, 734; m.p. 35 - 29 ºC; HRMS (EI) *m/z* calcd. $C_{16}H_{14}F_4O$: $[M]^+$ 298.0975 found: $[M]^+$ 298.0986.

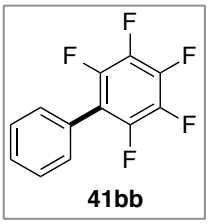

41bb

2,3,4,5,6-pentafluorobiphenyl (**41bb**)

The General Procedure 1 was applied with bromobenzene (52.7 μL, 0.50 mmol) and pentafluorobenzene (166.5 μL, 1.50 mmol). Column chromatography (hexane 100%) afforded the title product as a white solid (116.0 mg, 95%).

Spectroscopic data matched those previously reported.[166]

^{1}H NMR (400 MHz, $CDCl_3$): δ 7.52 - 7.45 (m, 3 H), 7.45 - 7.41 (m, 2 H); ^{13}C NMR (126 MHz, $CDCl_3$): δ 144.3 (dm, *J* = 247.5 Hz), 140.5 (dm, *J* = 252.7 Hz), 138.0 (dm, *J* = 250.6 Hz), 130.3, 129.4, 128.9, 126.5, 116.1 (app td, *J* = 17.4, 4.0 Hz); ^{19}F NMR (376 MHz, $CDCl_3$): δ –143.2 (dd, *J* = 22.9, 8.2 Hz, 2F), –155.6 (t, *J* = 21.1 Hz, 1F), –162.2 - –162.3 (m, 2F).

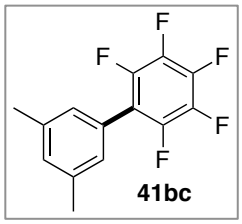

41bc

3',5'-dimethyl-2,3,4,5,6-pentafluorobiphenyl (**41bc**)

The General Procedure 1 was applied with 1-bromo-3,5-dimethylbenzene (67.9 μL, 0.50 mmol) and pentafluorobenzene (166.5 μL, 1.50 mmol). Column chromatography (hexane 100%) afforded the title product as a white solid (126.6 mg, 93%).

Spectroscopic data matched those previously reported.[167]

^{1}H NMR (400 MHz, $CDCl_3$): δ 7.10 (s, 1H), 7.02 (s, 2H), 2.38 (s, 6H); ^{13}C NMR (126 MHz, $CDCl_3$): δ 144.3 (dm, *J* = 247.1 Hz), 140.4 (dm, *J* = 253.3 Hz), 138.5, 137.9 (dm, *J* = 250.3 Hz), 131.1, 127.9, 126.3, 116.4, (app td, *J* = 17.6, 3.9 Hz), 21.4; ^{19}F NMR (376 MHz, $CDCl_3$) δ –143.0 (dd, *J* = 23.2, 8.2 Hz, 2F), –156.1 (t, *J* = 21.0 Hz, 1F), –162.5 (app td, *J* = 22.1, 7.6 Hz, 2F).

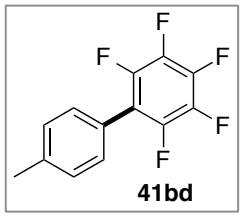

41bd

2,3,4,5,6-pentafluoro-4'-methylbiphenyl (**41bd**)

The General Procedure 1 was applied with 4-bromotoluene (61.5 μL, 0.50 mmol) and pentafluorobenzene (166.5 μL, 1.50 mmol). Column

chromatography (hexane 100%) afforded the title product as a white solid (108.4 mg, 84%).

Spectroscopic data matched those previously reported.[167]

^{1}H NMR (400 MHz, $CDCl_3$): δ 7.31 (app s, 4H), 2.42 (s, 3H); ^{13}C NMR (126 MHz, $CDCl_3$): δ 144.3 (dm, *J* = 247.5 Hz), 140.4 (dm, *J* = 253.0 Hz), 139.6, 138.0 (dm, *J* = 251.6 Hz), 130.1, 129.6, 123.5, 116.1 (app td, *J* = 17.3, 3.7 Hz), 21.5; ^{19}F NMR (376 MHz, $CDCl_3$) δ –143.4 (dd, *J* = 23.1, 8.2 Hz, 2F), –156.1 (t, *J* = 21.0 Hz, 1F), –162.4 (app td, *J* = 22.1, 8.0 Hz, 2F).

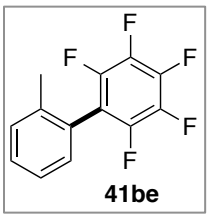

2,3,4,5,6-pentafluoro-2'-methylbiphenyl (**41be**)

The General Procedure 1 was applied with 2-bromotoluene (60.1 μL, 0.50 mmol) and pentafluorobenzene (166.5 μL, 1.50 mmol). Column chromatography (hexane 100%) afforded the title product as a colourless oil (56.8 mg, 44%)

Spectroscopic data matched those previously reported.[166]

^{1}H NMR (400 MHz, $CDCl_3$): δ 7.41 - 7.34 (m, 2H), 7.30 (app td, *J* = 7.3, 1.4 Hz, 1H), 7.19 (d, *J* = 7.5 Hz, 1H), 2.19 (s, 3H); ^{13}C NMR (126 MHz, $CDCl_3$): δ 144.2 (dm, *J* = 246.4 Hz), 140.7 (dm, *J* = 253.9 Hz), 137.8 (dm, *J* = 250.8 Hz), 137.5, 130.7, 130.6, 129.8, 126.1, 126.0, 115.6 (app td, *J* = 19.9, 4.2 Hz), 19.8; ^{19}F NMR (376 MHz, $CDCl_3$) δ -140.5 (dd, *J* = 23.3, 8.3 Hz, 2F), –155.3 (t, *J* = 20.9 Hz, 1F), –162.2 (app td, *J* = 22.1, 7.7 Hz, 2F).

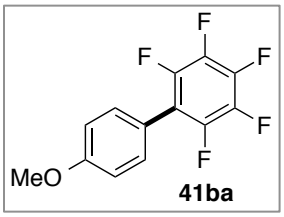

2,3,4,5,6-pentafluoro-4'-methoxybiphenyl (**41ba**)

The General Procedure 1 was applied with 4-bromoanisole (62.6 μL, 0.50 mmol) and pentafluorobenzene (166.5 μL, 1.50 mmol). Column chromatography (hexane 100%) afforded the title product as a white solid (117.9 mg, 86%).

Spectroscopic data matched those previously reported.[166]

^{1}H NMR (400 MHz, $CDCl_3$): δ 7.36 (d, *J* = 8.9 Hz, 2 H), 7.02 (d, *J* = 8.9 Hz, 2 H), 3.87 (s, 3H); ^{13}C NMR (126 MHz, $CDCl_3$): δ 160.4, 144.3 (dm, *J* = 246.7 Hz), 140.2 (dm, *J* = 252.5 Hz), 138.0 (dm, *J* = 250.6 Hz), 131.6, 118.5, 115.8 (app td, *J* = 17.1, 3.9 Hz), 114.3, 55.4; ^{19}F NMR (376 MHz, $CDCl_3$): δ –143.6 (dd, *J* = 23.2, 8.2 Hz, 2F), –156.5 (t, *J* = 21.0 Hz, 1F), –162.5 (app dt, *J* = 22.3, 7.6 Hz, 2F).

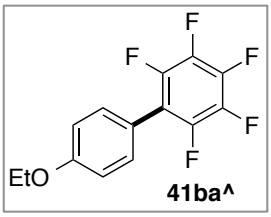

41ba^

4'-ethoxy-2,3,4,5,6-pentafluoro-1,1'-biphenyl (**41ba^**)

The General Procedure 1 was applied with 4-bromophenetole (71.4 μL, 0.50 mmol) and pentafluorobenzene (166.5 μL, 1.50 mmol). Column chromatography (hexane 100%) afforded the title product as a white solid (123.9 mg, 86%).

Spectroscopic data matched those previously reported.[168]

^{1}H NMR (500 MHz, $CDCl_3$): δ 7.35 (d, *J* = 8.8 Hz, 2 H), 7.00 (d, *J* = 8.8 Hz, 2 H), 4.09 (q, *J* = 7.0 Hz, 2H), 1.46 (t, *J* = 7.0 Hz, 3H); ^{13}C NMR (126 MHz, $CDCl_3$): δ 159.8, 144.3 (dm, *J* = 246.5 Hz), 140.1 (dm, *J* = 253.1 Hz), 138.0 (dm, *J* = 250.2 Hz), 131.5, 118.3, 115.9 (app td, *J* = 17.2, 4.0 Hz), 114.8, 63.7, 14.89; ^{19}F NMR (471 MHz, $CDCl_3$): δ –143.7 (dd, *J* = 23.2, 8.2 Hz, 2F), –156.7 (t, *J* = 21.2 Hz, 1F), –162.5 (app td, *J* = 22.6, 7.9 Hz, 2F).

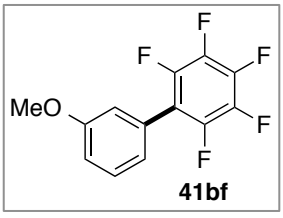

41bf

3'-methoxy-2,3,4,5,6-pentafluorobiphenyl (**41bf**)

The General Procedure 1 was applied with 3-bromoanisole (63.3 μL, 0.50 mmol) and pentafluorobenzene (166.5 μL, 1.50 mmol). Column chromatography (hexane 100%) afforded the title product as a white solid (109.7 mg, 80%).

Spectroscopic data matched those previously reported.[166]

^{1}H NMR (400 MHz, $CDCl_3$): δ 7.41 (app t, *J* = 8.0 Hz, 1H), 7.02 - 6.98 (m, 2H), 6.95 - 6.94 (m, 1H), 3.85 (s, 3H); ^{13}C NMR (126 MHz, $CDCl_3$): δ 159.8, 144.3 (dm, *J* = 247.7 Hz), 140.6 (dm, *J* = 253.6 Hz), 138.0 (dm, *J* = 249.5 Hz), 129.9, 127.6, 122.6, 116.2 - 115.8 (m,

2C), 115.0, 55.5; ^{19}F NMR (376 MHz, $CDCl_3$) δ –142.8 (dd, *J* = 23.0, 8.1 Hz, 2F), –155.5 (t, *J* = 20.9 Hz, 1F), –162.2 (app td, *J* = 22.1, 7.4 Hz, 2F).

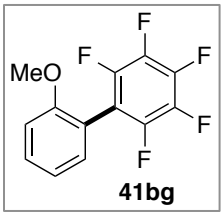

2,3,4,5,6-pentafluoro-2'-methoxybiphenyl (**41bg**)

The General Procedure 1 was applied with 2-bromoanisole (62.3 μL, 0.50 mmol) and pentafluorobenzene (166.5 μL, 1.50 mmol). Column chromatography (hexane 100%) afforded the title product as a colourless oil (91.8 mg, 67%).

Spectroscopic data matched those previously reported.[169]

^{1}H NMR (400 MHz, $CDCl_3$): δ 7.46 (ddd, *J* = 8.3, 7.5, 1.7 Hz, 1 H), 7.23 (dd, *J* = 7.5, 1.4 Hz, 1 H), 7.08 - 7.02 (m, 2H), 3.81 (s, 3H); ^{13}C NMR (126 MHz, $CDCl_3$): δ 157.3, 144.6 (dm, *J* = 247.1 Hz), 140.7 (dm, *J* = 252.5 Hz), 137.7 (dm, *J* = 249.8 Hz), 131.9, 131.3, 120.7, 115.4, 112.9 (app td, *J* = 19.2, 4.0 Hz), 111.4, 55.7; ^{19}F NMR (376 MHz, $CDCl_3$) δ –140.2 (dd, *J* = 23.0, 7.9 Hz, 2F), –156.2 (t, *J* = 20.9 Hz, 1F), –163.1 - –163.3 (m, 2F).

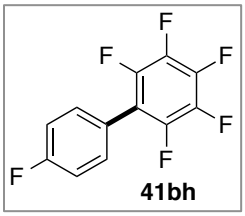

2,3,4,4',5,6-hexafluorobiphenyl (**41bh**)

The General Procedure 1 was applied with 1-bromo-4-fluorobenzene (54.9 μL, 0.50 mmol) and pentafluorobenzene (166.5 μL, 1.50 mmol). Column chromatography (hexane 100%) afforded the title product as a white solid (106.2 mg, 81%).

Spectroscopic data matched those previously reported.[166]

^{1}H NMR (400 MHz, $CDCl_3$): δ 7.44 - 7.40 (m, 2H), 7.19 (app t, *J*= 8.7 Hz, 2H); ^{13}C NMR (126 MHz, $CDCl_3$): δ 163.3 (d, *J* = 250.0 Hz), 144.3 (dm, *J* = 247.6 Hz), 140.6 (dm, *J* = 254.2 Hz), 138.0 (dm, *J* = 251.1 Hz), 132.2 (d, *J* = 8.4 Hz), 122.4, 116.1 (d, *J* = 21.9 Hz), 115.1, (app td, *J* = 17.1, 3.9 Hz); ^{19}F NMR (376 MHz, $CDCl_3$) δ –111.2 - –111.3 (m, 1F), –143.3 (dd, *J* = 22.9, 8.2 Hz, 2F), –155.1 (t, *J* = 21.0 Hz, 1F), –161.9 (app td, *J* = 21.9, 7.7 Hz, 2F).

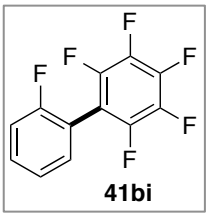

2,2',3,4,5,6-hexafluorobiphenyl (**41bi**)

The General Procedure 1 was applied with 1-bromo-2-fluorobenzene (54.7 μL, 0.50 mmol) and pentafluorobenzene (166.5 μL, 1.50 mmol). Column chromatography (hexane 100%) afforded the title product as a white solid (82.6 mg, 63%).

Spectroscopic data matched those previously reported.[170]

^{1}H NMR (400 MHz, $CDCl_3$): δ 7.51 - 7.47 (m, 1H), 7.35 (app t, *J* = 7.1 Hz, 1H), 7.28 (app t, *J* = 8.2 Hz, 1H), 7.23 (app t, *J* = 9.1 Hz, 1H); ^{13}C NMR (126 MHz, $CDCl_3$): δ 160.0 (d, *J* = 250.7 Hz), 144.5 (dm, *J* = 249.2 Hz), 141.2 (dm, *J* = 254.4 Hz), 137.9 (dm, *J* = 251.1 Hz), 132.1, 131.9 (d, *J* = 8.3 Hz), 124.5 (d, *J* = 3.6 Hz), 116.3 (d, *J* = 21.6 Hz), 114.3 (d, *J* = 15.9 Hz), 110.3 (app td, *J* = 18.6, 3.9 Hz); ^{19}F NMR (376 MHz, $CDCl_3$) δ –112.71 - –112.82 (m, 1F), –140.3 (app dt, *J* = 23.0, 9.1 Hz, 2F), –154.0 (t, *J* = 21.0 Hz, 1F), –162.0 (app td, *J* = 21.7, 7.4 Hz, 2F).

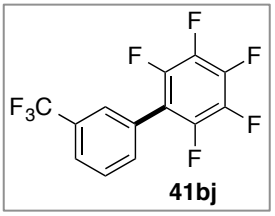

2,3,4,5,6-pentafluoro-3'-(trifluoromethyl)biphenyl (**41bj**)

The General Procedure 1 was applied with 3-bromobenzotrifluoride (69.7 μL, 0.50 mmol) and pentafluorobenzene (166.5 μL, 1.50 mmol). Column chromatography (hexane 100%) afforded the title product as a colourless oil (98.3 mg, 63%).

Spectroscopic data matched those previously reported.[169]

^{1}H NMR (400 MHz, $CDCl_3$): δ 7.75 - 7.71 (m, 2H), 7.66 - 7.62 (m, 2H); ^{13}C NMR (126 MHz, $CDCl_3$): δ 144.3 (dm, *J* = 248.7 Hz), 141.1 (dm, *J* = 253.4 Hz), 138.1 (dm, *J* = 251.3 Hz), 133.6, 131.5 (q, *J* = 32.9 Hz), 129.5, 127.4, 127.2, 126.3 (q, *J* = 3.6 Hz),123.8 (q, *J* = 272.5 Hz), 114.6 (td, *J* = 16.7, 4.4 Hz); ^{19}F NMR (376 MHz, $CDCl_3$) δ –62.8 (s, 3F), –143.0 (dd, *J* = 22.7, 8.2 Hz, 2F), –153.8 (t, *J* = 21.0 Hz, 1F), –161.4 (app td, *J* = 21.9, 7.9 Hz, 2F).

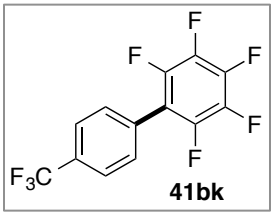

2,3,4,5,6-pentafluoro-4'-trifluoromethylbiphenyl (**41bk**)

The General Procedure 1 was applied with 4-bromobenzotrifluoride (70.0 μL, 0.50 mmol) and pentafluorobenzene (166.5 μL, 1.50 mmol). Column chromatography (hexane 100%) afforded the title product as a white solid (96.8 mg, 62%).

Spectroscopic data matched those previously reported.[166]

^{1}H NMR (400 MHz, $CDCl_3$): δ 7.77 (d, *J* = 8.1, 2H), 7.57 (d, *J*= 8.1, 2H); ^{13}C NMR (126 MHz, $CDCl_3$): δ 144.3 (dm, *J* = 249.1 Hz), 141.1 (dm, *J* = 255.2 Hz), 138.1 (dm, *J* = 251.9 Hz), 131.6 (q, *J* = 32.9 Hz), 130.8, 130.3, 125.9 (q, *J* = 3.6 Hz), 123.9 (q, *J* = 272.4 Hz), 114.7 (app td, *J* = 16.8, 4.1 Hz); ^{19}F NMR (376 MHz, $CDCl_3$) δ –62.9 (s, 3F), –142.9 (dd, *J* = 22.7, 8.2 Hz, 2F), –153.7 (t, *J* = 21.0 Hz, 1F), –161.3 (app td, *J* = 21.7, 7.6 Hz, 2F).

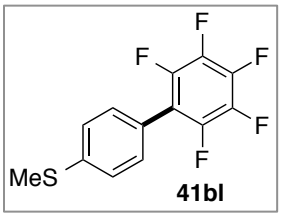

methyl(2',3',4',5',6'-pentafluoro-[biphenyl]-4-yl)sulfane (**41bl**)

The General Procedure 1 was applied with 4-bromothioanisole (101.6 mg, 0.50 mmol) and pentafluorobenzene (166.5 μL, 1.50 mmol). Column chromatography (hexane/EtOAc 99:1) afforded the title product as a white solid (104.4 mg, 72%).

Spectroscopic data matched those previously reported.[171]

^{1}H NMR (400 MHz, $CDCl_3$): δ 7.34 (app s, 4H), 2.53 (s, 3H); ^{13}C NMR (126 MHz, $CDCl_3$): δ 144.3 (dm, *J* = 247.9 Hz), 140.8, 140.4 (dm, *J* = 253.5 Hz), 138.0 (dm, *J* = 250.4 Hz), 130.5, 126.1, 122.7, 115.6 (app td, *J* = 17.0, 3.8 Hz), 15.3; ^{19}F NMR (376 MHz, $CDCl_3$) δ –143.3 (dd, *J* = 23.0, 8.1 Hz, 2F), –155.7 (t, *J* = 21.0 Hz, 1F), –162.1 (app td, *J* = 22.1, 7.6 Hz, 2F).

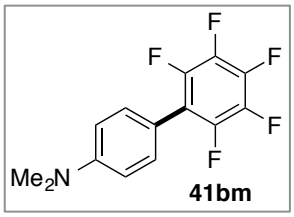

4'-dimethylamino-2,3,4,5,6-pentafluorobiphenyl (**41bm**)

The General Procedure 1 was applied with 4-bromo-*N*,*N*-dimethylaniline (100.0 mg, 0.50 mmol) and pentafluorobenzene

(166.5 μL, 1.50 mmol). Column chromatography (hexane/EtOAc 98:2) afforded the title product as a white solid (114.9 mg, 80%).

Spectroscopic data matched those previously reported.[167]

^{1}H NMR (400 MHz, $CDCl_3$): δ 7.31 (d, *J* = 8.9 Hz, 2H), 6.79 (d, *J* = 8.9 Hz, 2H), 3.02 (s, 6H); ^{13}C NMR (126 MHz, $CDCl_3$): δ 150.9, 144.3 (dm, *J* = 245.9 Hz), 139.6 (dm, *J* = 252.2 Hz), 138.0 (dm, *J* = 249.8 Hz), 131.1, 116.5 (app td, *J* = 17.0, 3.8 Hz), 113.4, 112.0, 40.3; ^{19}F NMR (376 MHz, $CDCl_3$) δ –144.1 (dd, *J* = 23.5, 8.1 Hz, 2F), –157.9 (t, *J* = 21.1 Hz, 1F), –163.0 (app td, *J* = 22.3, 7.6 Hz, 2F).

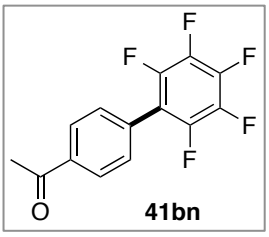

41bn

1-(2',3',4',5',6'-pentafluoro-biphenyl-4-yl)ethanone (**41bn**)

The General Procedure 1 applied with 4-bromoacetophenone (99.5 mg, 0.50 mmol) and pentafluorobenzene (166.5 μL, 1.50 mmol). Column chromatography (hexane/EtOAc 98:2) afforded the title product as a white solid (83.0 mg, 58%).

Spectroscopic data matched those previously reported.[169]

^{1}H NMR (400 MHz, $CDCl_3$): δ 8.08 (d, *J* = 8.5 Hz, 2 H), 7.55 (d, *J* = 8.5 Hz, 2 H), 2.66 (s, 3H); ^{13}C NMR (126 MHz, $CDCl_3$): δ 197.4, 144.2 (dm, *J* = 248.9 Hz), 141.0 (dm, *J* = 255.1 Hz), 138.3 (dm, *J* = 251.4 Hz), 137.6, 131.2, 130.6, 128.7, 115.0 (app td, *J* = 16.9, 3.9 Hz), 26.8; ^{19}F NMR (376 MHz, $CDCl_3$) δ –142.8 (dd, *J* = 22.6, 8.1 Hz, 2F), –153.9 (t, *J* = 21.0 Hz, 1F), –162.5 (app dt, *J* = 21.9, 7.8 Hz, 2F).

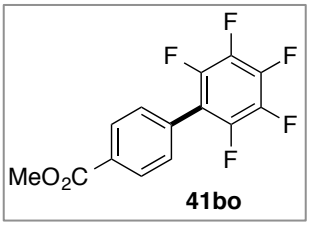

41bo

methyl 2',3',4',5',6'-pentafluorobiphenyl-4-carboxylate (**41bo**)

The General Procedure 1 was applied with methyl-4-bromobenzoate (107.5 mg, 0.50 mmol) and pentafluorobenzene (166.5 μL, 1.50 mmol). Column chromatography (hexane/EtOAc 98:2) afforded the title product as a white solid (89.1 mg, 59%).

Spectroscopic data matched those previously reported.[169]

^{1}H NMR (400 MHz, $CDCl_3$): δ 8.16 (d, *J* = 8.4 Hz, 2H), 7.51 (d, *J* = 8.4 Hz, 2H), 3.95, (s, 3H); ^{13}C NMR (126 MHz, $CDCl_3$): δ (1 carbon missing)[10] 166.5, 144.2 (dm, *J* = 248.7 Hz), 140.9 (dm, *J* = 255.1 Hz), 138.0 (dm, *J* = 251.0 Hz), 131.0, 130.4, 130.0, 115.1 (app td, *J* = 17.0, 3.9 Hz), 52.5; ^{19}F NMR (376 MHz, $CDCl_3$) δ –142.8 (dd, *J* = 22.7, 8.0 Hz, 2F), –154.1 (t, *J* = 20.9 Hz, 1F), –161.6 (app td, *J* = 22.1, 7.4 Hz, 2F).

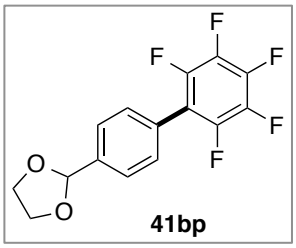

41bp

2-(2',3',4',5',6'-pentafluoro-[1,1'-biphenyl]-4-yl)-1,3-dioxolane (**41bp**)

The General Procedure 1 was applied with 1-Bromo-4-(1,3-dioxolan-2-yl)benzene (114.5 mg, 0.50 mmol) and pentafluorobenzene (166.5 μL, 1.50 mmol). Column chromatography (hexane/EtOAc 97:3) afforded the title product as a white solid (112.3 mg, 71%).

^{1}H NMR (400 MHz, $CDCl_3$): δ 7.62 (d, *J* = 8.2 Hz, 2H), 7.45 (d, *J* = 8.2, 2H), 5.88 (s, 1H), 4.20 - 4.04 (m, 4H); ^{13}C NMR (126 MHz, $CDCl_3$): δ 144.3 (dm, *J* = 248.0 Hz), 140.6 (dm, *J* = 254.2 Hz), 139.3, 138.0 (dm, *J* = 250.8 Hz), 130.4, 127.3, 126.9, 115.7 (app td, *J* = 17.2, 4.0 Hz), 103.3, 65.6; ^{19}F NMR (376 MHz, $CDCl_3$) δ –143.0 (dd, *J* = 22.9, 8.1 Hz, 2F), –155.2 (t, *J* = 21.0 Hz, 1F), –162.1 (app td, *J* = 22.0, 7.7 Hz, 2F); IR (ATR) 2886, 1491, 1093, 982, 834; m.p. 125-127 ºC; HRMS (EI) *m/z* calcd. $C_{15}H_9F_5O_2$: $[M+H]^+$ 317.0601; found: $[M+H]^+$ 317.0608.

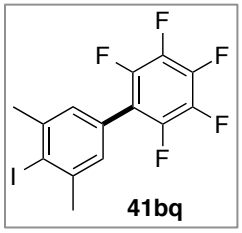

41bq

2,3,4,5,6-pentafluoro-4'-iodo-3',5'-dimethyl-1,1'-biphenyl (**41bq**)

The General Procedure 1 was applied with 5-bromo-2-iodo-*m*-xylene (155.5 mg, 0.50 mmol) and pentafluorobenzene (166.5 μL, 1.50 mmol). Column chromatography (hexane/EtOAc 95:5) afforded the title product as a white solid (165.2 mg, 83%).

^{1}H NMR (400 MHz, $CDCl_3$): δ 7.09 (s, 2H), 2.53 (s, 6H); ^{13}C NMR (126 MHz, $CDCl_3$): δ 144.1 (dm, *J* = 247.6 Hz), 143.0, 140.5 (dm, *J* = 254.5 Hz), 138.0 (dm, *J* = 249.9 Hz), 128.3,

125.8, 115.3 (app td, *J* = 17.5, 3.7 Hz), 110.0, 29.9; ^{19}F NMR (376 MHz, $CDCl_3$) δ –142.8 (dd, *J* = 22.9, 8.1 Hz, 2F), –115.2 (t, = 21.0 Hz, 1F), –162.0 (app dt, *J* = 22.1, 7.7 Hz, 2F); IR (ATR) 2953, 1521, 1496, 1026, 991; m.p. 68 - 70 °C; HRMS (EI) *m/z* calcd. $C_{14}H_8F_5I$: $[M]^+$ 397.9585; found: $[M]^+$ 397.9592.

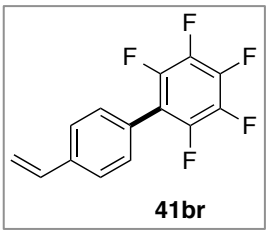

2,3,4,5,6-pentafluoro-4'-vinylbiphenyl (**41br**)

The General Procedure 1 was applied with 4-bromostyrene (65.4 μL, 0.50 mmol) and pentafluorobenzene (166.5 μL, 1.50 mmol). Column chromatography (hexane 100%) afforded the title product as a white solid (54.0 mg, 40%).

Spectroscopic data matched those previously reported.[172]

^{1}H NMR (400 MHz, $CDCl_3$): δ 7.53 (d, *J* = 8.2 Hz, 2H), 7.40 (d, *J* = 8.2 Hz, 2H), 6.77 (dd, *J* = 17.6, 10.9 Hz, 1H), 5.85 (dd, *J* = 17.6, 0.6 Hz, 1H), 5.36 (dd, *J* = 10.9, 0.6 Hz, 1H); ^{13}C NMR (126 MHz, $CDCl_3$): δ 144.3 (dm, *J* = 247.6 Hz), 140.5 (dm, *J* = 259.0 Hz), 138.7, 138.0 (dm, *J* = 250.4 Hz), 136.1, 130.5, 126.6, 125.7, 115.8 (app td, *J* = 17.2, 3.7 Hz), 115.6; ^{19}F NMR (376 MHz, $CDCl_3$) δ –143.2 (dd, *J* = 23.0, 8.1 Hz, 2F), –155.5 (t, *J* = 21.0 Hz, 1F), –162.2 (app td, *J* = 22.1, 7.7 Hz, 2F).

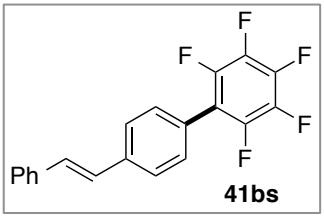

(*E*)-2,3,4,5,6-pentafluoro-4'-styryl-1,1'-biphenyl (**41bs**)

The General Procedure 1 was applied with 4-bromostilbene (129.6 mg, 0.50 mmol) and pentafluorobenzene (166.5 μL, 1.50 mmol). Column chromatography (hexane/EtOAc 95:5) afforded the title product as a white solid (117.7 mg, 68%).

^{1}H NMR (400 MHz, $CDCl_3$): δ 7.64 (d, *J* = 8.3 Hz, 2H), 7.55 (d, *J*= 7.3 Hz, 2H), 7.43 (d, *J* = 8.3 Hz, 2H), 7.39 (app t, *J* =7.4 Hz, 2H), 7.30 (tt, *J* = 7.4, 1.5 Hz, 1H), 7.21 (d, *J* = 16.3 Hz, 1H), 7.14 (d, *J* = 16.3 Hz, 1H); ^{13}C NMR (126 MHz, $(CD_3)_2CO$): δ 144.1 (dm, *J* = 247.0 Hz), 140.1 (dm, *J* = 250.6 Hz), 138.6, 137.7 (dm, *J* = 243.6 Hz), 137.1, 130.4, 130.1, 128.6, 127.8, 127.4, 126.7, 126.6, 125.1, 115.9 - 115.6, (m); ^{19}F NMR (376 MHz, $CDCl_3$) δ –143.2

(dd, *J* = 23.1, 8.1 Hz, 2F), –155.5 (t, *J* = 21.0 Hz, 1F), –162.1 (app td, *J* = 22.0, 7.7 Hz, 2F); IR (ATR) 2924, 1528, 1489, 982; m.p. 175 - 178 ºC; HRMS (EI) *m/z* calcd. $C_{20}H_{11}F_5$: $[M]^+$ 346.0775; found: $[M]^+$ 346.0775.

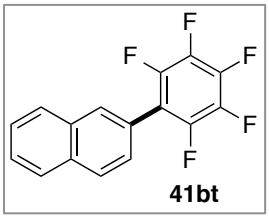

2-(perfluorophenyl)naphthalene (**41bt**)

The General Procedure 1 was applied with 2-bromonapthalene (103.5 mg, 0.50 mmol) and pentafluorobenzene (166.5 μL, 1.50 mmol). Column chromatography (hexane 100%) afforded the title product as a white solid (61.8 mg, 42%).

Spectroscopic data matched those previously reported.[166]

^{1}H NMR (400 MHz, $CDCl_3$): δ 7.97 - 7.89 (m, 4H), 7.60 - 7.49 (m, 3H); ^{13}C NMR (126 MHz, $CDCl_3$): δ 144.5 (dm, *J* = 248.3 Hz), 140.6 (dm, *J* = 252.3 Hz), 138.1 (dm, *J* = 250.6 Hz), 133.4, 133.2, 130.3, 128.6, 128.5, 127.9, 127.3, 127.2, 126.9, 123.9, 116.3 - 116.0 (m); ^{19}F NMR (376 MHz, $CDCl_3$) δ –143.0 (dd, *J* = 23.0, 8.2 Hz, 2F), –155.4 (t, *J* = 21.0 Hz, 1F), –162.1 (app td, *J* = 22.0, 7.6 Hz, 2F).

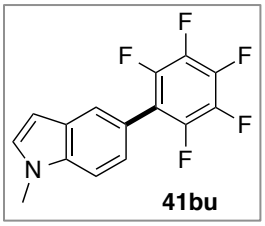

1-methyl-5-(perfluorophenyl)-*1H*-indole (**41bu**)

The General Procedure 1 was applied with 5-bromo-1-methylindole (105.0 mg, 0.50 mmol) and pentafluorobenzene (166.5 μL, 1.50 mmol). Column chromatography (hexane/EtOAc 98:2) afforded the title product as a white solid (87.7 mg, 59%).

Spectroscopic data matched those previously reported.[169]

^{1}H NMR (400 MHz, $CDCl_3$): δ 7.70 (s, 1H), 7.44 (d, *J*= 8.6 Hz, 1H), 7.27 - 7.24 (m, 1H), 7.14 (d, *J* = 3.1 Hz, 1H), 6.57 (d, *J* = 3.1 Hz, 1H), 3.84 (s, 3H); ^{13}C NMR (126 MHz, $CDCl_3$): δ 144.5 (dm, *J* = 246.4 Hz), 140.0 (dm, *J* = 254.9 Hz), 138.0 (dm, *J* = 250.1 Hz), 136.9, 130.0, 128.7, 123.4, 123.2, 117.4 (app td, *J* = 17.7, 3.7 Hz), 117.1, 109.6, 101.7, 33.0; ^{19}F NMR (376 MHz, $CDCl_3$) δ –143.4 (dd, *J* = 23.5, 8.1 Hz, 2F), –157.2 (t, *J* = 21.1 Hz, 1F), –162.9 (app td, *J* = 22.2, 7.3 Hz, 2F).

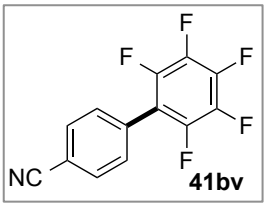

41bv

2',3',4',5',6'-pentafluoro-biphenyl-4-carbonitrile (**41bv**).

The General Procedure 1 was applied with $[Ru(^tBuCN)_6](BF_4)_2$ (31.0 mg, 0.040 mmol), 4-bromobenzonitrile (91.0 mg, 0.50 mmol) and pentafluorobenzene (166.5 μL, 1.50 mmol) for 1 h. Column chromatography (hexane/ CH_2Cl_2 95:5) afforded the title product as a white solid (33.6 mg, 25%).

Spectroscopic data matched those previously reported.[172]

^{1}H NMR (400 MHz, $CDCl_3$): δ 7.80 (d, *J* = 8.2 Hz, 2H), 7.57 (d, *J* = 8.2 Hz, 2H); ^{13}C NMR (126 MHz, $CDCl_3$): δ 144.2 (dm, *J* = 249.4 Hz), 141.3 (dm, *J* = 257.9 Hz), 138.1 (dm, *J* = 251.9 Hz), 132.6, 131.3, 131.1, 118.3, 114.2 (app td, *J* = 16.6, 4.0 Hz), 113.5; ^{19}F NMR (376 MHz, $CDCl_3$) δ –142.7 - –142.8 (m, 2F), –152.8 (t, *J* = 21.0 Hz, 1F), –160.8 - –161.0 (m, 2F).

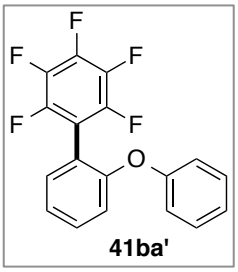

41ba'

2,3,4,5,6-pentafluoro-2'-phenoxy-1,1'-biphenyl (**41ba'**)

The General Procedure 1 was applied with 1-bromo-2-phenoxybenzene (124.6 mg, 0.50 mmol) and pentafluorobenzene (166.5 μL, 1.50 mmol). Column chromatography (hexane 100%) afforded the title product as a colourless oil (132.8 mg, 79%).

^{1}H NMR (400 MHz, $CDCl_3$): δ 7.43 - 7.40 (m, 1H), 7.37 - 7.32 (m, 3H), 7.21 (t, *J* = 7.6 Hz, 1H), 7.13 (t, *J* = 7.5 Hz, 1H) 7.01 - 6.97 (m, 3H); ^{13}C NMR (126 MHz, $CDCl_3$): δ 156.4, 155.8, 144.6 (dm, *J* = 247.5 Hz), 140.8 (dm, *J* = 253.6 Hz), 137.7 (dm, *J* = 250.3 Hz), 132.3, 131.3, 130.0, 124.1, 123.2, 119.5, 118.2, 117.6, 112.4 (app td, *J* = 19.0, 3.8 Hz); ^{19}F NMR (376 MHz, $CDCl_3$) δ –140.1 (dd, *J* = 23.0, 7.8 Hz, 2F), –155.3 (t, *J* = 21.0 Hz, 1F), –162.6 - –162.7 (m, 2F); IR (ATR) 2924, 1488, 1237, 1061, 987, 749; HRMS (EI) *m/z* calcd. $C_{18}H_9F_5O$: $[M]^+$ 336.0568 found: $[M]^+$ 336.0566.

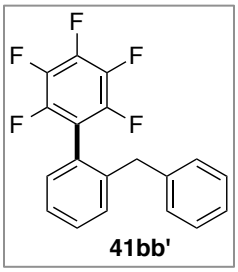

2'-benzyl-2,3,4,5,6-pentafluoro-1,1'-biphenyl (**41bb'**)

The General Procedure 1 was applied with 1-benzyl-2-bromobenzene (123.6 mg, 0.50 mmol) and pentafluorobenzene (166.5 μL, 1.50 mmol). Column chromatography (hexane 100%) afforded the title product as a colourless oil (70.2 mg, 42%).

^{1}H NMR (400 MHz, $CDCl_3$): δ 7.43 (t, *J* = 7.4 Hz, 1H), 7.36 - 7.31 (m, 2H), 7.20 - 7.13 (m, 4H), 6.91 (d, *J* = 7.2 Hz, 2H), 3.85 (s, 2H); ^{13}C NMR (126 MHz, $CDCl_3$): δ 144.1 (dm, *J* = 247.3 Hz), 140.8 (dm, *J* = 254.2 Hz), 140.7, 139.8, 137.6 (dm, *J* = 251.9 Hz), 131.1, 130.8, 130.0, 128.7, 128.4, 126.9, 126.4, 126.2, 115.6 - 115.3 (m), 39.9; ^{19}F NMR (376 MHz, $CDCl_3$) δ –140.1 (dd, *J* = 23.4, 8.1 Hz, 2F), –155.3 (t, *J* = 21.0 Hz, 1F), –162.3 - –162.5 (m, 2F); IR (ATR) 2921, 1521, 1494, 1060, 987, 736; HRMS (EI) *m/z* calcd. $C_{19}H_{11}F_5$ $[M]^+$ 334.0775 found: $[M]^+$ 334.0760.

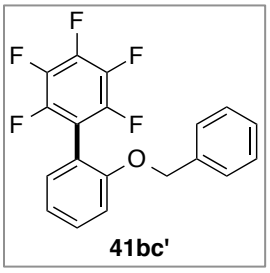

2'-(benzyloxy)-2,3,4,5,6-pentafluoro-1,1'-biphenyl (**41bc'**)

The General Procedure 1 was applied with 1-(benzyloxy)-2-bromobenzene (131.6 mg, 0.50 mmol) and pentafluorobenzene (166.5 μL, 1.50 mmol). Column chromatography (hexane 100%) afforded the title product as a colourless oil (117.3 mg, 67%).

^{1}H NMR (400 MHz, $CDCl_3$): δ 7.46 (td, *J* = 7.9, 1.6 Hz, 1H), 7.41 - 7.31 (m, 6H), 7.12 (t, *J* = 7.7 Hz, 2H), 5.14 (s, 2H); ^{13}C NMR (126 MHz, $CDCl_3$): δ 156.4, 144.6 (dm, *J* = 247.1 Hz), 140.6 (dm, *J* = 253.0 Hz), 137.7 (dm, *J* = 249.9 Hz), 136.7. 132.0, 131.2, 128.7, 128.1, 127.1, 121.1, 115.9, 113.2 - 112.8 (m, 2C), 70.6; ^{19}F NMR (376 MHz, $CDCl_3$) δ –139.9 (dd, *J* = 23.1, 7.9 Hz, 2F), –156.0 (t, *J* = 21.0 Hz, 1F), –163.1 - –163.3 (m, 2F); IR (ATR) 2924, 1490, 1449, 1061, 986, 865, 751; HRMS (EI) *m/z* calcd. $C_{19}H_{11}F_5O$ $[M]^+$ 350.0725 found: $[M]^+$ 350.0738.

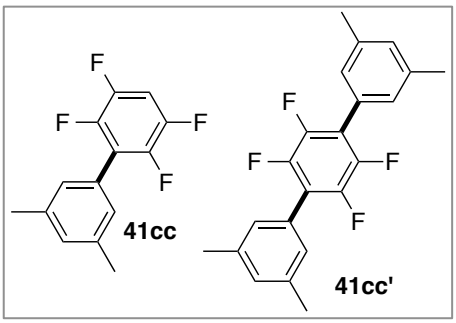

2,3,5,6-tetrafluoro-3',5'-dimethylbiphenyl (**41cc**) and 2',3',5',6'- tetrafluoro -3,3'',5,5''-tetramethyl-1,1':4',1''-terphenyl (**41cc'**)

The General Procedure 1 was applied with 1-bromo-3,5-dimethylbenzene (67.9 μL, 0.50 mmol) and 1,2,4,5-tetrafluorobenzene (167.5 μL, 1.50 mmol). Column chromatography (hexane 100%) afforded both 2,3,5,6-tetrafluoro-3',5'-dimethylbiphenyl (94.1 mg, 74%) and 2',3',5',6'-tetrafluoro-3,3'',5,5''-tetramethyl-1,1':4',1''-terphenyl (17.8 mg, 10%) as white solids.

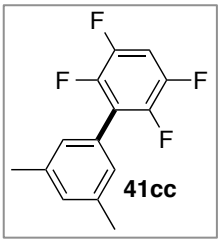

2,3,5,6-tetrafluoro-3',5'-dimethylbiphenyl (**41cc**)

^{1}H NMR (400 MHz, $CDCl_3$): δ 7.11 (s, 1H), 7.09 - 7.01 (m, 3H), 2.39 (s, 6H); ^{13}C NMR (126 MHz, $CDCl_3$): δ 146.3 (dm, *J* = 247.7 Hz), 143.9 (dm, *J* = 246.2 Hz), 138.3, 131.0, 127.9 (t, *J* = 1.7 Hz), 127.4 (t, *J* = 2.3 Hz), 122.0 (t, *J* = 16.9 Hz), 104.7 (t, *J* = 22.7 Hz), 21.4; ^{19}F NMR (376 MHz, $CDCl_3$) δ –139.4 (ddd, *J* =22.5, 12.8, 9.7 Hz, 2F), –143.6 (ddd, *J* = 21.9, 13.4, 7.9 Hz, 2F); IR (ATR) 2292, 1494, 1172, 929, 848, 705; m.p. 42-44 ºC; HRMS (EI) *m/z* calcd. $C_{14}H_{10}F_4$: $[M]^+$ 254.0707; found: 254.0713.

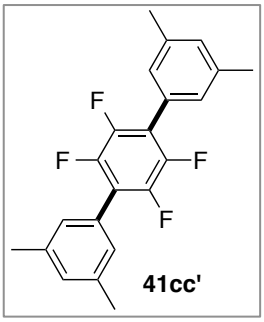

2',3',5',6'-tetrafluoro-3,3'',5,5''-tetramethyl-1,1':4',1''-terphenyl (**41cc'**)

^{1}H NMR (400 MHz, $CDCl_3$): δ 7.12 - 7.11 (m, 6H), 2.40 (s, 12H); ^{13}C NMR (126 MHz, $CDCl_3$): δ 144.2 (dm, *J* = 250.3 Hz), 138.3, 130.9, 128.0, 127.5, 119.9 – 119.7 (m); ^{19}F NMR (376 MHz, $CDCl_3$) δ –144.3 (s, 4F). IR (ATR) 2922, 1420, 984, 846; m.p. 214-215 ˚C; HRMS (EI) *m/z* calcd. $C_{22}H_{18}F_4$: $[M]^+$ 358.1339; found: $[M]^+$ 358.1335.

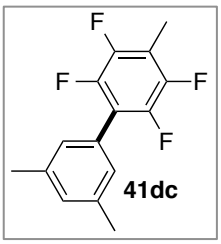

2,3,5,6-tetrafluoro-3',4,5'-trimethylbiphenyl (**41dc**)

The General Procedure 1 was applied with 1-bromo-3,5-dimethylbenzene (67.9 μL, 0.50 mmol) and 2,3,5,6-tetrafluorotoluene (182.7 μL, 1.50 mmol). Column chromatography (hexane 100%) afforded the title product

as a colourless oil (106.0 mg, 79%).

Spectroscopic data matched those previously reported.[167]

^{1}H NMR (400 MHz, $CDCl_3$): δ 7.07 - 7.05 (m, 3H), 2.37 - 2.31 (m, 9H); ^{13}C NMR (126 MHz, $CDCl_3$): δ 145.4 (dm, *J* = 243.7 Hz), 143.8 (dm, *J* = 245.2 Hz), 138.2, 130.7, 128.0, 127.6, 118.4 (t, *J* = 17.0 Hz), 114.9 (t, *J* = 19.2 Hz), 21.4, 7.60; ^{19}F NMR (376 MHz, $CDCl_3$) δ –144.4 (dd, *J* = 22.6, 12.6 Hz, 2F), –145.4 (dd, *J* = 22.3, 12.8 Hz, 2F). IR (ATR) 2923, 1482, 922, 851; HRMS (EI) *m/z* calcd. $C_{15}H_{12}F_4$: $[M]^+$ 268.0870; found: $[M]^+$ 268.0867.

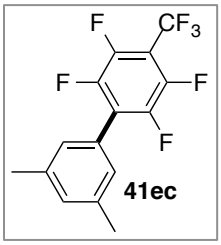

2,3,5,6-tetrafluoro-3',5'-dimethyl-4-(trifluoromethyl)biphenyl (**41ec**)

The General Procedure 1 was applied with 1-bromo-3,5-dimethylbenzene (67.9 μL, 0.50 mmol) and 2,3,5,6-tetrafluorobenzotrifluoride (204.3 μL, 1.50 mmol). Column chromatography (hexane 100%) afforded the title product as a white solid (106.3 mg, 58%).

^{1}H NMR (400 MHz, $CDCl_3$): δ 7.14 (s, 1H), 7.06 (s, 2H), 2.39 (s, 6H); ^{13}C NMR (126 MHz, $CDCl_3$): δ 145.6 - 143.2 (m, 2C), 138.7, 131.8, 127.7, 126.0, 125.5 (t, *J* = 16.8 Hz), 121.1 (q, *J* = 274.3 Hz), 108.8 -107.9 (m), 21.4; ^{19}F NMR (376 MHz, $CDCl_3$) δ –56.2 (t, *J* =21.2 Hz, 3F), –140.9 - –141.1 (m, 2F), –141.2 - –141.3 (m, 2F). IR (ATR) 2927, 1527, 1495, 1484, 1139, 990; m.p. 68-71 ºC; HRMS (EI) *m/z* calcd. $C_{15}H_9F_7$: $[M]^+$ 322.0587; found: $[M]^+$ 322.0582.

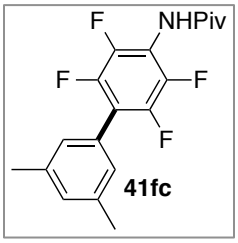

N-(2,3,5,6-tetrafluoro-3',5'-dimethyl-biphenyl-4-yl)pivalamide (**41fc**)

The General Procedure 1 was applied with 1-bromo-3,5-dimethylbenzene (67.9 μL, 0.50 mmol) and *N*-(2,3,5,6-tetrafluorophenyl)pivalamide (373.8 mg, 1.50 mmol) and pivalonitrile (332.6 μL, 3.00 mmol). Column chromatography with a 0-30% CH_2Cl_2-hexane gradient afforded the title product as a white solid (125.5 mg, 71%).

^{1}H NMR (400 MHz, $CDCl_3$): δ 7.26 (s, 1H) 7.08 (s, 1H), 7.03 (s, 2H), 2.37 (s, 6H), 1.36 (s, 9H); ^{13}C NMR (126 MHz, $CDCl_3$): δ 177.2, 144.0 (dm, *J* = 245.4 Hz), 142.7 (app dt, *J* =

249.0 15.8, 3.9 Hz), 138.3, 131.0, 127.9, 126.9, 119.1 (t, *J* = 17.3 Hz), 115.3 (tt, *J* = 14.7, 2.4 Hz), 39.7, 27.6, 21.4; ^{19}F NMR (376 MHz, $CDCl_3$) δ –144.1 (dd, *J* = 22.3, 9.8 Hz, 2F), –146.6 - –146.7 (m, 2F); IR (ATR) 3294, 2972, 1674, 1479, 1190, 988; m.p. 184 - 188 ºC; HRMS (EI) *m/z* calcd. $C_{16}H_{15}NF_4$: $[M]^+$ 353.1403; found: $[M+K]^+$ 392.1034.

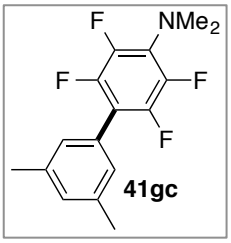

2,3,5,6-tetrafluoro-*N*,*N*,3',5'-tetramethyl-biphenyl-4-amine (**41gc**)

The General Procedure 1 was applied with 1-bromo-3,5-dimethylbenzene (67.9 μL, 0.50 mmol) and 2,3,5,6-tetrafluoro-*N*,*N*-dimethylaniline (289.7 mg, 1.50 mmol). Column chromatography with a 0-20% CH_2Cl_2-hexane gradient afforded the title product as a white solid (98.1 mg, 66%).

^{1}H NMR (400 MHz, $CDCl_3$): δ 7.06 (app s, 3H), 3.00 (s, 6H), 2.38 (s, 6H); ^{13}C NMR (126 MHz, $CDCl_3$): δ 144.6 (dm, *J* = 244.5 Hz), 142.6 (dm, *J* = 244.5 Hz), 138.2, 130.4 - 130.1 (m, 2C), 128.0, 127.7, 113.2 (t, *J* = 17.7 Hz), 43.5 (t, *J* = 3.8 Hz), 21.4; ^{19}F NMR (376 MHz, $CDCl_3$) δ –146.0 (dd, *J* = 21.2, 9.0 Hz, 2F), –151.9 - –152.0 (m, 2F); IR (ATR) 2923, 1650, 1488, 1450, 1437, 1077, 982; m.p. 83-84 ºC; HRMS (EI) *m/z* calcd. $C_{16}H_{15}NF_4$: $[M]^+$ 297.1135; found: $[M]^+$ 297.1126.

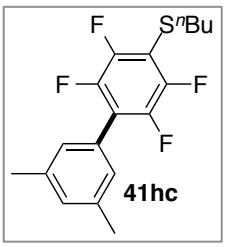

butyl(2,3,5,6-tetrafluoro-3',5'-dimethyl-[1,1'-biphenyl]-4-yl)sulfane (**41hc**)

The General Procedure 1 was applied with 1-bromo-3,5-dimethylbenzene (67.9 μL, 0.50 mmol) and butyl(2,3,5,6-tetrafluorophenyl)sulfane (357.4 mg, 1.50 mmol). Column chromatography (hexane 100%) afforded the title product as a colourless oil (111.3 mg, 65%).

^{1}H NMR (400 MHz, $CDCl_3$): δ 7.11 (s, 1H), 7.09 (s, 2H), 2.98 (t, *J* = 7.4 Hz, 2H), 2.40 (s, 6H), 1.61 (app quintet, *J* = 7.4 Hz, 2H), 1.48 (app sextet, *J* = 7.4 Hz, 2H), 0.95 (t, *J* = 7.3 Hz, 3H); ^{13}C NMR (126 MHz, $CDCl_3$): δ 147.4 (app ddt, *J* = 244.6, 14.8, 4.0 Hz), 142.4 (app ddt, *J* = 247.9, 15.5, 5.0 Hz), 138.3, 131.0, 127.9, 127.1, 120.9 (t, *J* = 17.2 Hz), 113.2 (t, *J* = 20.6 Hz), 34.6 (t, *J* = 2.5 Hz), 32.0, 21.7, 21.4, 13.7; ^{19}F NMR (376 MHz, $CDCl_3$) δ –134.7

(dd, *J* = 24.3, 11.9 Hz, 2F), –143.3 (dd, *J* = 24.0, 11.6 Hz, 2F); IR (ATR) 2960, 2929, 1604 1470, 974, 853, 725; HRMS (EI) *m/z* calcd. $C_{18}H_{18}F_4S_1$: $[M]^+$ 342.1060 found: $[M]^+$ 342.1075.

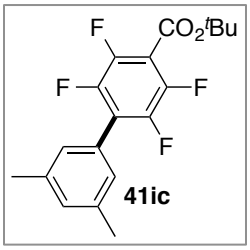

tert-butyl 2,3,5,6-tetrafluoro-3',5'-dimethyl-biphenyl-4-carboxylate (**41ic**)

The General Procedure 1 was applied with 1-bromo-3,5-dimethylbenzene (67.9 μL, 0.50 mmol) and *tert*-butyl 2,3,5,6-tetrafluorobenzoate (375.3 mg, 1.50 mmol) for 2 h. Column chromatography (hexane 100%) afforded the title product as a colourless oil (136.4 mg, 77%).

^{1}H NMR (400 MHz, $CDCl_3$): δ 7.11 (s, 1H), 7.05 (s, 2H), 2.38 (s, 6H), 1.62 (s, 9H); ^{13}C NMR (126 MHz, $CDCl_3$): δ 158.9, 144.6 (app ddt, *J* = 254.0, 15.9, 4.9 Hz), 143.9 (app ddt, 247.9, 14.0, 4.6 Hz), 138.5, 131.4, 127.8, 126.7, 123.3 (t, *J* = 16.9 Hz), 113.3 (t, *J* = 16.9 Hz), 84.7, 28.3, 21.4; ^{19}F NMR (376 MHz, $CDCl_3$) δ –141.4 - –141.5 (m, 2F), –142.6 - –142.8 (m, 2F); IR (ATR) 2982, 1732, 1478, 1328, 1288, 1142, 989; HRMS (EI) *m/z* calcd. $C_{19}H_{18}O_2F_4$: $[M]^+$ 354.1237; found: $[M]^+$ 354.1231.

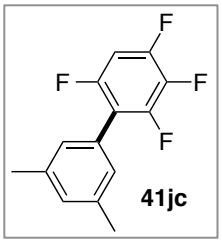

2,3,4,6-tetrafluoro-3',5'-dimethylbiphenyl (**41jc**)

The General Procedure 1 was applied with 1-bromo-3,5-dimethylbenzene (67.9 μL, 0.50 mmol) and 1,2,3,5-tetrafluorobenzene (161.6 μL, 1.50 mmol). Column chromatography (hexane 100%) afforded the title product as a colourless oil (94.0 mg, 74%).

^{1}H NMR (400 MHz, $CDCl_3$): δ 7.07 (s, 1H), 7.02 (s, 2H), 6.88 - 6.81 (m, 1H), 2.37 (s, 6H); ^{13}C NMR (126 MHz, $CDCl_3$): δ 154.4 (dm, *J* = 246.3 Hz), 149.8 (dm, *J* = 250.6 Hz), 149.1 (dm, *J* = 249.8 Hz), 138.3, 137.6 (dm, *J* = 248.0 Hz), 130.7, 128.0, 127.4, 116.7 - 116.4 (m), 100.9 (ddd, *J* = 29.2, 21.3, 3.9 Hz), 21.4; ^{19}F NMR (376 MHz, $CDCl_3$) δ –117.9 (app t, *J* = 10.0 Hz, 1F), –133.9 (ddd, *J* = 21.6, 9.8, 5.0, 1F), –135.2 (d, *J* = 20.0, 1F), –165.0 (app tdd, *J*

= 21.6, 11.0, 6.1 Hz, 1F); IR (ATR) 2921, 1515, 1049, 787; HRMS (EI) *m/z* calcd. $C_{14}H_{10}F_4$: $[M]^+$ 254.0713; found: $[M]^+$ 254.0720.

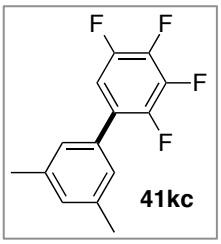

2,3,4,5-tetrafluoro-3',5'-dimethylbiphenyl (**41kc**)

The General Procedure 1 was applied with 1-bromo-3,5-dimethylbenzene (67.9 μL, 0.50 mmol) and 1,2,3,4-tetrafluorobenzene (160.8 μL, 5.00 mmol). Column chromatography (hexane 100%) afforded the title product as a white solid (99.2 mg, 80%).

^{1}H NMR (400 MHz, $CDCl_3$): δ 7.08 - 7.00 (m, 4H), 2.38 (s, 6H); ^{13}C NMR (126 MHz, $CDCl_3$): δ 147.1 (dm, *J* = 246.6 Hz), 145.0 (dm, *J* = 248.5 Hz), 141.3 (dm, *J* = 252.6 Hz), 139.7 (dm, *J* = 253.1 Hz), 138.6, 133.1, 130.5, 126.7 (d, *J* = 2.7 Hz), 126.0 - 125.8 (m), 111.5 (app dt, *J* = 19.6, 3.1 Hz), 21.4; ^{19}F NMR (376 MHz, $CDCl_3$) δ –139.8 - –140.0 (m, 1F), –143.5 - –143.6 (m, 1F), –155.4 (app t, *J* = 20.3 Hz, 1F), –157.5 - –157.6 (m, 1F); IR (ATR) 2926, 1526, 1487, 845; m.p. 86 - 87 ºC; HRMS (EI) *m/z* calcd. $C_{14}H_{10}F_4$: $[M]^+$ 254.0713; found: $[M]^+$ 254.0708.

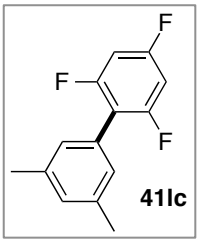

2,4,6-trifluoro-3',5'-dimethylbiphenyl (**41lc**)

The General Procedure 1 was applied with 1-bromo-3,5-dimethylbenzene (67.9 μL, 0.50 mmol) and 1,3,5-trifluorobenzene (517.1 μL, 5.00 mmol). Column chromatography (hexane 100%) afforded the title product as a colourless oil (56.7 mg, 48%).

^{1}H NMR (400 MHz, $CDCl_3$): δ 7.05 (s, 1H), 7.03 (s, 2H), 6.74 (dd, *J* = 8.6, 8.0 Hz, 2H), 2.37 (s, 6H); ^{13}C NMR (126 MHz, $CDCl_3$): δ 161.7 (dt, *J* = 248.7, 15.7 Hz), 160.4 (ddd, *J* = 249.1, 14.7, 9.9 Hz), 138.0, 130.2, 128.2, 128.1, 115.4 (td, *J* = 19.7, 4.8 Hz), 100.7 - 100.2 (m), 21.4; ^{19}F NMR (376 MHz, $CDCl_3$) δ –109.6 (tt, *J* =8.7, 5.9 Hz, 1F), –111.1 (app t, *J* = 6.6 Hz, 2F); IR (ATR) 2920, 1636, 1597, 1120, 1030, 1000, 839; HRMS (EI) *m/z* calcd. $C_{14}H_{11}F_3$: $[M]^+$ 236.0807; found: $[M]^+$ 226.0808.

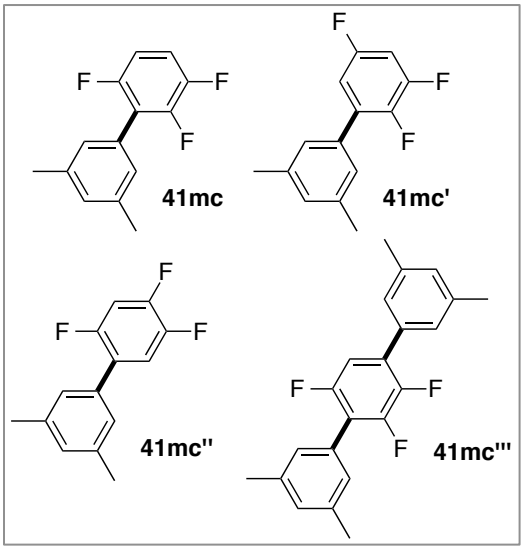

2,3,6-trifluoro-3',5'-dimethylbiphenyl (**41mc**), 2,3,5-trifluoro-3',5'-dimethylbiphenyl (**41mc'**), 2,4,5-trifluoro-3',5'-dimethylbiphenyl (**41mc''**), and 2',3',5'-trifluoro-3,3'',5,5''-tetramethylterphenyl (**41mc'''**)

The General Procedure 1 was applied with 1-bromo-3,5-dimethylbenzene (67.9 μL, 0.50 mmol) and 1,2,4-trifluorobenzene (522.5 μL, 5.00 mmol). Column chromatography (hexane, 100%) afforded a 1.00 : 0.95 : 0.13 mixture of 2,3,6-trifluoro-3',5'-dimethylbiphenyl, 2,3,5-trifluoro-3',5'-dimethylbiphenyl and 2,4,5-trifluoro-3',5'-dimethylbiphenyl respectively as a colourless oil (83.9. mg, 71%) , and 2',3',5'-trifluoro-3,3'',5,5''-tetramethylterphenyl as a white solid (6.1 mg, 5%). Milligrams (5 - 10 mg) of 2,3,6-trifluoro-3',5'-dimethylbiphenyl and a mixture of 2,3,5-trifluoro-3',5'-dimethylbiphenyl and 2,4,5-trifluoro-3',5'-dimethylbiphenyl were isolated as colourless oils by column chromatography (hexane, 100%) for analysis.

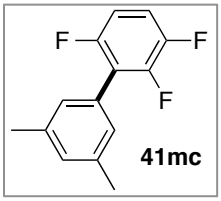

2,3,6-trifluoro-3',5'-dimethylbiphenyl (**41mc**)

^{1}H NMR (400 MHz, CD_2Cl_2): δ 7.18 - 7.10 (m, 2H), 7.06 (s, 2H), 6.94 (app tdd, *J* = 9.1, 3.9, 2.2 Hz, 1H), 2.37 (d, *J* = 0.8 Hz, 6H); ^{1}H {^{19}F} (500 MHz, CD_2Cl_2): δ 7.14 (d, *J* = 9.2 Hz, 1H), 7.10 (s, 1H), 7.06 (s, 2H), 6.94 (d, *J* = 9.1 Hz, 1H), 2.38 (s, 6H); ^{13}C NMR (126 MHz, CD_2Cl_2): δ 155.8 (ddd, *J* = 243.8, 5.0, 2.7 Hz), 148.2 (ddd, *J* = 248.4, 14.2, 7.5 Hz), 147.8 (ddd, *J* = 243.7, 13.8, 3.6 Hz), 138.5, 130.8, 128.4 (d, *J* = 2.1 Hz), 128.1 (t, *J* = 1.8 Hz), 120.9 (dd, *J* = 21.3, 15.7 Hz), 115.9 (ddd, J = 19.5, 9.9, 1.5 Hz), 111.2 (ddd, *J* = 25.7, 6.9, 4.1 Hz), 21.4; ^{19}F NMR (376 MHz, CD_2Cl_2) δ –120.1 - –120.2 (m, 1F), –138.6 (dd, *J* = 21.7, 8.6 Hz, 1F), –143.1 - –143.2 (m, 1F); ^{19}F {^{1}H} NMR (376 MHz, CD_2Cl_2) δ –120.2 (dd, *J* = 15.1, 3.6 Hz, 1F) –138.6 (dd, *J* = 21.7, 3.7 Hz, 1F), –143.2 (dd, *J* = 21.4, 15.1 Hz, 1F); IR (ATR) 2924, 1491, 1243, 786; HRMS (EI) *m/z* calcd. $C_{14}H_{11}F_3$: $[M]^+$ 236.0807; found: $[M]^+$ 236.0800.

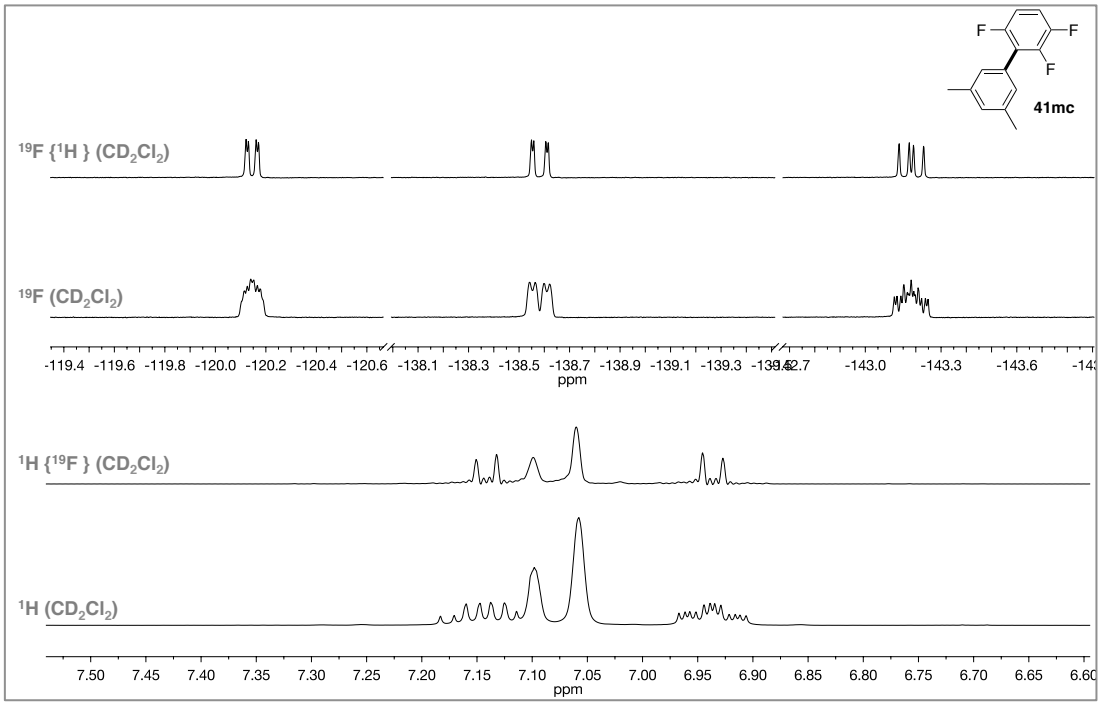

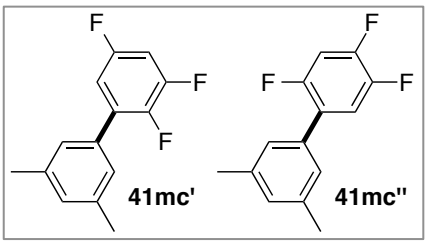

2,3,5-trifluoro-3',5'-dimethylbiphenyl (**3mb'**) and 2,4,5-trifluoro-3',5'-dimethylbiphenyl (**3mb''**)

^{1}H NMR (400 MHz, CD_2Cl_2): δ 7.26 (*minor*, ddd, *J* = 11.0, 8.9, 7.1 Hz, 1H) 7.14 (*major*, s, 2H), 7.10 (*minor*, s, 2H), 7.09 (*major*, s, 1H), 7.07 - 7.00 (*minor*, m, 1H) 7.05 (*minor*, s, 1H), 6.98 - 6.89 (*major*, m, 2H), 2.38 (*major*, d, *J* = 0.7 Hz, 6H), 2.37 (*minor*, d *J* = 0.7 Hz, 6H) ; ^{1}H {^{19}F} (500 MHz, CD_2Cl_2): δ 7.26 (*minor,* s, 1H), 7.14 (*major*, s, 2H), 7.10 (*minor*, s, 2H), 7.09 (*major*, s, 1H), 7.06 (*minor*, s, 1H), 7.03 (*minor*, s, 1H), 6.96 (*major*, d, *J* = 3.3 Hz, 1H), 6.93 (*major*, d, *J* = 3.3 Hz, 1H), 2.38 (*major*, s, 6H), 2.37 (*minor*, s, 6H) ; ^{13}C NMR (126 MHz, CD_2Cl_2): δ 158.0 (*major*, ddd, *J* = 244.2, 11.3, 3.3 Hz), 155.1 (*minor*, ddd, *J* = 246.1, 9.2, 2.4 Hz), 151.2 (*major*, ddd, *J* = 249.3, 15.5, 13.4 Hz), 149.6 (*minor*, ddd, *J* = 250.4, 14.5, 12.3 Hz), 147.2 (*minor*, ddd, *J* = 243.5, 12.4, 3.7 Hz), 145.0 (*major*, ddd, *J* = 244.3, 13.1, 4.1 Hz), 138.8 (*major*), 138.7 (*minor*), 134.2 (*minor*), 134.0 - 133.9 (*major* + *minor*, m), 132.6 (*major*, dd, *J*, = 12.3, 9.5 Hz), 130.7 (*major*), 130.2 (*minor*), 127.0 - 126.9 (*major* + *minor*, m), 118.6 (*minor*, dd, *J* = 19.7, 5.3 Hz), 112.1 (*major*, dm, *J* = 23.9 Hz), 106.3 (*minor*, dd, *J* = 29.2, 20.8 Hz), 104.3 (*major*, dd, *J* = 27.5, 21.4 Hz), 21.4 (*major* +

minor); ^{19}F NMR (376 MHz, CD_2Cl_2) δ –116.4 - –116.5 (*major*, m, 1F), –119.6 - –119.7 (*minor*, m, 1F), –134.3 (*major*, ddd, *J* = 20.0, 10.4, 2.9 Hz, 1F), –136.4 - –136.5 (*minor*, m, 1F), –143.8 - –144.0 (*minor*, m, 1F), –148.9 - –149.1 (*major*, m, 1F); ^{19}F {^{1}H} NMR (376 MHz, CD_2Cl_2) δ –116.4 (*major*, dd, *J* = 14.9, 3.3 Hz, 1F), –119.7 (*minor,* dd, *J* = 15.1, 3.8 Hz, 1F), –134.3 (*major*, dd, *J* = 20.7, 3.3 Hz, 1F), –136.5 (*minor*, dd, *J* = 21.7, 3.8 Hz, 1F), –143.9 (*minor*, dd, *J* = 21.7 15.1 Hz, 1F), –149.0 (*major*, dd, *J* = 20.7, 14.6, Hz, 1F); IR (ATR) 2924, 1600, 1496, 1113, 850, 786; HRMS (EI) *m/z* calcd. $C_{14}H_{11}F_3$: $[M]^+$ 236.0807; found: $[M]^+$ 236.0799.

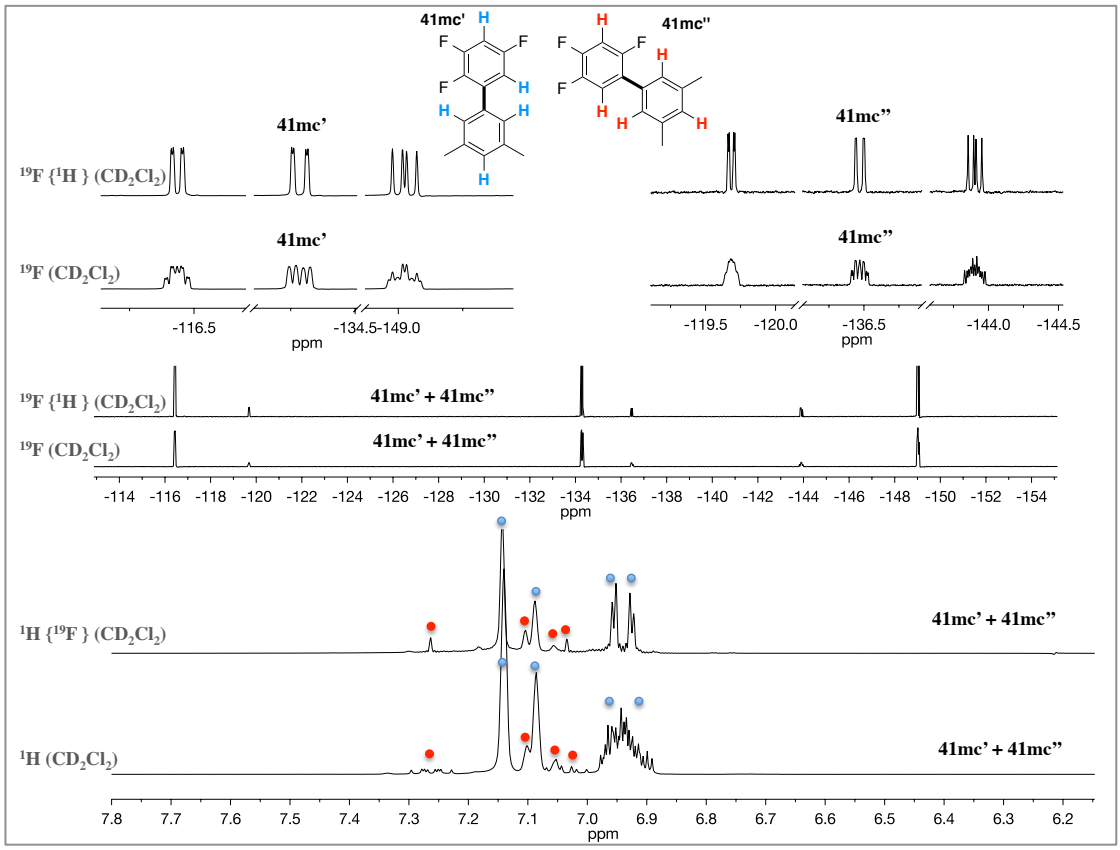

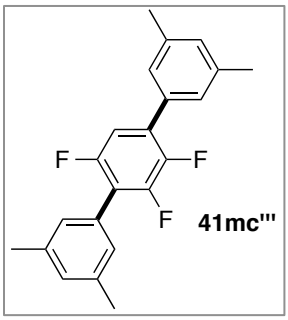

2',3',5'-trifluoro-3,3",5,5"-tetramethylterphenyl (**41mc'''**)

^{1}H NMR (400 MHz, CD_2Cl_2): δ 7.19 (app s, 2H), 7.11 - 7.08 (m, 4H), 7.05 (ddd, *J* = 10.3, 5.9, 2.2 Hz, 1H), 2.39 (s, 12H); ^{1}H {^{19}F} (500 MHz, CD_2Cl_2): δ 7.19 (s, 2H), 7.11 - 7.09 (s, 4H), 7.05 (s, 1H), 2.39 (s, 12H); ^{13}C NMR (101 MHz, CD_2Cl_2): δ 155.3 (ddd, *J* = 244.1,

6.9, 3.6 Hz), 148.8 (ddd, *J* = 248.5, 16.2, 9.1 Hz), 145.4 (ddd, *J* = 246.4, 15.2, 3.7 Hz), 138.8, 138.5, 133.9, 130.7, 130.6, 130.3 (dd, *J* = 12.0, 2.2 Hz), 128.4, 128.1, 126.9 (d, *J* = 2.9 Hz), 119.2 (dd, *J* = 21.3, 16.1 Hz), 111. 7 (dt, *J* = 25.8, 3.4), 21.4, 21.4; ^{19}F NMR (376 MHz, CD_2Cl_2) δ –120.9 - –120.9 (m, 1F), 138.6 (d, *J* = 20.8 Hz, 1F), –148.1 (ddd, *J* =20.5, 14.5, 5.6 Hz, 1F);^{19}F {^{1}H} NMR (471 MHz, CD_2Cl_2) δ –120.9 (dd, *J* = 14.8, 3.5 Hz), –138.6, (dd, *J* = 21.0, 4.0 Hz), –148.1 (dd, *J* = 21.2, 14.7 Hz); IR (ATR) 2972, 1501, 1218, 1133, 835; m.p. 200 - 203 ºC; HRMS (EI) *m/z* calcd. $C_{22}H_{19}F_3$: $[M]^+$ 340.1439; found: $[M]^+$ 340.1445.

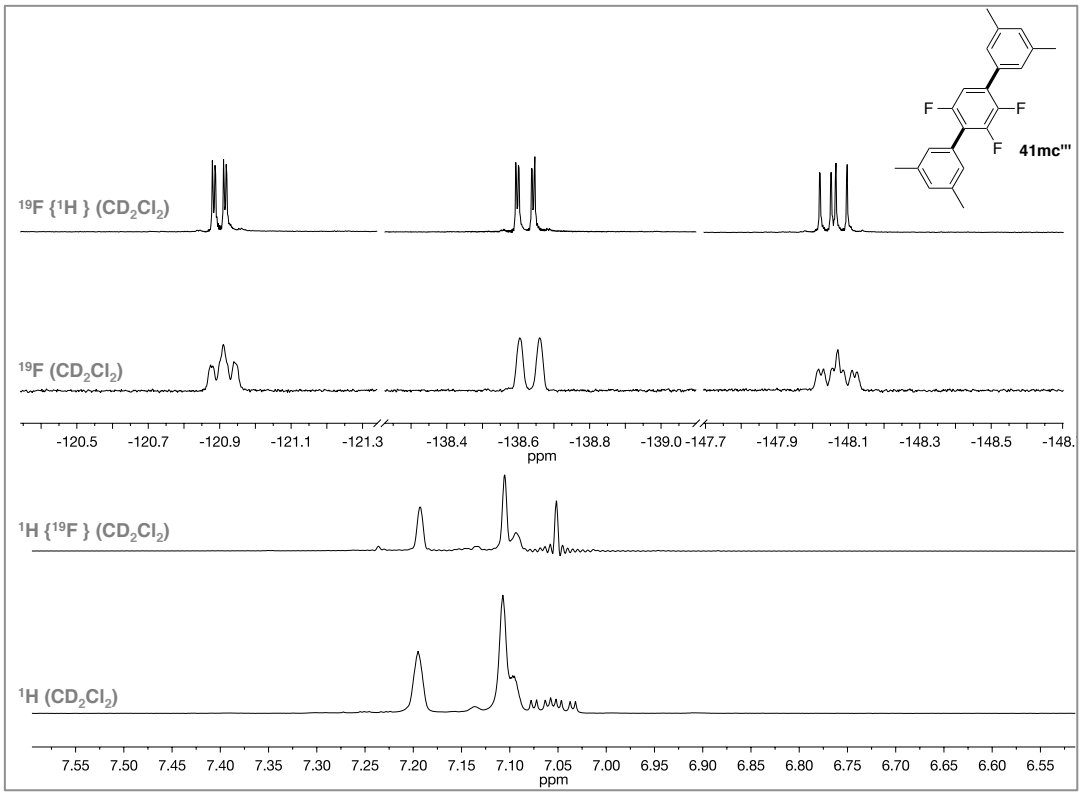

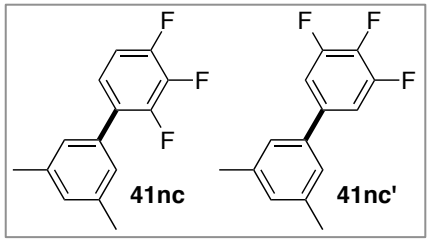

2,3,4-trifluoro-3',5'-dimethylbiphenyl (**41nc**) and 3,4,5-trifluoro-3',5'-dimethylbiphenyl (**41nc'**)

The General Procedure 1 was applied with 1-bromo-3,5-dimethylbenzene (67.9 μL, 0.50 mmol) and 1,2,3-trifluorobenzene (515.9 μL, 5.00 mmol). Column chromatography (hexane, 100%) afforded

a 1.0:0.3 mixture of 2,3,4-trifluoro-3',5'-dimethylbiphenyl and 3,4,5-trifluoro-3',5'-dimethylbiphenyl as a colourless oil (34.2 mg, 29%). Milligrams (5 - 10 mg) of each regioisomer were isolated by column chromatography (hexane, 100%): **41nc** as a colourless oil and **41nc'** as a white solid.

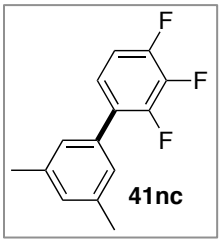

2,3,4-trifluoro-3',5'-dimethylbiphenyl (**41nc**)

^{1}H NMR (500 MHz, $CDCl_3$): δ 7.15 - 7.10 (m, 3H), 7.05 (s, 1H), 7.00 (app dtd, *J* = 9.2, 7.1, 2.0 Hz, 1H), 2.38 (s, 6H); ^{1}H {^{19}F} NMR (500 MHz, $CDCl_3$): δ 7.12 (d, *J* = 8.8 Hz, 1H), 7.10 (s, 2H), 7.05 (s, 1H), 7.01 (d, *J* = 8.8 Hz, 1H), 2.38 (s, 6H) ^{13}C NMR (126 MHz, $CDCl_3$): δ 150.9 (ddd, *J* = 157.8, 10.1, 3.1 Hz), 148.4 (ddd *J* = 159.2, 10.3, 3.2 Hz), 140.4, (dt, *J* = 250.7, 15.6 Hz), 138.4, 134.1, 130.0, 127.1 (dd, *J* = 11.0, 3.9 Hz), 126.8 (d, *J* = 2.9 Hz), 124.0 (dt, *J* = 7.8, 4.0 Hz), 112.1 (dd, *J* = 17.1, 4.0 Hz), 21.5; ^{19}F NMR (471 MHz, $CDCl_3$) δ –135.7 - –136.4 (m, 1F), –138.6 (app dt, *J* = 20.2, 6.9 Hz, 1F), –160.3 (app td, *J* = 20.7, 7.5 Hz, 1F); ^{19}F {^{1}H} NMR (471 MHz, $CDCl_3$) δ –136.2 (dd, *J* = 20.2, 6.8 Hz, 1F), –138.6 (dd, *J* = 20.7, 6.9 Hz, 1F), –160.3, (app t, *J* = 20.6 Hz, 1F); IR (ATR) 2924, 1511, 1039, 807, 706; HRMS (EI) *m/z* calcd. $C_{14}H_{11}F_3$: $[M]^+$ 236.0807 found: $[M]^+$ 236.0801.

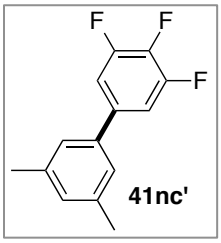

3,4,5-trifluoro-3',5'-dimethylbiphenyl (**41nc'**)

^{1}H NMR (500 MHz, CD_2Cl_2): δ 7.22 (app dd, *J* = 9.3, 6.5 Hz, 2H), 7.13 (s, 2H), 7.05 (s, 1H), 2.37 (s, 6H); ^{1}H {^{19}F} NMR (500 MHz, CD_2Cl_2): δ 7.22 (s, 2H), 7.13 (s, 2H), 7.04 (s, 1H), 2.36 (s, 6H) ^{13}C NMR (126 MHz, CD_2Cl_2): δ 151.7 (ddd, *J* = 248.1, 10.0, 4.3 Hz), 139.4 (dt, *J* = 249.8, 15.4 Hz), 139.2, 138.3 – 138.3 (m), 138.1 (td, *J* = 7.7 Hz), 130.4, 125.0, 111.3 (dd, *J* = 16.6, 4.9 Hz), 21.4; ^{19}F NMR (471 MHz, CD_2Cl_2) δ –135.5 - –135.6 (m, 2F), –164.3 (tt, *J* = 20.6, 6.2 Hz, 1F); ^{19}F {^{1}H} NMR (471 MHz, CD_2Cl_2) δ –135.5 (d, *J* = 19.9 Hz, 2F), –164.3 (t, *J* = 19.9 Hz, 1F); m.p. 35 - 37 °C; IR (ATR) 2930, 1487, 1039, 826, 751, 706; HRMS (EI) *m/z* calcd. $C_{14}H_{11}F_3$: $[M]^+$ 236.0807 found: $[M]^+$ 236.0799.

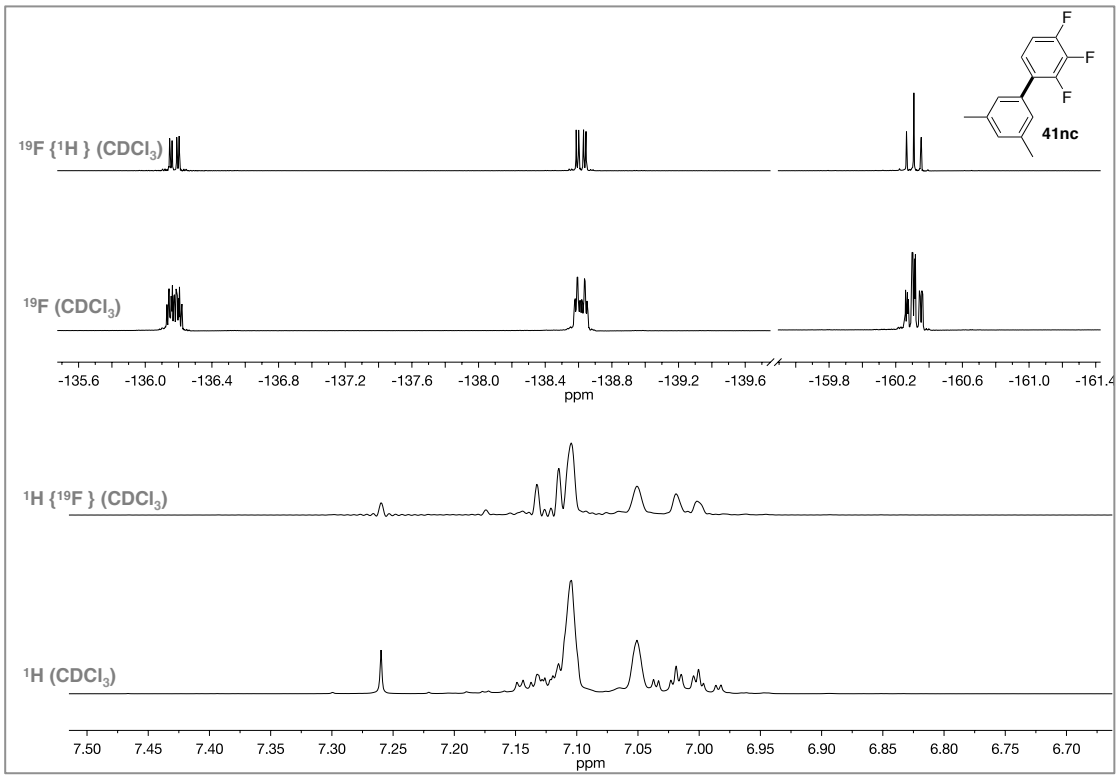
F
F
F
41nc
19F {1H } (CDCl3)
19F (CDCl3)
-135.6 -136.0 -136.4 -136.8 -137.2 -137.6 -138.0 -138.4 -138.8 -139.2 -139.6 -159.8 -160.2 -160.6 -161.0
ppm
1H {19F } (CDCl3)
1H (CDCl3)
7.50 7.45 7.40 7.35 7.30 7.25 7.20 7.15 7.10 7.05 7.00 6.95 6.90 6.85 6.80 6.75 6.70
ppm

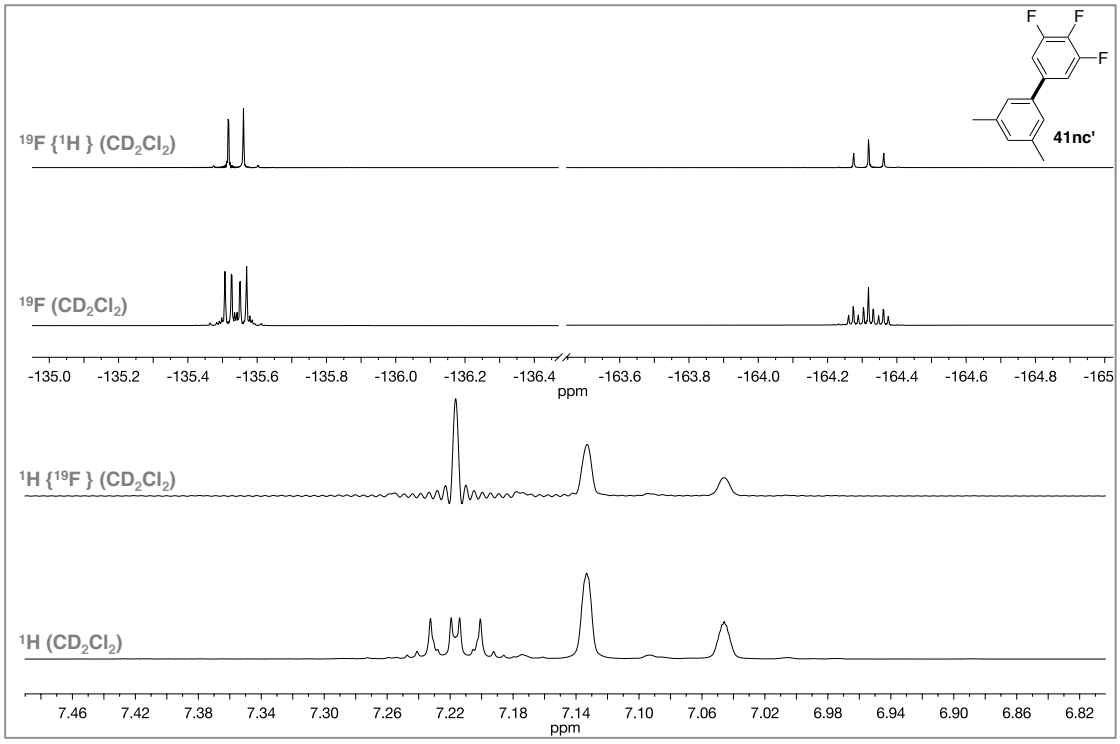
F
F
F
41nc'
19F {1H } (CD2Cl2)
19F (CD2Cl2)
-135.0 -135.2 -135.4 -135.6 -135.8 -136.0 -136.2 -136.4 -163.6 -163.8 -164.0 -164.2 -164.4 -164.6 -164.8
ppm
1H {19F } (CD2Cl2)
1H (CD2Cl2)
7.46 7.42 7.38 7.34 7.30 7.26 7.22 7.18 7.14 7.10 7.06 7.02 6.98 6.94 6.90 6.86 6.82
ppm

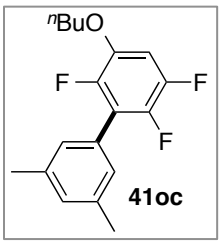

3-butoxy-2,5,6-trifluoro-3',5'-dimethyl-1,1'-biphenyl (**41oc**)

The General Procedure 1 was applied with 1-bromo-3,5-dimethylbenzene (67.9 μL, 0.50 mmol) and 1-butoxy-2,4,5-trifluorobenzene (510.5 mg, 2.50 mmol). Column chromatography (hexane 100%) afforded the title product as a colourless oil (63.2 mg, 41%).

^{1}H NMR (500 MHz, $CDCl_3$): δ 7.08 (app s, 3H), 6.81 (app dt, *J* = 11.5, 7.7 Hz, 1H), 4.02 (t, *J* = 6.5 Hz, 2H), 2.39 (s, 6H), 1.82 (app quintet, *J* = 7.0 Hz, 2H), 1.52 (app sextet, *J* = 7.5, 2H), 1.00 (t, *J* = 7.4, 3H); ^{1}H {^{19}F} NMR (500 MHz, $CDCl_3$): δ 7.08 (app s, 3H), 6.80 (s, 1H), 4.01 (t, *J* = 6.5 Hz, 2H), 2.38 (s, 6H), 1.81 (app quintet, *J* = 7.0 Hz, 2H), 1.52 (app sextet, *J* = 7.5, 2H), 1.00 (t, *J* = 7.4, 3H); ^{13}C NMR (126 MHz, $CDCl_3$): δ 146.5 (ddd, *J* = 243.6, 14.4, 4.0 Hz), 145.5 (app dt, *J* = 244.3, 3.8 Hz), 143.6 - 143.4 (m), 141.4 (ddd, *J* = 241.7, 14.1, 5.4 Hz), 138.0, 130.5, 128.4 (d, *J* = 1.8 Hz), 128.0, 120.9 (app t, *J* = 17.3 Hz), 102.4 (dd, *J* = 22.2, 2.1 Hz), 70.1, 31.3, 21.4, 19.2, 13.9; ^{19}F NMR (376 MHz, $CDCl_3$) δ –140.7, (dd *J* = 12.8, 7.7 Hz, 1F), –141.5 - –141.6 (m, 1F), –149.6 (dd, *J* = 23.0, 7.6 Hz, 1F); ^{19}F {^{1}H} NMR (471 MHz, $CDCl_3$) δ –140.6, (d, *J* = 13.0 Hz, 1F), –141.5 (dd, *J* = 22.9, 13.0 Hz, 1F), –149.6 (d, *J* = 22.9 Hz, 1F); IR (ATR) 2961, 1494, 1238, 1150, 929, 850; HRMS (EI) *m/z* calcd. $C_{18}H_{19}F_3O$: $[M]^+$ 308.1381 found: $[M]^+$ 308.1380.

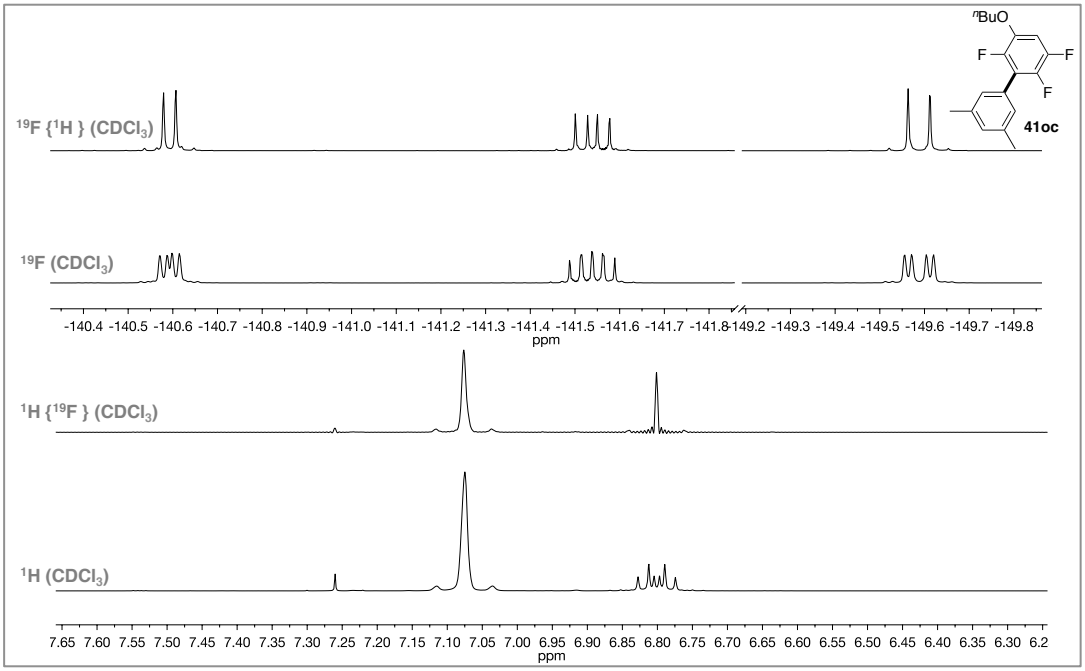

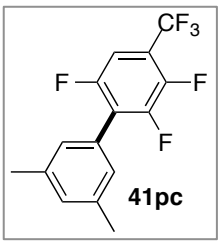

2,3,6-trifluoro-3',5'-dimethyl-4-(trifluoromethyl)-biphenyl (**41pc**)

The General Procedure 1 was applied with 1-bromo-3,5-dimethylbenzene (67.9 μL, 0.50 mmol) and 2,3,5-trifluorobenzotrifluoride (300.0 mg, 1.50 mmol). Column chromatography (hexane 100%) afforded the title product as a colourless oil (141.5 mg, 93%).

^{1}H NMR (400 MHz, $CDCl_3$): δ 7.23 (ddd, *J* = 8.7, 5.4, 2.3 Hz, 1H), 7.14 (s, 1H), 7.10 (s, 2H), 2.42 (s, 6H); ^{1}H {^{19}F} NMR (400 MHz, $CDCl_3$): δ 7.24 (s, 1H), 7.15 (s, 1H), 7.10 (s, 2H), 2.42 (s, 6H); ^{13}C NMR (100 MHz, $CDCl_3$): δ 154.7 (ddd, *J* = 247.4, 5.2, 3.3 Hz), 148.7 (ddd, *J* = 252.1, 13.2, 7.3 Hz), 145.4 (dm, *J* = 256.4 Hz), 138.5, 131.3, 127.8, 126.9, 124.8 (dd, *J* = 20.5, 15.6 Hz), 121.7 (app qt, *J* = 272.6, 2.8 Hz), 119.2 - 117.9 (m), 108.9 (app dquintet = 28.7, 4.4 Hz), 21.4; ^{19}F NMR (376 MHz, $CDCl_3$) δ –61.3 (d, *J* = 12.7 Hz, 3F), –116.7 - –116.8 (m, 1F), –134.3 (dd, *J* = 20.9, 2.3 Hz, 1F), –143.0 - –143.2 (m, 1F); ^{19}F {^{1}H} NMR (471 MHz, $CDCl_3$) δ –61.3 (d, *J* = 13.1 Hz, 3F), –116.7 (dd, *J* = 15.4, 4.9 Hz, 1F), –134.3 (dd, *J* = 20.9, 4.5 Hz, 1F), –143.1 - –143.2 (m, 1F) IR (ATR) 2924, 1365, 1177, 1142, 752; HRMS (EI) *m/z* calcd. $C_{15}H_{10}F_6$ $[M]^+$ 304.0681 found: $[M]^+$ 304.0681.

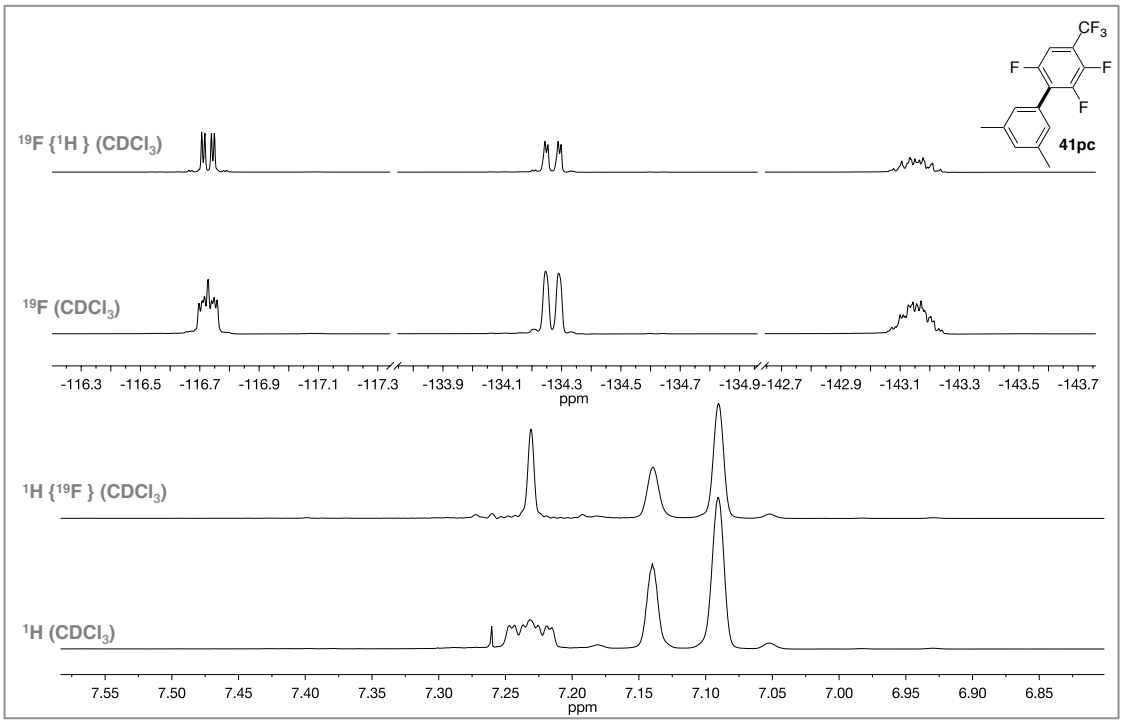

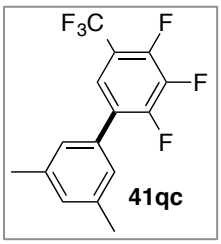

2,3,4-trifluoro-3',5'-dimethyl-5-(trifluoromethyl)-biphenyl (**41qc**)

The General Procedure 1 was applied with 1-bromo-3,5-dimethylbenzene (67.9 μL, 0.50 mmol) and 2,3,4-trifluorobenzotrifluoride (500.0 mg, 2.50 mmol). Column chromatography (hexane 100%) afforded the title product as a white solid (88.2 mg, 58%).

^{1}H NMR (400 MHz, $CDCl_3$): δ 7.44 (app t, *J* = 7.3 Hz, 1H), 7.09 (app s, 3H), 2.39 (s, 6H); ^{1}H {^{19}F} NMR (500 MHz, $CDCl_3$): δ 7.44 (s, 1H), 7.09 (app s, 3H), 2.39 (s, 6H); ^{13}C NMR (126 MHz, $CDCl_3$): δ 151.0 (dm, *J* = 256.1 Hz), 148.2 (dm, *J* = 260.4 Hz), 140.8 (ddd, *J* = 253.9, 16.1, 14.4 Hz), 138.7, 132.7, 130.8, 127.3 (dd, *J* = 11.8, 4.2 Hz), 126.7 (d, *J* = 2.4), 122.0 (q, *J* = 272.9 Hz), 121.8 - 121.7 (m), 115.7 (ddd, *J* = 34.3, 9.3, 4.3 Hz), 21.5; ^{19}F NMR (376 MHz, $CDCl_3$) δ –60.7 (d, *J* = 12.6 Hz, 3F), –130.9 - –131.0 (m, 1F), –136.4 - –136.6 (m, 1F), –156.5 (app t, *J* = 20.3 Hz, 1F); ^{19}F {^{1}H} NMR (471 MHz, $CDCl_3$) δ –60.7 (d, *J* = 12.6 Hz, 3F), –131.0 (dd, *J* = 20.6, 11.0 Hz, 1F) –136.4 - –136.6 (m, 1F), –156.6 (app t, *J* = 20.5 Hz, 1F); IR (ATR) 2924, 1488, 1371, 1211, 1136, 851, 646; m.p. 35 - 38 ºC; HRMS (EI) *m/z* calcd. $C_{15}H_{10}F_6$ [M]$^{+}$ 304.0687; found: [M]$^{+}$ 304.0700.

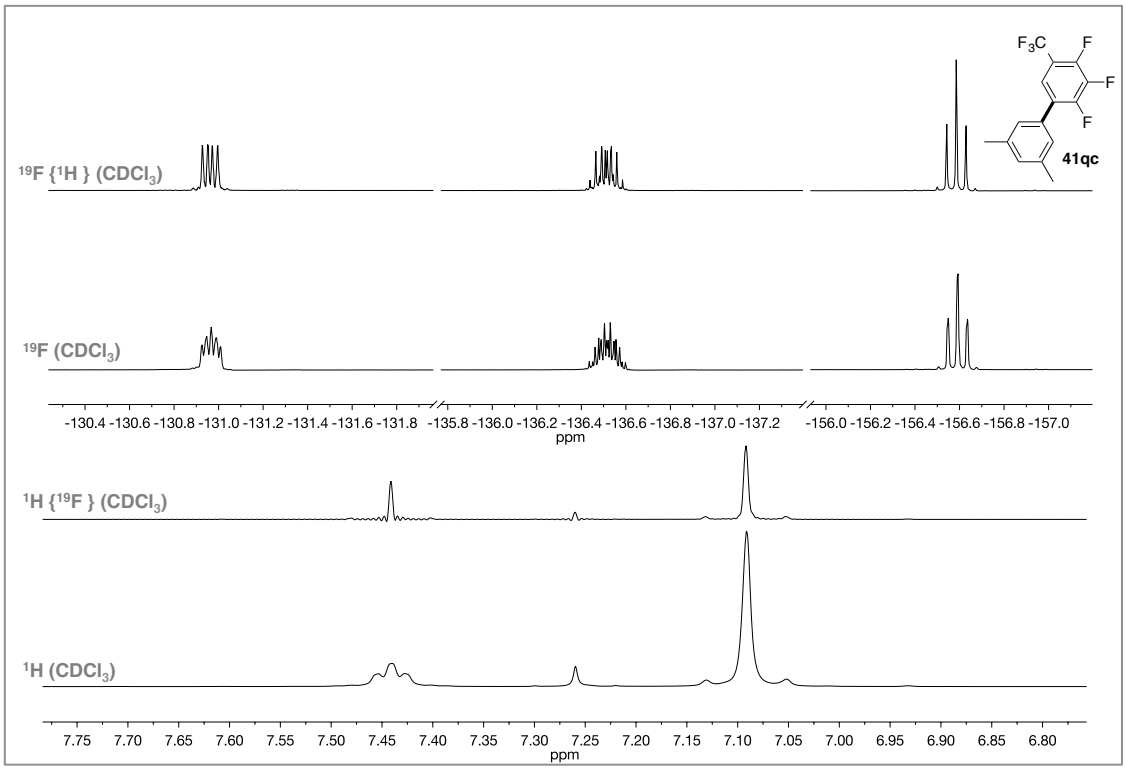

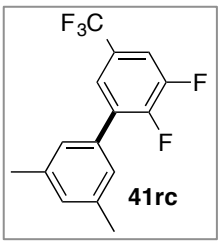

2,3-difluoro-3',5'-dimethyl-6-(trifluoromethyl)-biphenyl (**41rc**)

The General Procedure 1 was applied with 1-bromo-3,5-dimethylbenzene (67.9 μL, 0.50 mmol) and 3,4-difluorobenzotrifluoride (455.2 mg, 2.50 mmol). Column chromatography (hexane 100%) afforded the title product as a colourless oil (78.7 mg, 55%).

^{1}H NMR (500 MHz, $CDCl_3$): δ 7.50 (app d, *J* = 5.6 Hz, 1H), 7.44 - 7.40 (m, 1H), 7.16 (s, 2H), 7.10 (s, 1H), 2.41 (s, 6H); ^{1}H {^{19}F} (500 MHz, $CDCl_3$): δ 7.48 (d, *J* = 2.4 Hz, 1H), 7.48 (d, *J* = 2.4 Hz, 1H), 7.14 (s, 2H), 7.09 (s, 1H), 2.39 (s, 6H); ^{13}C NMR (126 MHz, $CDCl_3$): δ 151.0 (dd, *J* = 251.0, 14.3 Hz) 150.0 (dd, *J* = 255.7, 12.9 Hz), 138.6, 133.3, 132.7 (d, *J* = 11.6 Hz), 130.7, 127.3 - 126.4 (m, 2C), 123.2 (qd *J* = 272.2, 2.4 Hz), 123.0 - 122.9 (m), 113.5 (dq, *J* = 20.2, 3.3 Hz), 21.5; ^{19}F NMR (376 MHz, $CDCl_3$) δ –62.2 (s, 3F), –134.7 (dd, *J* = 20.7, 9.6 Hz, 1F), –136.9 - –137.0 (dm, *J* = 20.7 Hz, 1F); ^{19}F {^{1}H} NMR (471 MHz, $CDCl_3$) δ –62.3 (s, 3F), –134.7 (d, *J* = 20.7 Hz, 1F), –137.0 (d, *J* = 20.7 Hz, 1F); IR (ATR) 2923, 1371, 1294, 1129, 652; HRMS (EI) *m/z* calcd. $C_{15}H_{11}F_5$: $[M]^+$ 286.0775; found: $[M]^+$ 286.0774.

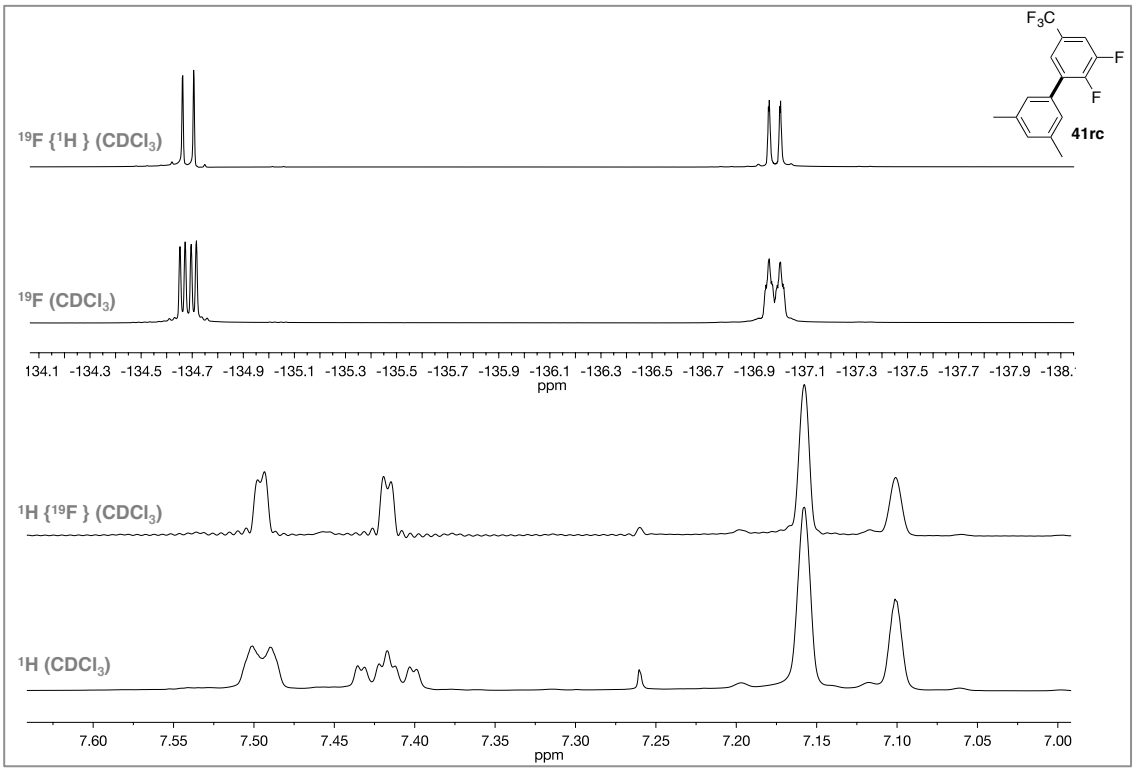

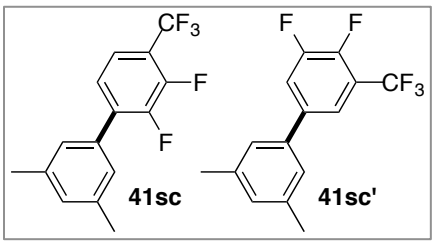

2,3-difluoro-3',5'-dimethyl-4-(trifluoromethyl)- biphenyl (**41sb**) and 3,4-difluoro-3',5'-dimethyl-5-(trifluoromethyl)-biphenyl (**41sb'**)

The General Procedure 1 was applied with 1-bromo-3,5-dimethylbenzene (67.9 μL, 0.50 mmol) and 2,3-difluorobenzotrifluoride (455.2 mg, 2.50 mmol). Column chromatography (hexane 100%) afforded a 1.00 : 0.03 mixture of 2,3-difluoro-3',5'-dimethyl-4-(trifluoromethyl)-biphenyl and 3,4-difluoro-3',5'-dimethyl-5-(trifluoromethyl)-biphenyl as a colourless oil (82.1 mg, 54%).

^{1}H NMR (400 MHz, $CDCl_3$): δ (minor isomer not observed) 7.44 - 7.39 (m, 1H), 7.32 - 7.27 (m, 1H), 7.17 (s, 2H) 7.12 (s, 1H), 2.41 (s, 6H); ^{1}H {^{19}F} NMR (500 MHz, $CDCl_3$): δ (minor isomer not observed) 7.40 (d, *J* = 8.3 Hz, 1H), 7.28 (d, 8.3 Hz, 1H), 7.15 (s, 2H) 7.09 (s, 1H), 2.39 (s, 6H); ^{13}C NMR (100 MHz, $CDCl_3$): δ (minor isomer not observed) 148.9 (dm, *J* = 258.7 Hz), 148.4 (dd, *J* = 251.5, 12.0 Hz), 138.6, 135.7 (d, *J* = 10.7 Hz), 133.4, 130.8, 126.8 (d, *J* = 2.8 Hz), 125.1 (dd, *J* = 3.8, 2.6 Hz), 122.3 (qd, *J* = 272.3, 3.2 Hz), 121.2 (app quintet *J* = 4.5 Hz), 118.7 (qd, *J* = 33.6, 9.7 Hz), 21.4; ^{19}F NMR (376 MHz, $CDCl_3$) δ –61.0 (*major*, d, *J* = 12.5 Hz, 3F), –61.0 (*minor*, d, *J* = 12.7 Hz, 3F), –135.3 (*minor*, dd, *J* = 20.8, 10.7, 1F), –138.8 - –139.0 (*major*, m, 1F), –140.8 (*major*, dd, *J* = 20.1, 6.2 Hz, 1F) –142.0 - –142.2 (*minor*, m, 1F); ^{19}F {^{1}H} NMR (376 MHz, $CDCl_3$) δ –61.0 (*major* d, *J* = 12.7 Hz, 3F), –61.0 (*minor*, d, *J* = 12.7 Hz, 3F), –135.3 (*minor*, d, *J* = 20.7 Hz, 1F), –138.8 (*major*, dq, *J* = 20.0, 12.3 Hz, 1F), –140.8 (*major*, d, *J* = 20.5, 1F), –142.1 (*minor*, dq, *J* = 20.7, 12.8 Hz, 1F); IR (ATR) 2923, 1477, 1328, 1137, 1118, 823; HRMS (EI) *m/z* calcd. $C_{15}H_{11}F_5$ $[M]^+$ 286.0775 found: $[M]^+$ 286.0774.

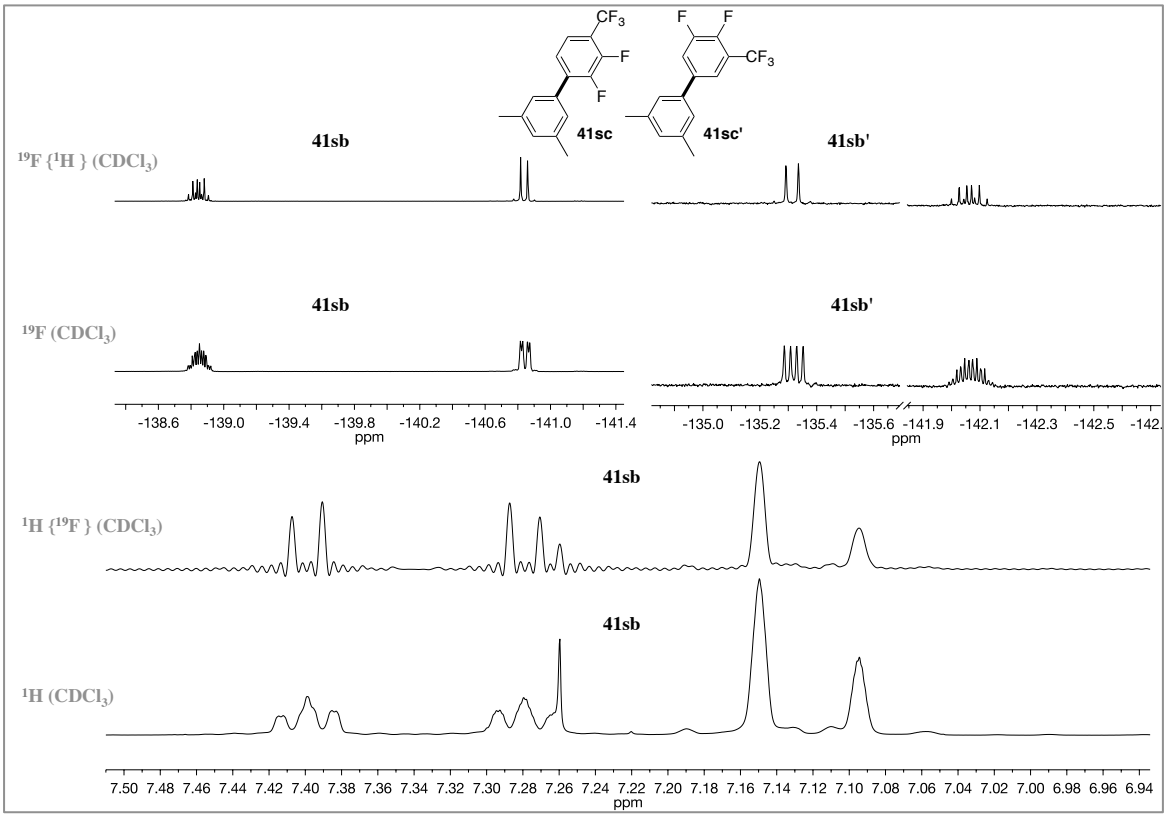

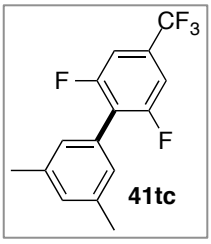

2,6-difluoro-3',5'-dimethyl-4-(trifluoromethyl)-biphenyl (**41tc**)

The general procedure was applied with 1-bromo-3,5-dimethylbenzene (67.9 μL, 0.50 mmol) and 3,5-difluorobenzotrifluoride (455.2 mg, 2.50 mmol). Column chromatography (hexane 100%) afforded the title product as a colourless oil (78.7 mg, 55%).

^{1}H NMR (400 MHz, $CDCl_3$): δ 7.28 (d, *J* = 6.7 Hz, 2H), 7.11 (s, 1H), 7.09 (s, 2H), 2.40 (s, 6H); ^{13}C NMR (126 MHz, $CDCl_3$): δ 160.1 (dd, *J* = 250.9, 7.5 Hz), 138.2, 131.2 (qt, *J* = 34.5 10.1 Hz), 130.9, 127.9, 127.6, 123.0 (qt, *J* = 272.3, 3.2 Hz), 122.7 (t, *J* = 18.9 Hz), 109.6 – 109.2 (m), 21.4; ^{19}F NMR (376 MHz, $CDCl_3$) δ – 63.0 (s, 3F), -110.5 (d, *J* = 6.4 Hz, 2F); IR (ATR) 2921, 1477, 1069, 918, 660; HRMS (EI) *m/z* calcd. $C_{15}H_{11}F_5$ $[M]^+$ 286.0775 found: $[M]^+$ 286.0764.

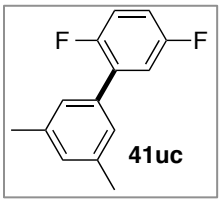

2,5-difluoro-3',5'-dimethyl-biphenyl (**41uc**)

The General Procedure 1 was applied with 1-bromo-3,5-dimethylbenzene (67.9 μL, 0.50 mmol) and 1,4-difluorobenzene (513.9 μL, 5.00 mmol). Column chromatography (hexane 100%) afforded the title product as a colourless oil (19.6 mg, 18%).

^{1}H NMR (400 MHz, $CDCl_3$): δ 7.15 - 7.05 (m, 5H) 7.00 - 6.95 (m, 1H), 2.39 (s, 6H); ^{13}C NMR (126 MHz, $CDCl_3$): δ 158.8 (dd, *J* = 242.0, 2.2 Hz) 155.9 (dd, *J* = 243.3, 2.4 Hz) 138.3, 134.8, 130.8 (dd, *J* = 16.0, 7.8 Hz), 130.0, 126.8, (d, *J* = 2.9 Hz), 117.3 – 117.0 (m, 2C), 115.0 (dd, *J* = 24.0, 8.6 Hz), 21.5; ^{19}F NMR (376 MHz, $CDCl_3$) δ –119.3 - –119.4 (m, 1F), –123.8 - –123.9 (m, 1F); IR (ATR) 2922, 1499. 1172, 851, 756; HRMS (EI) *m/z* calcd. $C_{14}H_{12}F_2$: $[M]^+$ 218.0902; found: $[M]^+$ 218.0900.

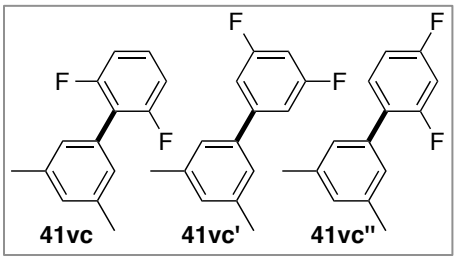

2,6-difluoro-3',5'-dimethyl-1,1'-biphenyl (**41vc**), 3,5-difluoro-3',5'-dimethylbiphenyl (**41vc'**) and 2,4-difluoro-3',5'-dimethyl-1,1'-biphenyl (**41vc''**)

The General Procedure 1 was applied with 1-bromo-3,5-dimethylbenzene (67.9 μL, 0.50 mmol) and 1,3-difluorobenzene (490.5 μL, 5.0 mmol). Column chromatography (hexane, 100%) afforded a 1.00 : 0.63 : 0.06 mixture of 2,6-difluoro-3',5'-dimethyl-1,1'-biphenyl, 3,5-difluoro-3',5'-dimethylbiphenyl and 2,4-difluoro-3',5'-dimethyl-1,1'-biphenyl respectively as a colourless oil (13.1 mg, 12%). Milligrams (<3 mg) of 2,6-difluoro-3',5'-dimethyl-1,1'-biphenyl, 3,5-difluoro-3',5'-dimethylbiphenyl and 2,4-difluoro-3',5'-dimethyl-1,1'-biphenyl were isolated for analysis by column chromatography (hexane 100%).

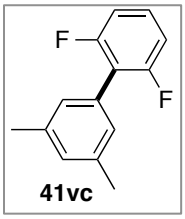

2,6-difluoro-3',5'-dimethyl-1,1'-biphenyl (**41vc**)

^{1}H NMR (500 MHz, (CD_2Cl_2): δ 7.30 (tt, *J* = 8.4, 6.3 Hz, 1H), 7.07 (s, 1H), 7.06 (s, 2H), 7.02 - 6.96 (m, 2H), 2.37 (s, 6H); ^{1}H {^{19}F} NMR (500 MHz, (CD_2Cl_2): δ 7.30 (t, *J* = 8.4, 6.3 Hz, 1H), 7.07 (s, 1H), 7.06 (s, 2H), 6.99 (d, *J* = 8.4, 2H), 2.37 (s, 6H); ^{13}C NMR (126 MHz, CD_2Cl_2): δ 160.5 (dd, *J* = 247.1, 7.3 Hz),

138.3, 130.3, 129.2 (d, *J* = 10.0 Hz), 129.1, 128.3, 119.1 (t, *J* = 19.3 Hz), 112.9 - 110.9 (m), 21.4; ^{19}F NMR (471 MHz, CD_2Cl_2) δ –115.0 (t, *J* = 6.8 Hz, 2F); ^{19}F {^{1}H} NMR (471 MHz, CD_2Cl_2) δ –115.0 (s, 2F); IR (ATR) 2921, 1468, 1230, 1013, 784; HRMS (EI) *m/z* calcd. $C_{14}H_{12}F_2$: $[M]^+$ 218.0902 found: $[M]^+$ 218.0907.

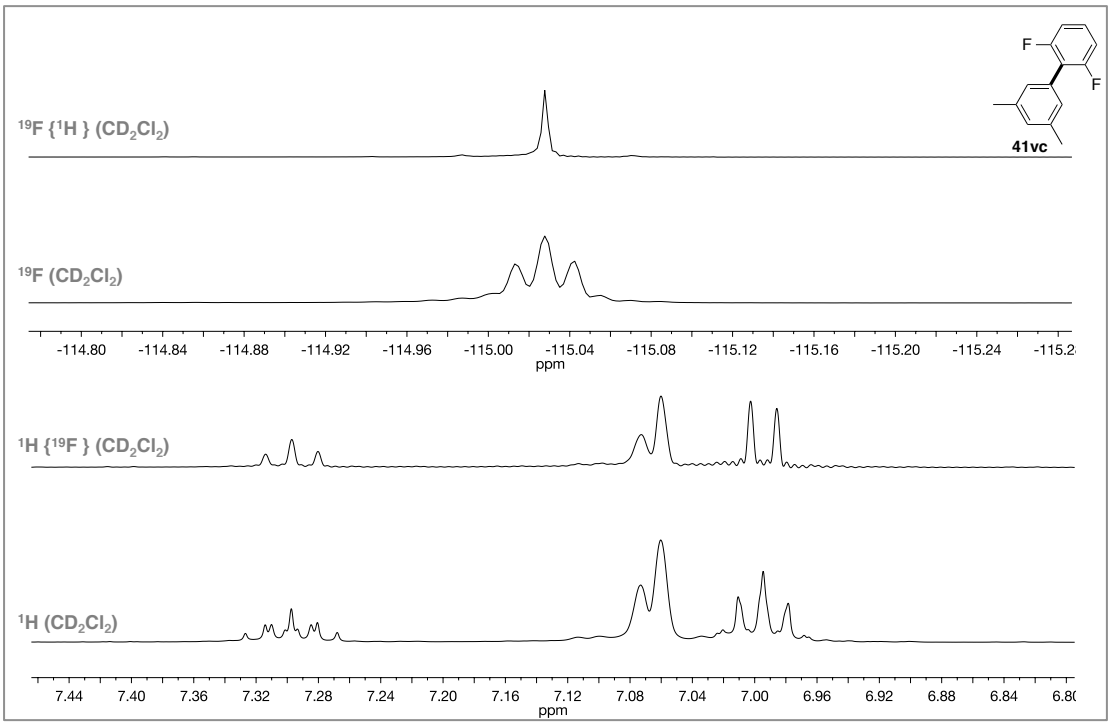

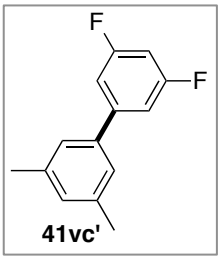

3,5-difluoro-3',5'-dimethylbiphenyl (**41vc'**)

^{1}H NMR (500 MHz, CD_2Cl_2): δ 7.18 (s, 2H), 7.15 - 7.11 (m, 2H), 7.05 (s, 1H), 6.70 (tt, *J* = 9.0, 2.3 Hz, 1H), 2.37 (s, 6H); ^{1}H {^{19}F} NMR (500 MHz, CD_2Cl_2): δ 7.18 (s, 2H), 7.13 (d, *J* = 2.3 Hz, 2H), 7.05 (s, 1H), 6.79 (t, *J* = 2.3 Hz, 1H), 2.37 (s, 6H); ^{13}C NMR (126 MHz, CD_2Cl_2): δ 163.6 (dd, *J* = 247.0, 13.2 Hz), 145.3 (t, *J* = 9.5 Hz), 139.1, 139.0 (t, *J* = 2.5 Hz), 130.5, 125.1, 110.6 - 109.7 (m), 102.5 (t, *J* = 25.6 Hz), 21.5; ^{19}F NMR (471 MHz, CD_2Cl_2) δ –110.8 (app t, *J* =8.6 Hz, 2F). ^{19}F {^{1}H} NMR (471 MHz, CD_2Cl_2) δ –110.8 (s, 2F). IR (ATR) 3025, 1599, 1589, 1117, 987, 843; HRMS (EI) *m/z* calcd. $C_{14}H_{12}F_2$: $[M]^+$ 218.0902 found: $[M]^+$ 218.0901.

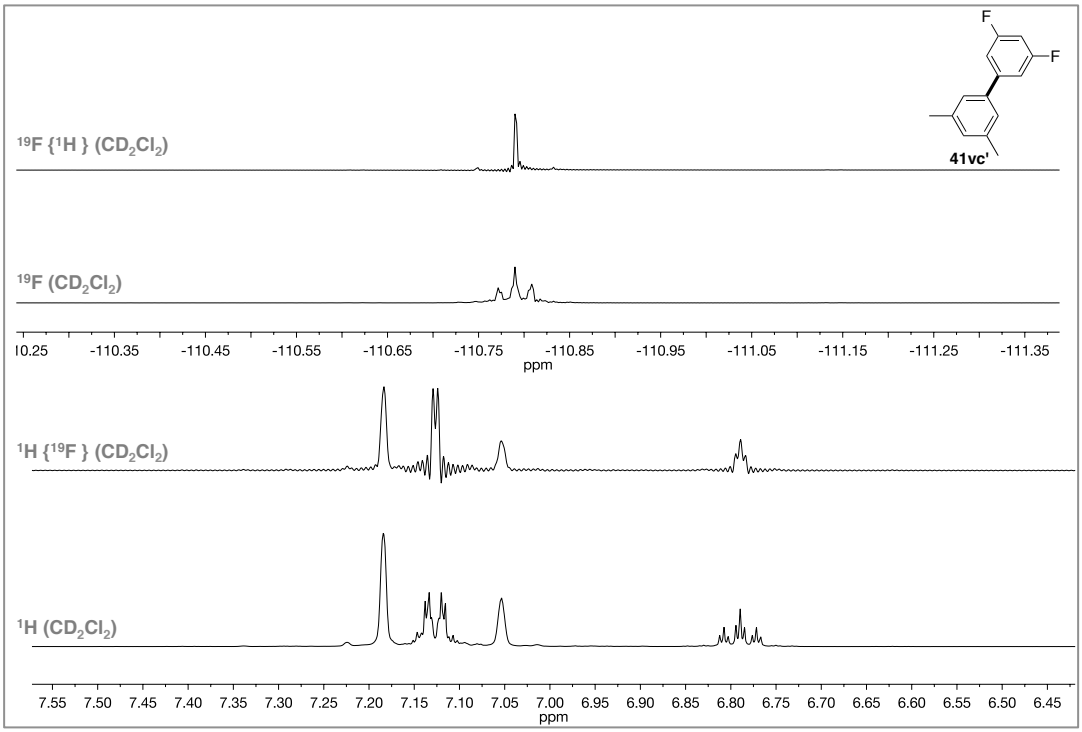

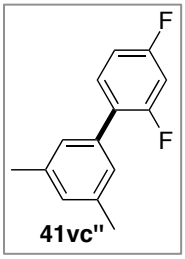

2,4-difluoro-3',5'-dimethyl-1,1'-biphenyl (**41vc''**)

^{1}H NMR (500 MHz, CD_2Cl_2): δ 7.40 (td, *J* = 8.7, 6.5 Hz, 1H), 7.10 (s, 2H), 7.03 (s, 1H), 6.98 - 6.89 (m, 2H), 2.36 (s, 6H); ^{1}H {^{19}F} NMR (500 MHz, CD_2Cl_2): δ 7.40 (d, *J* = 8.5 Hz, 1H), 7.10 (s, 2H), 7.03 (s, 1H), 6.96 (dd, *J* = 8.5, 2.9 Hz, 1H), 6.92 (d, *J* = 2.9 Hz, 1H), 2.36 (s, 6H) ^{13}C NMR (126 MHz, CD_2Cl_2): δ 162.5 (dd, *J* = 247.8, 11.9 Hz), 160.1 (dd, *J* = 249.4, 11.9 Hz), 138.5, 135.1, 132.0 (dd, *J* = 9.5, 5.1 Hz), 129.7, 127.0 (d, *J* = 2.6 Hz), 126.0 (dd, *J* = 13.9, 3.9 Hz), 111.8 (dd, *J* = 21.0, 3.9 Hz), 104.5 (dd, *J* = 27.0, 25.3, Hz), 21.4; ^{19}F NMR (471 MHz, CD_2Cl_2) δ –112.7 - –112.8 (m, 1F), –114.0 - –114.1 (m, 1F); ^{19}F {^{1}H} NMR (471 MHz, CD_2Cl_2) δ –112.8 (d, *J* = 7.4 Hz, 1F), –114.1 (d, *J* = 7.4 Hz, 1F);. IR (ATR) 2960, 1613, 1149, 990, 813; HRMS (EI) *m/z* calcd. $C_{14}H_{12}F_2$: $[M]^+$ 218.0902 found: $[M]^+$ 218.0908.

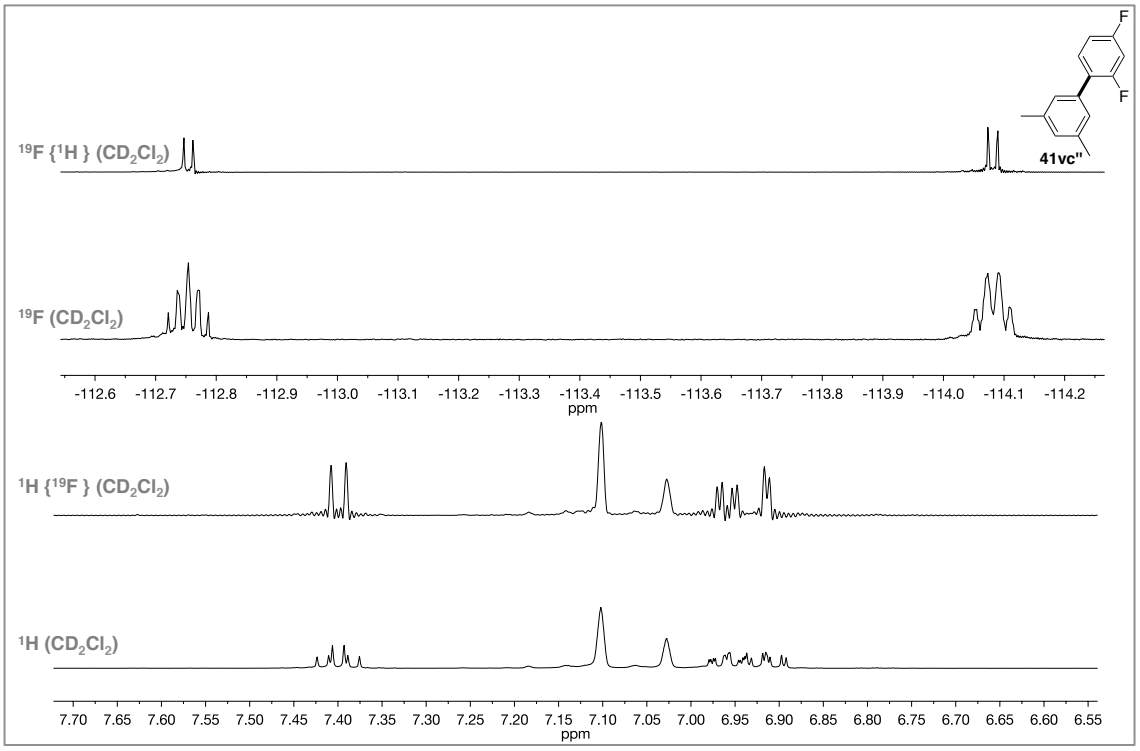

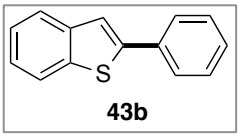

2-phenylbenzo*[b]*thiophene (**43b**)

The General Procedure 1 was applied with bromobenzene (52.7 μL, 0.50 mmol) and benzo[*b*]thiophene (201.3 mg, 1.50 mmol). Column chromatography (hexane 100%) afforded the title product as a white solid (29.4 mg, 28%).

Spectroscopic data matched those previously reported.[173]

^{1}H NMR (400 MHz, $CDCl_3$): δ 7.84 (d, *J* = 7.8 Hz, 1H), 7.78 (d, *J* = 7.6 Hz, 1H), 7.73 (d, *J* = 7.8 Hz, 2H), 7.55 (s, 1H), 7.43 (t, *J* = 7.6 Hz, 2H), 7.37 - 7.30 (m, 3H); ^{13}C NMR (126 MHz, $CDCl_3$): δ 144.4, 140.8, 139.6, 134.4, 129.1, 128.4, 126.6, 124.6, 124.5, 123.7, 122.4, 119.6.

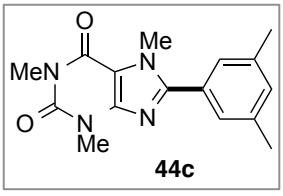

8-(3,5-dimethylphenyl) - 1,3,7-trimethyl-3,7-dihydro-1H-purine-2,6-dione (**44c**)

The General Procedure 1 was applied with 1-bromo-3,5-

dimethylbenzene (67.9 μL, 0.50 mmol), caffeine (291.3 mg, 1.50 mmol) and pivalonitrile (554.3 μL, 5.00 mmol). Column chromatography (hexane/CH_2Cl_2 100:0 – 40:60) afforded the title product as a white solid (88.6. mg, 59%).

Spectroscopic data matched those previously reported.[174]

^{1}H NMR (400 MHz, $CDCl_3$): δ 7.27 (s, 2H), 7.15 (s, 1H), 4.03 (s, 3H), 3.63 (s, 3H), 3.43 (s, 3H), 2.40 (s, 6H); ^{13}C NMR (126 MHz, $CDCl_3$): δ 155.7, 152.7, 151.9, 148.4, 138.8, 132.2, 128.3, 127.0, 108.6, 34.0, 29.9, 28.1, 21.5.

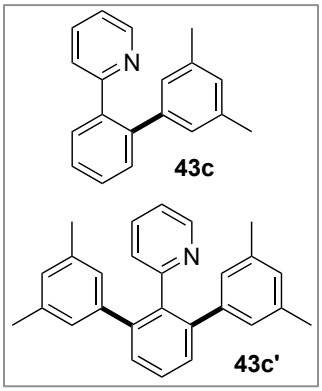

2-(3',5'-dimethyl-[biphenyl]-2-yl)pyridine (**43c**) and 2-(3,3",5,5"-tetramethyl-[1,1':3',1"-terphenyl]-2'-yl)pyridine (**43c'**)

The General Procedure 1 was applied with 1-bromo-3,5-dimethylbenzene (67.9 μL, 0.50 mmol) and 2-phenylpyridine (71.5 μL, 0.5 mmol). Column chromatography (hexane/CH_2Cl_2/AcOH 80:17:3) afforded 2-(3',5'-dimethyl-[biphenyl]-2-yl)pyridine as a clear oil (41.4 mg, 32% and 2-(3,3",5,5"-tetramethyl-[1,1':3',1"-terphenyl]-2'-yl)pyridine as a white solid (54.5. mg, 30%).

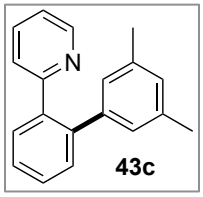

2-(3',5'-dimethyl-[biphenyl]-2-yl)pyridine (**43c**)

^{1}H NMR (400 MHz, $CDCl_3$): δ 8.64 (ddd, *J* = 4.9, 1.7, 0.9 Hz, 1H), 7.71 - 7.67 (m, 1H), 7.46 - 7.37 (m, 4H), 7.10 (ddd, *J* = 7.5, 4.9, 1.1 Hz, 1H), 6.91 (dt, *J* = 7.9, 1.0 Hz, 1H), 6.86 (s, 1H), 6.77 (s, 2H), 2.20 (s, 6H); ^{13}C NMR (126 MHz, $CDCl_3$): δ 159.5, 149.4, 141.3, 140.9, 139.5, 137.5, 135.2, 130.5, 130.5, 128.5, 128.4, 127.7, 127.5, 125.5, 121.3, 21.3; IR (ATR) 2918, 1584, 1461, 746; HRMS (EI) *m/z* calcd. $C_{19}H_{17}N$: $[M]^+$ 259.1356; found: $[M]^+$ 259.1350.

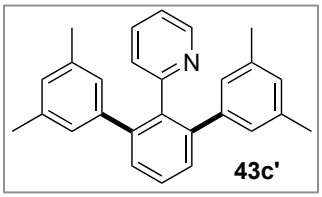

2-(3,3",5,5"-tetramethyl-[1,1':3',1"-terphenyl]-2'-yl) pyridine (**43c'**)

^{1}H NMR (400 MHz, $CDCl_3$): δ 8.34 (ddd, *J* = 4.9, 1.7, 1.0 Hz, 1H), 7.50 - 7.41 (m, 3H), 7.33 (td, *J* = 7.7, 1.8 Hz, 1H), 6.93 - 6.88 (m, 2H), 6.77 (s, 2H), 6.72 (s, 4H), 2.15 (s, 12H); ^{13}C NMR (126 MHz, $CDCl_3$): δ 159.5,

148.3, 142.0, 141.6, 138.6, 137.0, 134.8, 129.3, 128.1, 127.9, 127.7, 126.9, 120.8, 21.3; IR (ATR) 2916, 1587, 1454, 808, 707; m.p. 130 - 132 °C; HRMS (EI) *m/z* calcd. $C_{27}H_{25}N$: $[M]^+$ 363.1982; found: $[M]^+$ 363.1964.

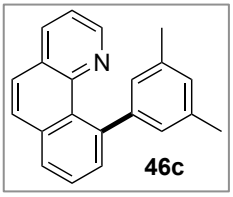

10-(3,5-Dimethylphenyl)benzo*[h]*quinolone (**45c**)

The General Procedure 1 was applied with 1-bromo-3,5-dimethylbenzene (67.9 μL, 0.50 mmol) and benzo[h]quinoline (89.6 mg, 0.50 mmol). Column chromatography (Et_2O 100%) afforded the title product as a viscous yellow oil (137.4 mg, 97%).

Spectroscopic data matched those previously reported.[175]

^{1}H NMR (400 MHz, $CDCl_3$): δ 8.47 (dd, *J* = 4.2, 1.9 Hz, 1H), 8.09 (dd, *J* = 8.0, 1.8 Hz, 1H), 7.90 (dd, *J* = 7.9, 1.2 Hz, 1H), 7.85 (d, *J* = 8.8 Hz, 1H), 7.70 - 7.65 (m, 2H), 7.56 (dd, *J* = 7.3, 1.4 Hz, 1H), 7.33 (dd, *J* = 8.0, 4.3 Hz, 1H), 7.00 (app s, 3H), 2.36 (s, 6H); ^{13}C NMR (126 MHz, $CDCl_3$): δ 147.0, 147.0, 146.3, 142.1, 136.7, 135.3, 135.2, 131.7, 129.2, 128.5, 127.9, 127.5, 127.3, 127.1, 126.7, 126.0, 121.2, 21.6.

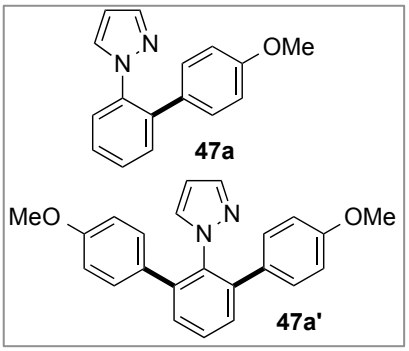

1-(4'-methoxy-[biphenyl]-2-yl)-1H-pyrazole (**47a**) and 1-(4,4''-dimethoxy-[terphenyl]-2'-yl)-1H-pyrazole (**47a'**)

The General Procedure 1 was applied with 4-bromoanisole (62.6 μL, 0.50 mmol) and 1-phenylpyrazole (66.1 μL, 0.5 mmol). Column chromatography (hexane/AcOH 90:10 – 40:60) afforded 1-(4'-methoxy-[biphenyl]-2-yl)-1H-pyrazole as a clear oil (38.8 mg, 31%) and 2-(4,4''-dimethoxy-[terphenyl]-2'-yl)-1H-pyrazole as a white solid (60.6 mg, 34%).

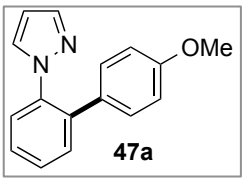

1-(4'-methoxy-[biphenyl]-2-yl)-1H-pyrazole (**47a**)

Spectroscopic data matched those previously reported.[150]

^{1}H NMR (500 MHz, $CDCl_3$): δ 7.54 (s, 1H), 7.49 - 7.48 (m, 1H), 7.35 - 7.33 (m, 3H), 7.00 (s, 1H), 6.92 (d, *J* = 7.9 Hz, 2H), 6.71 (d, J = 7.9 Hz, 2H), 6.10 (s, 1H),

3.68 (s, 3H); ^{13}C NMR (126 MHz, $CDCl_3$): δ 159.1, 140.2, 138.6, 136.5, 131.4, 131.0, 130.9, 129.7, 128.3, 128.0, 126.7, 114.0, 106.4, 55.2.

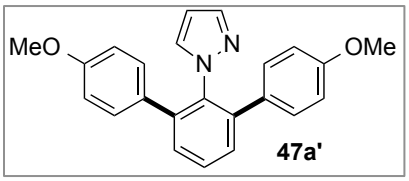

1-(4,4''-dimethoxy-[terphenyl]-2'-yl)-1H-pyrazole (**46a'**)

Spectroscopic data matched those previously reported.[176]

^{1}H NMR (500 MHz, $CDCl_3$): δ 7.47 (t, *J* = 7.6 Hz, 1H), 7.40 (s, 1H), 7.38 (d, *J* = 4.4 Hz, 2H), 7.05 (s, 1H), 6.98 (d, J = 7.5 Hz, 4H), 6.72 (d, J = 7.5 Hz, 4H), 6.04 (app d, *J* = 1.5 Hz, 1H), 3.73 (s, 6H); ^{13}C NMR (126 MHz, $CDCl_3$): δ 158.9, 140.2, 139.5, 136.4, 132.5, 131.3, 129.8, 129.5, 129.2, 113.0, 106.2, 55.2.

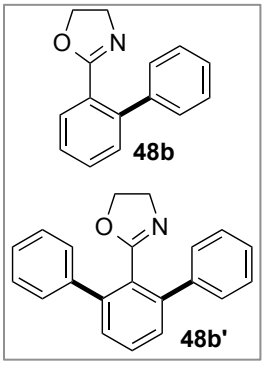

2-([1,1'-biphenyl]-2-yl)-4,5-dihydrooxazole (**48b**) and 2-([1,1':3',1''-terphenyl]-2'-yl)-4,5-dihydrooxazole (**48b'**)

The General Procedure 1 was applied with bromobenzene (52.5 μL, 0.50 mmol) and 2-phenyl-2-oxazoline (65.8 μL, 0.5 mmol). 10% yield of 2-([1,1'-biphenyl]-2-yl)-4,5-dihydrooxazole evaluated by ^{1}H-NMR. Column chromatography (hexane/AcOH 90:20 – 35:65) afforded 2-([1,1':3',1''-terphenyl]-2'-yl)-4,5-dihydrooxazole as a white solid (54.9 mg, 36%).

Spectroscopic data matched those previously reported.[147]

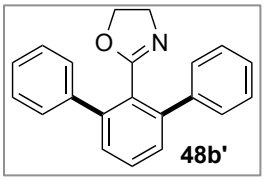

2-([1,1':3',1''-terphenyl]-2'-yl)-4,5-dihydrooxazole (**48b'**)

^{1}H NMR (500 MHz, $CDCl_3$): δ 7.53 (t, *J* = 7.6 Hz, 1H), 7.48 (d, *J* = 7.7 Hz, 4H), 7.40 (app t, *J* = 7.8 Hz, 6H), 7.35 (app t, *J* = 7.2 Hz, 2H), 3.90 (t, *J* = 9.4 Hz, 2H), 3.60 (t, *J* = 9.4 Hz, 2H); ^{13}C NMR (126 MHz, $CDCl_3$): δ 164.1, 142.4, 141.0, 129.7, 128.9, 128.7, 128.1, 127.6, 127.3, 67.4, 55.2.

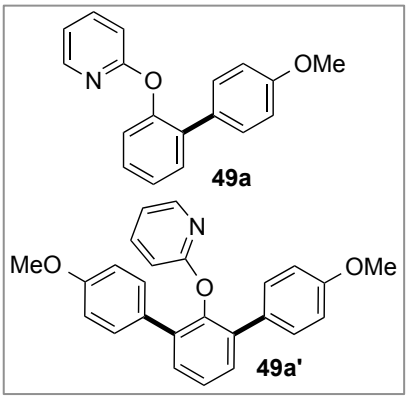

2-((4'-methoxy-[biphenyl]-2-yl)oxy)pyridine (**49a**) and 2-((4,4''-dimethoxy-[terphenyl]-2'-yl)oxy)pyridine (**49a'**)

The General Procedure 1 was applied with 4-bromoanisole (62.6 μL, 0.50 mmol) and 2-phenoxypyridine (85.6 mg, 0.5 mmol). Column chromatography (hexane/AcOH 90:10 – 40:60) afforded 2-((4'-methoxy-[biphenyl]-2-yl)oxy)pyridine (59.6 mg, 43%) and 2-((4,4''-dimethoxy-[terphenyl]-2'-yl)oxy)pyridine (40.3 mg, 21%) both as white solids.

Spectroscopic data matched those previously reported.[177]

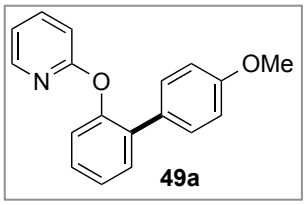

2-((4'-methoxy-[biphenyl]-2-yl)oxy)pyridine (**49a**)

^{1}H NMR (500 MHz, $CDCl_3$): δ 8.14 (d *J* = 4.6 Hz, 1H), 7.56 (t, *J* = 7.7 Hz, 1H), 7.45 (t, *J* = 9.1 Hz, 3H), 7.36, (t, *J* = 7.5 Hz, 1H), 7.29, (t, *J* 7.4 Hz, 1H), 7.17 (d, *J* = 8.0 Hz, 1H), 6.90 - 6.85 (m, 3H), 6.76 (d, *J* = 8.2 Hz, 1H), 3.78 (s, 3H); ^{13}C NMR (126 MHz, $CDCl_3$): δ 163.9, 158.9, 151.0, 147.8,139.2, 134.5, 131.2, 130.3 (2C), 128.3, 125.5, 122.8, 118.1, 113.6, 111.3, 55.3.

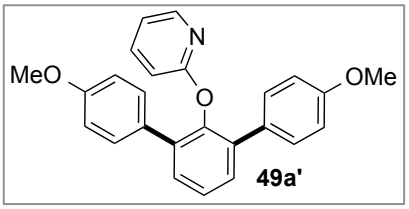

2-((4,4''-dimethoxy-[terphenyl]-2'-yl)oxy)pyridine (**49a'**)

^{1}H NMR (500 MHz, $CDCl_3$): δ 7.92 (d *J* = 3.9 Hz, 1H), 7.42 - 7.32 (m, 8H), 6.81 (d, *J* = 8.0 Hz, 4H), 6.66 (t, *J* = 5.8 Hz, 1H), 6.49 (d, *J* = 8.0 Hz, 1H), 3.76 (s, 6H); ^{13}C NMR (126 MHz, $CDCl_3$): δ 163.4, 158.8, 147.9, 147.3, 138.7, 135.9, 130.8, 130.4, 130.1, 125.9, 117.3, 113.5, 110.8.

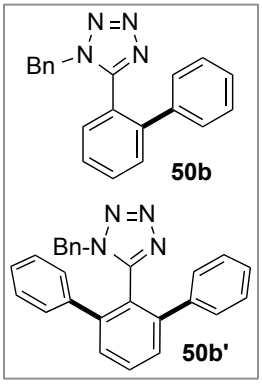

(5-([biphenyl]-2-yl)-1H-tetrazol-1-yl)(phenyl)methanone (**50b**) and (5-([terphenyl]-2'-yl)-1H-tetrazol-1-yl)(phenyl)methanone (**50b'**)

The General Procedure 1 was applied with bromobenzene (52.5 μL, 0.50 mmol) and 1-benzyl-5-phenyl-*1H*-tetrazole (118.1 mg, 0.5 mmol). Column chromatography (hexane/AcOH 90:20 – 40:60)

afforded (5-([biphenyl]-2-yl)-1H-tetrazol-1-yl)(phenyl)methanone (96.8 mg, 62%) and (5-([terphenyl]-2'-yl)-1H-tetrazol-1-yl)(phenyl)methanone (5.8 mg, 3%) both as white solids.

Spectroscopic data matched those previously reported.[178]

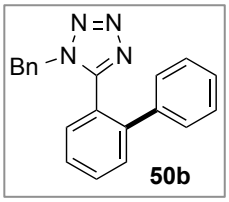

50b

(5-([biphenyl]-2-yl)-1H-tetrazol-1-yl)(phenyl)methanone (**50b**)

^{1}H NMR (500 MHz, $CDCl_3$): δ 7.62 (t, *J* = 7.5 Hz, 1H), 7.56 (d, *J* = 7.7 Hz, 1H), 7.40 (t, *J* = 7.5 Hz, 1H), 7.33 (d, *J* = 7.7 Hz, 1H), 7.29 - 7.26 (m, 3H), 7.19 - 7.11 (m, 5H), 6.74 (d, *J* = 7.6 Hz, 2H), 4.76 (s, 2H); ^{13}C NMR (126 MHz, $CDCl_3$): δ 154.7, 141.6, 138.8, 133.1, 131.6, 131.2, 130.3, 129.0, 128.7, 128.6, 128.6, 128.1, 128.1, 127.8 122.7, 50.8.

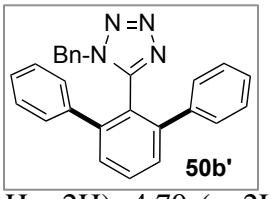

50b'

(5-([terphenyl]-2'-yl)-1H-tetrazol-1-yl)(phenyl)methanone (**50b'**)

^{1}H NMR (500 MHz, $CDCl_3$): δ 7.70 (t, *J* = 7.7 Hz, 1H), 7.50 (d, *J* = 7.7 Hz, 2H), 7.24 - 7.13 (m, 9H), 6.97 (d, *J* = 7.5 Hz, 4H), 6.69 (d, *J* = 7.5 Hz, 2H), 4.70 (s, 2H); ^{13}C NMR (126 MHz, $CDCl_3$): δ 153.1, 143.7, 139.1, 132.8, 131.3, 129.7, 129.1, 128.9, 128.8, 128.4, 128.4, 127.9, 121.5, 50.8.

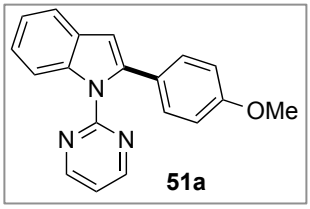

51a

2-(4-methoxyphenyl)-1-(pyrimidin-2-yl)-1H-indole (**51a**)

The General Procedure 1 was applied with 4-bromoanisole (62.6 μL, 0.50 mmol) and 1-(pyrimidin-2-yl)-*1H*-indole (97.6 mg, 0.5 mmol). Column chromatography (hexane/AcOH 90:10 – 30:70) afforded 2-(4-methoxyphenyl)-1-(pyrimidin-2-yl)-1H-indole (48.2 mg, 32%) as a colourless solid.

Spectroscopic data matched those previously reported.[162]

^{1}H NMR (500 MHz, $CDCl_3$): δ 8.66 (d, *J* = 4.8 Hz, 2H), 8.08 (d, J = 8.0 Hz, 1H), 7.61 (d, *J* = 7.5 Hz, 1H), 7.26 - 7.19 (m, 4H), 7.08 (t, *J* = 4.8 Hz, 1H), 6.82 (d, *J* = 8.4 Hz, 2H), 6.72 (s, 1H), 3.79 (s, 3H); ^{13}C NMR (126 MHz, $CDCl_3$): δ 159.0, 158.4, 158.3, 140.4, 138.1, 129.5, 129.5, 126.6, 123.3, 122.2, 120.6, 117.7, 113.8, 112.8, 107.4, 55.4.

Computational section: supplementary information

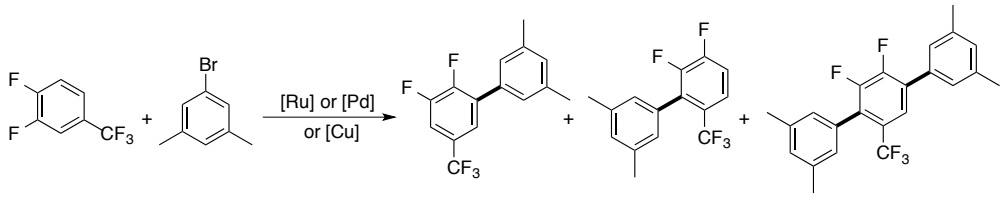

39r **40c** **41rc** **41rc'** **41rc''**

entry	[metal]	**41rc** (%)	**41rc'** (%)	**41rc''** (%)	ratio (**41rc**:**41rc'**:**41rc''**)
1[a]	[Ru]	55	-	-	1 : 0 : 0
2[b]	[Pd]	39	13	17	1 : 0.33 : 0.44
3[c]	[Cu]	10	5	1	1 : 0.5 : 0.1
4[d]	[Cu]	2	<1	-	1 : <0.5 : 0

[a] Reaction conditions: **Ru-C5** (15.5 mg, 0.020 mmol, 4 mol %), **39f** (325.2 μL, 2.50 mmol), **40c** (67.9 μL, 0.50 mmol), $(NMe_4)OPiv$ (35.1 mg, 0.20 mmol), (NMe_4) 4-fluorobenzoate (37.3 mg, 0.175 mmol), $(NMe_4)OC(CF_3)_3$ (386.5 mg, 1.250 mmol) and pivalonitrile (166.3 μL, 1.50 mmol) were stirred under N_2 in a closed vessel at 115 °C for 16 h; yield refers to isolated material (*see General Procedure 1*). [b] Reaction conditions: $Pd(OAc)_2$ (2.2 mg, 0.01 mmol, 5 mol %), $P^tBuMe{\cdot}HBF_4$ (5.0 mg, 0.02 mmol), **39f** (78.0 μL, 0.60 mmol), **40c** (27.2 mL, 0.20 mmol), K_2CO_3 (30.4 mg, 0.22 mmol) and DMA (78.0 μL) were stirred under N_2 in a closed vessel at 120 °C for 12 h; yield are evaluated by quantitative ^{19}F-NMR using C_6F_6 (11.5 μL, 0.10 mmol, 0.5 equiv) as internal standard (*see ref. 22)*. [c] Reaction conditions: CuI (3.8 mg, 0.02 mmol, 10 mol %), 1,10-phenanthroline (3.6 mg, 0.02 mmol), **39f** (78.0 μL, 0.60 mmol), 5-iodo-*m*-xylene (28.9 μL, 0.20 mmol), LiO^tBu (32.0 mg, 0.40 mmol) and DMF (200.0 μL) were stirred under N_2 in a closed vessel at 130 °C for 24 h; yield are evaluated by quantitative ^{19}F-NMR using C_6F_6 (11.5 μL, 0.10 mmol, 0.5 equiv) as internal standard (*see ref. 33a*). [d] Reaction conditions: CuI (3.8 mg, 0.02 mmol, 10 mol %), 1,10-phenanthroline (3.6 mg, 0.02 mmol), **1f** (78.0 μL, 0.60 mmol), 5-iodo-*m*-xylene (28.9 μL, 0.20 mmol), K_3PO_4 (106.1 mg, 0.50 mmol) and DMF (120.0 μL) were stirred under N_2 in a closed vessel at 130 °C for 24 h; yield are evaluated by quantitative ^{19}F-NMR using C_6F_6 (11.5 μL, 0.10 mmol, 0.5 equiv) as internal standard (*see ref. 33a*).

Table 2.41. Arylation of **39f** with **40c** with Ru-, Pd- or Cu-catalysts displaying different selectivity.

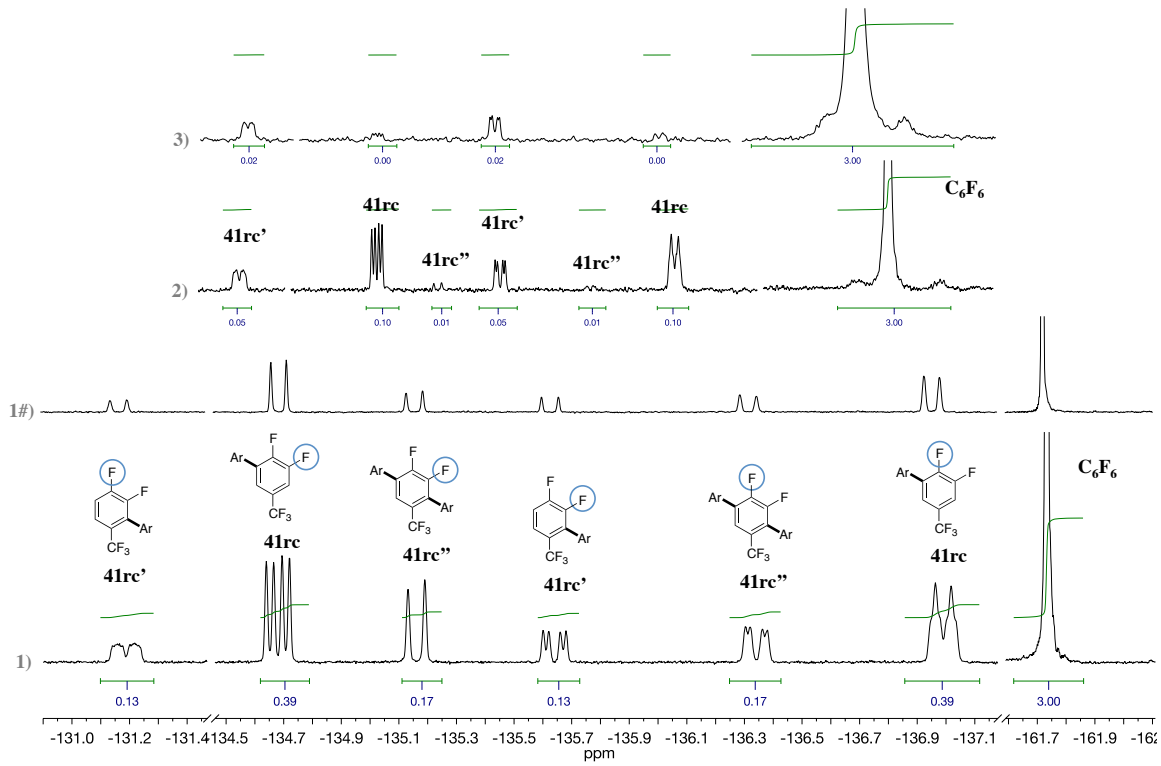

Figure 2.15. ^{19}F-NMR expansion of the reaction illustrated in Table 2.41 in: 1) entry 2 [Pd][b]; 1#) entry 2 [Pd][b], ^{19}F {^{1}H} NMR; 2) entry 3 [Cu][c]; 3) entry 4 [Cu][d] displaying **41rc**, **41rc'**, **41rc''** with relative integrations with respect to the internal standard C_6F_6.

Characterization of biaryls 41rc' and 41rc''

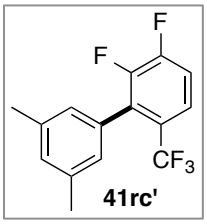

2,3-difluoro-3',5'-dimethyl-6-(trifluoromethyl)-1,1'-biphenyl (**41rc'**)

Milligrams were isolated for characterisation by column chromatography (hexane 100%).[22]

^{1}H NMR (500 MHz, CD_2Cl_2): δ 7.54 (ddd, *J* = 9.2, 4.8, 1.9, 1H), 7.30 (app q, *J* = 8.4 Hz, 1H) 7.11 (s, 1H), 6.91 (s, 2H), 2.36 (s, 6H); ^{1}H {^{19}F } NMR (500 MHz, CD_2Cl_2): 7.54 (d, *J* = 8.9 Hz, 1H), 7.30 (d, *J* = 8.9 Hz, 1H), 7.11 (s, 1H), 6.91 (s, 2H), 2.36 (s, 6H); ^{13}C NMR (126 MHz, $CDCl_3$): δ 152.6 (dd, *J* = 255.8, 13.7 Hz), 148.6 (dd, *J* = 247.0, 12.7 Hz), 137.6, 132.3 (d, *J* = 16.8 Hz), 130.6, 130.6, 127.4, 126.5 - 125.8 (m), 124.3 (only 1 peak of quartet observed for -CF_3), 122.3 - 122.1 (m), 116.0 (d, *J* = 17.8 Hz), 21.4; ^{19}F NMR (471 MHz, $CDCl_3$) δ –57.0 (s, 3F), –131.2 (dm, *J* = 24.7 Hz, 1F), –135.6 (dd, *J* = 22.5, 7.3

Hz, 1F); ^{19}F NMR (471 MHz, CD_2Cl_2) δ –57.3 (s, 3F), –132.1 (dm, *J* = 22.0 Hz, 1F), 136.7 (dd, *J* = 22.3, 7.3 Hz, 1F); ^{19}F {^{1}H} NMR (471 MHz, CD_2Cl_2) δ –57.3 (s, 3F), –132.1 (d, *J* = 22.0 Hz, 1F), 136.7 (dd, *J* = 22.0 Hz, 1F); IR (ATR) 2920, 1322, 1166, 1135; ; HRMS (EI) *m/z* calcd. $C_{15}H_{11}F_5$: $[M]^+$ 286.0775; found: $[M]^+$ 286.0782.

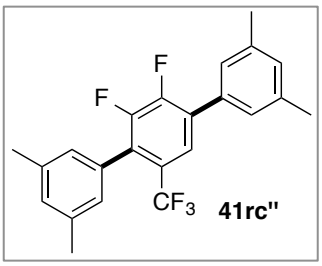

2',3'-difluoro-3,3'',5,5''- tetramethyl-5'-(trifluoromethyl)-1,1':4',1''-terphenyl (**41rc''**)

Milligrams were isolated for characterization by column chromatography (hexane 100%).[22]

^{1}H NMR (500 MHz, $CDCl_3$): δ 7.61 (d, *J* = 6.3 Hz, 1H), 7.20 (s, 2H), 7.10 (app s, 2H), 6.95 (s, 2H), 2.42 (s, 6H), 2.38 (s, 6H); ^{1}H {^{19}F} NMR (500 MHz, $CDCl_3$): δ 7.60 (s, 1H), 7.20 (s, 2H), 7.12 - 7.07 (m, 2H), 6.95 (s, 2H), 2.41 (s, 6H), 2.38 (s, 6H) ^{13}C NMR (126 MHz, $CDCl_3$): δ 149.8 (dd, *J* = 256.2, 14.5 Hz), 144.0 (dd, *J* = 246.8, 13.5 Hz), 138.6, 137.6, 133.5, 130.8, 130.6 (d, *J* = 11.3 Hz), 130.3, 130.2 (d, *J* = 11.5 Hz), 127.5, 126.8, 126.8, 125.9 - 125.1 (m), 123.3 (qd, *J* = 274.0, 3.2 Hz), 122.9 - 122.8 (m), 21.5, 21.5; ^{19}F NMR (471 MHz, $CDCl_3$) δ –56.9 (s, 3F), –135.1 (d, *J* = 22.0 Hz, 1F), –136.1 (dd, *J* = 22.0, 6.0 Hz, 1F); ^{19}F {^{1}H} NMR (471 MHz, $CDCl_3$) δ –56.9 (s, 3F), –135.2 (d, *J* = 22.0 Hz, 1F), –136.3 (d, *J* = 22.0 Hz, 1F); IR(ATR) 2920, 1364, 1294, 1132, 848; m.p. 185 - 187 ºC; HRMS (EI) *m/z* calcd. $C_{23}H_{19}F_5$: $[M]^+$ 390.1393 found: $[M]^+$ 390.1394.

Computational methods

All the calculations were performed at the DFT level with Gaussian 09, revision B.01[179] using the Becke three-parameter hybrid functional[180] with Lee, Yang and Parr correlation term.[181] Stuttgart/Dresden base and ECPs for transition metals[182] (Pd or Ru) and 6-31G basis set with polarization functions for all other atoms[183] (C, H, O, N, F and P). Stationary points were characterized as minima or saddle points by frequencies analysis, representative transition states were confirmed to correspond to the desired C–H activation step by optimization through the internal reaction coordinate to starting materials and products.[23184] Distortion-interaction analysis was performed by single point calculations on fragments of

the corresponding optimized transition states. Distortion of the starting complex ($\Delta E_{dist}(M)$) corresponds to the difference between the energy of the fragment containing the original metal complex in the TS geometry and that of its optimized (minimum) geometry. Distortion of the fluoroarene ($\Delta E_{dist}(Ar^FH)$) is the difference between the energy of the arene fragment in the TS geometry and that of the optimized arene. $\Delta E_{dist}(Ar^FH)$ could be further deconvoluted in C–H elongation energy ($\Delta E_{elong}(Ar^FH)$) and bending energy ($\Delta E_{bend}(Ar^FH)$), which correspond, respectively, to the energy cost of elongating the C–H bond to the distance it displays in the TS and the remaining cost of distortion, of which the main contribution is bending the C–H bond out of plane. Finally, interaction energy is the difference between the TS energy and the metal and arene individual fragments in the TS geometry.

Barriers for C–H activation of pentafluorobenzene with Ru complexes

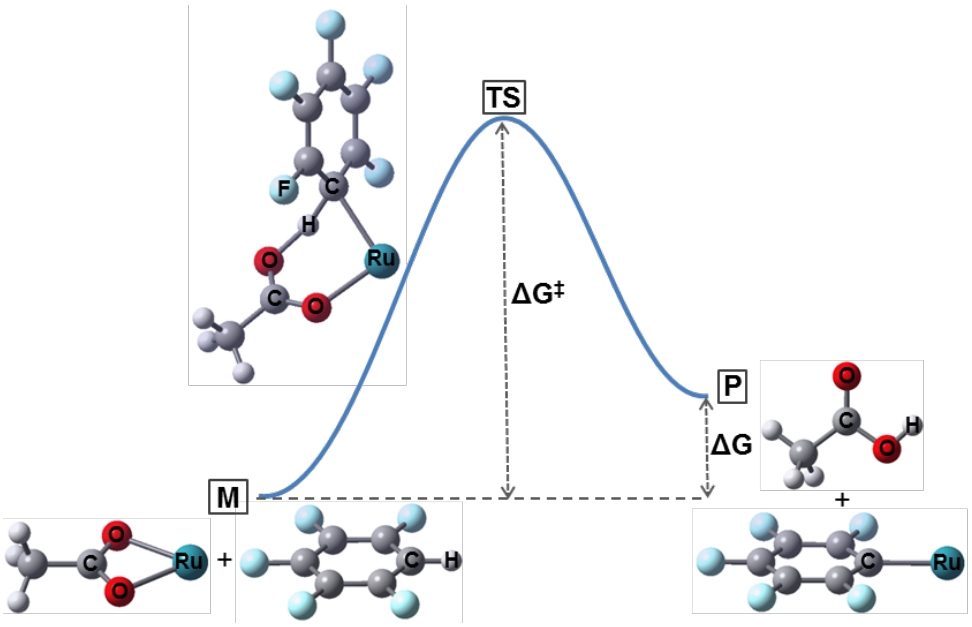

Figure 2.16. General scheme of the Ru-mediated CMD C–H activation. **M**: starting material, **TS**: transition state, **P**: product.

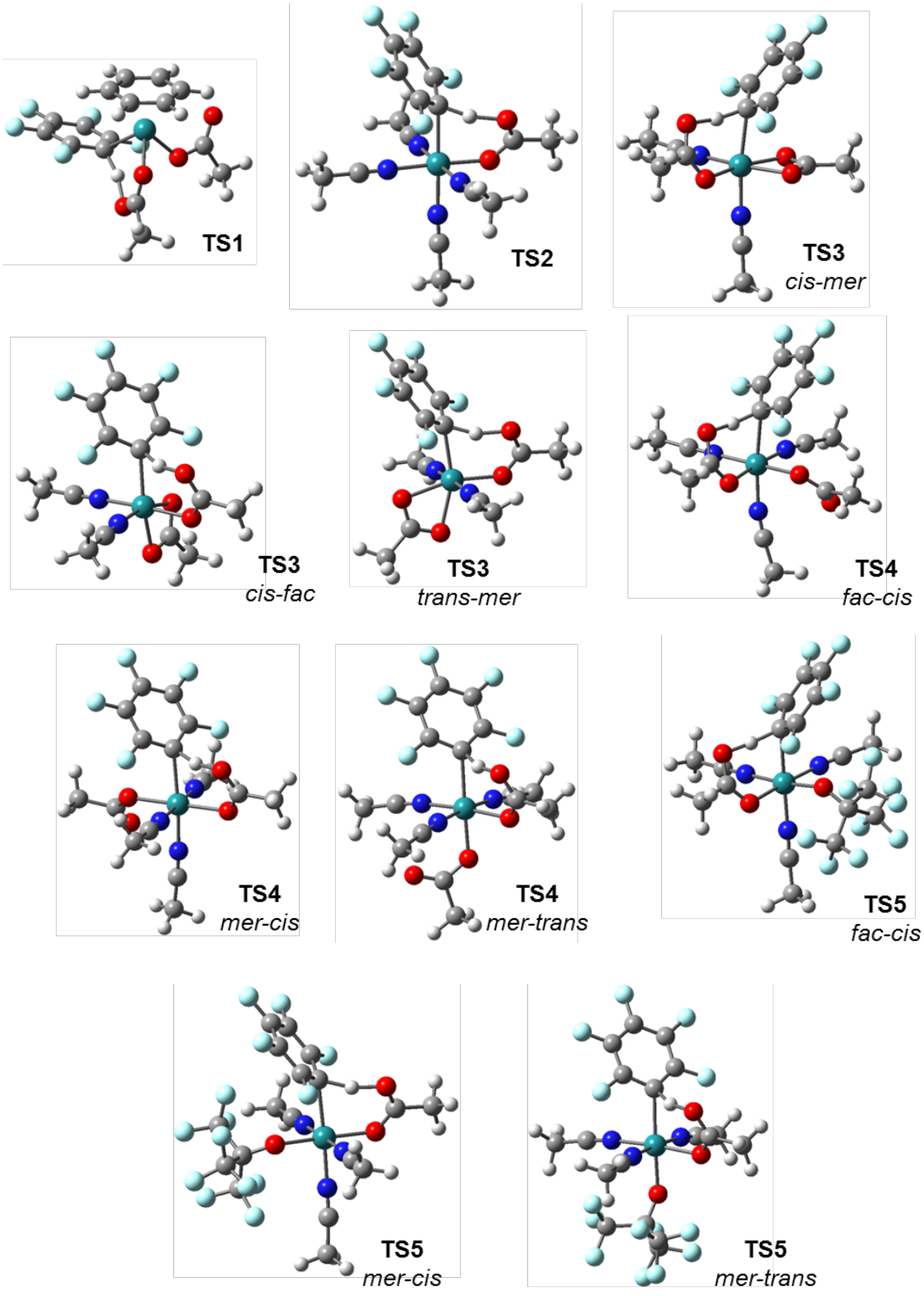

Figure 2.17. Optimised geometries of calculated transition states

M	TS geometry	TS		P	
		$\Delta E^{‡}$	$\Delta G^{‡}$	ΔE	ΔG
$Ru(\eta^6\text{-}C_6H_6)(OAc)_2$ (**M1**)		18.2	29.5	7.2	7.2
$[Ru(\varkappa^2\text{-}OAc)(MeCN)_4]^+$ (**M2**)		15.8	28.8	-1.8	12.1
$Ru(\varkappa^2\text{-}OAc)_2(MeCN)_2$ (**M3**)	*cis-mer*	9.8	21.1	-3.7	8.6
	trans-mer	11.2	23.0		
	cis-fac	12.2	23.9	-1.0	10.9
$Ru(\varkappa^2\text{-}OAc)(\varkappa^1\text{-}OAc)(MeCN)_3$ (**M4**)	*fac-cis*	13.8	24.4	1.3	13.4
	mer-cis	13.2	23.4		
	mer-trans	11.9	22.2	-0.5	10.0
$Ru(\varkappa^2\text{-}OAc)(OC(CF_3)_3)(MeCN)_3$ (**M5**)	*fac-cis*	14.4	25.0	2.0	12.8
	mer-cis	13.8	24.0		
	mer-trans	12.6	23.2	-3.4	7.2

Table 2.42. Energies in kcal/mol (relative to starting materials) of TS and products for the different Ru model complexes

Coordinates and energies of optimized structres

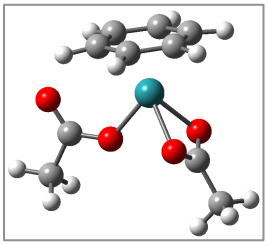

$[Ru(OAc)_2(\eta^6\text{-benzene})]$ (M1)

No Imaginary frequencies

E = -784.206282 Hartree

G = -784.044713 Hartree

C	-1.26410200	-1.81553100	-0.70714500
C	-1.26662500	-1.80508800	0.72656500
C	-1.87047600	-0.73350600	1.41977600
H	-0.69032000	-2.57525100	-1.21985900
H	-0.69521100	-2.55721100	1.25288900
H	-1.78707800	-0.67290700	2.49937500
C	-1.86449900	-0.75486700	-1.41912300
C	-2.49624800	0.32458700	-0.71410000
C	-2.50128400	0.33454600	0.69720300
H	-1.77743400	-0.71060600	-2.49916700
H	-2.88473800	1.17407400	-1.26435000
H	-2.89412400	1.19102300	1.23323800
Ru	-0.41071000	0.10460300	-0.00169800
O	0.40380500	1.76904800	1.09090000
C	0.77319600	2.32193700	0.00267300
O	0.39619300	1.77789300	-1.08731200
C	1.64667400	3.54234300	0.00471400
H	1.47185000	4.13399600	0.90522700
H	2.69344900	3.22043800	0.00070900
H	1.46691000	4.14054600	-0.89047100
O	1.57500100	-0.40278900	-0.01163300
C	2.06670900	-1.61755400	0.00029500
C	3.59160500	-1.62007200	-0.00808000

H	3.96059900	-1.09530400	-0.89445500
H	3.96963700	-1.08362900	0.86749100
H	3.96323600	-2.64530900	-0.00285800
O	1.42309500	-2.66705000	0.01682700

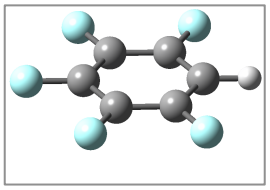

C_6HF_5

No Imaginary frequencies

E = -728.3743723 Hartree

G = -728.348383 Hartree

C	-0.00000400	-1.67785600	0.00019200
C	-1.19521700	-0.96888100	-0.00005500
C	1.19528300	-0.96863800	0.00016100
C	-1.20906300	0.42464600	0.00002500
C	1.20937800	0.42472400	-0.00000300
C	0.00002500	1.11815500	-0.00001500
F	-2.36604400	-1.62090200	-0.00018300
F	-2.36523100	1.09687300	0.00007200
F	2.36580200	-1.62131200	-0.00005800
F	2.36528600	1.09714600	-0.00011700
F	-0.00012900	2.45355300	0.00003400
H	0.00043700	-2.76112000	0.00044400

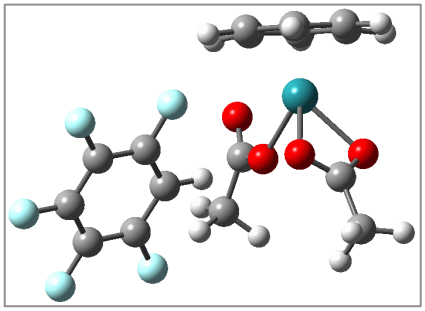

$Ru(OAc)_2(\eta^6\text{-benzene})] + C_6HF_5$

No Imaginary frequencies

E = -1512.591917 Hartree

G = -1512.386142 Hartree

C	-2.15424800	-1.12780600	-1.93640400
C	-1.64052800	-2.06316700	-1.01181700
C	-2.40892200	-2.40018600	0.15216500
H	-1.54071500	-0.76460500	-2.75002500
H	-0.63303900	-2.44414400	-1.12006700
H	-1.97195300	-3.03842500	0.91249000
C	-3.42768200	-0.51557200	-1.71902900
C	-4.17397800	-0.85849800	-0.56365400
C	-3.68736400	-1.83288300	0.36379600
H	-3.74623400	0.28477800	-2.37246400
H	-5.08844500	-0.31977600	-0.33843200
H	-4.23698900	-2.04397100	1.27355200
Ru	-2.18413800	-0.21420300	0.08657700
O	-2.78872200	1.10769600	1.66645800
C	-1.71899300	0.85917700	2.31386100
O	-0.95769900	-0.05576700	1.85368600
C	-1.35230700	1.63441200	3.54509300
H	-0.75358000	1.01793000	4.21825900
H	-0.75282800	2.50091200	3.24588600
H	-2.25043300	1.99507000	4.04972000
C	2.05316700	0.21056600	0.09099000
C	3.10556600	1.11619800	0.04041900
C	2.36099400	-1.14338800	0.07516400
C	4.43299200	0.69570800	-0.02434200
C	3.67611600	-1.59850000	0.01221900

C	4.71409300	-0.66944000	-0.03729400
F	2.86012100	2.43763500	0.05224200
F	5.43284700	1.58335100	-0.07290100
F	1.37814500	-2.06574700	0.12164400
F	3.94953600	-2.90898000	-0.00271900
F	5.98147800	-1.08921600	-0.09940500
H	1.02315600	0.55437700	0.14031900
C	-1.04329300	2.03846500	-1.56237300
O	-1.03359600	1.42783300	-0.39630000
O	-1.64597300	1.66688900	-2.56742400
C	-0.21711900	3.31856900	-1.55390200
H	0.77168200	3.14257600	-1.12353100
H	-0.12419000	3.70701700	-2.56876800
H	-0.71653100	4.06466800	-0.92676900

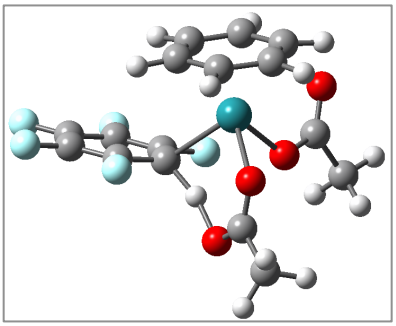

{[Ru(OAc)$_2$(η^6-benzene)]·C$_6$HF$_5$}‡ (TS1)

One imaginary frequency: i718.94

E = -1512.551581 Hartree

G = -1512.346057 Hartree

C	-0.98795300	0.85139400	-2.43292700
C	0.12509100	-0.01347200	-2.39660900
C	-0.04252400	-1.42754400	-2.22065000
H	-0.86831700	1.92464600	-2.48316300
H	1.12647400	0.40066900	-2.44193700
H	0.82125700	-2.07591800	-2.14256400
C	-2.29926000	0.30552000	-2.24420800
C	-2.47586300	-1.08359900	-2.04710700
C	-1.33498400	-1.95265300	-2.03152900
H	-3.13262100	0.98853700	-2.14962000
H	-3.45831500	-1.47933700	-1.81681600
H	-1.46134600	-3.00074300	-1.78446600
Ru	-1.05864000	-0.32770500	-0.53447900
O	-1.85027300	-1.61092900	0.93172400
C	-1.50851700	-1.55610400	2.16331200
O	-0.54645700	-0.87723600	2.61163800
C	-2.34523000	-2.36349700	3.13092100
H	-1.76669000	-2.60469700	4.02350300
H	-3.20873000	-1.75856700	3.42812900
H	-2.71624800	-3.27151700	2.65227700
C	0.97550600	-0.07875200	0.65537100
C	1.52339700	1.21290900	0.63916500
C	1.88654500	-1.11940500	0.41628600
C	2.86122300	1.46306700	0.34071300
C	3.22684900	-0.91657300	0.11865200
C	3.71409600	0.39143300	0.08182100
F	0.76274300	2.28454900	0.89893100
F	3.34149200	2.71236900	0.30517600
F	1.45559200	-2.39740800	0.45352900
F	4.05386700	-1.94164900	-0.12899500
F	4.99764700	0.61389400	-0.20286300
H	0.11532700	-0.37482500	1.54589000
C	-2.26473900	2.24999800	0.44932600
O	-1.82713400	1.05623900	0.76880300
O	-2.36192500	2.71332200	-0.68746900
C	-2.64210000	3.06755300	1.67804100
H	-1.72799200	3.34387300	2.21345500
H	-3.17216300	3.97180400	1.37644000
H	-3.25545800	2.47647600	2.36290600

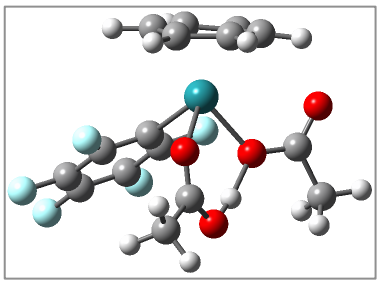

{[Ru(OAc)(η^6-benzene)(C_6F_5)]·(AcOH)}

No Imaginary frequencies

E = -1512.589868 Hartree

G = -1512.382497 Hartree

C	-2.28297400	0.85370800	-1.90879100
C	-1.21622500	0.18707300	-2.55156600
C	-1.08718300	-1.23647600	-2.43205600
H	-2.32800500	1.93410300	-1.89180100
H	-0.44715800	0.75984800	-3.05655800
H	-0.22845100	-1.74899300	-2.84847000
C	-3.30326700	0.10331200	-1.22255700
C	-3.18743200	-1.28330200	-1.10739200
C	-2.03454200	-1.94607700	-1.65931600
H	-4.08921800	0.64341500	-0.71118400
H	-3.89875100	-1.84688800	-0.51397100
H	-1.88000400	-3.00181200	-1.46514000
Ru	-1.17262900	-0.34021000	-0.41940100
O	-0.87953100	-1.78065500	1.17516900
C	-0.40112900	-1.62459100	2.31722800
O	-0.15581500	-0.46672800	2.85915200
C	-0.04163000	-2.82255500	3.15152300
H	1.03301600	-3.00708800	3.04462000
H	-0.24887300	-2.63314100	4.20632200
H	-0.58105100	-3.70130400	2.79850900
C	0.88620100	0.00032200	-0.37876100
C	1.42757000	1.28608000	-0.41862300
C	1.82585000	-1.02852700	-0.33055000
C	2.79630300	1.54738000	-0.37293300
C	3.20353500	-0.81637100	-0.28402500
C	3.69349700	0.48553600	-0.29981100
F	0.62031700	2.36955100	-0.53383400
F	3.25927600	2.80709400	-0.41009400
F	1.42462300	-2.32727400	-0.33662700
F	4.05884800	-1.85092800	-0.22878300
F	5.01356200	0.71412000	-0.25741600
H	-0.51311300	0.28065600	2.22726600
C	-1.94705700	2.11721900	1.30837500
O	-1.19578300	1.03330000	1.18763300
O	-2.79663600	2.46610700	0.50078900
C	-1.62837800	2.92474300	2.55672400
H	-0.64679100	3.39518100	2.43678600
H	-2.38264200	3.69864000	2.69999500
H	-1.57964700	2.28252200	3.44127700

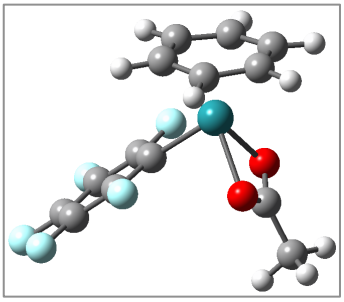

[Ru(OAc)(C_6F_5)(η^6-benzene)]

No Imaginary frequencies

E = -1283.481719 Hartree

G = -1283.328834 Hartree

C	-1.58302200	-2.07241800	-0.90492500
C	-1.59358200	-2.19801100	0.52225500
C	-2.52200500	-1.44538100	1.27936000
H	-0.81572300	-2.56510100	-1.48984400
H	-0.83507800	-2.78625300	1.02430300
H	-2.46736100	-1.45880300	2.36206800
C	-2.49996000	-1.19872600	-1.53530500
C	-3.51515900	-0.52707900	-0.76785500
C	-3.52840000	-0.65147200	0.62597000
H	-2.42860500	-1.02398300	-2.60287000
H	-4.20123800	0.15111900	-1.26301100

H	-4.22550100	-0.07199100	1.22096500
Ru	-1.38740100	-0.06818100	-0.00727100
O	-1.13109600	1.65334800	1.25341100
C	-1.00199100	2.40870900	0.23376900
O	-1.13613400	1.86482900	-0.91205900
C	-0.66384600	3.86414000	0.37491000
H	-1.05933100	4.25632700	1.31367600
H	0.42603300	3.97395300	0.38894400
H	-1.05411900	4.42827700	-0.47410900
C	0.68712900	-0.16798200	-0.01644000
C	1.42792400	-0.32490200	1.15215800
C	1.42884300	-0.07706000	-1.19145500
C	2.82146600	-0.36528700	1.17293700
C	2.82237900	-0.11239200	-1.21918900
C	3.52366400	-0.25550600	-0.02464100
F	0.79780000	-0.46150300	2.34480800
F	3.49200800	-0.51764900	2.32661300
F	0.79954400	0.03895200	-2.38640000
F	3.49369800	-0.01981500	-2.37873800
F	4.86403400	-0.29652100	-0.02853800

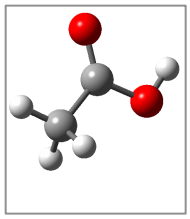

AcOH

No Imaginary frequencies

E = -229.0874096 Hartree

G = -229.052774 Hartree

C	1.39683000	-0.11058900	-0.00000700
H	1.91621200	0.84666800	-0.00006500
H	1.68286600	-0.69267600	-0.88103000
H	1.68292300	-0.69259600	0.88105100
C	-0.09241200	0.12509100	0.00003700
O	-0.64409100	1.20240500	-0.00001000
O	-0.77941000	-1.04562300	-0.00000500
H	-1.72050000	-0.80266900	-0.00002100

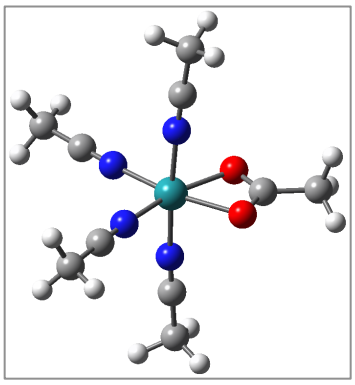

$[Ru(OAc)(MeCN)_4]^+$ (M2)

No Imaginary frequencies

E = -854.3873136 Hartree

G = -854.207582 Hartree

Ru	-0.00065500	0.07938600	0.00001000
N	-2.02657600	0.17044900	0.00066200
C	-3.17632600	0.29541600	0.00085900
N	-0.02200000	-1.33775400	-1.44707800
C	-0.03420300	-2.08531500	-2.33128700
N	-0.02081800	-1.33768100	1.44718400
C	-0.03200000	-2.08513700	2.33149500
N	2.02721500	0.11191400	-0.00072600
C	3.18051200	0.19898800	-0.00104500
C	-4.62363600	0.46386000	0.00110500
H	-4.93921600	0.97269000	0.91642700
H	-4.92851600	1.06359200	-0.86127700
H	-5.11697500	-0.51070800	-0.05183800
C	-0.04591500	-3.00766800	3.46006800
H	-0.96460700	-3.60104200	3.45038200
H	0.81149400	-3.68440100	3.40471700
H	0.00430700	-2.44856400	4.39902900
C	4.63268900	0.31879300	-0.00149100
H	5.09295200	-0.67324400	0.00154300
H	4.96150800	0.86006800	-0.89325200

H	4.96158500	0.86550500	0.88692100
C	-0.04962300	-3.00805300	-3.45967400
H	-0.87624200	-3.71674300	-3.35663100
H	-0.17365200	-2.45236600	-4.39380300
H	0.89001400	-3.56612300	-3.50248600
O	0.02297300	1.90228500	1.09053400
C	0.03502500	2.57169900	-0.00001200
C	0.09185800	4.06944100	-0.00003800
H	-0.38460900	4.46602300	-0.89818900
H	-0.38437800	4.46603500	0.89823100
H	1.13974200	4.38908200	-0.00017200
O	0.02207300	1.90228900	-1.09055900

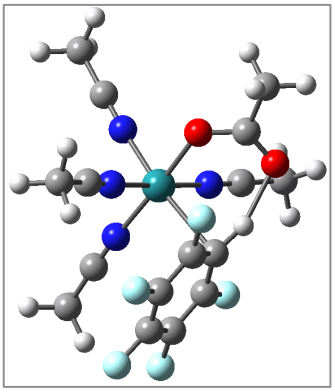

{[Ru(OAc)(MeCN)$_4$]·(C$_6$HF$_5$)}$^+$

No Imaginary frequencies

E = -1582.741487 Hartree

G = -1582.509953 Hartree

Ru	-0.82683700	-0.00760400	0.38358700
O	-1.96681500	1.27451100	-0.76891800
C	-2.24485300	1.09322700	-2.03333900
O	-1.79949500	0.18364200	-2.74618700
C	-3.17753200	2.15150900	-2.59955500
H	-2.65295200	3.11170900	-2.63991900
H	-3.49139300	1.87369800	-3.60587500
H	-4.04911600	2.28406500	-1.95318400
C	0.88016400	-0.15070000	-1.57045400
C	1.58601900	-1.30261300	-1.19596200
C	1.51552100	1.08344600	-1.37185100
C	2.82581600	-1.23399400	-0.57298700
C	2.75507100	1.18016900	-0.74735700
C	3.41069200	0.01469000	-0.35250500
F	1.05238300	-2.51107700	-1.39906900
F	3.44260900	-2.34276800	-0.14154200
F	0.91998600	2.21257500	-1.75489600
F	3.30172900	2.37576200	-0.49243200
F	4.58006200	0.09255300	0.27320700
H	-0.04395500	-0.20059400	-2.16992100
N	-1.71625100	-1.62102700	-0.46985100
C	-2.23541700	-2.46106200	-1.06835500
N	-2.28413300	0.11256200	1.71395400
C	-3.17854200	0.23083900	2.43665800
N	0.30390700	-1.21089300	1.60557100
C	0.96288600	-1.92047500	2.24123000
N	0.01880500	1.68246000	1.14563900
C	0.47515000	2.69069600	1.48058200
C	-2.88155500	-3.46961100	-1.89418500
H	-3.11456800	-3.02670400	-2.86744100
H	-2.21388000	-4.32340100	-2.03901600
H	-3.80632800	-3.81439000	-1.42376700
C	-4.31207900	0.38683700	3.33893700
H	-5.01749200	1.11235700	2.92362900
H	-4.82346200	-0.57111900	3.46906200
H	-3.97055400	0.74189400	4.31534500
C	1.83500400	-2.81818400	2.98808500
H	2.18935200	-2.33202000	3.90128000
H	1.29709000	-3.73159600	3.25691100
H	2.69446900	-3.08005400	2.36343900
C	1.09014600	3.95837700	1.84902600
H	1.30160000	3.98421400	2.92145100
H	2.02595100	4.07258400	1.29378300
H	0.42036400	4.78466200	1.59481500

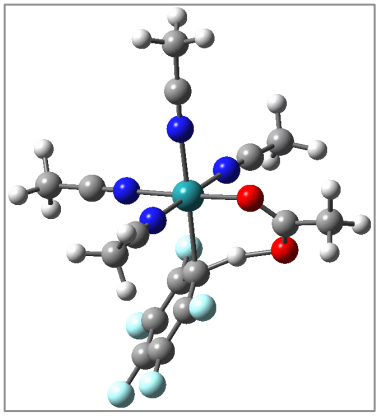

{[Ru(OAc)(C_6HF_5)($MeCN)_4$]$^+$}‡ (TS2)

One imaginary frequency: i492.18

E = -1582.736474 Hartree

G = -1582.510069 Hartree

Ru	-1.04769800	0.02030400	0.21402400
O	-1.83252900	1.16042000	-1.35038200
C	-1.36600300	1.03600800	-2.53814000
O	-0.38540900	0.29920900	-2.83537700
C	-2.02566400	1.85538400	-3.62235200
H	-1.43254500	2.76220600	-3.78259600
H	-2.03447600	1.29697300	-4.56015200
H	-3.03682600	2.14532400	-3.33517000
C	1.10659900	-0.05199500	-0.69269500
C	1.81655600	-1.24369700	-0.47093700
C	1.87850100	1.12102100	-0.62377400
C	3.16441000	-1.27745900	-0.13633800
C	3.22802900	1.13516700	-0.29614200
C	3.87327800	-0.07783500	-0.04995300
F	1.18791700	-2.43026200	-0.55029100
F	3.78790000	-2.43584600	0.10354900
F	1.30736100	2.30563800	-0.90062600
F	3.91179600	2.28090100	-0.22374100
F	5.16310200	-0.09173700	0.26603600
H	0.28439800	0.00111600	-1.63885700
N	-1.57159000	-1.66844600	-0.78979200
C	-1.85398500	-2.59571100	-1.41874700
N	-2.90026100	0.11340000	1.02732900
C	-3.97812800	0.20512900	1.43613700
N	-0.35088600	-1.06353100	1.79341100
C	0.04909100	-1.69564000	2.67687600
N	-0.58767500	1.76636400	1.14758100
C	-0.35534900	2.80107700	1.60700700
C	-2.17565000	-3.75867100	-2.23409700
H	-2.34277900	-3.44776200	-3.26939900
H	-1.34404400	-4.46874700	-2.20820700
H	-3.07729900	-4.25034500	-1.85879200
C	-5.34087800	0.32681800	1.93871300
H	-5.92891700	0.95753400	1.26583600
H	-5.80890600	-0.65976200	1.99921900
H	-5.33648100	0.77819700	2.93484000
C	0.56635500	-2.49900200	3.77795000
H	0.90416300	-1.85084100	4.59154300
H	-0.21374400	-3.16529100	4.15697900
H	1.41055200	-3.10329900	3.43314500
C	-0.03597800	4.11598200	2.14603200
H	0.27947300	4.03424000	3.18982100
H	0.77507000	4.56021300	1.56140500
H	-0.91233300	4.76760800	2.08811100
H	0.42036400	4.78466200	1.59481500

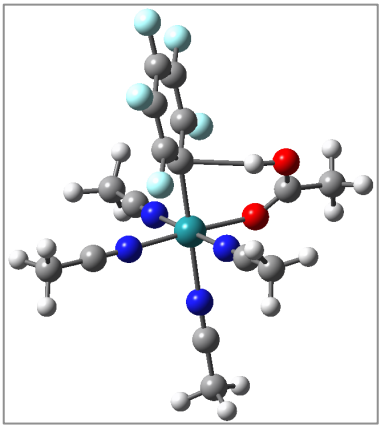

[Ru($MeCN)_4$(AcOH)(C_6F_5)]$^+$

No imaginary frequencies

E = -1582.758632 Hartree

G = -1582.526633 Hartree

Ru	-1.04915700	0.03804900	-0.13049600
O	-1.31832500	-1.56607100	1.27506400
C	-0.66621700	-1.81588600	2.29925500
O	0.38638400	-1.11603800	2.67714300
C	-1.01345800	-2.95469500	3.20692300
H	-0.24814900	-3.73143500	3.10581100
H	-1.00537100	-2.62281900	4.24811700
H	-1.98642700	-3.36476000	2.94073100
C	1.06267200	0.03435400	-0.01492100
C	1.82820200	1.20619800	0.05069800
C	1.83433800	-1.13117600	-0.11660900
C	3.22116500	1.23852600	0.00485700
C	3.22693800	-1.15484100	-0.16567500
C	3.93020100	0.04557100	-0.10984300
F	1.22098500	2.41673700	0.16093700
F	3.87996600	2.40281100	0.06729800
F	1.22580200	-2.34745100	-0.14000300
F	3.88915400	-2.31427400	-0.25987400
F	5.26354700	0.05223600	-0.15391800
H	0.61921300	-0.48656200	1.95340100
N	-1.16692600	1.40323000	1.36965800
C	-1.21839000	2.20008000	2.20733700
N	-3.17655200	0.00616300	-0.27301600
C	-4.33086800	-0.05131500	-0.33342600
N	-0.92378900	1.49840700	-1.49401600
C	-0.81836300	2.34653200	-2.27357300
N	-0.94789500	-1.34895400	-1.60867800
C	-0.86853600	-2.16476400	-2.42365100
C	-1.25084500	3.21173600	3.25533400
H	-1.15429900	2.73957400	4.23725000
H	-0.42152900	3.91158400	3.11638500
H	-2.19345200	3.76514500	3.21972400
C	-5.78499900	-0.13017200	-0.40737300
H	-6.12925000	-1.07821000	0.01546800
H	-6.23562900	0.69242600	0.15492600
H	-6.11239500	-0.06748300	-1.44895200
C	-0.65471400	3.42480600	-3.24022600
H	-0.44543100	3.01368300	-4.23186900
H	-1.56423900	4.02982500	-3.29334900
H	0.18049600	4.06451400	-2.94005000
C	-0.73231600	-3.21165200	-3.42751200
H	-0.57579800	-2.77055000	-4.41585500
H	0.12610600	-3.84351900	-3.18102400
H	-1.63325200	-3.83094300	-3.45370600

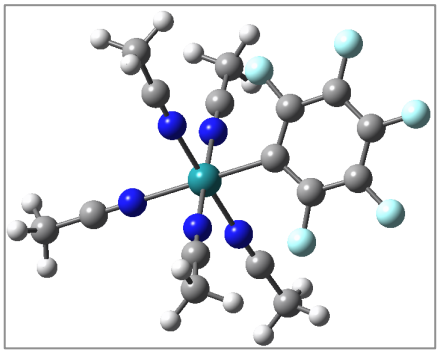

$[Ru(C_6F_5)(MeCN)_5]^+$ (P2)

No imaginary frequencies

E = -1486.43275 Hartree

G = -1486.217041 Hartree

Ru	1.04554500	-0.00012900	-0.00100800
N	1.02572300	-1.42588600	1.44633300
C	0.95647000	-2.24806500	2.25602700
N	1.02598900	1.42557500	1.44639100
C	0.95694300	2.24770400	2.25615300
N	3.19858200	-0.00023800	-0.00142700
C	4.35634900	-0.00010000	0.00027600
N	1.02389200	1.42542200	-1.44861300
C	0.95313700	2.24705900	-2.25872500
N	1.02361000	-1.42565200	-1.44862300
C	0.95265600	-2.24728500	-2.25872300
C	-1.05023000	0.00007300	0.00042700

C	-1.81567500	-1.16955400	0.00098800
C	-1.81545800	1.16984200	0.00099500
C	-3.20967500	-1.19685300	0.00203000
C	-3.20944800	1.19740800	0.00203300
C	-3.91858200	0.00034200	0.00256100
F	-1.21352600	-2.39184500	0.00054300
F	-1.21307300	2.39202500	0.00056300
F	-3.86908700	-2.36483500	0.00251400
F	-5.25541300	0.00047400	0.00355100
F	-3.86864800	2.36550600	0.00252500
C	0.82923800	3.29614000	3.25975400
H	-0.04015000	3.91854400	3.02803600
H	0.69400100	2.85500700	4.25126000
H	1.72422300	3.92445100	3.27072200
C	0.82331200	3.29478100	-3.26280600
H	-0.04646700	3.91644200	-3.03055700
H	1.71762200	3.92402700	-3.27510100
H	0.68751400	2.85291400	-4.25390900
C	0.82256200	-3.29499000	-3.26278200
H	1.71656500	-3.92467400	-3.27482000
H	-0.04758300	-3.91620600	-3.03071700
H	0.68723100	-2.85310600	-4.25394500
C	0.82850100	-3.29657000	3.25952700
H	0.69366700	-2.85550600	4.25112100
H	-0.04121300	-3.91855800	3.02791300
H	1.72320500	-3.92528600	3.27022700
C	5.81479200	0.00014800	0.00327700
H	6.19130400	0.90395200	-0.48392600
H	6.18813300	-0.02897900	1.03080500
H	6.19175500	-0.87431000	-0.53451000

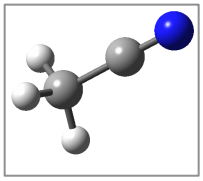

MeCN

No imaginary frequencies

E = -132.7556374 Hartree

G = -132.73318 Hartree

C	0.00000000	0.00000000	-1.18067200
H	0.00000000	1.02604600	-1.55948300
H	-0.88858100	-0.51302300	-1.55948300
H	0.88858100	-0.51302300	-1.55948300
C	0.00000000	0.00000000	0.28008700
N	0.00000000	0.00000000	1.44027900

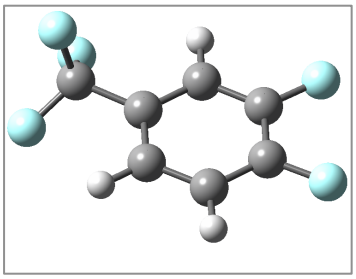

$C_6H_3F_2CF_3$ (39r)

No imaginary frequencies

E = -132.7556374 Hartree

G = -132.73318 Hartree

C	1.31406900	-1.61690500	-0.00716900
C	2.15033600	-0.50941400	0.00489400
C	-0.06812600	-1.43047700	-0.02840600
C	1.61769500	0.78095800	-0.00651200
C	-0.59803500	-0.13881100	-0.03892100
C	0.24645800	0.97611600	-0.02806600
F	3.48221500	-0.66048800	0.02273600
F	2.45468800	1.82939400	-0.00096900
H	-0.73098700	-2.28745900	-0.04518900
H	-0.14698600	1.98546200	-0.04513400

H	1.75501400	-2.60740700	-0.00327000
C	-2.08875900	0.06572100	0.00051500
F	-2.45360600	1.20699700	-0.62385400
F	-2.54687600	0.14959400	1.27093900
F	-2.74963000	-0.95369000	-0.58934500

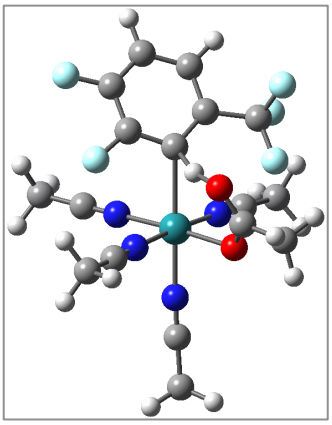

{[Ru(OAc)(39r)(MeCN)$_4$]$^+$}‡ (TS$^{Ru\text{-}a}$)

One imaginary frequency: i929.76

E = -1622.093791 Hartree

G = -1621.837613 Hartree

Ru	-0.95301600	-0.06153900	-0.19300600
O	-1.28950100	-1.53554100	1.24838300
C	-0.68968900	-1.44952400	2.37354100
O	0.17609900	-0.56476600	2.64031900
C	-1.01418900	-2.48756400	3.41873800
H	-0.21819700	-3.23980400	3.41503500
H	-1.02941600	-2.02990700	4.40981400
H	-1.96396000	-2.97778600	3.20379100
C	1.26859100	0.47209400	0.48795400
C	1.47277600	1.85800400	0.45777000
C	2.42211100	-0.29644800	0.16539000
C	2.66434400	2.45700300	0.05302900
C	3.62783000	0.29331600	-0.22396400
C	3.75455600	1.67892500	-0.29824700
F	0.48473300	2.70940600	0.80399000
F	2.73449100	3.79566700	0.00910900
H	0.56399300	-0.00551200	1.47976200
N	-1.78685800	1.25166200	1.12049800
C	-2.26156800	1.94972200	1.90903600
N	-2.80738600	-0.51185800	-0.86517600
C	-3.86833900	-0.82642500	-1.20085900
N	-0.73366900	1.37880200	-1.61844000
C	-0.61022300	2.21759300	-2.40617200
N	-0.21978600	-1.45313500	-1.48078000
C	0.14804500	-2.28136100	-2.19791800
C	-2.81421300	2.84186400	2.91888600
H	-2.11237800	3.65912700	3.10890500
H	-3.76582200	3.25986100	2.57931100
H	-2.97821200	2.29271400	3.85038000
C	-5.20579200	-1.23420100	-1.61257700
H	-5.22207300	-1.44543300	-2.68548600
H	-5.50186200	-2.13582300	-1.06869800
H	-5.92466500	-0.43857200	-1.39762000
C	-0.43786600	3.28729400	-3.38135200
H	0.24768800	4.04222600	-2.98523500
H	-0.02492300	2.88711900	-4.31161500
H	-1.40001600	3.76100000	-3.59577100
C	0.65207600	-3.34173100	-3.05912900
H	0.77063800	-2.97800900	-4.08345500
H	1.62281400	-3.66947800	-2.67795400
H	-0.04020200	-4.18820900	-3.05792500
H	4.48434800	-0.33164400	-0.45233000
H	4.68082600	2.15610400	-0.59861100
C	2.49744700	-1.80144500	0.29522000
F	2.82609000	-2.37427700	-0.90233400
F	1.36013800	-2.39126500	0.70385100
F	3.46675300	-2.16050900	1.15889100

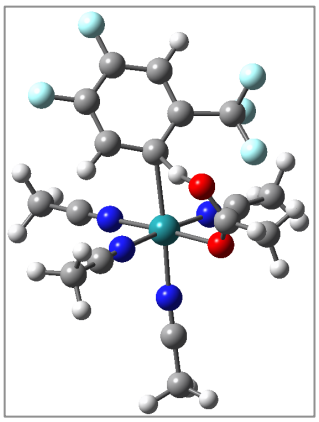

{[Ru(OAc)(39r)(MeCN)$_4$]$^+$}‡ (TS^{Ru-b})

One imaginary frequency: i1003.02

E = -1622.089229 Hartree

G = -1621.833131 Hartree

Ru	-1.06725900	0.16407800	-0.16906900
O	-1.78374900	-1.13384900	1.30676400
C	-1.17601600	-1.20550400	2.42722500
O	-0.10527300	-0.57730900	2.68049300
C	-1.75435000	-2.11125800	3.48514600
H	-1.15856400	-3.02952700	3.51772900
H	-1.67784700	-1.63694800	4.46577600
H	-2.78981900	-2.36691800	3.25990600
C	1.16923400	0.22467500	0.53098900
C	1.59818200	1.57199500	0.57977900
C	2.17628600	-0.72872200	0.23357600
C	2.89337100	1.95052500	0.27830700
C	3.49160600	-0.35256800	-0.06399000
C	3.84418900	0.98655200	-0.05929200
F	5.09094300	1.36582800	-0.34903800
H	0.37847800	-0.14274800	1.52036500
N	-1.49610400	1.71131100	1.08285000
C	-1.77405600	2.53222200	1.84960800
N	-2.98896100	0.19328000	-0.84798700
C	-4.09462300	0.16036000	-1.18574400
N	-0.47635300	1.41228200	-1.66788200
C	-0.13029900	2.11305900	-2.52175100
N	-0.74644500	-1.43521900	-1.37642600
C	-0.62176500	-2.37409100	-2.03808800
C	-2.10599100	3.55200000	2.83600800
H	-3.17436500	3.51681100	3.06729900
H	-1.53835400	3.37339600	3.75402600
H	-1.85810200	4.54558400	2.45208300
C	-5.49107300	0.10937500	-1.60074100
H	-6.05899200	-0.52488100	-0.91406700
H	-5.92305400	1.11405900	-1.59564200
H	-5.56845200	-0.30364700	-2.61041800
C	0.32571200	2.99667900	-3.58796000
H	0.50243400	2.42229400	-4.50177800
H	-0.42668400	3.76373000	-3.79198600
H	1.25883500	3.48520300	-3.29248900
C	-0.41743400	-3.58064100	-2.82673100
H	-0.30486700	-3.33088100	-3.88526700
H	0.49120400	-4.07663300	-2.47506100
H	-1.26797200	-4.25741600	-2.70726200
F	3.25288800	3.24298500	0.30336400
H	0.90695300	2.36089300	0.85059400
H	4.25765100	-1.09068800	-0.27523200
C	1.96023400	-2.22370500	0.27054100
F	2.04980100	-2.76339100	-0.98273600
F	0.76651300	-2.59380300	0.76958000
F	2.90862000	-2.83485700	1.00630000

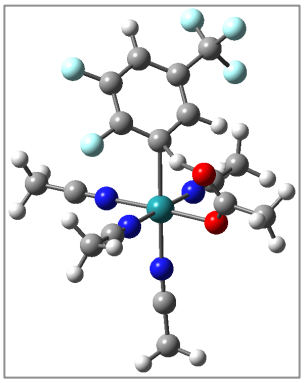

{[Ru(OAc)(39r)(MeCN)$_4$]$^+$}‡ (TS^{Ru-c})

One imaginary frequency: i880.00

E = -1622.09692 Hartree

G = -1621.842883 Hartree

Ru	-1.25194000	-0.25398500	-0.16648400
O	-1.58729700	-1.49915200	1.48430200
C	-1.18273500	-1.12756500	2.63966500
O	-0.48927200	-0.08669400	2.83321900
C	-1.54103200	-1.99477200	3.82183800
H	-0.62981600	-2.45956600	4.21123200
H	-1.95183100	-1.37308400	4.62129300
H	-2.25340300	-2.76948600	3.53922400
C	0.74741900	0.58602200	0.62112400
C	1.02833400	1.92778600	0.34291000
C	1.85624800	-0.28874300	0.60011900
C	2.30539600	2.36911700	-0.00705200
C	3.13154500	0.13418900	0.24002600
C	3.36598000	1.47990500	-0.07047200
F	0.05106200	2.85437800	0.36852300
F	2.48816800	3.66574400	-0.29913300
H	-0.03466100	0.31085900	1.61821200
N	-2.32606900	1.21317000	0.74001300
C	-2.90248500	2.04224600	1.30207000
N	-2.96067500	-1.05205600	-0.94147900
C	-3.93251800	-1.54989100	-1.32258500
N	-0.98726700	0.90820700	-1.81717800
C	-0.83345700	1.58690400	-2.74193100
N	-0.18401000	-1.76034600	-1.02213700
C	0.46213900	-2.60878700	-1.46930000
C	-3.59478600	3.09784000	2.02832400
H	-3.73172000	2.80108100	3.07210200
H	-3.00077700	4.01584300	1.99705000
H	-4.57372700	3.29007000	1.58071200
C	-5.15786700	-2.18614100	-1.78974800
H	-5.46245600	-2.96501900	-1.08482200
H	-5.95954400	-1.44652600	-1.86894800
H	-4.99623200	-2.63988700	-2.77158900
C	-0.62837800	2.45437700	-3.89541000
H	-0.05659000	1.92853700	-4.66527300
H	-1.59159400	2.75779500	-4.31524500
H	-0.07601300	3.34908800	-3.59360100
C	1.33904500	-3.64817000	-1.99198600
H	1.27250700	-3.69048300	-3.08257800
H	2.36877600	-3.41889400	-1.70143000
H	1.05776000	-4.62119300	-1.57964400
H	1.70408900	-1.32806000	0.86740300
H	4.34836500	1.83855500	-0.35567600
C	4.27027300	-0.85127200	0.22323600
F	3.83845800	-2.08811700	-0.15382800
F	4.83757500	-0.99452000	1.43443200
F	5.23720400	-0.48399800	-0.63919400

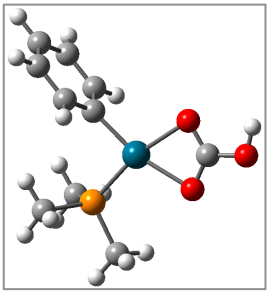

[Pd(O_2COH)(Ph)(PMe_3)]

No imaginary frequencies

E = -1085.153536 Hartree

G = -1084.967793 Hartree

Pd	-0.60014800	-0.19581700	-0.00123600
C	3.35131900	-1.32807800	1.20670200
C	2.03135300	-0.86312100	1.20749800
C	1.34958300	-0.64366200	0.00013000
C	2.02449900	-0.88654400	-1.20668800
C	3.34438600	-1.35123800	-1.20436900
C	4.01262400	-1.57067100	0.00155000
H	1.53082300	-0.69015300	2.15708900
H	3.84750900	-1.54327200	-2.14900900
H	5.03809100	-1.92937000	0.00199600
H	3.85978900	-1.50206800	2.15196500
H	1.51879600	-0.73130900	-2.15655300

P	-0.05813700	1.98202900	-0.00272200
C	0.95006700	2.58962700	-1.41705700
C	0.84345500	2.60192200	1.47688300
C	-1.58258600	3.01261800	-0.06397300
H	1.12337900	3.66750500	-1.33781400
H	1.90646000	2.06252900	-1.43065500
H	0.42621200	2.37702500	-2.35259300
H	1.03117500	3.67740300	1.39800500
H	0.24789500	2.40478800	2.37197800
H	1.79259600	2.06934800	1.56893600
H	-1.34116800	4.08037200	-0.04936800
H	-2.14127700	2.77443000	-0.97224100
H	-2.21816500	2.76636300	0.78994400
O	-1.60518200	-2.14588300	0.00277600
C	-2.72078800	-1.52953200	0.00305700
O	-2.80349700	-0.26651200	0.00072100
O	-3.86214800	-2.24018800	0.00601100
H	-3.60012100	-3.17371000	0.00754300

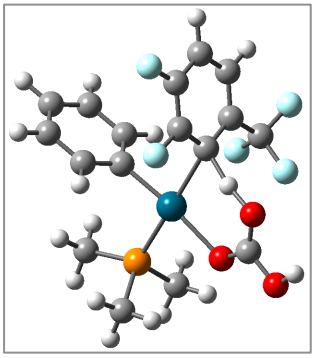

[Pd(O_2COH)(Ph)(39r)(PMe_3)]‡ ($TS^{Pd\text{-}a}$)

One imaginary frequency: i1051.79

E = -1852.871704 Hartree

G = -1852.614754 Hartree

Pd	0.79580200	-0.03654100	-0.20066200
C	-0.61357000	3.97887600	-0.72638900
C	-0.06605300	2.70704200	-0.92919900
C	0.02553600	1.78829100	0.12863300
C	-0.43844300	2.17564400	1.39503200
C	-0.98267700	3.44984100	1.59516200
C	-1.07005300	4.35674600	0.53772800
H	0.27450400	2.42905500	-1.92324400
H	-1.34117200	3.72915600	2.58322500
H	-1.49264000	5.34511000	0.69558100
H	-0.68300400	4.67222100	-1.56122000
H	-0.39376700	1.47973300	2.22734300
P	2.90536500	0.78126200	0.18837300
C	3.16549600	2.51832800	0.72837400
C	3.99440400	0.59613900	-1.28536600
C	3.74506400	-0.22722400	1.47975000
H	4.23121400	2.72035200	0.87424500
H	2.75860500	3.20045900	-0.02127600
H	2.62657900	2.69232500	1.66229300
H	5.03176800	0.85314400	-1.04707100
H	3.94003200	-0.44115000	-1.62359400
H	3.63802600	1.24495900	-2.08964400
H	4.79607600	0.06064500	1.58618200
H	3.23354800	-0.09312100	2.43636000
H	3.67432600	-1.27893600	1.19352000
O	1.82062000	-1.93619400	-0.62562100
C	1.17353700	-2.84513200	-1.19445500
O	-0.07466600	-2.83123700	-1.47186500
C	-2.04849900	-1.08285800	0.77255400
C	-1.33954700	-0.80564700	-0.42411100
C	-2.05895800	-0.13009700	-1.40534100
C	-3.38001400	0.28331100	-1.23395700
C	-4.04064500	0.01114600	-0.04671200
C	-3.36936400	-0.68232100	0.96502700
F	-1.47071000	0.15635500	-2.58609900
H	-0.56999700	-1.81944100	-0.96282800
F	-4.00363200	0.94190000	-2.22439600
H	-5.06865200	0.33608500	0.07188200
H	-3.88335400	-0.91390400	1.89045100
C	-1.34853400	-1.81546400	1.89041800
F	-2.21416700	-2.28612100	2.81518500

F	-0.47149000	-1.01493300	2.56157800
F	-0.62947400	-2.86940200	1.44478200
O	1.85890200	-3.94650400	-1.55383200
H	1.22085100	-4.55317300	-1.95916600

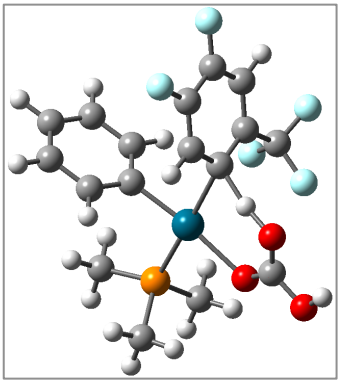

[Pd(O_2COH)(Ph)(39r)(PMe_3)]‡ ($TS^{Pd\text{-}b}$)

One imaginary frequency: i1054.85

E = -1852.863873 Hartree

G = -1852.607803 Hartree

Pd	0.91806100	-0.03485600	-0.25463700
C	-0.38740300	4.00157000	-0.89153500
C	0.15076600	2.71963700	-1.05145900
C	0.15136700	1.80134200	0.01113100
C	-0.39370000	2.20237100	1.24038300
C	-0.92852900	3.48621000	1.39867500
C	-0.92662300	4.39101300	0.33581700
H	0.56389400	2.43761700	-2.01736200
H	-1.35090600	3.77481800	2.35835600
H	-1.34324400	5.38646000	0.46107800
H	-0.38387800	4.69393200	-1.73013000
H	-0.41854800	1.50903500	2.07533300
P	3.02851900	0.77362100	0.19865400
C	4.16039500	0.61374300	-1.24672400
C	3.83715100	-0.25319100	1.49621100
C	3.27725600	2.50210300	0.77216700
H	5.18924200	0.87348100	-0.97651600
H	4.12324600	-0.41885000	-1.60151400
H	3.82327600	1.27215400	-2.05161800
H	4.88695500	0.02852700	1.62765100
H	3.30713700	-0.12692100	2.44386900
H	3.76733700	-1.30155300	1.19792600
H	4.33872400	2.70012400	0.95078000
H	2.89215200	3.19702900	0.02282300
H	2.71341000	2.66253300	1.69385800
O	1.95489100	-1.94826700	-0.62939500
C	1.32361900	-2.83006400	-1.25108700
O	0.09283100	-2.77336700	-1.60675800
C	-1.91356800	-1.08638800	0.64275100
C	-1.20384400	-0.76806500	-0.54075300
C	-1.94144900	-0.12702100	-1.55792900
C	-3.27795300	0.20120900	-1.39554700
C	-3.93319200	-0.10770600	-0.20458700
C	-3.26010500	-0.76000800	0.81855300
H	-0.39947200	-1.78972900	-1.09303300
F	-3.96449600	0.81564900	-2.37346500
F	-5.22825800	0.21327000	-0.06593800
H	-3.79813900	-1.01211800	1.72464100
H	-1.47302300	0.12786000	-2.50418600
C	-1.21253400	-1.78953800	1.78000500
F	-0.40844600	-0.94834600	2.49147200
F	-2.08184100	-2.32011500	2.66844400
F	-0.41965000	-2.79715100	1.35153700
O	1.99405100	-3.94571200	-1.58844200
H	1.36335800	-4.52961200	-2.03658000

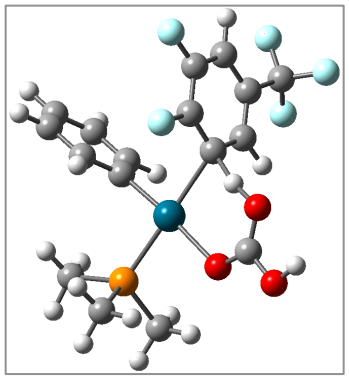

[Pd(O_2COH)(Ph)(39r)(PMe_3)]‡ ($TS^{Pd\text{-}c}$)

One imaginary frequency: i1011.22

E = -1852.865807 Hartree

G = -1852.610869 Hartree

Pd	-1.18562700	-0.27097000	-0.00398400
C	-0.39464200	3.78481400	1.16838400
C	-0.81871000	2.45107400	1.14753400
C	-0.59253500	1.64553400	0.02072600
C	0.06377300	2.20822400	-1.08465900
C	0.48505900	3.54272300	-1.06186300
C	0.25601400	4.33644000	0.06334200
H	-1.31225800	2.03863900	2.02352500
H	0.99745100	3.95748200	-1.92664600
H	0.58497100	5.37164800	0.08067500
H	-0.57193500	4.38954900	2.05453000
H	0.26273700	1.60616000	-1.96747900
P	-3.27578100	0.37586800	-0.74284700
C	-3.78151000	-0.58129000	-2.23303200
C	-3.61444700	2.12510400	-1.19495900
C	-4.58524900	-0.02604700	0.49008000
H	-4.82294900	-0.37621700	-2.50134700
H	-3.13445500	-0.31676200	-3.07346800
H	-3.65584000	-1.64487700	-2.01868200
H	-4.65408300	2.24707500	-1.51444000
H	-3.41290400	2.76909100	-0.33626700
H	-2.94431200	2.42929900	-2.00218000
H	-5.58313600	0.18541200	0.09196100
H	-4.51080000	-1.08564900	0.74592700
H	-4.42731000	0.56288800	1.39727300
O	-1.99375700	-2.32324700	-0.06658200
C	-1.38609600	-3.22485700	0.55164400
O	-0.24799400	-3.11399100	1.13053300
C	1.81469400	-0.95878000	-0.43516600
C	0.89727300	-0.82410300	0.63019100
C	1.37502800	-0.17818500	1.77069400
C	2.66787300	0.33459900	1.86277700
C	3.54359300	0.20815800	0.79662800
C	3.10948200	-0.44561600	-0.36353500
F	0.56703100	-0.01968500	2.83833100
H	0.17895500	-1.99940000	0.90699600
F	3.05923400	0.95839000	2.98766000
H	1.50348800	-1.47017300	-1.34112400
H	4.54285900	0.62015200	0.87677900
C	4.06737500	-0.64766100	-1.50414100
F	5.01392200	0.31708700	-1.54775400
F	4.72008700	-1.83073800	-1.41147900
F	3.43187200	-0.64779000	-2.69811900
O	-1.97762400	-4.43049300	0.61744000
H	-1.38106600	-5.01202000	1.11316800

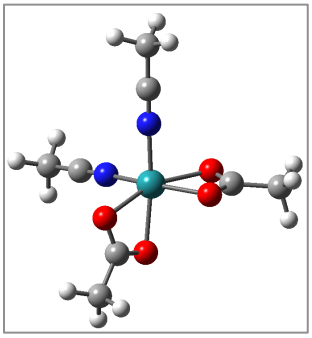

***cis*-Ru(κ^2-OAc)$_2$(MeCN)$_2$ (*cis*-M3)**

No imaginary frequencies

E = -817.5128659 Hartree

G = -817.364393 Hartree

Ru	-0.00005000	0.08310500	0.0000080
N	1.25064800	-1.27966900	-0.68972400

C	2.00839600	-2.04150100	-1.13033400
N	-1.25058100	-1.27988700	0.68963200
C	-2.00818600	-2.04187300	1.13022400
C	2.95242600	-2.98603500	-1.71440500
H	3.67857200	-2.45551400	-2.33814400
H	3.49408800	-3.52373200	-0.93011900
H	2.42580000	-3.71479300	-2.33844200
C	-2.95198600	-2.98678100	1.71408200
H	-3.75584100	-2.44828700	2.22550000
H	-3.39512700	-3.61791300	0.93761400
H	-2.44705200	-3.62964800	2.44188400
O	1.47103900	1.62306000	-0.26429700
C	1.89483000	1.42912200	0.92344800
C	2.95127400	2.31822700	1.52198200
H	3.48367100	1.79591200	2.31889000
H	3.64654900	2.65202900	0.74894900
H	2.46863900	3.20374700	1.94986300
O	1.37132100	0.48395200	1.60294900
O	-1.37132600	0.48418400	-1.60292200
C	-1.89492200	1.42922300	-0.92330700
O	-1.47125900	1.62295100	0.26451500
C	-2.95130900	2.31843100	-1.52178900
H	-3.64667800	2.65206000	-0.74876500
H	-2.46864200	3.20406500	-1.94940200
H	-3.48358900	1.79629000	-2.31888800

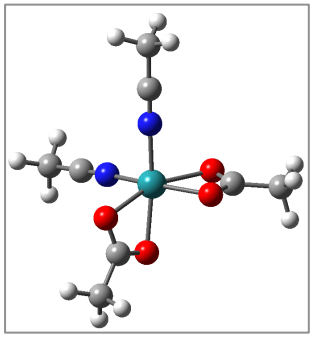

***trans*-Ru(κ^2-OAc)$_2$(MeCN)$_2$ (*trans*-M3)**

No imaginary frequencies

E = -817.5128646 Hartree

G = -817.368594 Hartree

Ru	-0.00661000	0.00027100	0.00000700
N	-2.00054500	-0.00140300	0.00002000
C	-3.15997100	-0.00267900	0.00000600
N	1.98715900	0.00152300	-0.00001700
C	3.14677700	0.00176600	-0.00002500
C	-4.61704700	-0.00479100	-0.00003900
H	-4.99607300	-0.51515100	-0.89065700
H	-4.99611400	-0.51922200	0.88821600
H	-4.99560000	1.02169000	0.00230800
C	4.60390200	0.00132900	-0.00002800
H	4.98158000	1.02816400	-0.00075900
H	4.98371300	-0.50988300	0.88979300
H	4.98370600	-0.51114300	-0.88912700
O	-0.00732500	-1.86077500	-1.09105200
C	-0.00172400	-2.51822800	0.00000100
C	0.04444200	-4.02456900	0.00000500
H	-0.43696300	-4.41811000	0.89734400
H	-0.43626700	-4.41810500	-0.89770500
H	1.08938500	-4.35382800	0.00043600
O	-0.00729000	-1.86077500	1.09105600
O	-0.01021400	1.86137100	-1.09105000
C	-0.00566700	2.51878600	0.00001500
O	-0.01017700	1.86136700	1.09107600
C	0.03799000	4.02523100	0.00000800
H	-0.44313800	4.41797500	0.89784400
H	1.08236100	4.35629200	-0.00066900
H	-0.44423100	4.41797700	-0.89724600

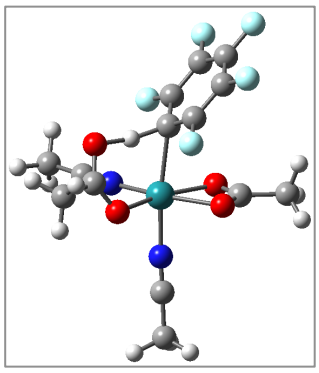

{[Ru(κ^2-OAc)$_2$(MeCN)$_2$]·C$_6$HF$_5$}‡ (TS3 *cis-fac*)

One imaginary frequency: i863.11

E = -1545.867826 Hartree

G = -1545.678837 Hartree

Ru	-1.08042200	-0.24291400	-0.0414930
O	-1.88899000	0.64517900	1.68698700
C	-1.36993800	1.71453000	2.13619500
O	-0.35756600	2.28438800	1.62341300
C	-1.98128500	2.32410100	3.37825000
H	-2.03921600	3.40998300	3.27208800
H	-2.96906800	1.90456700	3.57146600
H	-1.32922900	2.11045000	4.23168600
C	1.04274200	0.56574200	0.22761700
C	1.72158400	0.94873100	-0.93615700
C	1.83050100	-0.05994800	1.20592300
C	3.06738400	0.67691300	-1.15554300
C	3.17843900	-0.35042100	1.02919200
C	3.79657900	0.02312100	-0.16369500
F	1.07094600	1.59591500	-1.92147800
F	3.67470800	1.03677400	-2.29684900
F	1.27906500	-0.39441900	2.38257200
F	3.89367400	-0.96527100	1.98300000
F	5.09319800	-0.23980500	-0.35358100
H	0.20341400	1.39048000	0.78288600
N	-1.68831900	1.33031200	-1.08859900
C	-2.01434700	2.24172400	-1.72691500
N	-2.83088200	-1.16479500	-0.28818800
C	-3.83060400	-1.74120300	-0.39083100
C	-2.36046100	3.39173700	-2.55163100
H	-2.83113300	4.17152400	-1.94546200
H	-1.45481800	3.80226600	-3.00892500
H	-3.05225500	3.09894900	-3.34711500
C	-5.08716900	-2.47070000	-0.50447200
H	-5.32071200	-2.66753700	-1.55501500
H	-5.01439500	-3.42582400	0.02408600
H	-5.90292700	-1.88934500	-0.06475400
O	-0.29406900	-2.14047400	0.62482700
C	0.04900100	-2.42800100	-0.56888000
O	-0.20019400	-1.57770200	-1.48757300
C	0.76414800	-3.71616400	-0.87742100
H	1.82703300	-3.60014000	-0.63886500
H	0.36981900	-4.52379200	-0.25679500
H	0.66926700	-3.96283700	-1.93609000

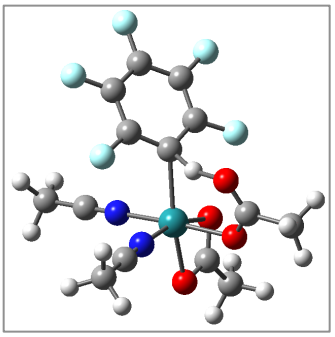

{[Ru(κ^2-OAc)$_2$(MeCN)$_2$]·C$_6$HF$_5$}‡ (TS3 *cis-mer*)

One imaginary frequency: i789.00

E = -1545.871638 Hartree

G = -1545.68335 Hartree

Ru	1.12402900	0.11168500	0.29871600
O	2.22879100	-0.96263400	-1.11874400
C	1.78845000	-1.06850100	-2.30765800
O	0.68156400	-0.59009700	-2.69931900
C	2.63079500	-1.84449100	-3.29609500
H	2.24884600	-2.86969200	-3.35078700
H	2.54682100	-1.40375700	-4.29154100
H	3.67247400	-1.87726500	-2.97428900

C	-0.92867400	-0.18283700	-0.65701500
C	-1.82226600	0.89558600	-0.70517700
C	-1.51795500	-1.43734600	-0.42886200
C	-3.18607100	0.76802100	-0.46738300
C	-2.87663800	-1.61028700	-0.18947900
C	-3.71413000	-0.49573400	-0.20931700
F	-1.37057200	2.13941700	-0.96436700
F	-3.99940100	1.83736100	-0.48718700
F	-0.75355300	-2.53813900	-0.44166000
F	-3.39540000	-2.82413000	0.04429300
F	-5.02449300	-0.63916000	0.01382500
H	-0.01069200	-0.24265100	-1.55844800
N	1.51551000	1.80096000	-0.67403700
C	1.81322600	2.76656400	-1.24224300
N	0.18476700	1.06678400	1.77636900
C	-0.34229700	1.58910700	2.66761400
C	2.17739200	3.97561200	-1.96899700
H	2.68250100	3.71376100	-2.90357900
H	1.28175600	4.55718300	-2.20752100
H	2.85107900	4.59472000	-1.36889500
C	-1.01196200	2.24218300	3.78560200
H	-1.48066500	1.49517600	4.43329000
H	-0.29241100	2.81647300	4.37680400
H	-1.78678600	2.92174600	3.41818500
O	1.24759300	-1.64188400	1.53105900
C	2.38810000	-1.26253900	1.95258100
O	2.82582100	-0.12756100	1.55843000
C	3.21461700	-2.13677200	2.85416100
H	3.81562800	-2.81203800	2.23563800
H	3.89079800	-1.53044600	3.45978400
H	2.56654200	-2.74369500	3.48958400

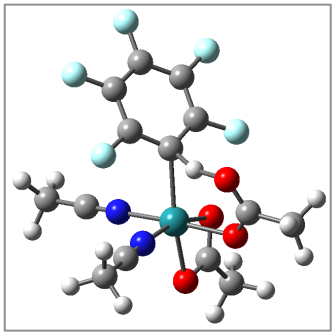

{[Ru(κ^2-OAc)$_2$(MeCN)$_2$]·C$_6$HF$_5$}‡ (TS3 *trans-mer*)

One imaginary frequency: i881.87

E = -1545.869318 Hartree

G = -1545.680318 Hartree

Ru	1.12045800	0.28390100	-0.12532500
O	1.66551300	1.05357600	1.75128400
C	1.12867700	0.55240300	2.79062000
O	0.22785300	-0.33939800	2.75793200
C	1.58215500	1.07307000	4.13648000
H	0.77129600	1.65778600	4.58278800
H	1.78716000	0.23513800	4.80778400
H	2.46728300	1.70111800	4.03235700
C	-0.97680400	-0.35839900	0.40501700
C	-1.41638200	-1.57359500	-0.14521000
C	-1.98943700	0.59558700	0.59683400
C	-2.72659100	-1.79922000	-0.55286400
C	-3.30955400	0.41157700	0.20505500
C	-3.68013000	-0.79830700	-0.37775800
F	-0.55316200	-2.58964100	-0.32840200
F	-3.08667200	-2.96802600	-1.10444300
F	-1.69718100	1.76510800	1.20392500
F	-4.22954800	1.37196200	0.39240500
F	-4.94612900	-1.00114200	-0.75778500
H	-0.18921300	-0.38094200	1.44450900
N	1.95475100	-1.47396100	0.36080900
C	2.47734000	-2.46847000	0.63922300
N	0.43261500	2.09890200	-0.63134600
C	0.09502700	3.16828400	-0.91710100
C	3.10598300	-3.73308700	0.99541500

H	2.65415800	-4.55009300	0.42501800
H	4.17763500	-3.70004000	0.77852000
H	2.96825800	-3.93177900	2.06237600
C	-0.35078500	4.51534600	-1.24579900
H	-0.62959800	4.57704300	-2.30172600
H	-1.22054000	4.77667800	-0.63561500
H	0.44828400	5.23609400	-1.04904800
O	2.84323400	0.70745500	-1.34219000
C	2.27311600	0.17999400	-2.35603000
O	1.09732100	-0.28770600	-2.21121000
C	2.98719700	0.08509200	-3.67843000
H	3.45745500	-0.90066300	-3.76355100
H	2.27463300	0.18887000	-4.49943100
H	3.76544600	0.84711800	-3.74645000

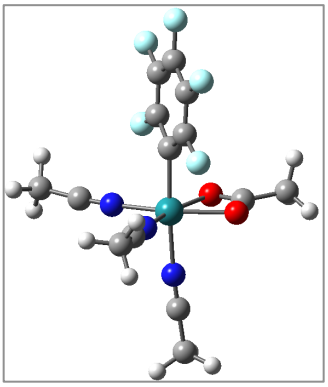

***fac*-[Ru(κ^2-OAc)(C_6F_5)($MeCN)_3$] (*fac*-M3)**

No imaginary frequencies

E = -1449.557092 Hartree

G = -1449.380049 Hartree

Ru	1.08747100	-0.00006500	-0.03180900
N	3.18948000	-0.00004500	-0.20161700
C	4.33457400	0.00014800	-0.38162500
N	1.12165400	-1.41429700	1.36223100
C	1.08389400	-2.29463500	2.11625400
N	1.12164400	1.41396700	1.36242100
C	1.08385000	2.29418200	2.11658700
C	-0.99539900	0.00003400	-0.01568300
C	-1.75617600	1.17151800	-0.04331900
C	-1.75622700	-1.17141700	-0.04346200
C	-3.14951100	1.19814900	-0.09065200
C	-3.14956300	-1.19799600	-0.09080200
C	-3.85601800	0.00009300	-0.11255700
F	-1.15051400	2.38822000	-0.02999100
F	-1.15061100	-2.38814500	-0.03028000
F	-3.81953600	2.36665100	-0.11078300
F	-5.19988700	0.00013000	-0.15227500
F	-3.81963300	-2.36646700	-0.11107900
C	5.77249000	0.00046300	-0.62377500
H	6.05307500	0.87161700	-1.22310600
H	6.31875700	0.03540400	0.32332800
H	6.06377400	-0.90521400	-1.16388500
C	0.97009700	-3.44113800	3.00825100
H	0.10536100	-4.04523100	2.71552900
H	1.86780800	-4.06426800	2.95196600
H	0.83529900	-3.11459600	4.04372100
C	0.97002300	3.44053400	3.00877200
H	1.86710600	4.06447700	2.95149100
H	0.10442200	4.04386500	2.71703800
H	0.83669100	3.11383900	4.04438400
O	1.00945500	1.09437800	-1.88459000
C	0.96055500	0.00003500	-2.53753100
O	1.00943600	-1.09436000	-1.88469100
C	0.80812600	0.00016600	-4.03517900
H	1.25402200	-0.89979200	-4.46323100
H	-0.25901400	0.00433500	-4.28297400
H	1.26073500	0.89659100	-4.46368100

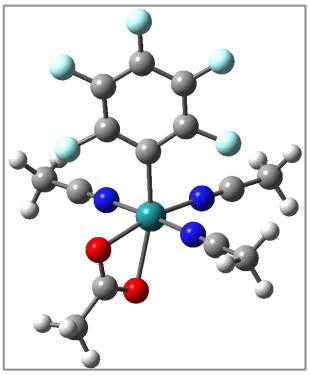

***mer*-[Ru(κ^2-OAc)(C_6F_5)($MeCN)_3$] (*mer*-M3)**

No imaginary frequencies

E = -1449.561357 Hartree

G = -1449.383707 Hartree

Ru	1.13133900	-0.13395500	0.1091040
N	1.01261900	-1.84379200	-0.93177500
C	0.94487700	-2.80814100	-1.56853300
N	0.86123200	-1.08346100	1.83443800
C	0.73562900	-1.64912600	2.83949000
N	1.30580700	1.61443100	1.07798600
C	1.41427300	2.64672500	1.59057200
C	-0.91668000	0.12450600	-0.08352300
C	-1.46881600	1.33489900	-0.51884200
C	-1.86764000	-0.87490700	0.14418900
C	-2.83278300	1.54778200	-0.71478700
C	-3.24006000	-0.71201900	-0.03841400
C	-3.73159500	0.51428700	-0.47173600
F	-0.66953900	2.39823700	-0.78653500
F	-1.48302000	-2.11267200	0.56656200
F	-3.29200400	2.74236500	-1.13288900
F	-5.05112400	0.69761600	-0.65140000
F	-4.09448700	-1.72625900	0.20148100
C	0.83414900	-4.01903300	-2.37081600
H	-0.05751600	-4.58147300	-2.07816600
H	0.75344100	-3.76069400	-3.43083600
H	1.71450400	-4.65300200	-2.22978600
C	0.55892400	-2.38019400	4.08766300
H	-0.33854400	-3.00426700	4.03301600
H	1.42289600	-3.02323400	4.28262000
H	0.44767600	-1.68421900	4.92459100
C	1.51931900	3.96687600	2.19739800
H	2.55760700	4.31114700	2.18415400
H	0.90382700	4.67881800	1.63902800
H	1.17165000	3.93948300	3.23421900
O	3.36779700	-0.07538600	-0.31004700
C	3.09496100	0.54723000	-1.38045900
O	1.87432400	0.79472500	-1.67290600
C	4.18884700	1.03027800	-2.30343500
H	3.88622700	0.90526000	-3.34583500
H	4.35742700	2.09940100	-2.13410300
H	5.11841800	0.49328400	-2.10797900

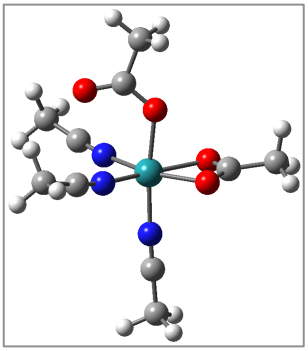

***fac*-Ru(κ^2-OAc)(κ^1-OAc)$(MeCN)_3$ (*fac*-M4)**

No imaginary frequencies

E = -950.2817677 Hartree

G = -950.095497 Hartree

Ru	-0.35095000	0.04598100	-0.0000010
N	-1.99123200	-1.10870900	0.00000100
C	-2.97199300	-1.72963200	-0.00000400
N	0.57041700	-1.02585900	1.40378200
C	1.21893500	-1.54583800	2.20937100
N	0.57042100	-1.02588000	-1.40376800
C	1.21895100	-1.54587600	-2.20933500
C	-4.21162900	-2.49683000	-0.00000200
H	-4.80581500	-2.25778700	-0.88740300
H	-3.99752300	-3.56988300	-0.00233500
H	-4.80371100	-2.26122400	0.88972200

C	2.12807000	-2.13286500	3.18322800
H	1.91743000	-1.74965300	4.18612700
H	2.03458200	-3.22266800	3.19655900
H	3.15401000	-1.86730200	2.90894400
C	2.12810900	-2.13292200	-3.18316000
H	1.91727600	-1.74999600	-4.18612700
H	3.15402000	-1.86707900	-2.90904400
H	2.03486000	-3.22274900	-3.19622100
O	-1.40576300	1.55813600	-1.09560500
C	-1.72088600	2.13114900	-0.00001200
O	-1.40576100	1.55814800	1.09558700
C	-2.41166600	3.46786900	-0.00001800
H	-3.02213800	3.58160900	0.89805600
H	-1.64993000	4.25498000	-0.00000700
H	-3.02211600	3.58161300	-0.89810600
O	1.18938700	1.42555600	-0.00000400
C	2.46282300	1.15596500	-0.00002200
O	2.99141900	0.03926000	-0.00005500
C	3.32084300	2.42423200	0.00001000
H	3.08958200	3.03252200	0.88022600
H	4.38096400	2.16463200	-0.00007200
H	3.08946900	3.03265200	-0.88008500

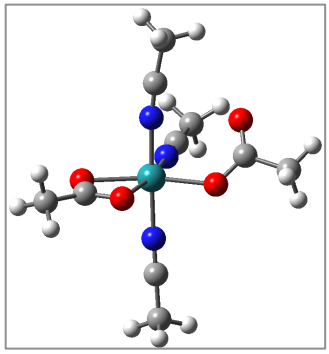

***mer*-Ru(κ^2-OAc)(κ^1-OAc)(MeCN)$_3$ (*mer*-M4)**

No imaginary frequencies

E = -950.27944 Hartree

G = -950.094136 Hartree

Ru	0.32757700	0.12075600	0.09254900
N	1.69615200	-1.33502200	-0.07106200
C	2.48578400	-2.16636700	-0.23411800
N	-0.71046200	-0.91631100	1.42618000
C	-1.37498500	-1.50273400	2.17225700
N	-1.04765900	1.58066500	0.14940700
C	-1.91033300	2.34943100	0.11625400
C	3.47873900	-3.20945400	-0.45621000
H	2.98583500	-4.17494300	-0.60362900
H	4.06968300	-2.97978600	-1.34789500
H	4.15281000	-3.28531300	0.40223100
C	-2.27779900	-2.23138700	3.05251000
H	-1.88644400	-3.23134800	3.26209600
H	-2.40454700	-1.70132200	4.00145400
H	-3.25468900	-2.32994700	2.56850000
C	-3.06022700	3.23715600	0.02753700
H	-3.27106000	3.69658600	0.99753000
H	-2.87646600	4.02864600	-0.70473600
H	-3.93029200	2.65360000	-0.28921500
O	1.75229800	1.37113000	1.18146500
C	2.16617100	1.85308800	0.07706700
O	1.64556300	1.43337600	-1.00889000
C	3.22834500	2.92346000	0.05056900
H	3.88222200	2.78372300	-0.81320800
H	2.74940800	3.90383400	-0.04775800
H	3.80733500	2.91043500	0.97554800
O	-0.67988400	-0.83343000	-1.45391000
C	-1.97143400	-0.97132300	-1.54140200
O	-2.82066700	-0.61669100	-0.71825300
C	-2.38858300	-1.65710200	-2.84685200
H	-1.91133400	-2.63903400	-2.92661900
H	-3.47340300	-1.77145300	-2.88295500
H	-2.05121000	-1.06593900	-3.70414400

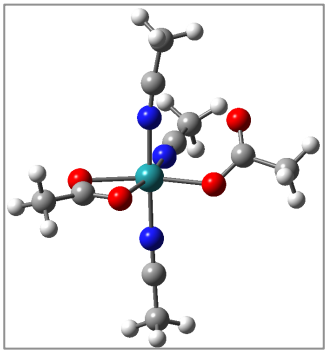

{[Ru(κ^2-OAc)(κ^1-OAc)(MeCN)$_3$]·C$_6$HF$_5$}‡

(TS4 *fac-cis*)

One imaginary frequency: i939.57

E = -1678.634087 Hartree

G = -1678.405054 Hartree

Ru	1.00457600	0.16843300	0.0649710
O	1.67919400	1.05909500	-1.72404400
C	1.04834800	2.04495500	-2.20980700
O	-0.01783400	2.53040000	-1.71013300
C	1.57840400	2.66390800	-3.48385100
H	0.99243200	2.28056600	-4.32601800
H	1.45238600	3.74855500	-3.45825200
H	2.62573100	2.40046400	-3.63575500
C	-1.23557700	0.69563800	-0.31406100
C	-1.98168200	0.95469200	0.84113500
C	-1.91248400	-0.01980000	-1.31390900
C	-3.26799500	0.46942200	1.04616200
C	-3.20075300	-0.52041900	-1.15476100
C	-3.87771500	-0.27578800	0.03834400
F	-1.45156600	1.68306300	1.84697500
F	-3.93143300	0.70844000	2.19095100
F	-1.33179200	-0.21177700	-2.50389200
F	-3.80752000	-1.21153300	-2.13118500
F	-5.11896800	-0.74162300	0.21218300
H	-0.49571700	1.62917300	-0.86922300
N	1.35162100	1.89527600	1.04965400
C	1.54175600	2.89748400	1.59998600
N	2.87512000	-0.48430300	0.33613200
C	3.88840700	-1.03228600	0.42476300
N	0.42977000	-0.81636700	1.71309500
C	0.14423900	-1.52509800	2.58117300
C	1.73737000	4.16981600	2.28281500
H	2.54377800	4.09214300	3.01798900
H	1.99480300	4.95012400	1.56031300
H	0.81750200	4.46127100	2.79888500
C	5.09131600	-1.84708400	0.50711100
H	5.75916400	-1.63195400	-0.33177000
H	5.62629400	-1.66143700	1.44264400
H	4.78921700	-2.89854600	0.46675600
C	-0.18766400	-2.50800500	3.60230800
H	0.12384600	-3.49538900	3.24710400
H	0.33083500	-2.28458100	4.53904500
H	-1.26518200	-2.51812300	3.79024800
O	0.63168000	-1.54212200	-1.05411900
C	1.00337900	-2.75405700	-0.76156500
O	1.61385500	-3.13192600	0.24601000
C	0.61011300	-3.75392400	-1.85204600
H	0.81122200	-4.77459900	-1.52170000
H	-0.44724300	-3.64289900	-2.10893700
H	1.18360300	-3.54751500	-2.76198500

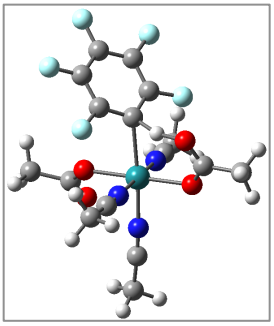

{[Ru(κ^2-OAc)(κ^1-OAc)(MeCN)$_3$]·C$_6$HF$_5$}‡

(TS4 *mer-cis*)

One imaginary frequency: i959.45

E = -1678.635181 Hartree

G = -1678.406554 Hartree

Ru	-1.00964100	0.09706300	0.12538400
O	-1.64078500	1.08672800	1.91069800
C	-0.98498700	2.09108900	2.31797600
O	0.08100900	2.52147700	1.76986300
C	-1.48372900	2.81756400	3.54846200
H	-0.80363300	2.61279100	4.38174900
H	-1.47000700	3.89655400	3.37443800
H	-2.48866000	2.48772900	3.81347600
C	1.23651400	0.68671400	0.30736100
C	1.87246400	1.02190800	-0.89513100
C	2.02474700	-0.04448800	1.20537600
C	3.15497400	0.59716900	-1.22566500
C	3.30877500	-0.49217600	0.92027400
C	3.87419400	-0.16937000	-0.31180500
F	1.25300900	1.79181700	-1.80667700
F	3.71328900	0.92178300	-2.40234800
F	1.54258000	-0.33801300	2.43114700
F	4.01281000	-1.21264500	1.80971100
F	5.11121700	-0.58058600	-0.60836700
H	0.51110600	1.59400600	0.93609100
N	-1.43462700	1.73775200	-0.95894100
C	-1.66110000	2.66586900	-1.61108600
N	-2.87555100	-0.56202500	-0.13380400
C	-3.91182100	-1.03852100	-0.32137000
N	-0.64079600	-1.59319900	1.15611700
C	-0.48190000	-2.61474900	1.67098700
C	-1.88294700	3.83950300	-2.44431800
H	-0.93087500	4.16735300	-2.87253900
H	-2.57246700	3.60345300	-3.25994100
H	-2.30308600	4.65674500	-1.85087500
C	-5.16172400	-1.72518000	-0.61397800
H	-4.93660500	-2.65159500	-1.15172700
H	-5.69362200	-1.96794100	0.31041900
H	-5.80795600	-1.09985200	-1.23656100
C	-0.27007500	-3.92765400	2.26197000
H	-0.40997900	-4.69562700	1.49520600
H	0.74506200	-4.00241100	2.66254700
H	-0.98200600	-4.10111800	3.07399200
O	-0.37799500	-0.80555900	-1.65185200
C	-0.73610800	-1.99335800	-2.04788600
O	-1.49117000	-2.77937900	-1.46750600
C	-0.10106000	-2.36902900	-3.39022400
H	-0.40686700	-3.37421900	-3.68524400
H	-0.40125000	-1.65193500	-4.16106200
H	0.98997300	-2.32147600	-3.31692100

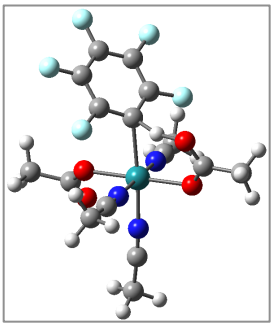

{[Ru(κ^2-OAc)(κ^1-OAc)(MeCN)$_3$]·C$_6$HF$_5$}‡

(TS4 *mer-trans*)

One imaginary frequency: i919.56

E = -1678.637241 Hartree

G = -1678.408426 Hartree

Ru	0.86916100	0.27809000	-0.05933600
O	1.36763600	1.82414300	1.28472200
C	0.75273700	1.90290700	2.39148300
O	-0.21587200	1.14990300	2.72677300
C	1.18512800	2.97850600	3.36408300
H	0.42482400	3.76634900	3.38362200
H	1.25047900	2.56296600	4.37273100
H	2.14172100	3.40791900	3.06530400
C	-1.35672400	0.03155400	0.65041700
C	-1.83652400	-1.28065700	0.74637600
C	-2.29802800	0.96683300	0.20030500
C	-3.11371800	-1.66289800	0.34835400
C	-3.58453400	0.63413000	-0.20817000

C	-3.99304900	-0.69604000	-0.13422500
F	-1.04459400	-2.26126400	1.22232900
F	-3.51209800	-2.94327000	0.42587300
F	-1.97372200	2.27569000	0.15642800
F	-4.43802900	1.56877100	-0.65733900
F	-5.22662400	-1.04141600	-0.51836200
H	-0.61784100	0.50503600	1.62091900
N	1.59577800	-1.05803600	1.25807200
C	2.11269800	-1.82426000	1.95029600
N	0.54970400	-1.18661000	-1.38733800
C	0.51274600	-2.06563100	-2.13828100
N	0.32917500	1.68782100	-1.39378300
C	0.12337400	2.54286500	-2.14451800
C	2.80235500	-2.80780300	2.77140200
H	3.19572600	-2.33929900	3.67803200
H	2.11741100	-3.61084400	3.05840200
H	3.63307600	-3.23266300	2.19983300
C	0.58987100	-3.19032400	-3.05943700
H	0.26215300	-2.89489600	-4.06023600
H	1.62967600	-3.52887500	-3.10876800
H	-0.03890200	-4.01558700	-2.71293500
C	-0.14784300	3.63954200	-3.06390900
H	-0.22365600	3.26813800	-4.08991400
H	-1.08839200	4.12927300	-2.79461000
H	0.66038600	4.37507500	-3.01535200
O	2.77233100	0.58134100	-0.82578100
C	3.62325100	-0.36414000	-1.10928400
O	3.45083700	-1.58261700	-1.01637600
C	4.96009300	0.20232000	-1.59793100
H	5.63868000	-0.61046700	-1.86221400
H	4.80296200	0.85071100	-2.46550700
H	5.41117100	0.81880800	-0.81399200

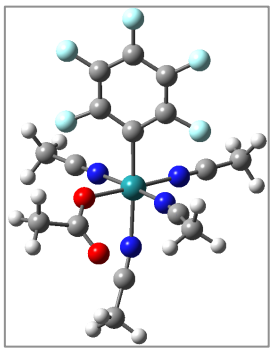

***cis*-[Ru(κ^1-OAc)(C_6F_5)($MeCN)_4$] (*cis*-P4)**

No imaginary frequencies

E = -1582.322308 Hartree

G = -1582.102974 Hartree

Ru	0.82707800	-0.12486900	0.46131400
N	1.03447700	-1.53822000	-0.95984000
C	1.24138100	-2.20915900	-1.87678900
N	2.95050200	-0.22663300	0.75976700
C	4.06131600	-0.17298900	0.44098000
N	0.40423100	-1.45748700	1.89524100
C	0.13714800	-2.25026700	2.69861300
N	0.67043500	1.40325600	1.76237200
C	0.56420000	2.33769500	2.43614200
C	-1.20276300	0.03545100	-0.01400300
C	-1.87038900	1.25278600	-0.19213200
C	-2.02255400	-1.08154200	-0.20433700
C	-3.21687900	1.36194500	-0.54124400
C	-3.37083200	-1.02434400	-0.55434100
C	-3.97823100	0.21371100	-0.72812500
F	-1.23107300	2.43501800	-0.01757500
F	-1.52509100	-2.34111800	-0.04592900
F	-3.79266400	2.57038700	-0.69239400
F	-5.27784000	0.29980500	-1.06222000
F	-4.09058300	-2.15195400	-0.72133000
C	1.55315500	-2.95830800	-3.08445500
H	0.64205400	-3.16361200	-3.65373900
H	2.23212500	-2.35536900	-3.69562600
H	2.03713600	-3.90797100	-2.83938900
C	-0.23661400	-3.26468700	3.67608100

H	-1.03528400	-3.89410500	3.27117900
H	0.62052400	-3.89957300	3.92047200
H	-0.59610100	-2.79500500	4.59664300
C	0.38080800	3.54682200	3.22719100
H	1.31522400	4.11285300	3.28294700
H	-0.38315600	4.17347900	2.75673100
H	0.05838200	3.29885400	4.24261600
C	5.40179100	-0.05766800	-0.11274900
H	5.94113100	-1.00562200	-0.03517100
H	5.27086700	0.21030300	-1.16683600
H	5.97245100	0.72063800	0.40123000
O	1.23354400	1.31857300	-1.01660000
C	2.12156100	1.28415300	-1.95767300
O	2.95821800	0.39502300	-2.18809400
C	2.06099900	2.52368800	-2.85745100
H	2.11124900	3.43472000	-2.25345900
H	2.87757900	2.51064100	-3.58192100
H	1.10344700	2.54587400	-3.38793600

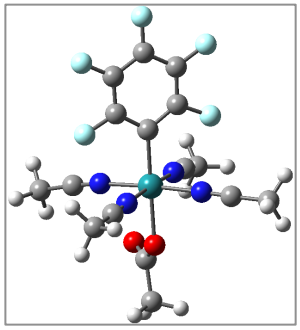

***trans*-[Ru(κ^1-OAc)(C_6F_5)($MeCN)_4$] (*trans*-P4)**

No imaginary frequencies

E = -1582.325198 Hartree

G = -1582.108401 Hartree

Ru	-0.77158200	-0.00001400	0.24737800
N	-0.62452200	1.42207800	1.6607740
C	-0.58000700	2.25288000	2.46474800
N	-0.62447300	-1.42221300	1.66067500
C	-0.57984500	-2.25311500	2.46453700
N	-1.05840300	-1.39627800	-1.17718500
C	-1.37832600	-2.12036300	-2.01793900
N	-1.05830800	1.39632900	-1.17711400
C	-1.37807800	2.12047900	-2.01787000
C	1.31099000	0.00000100	-0.05409000
C	2.07027000	1.16777800	-0.16792600
C	2.07028500	-1.16775800	-0.16801900
C	3.44896700	1.19686500	-0.37330700
C	3.44898100	-1.19681000	-0.37340000
C	4.14992800	0.00003600	-0.47751600
F	1.47322500	2.38927100	-0.07888500
F	1.47325800	-2.38926800	-0.07907200
F	4.11062700	2.36679900	-0.47035700
F	5.48012500	0.00005000	-0.67456000
F	4.11065800	-2.36672900	-0.47054100
C	-0.50359200	-3.31673500	3.45735800
H	0.25983000	-4.04484100	3.16705200
H	-0.24074100	-2.90498400	4.43614500
H	-1.46709000	-3.82820200	3.54036300
C	-1.88440400	-2.98013600	-3.07723400
H	-1.91566300	-4.02153800	-2.74463900
H	-2.89704500	-2.65406300	-3.33475000
H	-1.24815500	-2.91423000	-3.96439600
C	-1.88396000	2.98036800	-3.07716600
H	-2.89668400	2.65454200	-3.33466700
H	-1.91496500	4.02177900	-2.74457300
H	-1.24773500	2.91431200	-3.96433300
C	-0.50394000	3.31636800	3.45772500
H	-0.23805000	2.90489800	4.43580900
H	0.25726000	4.04622700	3.16599100
H	-1.46837200	3.82570100	3.54297900
O	-2.90664900	-0.00006800	0.66018200
C	-3.83843000	0.00002500	-0.23903800
O	-3.69871500	0.00011300	-1.47101500
C	-5.24984100	0.00007900	0.36657500
H	-6.00533500	-0.00031600	-0.42152200
H	-5.38481800	-0.87952700	1.00469600

H	-5.38501600	0.88022200	1.00392500

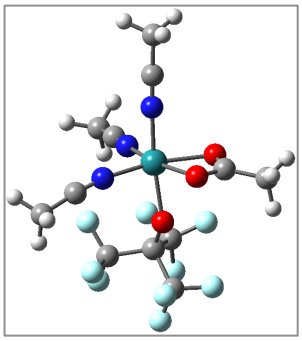

***fac*-Ru(κ^2-OAc)(OC(CF_3)$_3$)($MeCN$)$_3$ (*fac*-M5)**

No imaginary frequencies

E = -1848.002454 Hartree

G = -1847.820988 Hartree

Ru	1.44143700	0.08927300	-0.11080900
N	3.42097500	-0.09822500	-0.00686900
C	4.57851600	-0.14992600	0.05498500
N	1.22647300	-1.32063500	-1.51285000
C	0.93168000	-2.03422800	-2.37605000
N	1.20968200	-1.22953100	1.36476600
C	1.04747300	-1.92551200	2.27634800
C	6.03364800	-0.19940300	0.12708000
H	6.38451700	0.27104100	1.05071200
H	6.38271100	-1.23624000	0.10814800
H	6.47160800	0.33199700	-0.72334400
C	0.46454200	-2.89456700	-3.45427700
H	-0.62481100	-2.97400000	-3.38831600
H	0.73022600	-2.46705400	-4.42557900
H	0.90229600	-3.89365600	-3.37449300
C	0.74393400	-2.75647200	3.43318700
H	1.39139000	-2.49532900	4.27544900
H	-0.29804000	-2.59167800	3.72413400
H	0.88232000	-3.81539500	3.19639200
O	1.56690400	1.94179400	0.93031800
C	1.61113700	2.56803100	-0.18258900
O	1.68729700	1.88094400	-1.25447800
C	1.53305600	4.06779900	-0.22645200
H	2.05905800	4.45171200	-1.10282400
H	0.47914500	4.35596800	-0.30347200
H	1.94168400	4.49865900	0.68971700
O	-0.56871400	0.56737100	-0.41479200
C	-1.79353900	0.18979900	-0.02384200
C	-2.05301500	0.39167800	1.51916600
C	-2.13910600	-1.29802300	-0.38681500
C	-2.79790600	1.12386300	-0.79732300
F	-1.56804900	-0.65006100	2.24684800
F	-1.44373400	1.49677000	1.95801800
F	-3.36434000	0.48943500	1.82734800
F	-1.20160500	-2.15446000	0.07027700
F	-3.32326500	-1.70715800	0.11469500
F	-2.18979500	-1.46586200	-1.72958600
F	-2.48436200	1.18501400	-2.09863000
F	-4.08379300	0.71492000	-0.71320700
F	-2.73790900	2.37535300	-0.30189000

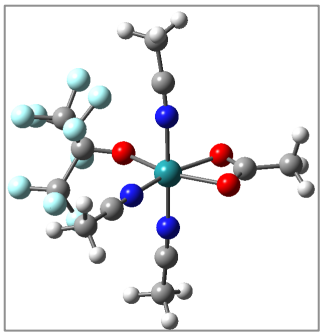

***mer*-Ru(κ^2-OAc)(OC(CF_3)$_3$)($MeCN$)$_3$ (*mer*-M5)**

No imaginary frequencies

E = -1848.000765 Hartree

G = -1847.82105 Hartree

Ru	1.48740600	0.02766000	0.09710000
N	1.56492000	-1.96760400	-0.10646900
C	1.51588400	-3.10633200	-0.30396200
N	0.99830800	-0.14336500	2.00619900
C	0.76915100	-0.24824400	3.13783500
N	1.30301200	2.02843000	0.14689900

C	1.05489300	3.15613900	0.07696900
C	1.39648400	-4.53280300	-0.57116000
H	0.34544300	-4.82831000	-0.49993900
H	1.75753400	-4.75726000	-1.57899700
H	1.97997400	-5.11133900	0.15074300
C	0.42972800	-0.38609700	4.54760100
H	-0.59838200	-0.74766500	4.64958800
H	1.10362200	-1.09497500	5.03825900
H	0.51251300	0.58017700	5.05419100
C	0.65287700	4.55122700	-0.03317200
H	1.05545300	4.98992800	-0.95061300
H	-0.43974700	4.59900100	-0.06705400
H	1.01233300	5.12791500	0.82370400
O	3.63673900	0.14833900	0.16494100
C	3.68459400	0.24895100	-1.10825800
O	2.59161800	0.22381100	-1.76045800
C	5.00332600	0.42871800	-1.81387500
H	4.95530000	0.00198900	-2.81757400
H	5.21770400	1.49900100	-1.90853200
H	5.80887300	-0.03130000	-1.23832200
O	-0.42716100	-0.03690400	-0.76636700
C	-1.71827200	-0.03566300	-0.40508400
C	-2.13570900	-1.30347400	0.43117300
C	-2.14499400	1.24391200	0.40060300
C	-2.54108200	-0.05974100	-1.74777600
F	-1.73551700	-1.20229000	1.72211100
F	-3.46801100	-1.51635100	0.45443000
F	-1.56034100	-2.41191800	-0.06894600
F	-2.42443600	-1.26262900	-2.34313300
F	-3.86096900	0.17503500	-1.56925500
F	-2.08315600	0.86462600	-2.60140800
F	-2.03793700	2.35112200	-0.37046300
F	-3.41434400	1.19127500	0.85651200
F	-1.35206800	1.44580000	1.47297800

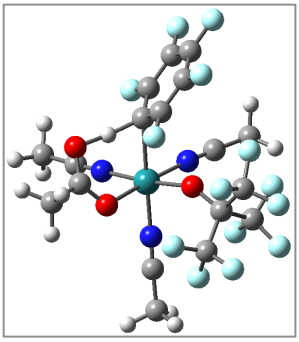

{[Ru(OAc)(OC(CF$_3$)$_3$)(MeCN)$_3$]·C$_6$F$_5$}‡ (TS5 *fac-cis*)

One imaginary frequency: i993.92

E = -2576.35387 Hartree

G = -2576.129488 Hartree

Ru	-0.38946500	1.24970100	0.12861600
O	0.01032300	1.94600500	-1.81559400
C	-0.90353900	1.95241900	-2.69292400
O	-2.08745000	1.52139500	-2.49913500
C	-0.55708200	2.47498000	-4.06778300
H	-0.34430700	1.61943200	-4.71765400
H	-1.40577300	3.01450400	-4.49354000
H	0.32724100	3.11188900	-4.02794200
C	-2.02595500	-0.25430700	-0.60154800
C	-3.04560600	-0.48238200	0.32877100
C	-1.59427600	-1.39112300	-1.30322000
C	-3.54515800	-1.74469800	0.62386300
C	-2.06806900	-2.67322500	-1.04654000
C	-3.04702900	-2.84638100	-0.07053500
F	-3.57484400	0.54699200	1.02801400
F	-4.49522700	-1.92057800	1.56018600
F	-0.71536100	-1.26244300	-2.30299800
F	-1.62073000	-3.73360300	-1.73111400
F	-3.52343000	-4.06738900	0.19140000
H	-2.05673500	0.77679900	-1.43519200
N	-1.73340400	2.71256100	0.35951700
C	-2.52309000	3.55327700	0.47167300
N	1.05772600	2.49358000	0.72833300
C	1.92418900	3.21078600	0.99643000

N	-0.65323600	0.52486700	1.98269000
C	-0.70786800	-0.00608900	3.00917700
C	-3.55331200	4.57622800	0.59523900
H	-3.25685800	5.33546000	1.32487700
H	-3.72015900	5.06242400	-0.37064900
H	-4.49205000	4.11984800	0.92369600
C	3.08052900	4.04178700	1.30076800
H	3.02691500	4.98795900	0.75490500
H	3.13152100	4.25277300	2.37268300
H	3.98687900	3.50839500	0.99911000
C	-0.71710300	-0.73581900	4.26945200
H	0.16611000	-1.38049000	4.30557800
H	-0.69370200	-0.04583000	5.11757200
H	-1.61482300	-1.35660500	4.34180400
O	0.84810400	-0.41102000	-0.19543700
C	2.10265700	-0.84276300	-0.02264300
C	2.55216700	-0.87620400	1.48247500
C	2.13020100	-2.32261200	-0.56693600
C	3.17349100	-0.02246000	-0.83802800
F	1.83175300	-1.78995700	2.17643200
F	2.34524400	0.31218600	2.09022800
F	3.85513200	-1.18002600	1.64886500
F	3.52643300	1.11908000	-0.18601000
F	2.68834900	0.33641700	-2.02875700
F	4.31813400	-0.70909100	-1.04379400
F	3.23377100	-3.00746800	-0.19318700
F	2.08360500	-2.32791300	-1.91004800
F	1.06560500	-3.00843100	-0.11843700

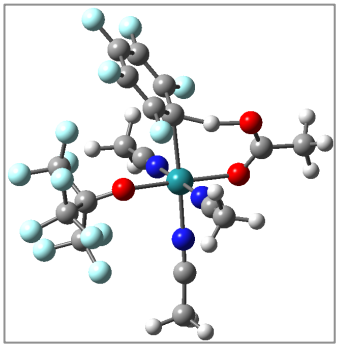

{[Ru(OAc)(OC(CF$_3$)$_3$)(MeCN)$_3$]·C$_6$F$_5$}‡

(TS5 *mer-cis*)

One imaginary frequency: i960.28

E = -2576.354908 Hartree

G = -2576.131142 Hartree

Ru	0.34161100	-1.36264300	-0.05860200
O	1.67244700	-2.96587400	-0.44747600
C	2.81401800	-2.97587600	0.10540000
O	3.26229500	-2.03503500	0.83477000
C	3.70817400	-4.17225700	-0.13193800
H	4.55576900	-3.86485600	-0.75279800
H	4.11330300	-4.52542200	0.81993000
H	3.16273500	-4.97269200	-0.63235000
C	2.01067200	0.20647100	0.36662400
C	1.78495800	1.09814000	1.42512800
C	2.68944100	0.75910600	-0.72830800
C	2.13302600	2.44371000	1.37979500
C	3.04868500	2.09688100	-0.82352000
C	2.76022900	2.94602900	0.24284200
F	1.22230800	0.67574700	2.56922200
F	1.87754000	3.26143200	2.41080400
F	3.05752800	-0.03585400	-1.75757900
F	3.67918900	2.57668900	-1.90860100
F	3.10193400	4.23568700	0.18008400
H	2.48878600	-0.99166300	0.65470800
N	0.24063100	-1.86726000	1.89642000
C	0.13324200	-2.09047900	3.02496400
N	-1.14788200	-2.64693200	-0.41725000

C	-2.02968700	-3.37312000	-0.59888600
N	0.39566700	-0.87151800	-2.00482700
C	0.41822100	-0.57364600	-3.12094200
C	0.01812200	-2.30077400	4.46101100
H	0.49658900	-1.46890700	4.98651700
H	-1.03519900	-2.34110700	4.75256000
H	0.50611300	-3.23452100	4.75430000
C	-3.20052600	-4.20829200	-0.82790500
H	-3.13905800	-4.69359000	-1.80610600
H	-3.27890500	-4.97992300	-0.05683300
H	-4.09605500	-3.58013100	-0.79600000
C	0.44904500	-0.12647600	-4.50535300
H	-0.23417300	0.71914100	-4.62847000
H	1.46165800	0.19350300	-4.76815600
H	0.14520500	-0.93284300	-5.17860100
O	-0.97783000	0.19614400	0.51326200
C	-2.01022400	0.91087000	0.04714600
C	-1.54482200	2.12160800	-0.85182700
C	-3.07826300	0.09707200	-0.76682900
C	-2.72634300	1.50518400	1.31976500
F	-0.45278500	2.70077900	-0.33169200
F	-1.21358900	1.71282200	-2.10379200
F	-2.48697000	3.07639500	-0.99366000
F	-1.93469600	2.41611100	1.91375300
F	-2.97045900	0.53246100	2.21514500
F	-3.90648600	2.10602600	1.05361200
F	-2.52726000	-0.55246600	-1.81387400
F	-4.06415900	0.87015300	-1.26683200
F	-3.66205900	-0.84459600	0.01140000

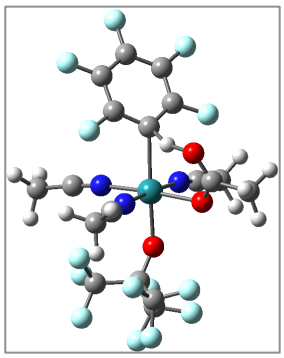

{[Ru(OAc)(OC(CF$_3$)$_3$)(MeCN)$_3$]·C$_6$F$_5$}‡

(TS5 *mer-trans*)

One imaginary frequency: i740.42

E = -2576.356679 Hartree

G = -2576.132428 Hartree

Ru	-0.28874700	0.23218700	0.1623500
O	0.02632800	1.78657600	1.53586700
C	-0.73002400	1.88065000	2.55360100
O	-1.73073800	1.13041200	2.76935700
C	-0.42249500	2.97654400	3.55083000
H	-1.17461700	3.76639700	3.45277800
H	-0.49211700	2.58341100	4.56811200
H	0.56734800	3.39639900	3.37068100
C	-2.58418000	0.05916000	0.52020700
C	-3.12623900	-1.23373800	0.51158200
C	-3.41261200	1.04944000	-0.02908700
C	-4.35028900	-1.54585200	-0.06985500
C	-4.64290100	0.78392100	-0.61900400
C	-5.11284900	-0.52795300	-0.63944200
F	-2.44746400	-2.26034300	1.05788100
F	-4.80801800	-2.80747600	-0.08797700
F	-3.02883200	2.33915100	0.01283100
F	-5.38589300	1.76541700	-1.15262800
F	-6.29391400	-0.80827400	-1.19771100
H	-1.98551300	0.47720000	1.57083500
N	0.11729400	-1.07507200	1.63241200
C	0.37147300	-1.77210000	2.51776200
N	-0.44591000	-1.21993900	-1.21597900

C	-0.40838700	-2.04281800	-2.02902200
N	-0.58865500	1.64530600	-1.26007500
C	-0.60887800	2.49613900	-2.04073000
C	0.74059200	-2.63447300	3.62991700
H	0.26579300	-2.28463500	4.55111300
H	0.42178300	-3.66259300	3.43643400
H	1.82691800	-2.61503900	3.75809700
C	-0.26668800	-3.08341400	-3.03821700
H	-0.71814300	-2.76788800	-3.98308900
H	0.79892200	-3.27329800	-3.19833900
H	-0.75005900	-4.00697600	-2.70704000
C	-0.62096300	3.58769100	-3.00454600
H	-0.71342400	3.19655800	-4.02163700
H	-1.46197000	4.25751500	-2.80355500
H	0.31173800	4.15395400	-2.92841300
O	1.68045600	0.54703300	-0.50015700
C	2.90522100	0.01623300	-0.36019700
C	3.00216400	-1.49799900	-0.76396500
C	3.82505400	0.83621400	-1.34321200
C	3.50219400	0.17787700	1.09070400
F	3.24458300	0.95078200	-2.54925700
F	4.02188800	2.08002900	-0.86802000
F	5.03892200	0.27764100	-1.53755700
F	3.14449000	1.35018200	1.62027700
F	4.85111400	0.10476800	1.11341800
F	3.05309400	-0.79557200	1.92610800
F	2.74240100	-1.65883000	-2.08404000
F	2.10239000	-2.25402300	-0.10232000
F	4.21630500	-2.03396600	-0.52526800

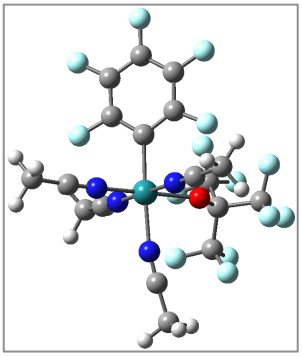

***cis*-Ru(C_6F_5)($OC(CF_3)_3$)($MeCN)_4$] (*cis*-P5)**

No imaginary frequencies

E = -2480.041832 Hartree

G = -2479.829319 Hartree

Ru	0.27643800	1.25087400	0.31019600
N	0.18076300	1.35752800	-1.69360100
C	0.13908300	1.36830900	-2.84826800
N	-1.37169700	2.59899500	0.50628400
C	-2.38607200	3.14638400	0.60611200
N	1.62718700	2.71100300	0.35601300
C	2.44181000	3.53649400	0.35890700
N	0.33254200	1.06643100	2.32691500
C	0.30261500	0.82947500	3.45732400
C	1.82737200	-0.14951300	0.14444600
C	1.92203800	-1.30449000	0.93093000
C	2.88090600	-0.01199500	-0.76462800
C	2.94662500	-2.24462700	0.81980900
C	3.92461000	-0.92389400	-0.91527800
C	3.95955600	-2.05822700	-0.11400700
F	0.99930600	-1.58547500	1.88115100
F	2.95428600	1.07485800	-1.58830600
F	2.97002800	-3.33142500	1.61360900
F	4.95703500	-2.95095100	-0.23256900
F	4.90094400	-0.71238500	-1.82037700
C	0.08275900	1.29649800	-4.30068900
H	1.09322500	1.20601100	-4.71004200
H	-0.49851100	0.41663100	-4.59178800
H	-0.39114800	2.19017300	-4.71642400

C	3.50034600	4.53798900	0.33463300
H	4.28788300	4.22773700	-0.35926800
H	3.10934300	5.50757400	0.01151400
H	3.93908400	4.65318900	1.33037100
C	0.26866400	0.43034300	4.85713200
H	-0.74574800	0.52781500	5.25407600
H	0.57757400	-0.61668400	4.93375300
H	0.94579100	1.04725600	5.45446200
C	-3.70910300	3.74894500	0.70353700
H	-3.79940100	4.59504800	0.01673700
H	-4.45177700	2.99007300	0.44125200
H	-3.89851900	4.09731000	1.72261400
O	-1.18820900	-0.26824400	0.49453100
C	-2.08142500	-0.98242200	-0.19267100
C	-3.23951300	-0.11184600	-0.80748800
C	-1.46989900	-1.85109100	-1.36097700
C	-2.72915400	-1.98102500	0.84120300
F	-2.75625600	0.91722600	-1.53561000
F	-3.99850500	0.43870900	0.17362600
F	-4.07173100	-0.80529300	-1.61172000
F	-1.29211500	-1.11320700	-2.49016400
F	-2.25569100	-2.89198200	-1.71094300
F	-0.27340700	-2.33887500	-1.01724000
F	-3.85953200	-2.56994000	0.38826100
F	-1.85968700	-2.95880200	1.15292900
F	-3.04737400	-1.34181000	1.97940200

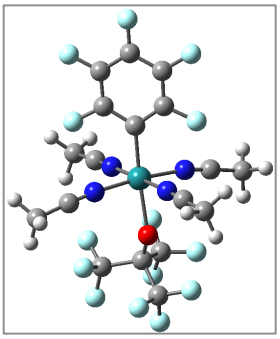

***trans*-Ru(C_6F_5)($OC(CF_3)_3$)($MeCN)_4$] (*trans*-P5)**

No imaginary frequencies

E = -2480.050539 Hartree

G = -2479.838312 Hartree

Ru	0.43676000	-0.10417600	0.14263800
N	0.36941400	1.34754300	1.53634900
C	0.19658200	2.17821300	2.32127600
N	0.54513600	-1.48537200	1.61355900
C	0.53114400	-2.28371500	2.44883100
N	0.29429100	-1.56323100	-1.24047400
C	0.04327100	-2.38675500	-2.01166800
N	0.29813000	1.27335300	-1.31428400
C	0.21601500	2.07820800	-2.13951500
C	2.51811100	-0.00886800	0.00496900
C	3.24047700	1.18769900	-0.03492600
C	3.32695900	-1.14852800	-0.04828300
C	4.62984400	1.26660700	-0.11959700
C	4.71823300	-1.12501500	-0.13253200
C	5.38109300	0.09727700	-0.16886500
F	2.59537400	2.38629700	0.01057700
F	2.76967800	-2.39018200	-0.01689900
F	5.25263800	2.46026000	-0.15300400
F	6.72152500	0.14799900	-0.25010000
F	5.42685100	-2.26922100	-0.17858300
C	0.50858500	-3.30267800	3.48958100
H	1.21479600	-4.10236900	3.24787500
H	0.78772900	-2.86686300	4.45316400
H	-0.49582600	-3.72775100	3.57323500

C	-0.35055400	-3.40989000	-2.96986700
H	-0.07424600	-4.40198200	-2.60173300
H	-1.43542500	-3.36735300	-3.10528200
H	0.13929900	-3.24293900	-3.93332500
C	0.07081600	3.10560100	-3.16061900
H	-0.95450400	3.48757900	-3.15558100
H	0.76082600	3.93161600	-2.96504500
H	0.28881500	2.69241400	-4.14960000
C	-0.07769900	3.23493900	3.28465800
H	0.11099900	2.88209000	4.30250800
H	0.55821000	4.10305900	3.08877500
H	-1.12731200	3.53266600	3.20218000
O	-1.71629500	-0.41092900	0.50044200
C	-2.91244200	-0.04305100	0.04424500
C	-3.18038400	1.50354200	0.18820600
C	-3.15017800	-0.43643000	-1.46128600
C	-3.99148400	-0.79352700	0.91210600
F	-4.01082300	-0.29844600	2.16700500
F	-3.70083500	-2.10186800	1.00246100
F	-5.24860800	-0.69617100	0.42351400
F	-4.31136400	0.02837900	-1.97037500
F	-3.15784500	-1.78313900	-1.60694400
F	-2.16263300	0.02766700	-2.25625800
F	-4.47933700	1.84757900	0.05711700
F	-2.77010500	1.94701600	1.39284200
F	-2.49335900	2.21196300	-0.74169800

Crystallographic section

Crystallographic data of Ru-C5

The crystal structure was deposit at the Cambridge Crystallographic Data Centre.

CCDC: 1420657

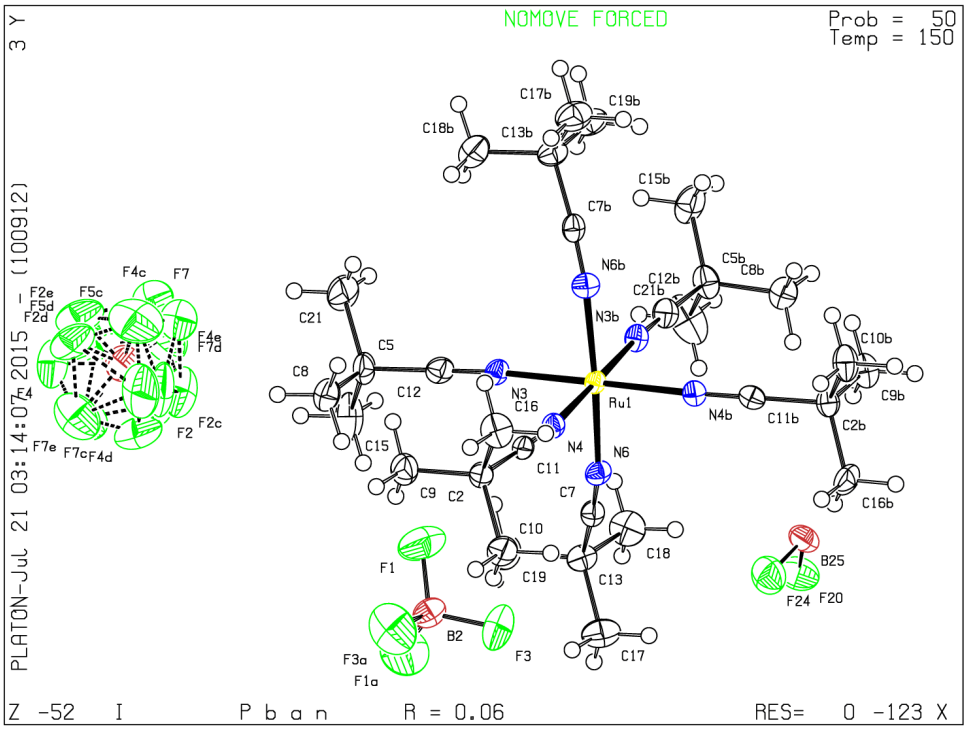

Table 1 Crystal data and structure refinement for Ru-C5

Empirical formula	$C_{30}H_{54}B_2F_8N_6Ru$
Formula weight	773.48
Temperature/K	150.03(10)
Crystal system	orthorhombic
Space group	Pban
a/Å	10.8977(3)
b/Å	34.0657(11)
c/Å	11.0451(4)
α/°	90
β/°	90
γ/°	90

Volume/Å^3	4100.4(2)
Z	4
ϱ_{calc}g/cm^3	1.253
μ/mm^{-1}	0.445
F(000)	1608.0
Crystal size/mm^3	0.27 × 0.25 × 0.15
Radiation	MoKα (λ = 0.71073)
2Θ range for data collection/°	7.054 to 58.492
Index ranges	-12 ≤ h ≤ 13, -26 ≤ k ≤ 45, -8 ≤ l ≤ 14
Reflections collected	16335
Independent reflections	4871 [R_{int} = 0.0735, R_{sigma} = 0.0954]
Data/restraints/parameters	4871/73/253
Goodness-of-fit on F^2	1.043
Final R indexes [I>=2σ (I)]	R_1 = 0.0573, wR_2 = 0.1217
Final R indexes [all data]	R_1 = 0.1126, wR_2 = 0.1505
Largest diff. peak/hole / e Å^{-3}	1.32/-1.07

Table 2 Fractional Atomic Coordinates (×10^4) and Equivalent Isotropic

Displacement Parameters (Å^2×10^3) for C5. U_{eq} is defined as 1/3 of the trace of the orthogonalised U_{IJ} tensor.

Atom	*x*	*y*	*z*	*U(eq)*
Ru1	2500	3958.5(2)	5000	17.77(14)
C2	169(4)	4797.7(12)	2636(4)	24(1)
N3	1525(3)	3555.1(10)	4081(3)	22.9(8)
N4	1530(3)	4363.2(10)	4058(3)	22.0(8)
C5	91(4)	3110.6(14)	2766(4)	31.5(11)
N6	1229(3)	3912.9(10)	6318(3)	24.0(8)
C7	562(4)	3787.2(12)	7008(4)	23.3(9)
C8	-618(4)	3390.2(13)	1931(4)	33.1(11)
C9	-619(4)	4519.0(14)	1873(4)	35.7(12)
C10	-639(4)	5069.9(13)	3415(4)	35.4(12)
C11	942(4)	4556.7(12)	3457(4)	21.9(9)
C12	910(4)	3357.1(13)	3526(4)	27.8(10)
C13	-236(4)	3562.5(13)	7867(4)	29.2(10)
C15	-798(5)	2889.8(15)	3596(5)	48.1(15)
C16	1018(4)	5040.2(14)	1824(4)	35.6(12)

C17	-1048(5)	3847.3(15)	8579(5)	43.3(13)
C18	613(4)	3330.2(15)	8700(5)	43.5(13)
C19	-1016(4)	3287.5(14)	7096(5)	38.5(12)
C21	886(5)	2828.8(16)	2009(6)	58.7(18)
F20	1897(5)	3947.1(16)	10830(5)	50.1(16)
F24	1660(5)	4408.4(17)	9423(5)	52.5(16)
B25	2500	4175(2)	10000	35(3)
B4	-2500	2500	0	52(3)
F5	-2620(20)	2897.4(11)	-160(19)	78(5)
F2	-2707(17)	2449(5)	1212(3)	61(4)
F7	-1281(4)	2430(6)	-204(17)	75(5)
B2	-2500	4097.1(12)	5000	34.9(17)
F1	-1638(3)	3868.4(11)	4440(3)	78.4(12)
F3	-1937(3)	4325.9(11)	5852(3)	78.3(12)
F4	-3284(11)	2300(4)	-742(11)	86(5)

Table 3 Anisotropic Displacement Parameters ($Å^2×10^3$) for Ru-C5

The Anisotropic displacement factor exponent takes the form: $-2\pi^2[h^2a^{*2}U_{11}+2hka^*b^*U_{12}+\ldots]$

Atom	U_{11}	U_{22}	U_{33}	U_{23}	U_{13}	U_{12}
Ru1	20.7(2)	14.5(2)	18.1(2)	0	-1.6(2)	0
C2	26(2)	22(2)	25(2)	-2(2)	-4.2(19)	3.3(17)
N3	28.0(19)	16.8(18)	23.8(19)	-1.4(16)	-2.8(17)	2.3(15)
N4	23.7(18)	18.5(18)	23.8(19)	-1.4(16)	-2.4(17)	0.1(15)
C5	33(2)	24(2)	37(3)	-7(2)	-12(2)	-1.4(19)
N6	27.8(19)	16.8(18)	27.5(19)	-2.8(17)	2.5(17)	-1.0(15)
C7	27(2)	17(2)	26(2)	-1(2)	-5(2)	2.7(17)
C8	41(3)	27(2)	31(3)	-2(2)	-6(2)	-2(2)
C9	36(3)	34(3)	37(3)	-3(2)	-9(2)	4(2)
C10	39(3)	29(3)	38(3)	-3(2)	-8(2)	14(2)
C11	21(2)	21(2)	24(2)	-5.9(19)	0.4(19)	-2.8(17)
C12	31(3)	21(2)	31(3)	-1(2)	-1(2)	5.6(18)
C13	33(3)	24(2)	30(2)	1(2)	6(2)	-1.0(19)
C15	65(4)	32(3)	47(3)	12(3)	-23(3)	-20(3)
C16	43(3)	28(3)	35(3)	14(2)	-4(2)	0(2)
C17	47(3)	40(3)	42(3)	2(3)	15(3)	4(2)

C18	49(3)	43(3)	39(3)	12(3)	1(3)	1(2)
C19	45(3)	34(3)	36(3)	4(2)	4(3)	-14(2)
C21	54(3)	41(3)	82(5)	-37(3)	-18(3)	17(3)
F20	43(3)	52(4)	55(4)	12(3)	13(3)	-4(3)
F24	49(4)	56(4)	53(4)	0(4)	-13(3)	8(3)
B25	23(7)	41(9)	40(9)	0	2(9)	0
B4	51(5)	68(6)	37(5)	0	0	0
F5	91(11)	86(6)	58(11)	16(5)	-44(8)	11(6)
F2	86(12)	46(10)	50(5)	-5(5)	5(5)	-39(7)
F7	62(5)	83(13)	80(13)	-27(8)	7(5)	0(5)
B2	45(4)	26(4)	34(4)	0	6(5)	0
F1	81(3)	78(3)	76(3)	-25(2)	15(2)	22(2)
F3	82(2)	85(3)	68(3)	-39(2)	-16(2)	-7(2)
F4	77(9)	109(11)	71(9)	-32(8)	-27(7)	-7(7)

Table 4 Bond Lengths for Ru-C5

Atom	*Atom*	*Length/Å*	*Atom*	*Atom*	*Length/Å*
Ru1	N3	2.012(3)	C7	C13	1.498(6)
Ru1	N3[1]	2.012(3)	C13	C17	1.530(6)
Ru1	N4[1]	2.025(3)	C13	C18	1.526(6)
Ru1	N4	2.025(3)	C13	C19	1.525(6)
Ru1	N6[1]	2.015(4)	F20	B25	1.370(2)
Ru1	N6	2.015(4)	F24	B25	1.369(2)
C2	C9	1.533(6)	B25	F20[2]	1.370(2)
C2	C10	1.540(6)	B25	F24[2]	1.369(2)
C2	C11	1.485(6)	B4	F5	1.372(2)
C2	C16	1.531(6)	B4	F2	1.369(2)
N3	C12	1.131(5)	B4	F7	1.369(2)
N4	C11	1.134(5)	B4	F4	1.366(2)
C5	C8	1.534(6)	B2	F1[3]	1.368(2)
C5	C12	1.485(6)	B2	F1	1.368(2)
C5	C15	1.531(7)	B2	F3	1.367(2)
C5	C21	1.539(6)	B2	F3[3]	1.367(2)
N6	C7	1.137(5)			

[1]1/2-X,+Y,1-Z; [2]1/2-X,+Y,2-Z; [3]-1/2-X,+Y,1-Z

Table 5 Bond Angles for Ru-C5

Atom	*Atom*	*Atom*	*Angle/°*	*Atom*	*Atom*	*Atom*	*Angle/°*
N3	Ru1	N3[1]	93.84(19)	C7	N6	Ru1	162.3(3)
N3[1]	Ru1	N4	179.36(14)	N6	C7	C13	171.3(4)
N3	Ru1	N4[1]	179.36(14)	N4	C11	C2	177.9(5)
N3	Ru1	N4	86.00(13)	N3	C12	C5	177.7(5)
N3[1]	Ru1	N4[1]	86.00(13)	C7	C13	C17	109.7(4)
N3	Ru1	N6	87.06(14)	C7	C13	C18	107.1(4)
N3[1]	Ru1	N6[1]	87.06(14)	C7	C13	C19	106.5(4)
N3	Ru1	N6[1]	86.90(14)	C18	C13	C17	111.7(4)
N3[1]	Ru1	N6	86.90(14)	C19	C13	C17	110.8(4)
N4	Ru1	N4[1]	94.17(19)	C19	C13	C18	110.9(4)
N6	Ru1	N4[1]	92.31(13)	F20[2]	B25	F20	110.8(7)
N6	Ru1	N4	93.71(14)	F24	B25	F20	108.6(4)
N6[1]	Ru1	N4	92.31(13)	F24[2]	B25	F20[2]	108.6(4)
N6[1]	Ru1	N4[1]	93.71(14)	F24[2]	B25	F20	109.8(4)
N6	Ru1	N6[1]	171.16(19)	F24	B25	F20[2]	109.8(4)
C9	C2	C10	111.1(3)	F24	B25	F24[2]	109.1(7)
C11	C2	C9	108.1(4)	F2	B4	F5	103.6(8)
C11	C2	C10	108.5(4)	F7	B4	F5	104.2(8)
C11	C2	C16	108.2(3)	F7	B4	F2	107.4(8)
C16	C2	C9	110.5(4)	F4	B4	F5	110.6(8)
C16	C2	C10	110.3(4)	F4	B4	F2	114.9(7)
C12	N3	Ru1	173.5(4)	F4	B4	F7	115.0(7)
C11	N4	Ru1	172.5(3)	F1[3]	B2	F1	110.5(4)
C8	C5	C21	110.1(4)	F3[3]	B2	F1[3]	109.2(2)
C12	C5	C8	106.9(4)	F3[3]	B2	F1	108.7(2)
C12	C5	C15	108.6(4)	F3	B2	F1	109.2(2)
C12	C5	C21	108.7(4)	F3	B2	F1[3]	108.8(2)
C15	C5	C8	110.2(4)	F3[3]	B2	F3	110.5(4)
C15	C5	C21	112.0(4)				

[1]1/2-X,+Y,1-Z; [2]1/2-X,+Y,2-Z; [3]-1/2-X,+Y,1-Z

Table 6 H-Atom Coordinates (Å×10^4) and Isotropic Displacement Parameters (Å^2×10^3) for Ru-C5

Atom	*x*	*y*	*z*	*U(eq)*
H8A	-1160	3241	1423	50
H8B	-1088	3570	2412	50
H8C	-50	3534	1436	50
H9A	-1128	4669	1335	54
H9B	-96	4350	1409	54
H9C	-1128	4364	2397	54
H10A	-1145	5228	2897	53
H10B	-1149	4914	3936	53
H10C	-125	5237	3896	53
H15A	-1333	2729	3115	72
H15B	-341	2727	4143	72
H15C	-1276	3075	4049	72
H16A	534	5198	1286	53
H16B	1523	5207	2317	53
H16C	1531	4867	1360	53
H17A	-1559	3702	9128	65
H17B	-540	4026	9028	65
H17C	-1555	3993	8027	65
H18A	131	3182	9266	65
H18B	1106	3155	8226	65
H18C	1136	3508	9133	65
H19A	-1546	3136	7610	58
H19B	-1502	3439	6542	58
H19C	-490	3114	6649	58
H21A	366	2668	1514	88
H21B	1429	2978	1502	88
H21C	1359	2665	2540	88

Table 7 Atomic Occupancy for Ru-C5

Atom	*Occupancy*	*Atom*	*Occupancy*	*Atom*	*Occupancy*
F20	0.5	F24	0.5	B25	0.5
F5	0.25	F2	0.25	F7	0.25
F4	0.25				

Crystallographic data of Ru-C5'

The crystal structure was deposit at the Cambridge Crystallographic Data Centre.

CCDC: 1420658

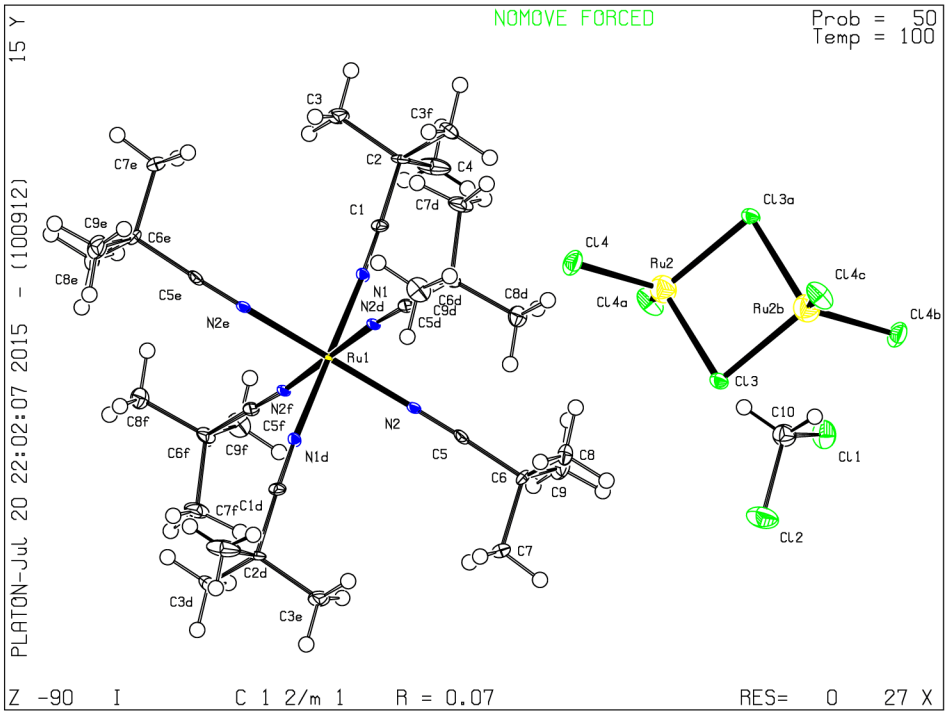

Table 1 Crystal data and structure refinement for Ru-C5'

Identification code	Ru-C5'
Empirical formula	$C_{32}H_{58}Cl_{10}N_6Ru_3$
Formula weight	1184.55
Temperature/K	100.(2)
Crystal system	monoclinic
Space group	C2/m
a/Å	21.221(7)
b/Å	13.810(4)
c/Å	9.163(3)
α/°	90
β/°	103.056(7)

γ/°	90
Volume/Å^3	2615.9(14)
Z	2
ϱ_{calc}g/cm^3	1.504
μ/mm^{-1}	1.393
F(000)	1188.0
Crystal size/mm^3	0.200 × 0.130 × 0.100
Radiation	MoKα (λ = 0.71073)
2Θ range for data collection/°	3.54 to 57.52
Index ranges	-28 ≤ h ≤ 27, -18 ≤ k ≤ 17, -12 ≤ l ≤ 12
Reflections collected	13063
Independent reflections	3453 [R_{int} = 0.0554, R_{sigma} = 0.0542]
Data/restraints/parameters	3453/0/139
Goodness-of-fit on F^2	1.092
Final R indexes [I>=2σ (I)]	R_1 = 0.0656, wR_2 = 0.2019
Final R indexes [all data]	R_1 = 0.0867, wR_2 = 0.2187
Largest diff. peak/hole / e Å^{-3}	3.59/-3.02

Table 2 Fractional Atomic Coordinates (×10^4) and Equivalent Isotropic Displacement Parameters (Å^2×10^3) for Ru-C5' U_{eq} is defined as 1/3 of of the trace of the orthogonalised U_{IJ} tensor

Atom	*x*	*y*	*z*	*U(eq)*
C1	5805(4)	5000	7496(9)	9.3(15)
C2	6261(4)	5000	6486(9)	9.4(15)
C3	6677(3)	5910(5)	6828(8)	17.5(12)
C4	5873(5)	5000	4859(11)	27(2)
C5	4092(3)	3272(4)	8635(6)	10.8(11)
C6	3685(3)	2394(4)	8227(7)	12.0(11)
C7	3106(3)	2498(5)	8987(8)	20.3(13)
C8	4093(3)	1504(4)	8823(7)	16.2(12)
C9	3451(3)	2358(5)	6517(7)	20.1(13)
C10	3186(5)	0	2554(11)	21.0(19)

Cl1	2815.1(13)	0	604(3)	26.3(5)
Cl2	2586.1(15)	0	3623(3)	34.8(6)
Cl3	4343(1)	0	5770(2)	14.6(4)
Cl4	5562.0(9)	2030.6(13)	6905.4(18)	25.0(4)
N1	5484(3)	5000	8333(7)	7.8(12)
N2	4396(2)	3930(3)	9004(5)	8.3(9)
Ru1	5000	5000	10000	4.0(2)
Ru2	5000	1178.8(7)	5000	31.3(3)

Table 3 Anisotropic Displacement Parameters ($Å^2×10^3$) for Ru-C5'

Atom	U_{11}	U_{22}	U_{33}	U_{12}	U_{13}	U_{23}
C1	5(3)	13(4)	10(3)	0	1(3)	0
C2	4(3)	17(4)	8(3)	0	3(3)	0
C3	18(3)	15(3)	25(3)	-2(2)	14(2)	3(2)
C4	12(5)	60(8)	10(4)	0	3(3)	0
C5	13(3)	10(3)	11(2)	2(2)	8(2)	-1(2)
C6	11(3)	10(3)	16(3)	-6(2)	5(2)	-4(2)
C7	15(3)	17(3)	33(4)	-7(2)	14(3)	-7(3)
C8	19(3)	10(3)	19(3)	-2(2)	5(2)	-3(2)
C9	22(3)	21(3)	16(3)	-6(3)	1(2)	-5(2)
C10	21(5)	24(5)	19(4)	0	5(4)	0
Cl1	34.4(14)	24.4(12)	19.2(11)	0	4.2(10)	0
Cl2	30.6(14)	47.1(17)	32.9(14)	0	19.9(11)	0
Cl3	15.9(10)	13.6(9)	17.3(9)	0	9.8(8)	0
Cl4	34.2(9)	23.6(8)	19.3(7)	-14.1(7)	10.5(7)	-8.2(6)
N1	10(3)	7(3)	7(3)	0	4(2)	0
N2	9(2)	7(2)	11(2)	0.2(17)	7.0(17)	0.4(17)
Ru1	4.4(4)	1.9(4)	7.5(4)	0	4.8(3)	0
Ru2	35.8(6)	28.9(5)	30.9(5)	0	11.2(4)	0

Table 4 Bond Lengths for Ru-C5'

Atom	*Atom*	*Length/Å*	*Atom*	*Atom*	*Length/Å*
C1	N1	1.135(11)	Cl3	Ru2	2.3528(17)
C1	C2	1.481(11)	Cl3	$Ru2^2$	2.3528(17)

C2	C3	1.527(8)	Cl4	Ru2	2.2167(17)
C2	C3[1]	1.527(8)	N1	Ru1	2.025(7)
C2	C4	1.531(12)	N2	Ru1	2.032(5)
C5	N2	1.122(8)	Ru1	N1[3]	2.025(7)
C5	C6	1.487(8)	Ru1	N2[3]	2.032(5)
C6	C8	1.531(9)	Ru1	N2[1]	2.032(5)
C6	C9	1.533(9)	Ru1	N2[4]	2.032(5)
C6	C7	1.551(8)	Ru2	Cl4[5]	2.2167(17)
C10	Cl2	1.773(10)	Ru2	Cl3[2]	2.3528(17)
C10	Cl1	1.782(10)			

Table 5 Bond Angles for Ru-C5'

Atom	*Atom*	*Atom*	*Angle/°*	*Atom*	*Atom*	*Atom*	*Angle/°*
N1	C1	C2	176.3(8)	N1	Ru1	N2	92.14(18)
C1	C2	C3	107.5(4)	N1[3]	Ru1	N2[3]	92.14(18)
C1	C2	C3[1]	107.5(4)	N1	Ru1	N2[3]	87.86(18)
C3	C2	C3[1]	110.8(7)	N2	Ru1	N2[3]	180.0
C1	C2	C4	109.0(7)	N1[3]	Ru1	N2[1]	87.86(18)
C3	C2	C4	111.0(5)	N1	Ru1	N2[1]	92.14(18)
C3[1]	C2	C4	111.0(5)	N2	Ru1	N2[1]	93.3(3)
N2	C5	C6	177.0(6)	N2[3]	Ru1	N2[1]	86.7(3)
C5	C6	C8	108.4(5)	N1[3]	Ru1	N2[4]	92.14(18)
C5	C6	C9	108.6(5)	N1	Ru1	N2[4]	87.86(18)
C8	C6	C9	111.4(5)	N2	Ru1	N2[4]	86.7(3)
C5	C6	C7	106.6(5)	N2[3]	Ru1	N2[4]	93.3(3)
C8	C6	C7	110.8(5)	N2[1]	Ru1	N2[4]	180.0
C9	C6	C7	110.7(5)	Cl4	Ru2	Cl4[5]	115.89(11)
Cl2	C10	Cl1	110.1(5)	Cl4	Ru2	Cl3[2]	110.70(7)
Ru2	Cl3	Ru2[2]	87.56(8)	Cl4[5]	Ru2	Cl3[2]	112.39(7)
C1	N1	Ru1	173.9(7)	Cl4	Ru2	Cl3	112.39(7)
C5	N2	Ru1	170.4(5)	Cl4[5]	Ru2	Cl3	110.70(7)
N1[3]	Ru1	N1	180.0	Cl3[2]	Ru2	Cl3	92.44(8)
N1[3]	Ru1	N2	87.86(18)				

Table 6 H-Atom Coordinates (Å×10^4) and Isotropic Displacement Parameters (Å^2×10^3) for Ru-C5'

Atom	*x*	*y*	*z*	*U(eq)*
H3A	6405	6484	6546	26
H3B	7015	5896	6255	26
H3C	6877	5934	7901	26
H4A	5680(50)	4480(70)	4760(110)	41
H4B	6190(80)	5000	4480(170)	41
H4C	5680(50)	5520(70)	4760(110)	41
H7A	3263	2478	10077	30
H7B	2801	1965	8668	30
H7C	2887	3116	8695	30
H8A	4474	1479	8386	24
H8B	3834	916	8549	24
H8C	4233	1546	9916	24
H9A	3165	2910	6179	30
H9B	3213	1754	6227	30
H9C	3824	2387	6054	30
H10A	3463	-581	2803	25
H10B	3463	581	2803	25

Table 7 Atomic Occupancy for C5'.

Atom	*Occupancy*	*Atom*	*Occupancy*	*Atom*	*Occupancy*
H4A	0.5	H4C	0.5	H10A	0.5
H10B	0.5				

Crystallographic data of Ru1-39c

The crystal structure was deposit at the Cambridge Crystallographic Data Centre.

CCDC: 1420695

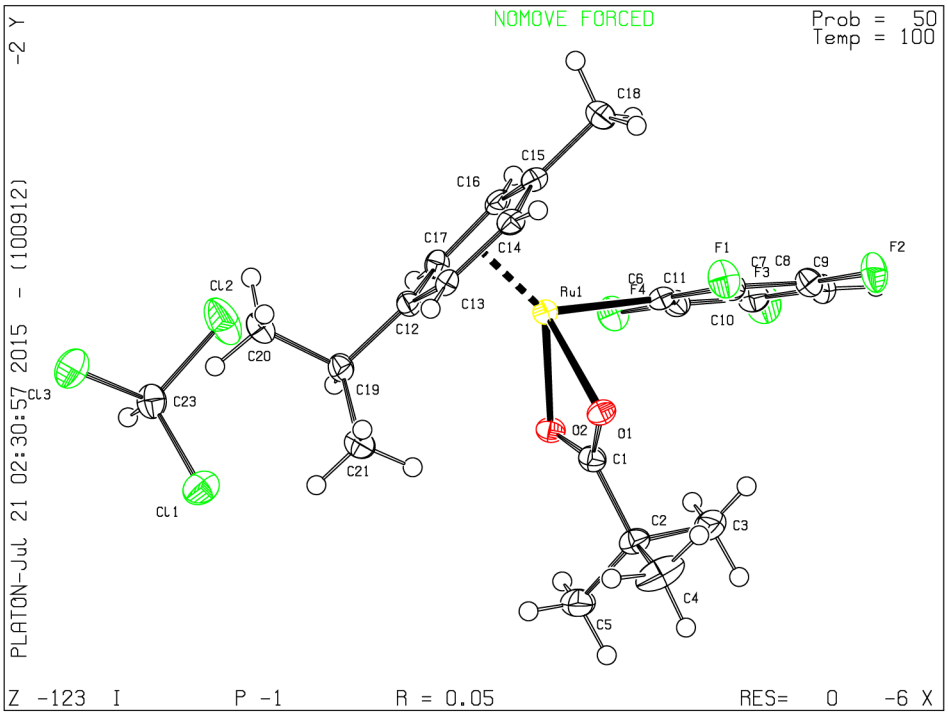

Table 1 Crystal data and structure refinement for Ru1-39c

Empirical formula	$C_{22}H_{25}Cl_3F_4O_2Ru$
Formula weight	604.84
Temperature/K	100.(2)
Crystal system	triclinic
Space group	P-1
a/Å	9.9568(11)
b/Å	10.1815(12)
c/Å	13.3346(15)
α/°	107.735(2)
β/°	99.041(2)
γ/°	94.998(3)

Volume/Å^3	1258.4(2)
Z	2
ϱ_{calc}g/cm^3	1.596
μ/mm^{-1}	0.988
F(000)	608.0
Crystal size/mm^3	0.360 × 0.100 × 0.090
Radiation	MoKα (λ = 0.71073)
2Θ range for data collection/°	3.26 to 56.94
Index ranges	-13 ≤ h ≤ 13, -13 ≤ k ≤ 13, -17 ≤ l ≤
Reflections collected	23196
Independent reflections	6301 [R_{int} = 0.0174, R_{sigma} = N/A]
Data/restraints/parameters	6301/0/295
Goodness-of-fit on F^2	1.045
Final R indexes [I>=2σ (I)]	R_1 = 0.0195, wR_2 = 0.0478
Final R indexes [all data]	R_1 = 0.0217, wR_2 = 0.0489
Largest diff. peak/hole / e Å^{-3}	0.64/-0.67

Table 2 Fract. Atom. Coord. (×10^4) and Equiv. Isotropic Displacement Parameters (Å^2×10^3) for Ru1-39c

Atom	*x*	*y*	*z*	*U(eq)*
C1	2471.2(13)	3133.3(13)	2885.9(11)	12.4(2)
C2	940.1(14)	3210.2(15)	2736.2(11)	15.5(3)
C3	240.1(16)	1709.3(17)	2122.8(16)	29.5(4)
C4	502.2(17)	3744(2)	3816.1(14)	34.8(4)
C5	569.9(16)	4143.3(19)	2059.4(15)	27.4(3)
C6	3740.6(13)	518.6(13)	2435.2(11)	11.9(2)
C7	3330.9(14)	-136.0(14)	3133.7(11)	14.8(3)
C8	2513.7(15)	-1419.1(15)	2789.7(12)	17.4(3)
C9	2063.6(15)	-2141.7(15)	1713.4(12)	18.5(3)
C10	2471.8(14)	-1520.6(15)	1001.1(11)	16.5(3)
C11	3278.7(14)	-235.2(14)	1355.6(11)	13.6(2)
C12	6390.5(13)	4334.6(13)	3054.4(10)	11.5(2)

C13	6493.5(13)	4191.5(14)	4077.2(10)	12.2(2)
C14	6656.8(13)	2875.9(14)	4228.4(10)	12.4(2)
C15	6769.2(13)	1695.3(14)	3368.7(11)	12.8(2)
C16	6627.7(13)	1822.4(14)	2320.9(11)	12.8(2)
C17	6412.3(13)	3107.6(14)	2172.8(10)	12.1(2)
C18	6968.7(15)	329.4(15)	3545.0(12)	19.1(3)
C19	6206.6(14)	5702.3(14)	2860.7(11)	15.1(3)
C20	7611.8(16)	6619.6(16)	3178.0(14)	23.9(3)
C21	5162.1(16)	6469.7(16)	3449.1(14)	22.7(3)
C22	7120.4(16)	7111.5(15)	236.5(12)	19.4(3)
Cl1	8537.7(4)	8338.4(5)	1024.0(3)	30.86(9)
Cl2	7421.7(6)	5414.9(4)	191.4(4)	43.07(13)
Cl3	5614.6(4)	7496.7(5)	742.3(3)	26.05(8)
F1	3742.5(10)	486.1(9)	4209.0(7)	21.32(18)
F2	2149.8(10)	-1982.4(10)	3526.0(8)	26.2(2)
F3	2073.9(10)	-2195.5(9)	-67.9(7)	25.1(2)
F4	3629.9(9)	291.6(9)	595.0(6)	18.89(17)
O1	3164.5(10)	3077.2(10)	3752.8(7)	13.27(18)
O2	3094.4(10)	3011.3(10)	2104.4(8)	13.30(18)
Ru1	4863.8(2)	2510.5(2)	2968.4(2)	8.98(3)

Table 3 Anisotropic Displacement Parameters ($Å^2×10^3$) for Ru1-39c

The Anisotropic displacement factor exponent takes the form: $-2\pi^2[h^2a^{*2}U_{11}+2hka^*b^*U_{12}+\ldots]$.

Atom	U_{11}	U_{22}	U_{33}	U_{12}	U_{13}	U_{23}
C1	11.5(6)	9.2(6)	14.5(6)	0.9(5)	2.8(5)	1.0(5)
C2	9.1(6)	17.3(6)	17.4(6)	2.1(5)	2.9(5)	1.6(5)
C3	13.2(7)	20.3(8)	48.6(11)	-1.5(6)	2.3(7)	4.5(7)
C4	15.2(7)	64.0(13)	20.8(8)	12.2(8)	7.5(6)	3.4(8)
C5	16.3(7)	31.9(9)	39.5(9)	10.0(6)	4.7(6)	18.0(7)
C6	9.6(6)	11.2(6)	15.1(6)	2.3(5)	2.1(5)	4.2(5)
C7	15.1(6)	14.7(6)	14.0(6)	1.4(5)	1.5(5)	4.5(5)
C8	17.3(7)	15.9(7)	22.5(7)	1.6(5)	5.0(5)	10.7(6)
C9	16.2(7)	11.8(6)	24.9(7)	-0.6(5)	1.5(5)	4.0(5)
C10	16.0(6)	14.4(6)	14.7(6)	2.8(5)	-0.3(5)	-0.3(5)

C11	13.6(6)	14.0(6)	14.1(6)	3.7(5)	4.0(5)	4.6(5)
C12	8.2(5)	11.4(6)	14.6(6)	-0.1(4)	2.4(4)	4.0(5)
C13	9.8(6)	11.6(6)	13.2(6)	0.7(5)	1.5(5)	1.8(5)
C14	9.4(6)	14.8(6)	12.3(6)	0.7(5)	0.7(5)	4.3(5)
C15	9.3(6)	12.6(6)	16.7(6)	2.2(5)	2.4(5)	5.1(5)
C16	9.8(6)	12.8(6)	15.1(6)	2.1(5)	4.8(5)	2.0(5)
C17	9.2(6)	15.4(6)	12.4(6)	1.2(5)	4.1(5)	4.5(5)
C18	20.2(7)	14.5(6)	24.7(7)	5.7(5)	4.4(6)	8.4(6)
C19	16.7(6)	12.6(6)	17.5(6)	3.0(5)	3.9(5)	6.6(5)
C20	20.6(7)	15.2(7)	38.8(9)	1.4(6)	7.4(6)	12.6(6)
C21	21.4(7)	18.0(7)	33.8(8)	8.8(6)	11.3(6)	11.0(6)
C22	23.1(7)	17.9(7)	16.7(6)	0.6(6)	4.8(6)	5.0(5)
Cl1	21.37(19)	33.4(2)	31.2(2)	-5.80(16)	2.07(15)	5.16(17)
Cl2	74.5(4)	19.09(19)	46.4(3)	14.4(2)	38.0(3)	10.98(18)
Cl3	18.59(17)	39.4(2)	23.08(18)	4.50(15)	4.33(14)	14.16(16)
F1	28.3(5)	21.8(4)	12.1(4)	-3.6(4)	1.4(3)	6.0(3)
F2	31.7(5)	22.7(5)	27.6(5)	-4.8(4)	6.6(4)	14.9(4)
F3	30.3(5)	20.6(4)	15.3(4)	-2.6(4)	-1.3(4)	-3.0(3)
F4	25.7(4)	19.3(4)	11.9(4)	1.0(3)	5.5(3)	4.9(3)
O1	10.5(4)	15.6(5)	12.0(4)	2.4(4)	3.1(3)	1.5(4)
O2	10.9(4)	16.2(5)	13.6(4)	3.0(4)	3.2(3)	5.2(4)
Ru1	8.28(5)	9.33(5)	8.96(5)	1.03(3)	2.30(3)	2.15(4)

Table 4 Bond Lengths for Ru1-39c

Atom	*Atom*	*Length/Å*	*Atom*	*Atom*	*Length/Å*
C1	O1	1.2699(17)	C12	C19	1.5126(18)
C1	O2	1.2744(16)	C12	Ru1	2.2576(13)
C1	C2	1.5181(18)	C13	C14	1.4330(18)
C1	Ru1	2.5125(13)	C13	Ru1	2.2291(13)
C2	C4	1.523(2)	C14	C15	1.4127(18)
C2	C5	1.527(2)	C14	Ru1	2.1701(13)
C2	C3	1.537(2)	C15	C16	1.4284(19)
C6	C7	1.3887(18)	C15	C18	1.5037(19)

C6	C11	1.3894(18)	C15	Ru1	2.1907(13)
C6	Ru1	2.0846(13)	C16	C17	1.4107(19)
C7	F1	1.3572(16)	C16	Ru1	2.1549(13)
C7	C8	1.3826(19)	C17	Ru1	2.1484(12)
C8	F2	1.3576(16)	C19	C21	1.527(2)
C8	C9	1.378(2)	C19	C20	1.534(2)
C9	C10	1.382(2)	C22	Cl1	1.7557(16)
C10	F3	1.3563(16)	C22	Cl2	1.7635(16)
C10	C11	1.3792(19)	C22	Cl3	1.7651(16)
C11	F4	1.3597(15)	O1	Ru1	2.1560(9)
C12	C13	1.4041(18)	O2	Ru1	2.1372(10)
C12	C17	1.4357(18)			

Table 5 Bond Angles for Ru1-39c

Atom	*Atom*	*Atom*	*Angle/°*	*Atom*	*Atom*	*Atom*	*Angle/°*
O1	C1	O2	116.92(12)	C12	C19	C20	108.68(11
O1	C1	C2	122.38(12)	C21	C19	C20	110.78(12
O2	C1	C2	120.48(12)	Cl1	C22	Cl2	110.39(9)
O1	C1	Ru1	59.10(7)	Cl1	C22	Cl3	110.53(8)
O2	C1	Ru1	58.25(7)	Cl2	C22	Cl3	110.45(8)
C2	C1	Ru1	168.97(9)	C1	O1	Ru1	90.54(8)
C1	C2	C4	110.90(12)	C1	O2	Ru1	91.28(8)
C1	C2	C5	110.10(12)	C6	Ru1	O2	83.64(4)
C4	C2	C5	110.49(14)	C6	Ru1	C17	122.54(5)
C1	C2	C3	105.32(11)	O2	Ru1	C17	99.98(4)
C4	C2	C3	110.56(14)	C6	Ru1	C16	94.19(5)
C5	C2	C3	109.34(13)	O2	Ru1	C16	125.51(4)
C7	C6	C11	114.34(12)	C17	Ru1	C16	38.27(5)
C7	C6	Ru1	122.56(10)	C6	Ru1	O1	83.59(4)
C11	C6	Ru1	123.02(10)	O2	Ru1	O1	60.67(4)
F1	C7	C8	117.11(12)	C17	Ru1	O1	147.31(4)
F1	C7	C6	119.77(12)	C16	Ru1	O1	173.26(4)
C8	C7	C6	123.11(13)	C6	Ru1	C14	115.97(5)

F2	C8	C9	119.23(13)	O2	Ru1	C14	156.57(5)
F2	C8	C7	119.41(13)	C17	Ru1	C14	80.72(5)
C9	C8	C7	121.35(13)	C16	Ru1	C14	68.53(5)
C8	C9	C10	116.67(13)	O1	Ru1	C14	106.69(4)
F3	C10	C11	119.51(13)	C6	Ru1	C15	91.35(5)
F3	C10	C9	119.13(13)	O2	Ru1	C15	162.91(4)
C11	C10	C9	121.36(13)	C17	Ru1	C15	69.02(5)
F4	C11	C10	117.13(12)	C16	Ru1	C15	38.37(5)
F4	C11	C6	119.72(12)	O1	Ru1	C15	135.13(4)
C10	C11	C6	123.15(13)	C14	Ru1	C15	37.80(5)
C13	C12	C17	117.36(12)	C6	Ru1	C13	153.49(5)
C13	C12	C19	122.31(12)	O2	Ru1	C13	120.60(4)
C17	C12	C19	120.29(11)	C17	Ru1	C13	67.28(5)
C13	C12	Ru1	70.66(7)	C16	Ru1	C13	80.54(5)
C17	C12	Ru1	66.91(7)	O1	Ru1	C13	98.61(4)
C19	C12	Ru1	132.02(9)	C14	Ru1	C13	37.99(5)
C12	C13	C14	120.73(12)	C15	Ru1	C13	68.37(5)
C12	C13	Ru1	72.87(7)	C6	Ru1	C12	160.47(5)
C14	C13	Ru1	68.77(7)	O2	Ru1	C12	98.40(4)
C15	C14	C13	121.54(12)	C17	Ru1	C12	37.93(5)
C15	C14	Ru1	71.89(8)	C16	Ru1	C12	68.72(5)
C13	C14	Ru1	73.23(7)	O1	Ru1	C12	114.45(4)
C14	C15	C16	117.99(12)	C14	Ru1	C12	67.66(5)
C14	C15	C18	120.90(12)	C15	Ru1	C12	81.02(5)
C16	C15	C18	121.05(12)	C13	Ru1	C12	36.47(5)
C14	C15	Ru1	70.31(7)	C6	Ru1	C1	80.31(5)
C16	C15	Ru1	69.46(7)	O2	Ru1	C1	30.47(4)
C18	C15	Ru1	129.60(9)	C17	Ru1	C1	127.35(5)
C17	C16	C15	119.99(12)	C16	Ru1	C1	155.47(5)
C17	C16	Ru1	70.62(7)	O1	Ru1	C1	30.36(4)
C15	C16	Ru1	72.17(7)	C14	Ru1	C1	135.30(5)
C16	C17	C12	122.18(12)	C15	Ru1	C1	163.59(5)
C16	C17	Ru1	71.11(7)	C13	Ru1	C1	114.52(4)
C12	C17	Ru1	75.16(7)	C12	Ru1	C1	111.14(4)
C12	C19	C21	113.56(11)				

Table 6 Hydrogen Bonds for Ru1-39c

D	*H*	*A*	*d(D-H)/Å*	*d(H-A)/Å*	*d(D-A)/Å*	*D-H-A/°*
C22	H22	O2[1]	1.00	2.07	3.0583(18)	170.7

Table 7 Torsion Angles for Ru1-39c

A	*B*	*C*	*D*	*Angle/°*	*A*	*B*	*C*	*D*	*Angle/°*
O1	C1	C2	C4	21.11(19)	C19	C12	C13	Ru1	128.13(12)
O2	C1	C2	C4	-164.48(14)	C12	C13	C14	C15	2.30(19)
Ru1	C1	C2	C4	115.4(5)	Ru1	C13	C14	C15	55.54(11)
O1	C1	C2	C5	143.71(14)	C12	C13	C14	Ru1	-53.24(11)
O2	C1	C2	C5	-41.88(18)	C13	C14	C15	C16	-3.92(19)
Ru1	C1	C2	C5	-122.0(5)	Ru1	C14	C15	C16	52.24(11)
O1	C1	C2	C3	-98.52(15)	C13	C14	C15	C18	178.76(12)
O2	C1	C2	C3	75.89(16)	Ru1	C14	C15	C18	-125.08(12)
Ru1	C1	C2	C3	-4.2(6)	C13	C14	C15	Ru1	-56.16(11)
C11	C6	C7	F1	178.65(12)	C14	C15	C16	C17	1.33(19)
Ru1	C6	C7	F1	-4.50(18)	C18	C15	C16	C17	178.65(12)
C11	C6	C7	C8	-1.0(2)	Ru1	C15	C16	C17	53.98(11)
Ru1	C6	C7	C8	175.84(11)	C14	C15	C16	Ru1	-52.65(11)
F1	C7	C8	F2	0.9(2)	C18	C15	C16	Ru1	124.67(12)
C6	C7	C8	F2	-179.47(13)	C15	C16	C17	C12	2.93(19)
F1	C7	C8	C9	-178.93(13)	Ru1	C16	C17	C12	57.64(11)
C6	C7	C8	C9	0.7(2)	C15	C16	C17	Ru1	-54.71(11)
F2	C8	C9	C10	-179.68(13)	C13	C12	C17	C16	-4.52(19)
C7	C8	C9	C10	0.1(2)	C19	C12	C17	C16	177.80(12)
C8	C9	C10	F3	179.08(13)	Ru1	C12	C17	C16	-55.78(11)
C8	C9	C10	C11	-0.6(2)	C13	C12	C17	Ru1	51.25(11)
F3	C10	C11	F4	0.24(19)	C19	C12	C17	Ru1	-126.42(11)
C9	C10	C11	F4	179.93(12)	C13	C12	C19	C21	-43.34(18)
F3	C10	C11	C6	-179.39(12)	C17	C12	C19	C21	134.21(13)
C9	C10	C11	C6	0.3(2)	Ru1	C12	C19	C21	49.09(17)

C7	C6	C11	F4	-179.12(12)	C13	C12	C19	C20	80.43(16)
Ru1	C6	C11	F4	4.04(17)	C17	C12	C19	C20	-102.01(15)
C7	C6	C11	C10	0.5(2)	Ru1	C12	C19	C20	172.87(10)
Ru1	C6	C11	C10	-176.33(10)	O2	C1	O1	Ru1	-7.44(12)
C17	C12	C13	C14	1.90(18)	C2	C1	O1	Ru1	167.16(11)
C19	C12	C13	C14	179.52(12)	O1	C1	O2	Ru1	7.50(12)
Ru1	C12	C13	C14	51.39(11)	C2	C1	O2	Ru1	-167.20(11)
C17	C12	C13	Ru1	-49.49(10)					

Table 8 H-Atom Coordinates (Å×10^4) and Isotropic Displacement Parameters (Å^2×10^3) for Ru1-39c

Atom	*x*	*y*	*z*	*U(eq)*
H3A	540	1379	1434	44
H3B	-759	1687	1994	44
H3C	494	1105	2549	44
H4A	730	3125	4234	52
H4B	-491	3765	3700	52
H4C	986	4687	4208	52
H5A	1042	5094	2438	41
H5B	-426	4150	1938	41
H5C	856	3785	1368	41
H9	1501	-3023	1473	22
H13	6455	4976	4676	15
H14	6690	2796	4923	15
H16	6679	1042	1724	15
H17	6277	3163	1466	15
H18A	7947	232	3628	29
H18B	6448	-437	2927	29
H18C	6641	303	4195	29
H19	5874	5498	2074	18
H20A	7927	6896	3957	36
H20B	7530	7453	2964	36
H20C	8276	6095	2815	36
H21A	4284	5853	3259	34
H21B	5031	7300	3241	34

H21C	5501	6748	4225	34
H22	6990	7158	-510	23

Crystallographic data of Ru2-39c

The crystal structure was deposit at the Cambridge Crystallographic Data Centre.

CCDC: 1420659

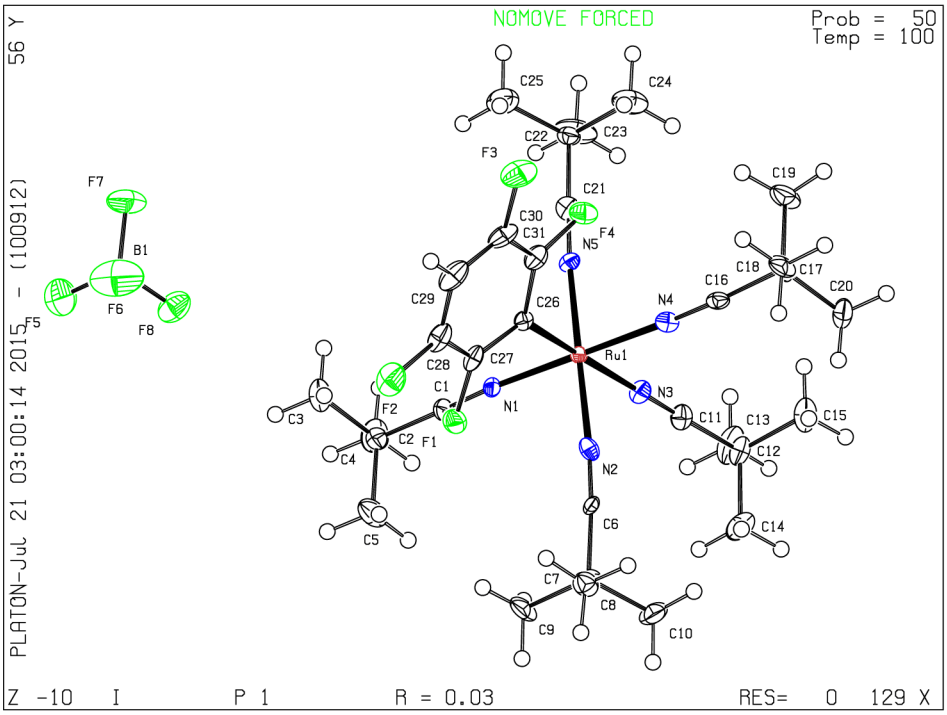

Table 1 Crystal data and structure refinement for Ru2-39c

Empirical formula	$C_{31}H_{46}BF_8N_5Ru$
Formula weight	752.61
Temperature/K	100.(2)
Crystal system	triclinic
Space group	P1
a/Å	9.1210(14)

b/Å	10.6390(16)
c/Å	11.3056(18)
α/°	67.036(4)
β/°	73.952(4)
γ/°	85.831(4)
Volume/Å^3	970.0(3)
Z	1
ϱ_{calc}g/cm^3	1.288
μ/mm^{-1}	0.468
F(000)	388.0
Crystal size/mm^3	0.200 × 0.100 × 0.050
Radiation	MoKα (λ = 0.71073)
2Θ range for data collection/°	4.06 to 56.7
Index ranges	-12 ≤ h ≤ 12, -14 ≤ k ≤ 14, -15 ≤ l ≤ 15
Reflections collected	17723
Independent reflections	8574 [R_{int} = 0.0265, R_{sigma} = 0.0396]
Data/restraints/parameters	8574/3/431
Goodness-of-fit on F^2	1.020
Final R indexes [I>=2σ (I)]	R_1 = 0.0293, wR_2 = 0.0679
Final R indexes [all data]	R_1 = 0.0302, wR_2 = 0.0684
Largest diff. peak/hole / e Å^{-3}	0.98/-0.45
Flack parameter	0.16(3)

Table 2 Fractional Atomic Coordinates (×10^4) and Equivalent Isotropic Displacement Parameters (Å^2×10^3) for Ru2-39c. U_{eq} is defined as 1/3 of of the trace of the orthogonalised U_{IJ} tensor.

Atom	*x*	*y*	*z*	*U(eq)*
B1	4619(6)	3390(5)	7079(5)	29.6(10)
C1	6094(7)	9510(7)	7642(6)	17.7(13)
C2	5118(7)	9385(7)	6836(7)	21.4(15)
C3	5181(8)	7915(8)	6928(7)	31.3(17)
C4	3471(7)	9723(8)	7405(7)	31.1(16)

C5	5754(8)	10383(8)	5400(7)	32.7(16)
C6	10124(7)	11960(6)	6283(6)	14.4(12)
C7	10659(7)	12994(7)	4910(6)	18.5(12)
C8	12274(7)	12627(7)	4257(6)	24.8(13)
C9	9523(7)	12943(8)	4143(6)	28.6(15)
C10	10713(8)	14392(7)	4993(7)	28.6(14)
C11	7143(4)	12441(4)	9588(4)	19.8(7)
C12	6982(4)	13793(4)	9693(4)	23.4(8)
C13	5292(5)	14017(6)	10252(6)	36.0(11)
C14	7618(5)	14880(5)	8287(5)	32.9(10)
C15	7945(5)	13798(5)	10608(5)	33.5(10)
C16	10801(7)	10040(7)	10596(6)	15.9(13)
C17	11751(7)	10111(7)	11440(6)	20.4(15)
C18	13340(7)	9649(7)	10948(6)	24.3(14)
C19	10949(8)	9159(8)	12879(6)	32.4(17)
C20	11806(9)	11603(7)	11322(8)	31.3(17)
C21	6679(7)	7661(7)	11911(7)	20.5(14)
C22	6045(7)	6629(7)	13283(6)	18.9(12)
C23	4511(8)	7040(8)	13934(7)	39.0(19)
C24	7199(8)	6560(8)	14057(7)	35.4(18)
C25	5938(10)	5233(8)	13199(7)	44(2)
C26	9664(6)	8155(7)	8691(6)	13.4(12)
C27	10010(4)	8038(4)	7469(4)	19.8(7)
C28	10896(4)	7029(4)	7163(4)	24.5(8)
C29	11495(5)	6036(5)	8087(5)	29.8(10)
C30	11162(4)	6101(4)	9331(4)	25.1(8)
C31	10276(4)	7114(4)	9615(4)	20.8(7)
F1	9506(2)	8967(2)	6442(2)	23.3(5)
F2	11152(3)	7026(3)	5922(3)	36.2(6)
F3	11698(3)	5142(3)	10302(3)	37.3(6)
F4	10047(3)	7054(2)	10878(2)	25.9(5)
F5	3671(5)	3334(4)	6363(4)	84.0(14)
F6	6087(5)	3123(4)	6438(4)	71.9(12)
F7	4256(4)	2458(3)	8358(3)	54.4(8)
F8	4663(3)	4707(3)	7029(3)	37.5(6)

N1	6905(6)	9557(5)	8223(5)	16.0(11)
N2	9634(5)	11128(6)	7320(5)	16.6(12)
N3	7414(6)	11419(6)	9482(6)	19.7(12)
N4	10018(5)	9940(6)	10001(5)	16.1(12)
N5	7263(6)	8407(5)	10878(5)	16.1(11)
Ru1	8472.1(4)	9739.9(4)	9099.2(4)	11.62(6)

Table 3 Anisotropic Displacement Parameters ($Å^2×10^3$) for Ru2-39c. The Anisotropic displacement factor exponent takes the form: $-2\pi^2[h^2a^{*2}U_{11}+2hka^*b^*U_{12}+\ldots]$.

Atom	U_{11}	U_{22}	U_{33}	U_{12}	U_{13}	U_{23}
B1	49(3)	20(3)	21(2)	-1(2)	-12(2)	-6.4(19)
C1	14(3)	20(3)	19(3)	-2(2)	-5(2)	-7(3)
C2	23(3)	22(4)	20(3)	-2(3)	-8(2)	-6(3)
C3	31(4)	37(5)	37(4)	-1(3)	-13(3)	-22(4)
C4	16(2)	36(4)	44(4)	0(2)	-7(2)	-19(3)
C5	27(3)	47(4)	25(3)	0(2)	-12(2)	-11(3)
C6	17(2)	9(2)	18(3)	-2.3(18)	-7.3(19)	-4(2)
C7	17(2)	16(3)	16(2)	-0.5(18)	-1.1(17)	-1(2)
C8	23(3)	29(3)	20(3)	-1(2)	-4(2)	-9(2)
C9	25(3)	42(4)	18(3)	-4(2)	-13(2)	-5(3)
C10	37(3)	13(3)	30(3)	-2(2)	-8(2)	-3(2)
C11	13.5(15)	23(2)	23.2(18)	-1.3(14)	-2.6(13)	-11.2(17)
C12	19.0(17)	21(2)	34(2)	0.2(14)	-5.0(15)	-16.4(18)
C13	24(2)	34(3)	59(3)	5(2)	-6(2)	-30(3)
C14	30(2)	20(2)	45(3)	-2.0(17)	-11.8(19)	-8(2)
C15	33(2)	37(3)	42(2)	-0.1(19)	-11.8(19)	-25(2)
C16	19(3)	13(3)	11(3)	1(2)	0(2)	-3(2)
C17	15(3)	33(4)	18(3)	-3(2)	-8(2)	-11(3)
C18	22(3)	30(4)	20(2)	3(2)	-14(2)	-4(2)
C19	29(3)	46(4)	14(3)	-10(2)	-4(2)	-2(3)
C20	40(4)	27(4)	37(4)	-2(3)	-16(3)	-18(3)
C21	17(2)	24(3)	21(3)	6(2)	-4(2)	-10(3)
C22	21(2)	19(3)	14(2)	-1.1(19)	-4.5(18)	-3(2)

C23	26(3)	49(4)	22(3)	10(3)	2(2)	0(3)
C24	25(3)	42(5)	25(3)	-2(3)	-5(2)	1(3)
C25	70(5)	29(4)	25(3)	-7(3)	-3(3)	-7(3)
C26	9(2)	15(3)	15(2)	-1.4(17)	-2.6(18)	-5(2)
C27	15.5(15)	17(2)	28.0(19)	-4.1(13)	-2.2(14)	-11.1(16)
C28	19.4(16)	22(2)	31(2)	-4.6(14)	5.0(15)	-15.6(18)
C29	21.0(19)	20(2)	44(3)	-0.4(17)	1.3(17)	-14(2)
C30	18.3(16)	13(2)	37(2)	2.1(14)	-4.5(15)	-3.8(17)
C31	15.1(15)	19(2)	26.6(18)	-1.3(13)	-2.3(14)	-9.0(16)
F1	27.2(11)	24.2(13)	19.7(10)	1.9(9)	-5.4(9)	-10.5(10)
F2	40.1(14)	35.7(16)	34.2(13)	0.1(11)	3.2(11)	-23.6(13)
F3	33.5(13)	23.7(15)	47.6(16)	12.0(11)	-15.7(12)	-4.9(12)
F4	27.7(11)	22.9(13)	24.6(11)	5.9(9)	-11.9(9)	-4.1(10)
F5	120(4)	63(3)	80(3)	-27(2)	-69(3)	-6(2)
F6	86(3)	54(2)	53(2)	31(2)	7.7(18)	-18.5(18)
F7	80(2)	41(2)	26.5(14)	-6.6(16)	-11.5(14)	3.4(13)
F8	40.3(14)	25.8(15)	43.0(15)	2.8(11)	-2.8(12)	-15.4(12)
N1	22(3)	14(3)	13(3)	-4(2)	-3(2)	-6(2)
N2	14(2)	22(3)	18(3)	4(2)	-9(2)	-10(3)
N3	20(2)	17(3)	22(3)	-1.3(19)	-4(2)	-8(2)
N4	10(2)	20(3)	15(3)	2(2)	-2(2)	-5(2)
N5	16(2)	14(3)	15(3)	-3(2)	-1(2)	-4(2)
Ru1	11.10(9)	11.89(12)	11.52(10)	-0.42(7)	-3.55(7)	-3.67(8)

Table 4 Bond Lengths for Ru2-39c

Atom	*Atom*	*Length/Å*	*Atom*	*Atom*	*Length/Å*
B1	F5	1.356(6)	C17	C20	1.544(10)
B1	F7	1.359(6)	C21	N5	1.128(8)
B1	F8	1.383(6)	C21	C22	1.488(9)
B1	F6	1.403(6)	C22	C23	1.511(9)
C1	N1	1.131(8)	C22	C24	1.526(9)
C1	C2	1.483(9)	C22	C25	1.537(10)
C2	C3	1.524(10)	C26	C27	1.382(7)

C2	C5	1.525(10)	C26	C31	1.400(7)
C2	C4	1.538(9)	C26	Ru1	2.075(6)
C6	N2	1.147(8)	C27	F1	1.368(4)
C6	C7	1.478(9)	C27	C28	1.391(5)
C7	C10	1.532(9)	C28	F2	1.358(5)
C7	C9	1.539(8)	C28	C29	1.370(6)
C7	C8	1.552(8)	C29	C30	1.382(6)
C11	N3	1.142(7)	C30	F3	1.355(5)
C11	C12	1.482(5)	C30	C31	1.385(5)
C12	C15	1.533(5)	C31	F4	1.361(4)
C12	C14	1.534(6)	N1	Ru1	2.009(5)
C12	C13	1.535(6)	N2	Ru1	2.020(5)
C16	N4	1.142(8)	N3	Ru1	2.105(6)
C16	C17	1.480(9)	N4	Ru1	2.020(5)
C17	C18	1.522(8)	N5	Ru1	2.011(5)
C17	C19	1.540(9)			

Table 5 Bond Angles for Ru2-39c

Atom	*Atom*	*Atom*	*Angle/°*	*Atom*	*Atom*	*Atom*	*Angle/°*
F5	B1	F7	114.1(4)	C23	C22	C25	111.7(6)
F5	B1	F8	108.6(4)	C24	C22	C25	108.6(6)
F7	B1	F8	111.4(4)	C27	C26	C31	112.4(5)
F5	B1	F6	107.2(4)	C27	C26	Ru1	124.4(4)
F7	B1	F6	107.7(4)	C31	C26	Ru1	123.2(4)
F8	B1	F6	107.6(4)	F1	C27	C26	120.5(4)
N1	C1	C2	175.6(7)	F1	C27	C28	114.9(3)
C1	C2	C3	107.3(5)	C26	C27	C28	124.6(4)
C1	C2	C5	108.2(6)	F2	C28	C29	119.7(4)
C3	C2	C5	111.0(6)	F2	C28	C27	118.9(4)
C1	C2	C4	109.3(5)	C29	C28	C27	121.5(4)
C3	C2	C4	110.5(6)	C28	C29	C30	116.0(4)
C5	C2	C4	110.4(6)	F3	C30	C29	119.3(4)
N2	C6	C7	175.3(6)	F3	C30	C31	119.0(4)

C6	C7	C10	108.0(5)	C29	C30	C31	121.6(4)
C6	C7	C9	107.5(5)	F4	C31	C30	115.2(3)
C10	C7	C9	111.7(6)	F4	C31	C26	120.9(4)
C6	C7	C8	108.5(5)	C30	C31	C26	123.9(4)
C10	C7	C8	110.5(5)	C1	N1	Ru1	174.9(6)
C9	C7	C8	110.5(5)	C6	N2	Ru1	171.7(5)
N3	C11	C12	173.4(4)	C11	N3	Ru1	165.7(5)
C11	C12	C15	106.9(3)	C16	N4	Ru1	174.7(5)
C11	C12	C14	107.5(3)	C21	N5	Ru1	174.7(6)
C15	C12	C14	110.2(3)	N1	Ru1	N5	91.0(2)
C11	C12	C13	109.8(3)	N1	Ru1	N2	88.5(2)
C15	C12	C13	111.8(3)	N5	Ru1	N2	178.0(3)
C14	C12	C13	110.5(4)	N1	Ru1	N4	178.9(3)
N4	C16	C17	176.5(7)	N5	Ru1	N4	88.5(2)
C16	C17	C18	108.5(5)	N2	Ru1	N4	92.0(2)
C16	C17	C19	106.4(5)	N1	Ru1	C26	90.5(2)
C18	C17	C19	111.9(6)	N5	Ru1	C26	90.5(2)
C16	C17	C20	108.0(5)	N2	Ru1	C26	91.4(2)
C18	C17	C20	111.2(6)	N4	Ru1	C26	90.5(2)
C19	C17	C20	110.7(6)	N1	Ru1	N3	92.7(2)
N5	C21	C22	174.9(7)	N5	Ru1	N3	92.0(2)
C21	C22	C23	110.7(5)	N2	Ru1	N3	86.1(2)
C21	C22	C24	106.4(6)	N4	Ru1	N3	86.3(2)
C23	C22	C24	110.7(6)	C26	Ru1	N3	175.9(3)
C21	C22	C25	108.5(5)				

Table 6 Hydrogen Bonds for Ru2-39c

D	*H*	*A*	*d(D-H)/Å*	*d(H-A)/Å*	*d(D-A)/Å*	*D-H-A/°*
C29	H29	F8[1]	0.95	2.42	3.254(5)	145.8

Table 7 Torsion Angles for Ru2-39c

A	*B*	*C*	*D*	*Angle/°*	*A*	*B*	*C*	*D*	*Angle/°*
C31	C26	C27	F1	180.0(3)	C28	C29	C30	F3	179.1(4)
Ru1	C26	C27	F1	-3.0(6)	C28	C29	C30	C31	-0.1(6)
C31	C26	C27	C28	-1.5(7)	F3	C30	C31	F4	1.0(5)
Ru1	C26	C27	C28	175.5(3)	C29	C30	C31	F4	-179.7(3)
F1	C27	C28	F2	-1.5(5)	F3	C30	C31	C26	179.9(4)
C26	C27	C28	F2	180.0(4)	C29	C30	C31	C26	-0.8(6)
F1	C27	C28	C29	179.3(3)	C27	C26	C31	F4	-179.6(4)
C26	C27	C28	C29	0.7(6)	Ru1	C26	C31	F4	3.4(6)
F2	C28	C29	C30	-179.1(3)	C27	C26	C31	C30	1.5(7)
C27	C28	C29	C30	0.2(6)	Ru1	C26	C31	C30	-175.5(3)

Table 8 H-Atom Coordinates (Å×10^4) and Isotropic Displacement Parameters (Å^2×10^3) for Ru2-39c

Atom	*x*	*y*	*z*	*U(eq)*
H3A	6244	7701	6606	47
H3B	4576	7805	6379	47
H3C	4765	7294	7859	47
H4A	3094	9100	8340	47
H4B	2818	9617	6889	47
H4C	3451	10667	7348	47
H5A	5659	11321	5360	49
H5B	5180	10258	4835	49
H5C	6832	10211	5080	49
H8A	12987	12683	4744	37
H8B	12618	13270	3326	37
H8C	12237	11696	4288	37
H9A	9560	12055	4064	43
H9B	9796	13672	3251	43
H9C	8488	13069	4627	43
H10A	9686	14607	5409	43
H10B	11089	15092	4093	43
H10C	11400	14371	5531	43

H13A	4708	13973	9659	54
H13B	5190	14916	10310	54
H13C	4899	13305	11142	54
H14A	8654	14656	7901	49
H14B	7644	15776	8338	49
H14C	6962	14902	7724	49
H15A	7551	13079	11494	50
H15B	7889	14688	10685	50
H15C	9009	13632	10231	50
H18A	13267	8715	10997	36
H18B	13977	9673	11510	36
H18C	13798	10261	10023	36
H19A	9991	9553	13200	49
H19B	11615	9056	13456	49
H19C	10730	8263	12897	49
H20A	12268	12199	10391	47
H20B	12418	11674	11884	47
H20C	10767	11885	11616	47
H23A	4616	7947	13941	59
H23B	4140	6375	14853	59
H23C	3783	7063	13431	59
H24A	8178	6273	13632	53
H24B	6822	5900	14977	53
H24C	7337	7464	14061	53
H25A	5228	5272	12676	66
H25B	5568	4534	14100	66
H25C	6950	5003	12769	66
H29	12104	5344	7885	36

References

[1] a) Bringmann, G.; Günther, C.; Ochse, M.; Schupp, O.; Tasler, S. Biaryls in Nature: A Multi-Facetted Class of Stereochemically, Biosynthetically, and Pharmacologically Intriguing Secondary Metabolites; In *Progress in the Chemistry of Organic Natural Products*; Herz, W., Falk, H., Kirby, G. W., Moore, R. E., Eds.; Springer Vienna: 2001; Vol. 82, pp 1-249; b) Hassan, J.; Sévignon, M.; Gozzi, C.; Schulz, E.; Lemaire, M. *Chem. Rev.* **2002**, *102*, 1359; c) Horton, D. A.; Bourne, G. T.; Smythe, M. L. *Chem. Rev.* **2003**, *103*, 893; d) Bringmann, G.; Price Mortimer, A. J.; Keller, P. A.; Gresser, M. J.; Garner, J.; Breuning, M. *Angew. Chem. Int. Ed.* **2005**, *44*, 5384.

[2] a) Ullmann, F.; Bielecki, J. *Ber. Dtsch. Chem. Ges.* **1901**, *34*, 2174; b) Ullmann, F. *Ber. Dtsch. Chem. Ges.* **1903**, *36*, 2382; c) Ullmann, F.; Sponagel, P. *Ber. Dtsch. Chem. Ges.* **1905**, *38*, 2211; d) Goldberg, I. *Ber. Dtsch. Chem. Ges.* **1906**, *39*, 1691.

[3] de Meijere, A.; Diederich, F. *Metal-Catalyzed Cross-Coupling Reactions*; Wiley-VCH: Weinheim, 2004.

[4] http://www.nobelprize.org/nobel_prizes/chemistry/laureates/2010/

[5] Sheldon, R. A. *Green Chem.* **2007**, *9*, 1273.

[6] Trost, B. M. *Angew. Chem. Int. Ed.* **1995**, *34*, 259.

[7] Representative reviews on C–H activation: a) Alberico, D.; Scott, M. E.; Lautens, M. *Chem. Rev.* **2007**, *107*, 174; b) Ackermann, L.; Vicente, R.; Kapdi, A. R. *Angew. Chem. Int. Ed.* **2009**, *48*, 9792; c) Gutekunst, W. R.; Baran, P. S. *Chem. Soc. Rev.* **2010**, *40*, 1976; d) Lyons, T. W.; Sanford, M. S. *Chem. Rev.* **2010**, *110*, 1147; e) Boorman, T. C.; Larrosa, I. *Chem. Soc. Rev.* **2011**, *40*, 1910; f) Wencel-Delord, J.; Droge, T.; Liu, F.; Glorius, F. *Chem. Soc. Rev.* **2011**, *40*, 4740; g) Arockiam, P. B.; Bruneau, C.; Dixneuf, P. H. *Chem. Rev.* **2012**, *112*, 5879; h) Engle, K. M.; Mei, T.-S.; Wasa, M.; Yu, J.-Q. *Acc. Chem. Res.* **2012**, *45*, 708; i) Girard, S. A.; Knauber, T.; Li, C. J. *Angew. Chem. Int. Ed.* **2014**, *53*, 74; l) Kakiuchi, F.; Kochi, T.; Murai, S. *Synlett* **2014**, *25*, 2390; m) Tani, S.; Uehara, T. N.; Yamaguchi, J.; Itami, K. *Chem. Sci.* **2014**, *5*, 123; n) Zhang, X.-S.; Chen, K.; Shi, Z.-J. *Chem. Sci.* **2014**, *5*, 2146.

[8] Selected examples and reviews: a) Yamaguchi, J.; Muto, K.; Itami, K. *Eur. J. Org. Chem.* **2013**, 19; b) Sun, Y.; Sun, H.; Jia, J.; Du, A.; Li, X. *Organometallics* **2014**, *33*, 1079; c) Aihara, Y.; Chatani, N. *J. Am. Chem. Soc.* **2014**, *136*, 898; d) Yokota, A.; Aihara, Y.; Chatani, N. *J. Org. Chem.* **2014**, *79*, 11922.

[9] a) Join, B.; Yamamoto, T.; Itami, K. *Angew. Chem. Int. Ed.* **2009**, *48*, 3644; b) Junker, A.; Yamaguchi, J.; Itami, K.; Wünsch, B. *J. Org. Chem.* **2013**, *78*, 5579.

[10] Lane, B. S.; Sames, D. *Org. Lett.* **2004**, *6*, 2897.

[11] Lane, B. S.; Brown, M. G.; Sames, D. *J. Am. Chem. Soc.* **2005**, *127*, 8050.

[12] a)Yanagisawa, S.; Sudo, T.; Noyori, R.; Itami, K. *J. Am. Chem. Soc.* **2006**, *128*, 11748; b) Yanagisawa, S.; Sudo, T.; Noyori, R.; Itami, K. *Tetrahedron* **2008**, *64*, 6073.

[13] Ciana, C.-L.; Phipps, R. J.; Brandt, J. R.; Meyer, F.-M.; Gaunt, M. J. *Angew. Chem. Int. Ed.* **2011**, *50*, 458.

[14] a) Phipps, R. J., Gaunt, M. J. *Science* **2009**, *323*, 1593; b) Duong, H. A.; Gilligan, R. E.; Cooke, M. L.; Phipps, R. J.; Gaunt, M. J. *Angew. Chem. Int. Ed.* **2011**, *50*, 463.

[15] a) Kita, Y.; Morimoto, K.; Ito, M.; Ogawa, C.; Goto, A.; Dohi, T. *J. Am. Chem. Soc.* **2009**, *131*, 1668; b) Malmgren, J.; Santoro, S.; Jalalian, N.; Himo, F.; Olofsson, B. *Chem. Eur. J.* **2013**, *19*, 10334.

[16] a) Ball, L. T.; Lloyd-Jones, G. C.; Russell, C. A. *Science* **2012**, *337*, 1644; b) Ball, L. T.; Lloyd-Jones, G. C.; Russell, C. A. *J. Am. Chem. Soc.* **2014**, *136*, 254.

[17] Ryabov, A. D.; Sakodinskaya, I. K.; Yatsimirsky, A. K. *J. Chem. Soc., Dalton Trans*. **1985**, 2629.

[18] Davies, D. L.; Donald, S. M. A.; Macgregor, S. A. *J. Am. Chem. Soc*. **2005**, *127*, 13754.

[19] a) Campeau, L.-C.; Rousseaux, S.; Fagnou, K. *J. Am. Chem. Soc*. **2005**, *127*, 18020; b) Leclerc, J.-P. ; Fagnou, K. *Angew. Chem. Int. Ed*. **2006**, *45*, 7781; c) Campeau, L.-C.; Bertrand-Laperle, M.; Leclerc, J.-P.; Villemure, E.; Gorelsky, S.; Fagnou, K. *J. Am. Chem. Soc*. **2008**, *130*, 3276; d) Campeau, L.-C.; Stuart, D. R.; Leclerc, J.-P.; Bertrand-Laperle, M.; Villemure, E.; Sun, H.-Y.; Lasserre, S.; Guimond, N.; Lecavallier, M.; Fagnou, K. *J. Am. Chem. Soc*. **2009**, *131*, 3291.

[20] a) García-Cuadrado, D.; Braga, A. A. C.; Maseras, F.; Echavarren, A. M. *J. Am. Chem. Soc*. **2006**, *128*, 1066; b) García-Cuadrado, D.; de Mendoza, P.; Braga, A. A. C.; Maseras, F.; Echavarren, A. M. *J. Am. Chem. Soc*. **2007**, *129*, 6880.

[21] Campeau, L.-C.; Parisien, M.; Leblanc, M.; Fagnou, K. *J. Am. Chem. Soc*. **2004**, *126*, 9186-9187.

[22] Lafrance, M.; Rowley, C. N.; Woo, T. K.; Fagnou, K. *J. Am. Chem. Soc*. **2006**, *128*, 8754.

[23] a) Huang, Q.; Fazio, A.; Dai, G.; Campo, M. A.; Larock, R. C. *J. Am. Chem. Soc*. **2004**, *126*, 7460. b) Zhao, J.; Yue, D.; Campo, M. A.; Larock, R. C. *J. Am. Chem. Soc*. **2007**, *129*, 5288.

[24] Wang, X.; Lane, B. S.; Sames, D. *J. Am. Chem. Soc*. **2005**, *127*, 4996.

[25] Lafrance, M.; Fagnou, K.; *J. Am. Chem. Soc*. **2006**, *128*, 16496.

[26] a) Pascual, S.; de Mendoza, P.; Braga, A. A. C.; Maseras, F.; Echavarren, A. M. *Tetrahedron* **2008**, *64*, 6021; b) Lafrance, M.; Lapointe, D.; Fagnou, K. *Tetrahedron* **2008**, *64*, 6015.

[27] a) Huestis, M. P.; Fagnou, K. *Org. Lett*. **2009**, *11*, 1357; b) Schipper, D. J.; El-Salfiti, M.; Whipp, C. J.; Fagnou, K.; *Tetrahedron* **2009**, *65*, 4977; c) Caron, L.; Campeau, L.-C.; Fagnou, K. *Org. Lett*. **2008**, *10*, 4533.

[28] a) Gorelsky, S. I.; Lapointe, D.; Fagnou, K. *J. Am. Chem. Soc*. **2008**, *130*, 10848; b) Liégault, B.; Petrov, I.; Gorelsky, S. I.; Fagnou, K. *J. Org. Chem*. **2010**, *75*, 1047; c) Liégault, B.; Lapointe, D.; Caron, L.; Vlassova, A.; Fagnou, K. *J. Org. Chem*. **2009**, *74*, 1826; d) Lapointe, D.; Fagnou, K. *Org. Lett*. **2009**, *11*, 4160; e) René, O.; Lapointe, D.; Fagnou, K.; *Org. Lett*. **2009**, *11*, 4560; f) Ackermann, L.; Vicente, R.; Born, R. *Adv. Synth. Catal*. **2008**, *350*, 741; g) Ackermann, L.; Althammer, A.; Fenner, S. *Angew. Chem. Int. Ed*. **2009**, *48*, 201; h) Zhao, D.; Wang, W.; Lian, S.; Yang, F.; Lan, J.; You, J. *Chem. Eur. J*. **2009**, *15*, 1337.

[29] a) Gorelsky, S. I.; Lapointe, D.; Fagnou, K. *J. Am. Chem. Soc*. **2008**, *130*, 10848; b) Lapointe, D.; Markiewicz, T.; Whipp, C. J.; Toderian, A.; Fagnou, K. *J. Org. Chem*. **2011**, *76*, 749.

[30] a) Stuart, D. R.; Fagnou, K. *Science* **2007**, *316*, 1172; b) Stuart, D. R.; Villemure, E; Fagnou, K. *J. Am. Chem. Soc*. **2007**, *129*, 12072; c) Potavathri, S.; Pereira, K. C.; Gorelsky, S. I.; Pike, A.; LeBris, A. P.; DeBoef, B. *J. Am. Chem. Soc*. **2010**, *132*, 14676; d) Meir, R.; Kozuch, S.; Uhe, A.; Shaik, S. *Chem. Eur. J*. **2011**, *17*, 7623.

[31] a) Gorelsky, S. I.; Lapointe, D.; Fagnou, K. *J. Org. Chem*. **2012**, *77*, 658; b) Gorelsky, S. I. *Coord. Chem. Rev*. **2013**, *257*, 153.

[32] a) Liégault, B.; Petrov, I.; Gorelsky, S. I.; Fagnou, K. *J. Org. Chem*. **2010**, *75*, 1047; b) Gorelsky, S. I. *Organometallics* **2012**, *31*, 794.

[33] a) Do, H.-Q.; Daugulis, O. *J. Am. Chem. Soc*. **2008**, *130*, 1128; b) Do, H.-Q.; Khan, R. M. K.; Daugulis, O. *J. Am. Chem. Soc*. **2008**, *130*, 15185.

[34] Lu, P.; Boorman, T. C.; Slawin, A. M. Z.; Larrosa, I. *J. Am. Chem. Soc*. **2010**, *132*, 5580.

[35] Cambeiro, X. C.; Boorman, T. C.; Lu, P.; Larrosa, I. *Angew. Chem. Int. Ed*. **2013**, *52*, 1781.

[36] Cambeiro, X. C.; Ahlsten, N.; Larrosa I. *J. Am. Chem. Soc.* **2015**, *137*, 15636.

[37] a) Yang, J. *Org. Biomol. Chem.* **2015**, *13*, 1930; b) Sharma, R.; Thakur, K.; Kumar, R.; Kumar, I.; Sharma, U. *Cat. Rev. - Sci. Eng.* **2015**, *57*, 345.

[38] Selected examples and reviews: a) Punji, B.; Song, W.; Shevchenko, G. A.; Ackermann, L. *Chem. Eur. J.* **2013**, *19*, 10605; b) Ackermann, L. *J. Org. Chem.* **2014**, *79*, 8948; c) Gao, K.; Yoshikai, N. *Acc. Chem. Res.*, **2014**, *47*, 1208.

[39] Selected examples and reviews: a) Norinder, J.; Matsumoto, A.; Yoshikai, N.; Nakamura, E. *J. Am. Chem. Soc.* **2008**, *130*, 5858; b) Sun, C.-L.; Li, B.-J.; Shi, Z.-J. *Chem. Rev.* **2011**, *111*, 1293; c) Gu, Q.; Al Mamari, H. H.; Graczyk, K.; Diers, E. Ackermann, L. *Angew. Chem. Int. Ed.* **2014**, *53*, 3868.

[40] a) Kitahara, M.; Umeda, N.; Hirano, K; Satoh, T.; Miura, M. *J. Am. Chem. Soc.* **2011**, *133*, 2160; b) Nishino, M.; Hirano, K.; Satoh, T.; Miura, M. *Angew. Chem. Int. Ed.* **2012**, *51*, 6993; c) Hirano, K.; Miura, M. *Chem. Commun.* **2012**, *48*, 10704; d) Nishino,M.; Hirano, K.; Satoh, T.; Miura, M. *Angew. Chem. Int. Ed.* **2013**, *52*, *4457*.

[41] a) Shin, K.; Park, S.-W.; Chang, S. *J. Am. Chem. Soc.* **2015**, *137*, 8584; b) Huang, L.; Hackenberger, D.; Gooßen, L. J. *Angew. Chem. Int. Ed.* **2015**, *54*, 12607; c) Gao, P.; Guo, W.; Xue, J.; Zhao, Y.; Yuan, Y.; Xia, Y.; Shi, Z.-J. *J. Am. Chem. Soc.* **2015**, *137*, 12231.

[42] Tremont, S. J.; Rahaman, H. U. *J. Am. Chem. Soc.* **1984**, *106*, 5760.

[43] Kalyani, D.; Deprez, N. R.; Desai, L. V; Sanford, M. S. *J. Am. Chem. Soc.* **2005**, *127*, 7330.

[44] a) Daugulis, O.; Zaitsev, V. G. *Angew. Chem. Int. Ed.* **2005**, *44*, 4046; b) Shabashov, D.; Daugulis, O. *Org. Lett.* **2005**, *7*, 3657.

[45] Canty, A. J.; Patel, J.; Rodemann, T.; Ryan, J. H.; Skelton, B. W.; White, A. H. *Organometallics* **2004**, 3466.

[46] a) Dick, A. R.; Hull, K. L.; Sanford, M. S. *J. Am. Chem. Soc.* **2004**, *126*, 2300; b) Dick, A. R.; Sanford, M. S. *Tetrahedron* **2006**, *62*, 2439; c) Muñiz, K. *Angew. Chem. Int. Ed.* **2009**, *48*, 9412; d) Hickman, A. J.; Sanford, M. S. *Nature* **2012**, *484*, 177.

[47] Vicente, J.; Arcas, A.; Juliá-Hernández, F.; Bautista, D. *Angew. Chem. Int. Ed.* **2011**, *50*, 6896.

[48] a) Shabashov, D.; Daugulis, O. *Org. Lett.* **2006**, *8*, 4947; b) Shabashov, D.; Daugulis, O. *J. Org. Chem.* **2007**, *72*, 7720.

[49] Daugulis, O.; Do, H.-Q.; Shabashov, D. *Acc. Chem. Res.* **2009**, *42*, 1074.

[50] Fauvarque, J.-F.; Pflüger, F.; Troupel, M. *J. Organomet. Chem.* **1981**, *208*, 419.

[51] Thirunavukkarasu, V. S.; Parthasarathy, K.; Cheng, C.-H. *Angew. Chem. Int. Ed.* **2008**, *47*, 9462.

[52] Thirunavukkarasu, V. S.; Cheng, C.-H. *Chem. Eur. J.* **2011**, *17*, 14723.

[53] Chiong, H.; Pham, Q.-N.; Daugulis, O. *J. Am. Chem. Soc.* **2007**, *129*, 9879.

[54] Cornella, J.; Righi, M.; Larrosa, I. *Angew. Chem. Int. Ed.* **2011**, *50*, 9429.

[55] a) Luo, J.; Preciado, S.; Larrosa, I. *J. Am. Chem. Soc.* **2014**, *136*, 4109; b) Luo, J.; Preciado, S.; Larrosa, I. *Chem. Commun.* **2015**, *51*, 3127; c) Luo, J.; Araromi, S.; Preciado, S.; Larrosa, I. *Chem. Asian J.* doi: 10.1002/asia.2015 00506.

[56]Arroniz, C.; Ironmonger, A.; Rassias, G.; Larrosa, I. *Org. Lett.* **2013**, *15*, 910.

[57] Arroniz, C.; Denis, J. G.; Ironmonger, A.; Rassias, G.; Larrosa, I. *Chem. Sci.* **2014**, *5*, 3509.

[58] Giri, R.; Maugel, N.; Li, J.-J.; Wang, D.-H.; Breazzano, S. P.; Saunders, L. B.; Yu, J.-Q. *J. Am. Chem. Soc.* **2007**, *129*, 3510.

[59] Wang, D.-H.; Mei, T.-S.; Yu, J.-Q. *J. Am. Chem. Soc.* **2008**, *130*, 17676.

[60] Zhu, C.; Zhang, Y.; Kan, J.; Zhao, H.; Su, W. *Org. Lett.* **2015**, *17*, 3418.

[61] a)Yang, S.; Li, B.; Wan, X.; Shi, Z. *J. Am. Chem. Soc.* **2007**, *129*, 6066; b) Shi, Z.; Li, B.; Wan, X.; Cheng, J.; Fang, Z.; Cao, B.; Qin, C.; Wang, Y. *Angew. Chem. Int. Ed.* **2007**, *46*, 5554; c) Li, B.-J.; Tian, S.-L.; Fang, Z.; Shi, Z.-J. *Angew. Chem. Int. Ed.* **2008**, *47*, 1115; d) Brache, G.; Garcia-Fortanet, J.; Buchwald, S. L. *Org. Lett.* **2008**, *10,* 2207; e) Yeung, C. S.; Zhao, X.; Borduas, N.; Dong, V. M. *Chem. Sci.* **2010**, *1*, 331; f) Wang, X.; Leow, D.; Yu, J.-Q. *J. Am. Chem. Soc.* **2011**, *133*, 13864.

[62] a) Kametani, Y.; Satoh, T.; Miura, M.; Nomura, M. *Tetrahedron Lett.* **2000**, *41*, 2655; b) Shabashov, D.; Molina Maldonado, J. R.; Daugulis, O. *J. Org. Chem.* **2008**, *73*, 7818; c) Li, D.-D.; Yuan, T.-T.; Wang, G.-W. *J. Org. Chem.* **2012**, *77*, 334.

[63] Sun, C.-L.; Liu, N.; Li, B.-J.; Yu, D.-G.; Wang, Y.; Shi, Z.-J. *Org. Lett.* **2010**, *12*, 184.

[64] a) Hull, K. L.; Lanni, E. L.; Sanford, M. S. *J. Am. Chem. Soc.* **2006**, *128*, 14047; b) Xia, J.; You, S. *Organometallics* **2007**, *26,* 4869; c) Hull, K. L.; Sanford, M. S. *J. Am. Chem. Soc.* **2007**, *129*, 11904; d) Hull, K. L.; Sanford, M. S. *J. Am. Chem. Soc.* **2009**, *131*, 9651; e) Lyons, T. W.; Hull, K. L.; Sanford, M. S. *J. Am. Chem. Soc.* **2011**, *133*, 4455; f) Yu, M.; Liang, Z.; Wang, Y.; Zhang, Y. *J. Org. Chem.* **2011**, *76*, 4987; g) Aihara, Y.; Chatani, N. *Chem. Sci.* **2013**, *4*, 664.

[65] a) Bedford, R. B.; Webster, R. L.; Mitchell, C. J. *Org. Biomol. Chem.* **2009**, *7*, 4853; b) Zhao, X.; Yeung, C. S.; Dong, V. M. *J. Am. Chem. Soc.* **2010**, *132*, 5837.

[66] Nishikata, T.; Abela, A. R.; Huang, S.; Lipshutz, B. H. *J. Am. Chem. Soc.* **2010**, *132*, 497.

[67] Shao, J.; Chen, W.; Giulianotti, M. A.; Houghten, R. A.; Yu, Y. *Org. Lett.* **2012**, *14*, 5452.

[68] a) Satoh, T.; Kametani, Y.; Terao, Y.; Miura, M.; Nomura, M. *Tetrahedron Lett.* **1999**, *40*, 5345; b) Terao, Y.; Kametani, Y.; Wakui, H.; Satoh, T.; Miura, M.; Nomura, M. *Tetrahedron* **2001**, *57*, 5967.

[69] Gürbüz, N.; Özdemir, I.; Çetinkaya, B. *Tetrahedron Lett.* **2005**, *46*, 2273.

[70] a) Satoh, T.; Kawamura, Y.; Miura, M.; Nomura, M. *Angew. Chem. Int. Ed. Engl.* **1997**, *36*, 1740; b) Kawamura, Y.; Satoh, T.; Miura, M.; Nomura, M. *Chem. Lett.* **1998**, *27*, 931.

[71] Terao, Y.; Wakui, H.; Nomoto, M.; Satoh, T.; Miura, M.; Nomura, M. *J. Org. Chem.* **2003**, *68*, 5236.

[72] a) Chan, L. Y.; Cheong L.; Kim S. *Org. Lett.* **2013**, *15*, 2186; b) Jeon, W. H.; Lee, T. S.; Kim, E., J.; Moon, B.; Kang, J. *Tetrahedron* **2013**, *69*, 5152.

[73] a) Lazareva, A.; Daugulis, O. *Org. Lett.* **2006**, *8*, 5211; b) Gao, D.-W.; Shi, Y.-C.; Gu, Q.; Zhao, Z.-L.; You, S.-L. *J. Am. Chem. Soc.* **2013**, *135*, 86.

[74] a) Trost, B. M.; Toste, F. D.; Pinkerton, A. B. *Chem. Rev.* **2001**, *101*, 2067; b) De Sarkar, S.; Liu, W.; Kozhushkov, S. I.; Ackermann, L. *Adv. Synth. Catal.* **2014**, *356*, 146.

[75] Lewis, L. N.; Smith, J. F. *J. Am. Chem. Soc.* **1986**, *108*, 2728.

[76] Murai, S.; Kakiuchi, F.; Sekine, S.; Tanaka, Y.; Kamatani, A.; Sonoda, M.; Chatani, N. *Nature* **1993**, 529; b) Kakiuchi, F.; Yamamoto, Y.; Chatani, N.; Murai, S. *Chem. Lett.* **1995**, 681; c) Kakiuchi, F.; Murai, S. *Acc. Chem. Res.* **2002**, *35*, 826.

[77] a) Kakiuchi, F.; Kan, S.; Igi, K.; Chatani, N.; Murai, S. *J. Am. Chem. Soc.* **2003**, *125*, 1698; b) Kakiuchi, F.; Matsuura, Y.; Kan, S.; Chatani, N. *J. Am. Chem. Soc.* **2005**, *127*, 5936.

[78] a) Oi, S.; Fukita, S.; Hirata, N.; Watanuki, N.; Miyano, S.; Inoue, Y. *Org. Lett.* **2001**, *3*, 2579; b) Oi, S.; Ogino, Y.; Fukita, S.; Inoue, Y. *Org. Lett.* **2002**, *4*, 1783.

[79] a) Ackermann, L. *Org. Lett.* **2005**, *7*, 3123; b) Ackermann, L.; Althammer, A.; Born, R. *Angew. Chem. Int. Ed.* **2006**, *45*, 2619.

[80] Özdemir, I.; Demir, S.; Çetinkaya, B.; Gourlaouen, C.; Maseras, F.; Bruneau, C.; Dixneuf, P. H. *J. Am. Chem. Soc.* **2008**, *130*, 1156.

[81] Ackermann, L.; Vicente, R.; Althammer, A. *Org. Lett.* **2008**, *10*, 2299.

[82] a) Chinnagolla, R. K.; Jeganmohan, M. *Org. Lett.* **2012**, *14*, 5246; b) Chinnagolla, R. K.; Jeganmohan, M. *Chem. Commun.* **2014**, *50*, 2442.

[83] a) Hubrich, J.; Himmler, T.; Rodefeld, L.; Ackermann, L. *Adv. Synth. Catal.* **2015**, *357*, 474; b) Ackermann. L. *Org. Process Res. Dev.* **2015**, *19*, 260 and ref. therein.

[84] Oi, S.; Fukita, S.; Inoue Y. *Chem. Commun.* **1998**, 2439.

[85] a) Ueura, K.; Satoh, T.; Miura, M. *Org. Lett.* **2005**, *7*, 2229; b) Miyamura, S.; Tsurugi, H.; Satoh, T.; Miura, M. *J. Organomet. Chem.* **2008**, *693*, 2438.

[86] Vogler, T.; Studer, A. *Org. Lett.* **2008**, *10*, 129.

[87] a) Lu, M.-Z.; Lu, P.; Xu, Y.-H.; Loh, T.-P. *Org. Lett.* **2014**, *16*, 2614; b) Wang, L.; Qu, X.; Li, Z.; Peng, W.-M. *Tetrahedron Lett.* **2015**, *56*, 3754.

[88] a) Bedford, R. B.; Coles, S. J.; Hursthouse, M. B.; Limmert, M. E. *Angew. Chem., Int. Ed.* **2003**, *42*, 112; b) Bedford, R. B.; Limmert, M. E. *J. Org. Chem.* **2003**, *68*, 8669; c) Bedford, R. B.; Betham, M.; Caffyn, A. J. M.; Charmant, J. P .H.; Lewis-Alleyne, L. C.; Long, P. D.; Polo-Cerón, D.; Prashar, S. *Chem. Commun.* **2008**, 990.

[89] Oi, S.; Watanabe, S.; Fukita, S.; Inoue, Y. *Tetrahedron Lett.* **2003**, *44*, 8665.

[90] Zhao, X.; Yu, Z. *J. Am. Chem. Soc.* **2008**, *130*, 8136.

[91] a) Wencel-Delord, J.; Nimphius, C.; Patureau, F. W.; Glorius, F. *Angew. Chem., Int. Ed.* **2012**, *51*, 2247; b) Kuhl, N.; Hopkison, M. N.; Glorius, F. *Angew. Chem. Int. Ed.* **2012**, *51*, 8230; c) Wencel-Delord, J.; Nimphius, C.; Wang, H. G.; Glorius, F. *Angew. Chem. Int. Ed.* **2012**, *51*, 13001.

[92] Kuhl, N.; Hopkinson, M. N.; Wencel-Delord, J.; Glorius, F. *Angew. Chem. Int. Ed.* **2012**, *51*, 10236.

[93] Dong, J. X.; Long, Z.; Jie, S. F.; Wu, N. J.; Guo, Q.; Lan, J. B.; You, J. S. *Angew. Chem. Int. Ed.* **2013**, *52*, 580.

[94] Phipps, R. J.; Grimster; N. P.; Gaunt, M. J. *J. Am. Chem. Soc.* **2008**, *130*, 8172.

[95] Phipps, R. J.: Gaunt, M. J. *Science*, **2009**, *323*, 1593.

[96] Chen, B.; Hou, X.-L.; Li, Y.-X.; Wu, Y.-D. *J. Am. Chem. Soc.* **2011**, *133*, 7668.

[97] Leow, D.; Li, G.; Mei, T.-S.; Yu, J.-Q. *Nature* **2012**, *486*, 518.

[98] Yang, Y.-F.; Cheng, G.-J.; Liu, P.; Leow, D.; Sun, T.-Y.; Chen, P.; Zhang, X.; Yu, J.-Q.; Wu; Y.-D.; Houk, K. N. *J. Am. Chem. Soc.* **2014**, *136*, 344.

[99] Wan, L.; Dastbaravardeh, N.; Li G.; Yu, J.-Q. *J. Am. Chem. Soc.* **2013**, *135*, 18056.

[100] Yang, G.; Lindovska, P.; Zhu, D.; Kim, J.; Wang, P.; Tang, R.Y.; Movassaghi, M.; Yu, J.-Q. *J. Am. Chem. Soc.* **2014**, *136*, 10807.

[101] Cheng, G.-J.; Yang, Y.-F.; Liu, P.; Chen, P.; Sun, T.-Y.; Li, G.; Zhang, X.; Houk, K. N.; Yu, J.-Q.; Wu, Y.-D. *J. Am. Chem. Soc.* **2014**, *136*, 894.

[102] a) Dai, H. X.; Li, G.; Zhang, X. G.; Stepan, A. F.; Yu, J.-Q. *J. Am. Chem. Soc.* **2013** *135*, 7567; b) Lee, S.; Lee H.; Tan, K. L. *J. Am. Chem. Soc.* **2013**, *135*, 18778; c) Bera, M.; Modak, A.; Patra, T.; Maji, A.; Maiti, D. *Org. Lett.* **2014**, *16*, 5760; d) Tang, R.Y.; Li, G.; Yu, J.-Q. *Nature* **2014**, *507*, 215; e) Deng, Y.; Yu, J.-Q. *Angew. Chem. Int. Ed.* **2015**, *54*, 888.

[103] a) Catellani, M. *Top. Organomet. Chem.* **2005**, *14*, 21; b) Ye, J.; Lautens, M. *Nat. Chem.* **2015**, *7*, 863.

[104] a) Wan, X.-C.; Gong, W.; Fang, L.-Z.; Zhu, R.-Y.; Li, S.; Engle, K. M.; Yu, J.-Q. *Nature*, **2015**, *519*, 334; b) Shen, P.-X.; Wang, X.-C.; Wang, P.; Zhu, R.-Y.; Yu, J.-Q. *J. Am. Chem. Soc.* **2015**, *137*, 11574.

[105] Dong, Z.; Wang, J.; Dong, G. *J. Am. Chem. Soc.* **2015**, *137*, 5887.

[106] Maestri, G.; Motti, E.; Della Ca', N.; Malacria, M.; Derat, E.; Catellani, M. *J. Am. Chem. Soc.* **2011**, *133*, 8574.

[107] Juliá-Hernández, F.; Simonetti, M.; Larrosa, I. *Angew. Chem. Int. Ed.* **2013**, *52*, 11458.

[108] a) Saidi, O.; Marafie, J.; Ledger, A. E.; Liu, P. M.; Mahon, M. F.; Kociok-Kohn, G.; Whittlesey, M. K.; Frost, C. G. *J. Am. Chem. Soc.* **2011**, *133*, 19298; b) Paterson, A. J.; St John-Campbell, S.; Mahon, M. F.; Press; N. J.; Frost, C. G. *Chem. Commun.* **2015**, *51*, 12807.

[109] a) Hofmann, N.; Ackermann, L. *J. Am. Chem. Soc.* **2013**, *135*, 5877; b) Li, J.; Warratz, S.; Zell, D.; De Sarkar, S.; Ishikawa, E. E.; Ackermann, L. *J. Am. Chem. Soc.* **2015**, *137*, 13894.

[110] Teskey, C. J.; Lui, A. Y. W.; Greaney, M. F. *Angew.Chem. Int. Ed.* **2015**, *54*, 11677.

[111] Yu, Q.; Hu, L.; Wang, Y.; Zheng, S.; Huang, J. *Angew. Chem. Int. Ed.* **2015**, *54*, 15284.

[112] Gagliardo, M.; Snelders, D. J.; Chase, P. A.; Klein Gebbink, R. J.; van Klink, G. P.; van Koten, G. *Angew. Chem. Int. Ed.* **2007**, *46*, 8558.

[113] a) Beley, M.; Collin, J.-P.; Louis, R.; Metz, B.; Sauvage, J.-P. *J. Am. Chem. Soc.* **1991**, *113*, 8521; b) Espinet, P.; Alonso, M. Y.; Garcia-Herbosa, G.; Ramos, J. M.; Jeannin, Y.; Philoche-Levisalles, M. *Inorg. Chem.* **1992**, *31*, 2501; c) Beley, M.; Collin, J.-P.; Sauvage, J.-P. *Inorg. Chem.* **1993**, *32*, 4539; d) Sutter, J.-P.; Grove, D. M.; Beley, M.; Collin, J.-P.; Veldman, N.; Spek, A. L.; Sauvage, J.-P.; van Koten, G. *Angew. Chem. Int. Ed.* **1994**, *33*, 1282; e) Wadman, S. H.; Havenith, R. W.; Lutz, M.; Spek, A. L.; van Klink, G. P.; van Koten, G. *J. Am. Chem. Soc.* **2010**, *132*, 1914.

[114] a) Clark, G. R.; Headford, C. E. L.; Roper, W. R.; Wright, L. J.; Yap; V. P. D. *Inorg. Chim. Acta* **1994**, *220*, 261; b) Clark, A. M.; Rickard, C. E. F.; Roper, W. R.; Wright, L. J. *Organometallics* **1999**, *18*, 2813; c) Clark, A. M.; Rickard, C. E. F.; Roper, W. R.; Wright, L. J. *J. Organomet. Chem.* **2000**, *598*, 262; d) Stoessel, P.; Spreitzer, H.; Bach, I. **2004**, WO 2004/037836A1.

[115] a) Gagliardo, M.; Amijs, C. H.; Lutz, M.; Spek, A. L.; Havenith, R. W.; Hartl, F.; van Klink, G. P.; van Koten, G. *Inorg. Chem.* **2007**, *46*, 11133; b) Stoessel, P.; Spreitzer, H. Becker, H. **2002**, DE 101 09 027A1; c) Stoessel, P.; Spreitzer, H.; Becker, H. **2002**, WO 02/068435A1.

[116] a) Clark, A. M.; Rickard, C. E. F.; Roper, W. R.; Wright, L. J. *Organometallics* **1998**, *17*, 4535; b) Coudret, C.; Fraysse, S. *Chem. Commun.* **1998**, 663; c) Lau, M.-K.; Zhang, Q.-F.; Chim, J. L. C.; Leung, W.-H.: Wong, W.-T. *Chem. Commun.* **2001**, 1478; d) Arm, K. J.; Williams, J. A. *Chem. Commun.* **2005**, 230; e) Cheung, K.-

M.; Zhang, Q.-F.; Chan, K.-W.; Lam, M. H. W.; Williams, I. D.; Leung, W.-H. *J. Organomet. Chem.* **2005**, *690*, 2913.

[117] a) Slagt, M. Q.; Klein Gebbink, R. J. M.; Lutz, M.; Spek, A. L.; van Koten, G. *J. Chem. Soc. Dalton Trans.* **2002**, 2591; b) Slagt, M. Q.; Rodríguez, G.; Grutters, M. M. P.; Klein Gebbink, R. J. M.; Klopper, W.; Jenneskens, L. W.; Lutz, M.; Spek, A. L.; van Koten, G. *Chem. Eur. J.* **2004**, *10*, 1331.

[118] Stoessel, P.; Spreitzer, H.; Becker, H. **2003**, WO 03/040160A1.

[119] Ackermann, L.; Novak, P.; Vicente, R.; Hofmann, N. *Angew. Chem. Int. Ed.* **2009**, *48*, 6045.

[120] Ackermann, L.; Novák, P.; Vicente, R.; Pirovano, V.; Potukuchi, H. K. *Synthesis* **2010**, 2245.

[121] Na, Y.; Park, S.; Han, S. B.; Han, H.; Ko, S.; Chang, S. *J. Am. Chem. Soc.* **2004**, *126*, 250.

[122] a) Ezbiansky, K.; Djurovich, P. I.; LaForest, M.; Sinning, D. J.; Zayes, R.; Berry, D. H. *Organometallics* **1998**, *17*, 1455; b) Ishiyama, T.; Sato, K.; Nishio, Y.; Miyaura, N. *Angew. Chem. Int. Ed.* **2003**, 42, 5346; c) Ishiyama, T.; Sato, K.; Nishio, Y.; Miyaura, N. *Angew. Chem.* **2003**, *115*, 5504; d) Tsukada, N.; Hartwig, J. F. *J. Am. Chem. Soc.* **2005**, *127*, 5022; e) Saiki, T.; Nishio, Y.; Ishiyama, T.; Miyaura, N. *Organometallics* **2006**, *25*, 6068; f) Murata, M.; Fukuyama, N.; Wada, J.; Watanabe, S.; Masuda, Y. *Chem. Lett.* **2007**, *36*, 910; g) Cheng, C.; Hartwig, J. F. *Science* **2014**, *343*, 853; h) Cheng, C.; Hartwig, J. F. *J. Am. Chem. Soc.* **2014**, *136*, 12064.

[123] a) Iverson, C. N.; Smith, M. R. *J. Am. Chem. Soc.* **1999**, *121*, 7696; b) Chen, H.; Schlecht, S.; Semple, T. C.; Hartwig, J. F. *Science* **2000**, *287*, 1995; c) Cho, J.-Y.; Iverson, C. N.; Smith, M. R. *J. Am. Chem. Soc.* **2000**, *122*, 12868; d) Cho, J.-Y.; Tse, M. K.; Holmes, D.; Maleczka, R. E.; Smith, M. R. *Science* **2002**, *295*, 305; e) Ishiyama, T.; Takagi, J.; Ishida, K.; Miyaura, N.; Anastasi, N.; Hartwig, J. F. *J. Am. Chem. Soc.* **2002**, *124*, 390; f) Ishiyama, T.; Takagi. J.; Hartwig, J. F.; Miyaura, N. *Angew. Chem. Int. Ed.* **2002**, 41, 3056; g) Ishiyama, T.; Nobuta, Y.; Hartwig, J. F.; Miyaura, N. *Chem. Commun.* **2003**, 2924; h) Tamura, H.; Yamazaki, H.; Sato, H.; Sakaki, S. *J. Am. Chem. Soc.* **2003**, *125*, 16114; i) Boller, T. M.; Murphy, J. M.; Hapke, M.; Ishiyama, T.; Miyaura, N.; Hartwig, J. F. *J. Am. Chem. Soc.* **2005**, *127*, 14263; l) Saito, Y.; Segawa, Y.; Itami, K. *J. Am. Chem. Soc.* **2015**, *137*, 5193.

[124] Mkhalid, I. A. I.; Barnard, J. H.; Marder, T. B.; Murphy, J. M.; Hartwig, J. F. *Chem. Rev.* **2009**, *110*, 890; b) Hartwig, J. F. *Acc. Chem. Res.* **2012**, *45*, 864.

[125] Furukawa, T.; Tobisu, M.; Chatani, N. *Chem. Commun.* **2015**, *51*, 6508.

[126] a)Waltz, K. M.; He, X.; Muhoro, C.; Hartwig, J. F. *J. Am. Chem. Soc.* **1995**, *117*, 11357; b) Hatanaka, T.; Ohki, Y.; Tatsumi, K. *Chem. Asian J.* **2010**, *5*, 1657; c)Yan, G.; Jiang, Y.; Kuang, C.; Wang, S.; Liu, H.; Zhang; Y.; Wang, J. *Chem. Commun.* **2010**, *46*, 3170; e) Mazzacano, T. J.; Mankad, N. P. *J. Am. Chem. Soc.* **2013**, *135*, 17258.

[127] Obligacion, J. V.; Semproni, S. P.; Chirik. P. J. *J. Am. Chem. Soc.* **2014**, *136*, 4133.

[128] Furukawa, T.; Tobisu, M.; Chatani, N. *J. Am. Chem. Soc.* **2015**, *137*, 12211.

[129] Hartwig, J. F. *Chem. Soc. Rev.* **2011**, *40*, 1992.

[130] Kuninobu, Y.; Ida, H.; Nishi, M.; Kanai, M. *Nature Chem.* **2015**, *7*, 712.

[131] Haynes, William M., and David R. Lide. *CRC Handbook of Chemistry and Physics: A Ready-Reference Book of Chemical and Physical Data*; Boca Raton, Fla: CRC, 2010.

[132] Average price and global demand of palladium and ruthenium from 2005 to 2013. Johnson Matthey Precious Metals Management Home Page. http://www.platinum.matthey.com (accessed Nov 10, 2015).

[133] a) Kakiuchi, F.; Matsumoto, M.; Sonoda, M.; Fukuyama, T.; Chatani, N.; Murai, S.; Furukawa, N.; Seki, Y. *Chem. Lett.* **2000**, 750; b) Kakiuchi, F.; Igi, K.; Matsumoto, M.; Chatani, N.; Murai, S. *Chem. Lett.* **2001**, 422.

[134] For other Ru-catalysed C_{Ar}–H functionalization reactions without directing groups, see: 1) Intra- and intermolecular hydroarylation of alkenes and alkynes with aromatic compounds: a) Lail, M.; Arrowood, B. N.; Gunnoe, T. B. *J. Am. Chem. Soc.* **2003**, *125*, 7506; b) Youn, S. W.; Pastine, S. J.; Sames, D. *Org. Lett.* **2004**, *6*, 581; c) Pittard, K. A.; Lee, J. P.; Cundari, T. R.; Gunnoe, T. B.; Petersen, J. L. *Organometallics* **2004**, *23*, 5514; d) Cadierno, V.; Francos, J.; Gimeno, J. *Chem. Commun.* **2010**, *46*, 4175; e) Tan, S. T.; Teo, Y. C.; Fan, W. Y. *J. Organomet. Chem.* **2012**, *708-709*, 58; 2) Allylation of arenes with Ru(IV)-based catalysts: f) Nishibayashi, Y.; Yamanashi, M.; Takagi, Y.; Hidai, M. *Chem. Commun.* **1997**, 859; g) Fernandez, I.; Hermatschweiler, R.; Breher, F.; Pregosin, P. S.; Veiros, L. F.; Calhorda, M. J. *Angew. Chem. Int. Ed.* **2006**, *45*, 6386; h) Bruneau, C.; Achard, M. *Coord. Chem. Rev.* **2012**, *256*, 525; 3) Propargylation of aromatic compounds with propargyl alcohols: i) Bustelo, E.; Dixneuf, P. H. *Adv. Synth. Catal.* **2005**, *347*, 393; (j) Fischmeister, C.; Toupet, L.; Dixneuf, P. H. *New J. Chem.* **2005**, *29*, 765; k) Thies, N.; Hrib, C. G.; Haak, E. *Chem. Eur. J.* **2012**, *18*, 6302; 4) Oxidative cross-coupling of benzene derivatives with cycloalkanes: l) Guo, X.; Li, C.-J. *Org. Lett.* **2011**, *13*, 4977; 5) Oxidative coupling of arenes with alkenes using bimolecular oxygen as terminal oxidant: m) Weissman, H.; Song, X.; Milstein, D. *J. Am. Chem. Soc.* **2001**, *123*, 337; 6) C-3 selective C–H silylation of indoles: n) Klare, H. F.; Oestreich, M.; Ito, J.; Nishiyama, H.; Ohki, Y.; Tatsumi, K. *J. Am. Chem. Soc.* **2011**, *133*, 3312; 7) Dehydrogenative C–N cross- and homo-coupling of carbazole-type derivatives: o) Louillat, M.-L.; Patureau, F. W. *Org. Lett.* **2013**, *15*, 164; p) Louillat, M. L.; Biafora, A.; Legros, F.; Patureau, F. W. *Angew. Chem. Int. Ed.* **2014**, *53*, 3505; and 8) *para*-Hydroxylation of anisole-type substrates with iodine(III)species: q) Liu, W.; Ackermann, L. *Org. Lett.* **2013**, *15*, 2013.

[135] a) Ackermann, L.; Vicente, R.; Potukuchi, H. K.; Pirovano, V. *Org. Lett.* **2010**, *12*, 5032; b) Ackermann, L. *Chem. Rev.* **2011**, *111*, 1315; c) Ackermann, L. *Acc. Chem. Res.* **2014**, *47*, 281.

[136] a) Jessop, P. G.; Morris, R. H. *Coord. Chem. Rev.* **1992**, *121*, 155; b) Prechtl, M. H.; Holscher, M.; Ben-David, Y.; Theyssen, N.; Loschen, R.; Milstein, D.; Leitner, W. *Angew. Chem. Int. Ed.* **2007**, *46*, 2269.

[137] Ferrer Flegeau, E.; Bruneau, C.; Dixneuf, P. H.; Jutand, A. *J. Am. Chem. Soc.* **2011**, *133*, 10161.

[138] Dyatkin, B. L.; Mochalina, E. P.; Knunyants, I. L. *Tetrahedron* **1965**, *21*, 2991.

[139] Lomas, J. S. *J. Phys. Org. Chem.* **2012**, *25*, 620.

[140] Hydrogen atoms and $CHCl_3$ deriving from crystallization (see crystallographic section) were removed for clarity from the X-ray structure of **Ru1-39c** (Figure 2.3).

[141] Fernandez, S.; Pfeffer, M.; Ritleng, V.; Sirlin, C. *Organometallics* **1999**, *18*, 2390.

[142] Hansch, C.; Leo, A.; Taft, R. W. *Chem. Rev.* **1991**, *91*, 165.

[143] a) Zelonka, R. A.; Baird, M. C. *J. Organomet. Chem.* **1972**, *44*, 383; b) Bennett, M. A.; Smith, A. K. *J. Chem. Soc. Dalton Trans.* **1974**, 233; c) Weber, W.; Ford, P. C. *Inorg. Chem.* **1986**, *25*, 1088.

[144] Sollert, C.; Devaraj, K.; Orthaber, A.; Gates, P. J.; Pilarski, L. T. *Chem. Eur. J.* **2015**, *21*, 5380.

[145] Hydrogen atoms and BF_4 counteranion of **Ru2-39c** (see crystallographic section) were removed for clarity from the X-ray structure of **Ru2-39c** (Figure 2.3).

[146] Hydrogen atoms and BF_4 counteranions of **Ru-C5** (see crystallographic section) were removed for clarity from the X-ray structure of of **Ru-C5** (Figure 2.6).

[147] Fabre, I.; von Wolff, N.; Le Duc, G.; Ferrer Flegeau, E.; Bruneau, C.; Dixneuf, P. H.; Jutand, A. *Chem. Eur. J.* **2013**, *19*, 7595.

[148] Campeau, L.-C.; Parisien, M.; Jean, A.; Fagnou, K. *J. Am. Chem. Soc.* **2006**, *128*, 581.

[149] Sun, C. L.; Li, H.; Yu, D. G.; Yu, M.; Zhou, X.; Lu, X. Y.; Huang, K.; Zheng, S. F.; Li, B. J.; Shi, Z. J. *Nat. Chem.* **2010**, *2*, 1044.

[150] Ackermann, L.; Vicente, R.; Potukuchi, H. K.; Pirovano, V. *Org. Lett.* **2010**, *12*, 5032.

[151] Aihara, Y.; Chatani, N. *Chem. Sci.* **2013**, *4*, 664.

[152] Hubrich, J.; Himmler, T.; Rodefeld, L.; Ackermann, L. *ACS Catal.* **2015**, *5*, 4089.

[153] Calculations performed with G09 using B3LYP functional and 6-31G basis set with polarization functions for C, H, O, N and F atoms, SDD base and ECPs for Ru (see computational section).

[154] Other models studied are *fac*- and *mer*-$Ru(OAc)_2(MeCN)_2$, and $Ru[(OC(CF_3)_3](OAc)(MeCN)_3$. All of them provided similar barriers (see computational section).

[155] Espenson, J. H. *Chemical Kinetics and Reaction Mechanisms*, 2nd ed. McGraw-Hill: New York, 1995.

[156] a) Sagel, I. H. *Enzyme Kinetics: Behavior and Analysis of Rapid Equilibrium and Steady-State Enzyme Systems;* Wiley-Interscience: New York, 1975; b) Diao, T.; Stahl, S. S. *J. Am. Chem. Soc.* **2011**, *133*, 14566; c) Pun, D.; Diao, T.; Stahl, S. S. *J. Am. Chem. Soc.* 2013, 135, 8213.

[157] Do, H.-Q.; Daugulis, O. *J. Am. Chem. Soc.* **2009**, *131*, 17052.

[158] Kumar, A.; Bhakuni, B. S.; Prasad, C. D.; Kumar, S.; Kumar, S. *Tetrahedron* **2013**, *69*, 5383.

[159] Julich-Gruner, K. K.; Kataeva, O.; Schmidt, A. W.; Knolker, H. J. *Chem. Eur. J.* **2014**, *20*, 8536.

[160] Maiti, D.; Buchwald, S. L. *J. Org. Chem.* **2010**, *75,* 1791.

[161] Masahiko, S. **2012**, US 2012/232283 A1

[162] Ackermann, L.; Lygin, A. V. *Org. Lett.* **2011**, *13*, 3332.

[163] Molina de la Torre, J. A.; Espinet, P.; Albéniz, A. C. *Organometallics* **2013**, *32*, 5428.

[164] Arockiam, P. B.; Fischmeister, C.; Bruneau, C.; Dixneuf, P. H. *Angew. Chem. Int. Ed.* **2010**, *49*, 6629.

[165] Bruce, D. W.; Metrangolo, P.; Meyer, F.; Pilati, T.; Prasang, C.; Resnati, G.; Terraneo, G.; Wainwright, S. G.; Whitwood, A. C. *Chem. Eur. J.* **2010**, *16*, 9511.

[166] Korenaga, T.; Kosaki, T.; Fukumura, R.; Ema, T.; Sakai, T. *Org. Lett.* **2005**, *7*, 4915.

[167] Ye Wei; Kan, J.; Wang, M.; Su, W.; Hong, M. *Org. Lett.* **2009**, *11*, 3346.

[168] Xingyi, Z.; Feng, L.; Weike, S. *Tetrahedron Lett.* **2013**, *54*, 1285.

[169] Rene, O.; Fagnou, K. *Org. Lett.* **2010**, *12*, 2116.

[170] Lafrance, M.; Shore, D.; Fagnou, K. *Org. Lett.* **2006**, *8*, 5097.

[171] Shang, R.; Xu, Q.; Jiang, Y. Y.; Wang, Y.; Liu, L. *Org. Lett.* **2010**, *12*, 1000.

[172] Yuen, O. Y.; Charoensak, M.; So, C. M.; Kuhakarn, C.; Kwong, F. Y. *Chem. Asian. J.* **2015**, *10*, 857.

[173] Hari, D. P.; Hering, T.; König, B. *Org. Lett.* **2012**, *14*, 5334.

[174] Chiong, H. A.; Daugulis, O. *Org. Lett.* **2007**, *9*, 1449.

[175] Kim, M.; Kwak, J.; Chang, S. *Angew. Chem. Int. Ed.* **2009**, *48*, 8935.

[176] Luo, N.; Yu, Z. *Chem. Eur. J.* **2010**, *16*, 787.

[177] Ackermann, L.; Diers, E.; Manvar, A. *Org. Lett.* **2012**, *14*, 1154.

[178] Ding, Y.-J.; Li, Y.; Dai, S.-Y.; Lana, Q.; Wang, X.-S. *Org. Biomol. Chem.* **2015**, *13*, 3198.

[179] M. J. Frisch, G. W. Trucks, H. B. Schlegel, G. E. Scuseria, M. A. Robb, J. R. Cheeseman, G. Scalmani, V. Barone, B. Mennucci, G. A. Petersson, H. Nakatsuji, M. Caricato, X. Li, H. P. Hratchian, A. F. Izmaylov, J. Bloino, G. Zheng, J. L. Sonnenberg, M. Hada, M. Ehara, K. Toyota, R. Fukuda, J. Hasegawa, M. Ishida, T. Nakajima, Y. Honda, O. Kitao, H. Nakai, T. Vreven, J. A. Montgomery, Jr., J. E. Peralta, F. Ogliaro, M. Bearpark, J. J. Heyd, E. Brothers, K. N. Kudin, V. N. Staroverov, T. Keith, R. Kobayashi, J. Normand, K. Raghavachari, A. Rendell, J. C. Burant, S. S. Iyengar, J. Tomasi, M. Cossi, N. Rega, J. M. Millam, M. Klene, J. E. Knox, J. B. Cross, V. Bakken, C. Adamo, J. Jaramillo, R. Gomperts, R. E. Stratmann, O. Yazyev, A. J. Austin, R. Cammi, C. Pomelli, J. W. Ochterski, R. L. Martin, K. Morokuma, V. G. Zakrzewski, G. A. Voth, P. Salvador, J. J. Dannenberg, S. Dapprich, A. D. Daniels, O. Farkas, J. B. Foresman, J. V. Ortiz, J. Cioslowski, and D. J. Fox, Gaussian, Inc., Wallingford CT, **2010**.

[180] Becke, A. D. *J. Chem. Phys.* **1993**, *98*, 5648.

[181] a) Lee, C.; Yang, W.; Parr, R. G. *Phys. Rev. B* **1988**, *37*, 785; b) Miehlich, B.; Savin, A.; Stoll, H.; Preuss, H. *Chem. Phys. Lett.* **1989**, *157*, 200.

[182] Andrae, D.; Haeussermann, U.; Dolg, M.; Stoll, H.; Preuss, H. *Theor. Chem. Acc.* **1990**, *77*, 123.

[183] a) Hariharan, P. C.; Pople, J. A. *Mol. Phys.* **1974**, *27*, 209; b) Francl, M. M.; Pietro, W. J.; Hehre, W. J.; Binkley, J. S.; DeFrees, D. J.; Pople, J. A.; Gordon, M. S. *J. Chem. Phys.* **1982**, *77*, 3654; c) Rassolov, V. A.; Ratner, M. A.; Pople, J. A.; Redfern, P. C.; Curtiss, L. A., *J. Comp. Chem.* **2001**, *22*, 976.

[184] a) Fukui, K. *Acc. Chem. Res.* **1981**, *14*, 363; b) Hratchian, H. P.; Schlegel, H. B., *J. Chem. Theor. Comput.* **2005**, *1*, 61.